



# **Novel Pronucleotide Reporters for bioorthogonal Labeling of Nucleic Acids**

## **Dissertation**

to obtain the Scientific Doctoral Degree

by

**Vincente Tassilo Sterrenberg**

(born in Husum)

presented to

the Department of Chemistry of the Faculty of Sciences at  
University of Hamburg



First Reviewer: Prof. Dr. Chris Meier

Second Reviewer: Prof. Dr. Volkmar Vill

Third Reviewer: Prof. Dr. Piet Herdewijn

Disputation Date: 17.02.2023



The presented work was compiled in the group of Prof. Dr. Chris Meier at the Institute of Organic Chemistry in the Department of Chemistry at the University of Hamburg from October 2017 until October 2022.



## Abstract

Recent technological advances in fluorescence microscopy provide the opportunity to visualize cellular or viral processes in living systems with high spatiotemporal resolution. Next to these technological advancements, there was significant progress in the field of catalyst-free bioorthogonal reactions. The inverse electron demand Diels-Alder reaction (**DA<sub>INV</sub>**) provides exceptional reaction rates between two reactive partners, while being highly specific, thus enabling the tracking of labeled biomolecules in living cells. The attachment of synthetic fluorophores, which meet the demand of modern fluorescence microscopy, to biomolecules of interest, provides an exciting opportunity to study live-cell dynamic processes. A significant advantage of the **DA<sub>INV</sub>** is its high adjustability regarding reaction kinetics, biocompatibility, and stability. By identifying the individual most suitable reaction partners, this work aims to develop application-orientated nucleoside and pronucleotide reporters, which enable the visualization of cellular and – especially – viral nucleic acids in living systems. Combining the latest developments in the field of bioorthogonal reactions with our expertise in pronucleotide systems achieved an eagerly awaited breakthrough in live-cell imaging of *in vivo* labeled nucleic acids.





## Überblick

Neue technologische Fortschritte im Bereich der Fluoreszenzmikroskopie eröffnen die Möglichkeit einen Einblick in zelluläre und virale Prozesse in lebenden Systemen zu gewinnen mit einer hohen räumlich-zeitlichen Auflösung. Neben technischen Verbesserungen im Bereich der Mikroskopie gab es auch einen spannenden Fortschritt im Feld der bioorthogonalen *Click*-Reaktionen. Die Diels-Alder Reaktion mit inversem Elektronenbedarf (**DA<sub>INV</sub>**) eröffnet nie dagewesene Reaktionskinetiken zwischen zwei reaktiven Partnern, mit hoher Spezifität, und ermöglicht somit die Verfolgung von markierten Biomolekülen in lebenden Zellen. Das Anbringen von synthetischen Fluorophoren, welche den Anforderungen von modernen Fluoreszenzmikroskopen gewachsen sind, an das Biomolekül von Interesse, erlaubt die spannende Möglichkeit dynamische Prozesse in lebenden Systemen zu studieren. Ein großer Vorteil der **DA<sub>INV</sub>** liegt in der Anpassungsfähigkeit der Reaktionspartner und in der Möglichkeit die Reaktivität, die Biokompatibilität und die Stabilität für die vorliegende Fragestellung anzupassen. Diese Arbeit erhebt den Anspruch, anwendungsorientierte Pronukleotide zu entwickeln, welche die Visualisierung von zellulären und – im Speziellen – von viralen Nukleinsäuren in lebenden Systemen ermöglicht. Die Kombination der Entwicklungen im Bereich der bioorthogonalen Reaktionen mit unserer Expertise im Bereich der Pronukleotid-Chemie ermöglichte den lang ersehnten Durchbruch im *live-cell imaging* von *in vivo* markierten Nukleinsäuren.



# Table of Contents

<b>Abstract</b> .....	<b>I</b>
<b>Überblick</b> .....	<b>III</b>
<b>Table of Contents</b> .....	<b>V</b>
<b>List of Abbreviations</b> .....	<b>IX</b>
<b>1 Introduction</b> .....	<b>1</b>
<b>2 Theory</b> .....	<b>2</b>
2.1 Viral replication.....	2
2.2 Human immunodeficiency virus .....	3
2.3 Herpes simplex virus.....	7
2.4 Fluorescence imaging .....	10
2.5 Nucleoside reporters .....	13
2.6 The inverse electron demand Diels-Alder reaction (DA <sub>INV</sub> ) .....	16
2.6.1 Tuning the diene .....	19
2.6.2 Tuning the dienophile.....	19
2.6.3 Vinyl-label .....	21
2.6.4 Norbornene-label .....	23
2.6.5 1MCP-label.....	24
2.6.6 TCO-label.....	25
2.6.7 Tetrazine-label .....	27
2.6.8 Reflection.....	28
2.7 Synthetic Fluorophores.....	32
2.8 Pronucleotide concept.....	36
<b>3 Objectives</b> .....	<b>45</b>
<b>4 Results and discussions</b> .....	<b>48</b>
4.1 Synthesis of vinyl-modified nucleosides and their TriPPPPro's.....	48
4.2 $\gamma$ -alkylated triphosphates and their prodrugs .....	67
4.3 Design and synthesis of 1MCP-pronucleotide reporters – finding the motif.....	74
4.4 Design and synthesis of rapid pronucleotide reporters .....	84
4.4.1 Deoxycytidine multitool precursor .....	84
4.4.2 Nicotinic acid-conjugated TriPPPPro compound .....	86
4.4.3 TCO/BCN-conjugated TriPPPPro compounds – finding the motif .....	90
4.4.4 $\gamma$ -(C9C9AB)-MeTz-(E)-dUTP synthesis.....	99
4.5 Synthesis of a dye-conjugated TriPPPPro compound.....	106

---

4.6	Building dye-tetrazine conjugates .....	111
4.7	Imaging.....	120
4.7.1	TriPPPPro stability .....	122
4.7.2	TriPPPPro screening .....	125
4.7.3	Evaluation and comparison of the 1MCP and 2TCO $\alpha$ label .....	134
4.7.4	Evaluation of the TriPPPPro concept .....	144
4.7.5	Evaluation of live-cell applications.....	148
4.7.6	Evaluation of vinyl functionalized pronucleotides.....	155
4.8	Study and production of genome labeled HSV-1.....	160
4.9	Study and production of genome labeled HIV-1.....	172
<b>5</b>	<b>Summary .....</b>	<b>181</b>
<b>6</b>	<b>Experimental Part .....</b>	<b>186</b>
6.1	General.....	186
6.2	Imaging.....	188
6.2.1	HSV-1 Virus.....	188
6.2.2	Vero cell culture .....	188
6.2.3	Spinning-disk fluorescence microscopy .....	188
6.2.4	Dual-labeled HSV-1 virus production .....	189
6.2.5	Imaging in fixed cells .....	190
6.2.6	Live-cell imaging.....	190
6.2.7	Dose curve for virus production .....	191
6.2.8	Plaque Assay .....	191
6.2.9	Labeled virus genome detection in virions .....	191
6.2.10	Infection of cells with HSV-1 <sup>2TCO</sup> .....	192
6.2.11	Infection of cells with HSV-1 <sup>TriPPPPro+dye</sup> .....	192
6.2.12	Cell culture and production of genome labeled HIV-1 $\Delta$ env viral particles.....	192
6.2.13	Quantification of light signals and colocalization with confocal laser microscope 193	
6.2.14	Live-cell imaging with dual-labeled HIV-1.....	193
6.2.15	Correlative light-electron microscopy.....	194
6.2.16	Statistical analysis for HIV-1 particle labeling .....	194
6.3	Synthesis .....	195
6.3.1	Preparation of masking units .....	200
6.3.2	7-Deaza-7-vinyl-2'-deoxyadenosine series .....	206
6.3.3	7-Deaza-7-vinyladenosine series .....	218
6.3.4	5-Vinyl-2'-deoxyuridine series .....	230
6.3.5	5-Vinyluridine series.....	242
6.3.6	Preparation of $\gamma$ -(C9C9AB)-MeTz-(E)-dUTP .....	252
6.3.7	Preparation of the 3,6-di-2-pyridyl-1,2,4,5-tetrazine motifs.....	258

Table of Contents

---

6.3.8	Preparation of rhodamine-tetrazine-conjugates.....	265
6.3.9	Preparation of $\gamma$ -(C9C9AB)-SiR-dCTP .....	273
6.3.10	Preparation of 1MCP-modified pronucleotides .....	278
6.3.11	Preparation of rapid pronucleotide reporters.....	295
6.3.12	Preparation of the $\gamma$ -(C9C9AB)-NcTz-dCTP .....	308
<b>7</b>	<b>References .....</b>	<b>312</b>
<b>8</b>	<b>Hazardous substance register .....</b>	<b>330</b>
	<b>Acknowledgements .....</b>	<b>347</b>
	<b>Declaration on Oath.....</b>	<b>349</b>



**List of Abbreviations**

1MCP	1-methylcyclopropene
2TCO $\alpha$	2-ene <i>trans</i> -cyclooctene, <i>axial</i>
3TCO	3-ene <i>trans</i> -cyclooctene
4TCO	4-ene <i>trans</i> -cyclooctene
A	adeonsine
AB	acyloxybenzyl
AC	adenylyl cyclase
Ac	acetyl
AF488	AlexaFluor488
AHA	L-azidohomoalanine
AIDS	acquired immune deficiency syndrome
AsPh <sub>3</sub>	triphenylarsine
BAB	bis(acyloxybenzyl)
BBB	blood-brain barrier
BCN	bicyclo[6.1.0]nonyne
Bn	benzyl
BODIPY	boron-dipyrromethene class
bp	base pair
Bu	butyl
Bz	benzoyl
C	cytidine
CA	capsid
CCO	<i>cis</i> -cyclooctene
CD4 <sup>+</sup>	cluster of differentiation 4
CEM/0	cell line derived from human T cells
cryo-ET	cryo-electron tomography
CSSB	Centre for Structural Systems Biology
CuAAC	copper-catalyzed azide-alkyne cycloaddition,
Cy5	Cyanine 5
<i>cycloSal</i>	<i>cycloSaligenyl</i>

d	doublet (NMR)
d4T	Stavudin
DA <sub>INV</sub>	inverse electron demand Diels-Alder reaction
DCC	<i>N,N'</i> -Dicyclohexylcarbodiimid
DCI	4,5-dicyanoimidazole
dd	douplet of douplet (NMR)
ddBCNA-TP	2',3'-dideoxy-bicyclic-nucleoside triphosphate
ddd	douplet of douplet of douplet (NMR)
ddt	douplet of douplet of triplets (NMR)
DIPEA	<i>N,N'</i> -Diisopropylethylamine
DiPPro	a nucleoside diphosphate prodrug
DMAP	4-Dimethylaminopyridine
DMEM	Dulbecco's Modified Eagle's Medium
DMF	<i>N,N'</i> -Dimethylformamide
DMSO	dimethyl sulfoxide
DNA	deoxyribonucleic acid
DNA pol $\gamma$	mitochondrial deoxyribonucleic acid polymerase $\gamma$
DPP	diphenyl phosphine
dt	douplet of triplets (NMR)
dTCO	dioxolane-fused <i>trans</i> -cyclooctene
DTE	dithiodiethanol
dTTP	2'-deoxythymidine triphosphate
dUMP	2'-deoxyuridine monophosphate
dUTP	2'-deoxyuridine triphosphate
dUTPase	dUTP diphosphatase
E	delayed early
EE	early endosomes
EM	electron microscopy
Equiv	equivalent
ER	endoplasmic reticulum
ESI	electro spray ionization



Et	ethyl
FBS	fetal bovine serum
FDA	food and Drug Administration
FISH	fluorescence In Situ Hybridization
Fm	fluorenylmethyl
Fm	9-Fluorenylmethyl
FP	fluorescent protein
FRET	Förster resonance energy transfer
G	guanosine
Gag	group-specific antigen
GCE	genetic code expansion
GFP	green fluorescent protein
<i>H,H</i> -COSY	proton correlative spectroscopy
HATU	<i>O</i> -(7-Azabenzotriazol-1-yl)- <i>N,N,N',N'</i> -tetramethyluronium-hexafluorophosphat
HDP	hexadecyloxypropyl
HIV-1	human immunodeficiency virus
HMBC	heteronuclear multiple-bond correlation
HOMO	highest occupied molecular orbital
HPI	Heinrich-Pette-Institut
hpi	hours post infection
HPLC	high performance liquid chromatography
HRMS	high resolution mass spectrometry
HSQC	heteronuclear single-quantum correlation
HSV-1	herpes simplex virus type 1
ICP8	viral replication protein 8
IE	immediate-early
IFN	interferone
IN	integrase
<i>i</i> Pr	<i>iso</i> -propyl
IR	infrared spectroscopy

<i>J</i>	coupling constant (NMR)
JF526/549	Janelia Fluor 526/549
kbp	kilo base pairs
L	late
LUMO	lowest unoccupied molecular orbital
m	multiplet (NMR)
M	molar (mol·L <sup>-1</sup> )
MALDI	matrix assisted laser desorption ionization
mCh	mCherry
MOI	multiplicity of infection
mRNA	messenger ribonucleic acid
MS	mass spectrometry
Ms	mesyl
Nc	nicotinic acid
ncAAs	noncanonical amino acids
NCS	<i>N</i> -Chlorosuccinimide
NcTz	6-(6-methyl-1,2,4,5-tetrazine-3-yl)nicotinic acid
NDP	nucleoside diphosphate
NHS	<i>N</i> -hydroxysuccinimide
NMP	nucleoside monophosphate
NMR	nuclear magnetic resonance
NP	normal phase
NPC	nuclear pore complex
NTC	nuclear transport complex
NTP	nucleoside triphosphate
PAGE	polyacrylamide gel electrophoresis
PBS	phosphate buffer saline
PCR	polymerase chain reaction
PEX	primer extension experiments
PIC	pre-integration complex
POC	isopropylloxymethyl carbonate

POM	pivaloyloxymethyl group
PR	protease
Pr55	Gag precursor polyprotein
ProTide	a nucleoside phosphoramidate prodrug
Py <sub>2</sub> Tz	6-di-2-pyridyl-1,2,4,5-tetrazine
RC	replication compartments
RNA	ribonucleic acid
RP	reversed phase
RT	reverse transcriptase
rt	room temperature
RTC	reverse transcription complex
SATE	S-acylthioethyl ester
SiR	silicon-rhodamine
SPAAC	strain-promoted azide-alkyne cycloaddition
SPIEDAC	strain-promoted inverse electron-demand Diels-Alder cycloaddition
ssDNA	single-stranded DNA
T	thymidine
t	triplet (NMR)
TAMRA	carboxytetramethylrhodamine
TBET	through bond energy transfer
<i>t</i> Bu	<i>tert</i> -butyl
TCO	<i>trans</i> -cyclooctene
TDA-1	<i>tris</i> -[2-(2-methoxyethoxy)-ethyl]amine
TEAH	triethylamine
TEAB	triethylammonium bicarbonate
TEP	triethyl phosphate
Tf	triflate
TFA	trifluoroacetic acid
TFAA	trifluoroacetic anhydride
TFP	tri-(2-furyl) phosphine

THF	tetrahydrofuran
TLC	thin layer chromatography
TMP	trimethyl phosphate
TMS	trimethylsilyl
TNG	trans-Golgi network
Tol	toloyl
TPP	triphenylphosphine
TreatHF	triethylamine trihydrofluorid
TriPPPPro	nucleoside triphosphate prodrug
Tz	1,2,4,5-tetrazine
U	uridine
UL2	gene for uracil <i>N</i> -glycosylase
UL50	gene for deoxyuridine 5'-triphosphate nucleotidohydrolase
VACV	vaccinia virus
vDNA	viral DNA
VP26mCh	virion polypeptide 26 fused with mCherry
VP-SFM	Virus production serum-free medium
vRNA	viral RNA
WHO	World Health Organization

# 1 Introduction

The coronavirus outbreak in late 2019, leading to the great pandemic with countless deaths and a global economic crisis, reminded the world once again how essential it is to join forces against infectious diseases. In a globalized world, where people move closer together, infectious diseases can spread at a devastating speed and threaten lives, our way of living, and free movement. Fortunately, the scientific world combined their knowledge to face the great danger without precedent.

By the paradigm *know your enemy*, it is of utmost importance to gain deep insights into viral processes inside the cellular machinery in order to inhibit viral diseases by finding the targets of tomorrow.

This work aims to provide chemical reporters to visualize viral genomes in living cells via fluorescence microscopy (live-cell imaging of single particles) by combining novel developments in the field of bioorthogonal reactions and our expertise in pronucleotide chemistry.

Collaborations with the Leibnitz-Institut for experimental virology (LIV), Hannover Medical School (MHH), and the Centre for Structural Systems Biology (CSSB) in Hamburg offered the unique opportunity to develop application-based pronucleotide reporters with the promising outlook of providing much-needed tools to gain deep insights into virus-cell interactions.

## 2 Theory

### 2.1 Viral replication

Humans live in a natural balance with bacteria and other microorganisms, constructing a deeply interdependent synergy.<sup>1,2</sup> Alongside this collaborative life, something else evolved—a defect of life itself. Viruses arose from ancient cells to ultimately destroy their origin.<sup>3</sup> Understanding viruses is vital in finding targets for novel antiviral therapeutics and understanding life itself. Originated from cells, viruses make use of the cellular machinery and provide insights into cellular dynamic processes, which are yet unknown.<sup>4</sup>

Viral particles of different families can differ significantly in size, morphology, structure, and function. Non-enveloped virions consist of nucleic acids protected by structural proteins, called the capsid core. Enveloped particles are further surrounded by a phospholipid membrane derived from the host cell. Viral glycoproteins are expressed on the membrane surface and are required for cell attachment and host-cell entry. While viruses supply some enzymes and accessory proteins, they lack the self-sustainability to translate new proteins. Therefore, they widely use the cellular machinery and resources to reproduce and spread.

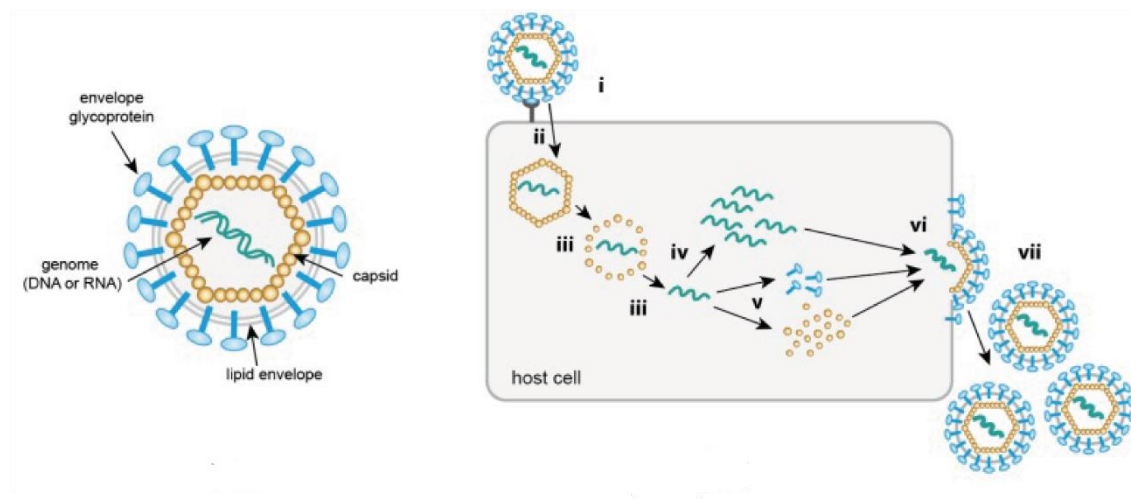


Figure 1: General structure of an enveloped virus (left) and schema of the viral replication process inside the host-cell (right).<sup>4</sup>

After attachment (i) and fusion or endocytosis of the virion with the host cell (ii), the pathogen undergoes a dynamic change in physical structure under complex interactions with cellular components, which can vary significantly between virus families. The uncoating or destabilization of the structural proteins (iii) occurs in the cytoplasm or at

the nucleus. The viral genome is transcribed or replicated (iv) either in the cytoplasm or inside the cell nucleus. Viral proteins are being translated by the cellular machinery (v) and subsequently assembled into progeny viral particles together with the replicated viral genome. This process occurs in the cytoplasm or directly at the cell membrane (vi). Viral particles are released via exocytosis, lysis, or viral budding (vii).<sup>4</sup>

During the early infection cycle, the virion undergoes a disassembly process and the initial viral structure disintegrates into subviral structures, which are under continuous transformation throughout viral reproduction in the host cell. Imaging techniques like electron microscopy (EM) or x-ray crystallography rely on detectable morphologies and highly consistent structures, which makes it difficult to identify subviral structures inside of the host cell environment. Furthermore, EM techniques only give a snapshot rather than capturing dynamic processes, which is essential for understanding the well-orchestrated virus-host interactions.

Although viral particle size ranges from 20 – 300 nm and is below the resolution limit of light microscopy, the attachment of a fluorophore to viral substructures of interest allows their localization inside the cell. To date, bioorthogonal labeling of nucleic acids inside of cells mostly requires fixation and permeabilization of the samples to obtain a sufficient signal-to-noise ratio of the image. However, this approach only allows taking a snapshot at a particular time point and impedes the visualization of dynamic processes. Therefore, the development of novel reporters, which enable live-cell imaging of dynamic processes, is highly desirable. The emerging interest to investigate dynamic processes in living cells or tissues is fueled by increasingly powerful light microscopy. Confocal and light sheet microscopy enable 3D tracking of objects over time and visualize dynamic processes with high temporal resolution in living cells.<sup>4</sup> Furthermore, newly emerging super-resolution microscopy techniques make fluorescent microscopy a promising imaging procedure for the foreseeable future.<sup>5</sup>

## **2.2 Human immunodeficiency virus**

The human immunodeficiency virus (HIV-1) causes the acquired immunodeficiency syndrome (AIDS) in patients who do not receive antiretroviral therapy. Like lentiviruses, HIV-1 can infect non-dividing cells, which is in contrast to retroviruses from other genera that rely on the breakdown of nuclear membranes during cell division. The virus infects CD4<sup>+</sup> cells, which play a significant role in the human immune response (Figure 2). After

fusion of the membranes, the conical capsid core, which contains the viral RNA genome (vRNA) of the retrovirus and viral enzymes such as the reverse transcriptase (RT), the integrase (IN), and the protease (PR) are released into the cytoplasm of the cell.<sup>6,7</sup>

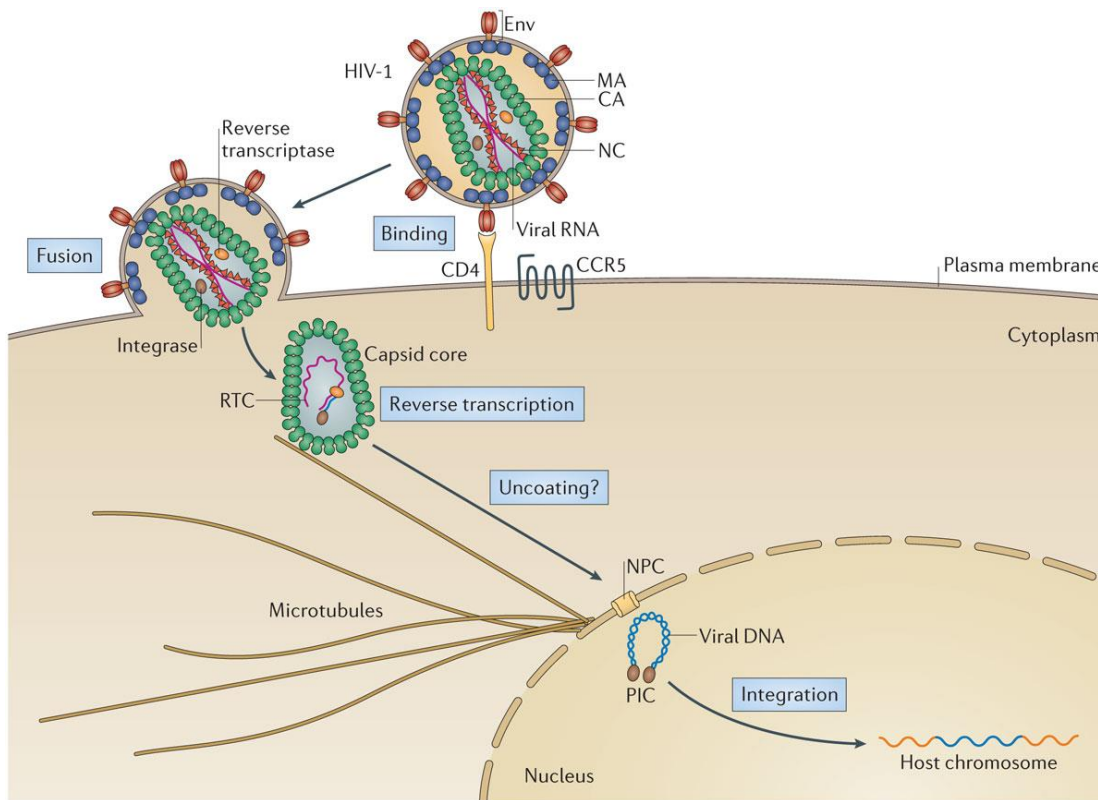


Figure 2: Schema of the early infection cycle of HIV-1 with the host cell with the reverse transcription complex (RTC), the pre-integration complex (PIC), and the nuclear pore complex (NPC).<sup>7</sup>

The cytoplasm is a hostile environment for retroviral genome replication since sensing of viral DNA (vDNA) by cytosolic nucleic acid sensors induces innate immunity, thereby preventing viral infection.<sup>8,9</sup> Therefore, the capsid (CA) plays a significant role in protecting the viral genome from host cell factors and in transporting the viral information to the nucleus.<sup>10</sup> The subviral protective shell consists of ~1200–1500 CA molecules assembled into hexamers and pentamers, giving the virion its structural integrity.<sup>11,12</sup> Overall, the capsid functions as a compartment that protects the reverse transcription complex (RTC) from cellular factors to ensure the unimpaired reverse transcription of the vRNA to the nascent double-stranded vDNA. While it has been established that the RT initiates reverse transcription in the cytoplasm, recent evidence suggests that the vDNA synthesis is completed inside the nucleus.<sup>13–15</sup>

Since the HIV-1 capsid has a length of ~120 nm and a width of ~60 nm, it presumably exceeds the dimensions of the nuclear pore complex (NPC) channel, which has a reported maximal diameter of ~40 nm.<sup>16</sup> This implies that the CA-lattice should – at



least partially – break down before nuclear entry of the RTC.<sup>10</sup> Until recently, there were three models for viral uncoating (Figure 3): Firstly, the immediate uncoating, where the capsid proteins disassemble shortly after the fusion near the cell membrane. Secondly, the cytoplasmic uncoating, where measurable CA remains associated with the RTC. Finally, the NPC uncoating, arguing that the capsid core is largely intact while interacting with the NPC.<sup>7</sup>

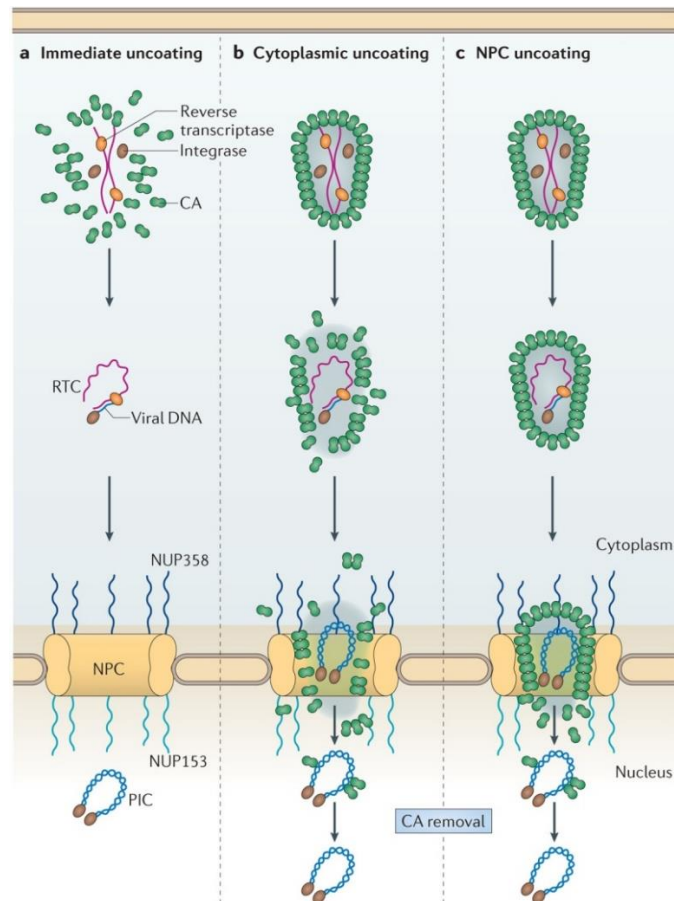


Figure 3: Schema for the three models for viral uncoating. The immediate (a), the cytoplasmic (b), and the nuclear pore complex (NPC, c) uncoating.<sup>7</sup>

However, more recent publications report the presence of intact capsid lattice<sup>10,14,15</sup> and capsid-like structures<sup>17</sup> inside the cell nucleus. Additionally, more recent cryo-electron tomography (cryo-ET) of intact human cells suggests an average NPC diameter of ~64 nm, suggesting that the HIV-1 CA-lattice would be small enough for nuclear entry.<sup>17–19</sup> These new findings contradict the current models of capsid disassembly and open up the discussion of the early HIV-1 replication mechanisms.

After the release of the RTC into the nucleus, it is referred to as the pre-integration complex (PIC, Figure 3). The viral integrase – transported into the nucleus by host factors – incorporates nascent vDNA into actively transcribing regions of the host cell

genome.<sup>20–22</sup> The proviral DNA is transcribed into nascent spliced and unspliced viral mRNA. The spliced mRNA is translated into viral proteins by the cellular translation machinery. The assembly of the unspliced vRNA and the translated proteins is promoted by the Gag precursor polyprotein Pr55<sup>Gag</sup> at the cell membrane. Subsequent budding releases the viral particle from the host cell. Finally, the viral protease cleaves the Gag and GagPol polyprotein precursors resulting in a mature virion, which is ready for the next pathogenic cycle.

A detailed understanding of the transcription and transport of viral genetic information from the cell surface to the cellular core may have important therapeutic implications. Attacking the integrity of the capsid core by therapeutic agents could improve cellular response due to IFN-stimulated genes. Triggering the antiviral state would make the cells more resistant to viral infections.<sup>7</sup> However, the uncoating of the capsid core is still poorly understood and under debate in current literature. The development of innovative nucleoside reporter molecules – that overcome present limitations – could significantly contribute to the investigation of the intricate interplay of viral-host interactions with novel fluorescence microscopy techniques and enable the visualization of dynamic processes in living systems on a single particle level.<sup>4</sup>

## 2.3 Herpes simplex virus

The different viruses of the large herpesviridae family infect most of the human population and are responsible for many mild to severe diseases. Typical for herpesviruses is their ability to establish both lytic and latent infection cycles, which leads them to becoming especially harmful to immune-deficient patients by complicating their initial treatment. For alphaherpesviruses, lytic infection occurs in epithelial cells, whereas life-long latent infection is inherent in sensory neurons.<sup>23</sup> The most prevalent virus of this family is the herpes simplex virus type-1 (HSV-1).<sup>24</sup> Its viral genome consists of a linear double-stranded G+C rich (G+C, 67%) DNA sequence with around 150 kilo base pairs (kbp).<sup>25</sup> The genome is protected by a T= 16 icosahedral capsid consisting of 162 capsomers. The capsid is surrounded by ~20 protein species, which are defined as the tegument and play a key role in subverting the antiviral immune response of the host cell.<sup>26</sup> The tegument, in turn, is surrounded by the lipid bilayer envelope embedded with numerous viral glycoproteins protruding from the membrane surface.<sup>25,26</sup>

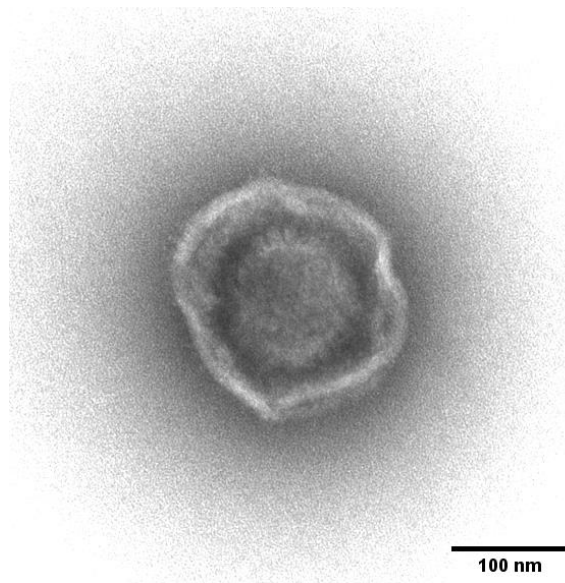


Figure 4: Transmission electron microscopy (TEM) image of HSV-1.

Herpesviruses enter the host cell by fusion with the membrane. The capsid is released into the cytoplasm. Since the capsids are too large to diffuse efficiently through the cytosol, the incoming capsids use cellular microtubules for transportation to the nuclear pore complex (NPC).<sup>27</sup> Here, the capsid uncoating occurs, and the dsDNA is injected through the NPC into the nucleus. In the nucleus, HSV-1 creates replication compartments (RC) which leads to an increase of the nuclear volume and displaces the

host chromatin to the nuclear periphery.<sup>28</sup> The rearrangement of the nucleus enables the efficient synthesis of large amounts of progeny DNA, transcription to mRNA, expression of viral proteins, and the assembly of new capsids. These distinct intranuclear sites provide an ideal environment for viral gene expression and replication.<sup>23,29</sup> The viral genome is transcribed sequentially and this can be divided into three phases: immediate-early (IE), delayed early (E), and late (L). Viral DNA is transcribed by host RNA polymerase II supported by viral factors throughout all stages of infection.<sup>26</sup> The translation to the viral gene products is thoroughly orchestrated, whereby the  $\alpha$  (or IE) genes are expressed first in the absence of *de novo* viral protein synthesis. The  $\alpha$  gene products are involved in repelling the host cell immune response and activating the expression of the  $\beta$  (or E) genes. Furthermore, a variety of the  $\beta$  gene products are enzymes and DNA-binding proteins, which are involved in viral DNA replication. After successful viral DNA replication, the  $\gamma$  (or L) gene products are translated efficiently and are involved mainly in the assembly of the progeny viral particles.<sup>29</sup> The *de novo* synthesized viral genomes are packed into new progenitor capsids, which egress from the nucleus by an envelopment-deenvelopment step at the inner and outer nuclear membrane.<sup>30</sup> The capsids are then transported to the cellular membrane for the final envelopment, followed by subsequent exocytosis.<sup>26</sup>

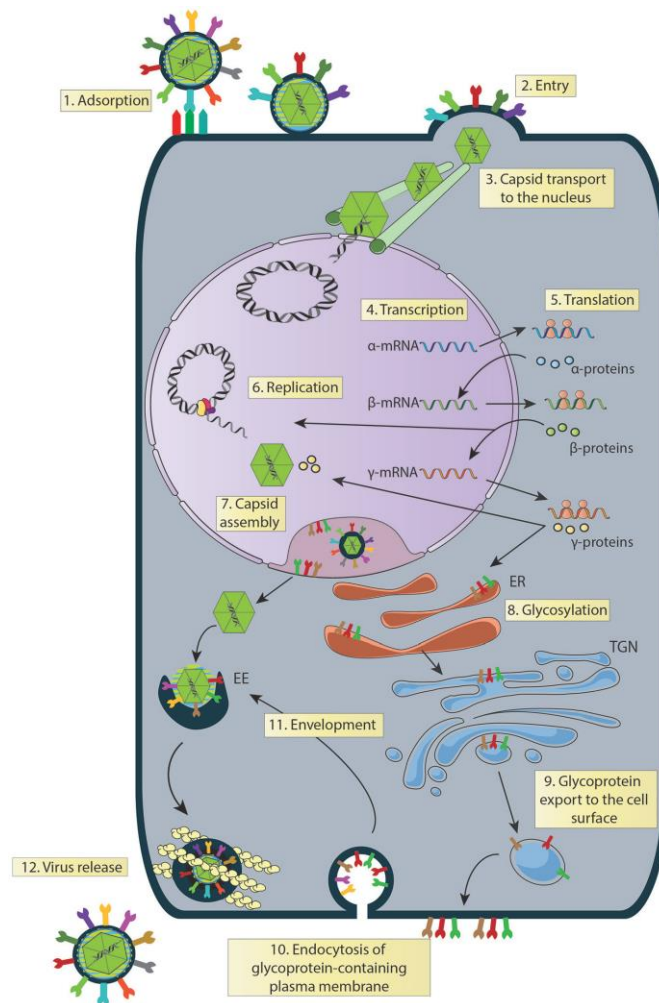


Figure 5: Illustration of the replication cycle of the herpes simplex virus type 1.<sup>26</sup>

The composition of herpes viruses is relatively complex, e.g., HSV-1 consists of more than 40 viral proteins as well as cellular proteins.<sup>25</sup> A variety of these proteins encoded by the viral genome regulate nucleotide metabolism (thymidine kinase, thymidylate synthase, dUTPase, ribonucleotide reductase), DNA replication (DNA polymerase, helicase, primase), DNA repair (uracil *N*-glycosylase, UL2), and posttranslational modifications (protein kinases). These enzymes ensure sufficient vDNA synthesis by simultaneously suppressing the host cell replication process and some potentially could influence the metabolic labeling process with unnatural nucleotide probes.

HSV-1 DNA polymerase is the key enzyme for vDNA replication and belongs to the family of B polymerases.<sup>24</sup> In the context of this work, the herpes polymerase is one major target enzyme regarding the visualization of viral DNA by employing nucleotide probes. The transcription to the respective vRNA is catalyzed by the host cell enzyme RNA polymerase II, which is the same polymerase responsible for transcribing the provirus of

HIV into its vRNA. Regarding RNA labeling, the RNA pol II is thus also a target enzyme during this work.

To analyze the virally induced remodeling events and understand the crucial steps in the viral replication cycle, additional tools that help to systematically study these events concerning their spatiotemporal occurrence in living cells are highly anticipated. A new generation of pronucleotide reporters that meet those demands could significantly contribute to gain deeper insight into the viral replication cycle.

## 2.4 Fluorescence imaging

Fluorescence imaging can bring us closer to a more comprehensive understanding of living matter by enlightening cellular and viral processes and dynamics at a single-cell level. Today, an increasing variety of fluorescent sensors enable the visualization of biomolecules with diverse approaches to target the biomolecule of interest.

*Immunolabeling* is widely used in identifying endogenous proteins linked to a primary antibody, which is often amplified by a secondary antibody conjugated to fluorophores. Recognition highly depends on the specificity of the primary antibody binding. Due to the inability of the antibodies to penetrate intact cells, this technique is usually restricted to permeabilized cells or the visualization of extracellular targets. Additionally, the multivalency of these probes can lead to oligomerization of the target proteins on cells.<sup>31</sup>

Via *genetic tagging*, fluorescent proteins (FP) can be fused to a protein. This imaging technique has its origin in discovering the green fluorescent protein (GFP) of the jellyfish *Aequorea victoria* and the technical feasibility to fuse it to the protein of interest by heterologous expression.<sup>32,33</sup> Since the discovery of GFP, numerous FP have been isolated and improved by protein engineering to advance their fluorescent and biochemical properties.<sup>34</sup> Due to the covalent attachment, the fluorescent signal is highly specific. However, the perturbation of the natural function of the labeled protein remains a concern and must be investigated for each application.<sup>35</sup> In addition, the photophysical properties required for advanced fluorescence microscopy are often unfulfilled by FPs.<sup>4</sup>

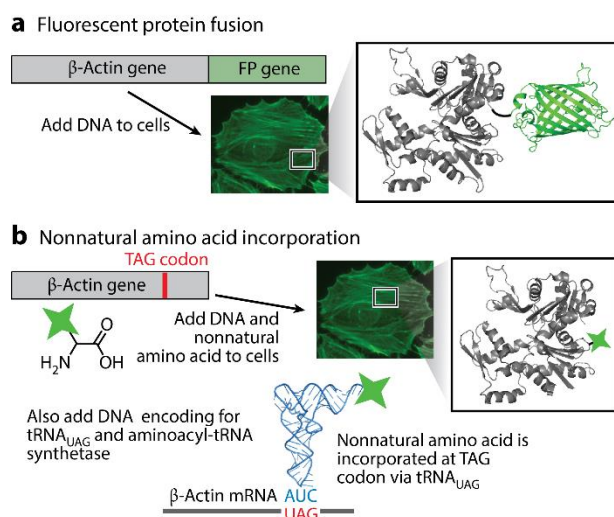


Figure 6: Two methods for obtaining fluorescently labeled proteins demonstrated on the example of beta-actin. FPs can be fused at the N- or C-termini of the target protein (a). The genetic code expansion (GCE) technology enables the introduction of nonconical amino acids (ncAAs) at any position of the protein of interest (b).<sup>35</sup>

To address this issue, unnatural amino acids can be incorporated into specific sites of the protein of interest and subsequently labeled by small-size fluorophore molecules, which meet the demands of advanced fluorescence imaging. These noncanonical amino acids (ncAAs) can be introduced into any protein position of interest via genetic code expansion (GCE) technology. A native codon is replaced by a rare amber (TAG) stop codon at the desired site of the gene to build in the ncAA during the expression of the protein of choice. The cellular translation machinery expresses the modified protein along with a tRNA–tRNA synthetase pair (tRNA-RS). The active side of the rRNA synthetase is genetically modified in order to only accept the specific ncAA, which is incorporated into the tRNA that recognizes the TAG codon. The appropriate DNA strands are transfected into the cells while the ncAA is added to the growth medium.<sup>36</sup> Either the fluorophore is already attached to the synthetic amino acid before incorporation, or an introduced functionality is chemo-selectively labeled post-synthetically by a fluorophore agent. Due to the absence of a bulky FP attachment, perturbation of the protein is less likely. The attachment of a synthetic fluorophore via a fast and specific bioorthogonal reaction is the least invasive strategy. However, unspecific binding or excess of the fluorophore conjugate might hamper the potential for live-cell imaging due to the high background signal.

The labeling of viral proteins is widely used in virology today and contributes significantly to understanding viral dynamics and the complex virus-cell interactions.

Next to the side-specific incorporation of fluorophores, a variety of non-specific stoichiometric labeling approaches were applied to study viral host-cell entry. The fluorescent dye-dequenching assay is frequently used to study viral fusion with the host cell. Here, alkyl chain carrying, intercalating membrane dyes, such as DiD, Octadecyl Rhodamin B (R18), or Texas Red™ DHP, are used to label viral membranes *in vitro* before host cell infection. The fluorophores undergo a self-quenching mechanism at higher dye concentrations, resulting in reduced fluorogenic viral particles. The fusion event with the cellular membrane results in a dequenching mechanism due to the distribution of the membrane-bound dye. The fluorescent enhancement mechanism allows the visualization of the spatiotemporal resolved single viral entry event into the live host cell. In addition to membrane fusion events, this methodology also provides insights into endocytic entry pathways.<sup>37</sup>

Besides intercalating dyes, amine-reactive dyes are used to covalently but non-specifically stain viral surface biomolecules.<sup>38</sup> Frequently used fluorophore-NHS-esters, can react with primary amines of lysine or thiol groups. For example, pH-sensitive dyes can be utilized to study the pH-dependent endocytic pathway of viruses.<sup>39</sup>

A combined weakness of these non-specific labeling approaches is that they cannot distinguish between infectious, genome-containing virions and empty, non-infectious particles. This disadvantage undermines the informative value of the visualized event and needs additional proof to verify an infectious pathway.

Shifting the focus on nucleic acid labeling, Fluorescence In Situ Hybridization (FISH) contributed significantly to finding specific DNA sequences in genomes by *in situ* hybridization with complementary DNA or RNA sensor probes. Historically, the methodology significantly contributed to mapping genes on the human chromosome. In virology, the detection of vDNA or vRNA via FISH played a crucial part in understanding basic virology today.<sup>4</sup> The advantage of the FISH methodology is the possibility of detecting specific sites in the genome. However, the technique can only be applied to fixed and denaturated samples. The harsh treatment required often interferes with immunofluorescence staining, and additionally, extensive cytoplasmatic extraction may result in an underrepresentation of subviral structures. Moreover, in most cases, FISH does not allow the discrimination between incoming viral genome and *de novo* synthesized viral nucleic acids deriving from viral genome transcription or the translation machinery.<sup>4</sup>



In contrast to the described labeling approaches for proteins, there is no comparable and efficient system in place for the metabolic labeling of nucleic acids in living systems. Direct chemical labeling of incoming newly-transcribed viral genome could overcome present limitations of the FISH technique<sup>4</sup> and simultaneously allow the differentiation between infectious and empty particles. Additionally, fast chemical nucleoside reporters would enable the visualization of tagged nucleic acids and their dynamic movement in same cell experiments.

Hence, this thesis aims to develop novel metabolic nucleoside reporters, which allow the visualization of *de novo* synthesized cellular or viral nucleic acids in or for living systems. However, the implementation of tools, which provide the ability to label single particles in live cells and simultaneously satisfy the demands of advanced fluorescence imaging, is challenging. The following chapters will give the reader an overview of nucleoside reporters and their limitation and unfold challenges and opportunities in the context of live-cell imaging.

## 2.5 Nucleoside reporters

In 1988, KNIPE *et al.* used 5-bromo-2'-deoxyuridine (BrdU) to label viral DNA in HSV-1 infected cells showing that the viral replication protein ICP8 organizes the formation of viral replication compartment within the cell nucleus.<sup>40</sup> The incorporated nucleoside reporter is detected by an immunofluorescent staining method with a BrdU-antibody. This methodology requires extensive denaturation of the fixed cells to make the labeled DNA accessible to the large antibody.<sup>41</sup>

Two decades later, 5-ethynyl-2'-deoxyuridine (**1**, EdU) was designed to overcome these limitations by introducing a small metabolic handle – the alkyne function.<sup>42</sup> The alkyne group reacts in a Cu(I)-catalyzed [3 + 2] cycloaddition reaction with an azide-fluorophore-conjugate (copper-catalyzed azide-alkyne cycloaddition, **CuAAC**,  $k' = 10^1$ – $10^2 \text{ M}^{-1}\text{s}^{-1}$ ). This first nucleoside reporter molecule for bioorthogonal labeling is still widely used in virology today.<sup>4</sup> Between 2011 and 2012, the derivatives 5-ethynyl-2'-deoxycytidine (**2**, EdC)<sup>43</sup> and 7-deaza-7-ethynyl-2'-deoxyadenosine (**3**, EdA)<sup>44</sup> were introduced and validated for labeling applications.

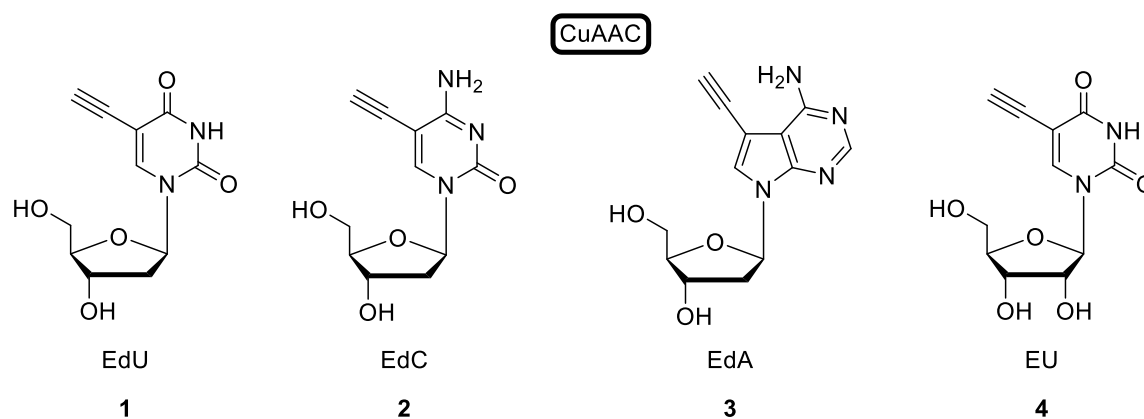


Figure 7: The ethynyl-modified nucleoside reporters of 5-ethynyl-2'-deoxyuridine (**1**, EdU), 5-ethynyl-2'-deoxycytidine (**2**, EdC), 7-deaza-7-ethynyl-2'-deoxyadenosine (**3**, EdA), and 5-ethynyluridine (**4**, EU).

Choosing the most suited nucleoside reporter is challenging and depends on several factors that must be considered before the experiment. After cell-uptake, the nucleoside analog must be phosphorylated efficiently to the corresponding active triphosphate by endogenous kinases. Subsequently, the nucleotide probe must be incorporated into the nascent nucleic acid by the catalyzing polymerase with sufficient substrate specificity. However, the metabolic phosphate intermediates or the active nucleoside triphosphate are potential substrates for cellular or viral enzymes, which ultimately affect the bioavailability of the active reporter or might induce cytotoxicity.<sup>4,45</sup> These metabolic crossovers can differ between cell types and viruses. To give an example, DELUCA *et al.* used UL2/UL50 HSV-1 viruses that are defective for the viral uracil glycosylase (UL2; cleaves uracil from DNA-strands) and dUTPase (UL50, hydrolyses UTP to UMP+PP), resulting in greater incorporation of EdU **1** in the HSV-1 genome, leading to improved experimental results.<sup>45</sup> Furthermore, the viral genome of interest can differ significantly in nucleobase content, making it beneficial to use the appropriate reporter molecule. For example, the herpes simplex virus type-1 (HSV-1) has a G+C rich content of 67%<sup>25,26</sup>, making EdC **2** the most suitable candidate for labeling the HSV-1 wild type.<sup>46</sup> Naturally, not only the base composition can impact the incorporation of nucleoside reporters but also the viral genome size. Thus, HSV-1 with a large dsDNA genome of 150 kbp is potentially easier to detect compared to reverse transcribed HIV-1 cDNA with two molecules of  $\sim 10^4$  bp each.<sup>4</sup> Figure 8 gives an overview of genome sizes of different virions.

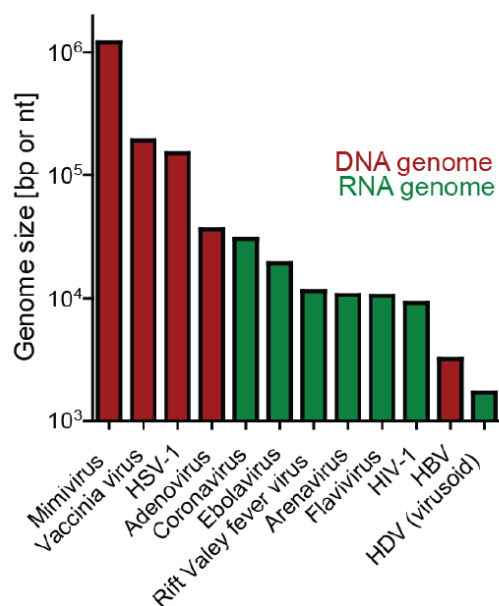


Figure 8: Overview of viral genome sizes for common viruses.<sup>4</sup>

The concept is not only limited to DNA detection. Cellular RNA transcription or viral RNA genome can be labeled by transferring the alkyne group to the ribonucleoside analog. In 2008, 5-ethynyl uridine (**4**, EU) was used for the first time to visualize newly synthesized cellular RNA.<sup>47</sup> Five years later, EU-labeled RNA of HIV-1 virions was successfully used to study capsid protein dissociation of the capsid core after infection. The staining of the incorporated EU-reporter with an azide-fluorophore-conjugate was only feasible shortly after viral fusion, giving evidence for destabilization of the capsid core, which leads to permeability for the small azide-dye-conjugate. Further evidence was accumulated in *in vitro* experiments. Isolated EU-labeled viral particles were fixed to slides and stained *in situ* with an azide-dye-conjugate in a buffer solution, which permeabilizes the viral membrane. Only a few particles were stained for vRNA, indicating an intact capsid core. Using normal cell lysate increased the labeling efficiency of vRNA, suggesting a destabilization of the viral core in the cytoplasm.<sup>48</sup>

In the past decades, the **CuAAC** of nucleoside reporters with azide-conjugated-fluorophores was a powerful tool to investigate the viral machinery in host cells.<sup>46,49–53</sup> However, due to the cytotoxicity of the Cu(I)-catalyst for bacteria and eukaryotic cells, labeled cells must be fixed before staining with labeling agents. Therefore, applying this method only allows to take snapshots at a particular time point per sample (often called hours post-infection, hpi), resulting in high sample preparation and low spatiotemporal resolution of the experiment. Overcoming these limitations, the catalyst-free inverse electron demand Diels-Alder reaction (**DA<sub>INV</sub>**) found increasing attention in the past

decade and will potentially pave the way for live-cell imaging of nucleic acids in the future.

## 2.6 The inverse electron demand Diels-Alder reaction ( $\text{DA}_{\text{INV}}$ )

Studying biomolecules and their function in the cellular environment is a demanding task because of the enormous complexity of the system. The selective modification of biomolecules in their native environment was a critical step that provided a tremendous range of new insights on cellular life. The term *bioorthogonal reaction* was coined by C.R. BERTOZZI and describes the challenging technique of a chemical reaction between two components, which “*must react rapidly and selectively with each other under physiological conditions in the presence of the plethora of functionality found within living systems.*”<sup>54</sup> The value of *bioorthogonal reaction* lies in the opportunity to introduce a wide variety of functionalities (e.g., synthetic fluorophores, biomolecules, biotin, radioactive tracers, etc.) to the biomolecule of interest at a chosen timepoint. The first step is the introduction of a relatively small chemical label to the biomolecule of interest, ideally not interfering with its natural function. The introduced label now opens the possibility of functionalizing the biomolecule with a sensor molecule carrying the complementary reactive group.

The catalyst-free Diels–Alder cycloaddition with inverse electron demand ( $\text{DA}_{\text{INV}}$ ) became the most significant *bioorthogonal reaction* in the last decade due to its high biocompatibility, high adjustability, nontoxic reagents, superior reaction rates, and increasing commercial availability of its “click-chemistry” reagents.

Mechanistically, the  $\text{DA}_{\text{INV}}$  is a reaction cascade between a 1,2,4,5-tetrazine **5** and a dienophile **6** in an inverse electron demand hetero-Diels–Alder / *retro*-Diels–Alder reaction resulting in dihydropyridazines **7** and **8**, which can further oxidize to the pyridazine **9**. The first reaction step is a concerted reaction between the  $4\pi$ -electrons of the diene and the  $2\pi$ -electrons of the dienophile to form a highly strained bicyclic adduct **10**. Due to the concerted nature of the first step, the reaction is described as a second-order reaction. The highly strained adduct **10** is rapidly converted by a *retro*-Diels–Alder reaction into the 4,5-dihydropyridazine **11** under the release of nitrogen as the only by-product making the reaction irreversible and entropically favored. The 1,3-prototropic isomerization forms the corresponding 1,4-dihydro-isomers **7** and **8**, which might oxidize to the pyridazine product **9**.<sup>55,56</sup>

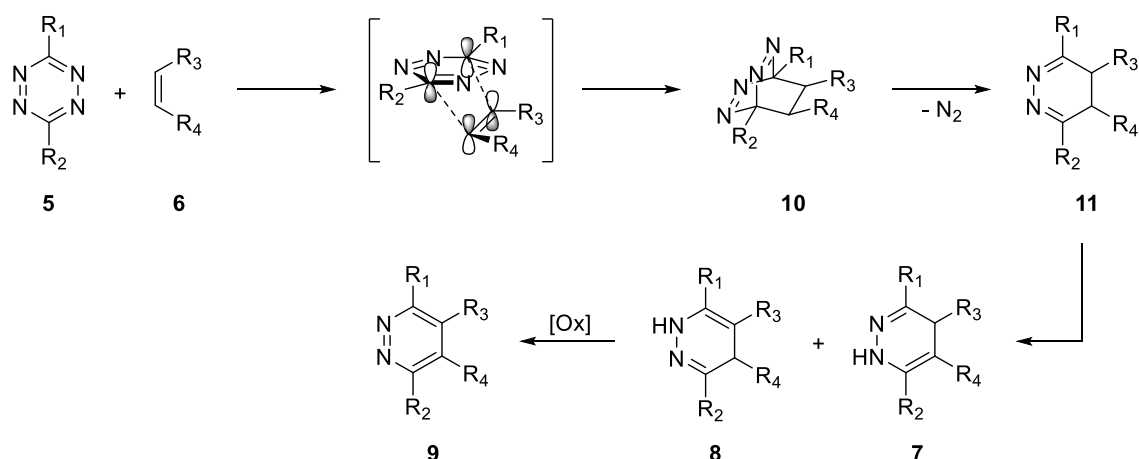


Figure 9: Mechanism of the inverse electron-demand Diels-Alder cycloaddition.

In contrast to the Diels-Alder with normal electron demand, where  $\Delta E$  is added from the HOMO of the electron-rich diene **12** and the LUMO of the electron-poor dienophile **13**, the  $DA_{INV}$  requires an electronically poor diene **14** and an electron-rich dienophile **15** (Figure 10). Electron-rich olefins are less prone to react with biological nucleophiles in a Michael-addition, thus meeting the selectivity needed for bioorthogonal reactions.

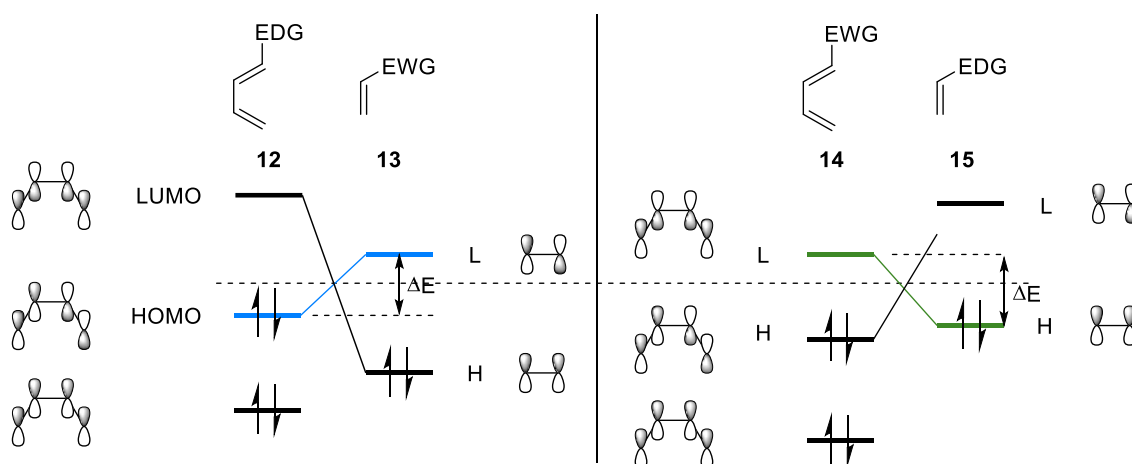


Figure 10: Frontier orbital interactions of the normal electron demand Diels-Alder (left) and the inverse electron demand Diels-Alder (right).

Figure 11 shows a comparison between the established **CuAAC**, mentioned in Chapter 2.6, and the  $DA_{INV}$  between 1,2,4,5-tetrazines and olefins.

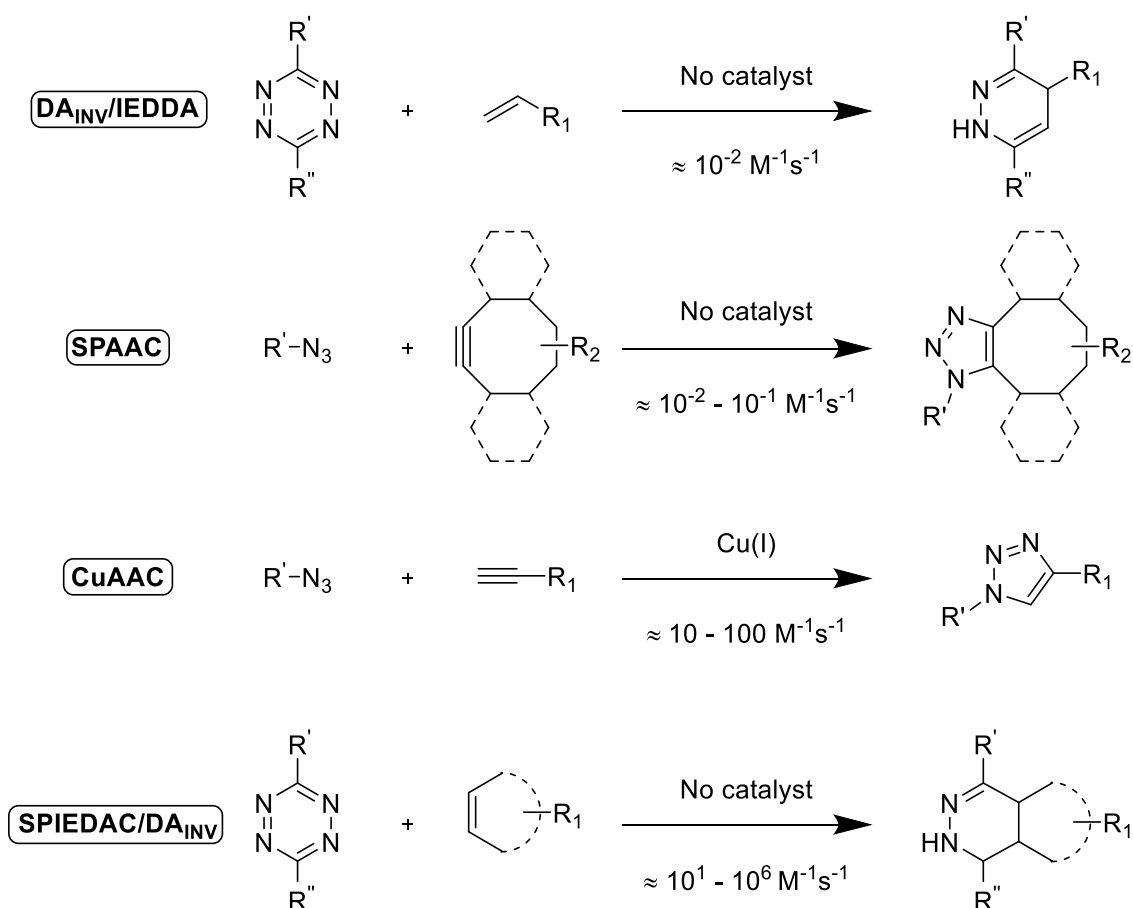


Figure 11: Comparison of the **DA<sub>INV</sub>** and the **CuAAC** and their strain-promoted variants **SPIEDAC** and **SPAAC**.

The smallest possible function of the **DA<sub>INV</sub>** is the vinyl group, which provides exceptional biocompatibility, but led to only low reaction rates ( $k' \sim 10^{-2} \text{ M}^{-1}\text{s}^{-1}$ ). The **CuAAC** displays reaction rates of  $10\text{-}100 \text{ M}^{-1}\text{s}^{-1}$ ; however, the dependency of the cytotoxic Cu-catalyst prevents the applicability of the 'click-labeling' process in living systems. The strain-promoted azide-alkyne cycloaddition (**SPAAC**) is independent of copper, but suffers from modest reaction rates ( $k' \sim 10^{-1}\text{-}10^{-2} \text{ M}^{-1}\text{s}^{-1}$ ). Fortunately, the strain-promoted effect is not only applicable to the azide-alkyne cycloaddition, but can also be applied to the **DA<sub>INV</sub>**, resulting in the fastest bioorthogonal reaction kinetics described today.<sup>57</sup> The high adjustability of the strain-promoted **DA<sub>INV</sub>** (**SPIEDAC**) and the challenge to balance reaction rates, stability, and biocompatibility of the bioorthogonal partners – with the focus on nucleoside reporters – is the basis of this work and will be described in detail in the following chapters.

### 2.6.1 Tuning the diene

To enhance the reactivity of the 1,2,4,5-tetrazine, electron-withdrawing groups (EWG), such as pyridyl (Py) or pyrimidyl (Y), are introduced at the 3- and 6-position of the tetrazine. The decrease of electron density in the tetrazine lowers the LUMO of the diene and decreases the  $\text{HOMO}_{\text{dienophile}}\text{-LUMO}_{\text{diene}}$  energy gap  $\Delta E$ , causing faster  $\text{DA}_{\text{INV}}$  reactions. Alkyl substituents at the 3- or 6-position reduce the reactivity due to donor effects and steric hindrance (raising LUMO). Hence, unsubstituted tetrazines react slightly faster than their alkylated analogs.

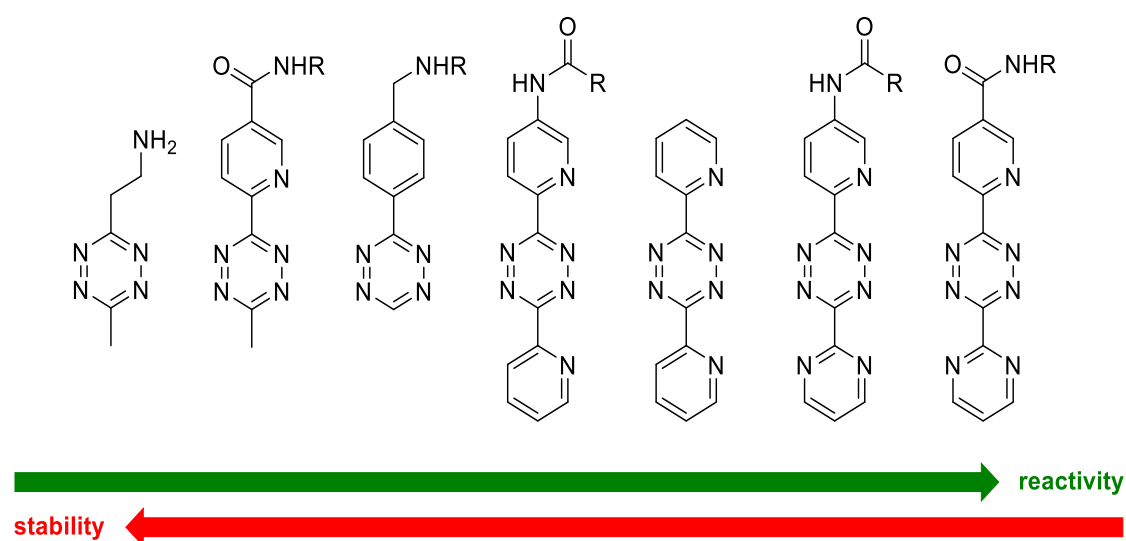


Figure 12: Conflicting correlation between the stability and the reactivity of 1,2,4,5-tetrazine depending on the 3,6-substitution motifs. EWGs increase reactivity (left to right), while EDGs and steric hindrance have a stabilizing effect.<sup>55</sup>

However, electron-withdrawing groups destabilize the aromatic ring, making the tetrazines prone for decomposition.<sup>58,59</sup> Therefore, it must be evaluated if the labeling experiment requires fast reaction kinetics or a more stable tetrazine motif since the compound stays in a physiological environment over extended periods.

### 2.6.2 Tuning the dienophile

The smallest dienophile is the vinyl function that provides modest reaction rates (Figure 14) but excellent biocompatibility when introduced to nucleosides (Chapter 2.6.3). In contrast to terminal olefines, strained alkenes offer an enormous increase in reaction rates with an increase of ring-strain: cyclooctene < cyclohexene < cyclopentene < cyclobutene < cyclopropene.<sup>60</sup> Moreover, forcing strained olefins in more reactive conformations increases the reaction rates and can exceed ring-strain effects. The *trans*-

cyclooctene (TCO) adopts different conformations with the “crown” conformation being the lowest in energy. The conducted *ab initio* calculations predicted an increase in energy for the “half-chair” conformation by 5.6 kcal/mol making it an even more reactive conformer (Figure 13).

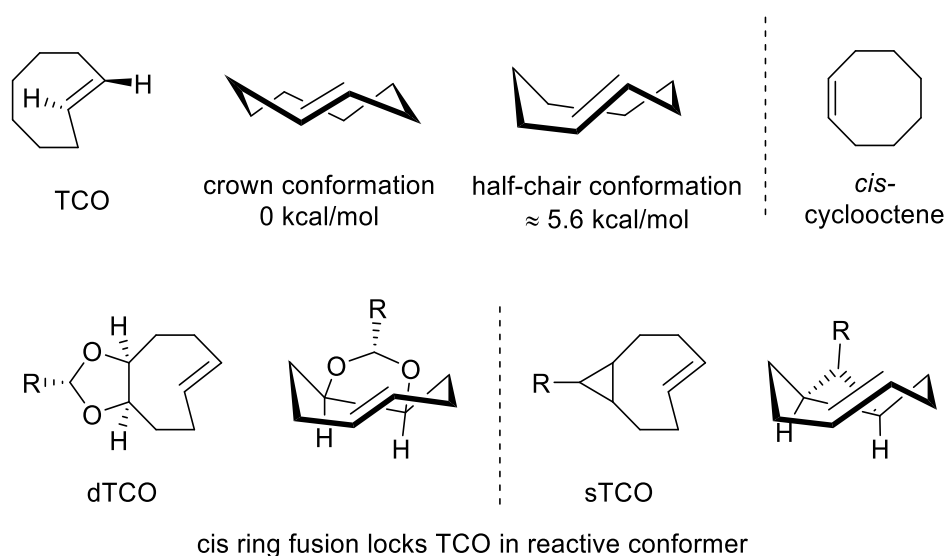


Figure 13: The “crown” conformation of TCO is 7 orders of magnitudes more reactive than the *cis*-cyclooctene (top-right). The “half-chair” conformation is even higher in energy compared to the “crown” conformation. Strained-ring fusion of *cis*-dioxolane or cyclopropane with TCO locks the strained olefines in a non-crown conformation, thus increasing reactivity even further.<sup>56</sup>

Both conformers of TCO give an enormous rate difference compared to *cis*-cyclooctene or cyclic olefins, with a higher ring strain (e.g., norbornene or 1MCP). Later, it was calculated and experimentally proven that the fusion of a *cis*-dioxolane (dTCO) or a cyclopropane ring (sTCO) with *trans*-cyclooctene locks the cyclooctene in a more reactive “half-chair”-like conformation (Figure 13). The conformational constrain brought forth the fastest  $DA_{INV}$  labels described today (Figure 14).<sup>56,57,61</sup>

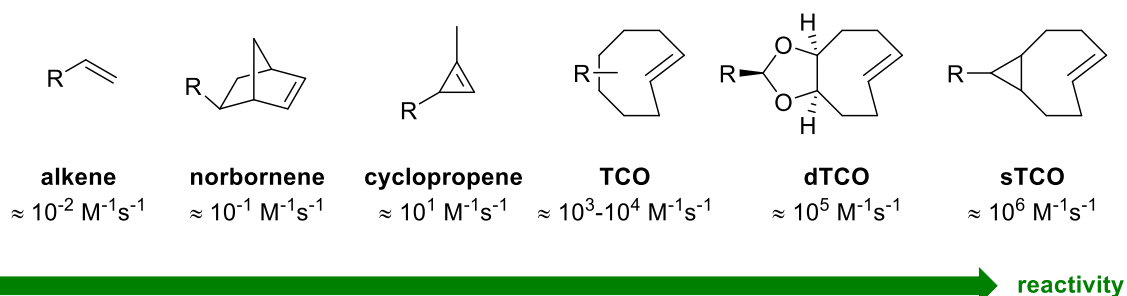


Figure 14: Increasing reactivity of strained olefins compared to terminal alkenes (left to right).

The following pages will briefly overview modified nucleoside and nucleotide probes, which utilize the  $DA_{INV}$  for metabolic labeling. The advantages and disadvantages of each



label will be highlighted. Furthermore, shortcomings of available tool systems to achieve live-cell imaging of nucleic acids are identified.

### 2.6.3 Vinyl-label

In 2014, LUEDTKE *et al.* introduced 5-vinyl-2'-deoxyuridine (**16**, VdU) as the first bioorthogonal probe for cellular DNA labeling, which employed the catalyst-free **DA<sub>INV</sub>** and a fluorescent tetrazine conjugate. After cell-uptake, VdU **16** is phosphorylated to the corresponding triphosphate and subsequently incorporated into newly synthesized cellular DNA by an endogenous DNA polymerase. Herein, VdU **16** showed advanced cytotoxicity properties compared to the azide-alkyne derivative EdU **1** – exhibited the advanced biocompatibility of the vinyl function for the first time. The evaluation of the reaction rates with 3,6-di-2-pyridyl-1,2,4,5-tetrazine (Py<sub>2</sub>Tz) in an aqueous solution displayed a reaction rate of  $2.1 \times 10^{-2} \text{ M}^{-1}\text{s}^{-1}$ . Due to the relatively low reaction rates, denaturation of the fixed and permeabilized samples was required to enable successful staining after four hours of incubation with a TAMRA-Py<sub>2</sub>Tz fluorophore.<sup>62</sup>

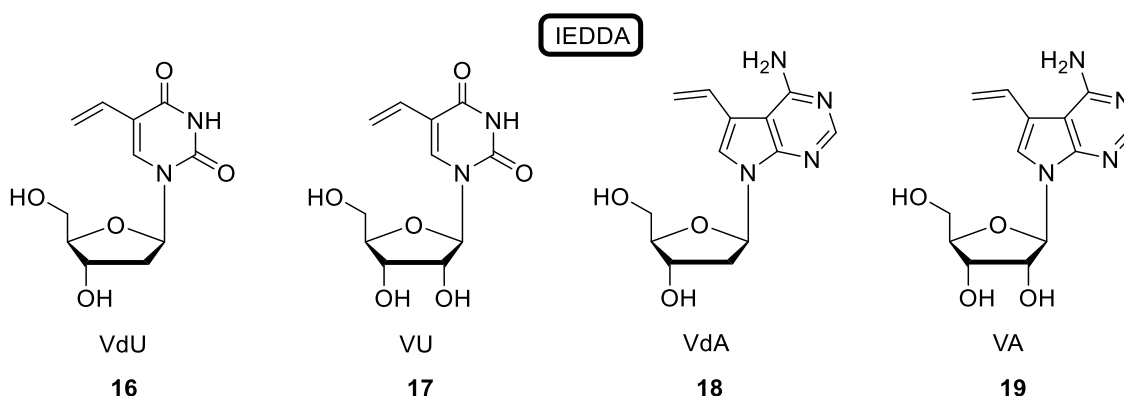


Figure 15: The vinyl-modified nucleoside reporters of 5-vinyl-2'-deoxyuridine (**16**, VdU), 5-vinyluridine (**17**, VU), 7-deaza-7-vinyl-2'-deoxyadenosine (**18**, VdA), and 7-deaza-7-vinyladenosine (**19**, VA).

In 2017, the metabolic incorporation of VdU **16** in the vaccinia virus (VACV) genome was evaluated. The VACV is an enveloped virus with a large genome ( $2 \times 10^5$  bp). An optimized timeline had to be implemented to affect neither the cell viability nor the virus' replication and to ensure efficient incorporation and subsequent staining of the nucleoside reporter. Therefore, VdU **16** was added 24 h post VACV infection and incubated for a further 12 h to ensure the incorporation of the reporter nucleoside. Then, a polar Cy5-tetrazine fluorophore was added. The membrane permeability for the dye-tetrazine-conjugate was assured due to damages to the cell membrane caused by the viral replication process. The cells were incubated for further 12 h for sufficient

staining of the incorporated vinyl-label. The fluorescently labeled VACV particles were isolated, and excess of fluorophore was removed. The labeled viral particles were available to study a new infection cycle via fluorescence imaging (Figure 16).<sup>63</sup>

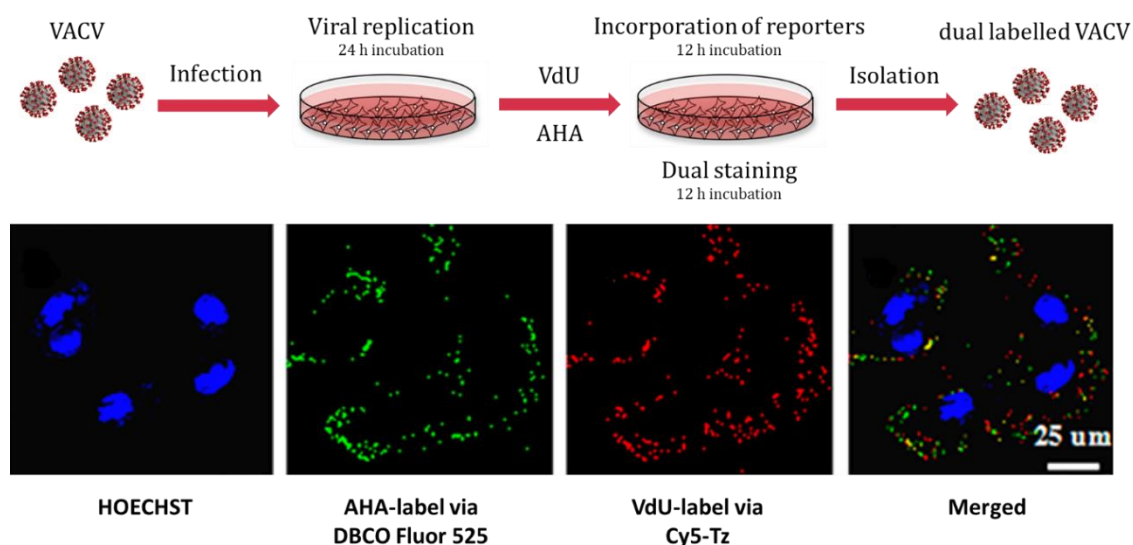


Figure 16: In this study by Xie *et al.*, Vero cells were infected by VACV (MOI= 1) in methionine-free medium. After, 24 h *L*-azidohomoalanine (AHA, 400 μM) and VdU (**16**, 40 μM) were added and incubated for 12 h. Subsequently, viral nucleic acid was stained by Cy5-MeTz (5 μM, red) at 37 °C for further 12 h via  $DA_{INV}$ . After three rounds of freezing–thawing, the cell debris was removed. The viral envelope proteins containing AHA were stained by cell-impermeable DBCO-Fluor 525 (5 μM, green) via SPAAC. The viral particles were isolated by centrifugation in a sucrose gradient. Subsequently, Vero cells were infected with the dual labeled virus to track the dynamic movement of the VACV.<sup>63</sup>

This study illustrates the feasibility of labeling viral genomes in infected cells using minimally invasive vinyl modifications. Briefly summarized, VdU **16** was successfully phosphorylated by endogenous kinases and subsequently incorporated into the viral genome by the VACV DNA polymerase. Moreover, the cell viability was not impaired due to the well tolerated cytotoxicity properties of the nucleoside reporter. Hence, the VdU reporter **16** exhibited overall good biocompatibility. Its disadvantage of slow reactivity has been compensated through long staining times. The excess addition of Cy5-fluorophore to the infected cells, which would have caused a significant background in same cell imaging experiments, was not a concern since labeled viral particles were isolated.

However, it must be stated that this approach is not necessarily applicable to different virus types. The labeling agent's cell permeability and bioavailability are not guaranteed and must be validated individually (i). After cellular uptake of the nucleoside reporter, it must be sufficiently phosphorylated to its triphosphate, and the metabolic pathway is not hampered by cellular or viral enzymes (ii). Differences in genome size or base

content could decrease incorporation rates of the nucleoside reporter and ultimately influence the labeling efficiency (iii). The introduced label/fluorophore modification is not perturbing viral particle assembly or viral infectivity (iv). The viral assembly process is accessible to the labeling agent and not hindered by viral compartments or - as an alternative - it is possible to stain the viral genome *in situ* after virion isolation (v).

Shortly after VdU, 7-deaza-7-vinyl-2'-deoxyadenosine (**18**, VdA) was introduced and showed enhanced reaction kinetics compared to the 2'-deoxyuridine derivative (14-fold), which was in agreement with performed molecular orbital calculations.<sup>64</sup> Recently, 5-vinyl uridine (**17**, VU) and 7-deaza-7-vinyladenosine (**19**, VA) were evaluated as RNA metabolic probes. The cytotoxicity and genotoxicity of VU **17** were compared to EU **4** in cell proliferation and gene expression assays to validate the probe's quality for metabolic labeling application. Cells treated with EU **4** showed a decrease in proliferation of nearly 50% after 48 h, whereas VU **17** had no significant effect on cell viability. In accordance with these results, 200 genes were differentially expressed under EU **4** exposure compared to 18 genes for the VU derivative **17**. These findings are comparable to the results for the vinyl and alkynyl DNA derivatives, demonstrating that the DA<sub>INV</sub> probes are favorable regarding cell viability. Labeling of cells with both VU **17** and VA **19** showed similar imaging results underlining their potential in minimally invasive RNA labeling *in vivo* (Figure 17).<sup>65</sup>

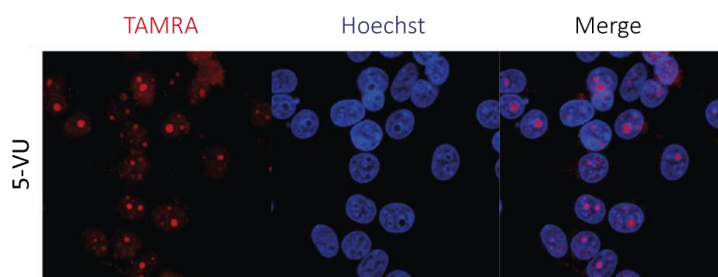


Figure 17: HEK293T cells were treated with 1 mM VU **17** for 5 h, followed by fixation, permeabilization, and incubation with TAMRA-Tz for 3 h. Fluorescence imaging was performed after washing out excess fluorophore probe: TAMRA-labeled RNA (*red*), staining of the cell nucleus with Hoechst (*blue*), and merged images.<sup>65</sup>

#### 2.6.4 Norbornene-label

Norbornenes provide the slowest reaction kinetics of the strained olefins, but exhibit excellent stability in physiological media. They were first introduced in 2008 by HILDERBRAND *et al.*<sup>66</sup> and are mainly used in protein labeling.<sup>67</sup> Moreover, the

norbornene label was introduced to C<sub>5</sub>-modified pyrimidine (dU **20**, dC **21**) and C<sub>7</sub>-modified 7-deazapurine (deaza-dA **22**) nucleoside triphosphates (Figure 18).<sup>68</sup>

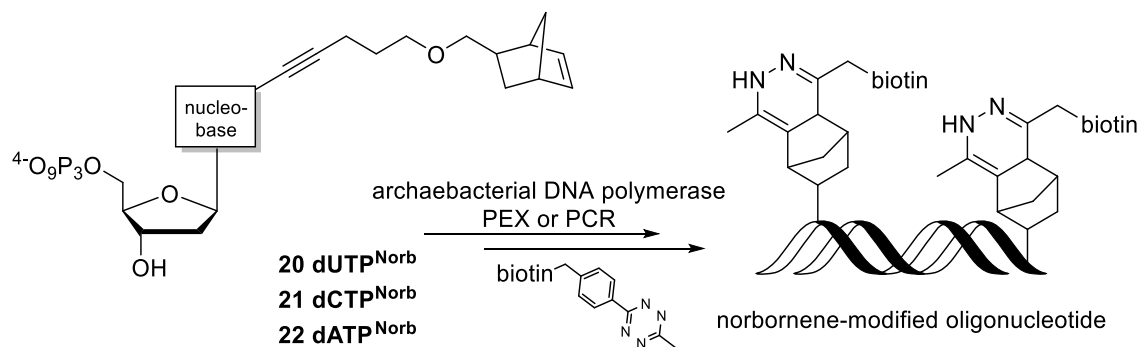


Figure 18: *In vitro* labeling of norbornene-modified DNA products, synthesized either by primer extension experiments (PEX) or polymerase chain reaction (PCR).<sup>68</sup>

Primer extension experiments (PEX) or polymerase chain reaction (PCR) with an archaeobacterial DNA polymerase resulted in norbornene-modified template strands. Successful functionalization of the modified DNA by **DA<sub>INV</sub>** was carried out with a tetrazine-biotin-conjugate for one hour at room temperature. The use of nucleoside triphosphates as substrates and the need for engineered polymerases for DNA synthesis limits the applicability of this technique to *in vitro* studies only.<sup>68</sup>

## 2.6.5 1MCP-label

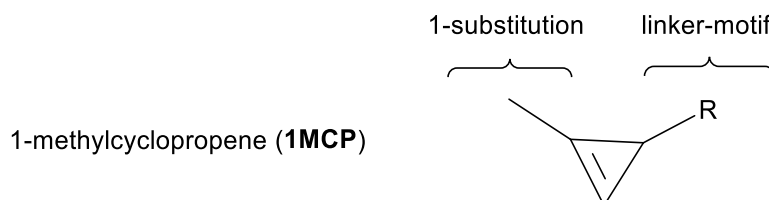


Figure 19: Illustration of the 1-methylcyclopropene label.

PATTERSON<sup>69</sup> and DEVARAJ<sup>70</sup> developed the faster and relatively small bioorthogonal 1-methylcyclopropene (1MCP) handle. Substitution and linker motifs significantly impact the stability of the motif and its reactivity towards tetrazines. Unsubstituted cyclopropenes are prone to nucleophilic attacks and polymerization by ene-ene reaction.<sup>71</sup> Introducing a methyl group increases the stability and makes 1MCP accessible for bioorthogonal labeling. By selecting a suitable 3-substitution motif, dimerization by ene-ene reaction can be reduced at the expense of higher reaction rates.<sup>72,73</sup> Due to the excellent compromise between size and reaction kinetics of 1MCP, the motif is frequently used for protein labeling with modified amino acids or sugar moieties of glycoproteins both *in vitro* and *in vivo*.<sup>56,69,74,75</sup> Furthermore, 1MCP-modified

nucleoside triphosphates were synthesized for *in vitro* labeling of DNA and RNA primer extension products (Figure 20).<sup>76–78</sup>

The carbamate-linked 1MCP-dUTP **23** was synthesized and used as a substrate in a primer extension experiment with Hemo Klen Taq, Vent (exo-), and Deep Vent (exo-) polymerases. Successful incorporation of the 1MCP-label was verified by reaction of the PEX product with a TAMRA-tetrazine-conjugate and subsequent PAGE analysis (Figure 20).<sup>78</sup>

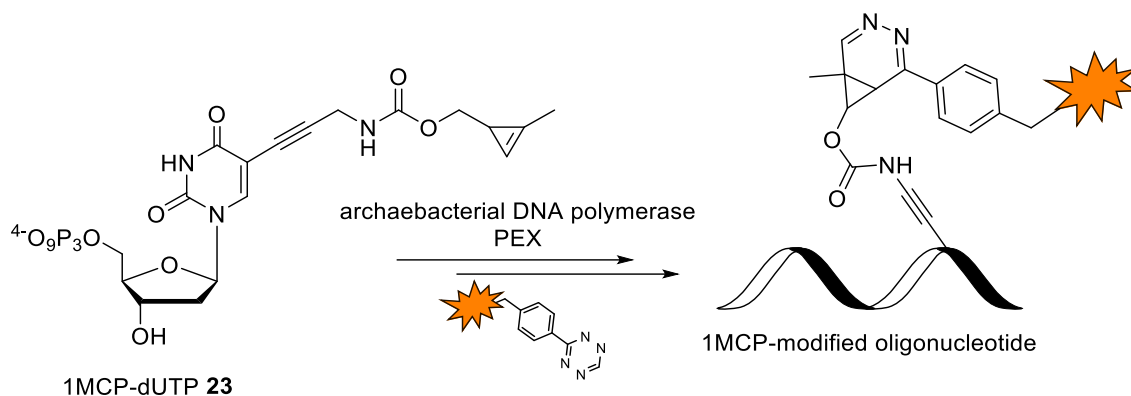


Figure 20: The carbamate-linked 1MCP-dUTP **23** is a substrate for the archaeobacterial DNA polymerases Hemo Klen Taq, Vent (exo-), and Deep Vent (exo-) polymerase in primer extension experiments (PEX). The PEX product was successfully stained with a tetrazine-TAMRA-conjugate and visualized by PAGE analysis.<sup>78</sup>

PATTERSON and DEVARAJ transferred the motif to the 7-deazapurines (deaza-dA) nucleoside triphosphates. The 1MCP-functionalized dATP analog was successfully incorporated into the primer extension product at higher rates than the dUTP derivative. The subsequent post-synthetic fluorescent staining of the PEX product was efficient according to PAGE analysis. Furthermore, 1MCP-modified primer extension products were transfected into living HeLa cells for 24 h, followed by fluorescent staining with a TAMRA-tetrazine conjugate. No-wash conditions were achieved by reducing the dye concentration to a picomolar level (incubation for 3 h), resulting in a low unspecific background.<sup>76</sup> The transfection of the oligonucleotide into living cells and subsequent fluorescent labeling proves the feasibility of live-cell imaging. However, 1MCP-modified metabolic nucleotide probes enabling the *in vivo* incorporation into nucleic acids are still missing.

### 2.6.6 TCO-label

The strained *trans*-cyclooctene (4TCO) provides one of the highest reaction rates toward tetrazines but tends to isomerize to the unreactive *cis*-isomer in the presence of high thiol concentrations.<sup>79</sup> Therefore, their application in physiological media is restricted to

time-limited experiments. The conformationally-strained dioxolane-fused trans-cyclooctene (dTCO) derivative is more stable and exhibits improved reactivities towards tetrazines one order of magnitude higher than 4TCOs (Figure 14).<sup>57</sup> However, the improved dTCO motif is still missing as a frequently applied label, potentially due to the higher synthetic effort. Today, the sTCO label is frequently used in *in vitro* and *in vivo* applications that provide fast bioorthogonal labeling.<sup>80,81</sup> Similar to the cyclopropene and norbornene modifications, 4TCO was introduced in 2'-deoxyuridine **24**<sup>82</sup>, and cytidine **25**<sup>83</sup> triphosphates to label enzymatically synthesized DNA PCR products (Figure 21) and newly transcribed RNA strands (Figure 22).

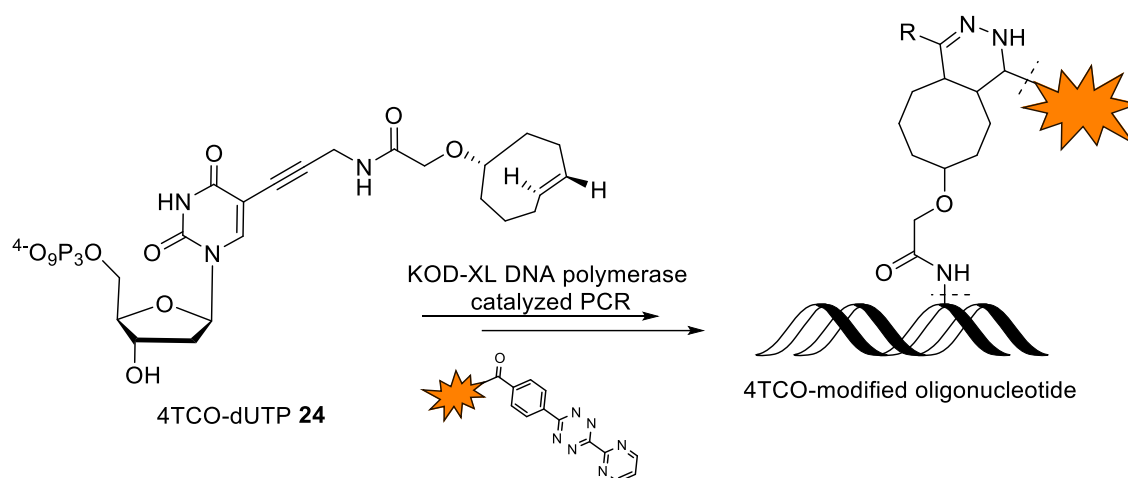


Figure 21: The 4TCO-dUTP **24** is a substrate for the KOD-XL polymerase in a polymerase chain reaction (PCR). The PCR product was successfully stained with a tetrazine-dye-conjugate and visualized by PAGE analysis.<sup>82</sup>

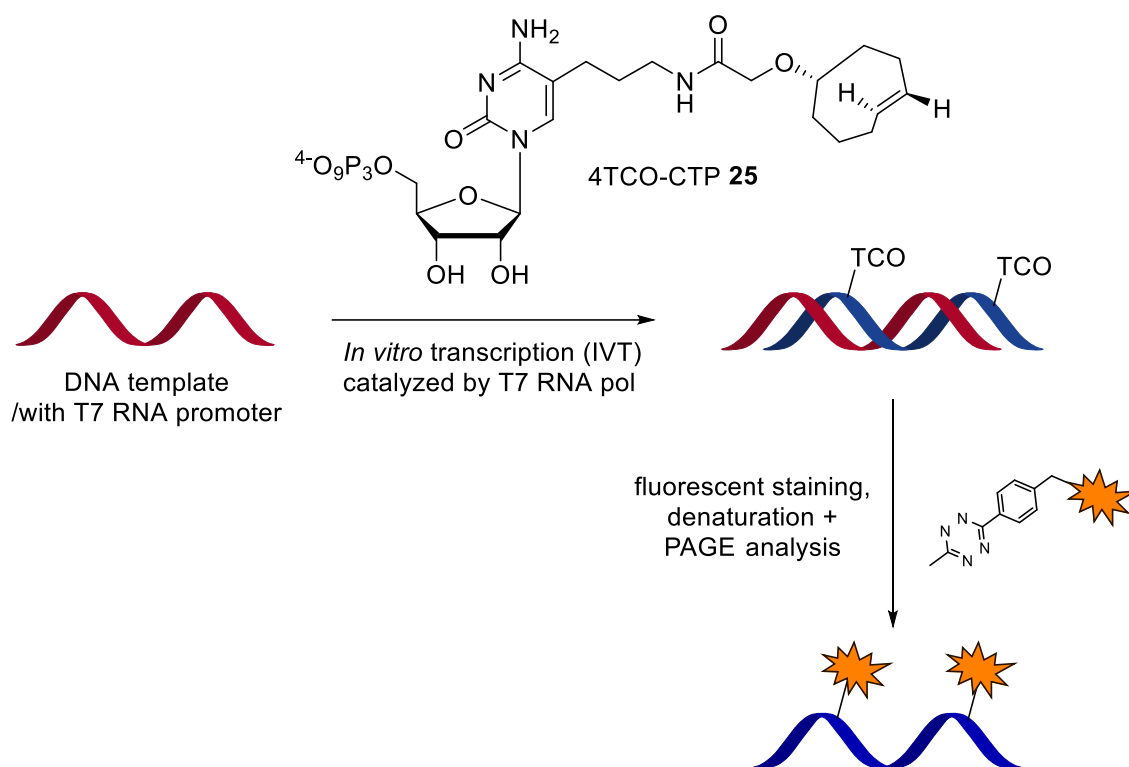


Figure 22: The 4TCO-CTP **25** is a substrate for the T7 RNA polymerase in an *in vitro* transcription of a DNA template. The transcription product was stained with a tetrazine-dye-conjugate, denatured, and visualized by PAGE analysis.<sup>83</sup>

### 2.6.7 Tetrazine-label

Moreover, WAGENKNECHT *et al.* changed the bioorthogonal approach by introducing two different tetrazine motifs to uridine triphosphates, which would allow rapid and efficient labeling with TCOs or bicyclo[6.1.0]nonyne (BCN) fluorophore conjugates. However, it was found that the tetrazine groups are not stable under the relatively harsh conditions of the PCR, which led to partial decomposition of the metabolic handle resulting in low post-synthetic labeling yields (Figure 23).<sup>78</sup>

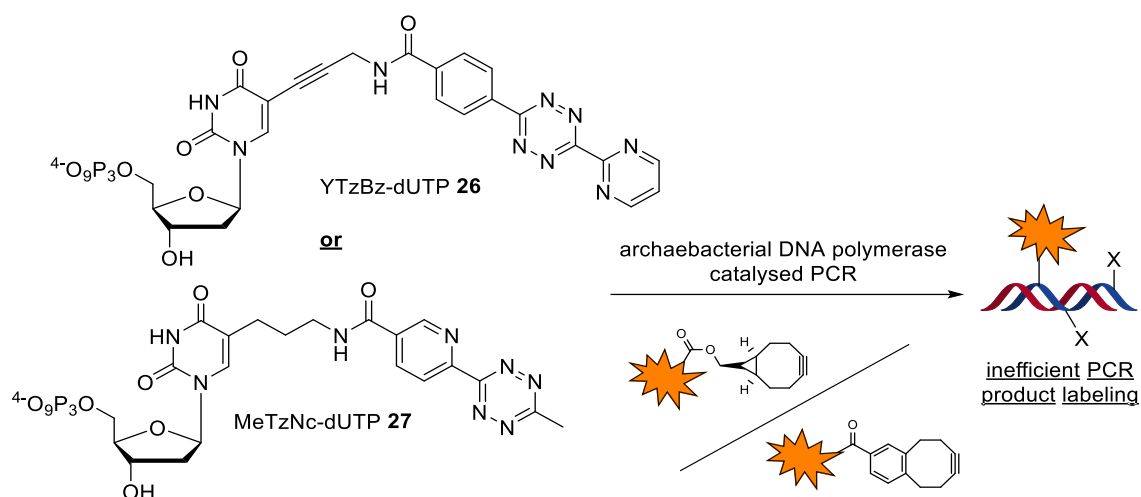


Figure 23: The modified dNTPs YTzBz-dUTP **26** and MeTzNC-dUTP **27** were used as substrates for archaeobacterial DNA polymerases in PCR reactions. However, the relatively harsh reaction conditions of the PCR led to partial decomposition of the tetrazine motifs, which resulted in inefficient fluorescent labeling of the PCR products.<sup>78</sup>

Nevertheless, a different study demonstrated the potential of this bioorthogonal approach. A tetrazine-labeled GFP was successfully stained within minutes using stoichiometric amounts of a 4TCO-conjugated fluorophore in cell lysate. These results underline that fast and efficient staining potentially enables no-wash conditions for future live-cell applications.<sup>84</sup> As mentioned above, 4TCOs suffer from isomerization to the respective less reactive *cis*-cyclooctene scaffolds in the presence of thiols under physiological conditions. Therefore, introducing the tetrazine motif to the nucleotide has the critical advantage of reducing the time the 4TCO (attached to the fluorophore) is exposed to the cellular environment. This methodology could ensure high labeling efficiency based on the premise of selecting a stable tetrazine motif.

### 2.6.8 Reflection

To summarize, vinyl modifications stand out due to their excellent biocompatibility. Once incorporated into nascent nucleic acids, the modification induces reduced genotoxicity compared to their alkyne-modification counterparts. Without a cytotoxic copper-catalyst, bioorthogonal labeling inside of living cells becomes feasible – as displayed for the VACV genome labeling. Unfortunately, reaction rates between the vinyl function and tetrazines are comparably slow ( $k' \sim 10^{-2} \text{ M}^{-1}\text{s}^{-1}$ ), resulting in low labeling efficiency. In general, a few compensating measures might have to be applied: Initially, the reaction times need to be increased during staining (i), which prevents the visualization of dynamic processes. Moreover, a significant excess of the dye must be used (ii) to maximize labeling efficiency, and to achieve sufficient signal-to-noise ratios,



repeated washing of fixed and permeabilized samples is indispensable. Lastly, the bio samples might need to be denatured (iii) in order to make the incorporated modification more accessible to the fluorophore.

The general concept to overcome these limitations and enable no-wash live-cell imaging is to enhance the bioorthogonal reaction's labeling efficiency drastically. It is presumed that the ideal intracellular bioorthogonal reaction requires a rate of  $k' > 10^4 \text{ M}^{-1}\text{s}^{-1}$  to reach completion within seconds to minutes at biological concentrations (mM to nM) of the bioorthogonal target.<sup>84</sup> To reach or – at least – approach this hypothetical mark, strain-promoted **DA<sub>INV</sub>** must be introduced to nucleoside reporters. As briefly discussed, there is a variety of strained olefin modified nucleotides described in recent literature. Regarding live-cell applications, WAGENKNECHT *et al.* showed encouraging results by fluorescently labeling transfected, cyclopropene-modified oligonucleotides inside of living cells under no-wash conditions.<sup>76</sup>

Transferring the labeling experiment with strained olefin labels from *in vitro* approaches to living systems is a challenging task to fulfill, but crucial to enlighten the dynamics of cellular and viral nucleic acids in real-time. The challenge is tripartite and can be divided into reaction kinetics, stability, and biocompatibility (invasiveness) (Figure 24).

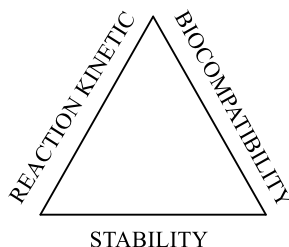


Figure 24: Illustration of the tripartite challenge to consider for live-cell imaging.

As repeatedly mentioned, the vinyl label exhibits superior biocompatibility and stability, but lacks sufficient reaction rates towards tetrazines. This deficiency impedes the efficient fluorescent labeling needed for no-wash live-cell imaging conditions. Yet, once incorporated into nucleic acids, the small-sized label is less likely to disturb the natural function of the labeled polynucleotide - resulting in reduced cytotoxicity and genotoxicity. Prolonged incubation times of the metabolic probe in (infected) cells become feasible.

Next to the biocompatibility of the incorporated label and the ability of the labeled polynucleotide to fulfill its natural function, the nucleoside reporters first need to be taken up by the cell and be phosphorylated by endogenous kinases to the active NTP,

i.e., the cell's metabolic machinery must accept these modified versions as good enough substrates. Once phosphorylated, the modification must be further tolerated by the respective polymerase that catalyzes the synthesis of the polynucleotide of interest. Hence, the biocompatibility of the nucleoside reporter is twofold. The modification must be compatible regarding substrate specificity towards kinases and polymerases, and once incorporated, the label ideally does not affect the natural function of the nucleic acid biopolymer.

Naturally, the vinyl function's biocompatibility is superior to modifications carrying strained-olefins – simply due to their difference in size. Successful labeling experiments with vinyl-modified nucleosides demonstrate their suitable substrate properties towards endogenous kinases. The absence of reporter nucleoside reporters with strained olefin labels for *in vivo* applications can most likely be attributed to the 'bottleneck' kinases. The narrow substrate specificity of endogenous kinases often limits efficient phosphorylation to the respective nucleotides. This obstacle is well known in nucleoside-based drug discovery and intensified the interest and application of nucleoside prodrugs in the past decades. Here, our expertise in developing pronucleotide technologies becomes exciting and is the subject of Chapter 2.8.

Under the premise that the modified NTPs are successfully generated inside the cell, the modification still must be tolerated by the respective polymerase for successful incorporation. Once incorporated, the bulkiness of the label might induce genotoxicity by interfering with the natural structure / function of the polynucleotide. In case of viral genome labeling, the modification might hamper viral replication and thus interfere with the viral process of interest. Additionally, the reactive label might decompose over time due to insufficient stability in physiological media, which would ultimately reduce the labeling efficiency and needs some consideration during the design of the experiment. However, once efficiently incorporated, fast reacting labels would allow rapid staining of the target with reduced fluorophore concentration, allowing the visualization of dynamic processes under no-wash live-cell imaging conditions (illustrated in Figure 25).

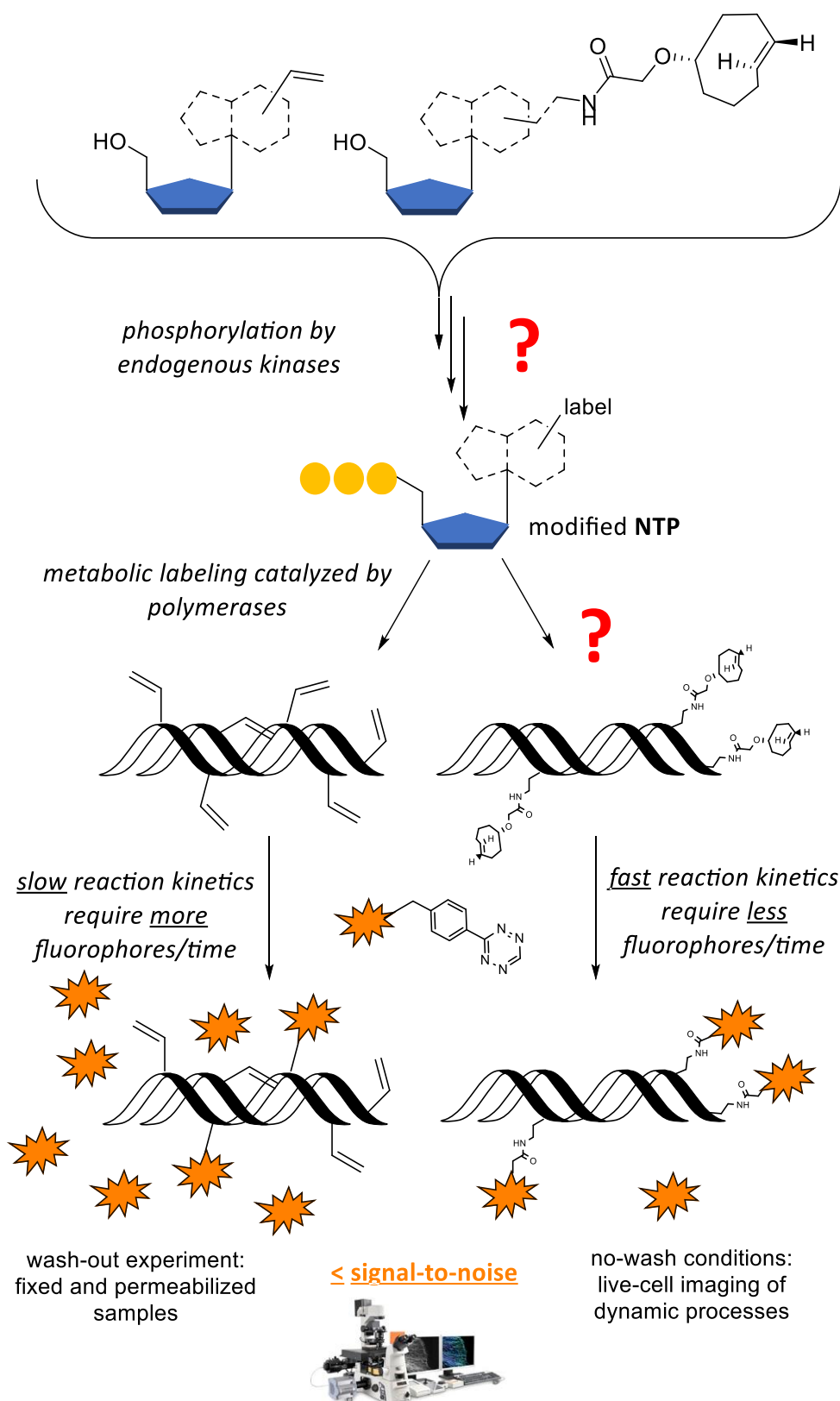


Figure 25: Illustration of the challenges for live-cell imaging of nucleic acids on the example of vinyl- or 4TCO-modified nucleoside reporters. The bulky TCO-modification potentially hampers the efficient phosphorylation of the nucleoside reporter to the corresponding NTP. Yet, incorporation of the 4TCO modification into *de novo* nucleic acid would enable rapid and efficient fluorogenic labeling of dynamic processes. Efficient labeling reduces the need for a large excess of the fluorogenic probe. Lower nonspecific background allows no-wash condition, thus live-cell imaging.

Furthermore, the challenge to distinguish between the viral and host-cell transcription process needs to be addressed. To date, described nucleoside reporters used in *in vitro* applications are both substrates towards viral and cellular polymerases, thus preventing specific labeling of viral transcription. Small molecule inhibitors can inhibit cellular transcription, thus reducing background deriving from the host cell machinery (e.g., aphidicolin for host cell DNA polymerase; actinomycin D for host cell transcription). However, this approach might interfere with the pathogenic pathway, which would put the obtained results into question. Thus, molecular probes that specifically target the viral polymerase of interest and – in addition – bypass their dependency on endogenous kinases could become the reporters of the future.

## 2.7 Synthetic Fluorophores

Finding the appropriate fluorophore for labeling cellular targets for no-wash live-cell microscopy is challenging. Usually, fluorescent probes suffer from low cell-permeability or unspecific hydrophobic binding to cellular components. Labeling agents are eagerly awaited, which easily pass-through biological membranes and whose conjugates allow rapid reaction kinetics even in small concentrations.

Cell-permeability by a diffusion-mediated process highly depends on the polarity of the probe. Endocytic cellular uptake leads to bright fluorescent particles inside the cell, which likely perturb the experiment. Polar or net-charged fluorescent probes are presumably cell-impermeable by diffusion-mediated cellular uptake. These fluorophores are suitable for extracellular targets or wash-out applications (cyanine dyes, e.g., Cy5 **28**).<sup>36</sup> On the other hand, hydrophobic fluorophores (e.g., BODIPY dyes **29**) tend to nonspecific, hydrophobic binding to cellular components, which results in poor cellular distribution and an increase in background signal.<sup>81</sup> More suited for live-cell imaging of cellular targets are rhodamine-based fluorophores. These xanthene probes exist in a dynamic equilibrium between the non-fluorescent spirolactone and the fluorescent zwitterionic counterpart (Figure 26). The equilibrium of the rhodamine dye responds to the environment's polarity to different degrees depending on the rhodamine motif.<sup>85</sup> A hydrophobic environment favors the non-fluorescent spirolactone form, which enables the cellular uptake of the probe, whereas more polar interactions favor the open fluorogenic zwitterion. Therefore, after binding to proteins, the fluorophore usually exists predominately in its fluorescent zwitterionic form.<sup>86</sup>

The design of silicon-rhodamines (**30**, SiR) enhances this effect by pushing the equilibrium to the spirolactone form, which enables improved cell-permeability of the probe. The binding to the target results in a more polar environment leading to a substantial increase in fluorescence. Additionally, nonspecific binding to hydrophobic surfaces favors the formation of the non-fluorescent spirolactone, which reduces the background signal and ultimately improves the signal-to-noise ratio of the experiment.<sup>81,87</sup> Due to this property, SiR probes are increasingly used in live-cell imaging applications.<sup>36,88–90</sup>

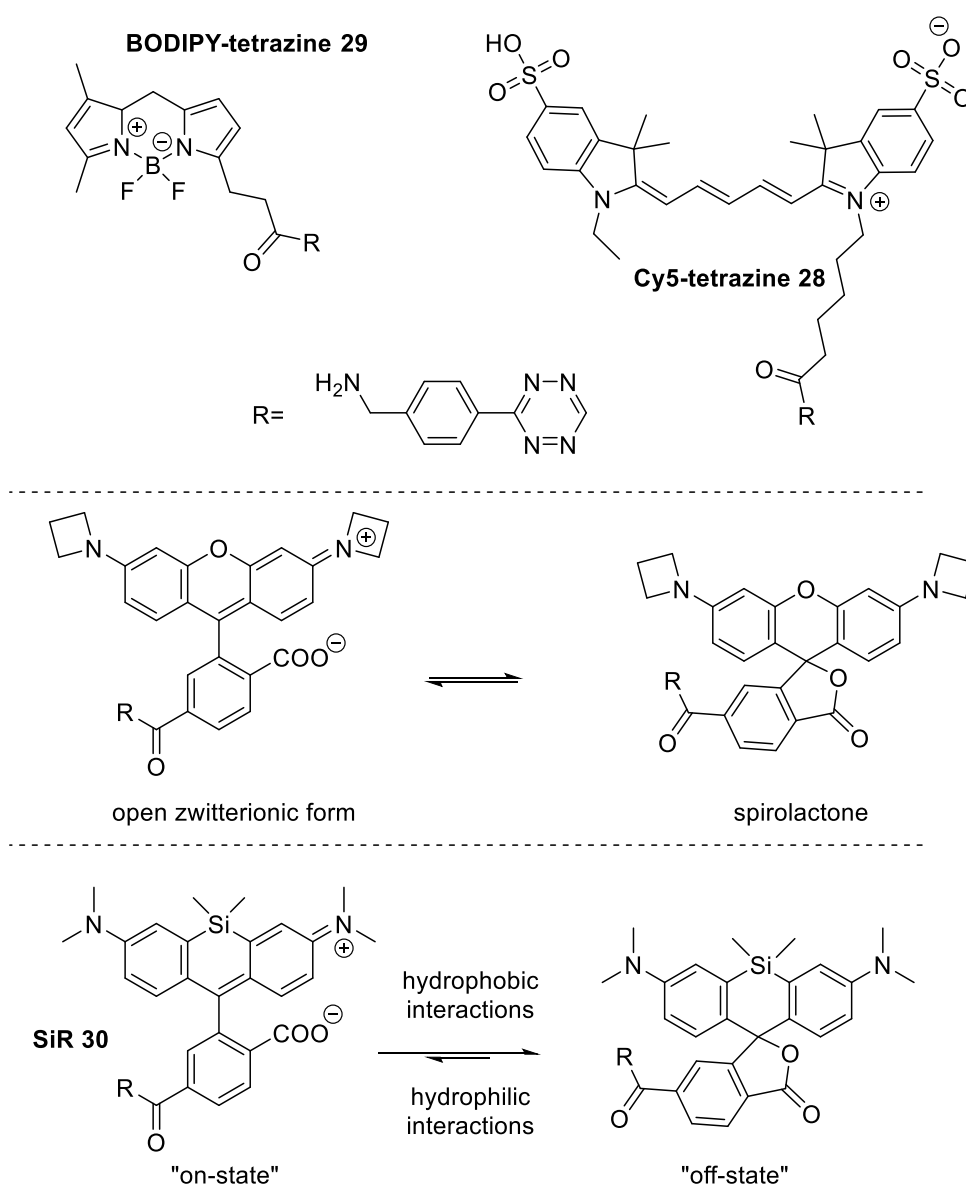


Figure 26: Four examples of fluorophore-tetrazine-conjugates. BODIPY (**29**, top left), cyanine (**28**, top right), and xanthene (middle and bottom)-based synthetic dyes.

Since the signal-to-noise ratio is crucial for fluorescence microscopy and no-wash live-cell imaging applications predominantly face the issue of nonspecific background staining, it is interesting to find fluorescent probes, which “turn-on” fluorescence intensity after successfully targeting the biomolecule of interest. Fortunately, tetrazines are chromophores with a broad absorption spectrum, which peaks around 515 nm, resulting in an effective quenching of a variety of fluorophores with emissions between 400-600 nm. Upon reaction with olefins and the “destruction” of the tetrazine motif, the fluorogenic properties of the dyes are restored, resulting in a “turn-on” of intensity.<sup>91</sup> In 2010, DEVARAJ and WEISSLEDER reported two examples of “turn-on” probes shown in Figure 27. Upon reaction with *trans*-cyclooctene, the BODIPY **31** and OregonGreen488-tetrazine **32** conjugates showed a 15-fold and 18.5-fold increase in fluorescence. In the “off state”, the probes were quenched by *Förster resonance energy transfer* (FRET), which accepts flexible alkyl-chain linkage.<sup>91</sup> Later, WEISSLEDER *et al.*<sup>92</sup> designed a variety of BODIPY-tetrazine “turn-on” probes, which are more efficiently quenched by *through-bond energy transfer* (TBET). TBET requires the energy donor (fluorophore) and acceptor (tetrazine) moieties to be connected through a connected  $\pi$ -electron system (Figure 27, **33**).<sup>93</sup> In 2014, DEVARAJ *et al.*<sup>94</sup> transferred this concept to rhodamine-based fluorophores by covalently attaching the tetrazine via double bond using a Heck-elimination reaction, resulting in efficient quenching of the rhodamine-core (Figure 27, **34**). Note that the change of the tetrazine motif (compared to the benzylamino tetrazine) reduces its reactivity towards olefins to the expense of labeling efficiency.

Overall, the requirements for fluorescent dyes are versatile, and the selection of the fluorescent probe needs careful consideration. Cellular, as well as photophysical properties, must be addressed to obtain optimal experimental results. Cellular properties such as membrane permeability, unspecific binding (retention), or intracellular distribution significantly affect the labeling efficiency and specificity, which ultimately impacts the signal-to-noise ratio of the fluorescent image. Furthermore, the photophysical properties of the bright synthetic fluorophores must fit the fluorescent experiment. For example, autofluorescence of naturally occurring fluorophores can be reduced by using red/far-red excitable probes, preferably with a large Stokes shift.

Additionally, the photostability of the dye must be ensured to enable 3D tracking of particles over time while retaining an overall brightness. Summarized, the wish list for fluorophore-tetrazine-conjugates is long. Finding the most suitable probe needs some consideration and, most likely, compromise solutions.

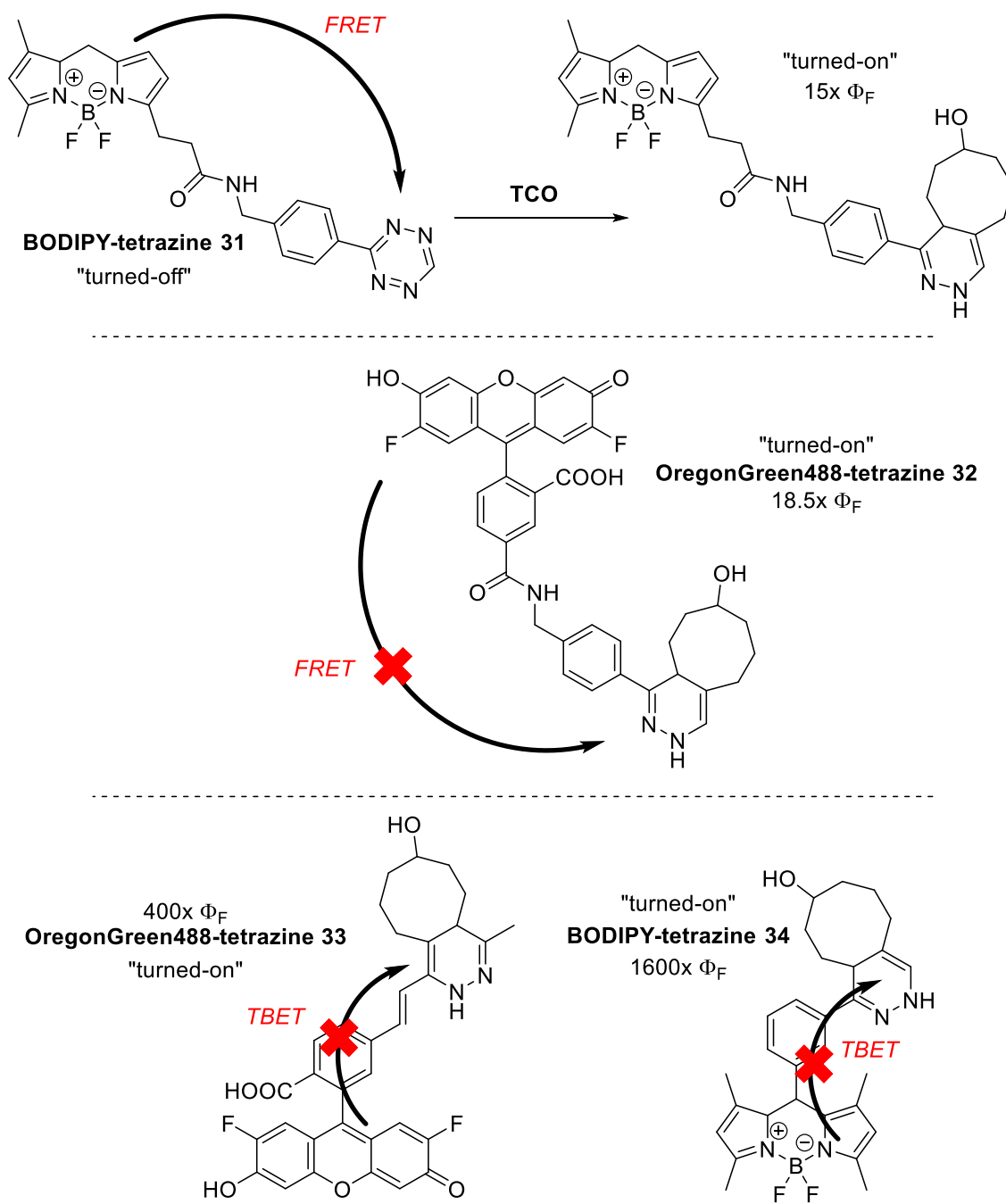


Figure 27: "Turn-on" of a BODIPY fluorophore and OregonGreen488 upon the reaction of the benzylamine tetrazine motif with TCO (top and middle). The quenching of the fluorophores occurs via FRET. The attachment of the tartrazine through connected  $\pi$ -system results in more efficient quenching of the fluorophore via TBET (bottom).

## 2.8 Pronucleotide concept

Bioactive compounds can show limitations during drug discovery in form of low solubility, toxic side effects, insufficient first pass-effect, poor bioavailability, or the inability to pass the blood-brain barrier. Overcoming these limitations, the drug is bio-reversibly converted into an inactive form, which displays improved pharmacokinetic and physiochemical properties. Improved solubility or increased drug absorption provides a higher bioavailability of the parent drug. In some cases, introducing specific bioreversible groups prevent uncontrolled drug distribution in the body or even allows specific drug accumulation in the target tissue, thus increasing bioavailability.<sup>95-97</sup> After cellular uptake of nucleoside analogs, they need to be phosphorylated to their corresponding triphosphates by endogenous kinases. Limitation during the phosphorylation steps to the active nucleotide can be attributed to the substrate specificity of the endogenous kinases. Due to low conversion, successful phosphorylation can stay out entirely or lack efficiency at a single phosphorylation step. This 'bottleneck' has an adverse effect on the bioavailability of the corresponding active nucleotide. However, the negative charge of the phosphates at physiological pH prevents cell permeability through biological membranes. Therefore, the general approach of nucleotide prodrugs is to protect the phosphates with biologically reversible masks. These lipophilically masked compounds can permeate into the cell, increasing bioavailability the parent drug's active metabolite after intracellular demasking.

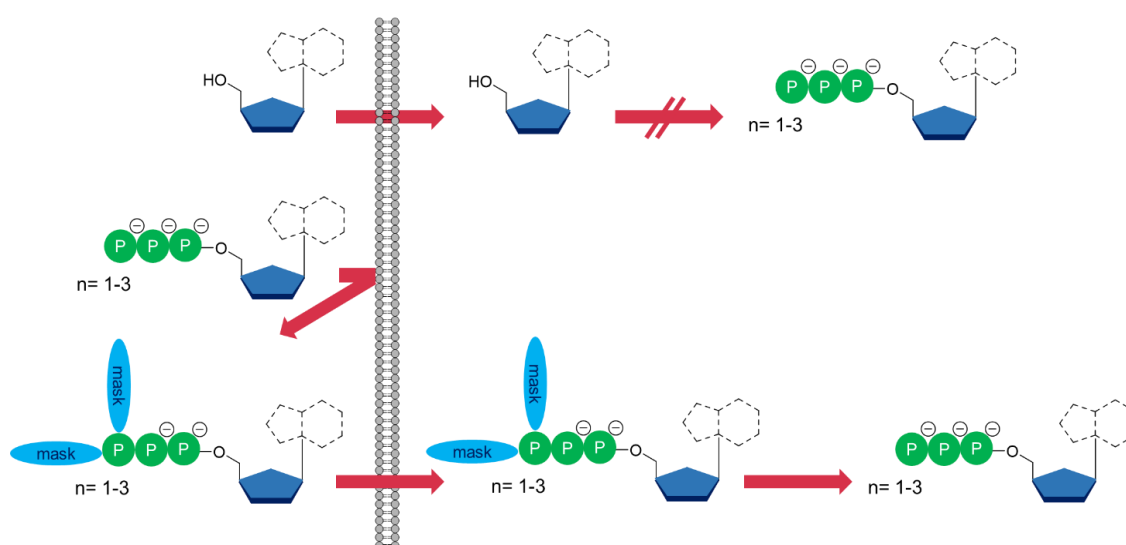


Figure 28: Pronucleotide concept in the light of cell permeability and intracellular phosphorylation processes.



Driven by the therapeutic significance of nucleoside analogs, several different pronucleotide concepts for nucleoside mono-, di- and triphosphates have been reported.

The starting point for the development of several concepts was the report of FARQUHAR *et al.* in 1983.<sup>98</sup> They described the protection of the phosphates by acyloxymethyl groups under the assumption that the uncharged phosphate-polyesters would allow cellular uptake of the monophosphate prodrug. The pivaloyloxymethyl group (POM) showed superior properties in chemical and enzymatic hydrolysis studies compared to a variety of tested acyloxymethyl esters giving the bisPOM concept its name. Enzymatical cleavage of the ester results in an unstable hydroxymethyl alcoholate, which decomposes to formaldehyde and the mono-masked monophosphate. After a second cycle, the desired nucleoside monophosphate is released.<sup>98,99</sup> Further developments of the concept led to the report of the isopropoxyloxymethyl carbonate (POC) group, which undergoes a similar cleavage mechanism. After the enzymatical attack, the unstable carboxylate forms, decomposing to carbon dioxide and formaldehyde.<sup>100</sup> In 2001 and 2002, the FDA approved the bisPOC prodrug Tenofovir disoproxil fumarate **35** (Viread) and the bisPOM pronucleotide Adefovir dipivoxil **36** (Hepsera), demonstrating the therapeutic value of these concepts.<sup>101</sup>

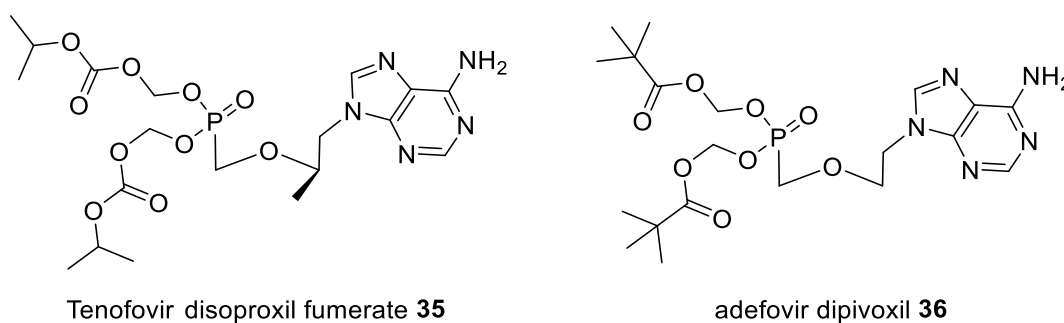


Figure 29: Tenofovir disoproxil fumarate **35** and Adefovir dipivoxil **36** as examples for the bis(POC) and the bis(POM) concept, respectively.

In the following decades, several nucleoside prodrugs were developed. In most cases, an enzymatic change in the masking unit initiates the formation of an unstable intermediate, which allows the intracellular release of the monophosphate. The bis(SATE)- and the bis(DTE)-concepts were described by PÉRIGAUD *et al.* and contained sulfur in their respective masking units.<sup>102</sup> Enzymatic cleavage of the respective thioester leads to the unstable *O*-2-mercaptoethylphosphotriester. The intermediate decomposes spontaneously via intramolecular nucleophilic displacement to the

respective phosphodiester under the release of ethylene sulfide. Removal of the second mask follows a similar mechanism resulting in the nucleoside monophosphate.<sup>103</sup>

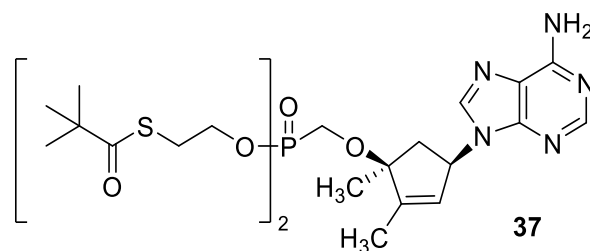


Figure 30: Example of the bis(SATE) concept of a nucleotide analog **37**.<sup>104</sup>

Besides these symmetric diester prodrugs, where both negative charges were masked by small lipophilic esters, monoester prodrugs with larger lipid-like substituents became increasingly attractive. Once designed by HOSTETLER *et al.* for nucleotide monophosph(on)ate prodrugs<sup>105</sup>, the concept was recently applied to acyclic nucleoside phosphonates. The hexadecyloxypropyl-(HDP) ester mimics naturally occurring lysophospholipid structures and is later cleaved intracellularly by phospholipase enzymes. Brincidofovir (**38**, CMX001) showed promising results for the treatment of cytomegalovirus; however, it failed FDA approval in phase III of their clinical trials.<sup>106</sup> HDP-HPMPA (**39**, CMX157) is in clinical trial against HIV, showing the overall potential of the concept for future antiviral applications.<sup>104,107</sup>

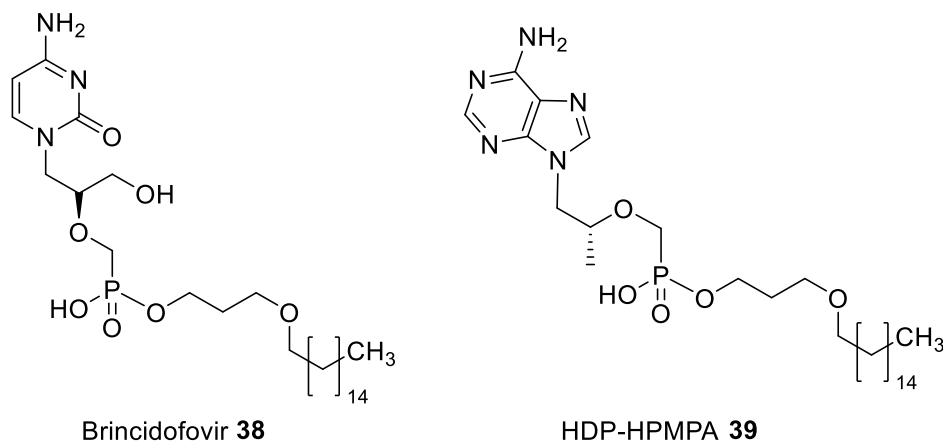


Figure 31: Two examples of the HDP concept as candidates for antiviral therapy.

In the 1990's, MCGUIGAN *et al.* developed a phosphoramidate prodrug system with a mixed amidate/ester protection system, which successfully delivers monophosphates into cells.<sup>108</sup> These so-called ProTides contain an *L*-alanine isopropyl amidate, which can be enzymatically activated by an ester cleavage of the amino acid. In the next step, the resulting carboxylate attacks the phosphorous atom by forming a five-membered ring

under the elimination of the second masking unit - the aryl alcohol. Aqueous hydrolysis induces ring-opening, followed by phosphoramidase cleavage of the amino acid leading to the formation of the desired nucleotide.<sup>109</sup> An example of the ProTide approach is Tenofovir alafenamide **40**, approved for HIV/AIDS and chronic hepatitis B treatment in 2015.<sup>110</sup> In 2013, the FDA approved Sofosbuvir **41**, which has since become a member of the WHO's list of essential medicines, due to its significance in treating hepatitis C.<sup>111</sup>

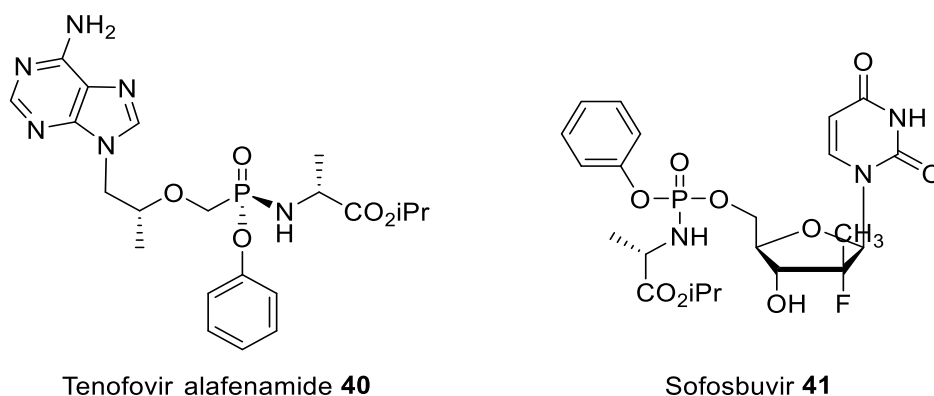


Figure 32: The FDA-approved antiviral active ProTide compounds Tenofovir alafenamide **40** and Sofosbuvir **41**.

Building on this pronucleotide technology, ROYZEN *et al.* recently described the first example of a 4TCO-conjugated nucleoside analog, which functions as a ribosomal RNA reporter in living cells.<sup>112</sup> The phosphoramidate prodrug of the modified adenosine monophosphate **42** facilitates the cellular uptake of the reporter molecule. Subsequent intracellular demasking releases the desired nucleotide, which is then phosphorylated to its active nucleoside triphosphate. Successful incorporation into newly synthesized ribosomal RNA was demonstrated by highly sensitive UHPLC-MS/MS of the pooled cellular RNA. No signal was observed for the incorporation into messenger RNA. Fluorescent labeling of the incorporated bioorthogonal reporter in living mammalian cells was achieved by treatment with a tetrazine-conjugated OregonGreen488 fluorophore (5  $\mu$ M) for two hours.

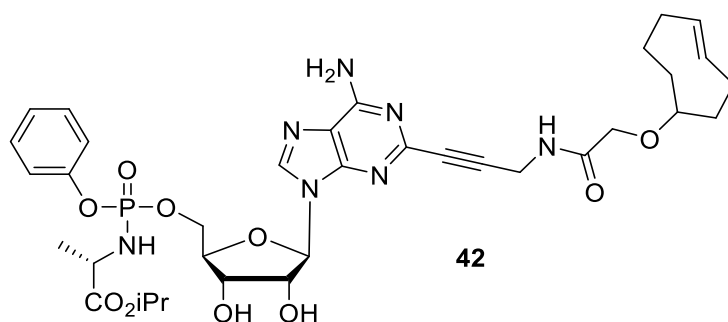


Figure 33: The phosphoramidate pronucleotide of a 4TCO-modified adenosine for bioorthogonal labeling.

The development of the *cycloSal* concept by MEIER *et al.* followed a different strategy independent from enzymatically induced cleavage of the masking groups. By introducing a saligenyl-moiety to cover the negative charges of the phosphate, a cyclic triester **43** is formed, which releases the desired nucleoside monophosphate **44** after chemical activation inside the cell.<sup>113–115</sup> At *pH*-values >7, the aryl ester bond is hydrolyzed, which induces a spontaneous cleavage of the benzyl ester under the elimination of *ortho*-quinone. The only by-product is hydrolyzed to the salicyl alcohol **45**. The hydrolysis rate can be increased by destabilizing the phenol ester with electron-withdrawing groups like nitro- or chloro-substituents. In contrast, stabilizing substituents like alkyl groups increase the stability of the *cycloSal* compounds and therefore prolong their half-lives in physiological media.<sup>116,117</sup>



Figure 34: Chemical activation pathway of the *cycloSal* concept.

Further developments addressed the concern that the *cycloSal* prodrugs might re-diffuse out of the cell due to slow cleavage of the saligenyl mask, which would result in a limited increase in potency. The design of the so-called “lock-in” *cycloSal*-prodrugs

contains a carbonyloxymethyl group, which is rapidly cleaved by enzymes inside the cell under the formation of a more polar carboxylic acid.

Later attempts to transfer the *cycloSal* concept to nucleoside diphosphates demonstrated unsatisfying results in implemented hydrolysis studies. These studies revealed the predominant formation of the nucleoside monophosphate in contrast to the desired release of the diphosphate. This observation is attributed to the fast cleavage of the energy-rich phosphate-phosphate anhydride bond, which is kinetically stable only because of the negative charges preventing nucleophilic attacks. Attempts to protect the terminal phosphate of di- and triphosphates with glycerin- or acyl groups led to similar results, namely pyrophosphate bond cleavage rather than the formation of the desired nucleotides.

The MEIER group achieved a breakthrough by using the bis(acyloxybenzyl) (BAB) concept, once designed as a nucleoside monophosphate prodrug system. In 1993, THOMSON *et al.* reported the BAB-AZT-MP, where two *para*-acyloxybenzyl moieties protect the phosphate.<sup>118</sup> The AB group is activated by esterases via cleavage of the acyl function. The resulting electron-donating phenolate induces a 1,6-elimination releasing the phosphate and a quinone methide. The quinone methide is further converted to 4-hydroxybenzyl alcohol in the presence of water.

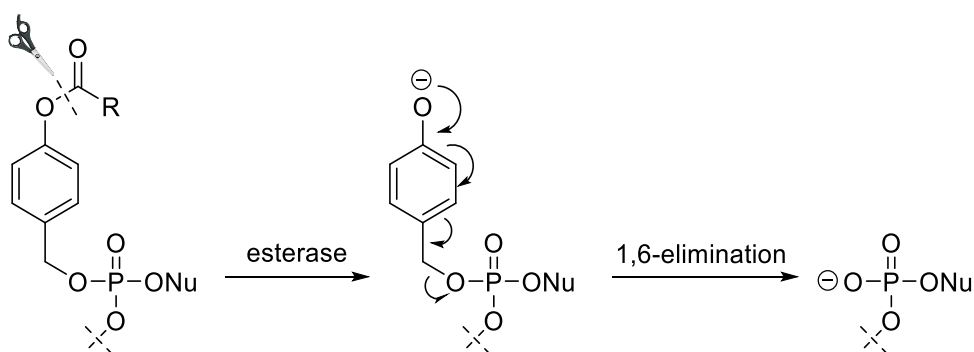


Figure 35: Enzymatic activation pathway of the BAB concept.

In 2008, the BAB concept was successfully transferred to nucleoside diphosphates (DiPPro concept) initiating the starting point of extensive research regarding the development of nucleoside-diphosphate and nucleoside-triphosphate prodrug systems. Synthetically, the DiPPro compounds were accessible by coupling a symmetrical bis(acyloxybenzyl) phosphoramidite with an appropriate NMP and subsequent oxidation of the phosphorous atom. Hydrolysis studies of these DiPPro compounds demonstrated high chemical stability and fast and highly selective enzymatic cleavage

in cell extracts to deliver the desired NDPs. The assumption was made that the successful release of the NDP can be attributed to a fast enzyme-catalyzed cleavage in the para-position of the first AB-mask without the involvement of the phosphate anhydride bond. The formation of a second negative charge at the mono-masked AB-NDP intermediate significantly increases the kinetic stability of the pyrophosphate bond due to electrostatic repulsion. The electrostatic repulsion contributes to the predominant release of the NDP after the second AB-cleavage.<sup>119</sup>

Since then, various DiPPro compounds bearing different symmetrical and non-symmetrical masking units were synthesized and evaluated to determine the most effective modification based on stability, nucleoside diphosphate release, and antiviral activity.<sup>120</sup> In general, these DiPPro compounds illustrated that the pronucleotide can penetrate biological membranes, followed by intracellular release of the phosphorylated metabolites – most likely the diphosphate nucleoside.<sup>119–124</sup>

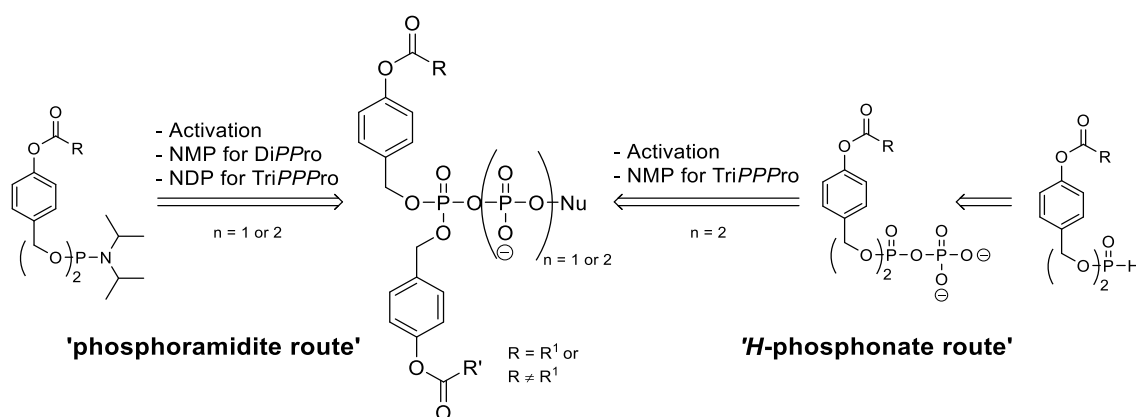


Figure 36: Synthetic routes for DiPPro- and TriPPPro compounds.

Later, this approach was successfully transferred to triphosphates (TriPPPro concept). Currently, there are two synthetic approaches available for the synthesis of BAB triphosphate prodrugs. The first approach consists of the coupling of the bis(AB) phosphoramidite with the appropriate NDP followed by the oxidation of the terminal phosphorus atom.<sup>125</sup> Since the synthesis of NDPs is often time-consuming or entirely unfeasible, a further synthetic approach was developed. The coupling between a dimasked pyrophosphate and an NMP enabled a convenient approach to synthesize numerous TriPPPro compounds with various nucleoside derivatives. The first synthetic step is the oxidative chlorination of the bis(AB)-H-phosphonate using *N*-chlorosuccinimide. The coupling of the reactive intermediate with tetrabutylammonium phosphate results in the corresponding dimasked

pyrophosphates. The pyrophosphate is then activated stepwise with trifluoroacetic anhydride (TFAA) and 1-methylimidazole before the final coupling with a NMP.<sup>126</sup>

Antiviral studies of these TriPPPro compounds revealed increased potency against HIV compared to their parent nucleosides. Especially significant was the observation that thymidine-base pronucleotides were active in thymidine kinase-deficient cells, in which the parent nucleosides were inactive – demonstrating metabolic bypass. Furthermore, hydrolysis studies of prodrugs in CEM/0 cell extract displayed NTP release, which strongly indicated the successful intracellular release of the active metabolite. Further evidence for intracellular accumulation of the demasked triphosphates was collected by incubating T-lymphocytes with fluorescent 2',3'-dideoxy-bicyclic-nucleoside triphosphate (ddBCNA-TP)-prodrugs. Subsequently, cell washing and lysis of the cell samples allowed for the detection of intracellularly present BCNA-triphosphates and lower nucleotide metabolites.<sup>126</sup>

A new generation of TriPPPro compounds was described by MEIER and co-workers recently. The design comprised only one cleavable AB-mask and a non-cleavable  $\gamma$ -alkyl group at the terminal  $\gamma$ -phosph(on)ate (Figure 37). After the cell-uptake of these asymmetrical prodrugs and the subsequent intracellular demasking of the bioreversible AB group, the  $\gamma$ -alkyl nucleoside triphosphate or  $\gamma$ -C-(alkyl)-nucleoside triphosphate are released, respectively.<sup>127,128</sup>

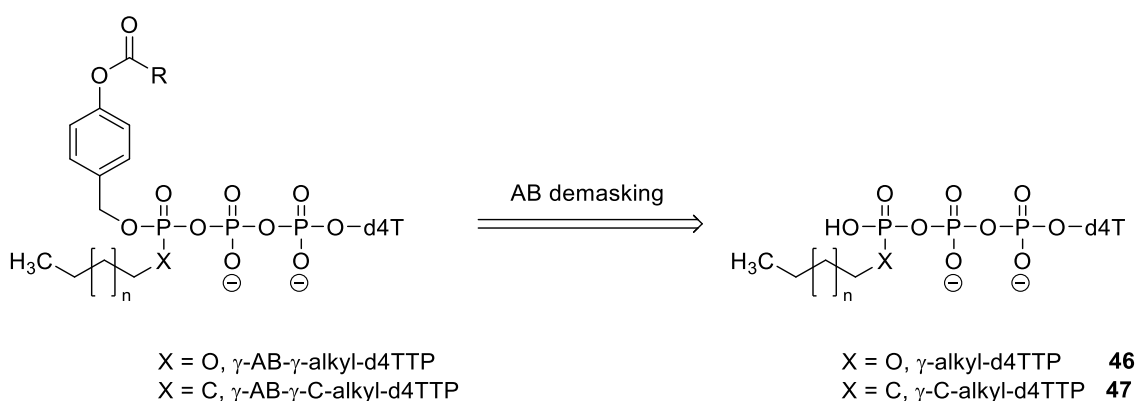


Figure 37: Illustration of the new generation of TriPPPro compounds.

Antiviral activities of these nucleotide prodrug analogs of d4T generally exhibited similar or increased potency against HIV in cell assays compared to the parent d4T analog. Furthermore, hydrolysis studies in CEM/0 cell extract provided the selective release of the  $\gamma$ -alkylated nucleotides, which displayed markedly increased stability against dephosphorylation by phosphatases compared to d4TTP. Moreover, primer extension

assays confirmed that  $\gamma$ -alkyl-d4TTP **46** and  $\gamma$ -C-alkyl-d4TTP **47** are substrates for the reverse transcriptase (RT), but not for the cellular polymerases  $\alpha$ ,  $\beta$ , and  $\gamma$ . Preliminary evidence indicates that the substrate specificity towards endogenous polymerases as well as RT depends on the length of the  $\gamma$ -alkyl chain. Since the RT tolerates higher chain lengths, a therapeutic window opens, in which the HIV-enzyme can be discriminated from endogenous polymerases.



### 3 Objectives

This work aims to synthesize triphosphate pronucleotides containing various chemical handles applicable in the bioorthogonal and catalyst-free **DA<sub>INV</sub>** to provide a toolbox for metabolic labeling of nucleic acids, with a special focus on live-cell (no-wash) applications.

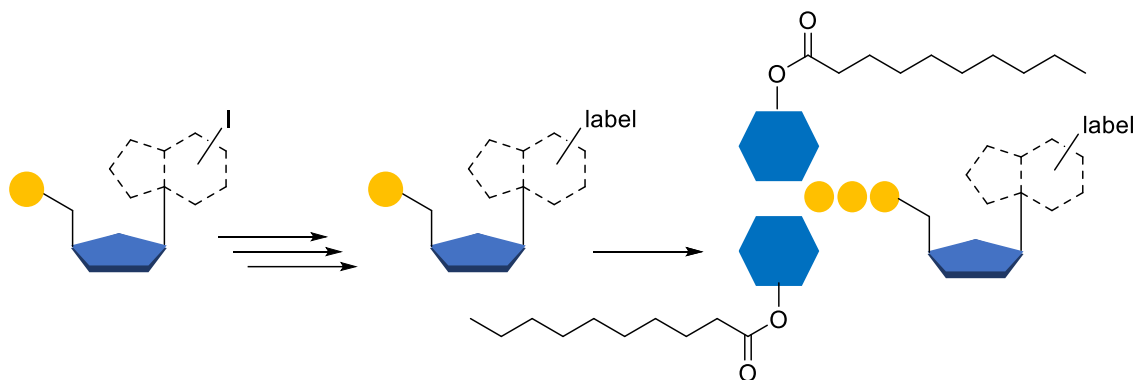


Figure 38: Illustration of the robust synthetic approach developed to synthesize TriPPP compounds with various labels.

The first part of this thesis explores the vinyl label and introduces this smallest possible function to C5-pyrimidine and C7-purine derivatives of uridine and 7-deazaadenine analogs. At first, the synthetic approach implemented in prior studies is employed. This method comprises the introduction of protective groups to increase the solubility of the nucleoside analogs and to allow their regioselective 5'-*O*-monophosphorylation.

However, being rather time-consuming and economically unfavorable, the synthetic approach was to be improved to a more sophisticated reaction route, which does not rely on a protective group strategy and enables simple access to more demanding nucleotide probes.

Besides to the synthesis of symmetric bis(AB) vinyl functionalized pronucleotides, this work aims to deliver asymmetric  $\gamma$ -alkyl modified (AB) pronucleotides to explore the applicability of this second generation triphosphate pronucleotide technology for metabolic labeling of nucleic acids. As described, the  $\gamma$ -alkyl moiety improves the stability of the intracellular released triphosphate and allows the discrimination between endogenous and viral polymerases depending on the alkyl chain length.

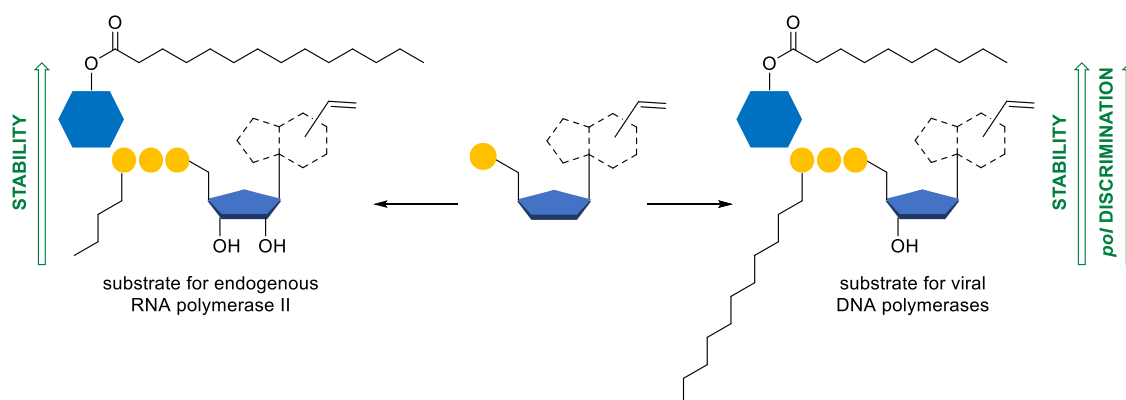


Figure 39: Illustration of  $\gamma$ -alkyl modified TriPPP compounds and their applications.

The rational concept here was to introduce a short C4 chain to the AB-pronucleotide of vinyl-ribonucleoside triphosphates to benefit from increased intracellular stability of the triphosphate without interfering with the substrate affinity towards the endogenous RNA polymerase II. In other words, this approach was designed to answer the question: is the C4 chain positively influencing the bioavailability of the reporter probe and ultimately improving the labeling capacity?

In contrast, a C11 chain was introduced to vinyl functionalized DNA pronucleotide reporters to study the potential of discriminating viral polymerases from cellular enzymes. To put it differently, these probes were envisaged to showcase: is it possible to visualize newly synthesized viral DNA without labeling the cellular DNA products?

With a robust synthetic approach at hand, the aim was to prepare various TriPPP compounds with strained functionalities such as 1MCPs, TCOs, and BCN. Moreover, 1,2,4,5-tetrazine motifs should be introduced to the nucleoside reporters to study the applicability of a reversed labeling approach. Additionally, a fluorogenic pronucleotide reporter with a silicon-rhodamine dye attached to the nucleobase via a long spacer should be synthesized.

Since bioorthogonal labeling strategies rely on a labeling dye, this work also aimed to synthesize various known and novel rhodamine-tetrazine conjugates for live-cell imaging applications. The aspiration was to synthesize a fluorogenic sensor molecule, which provides cell permeability, reduced background, and fast reaction kinetics.

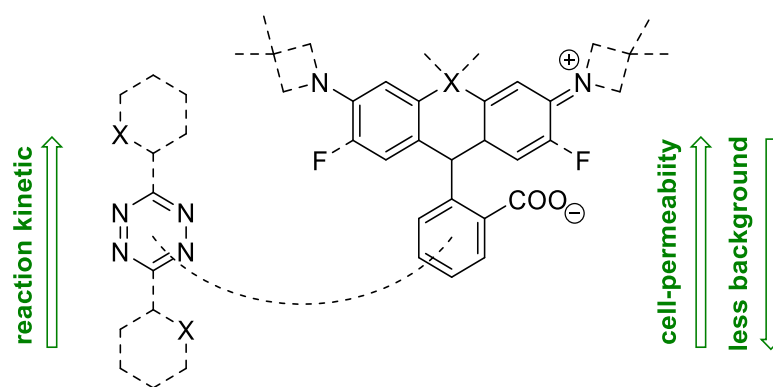


Figure 40: Illustration of the design of rhodamine-tetrazine conjugates.

Finally, the metabolic probes should be tested in imaging experiments to examine the applicability of these united concepts. Novel imaging assays and conditions were therefore to be set up and evaluated. Here, HSV-1 should be utilized as a model virus to investigate the metabolic labeling of viral DNA and RNA in host cells. A particular objective of this work was the metabolic labeling of viral nucleic acid in living cells and producing genome-labeled viral particles to enable the visualization of both late and early viral infection.

Taken together, this work aimed to provide the first benchmark for metabolic nucleic acid imaging in live-cell applications by combining the *TriPPP* concept and the latest developments in the field of “click-chemistry”.

## 4 Results and discussions

### 4.1 Synthesis of vinyl-modified nucleosides and their TriPPPPro's

The first aim of this work was to establish a synthetic approach to the preparation of various vinylated (BAB)-pronucleotides. As described in Chapter 2.8, the *H*-phosphonate route provides simple access to different TriPPPPro compounds if the respective NMPs are available. The first objective was hence to find a viable method to synthesize the vinylated NMPs.

Early results revealed three obstacles that needed to be addressed. Initially, the low solubility of the appropriate nucleoside derivatives in organic solvents complicated the synthetic workflow (i). Furthermore, similar physical properties of the iodo- and vinyl-bearing nucleoside derivatives during column chromatography impeded simple isolation of the vinylated nucleoside when the cross-coupling reaction didn't proceed to complete conversion of the iodized nucleoside starting material. (ii). Lastly, the vinyl function is unstable under acidic conditions, hence demanding the applied phosphorylation method's compliance to obtain the respective vinylated nucleoside monophosphate (iii).

The first rational reaction design comprised the introduction of protective groups at the hydroxyl functions of the iodized nucleosides, which significantly improved their overall solubility in organic solvents. Moreover, by applying an orthogonal protective group strategy, the selective deprotection of the 5'-hydroxyl function was feasible. Later, this approach allowed the regioselective 5'-*O*-monophosphorylation without significant loss of solubility in organic solvents due to the remaining 2'-(and 3'-) protective group(s). The retrosynthetic scheme is shown in Figure 41.

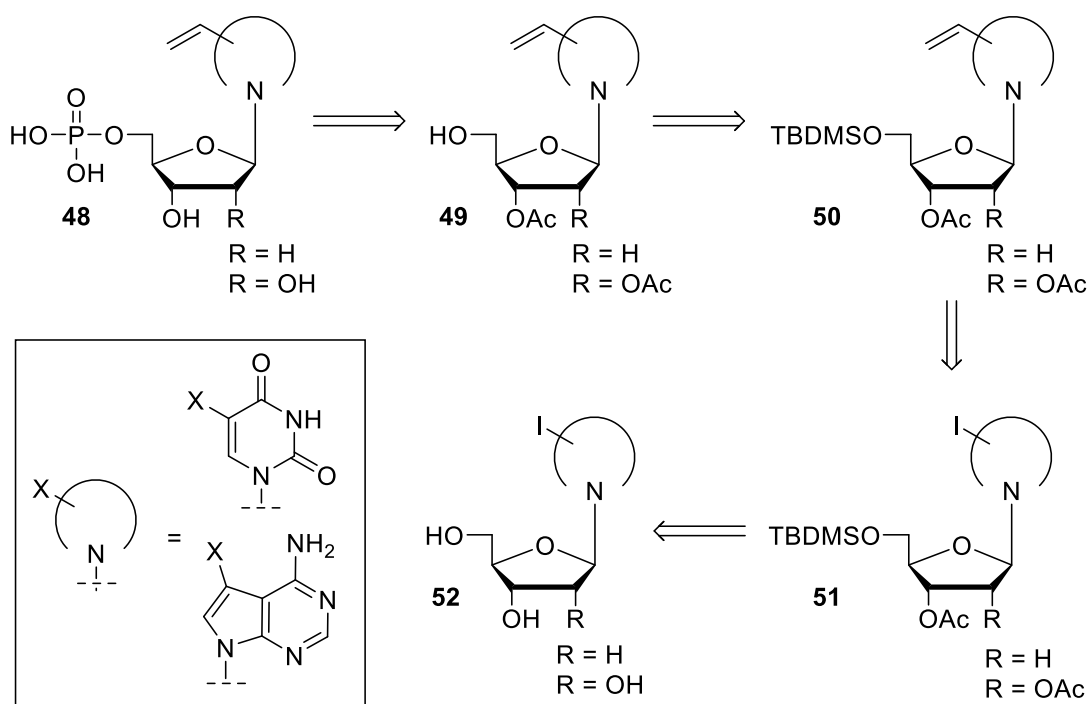


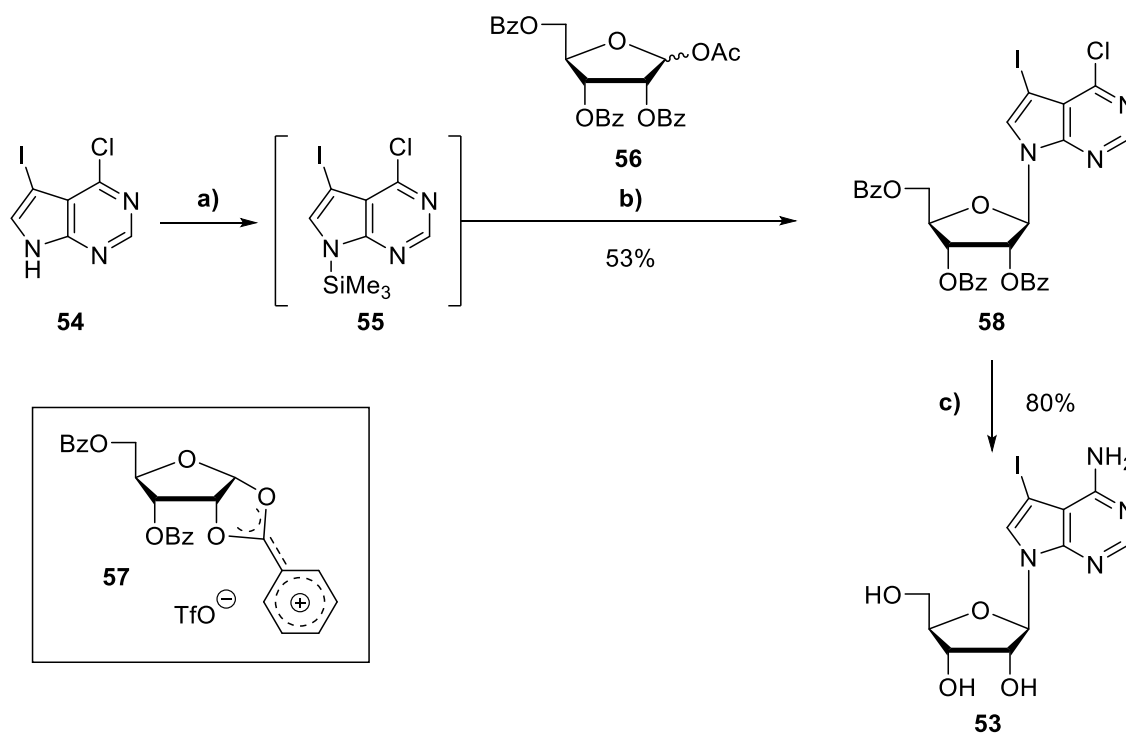
Figure 41: Retrosynthetic schema for the synthesis of the vinylated nucleoside monophosphates.

The vinyl-modified NMPs **48** should be obtained by 5'-*O*-phosphorylation of the 5'-deprotected nucleosides **49**, which are prepared from fully protected nucleosides **50** by fluoride-mediated desilylation. The introduction of the vinyl group is generated from the protected nucleosides **51** under STILLE cross-coupling conditions. The protected nucleoside derivatives **51** are prepared from the respective iodized C<sub>5</sub>-pyrimidine and the C<sub>7</sub>-deazapurine nucleosides **52** (5-iodouridine or 7-iodo-7-deazaadenine and their 2'-deoxyribonucleosides).

In terms of retaining substrate properties towards polymerase enzymes in general, the positions the C<sub>5</sub> position of pyrimidines and the C<sub>7</sub> position of 7-deazapurines were reported to be best suited for the introduction of the bioorthogonal handle.<sup>129–134</sup>

The 5-iodouridine analogs were commercially available, whereas the 7-iodo-7-deazaadenine derivatives were synthesized according to literature:

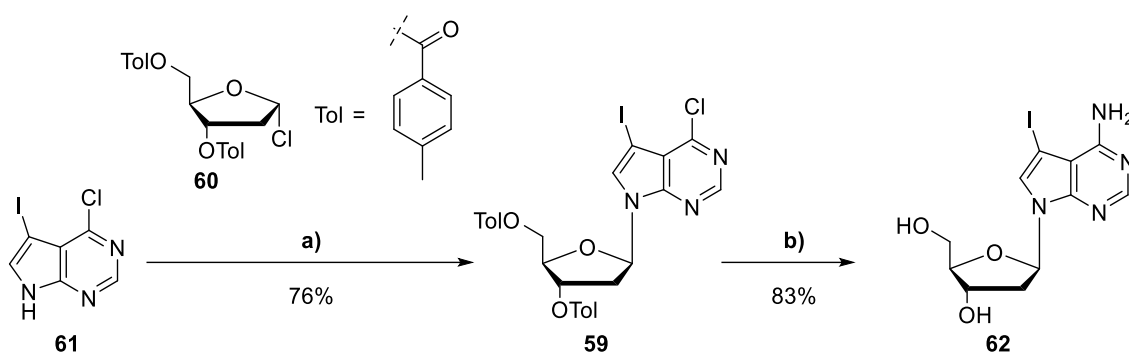
The synthesis of 7-deaza-7-iodoadenosine (**53**, IA) was performed according to SEELA *et al.*<sup>135</sup> The silyl-Hilbert-Johnson reaction involves the silylation of the relatively insoluble 6-chloro-7-iodo-7-deazapurine **54** into the lipophilic silyl intermediate **55**, which is readily soluble in acetonitrile. As described in the literature, BSA was employed as a silylation reagent, and TMSOTf was used as the glycosylation catalyst (Vorbrüggen conditions) and reacted with 1-*O*-acetyl-2,3,5-tri-*O*-benzoyl- $\beta$ -D-ribofuranose **56** to the oxo-carbenium intermediate **57**. Due to the electron-releasing properties of silicon, the silylated purine **55** is a good nucleophile and attacks the intermediate **57** under the formation of the glycosylation product **58**.<sup>135,136</sup> Deprotection of **58** and simultaneous substitution of the chloro-substituent by an NH<sub>2</sub> group was carried out in an autoclave (120 °C) with aqueous ammonia in dioxane. After recrystallization from methanol, IA **53** was obtained in 80% yield. Previous attempts to isolate **53** by column chromatography resulted in unsatisfying results due to its low solubility in organic solvents.



Scheme 1: Synthesis of 7-deaza-7-iodoadenosine **53** described by SEELA *et al.*<sup>135</sup> **Reagents and conditions:** **a)** BSA, CH<sub>3</sub>CN, 0 °C, 15 min; **b)** 1-*O*-Acetyl-2,3,5-tri-*O*-benzoyl- $\beta$ -D-ribofuranose, TMSOTf, rt to 80 °C, 90 min; **c)** dioxane/25% NH<sub>4</sub>OH<sub>(aq)</sub> (1:2 v/v), autoclave, 120 °C, o/n.

In analogy to SEELA *et al.*, the liquid-liquid phase transfer glycosylation was employed to synthesize the *P*-toluoyl protected 7-deaza-6-chloro-7-iodo-2'-deoxyadenosine **59**.<sup>137</sup> The reaction was carried out under standard conditions with 2-deoxy-3,5-di-*O*-(toluoyl)- $\alpha$ -D-*erythro*-pentofuranosyl chloride **60** as the sugar component and 6-chloro-7-iodo-7-deazapurine **61** as the nucleobase. The nucleobase anion was generated with powdered

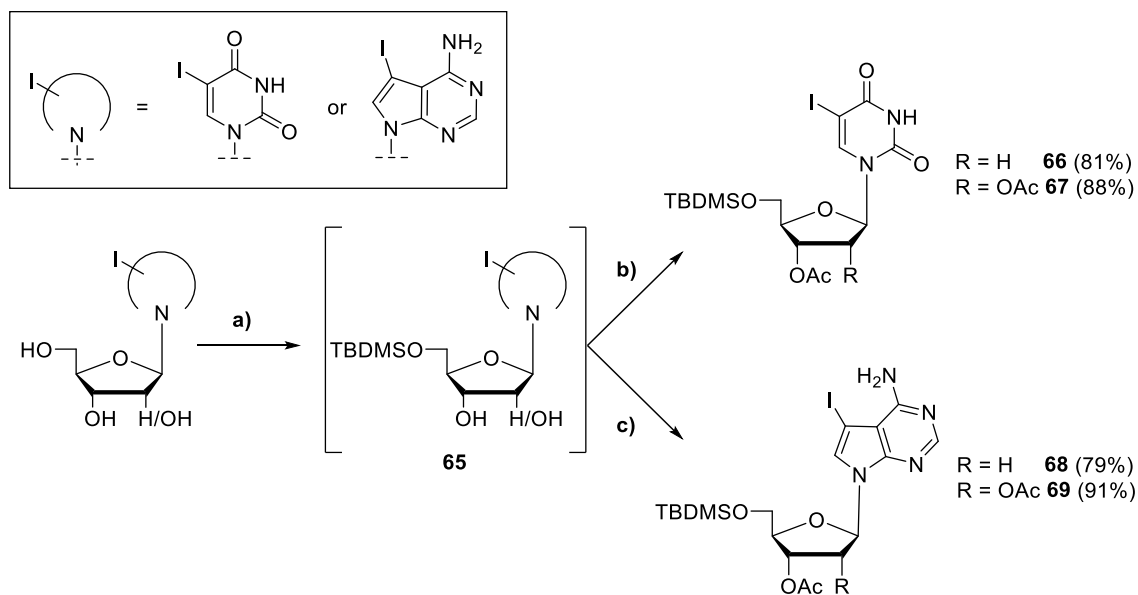
KOH and tris-[2-(2-methoxyethoxy)-ethyl]-amin (TDA-1) as a phase-transfer catalyst in acetonitrile. The  $\beta$ -nucleoside **59** was obtained in 76% yield which is in accordance with reported yields by SEELA *et al.*<sup>137,138</sup> No traces of the  $\alpha$ -anomer were detectable by NOESY. The displacement of the 6-chloro substituent by an NH<sub>2</sub> group and simultaneous deprotection of the *P*-toluoyl groups was performed as described above in an autoclave (120 °C) with aqueous ammonia in dioxane. Recrystallization from methanol resulted in the deprotected 7-deaza-7-iodo-2'-deoxyadenosine (**62**, IdA) with a similar yield as above in a yield of 83%.



Scheme 2: Synthesis of 7-deaza-7-iodo-2'-deoxyadenosine **62** according to SEELA *et al.*<sup>137–140</sup> **Reagents and conditions:** a) i) KOH, TDA-1, CH<sub>3</sub>CN, 10 min, rt ii) 2-deoxy-3,5-di-O-(toluoyl)- $\alpha$ -d-erythro-pentofuranosyl chloride, 20 min, rt; b) dioxane/25% NH<sub>4</sub>OH<sub>(aq)</sub> (1:2 v/v), autoclave, 120 °C, o/n.

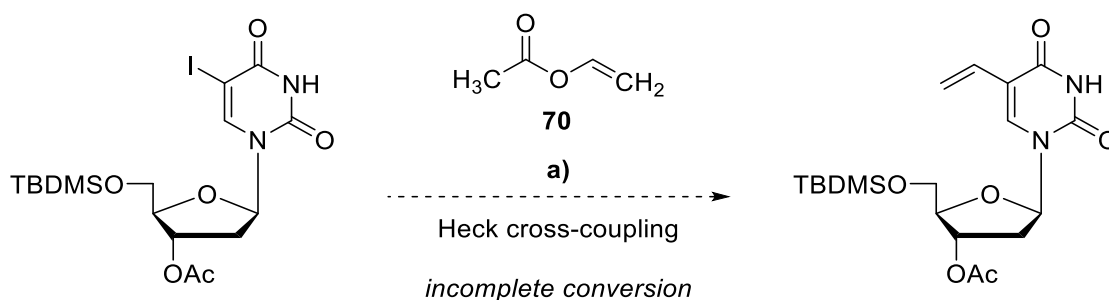
Since 5-iodo-2'-deoxyuridine (**63**, IdU) and 5-iodouridine (**64**, IU) were commercially available and IdA **62** and IA **53** were successfully synthesized, the next step was to introduce the protective groups. The *tert*-butyldimethylsilyl ether protection of the 5'-position and subsequent acetylation of the remaining hydroxyl functions is a widely applied orthogonal protective strategy in nucleoside chemistry because it allows the simple differentiation between the primary and secondary alcohol functions. Silylation of the 5'-hydroxyl group was achieved with a slight excess of TBDMSCl in pyridine to form the intermediate **65**. For the uridine nucleoside derivatives, an excess of acetic anhydride was added to yield the protected nucleosides **66** and **67** in good yields of 81% and 88%, respectively.

To prevent *N*-acetylation at the purine base, a regioselective *O*-acetylation method described by MATSUDA *et al.* was employed.<sup>141</sup> By changing the solvent from pyridine to acetonitrile with catalytic amounts of DMAP and triethylamine as a base, the acetylation reaction was accelerated and selectively produced the *O*-acetylated products **68** and **69** in good to excellent yields of 79% and 91%, respectively. As mentioned above, the overall solubility of the protected nucleoside derivatives in organic solvents improved significantly, simplifying the general synthetic workflow.



Scheme 3: Preparation of the protected nucleosides. **Reagents and conditions:** a) TBDMSCl, pyridine, rt, o/n; b) Ac<sub>2</sub>O, pyridine, rt, o/n; c) DMAP, Et<sub>3</sub>N, Ac<sub>2</sub>O, rt, 1 h.

In general, the 5-vinylation at the 5-iodouracil moiety can be achieved by Heck cross-coupling with vinyl acetate **70** as a vinylation reagent or under STILLE conditions that employ tributyl(vinyl)tin. Based on the toxicity of the tin reagent used under STILLE conditions, the Heck cross-coupling seemed to be the more appropriate starting-candidate (Scheme 4). However, the Heck cross-coupling reaction did not prove to be a reliable method to reproduce complete conversion of starting material, potentially due to insufficient stability of the catalyst/ligand system. This assumption was based on the relatively quick disappearance of the dark red color that typically indicates complete catalyst activation before cross-coupling. Moreover, elevated reaction times did not improve reaction conversion, giving further evidence for early catalyst deactivation. As mentioned above, it was not possible to separate the vinylated product from the starting material via chromatography due to their similar physical properties.



Scheme 4: Heck cross-coupling of **66** with vinyl acetate **70** according to E.deCLERCK *et al.*<sup>142</sup> **Reagents and conditions:** a) i) Pd(OAc)<sub>2</sub> (20 mol%), PPh<sub>3</sub> (40 mol%), Et<sub>3</sub>N, DMF, 70 °C; ii) **70**, DMF, 70 °C, o/n.



Moreover, when monitored by thin-layer chromatography, elongated reaction times showed the increasing formation of by-products, which ultimately would have lowered yields following comparable literature values.<sup>143,144</sup> Based on these unsatisfying results, the focus was now on the STILLE cross-coupling that proved to be a reliable method.

The catalyst/ligand system applied in this work, not only for the STILLE cross-coupling described here but also later for a variety of performed SONOGASHIRA cross-coupling reactions, was selected based on the work of FARINA *et al.*<sup>145</sup> They systematically screened weakly donating ligands for STILLE cross-coupling reactions and found that ligands with lower donor ability, such as P(C<sub>6</sub>F<sub>5</sub>)<sub>3</sub>, AsPh<sub>3</sub>, or tri-(2-furyl) phosphine (TFP), show significant reaction rate enhancement over triphenylphosphine-based catalysts. It was postulated that a pre-equilibrium exist between a fully coordinated species **71** and an unsaturated intermediate **72** (Figure 42). Strong electron-donating ligands, therefore, hamper the reaction by lowering the concentration of the reactive species **72**.<sup>146</sup>

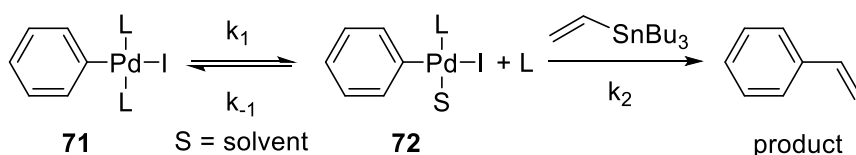


Figure 42: Illustration of the postulated preequilibrium between the fully-coordinated species **71** and the coordinatively unsaturated intermediate **72**.<sup>145</sup>

In addition, the study confirmed that ligands with low donor ability generally produce less stable catalyst systems. However, TFP proved to be an excellent compromise between increased reactivity and catalyst stabilization. Furthermore, FARINA *et al.* successfully synthesized 5-vinyluracil **74** from 5-iodouracil **73** with different ligands in *N*-methyl pyrrolidone under mild conditions (Figure 43).

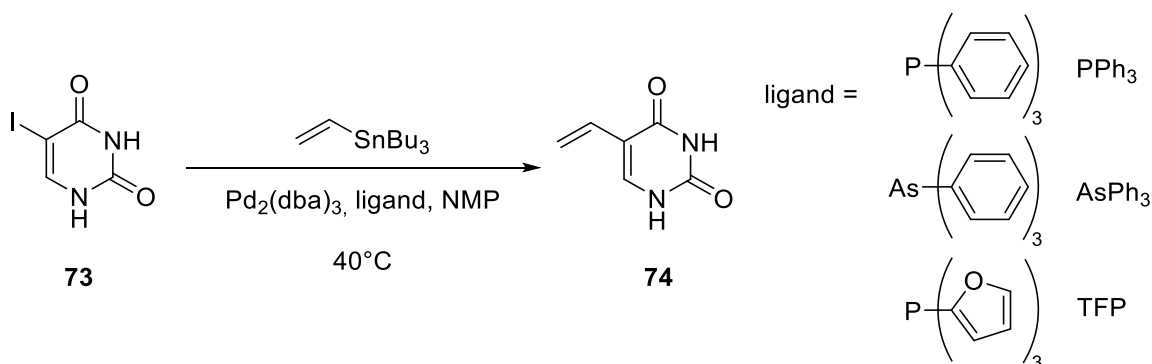
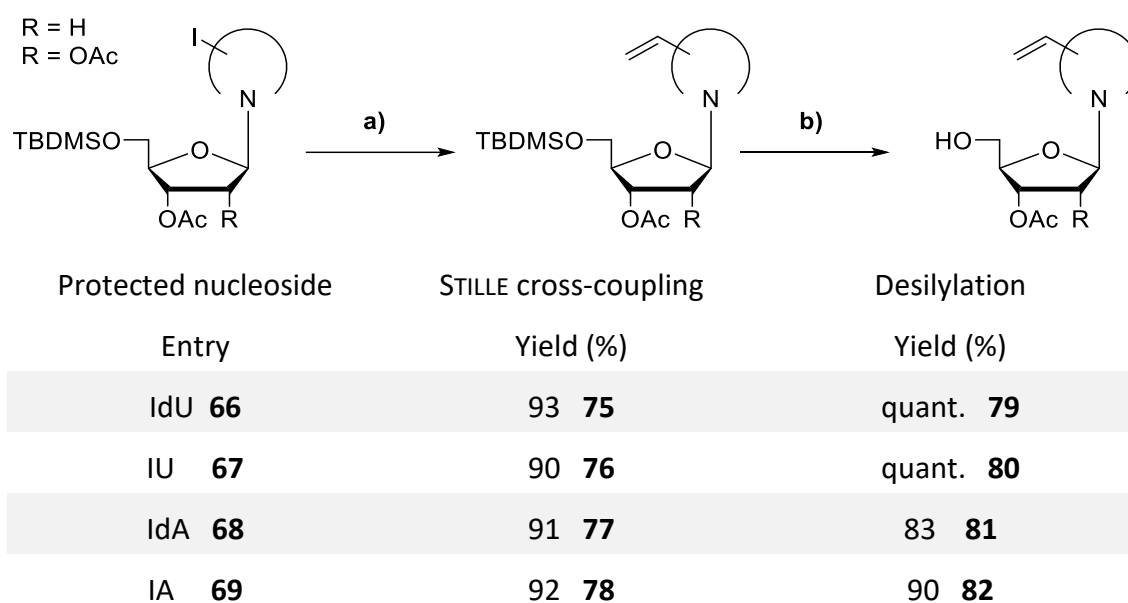


Figure 43: STILLE cross-coupling of 5-vinyluracil **74** under the screening of PPh<sub>3</sub>, AsPh<sub>3</sub>, and TFP as catalysts under mild conditions.<sup>145</sup>

As expected, the weakest electron donor ligand  $\text{AsPh}_3$  displayed the fastest kinetics followed by the TFP. Interestingly,  $\text{PPh}_3$  gave rise to an unstable catalyst that prevented complete conversion from **73** to **74**, whereas TFP demonstrated the most advanced stability.<sup>145</sup>

Later, ENGEL *et al.* prepared vinylated ribonucleoside derivatives in excellent yields utilizing the catalyst system  $\text{Pd}_2(\text{dba})_3/\text{TFP}$ . Thus, their refined reaction conditions were applied to the vinylation of the  $\text{C}_5$ -iodo-pyrimidine and  $\text{C}_7$ -iodo-deazapurine nucleosides **66-69** (Scheme 5).<sup>147</sup>



Scheme 5: STILLE cross-coupling reaction of the  $\text{C}_5$ -iodo-pyrimidine and  $\text{C}_7$ -iodo-deazapurine nucleosides and subsequent desilylation in order to gain vinyl functionalized nucleosides **79-82**. **Reagents and conditions:** a)  $\text{Pd}_2(\text{dba})_3$  (5.4 mol%), tri(2-furyl) phosphine (12 mol%), tributyl(vinyl) tin, DMF, 60 °C, 2-3 h;<sup>147</sup> b) TreatHF, THF, rt, o/n.

In each case,  $^1\text{H-NMR}$  spectra confirmed the complete conversion of starting material without any observable by-products. Due to the improved lipophilicity of the protected nucleosides, isolation of vinylated nucleosides **75**, **76**, **77**, and **78** by column chromatography was smoothly realized, resulting in overall excellent yields from 85-88%. Subsequent desilylation with triethylamine trihydrofluorid (TreatHF) in THF at room temperature resulted in good to excellent yields of the 5'-deprotected nucleosides **79**, **80**, **81**, and **82**. Fortunately, after TBDMS-deprotection the nucleosides still exhibited sufficient solubility in organic solvents due to the remaining acetyl group(s).

A prior attempt to synthesize 5-vinyluridine monophosphate (VUMP) via the phosphorylation method of SOWA & OUCHI led to the decomposition of the vinyl group due to the harsh acidic reaction conditions. The nucleoside monophosphates **83**, **84**, **85**,

and **86** were therefore prepared using bis(fluorenylmethyl) phosphoramidite **87**. The reagent was used by JESSEN *et al.* for the iterative synthesis of nucleoside oligophosphates starting from NMPs. Besides, this phosphoramidite route proved to be a reliable phosphorylation method for the preparation of 5'-*O*-nucleoside monophosphates.<sup>148</sup>

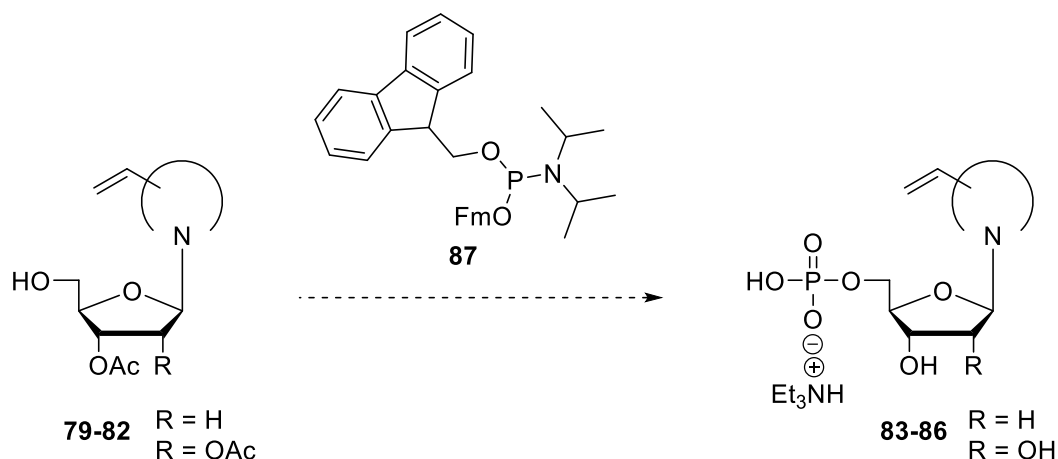
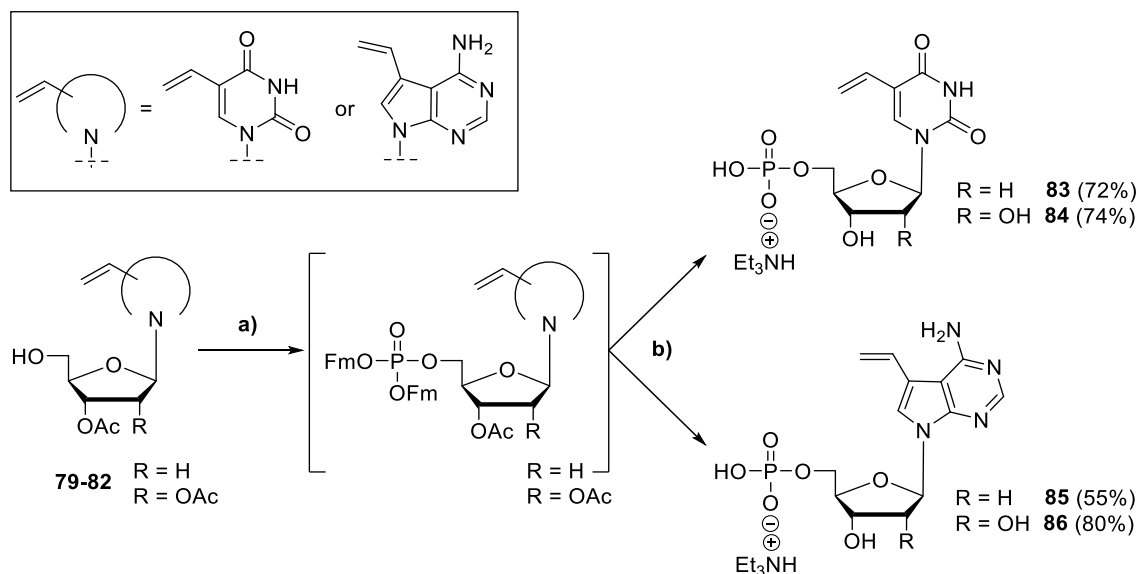


Figure 44: Preparation of the vinylated NMPs by bis(Fm)phosphoramidite **87** described by JESSEN *et al.*<sup>148</sup>

The phosphoramidite **87** was synthesized according to literature from phosphorus trichloride, diisopropylamine, and fluorenylmethanol.<sup>149</sup> The reaction of the phosphoramidite with the acetyl-protected nucleoside derivatives **79-82** is mediated by 4,5-dicyanoimidazole (DCI) in acetonitrile. After full – or stopped – conversion, the P<sup>III</sup>-intermediate is oxidized by *tert*-butyl hydroperoxide to the monophosphate triester **88**. Subsequent treatment with a mixture of H<sub>2</sub>O/CH<sub>3</sub>CN or CH<sub>3</sub>OH/Et<sub>3</sub>N (1:1:1 v/v/v) resulted in cleavage of the Fm-groups as well as the acetyl group(s). The TEAH salts of the nucleoside monophosphates were obtained with moderate to excellent yields between 55-80%.



Scheme 6: Monophosphorylation of **79-82** according to JESSEN *et al.*<sup>148</sup> **Reagents and conditions:** a) i) bis(fluorenylmethyl)phosphoramidite in  $\text{CH}_2\text{Cl}_2$ , 0.25 M DCl in  $\text{CH}_3\text{CN}$ ,  $\text{CH}_3\text{CN}$ , rt; ii) 5.5 M *t*-BuOOH in decane,  $\text{CH}_3\text{CN}$ , rt; b)  $\text{H}_2\text{O}/\text{CH}_3\text{OH}$  or  $\text{CH}_3\text{CN}/\text{Et}_3\text{N}$  (1:1: v/v/v), rt.

Briefly, the described reaction route to the vinyl-modified NMPs **83-86** is a simple solution to increase the solubility of the parent nucleosides, which improves the overall manageability during the synthetic workflow. Moreover, the selective desilylation allows the regioselective 5'-*O*-monophosphorylation with bis(Fm)phosphoramidite **87** in excellent yields under simultaneous cleavage of both the Fm- and the acetyl groups.

However, the additional protection/deprotection and subsequent purification steps are time-consuming and of low atom economy, hence, a more direct approach was implemented (Figure 45): The iodized NMPs should be synthesized first, avoiding the instability of the vinyl group under the acidic condition, and thus allowing simple and economic monophosphorylation protocols. The introduction of a phosphate group, combined with a suitable choice of counter ions, should improve the nucleotides' solubility in organic solvents as well as simplify purification methods. Successive vinylation under STILLE cross-coupling conditions should allow for simple access to the vinylated NMPs **83-86**.

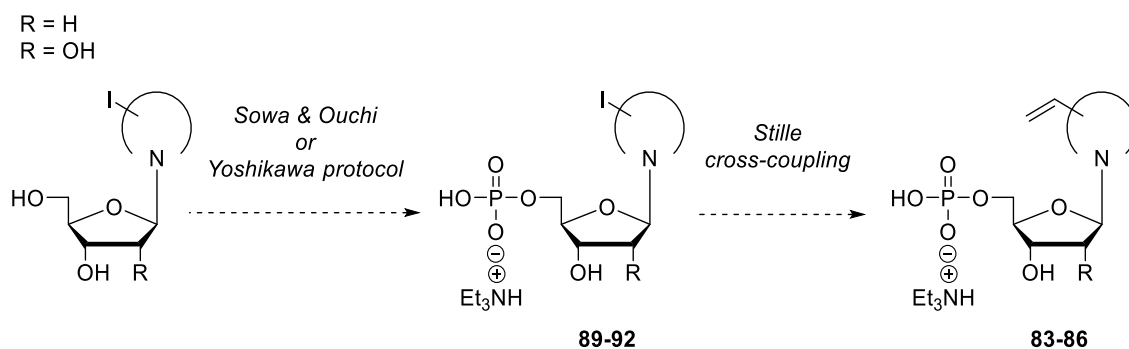
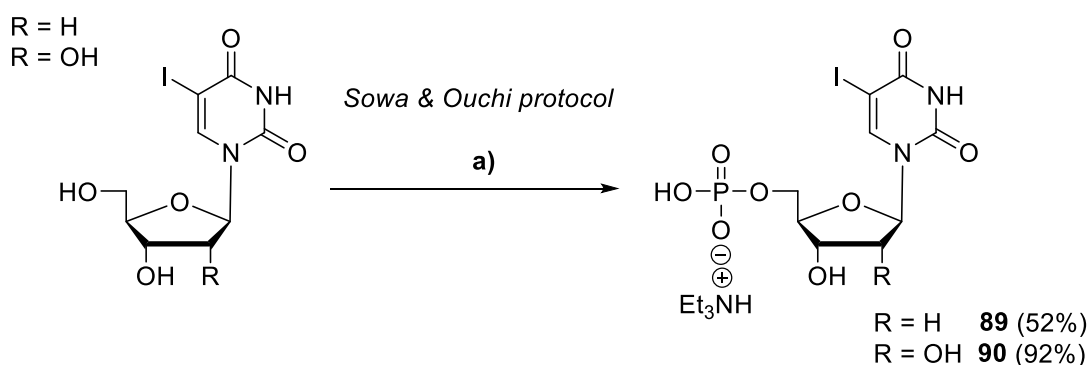


Figure 45: Novel synthetic approach with initial 5'-O-monophosphorylation.

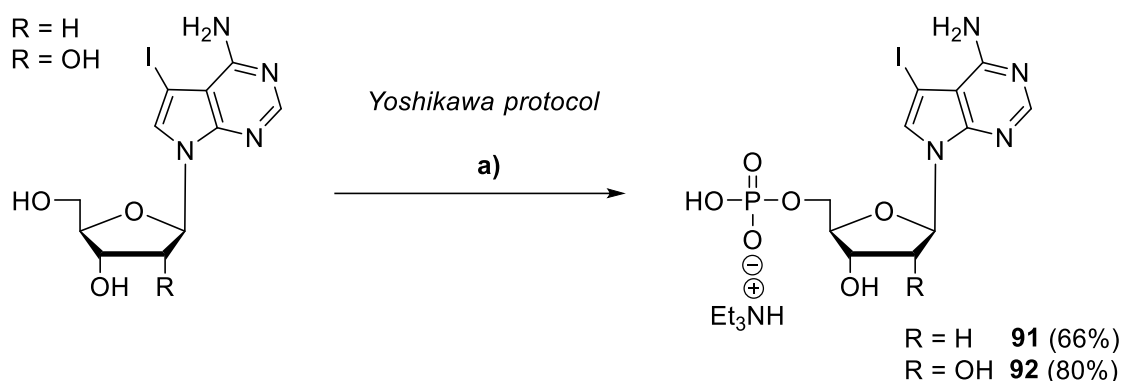
Following this approach, in a first step IdU **63** and IU **64** were phosphorylated to their respective nucleoside 5'-O-monophosphates applying the SOWA & OUCHI protocol.<sup>150</sup> Therefore, the appropriate nucleosides were converted with POCl<sub>3</sub>, pyridine, and water in acetonitrile at 0 °C. After neutralization with ammoniumbicarbonate and RP<sub>18</sub> column chromatography, the counter ions were exchanged from ammonia to TEAH by simple triethylamine addition and subsequent evaporation. 5-iodo-2'-deoxyuridine monophosphate (**89**, IdUMP) and 5-iodouridine monophosphate (**90**, IUMP) were isolated in good to excellent yields of 52% and 92%, respectively. The significantly lower yield of the 2'-deoxyribonucleoside derivative **89** is reasoned in the formation 3',5'-O-bis(phosphates). YOSHIKAWA *et al.* reported that the competitive phosphorylation of the 2' (or 3')-hydroxyl group is strongly inhibited in acidic media, which is easily achieved by traces of water. Noticeable, this effect is more significant for ribonucleoside derivatives resulting in overall better yields of monophosphorylated ribonucleosides.<sup>150,151</sup>



Scheme 7: 5'-O-monophosphorylation applying the protocol by SOWA & OUCHI.<sup>150</sup> **Reagents and conditions:** a) i) POCl<sub>3</sub> (4.4 equiv), pyridine (4.8 equiv), H<sub>2</sub>O (2.8 equiv) in CH<sub>3</sub>CN (18.9 equiv), 0 °C, 10 min; ii) nucleoside, 0 °C; iii) ice water, NH<sub>4</sub>HCO<sub>3</sub> (pH = 8); iv) ion-exchange to TEAH.

Since the iodized C<sub>7</sub>-deazapurine derivatives displayed poor solubility under SOWA & OUCHI conditions, the phosphorylation method by YOSHIKAWA *et al.* was employed. Trialkyl phosphates were found to be powerful phosphorylation accelerators and useful

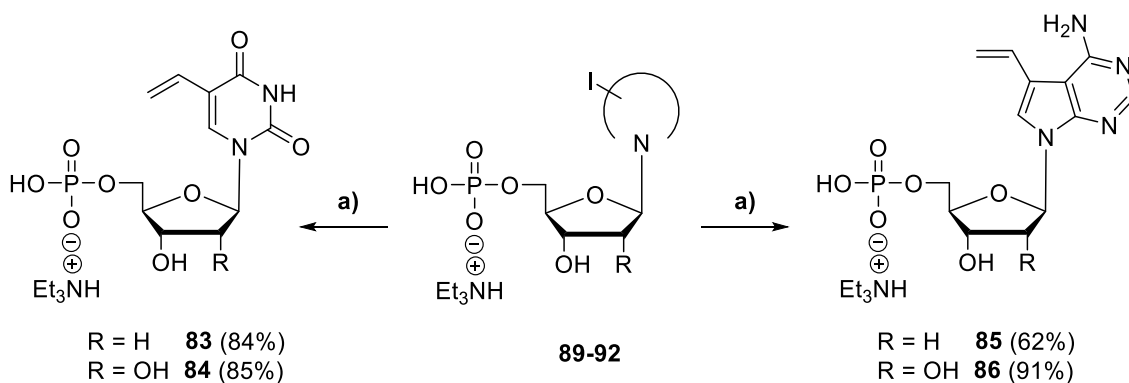
solvents for a variety of nucleosides.<sup>151</sup> Here, triethyl phosphate (TEP) was used, which is less toxic than trimethyl phosphate (TMP), and showed to be a suitable solvent for both IdA **62** and IA **53**.



Scheme 8: 5'-O-monophosphorylation applying the protocol by Yoshikawa. **Reagents and conditions:** a) i) nucleoside **62** and **53** solved in TEP, gentle heating; ii)  $POCl_3$ ;  $-10$  °C to  $-20$  °C; iii) ice water,  $NH_4HCO_3$  (pH = 8).

After the conversion of **62** and **53** with  $POCl_3$  at low temperatures ( $-10$  to  $-20$  °C) and subsequent hydrolysis and neutralization, it was crucial to establish a method that allows the removal of TEP (vapor pressure: 1 mmHg at 40 °C). The most significant proportion of TEP was removed by extraction with dichloromethane from water. The water removal under reduced pressure resulted in a residue, which might still contain smaller amounts of TEP. It was found that the addition of small volumes of dichloromethane to this residue led to the precipitation of the respective nucleotides. Subsequent purification of the collected precipitate by  $RP_{18}$  column chromatography with an acetonitrile gradient in 0.05 M triethylammonium bicarbonate (TEAB) buffer ensured the isolation of the appropriate nucleoside monophosphates **91** and **92** without any detectable traces of TEP impurity ( $^{31}P$ -NMR spectra) in good to excellent yields of 66% and 80%, respectively.

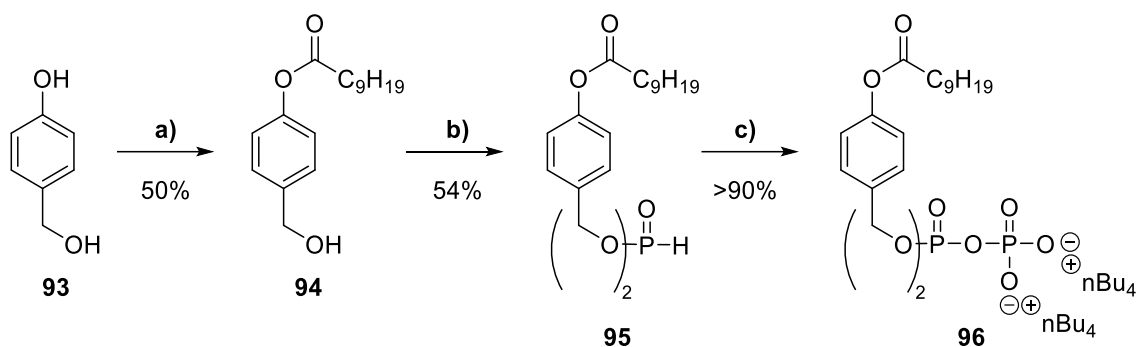
Since the NMPs showed good solubility in DMF due to the lipophilicity provided by the TEAH counter ions, the same STILLE conditions were applied as described before. All reactions showed completion within two hours at 60 °C monitored by  $^1H$ -NMR spectra. No observable by-products were detected, and after filtration to remove the catalyst and subsequent  $RP_{18}$  column chromatography, the vinylated NMPs **83-86** were obtained in good to excellent yields of 62-91%. Noteworthy, during this work, it was observed that  $Na^+$  or  $NH_4^+$  counter ions might hamper the cross-coupling reaction, whereas TEAH or  $NBu_4^+$  counter ions led to complete conversions within hours.



Scheme 9: STILLE cross-coupling reaction of **89-92**. Reagents and conditions: a)  $\text{Pd}_2(\text{dba})_3$  (5.4 mol%), tri(2-furyl) phosphine (12 mol%), tributyl(vinyl) tin, DMF, 60 °C, 2 h.

For the synthesis of the TriPPPro compounds by the *H*-phosphonate route, the bis(acyloxybenzyl)-*H*-phosphonate **95** was synthesized according to literature procedures.<sup>126,152</sup> The decanoyl moiety was chosen since it showed good properties on the model nucleoside d4T in early studies. The lipophilicity of the alkyl moiety enables cell permeability of the charged pronucleotide without complicating the synthesis and purification of the TriPPPro compounds in terms of solubility, which is often the case for longer chain lengths. First, the hydroxy benzyl alcohol **93** was acylated with decanoyl chloride and resulted in 4-(hydroxymethyl)phenyl decanoate **94** in 50% yield. Next, bis(4-decanoyloxybenzyl)-phosphonate **95** was prepared by displacing the phenyl groups of diphenyl phosphonate by 4-(hydroxymethyl)phenyl decanoate **94** in pyridine. The storage-stable bis(acyloxybenzyl)-*H*-phosphonate **95** was obtained in 54% yield after recrystallization from *i*-PrOH. The preparation of TriPPPro compounds under *H*-phosphonate route conditions involved coupling the NMP with the appropriate dimasked pyrophosphate. In 2005, MOHAMADY *et al.* subjected NMPs to trifluoroacetic anhydride (TFAA) followed by 1-methylimidazole for stepwise activation and successfully coupled these NMPs to various electron-deficient diphosphonates.<sup>153</sup> Since here, the coupling of activated NMP and dimasked pyrophosphate gave no conversion, GOLLNEST *et al.* reversed the activation approach by activating the pyrophosphate with TFAA and 1-methylimidazole before coupling with a variety of NMPs, which resulted in the corresponding TriPPPro derivatives.<sup>126</sup> Therefore, bis(acyloxybenzyl)-*H*-phosphonate **95** was oxidatively chlorinated with *N*-chlorosuccinimide (NCS) and treated with an excess of tetrabutylammonium phosphate in acetonitrile that provided pyrophosphate **96** in nearly quantitative yield. The isolation was achieved by extraction with dichloromethane from ammonium acetate, where centrifugation was crucial to

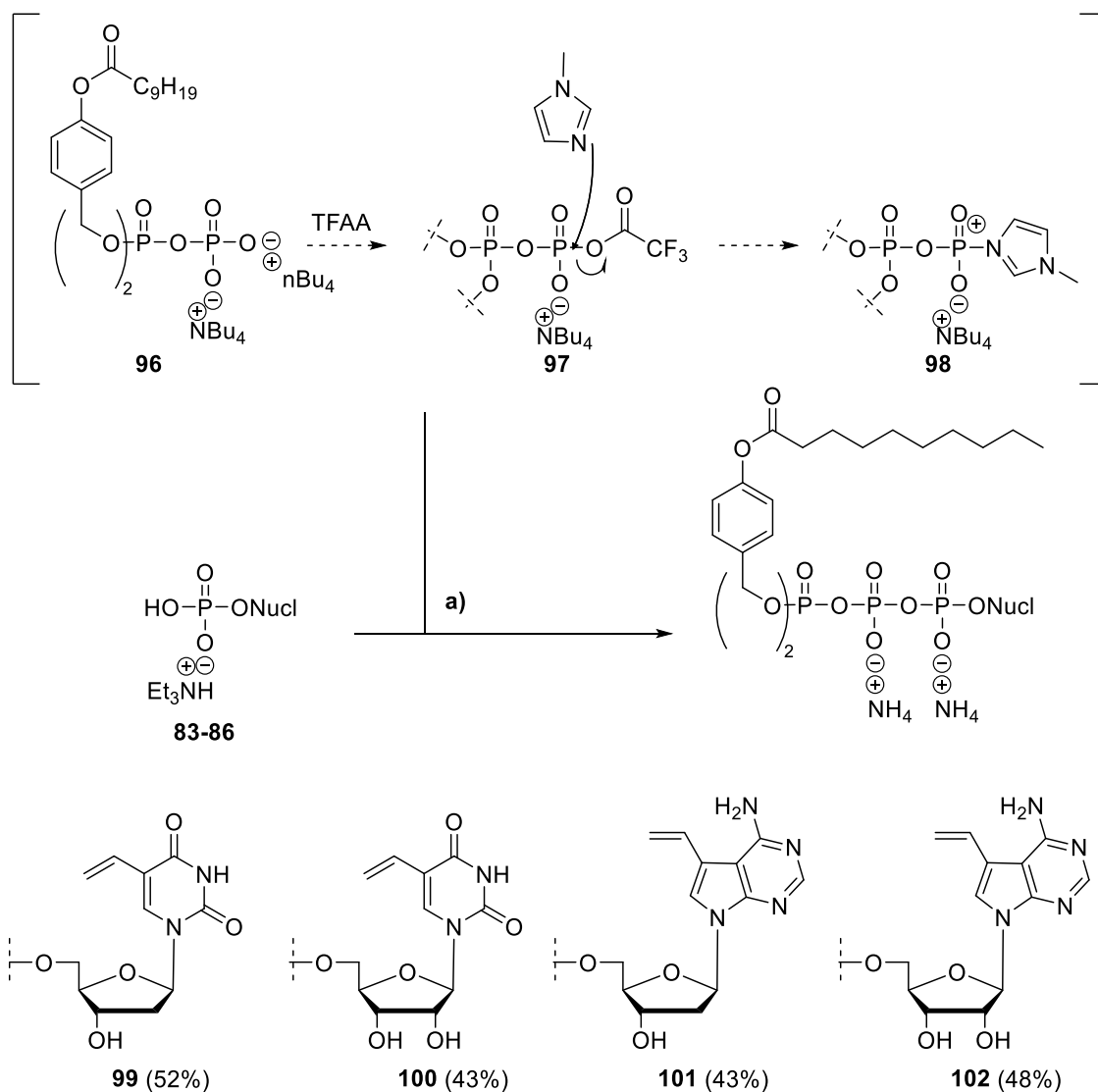
achieve phase separation. Since the purity was generally sufficient, the freshly prepared pyrophosphate was directly used as crude material.



Scheme 10: Preparation of bis(acyoxybenzyl)-*H*-phosphonate **95** and its pyrophosphate **96** according to GOLLNEST *et al.*<sup>125,126</sup> **Reagents and conditions:** a) decanoylchlorid, Et<sub>3</sub>N, THF, 0 °C to rt; b) diphenyl phosphonate, pyridine, 40 °C; c) i) NCS, CH<sub>3</sub>CN, 50-60 °C; ii) 0.4 M mono-tetrabutylammonium phosphate in CH<sub>3</sub>CN, rt.

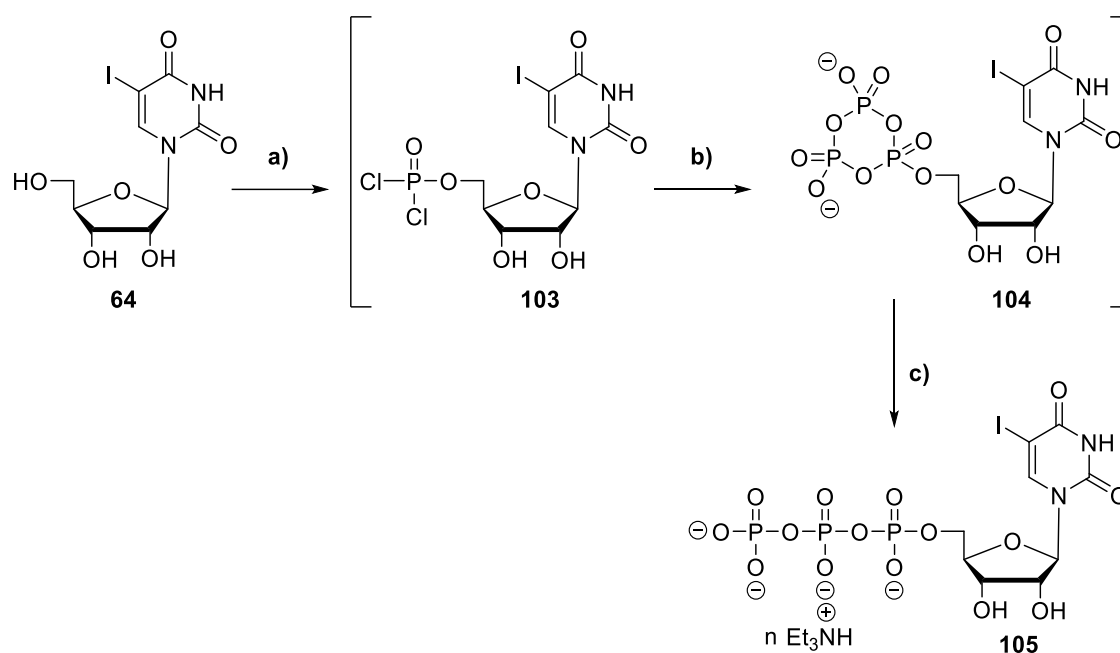
More specifically, the pyrophosphate **96** was reacted with TFAA in acetonitrile at 0 °C. The mixed anhydride **97** formed, which acted as a leaving group in the following activation step. The addition of 1-methylimidazole initiated a nucleophilic attack at the phosphorus center under the displacement of trifluoroacetic acid. The now activated pyrophosphate methylimidazolide **98** was then coupled with the appropriate NMP at room temperature. The NMPs (TEAH salt) were dissolved in DMF before addition, ensuring a homogenous reaction. Reaction progress was monitored by RP<sub>18</sub> HPLC. After the complete conversion of NMP, or no later than three hours after NMP addition, all volatiles were removed under reduced pressure. RP<sub>18</sub> column chromatography and ion exchange to ammonia obtained the desired  $\gamma$ -(C9C9AB)-TriPPP compounds **99**, **100**, **101**, and **102** in good yields between 43-52%.





Scheme 11: Synthesis of  $\gamma$ -(C9C9AB)-TriPPPPro compounds **99-102** by *H*-phosphonate route.<sup>126</sup> **Reagents and conditions:** a) i) **96**, TFAA, Et<sub>3</sub>N, CH<sub>3</sub>CN, 0 °C, 10 min; ii) 1-methylimidazole, Et<sub>3</sub>N, CH<sub>3</sub>CN, 0 °C to rt; iii) NMP (TEAH salt) in DMF, CH<sub>3</sub>CN, rt; iv) RP<sub>18</sub> column chromatography, ion-exchange to ammonia, RP<sub>18</sub> column chromatography.

To also enable studies with the non-prodrug (“naked”) vinylated nucleoside triphosphates, a simple protocol for their preparation was sought after. The natural choice was to design a similar approach compared to the vinylation of the corresponding NMPs. Therefore, the first step was the preparation of the iodized NTPs followed by the vinylation under STILLE conditions. The LUDWIG & ECKSTEIN protocol<sup>154</sup> enables the direct “one-pot, three-step” phosphorylation to the corresponding nucleoside triphosphates. In an initial step, the nucleoside reacts in a Yoshikawa-like protocol to the corresponding nucleoside dichlorophosphoridate **103** followed by conversion with bis-(tri-*n*-butylammonium) pyrophosphate salt and hydrolysis of the resulting cyclic intermediate **104** to the final nucleoside triphosphate **105**. A disadvantage of the LUDWIG & ECKSTEIN protocol is the possible formation of various phosphorylated by-products.<sup>155</sup> Especially the first monophosphorylation step to the dichlorophosphoridate **103** is crucial for a successful triphosphate synthesis. Here, the choice of base influences the regioselectivity and reaction rate and varies from nucleoside to nucleoside.<sup>156</sup>

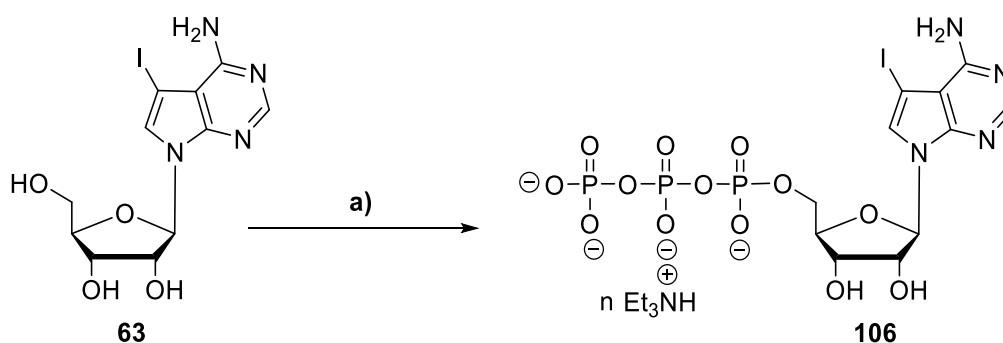


Scheme 12: Synthesis of 5-iodouridine triphosphate **105** under LUDWIG & ECKSTEIN conditions. **Reagents and conditions:** **a)**  $\text{POCl}_3$ , proton sponge, TMP,  $0^\circ\text{C}$ , 48 h; **b)**  $(\text{nBu}_3)_2\text{P}_2\text{O}_7$  in  $\text{CH}_3\text{CN}$ ,  $\text{nBu}_3$ , TMP,  $0^\circ\text{C}$ , 10 min; **c)** i) ice water,  $0^\circ\text{C}$ ; ii) extraction; iii) DEAD Sephadex A25 (0-1 M TEAB); iv)  $\text{RP}_{18}$  column chromatography.

For both ribonucleoside derivatives IU **64** and IA **53** proton sponge (1,8-bis(*N,N*-dimethylamino)naphthalin) was selected as a base. Because ribonucleosides show better regioselectivity towards 5'-monophosphorylation than their 2'-deoxyribonucleoside derivatives, two equivalents of  $\text{POCl}_3$  were employed. The reaction was carried out at  $0^\circ\text{C}$ . IU **64** showed slow reaction rates and only half

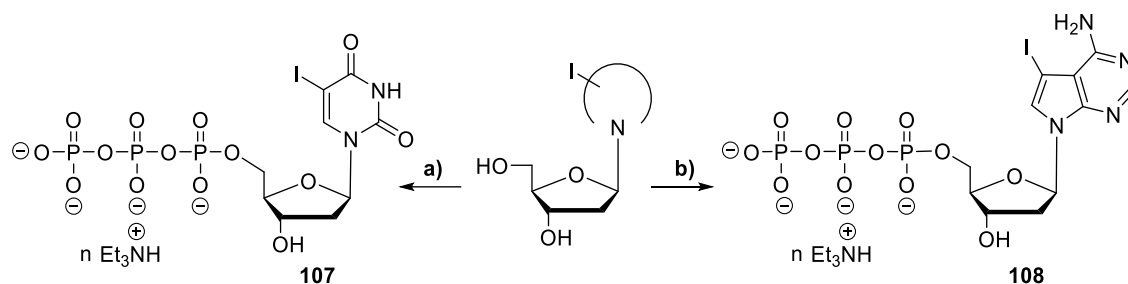
conversion to the respective intermediate after two days (RP<sub>18</sub> HPLC monitoring) with minimal formation of by-products. Since the yield was not the primary focus, the phosphorodichloridate **103** was converted with bis-(tri-*n*-butylammonium) pyrophosphate salt in acetonitrile followed by hydrolysis with ice water. Removal of TMP by dichloromethane extraction and subsequent DEAD Sephadex A25 ion strength chromatography resulted in crude 5-iodouridine triphosphate (**105**, IUTP). However, the <sup>31</sup>P-NMR spectra revealed trimetaphosphate salt impurity, which was successfully removed after RP<sub>18</sub> column chromatography. The triphosphate **105** was obtained in an expectedly low yield of 29%, caused by the incomplete monophosphorylation in the first step.

IA **53** showed approx. 50% conversion after two hours with good regioselectivity. However, after DEAD Sephadex A25 ion strength chromatography trimetaphosphate salt impurity was detected, which again was separated from the nucleotide by RP<sub>18</sub> column chromatography. 7-Deaza-7-iodoadenine triphosphate (**106**, IATP) was obtained in 27% yield.



Scheme 13: Synthesis of 7-iodo-7-deazaadenine triphosphate **106** under LUDWIG & ECKSTEIN conditions. **Reagents and conditions:** a) i) POCl<sub>3</sub>, proton sponge, TMP, 0 °C, 2 h; ii) (nBu<sub>3</sub>)<sub>2</sub>P<sub>2</sub>O<sub>7</sub> in CH<sub>3</sub>CN, nBu<sub>3</sub>, TMP, 0 °C, 0 min; iii) ice water, 0 °C; iv) extraction; v) DEAD Sephadex A25 (0-1 M TEAHHB); vi) RP<sub>18</sub> column chromatography.

For the 2'-deoxyribonucleoside derivatives, the reaction temperature of the monophosphorylation step was lowered to -20 °C to improve regioselectivity. Furthermore, to reduce formation of trimetaphosphate the reaction temperature in the second step was reduced to -15 °C, and the reaction time was prolonged to two hours, as reported by GILLERMANN & FISCHER in their improved procedure.<sup>155</sup> The reaction conditions applied are summarized in Scheme 14.



Scheme 14: Synthesis of the 2'-deoxynucleoside triphosphates **107** and **108** by LUDWIG & ECKSTEIN conditions. **Reagents and conditions:** a) i)  $\text{POCl}_3$ ,  $n\text{Bu}_3$ , TMP,  $-20^\circ\text{C}$ , 48 h; ii)  $(n\text{Bu}_3)_2\text{P}_2\text{O}_7$  in  $\text{CH}_3\text{CN}$ ,  $n\text{Bu}_3$ , TMP,  $-15^\circ\text{C}$ , 2 h; iii) ice water,  $0^\circ\text{C}$ ; iv) extraction; v) DEAD Sephadex A25 (0-1 M TEAB); vi)  $\text{RP}_{18}$  column chromatography; b) i)  $\text{POCl}_3$ , TMP,  $-20^\circ\text{C}$ , 48 h; ii)  $(n\text{Bu}_3)_2\text{P}_2\text{O}_7$  in  $\text{CH}_3\text{CN}$ ,  $n\text{Bu}_3$ , TMP,  $-15^\circ\text{C}$ , 2 h; iii) ice water,  $0^\circ\text{C}$ ; iv) extraction; v) DEAD Sephadex A25 (0-1 M TEAB).

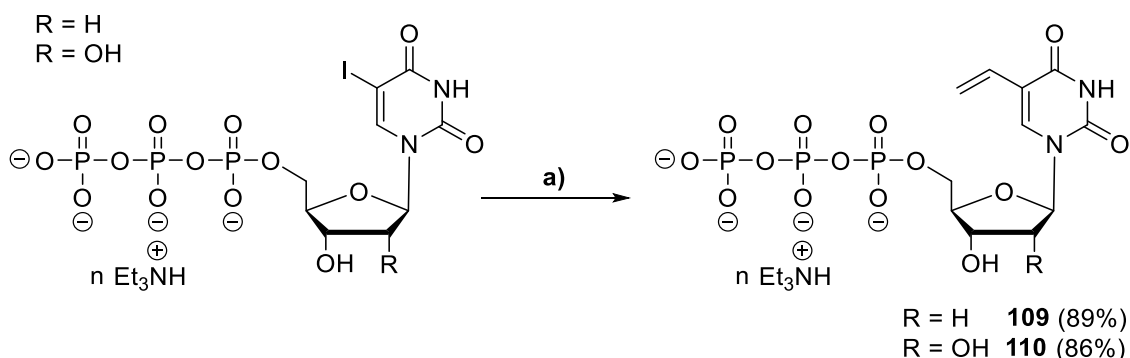
IdU **63** was converted with  $\text{POCl}_3$  (1.2 equiv.) in trimethyl phosphate (TMP) at  $-20^\circ\text{C}$  in the presence of tri-*n*-butylamine as a base. Due to low reaction rates, the mixture was stirred for two days. Around two-thirds of the nucleoside reacted with satisfying regioselectivity, as analyzed by HPLC. Thus, bis-(tri-*n*-butylammonium) pyrophosphate salt was added, and the reaction mixture was stirred for two hours at  $-15^\circ\text{C}$  as described above. After DEAD Sephadex A25 ion strength chromatography, no trimetaphosphate was detectable but pyrophosphate salt impurity. Therefore, further  $\text{RP}_{18}$  column chromatography purifications had to be performed to result pure 5-iodo-2'-deoxyuridine triphosphate (**107**, IdUTP) in 31% yield.

IdA **62** was treated with  $\text{POCl}_3$  (1.2 equiv.) in absence of a base. Surprisingly, after two days at  $-20^\circ\text{C}$ , almost complete nucleoside conversion to the triphosphate was observed under minimal formation of by-products. DEAD Sephadex A25 ion strength chromatography resulted in the desired 7-deaza-7-iodo-2'-deoxyadenine triphosphate (**108**, IdATP) in an excellent yield of 87%.

In short, the LUDWIG & ECKSTEIN procedure allows the simple preparation of nucleoside triphosphates without requirements of any protective strategy regarding the nucleoside. By improving the first phosphorylation step with respect to conversion and regioselectivity, good to excellent yields are achievable. Especially, use of the appropriate base can significantly enhance regioselectivity and reaction rates<sup>156</sup>, providing room for improvements.

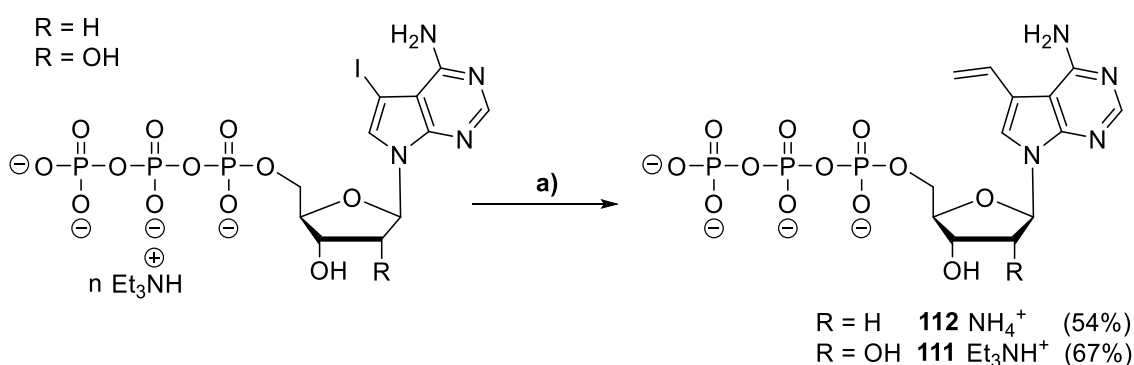
Next, the STILLE cross-coupling reaction was employed to introduce the 5-vinyl function to the  $\text{C}_5$ -pyrimidine NTPs with slightly adjusted conditions compared to the vinylation of the corresponding NMP analogs. The reaction temperature was lowered from  $60^\circ\text{C}$  to  $40^\circ\text{C}$  to ensure the stability of the triphosphates. Hence, the reaction time was

prolonged to five hours, after which complete conversion was achieved ( $^1\text{H-NMR}$  spectroscopic monitoring). Simple filtration and  $\text{RP}_{18}$  column chromatography resulted in the triphosphates **109** and **110** in excellent yields of 89% and 86%, respectively.



Scheme 15: STILLE cross-coupling reaction of NTPs **109** and **110**. Reagents and conditions: a)  $\text{Pd}_2(\text{dba})_3$  (10 mol%), tri(2-furyl) phosphine (24 mol%), tributyl(vinyl) tin, DMF, 40 °C, 5 h.

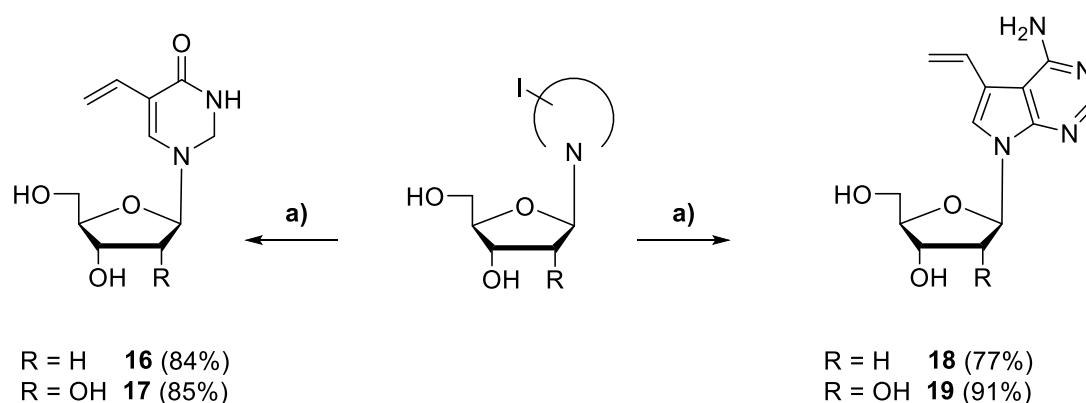
For the  $\text{C}_7$ -deazapurine derivatives, 10 vol% water was added to DMF to ensure the triphosphates' solubility. The increase of the solvent's hydrophilicity resulted in an inhomogeneous reaction mixture, and therefore, the cross-coupling was stirred overnight to ensure complete conversion. Filtration and  $\text{RP}_{18}$  column chromatography resulted in triphosphate VATP **111** in 67% yield. For the VdATP **112** a Dowex ion exchange to ammonia was employed to improve its solubility in water, which resulted in **112** as its ammonia salt in 54% yield. Lower yields for the  $\text{C}_7$ -deazapurine derivatives can be attributed to their low solubility in organic solvents and, in the case of **112**, to further loss during ion-exchange chromatography.



Scheme 16: STILLE cross-coupling reaction of NTPs **111** and **112**. Reagents and conditions: a)  $\text{Pd}_2(\text{dba})_3$  (10 mol%), tri(2-furyl) phosphine (24 mol%), tributyl(vinyl) tin, DMF/ $\text{H}_2\text{O}$  9:1 v/v, 40 °C, 16 h, ion-exchange to ammonia (for **112**).

For the direct synthesis of the vinylated nucleosides **16-19**, a workup procedure needed to be established that addressed the low solubility of these nucleosides in organic solvents. The STILLE cross-coupling reaction was performed in DMF under the standard

conditions employed in this work, and complete conversion was monitored by  $^1\text{H-NMR}$  spectroscopic measurement. After complete conversion of starting materials, the respective reaction mixtures were concentrated under reduced pressure, and the resulting residues were dissolved in dichloromethane/methanol-mixtures (4:1 v/v). The crude products were then adsorbed on Celite<sup>®</sup> and packed into small flash columns. The dry-loaded columns were subsequently stacked onto RP<sub>18</sub> flash columns before performing automated RP<sub>18</sub> column chromatography with an acetonitrile gradient in water. The vinylated nucleosides **16-19** were obtained in overall good yields between 78-83%.



Scheme 17: STILLE cross-coupling reaction to the vinyl functionalized nucleosides **16-19**. **Reagents and conditions: a)** Pd<sub>2</sub>(dba)<sub>3</sub> (5.4 mol%), tri(2-furyl) phosphine (12 mol%), tributyl(vinyl) tin, DMF, 60 °C, 2 h.

Briefly, a reliable synthetic approach to the described vinylated nucleosides, their triphosphates and TriPPPPro nucleotides was established. Here, the catalyst system of Pd<sub>2</sub>(dba)<sub>3</sub> and TFP proved to be the system of choice and provided full conversions of iodized starting materials under various conditions. By first phosphorylating the iodized nucleosides, the solubility of their corresponding nucleotides in organic solvents increases due to the lipophilicity of the TEAHH counter ions. Subsequent vinylation readily provides the starting material for the preparation of the desired TriPPPPro compounds. In the next chapter, the synthesis of vinylated, next generation  $\gamma$ -alkylated TriPPPPro compounds and their respective cellular metabolites will be discussed.

## 4.2 $\gamma$ -alkylated triphosphates and their prodrugs

One aim of antiviral therapy is to target the viral polymerase without disturbing cellular transcription. Nucleoside drugs that specifically inhibit viral transcription will have reduced cytotoxic effects and, therefore, minimal side effects on human health. Transferred to the visualization of viral transcription in host cells, it is the overall aim not only to target viral enzymes specifically and minimize interference with cellular processes but also to ensure a minimal impact on viral replication itself. In short, finding a concept that allows the discrimination between host cell and viral polymerases, while not perturbing cellular/viral processes, would have great value.

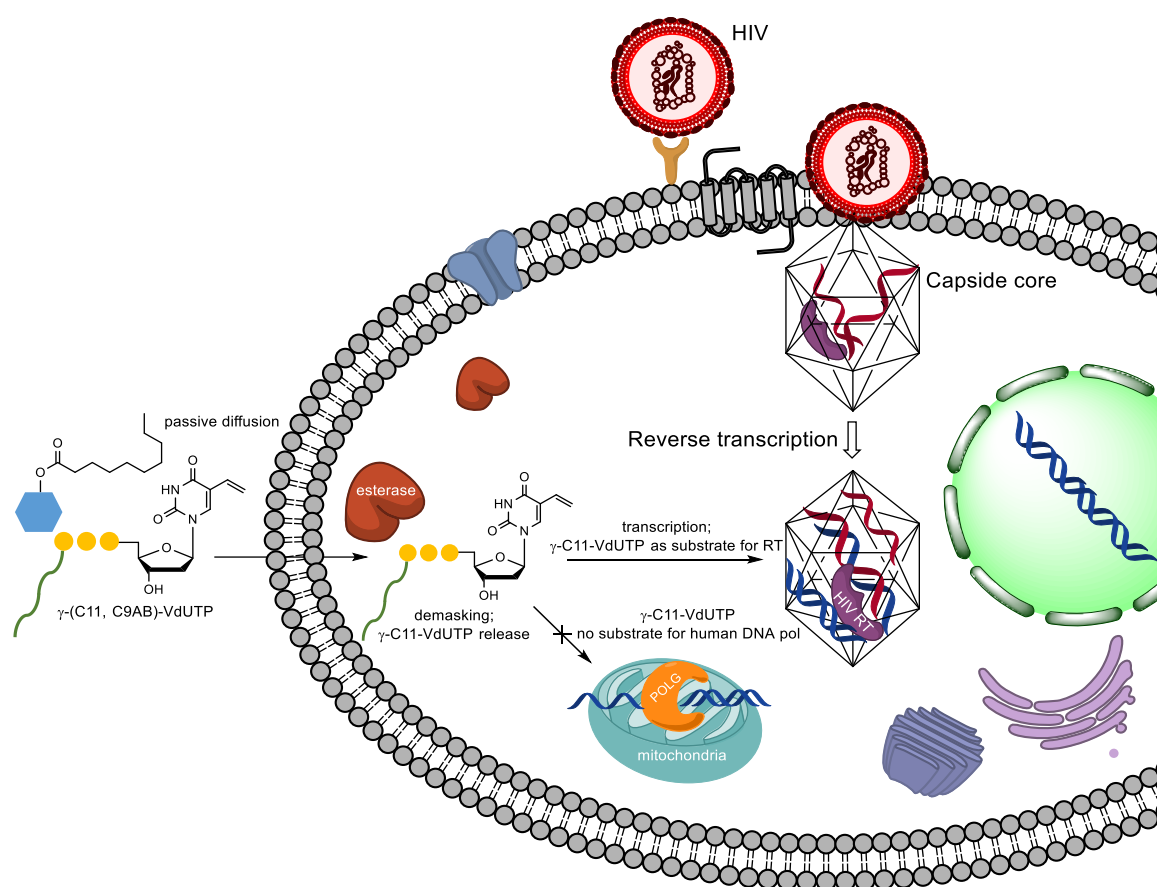


Figure 46: Illustration of the cellular uptake and intracellular release of a  $\gamma$ -alkyl modified vinyl-NTP (e.g.,  $\gamma$ -C11-VdUTP) for specific labeling of newly synthesized viral HSV-1 genome by discriminating between the human DNA polymerase (DNA pol) and the reverse transcriptase (RT).

As described in Chapter 2.8, discrimination between HIV-RT and human DNA polymerases becomes possible by capping the terminal phosphate groups of NTPs. The concept for specific viral DNA labeling is illustrated in Figure 46 for an HIV-1 infected host cell. Potentially, the concept is also applicable to other viral polymerases, e.g., herpes polymerases.<sup>127</sup> The introduction of a  $\gamma$ -alkyl chain to the terminal phosphate group to various NTPs is easily achieved by applying the above-described

*H*-phosphonate route.

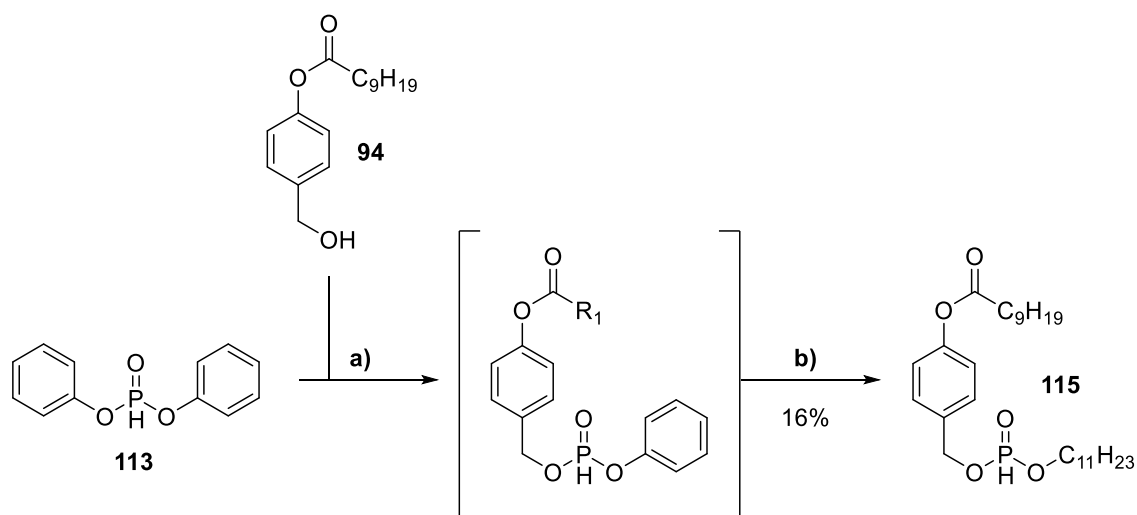
Additionally, combining the  $\gamma$ -alkyl cap with an (AB)-mask would increase the lipophilicity of the pronucleotide, thus allowing cell permeation of the nucleotide reporter and intracellular release of the  $\gamma$ -alkylated nucleoside triphosphate after enzymatic cleavage of the lipophilic mask.

Moreover, the  $\gamma$ -alkyl chain improves the overall chemical and enzymatic stability of the NTP in the cellular environment. The improved stability potentially leads to a significant increase in bioavailability of the nucleotide reporter in the host cell and thus positively influences labeling efficiency.

The objective was to synthesize thus designed DNA reporter nucleotides in order to study if this concept is applicable for visualizing viral transcription inside of their host cell. Therefore, the  $\gamma$ -alkyl modified triphosphates of VdU **16** and VdA **18** were synthesized with a chain length of  $\gamma$ -C11 as well as their asymmetrical  $\gamma$ -(C11,C9AB)-TriPPP compounds. The  $\gamma$ -C11 alkyl chain was selected as a starting point with the general objective to achieve a good trade-off between discrimination of human versus viral polymerases and substrate specificity toward viral polymerases to ensure low cytotoxicity, low background and efficient labeling.

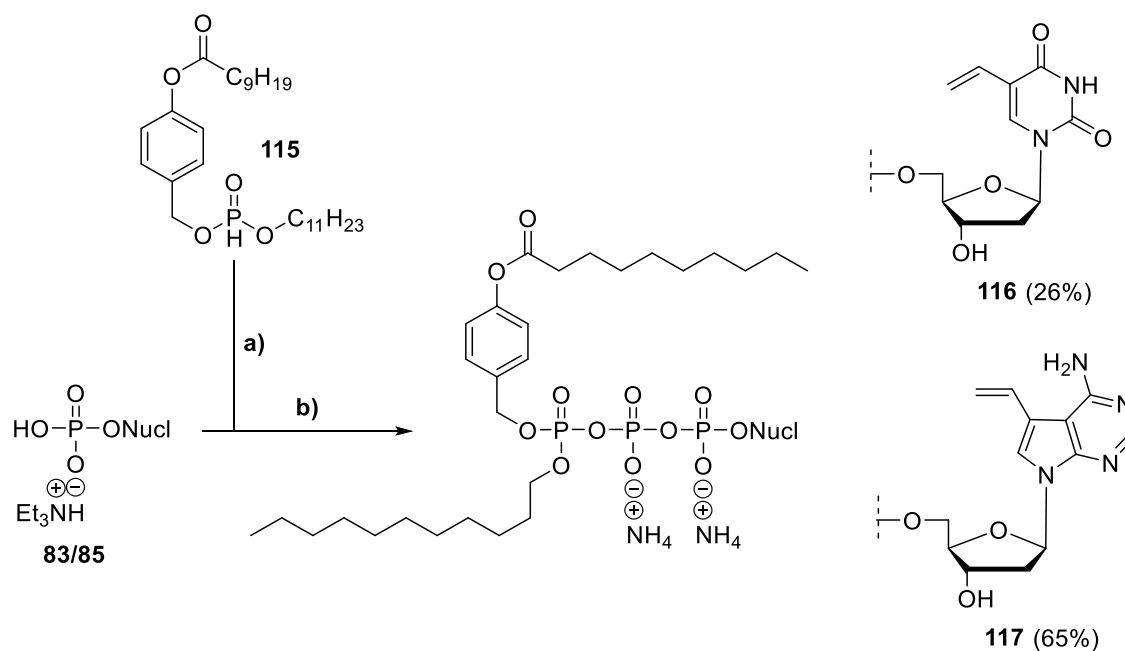
For the latter, the appropriate (C11,C9AB)-*H*-phosphonate **115** had to be prepared. First, one phenyl group of the diphenyl phosphonate **113** (1.3 equiv) was displaced by 4-(hydroxymethyl)phenyl decanoate **94** (1 equiv) in pyridine at -10 °C to provide the intermediate **114**. The addition of 1-undecanol at room temperature resulted in the asymmetric (C11,C9AB)-*H*-phosphonate **115** after several purifications on silica gel and final recrystallization from *i*-PrOH in a low yield of 16%. In future, the diphenyl phosphonate **113** should be examined for purity by <sup>31</sup>P-NMR spectroscopy before usage, and recrystallization from *i*-PrOH should be employed as the single purification method.





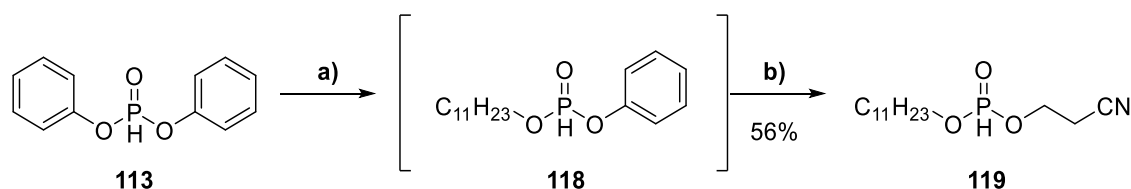
Scheme 18: Preparation of (C11,C9AB)-H-phosphonate **115**. Reagents and conditions: **a)** **94**, pyridine, -10 °C; **b)** 1-undecanol, pyridine, rt.

The preparation of both the  $\gamma$ -(C11,C9AB)-TriPPPPro compounds of **16** and **18** were realized by standard procedures described in Chapter 4.1 and in accordance to ZHAO *et al.*, who initially reported on the concept.<sup>127</sup> First, the (C11,C9AB)-H-phosphonate **115** was transformed to its pyrophosphate by NCS activation and subsequent coupling with tetrabutylammonium phosphate salt in acetonitrile. After the stepwise activation of the pyrophosphate salt mediated by TFAA and 1-methylimidazole, the appropriate NMP was added for coupling. Purification on RP<sub>18</sub> silica gel and ion exchange to ammonium yielded **116** and **117** with a conversion rate of 26% and 65%, respectively.



Scheme 19: Synthesis of  $\gamma$ -(C11,C9AB)-TriPPPro compounds **116** and **117** by *H*-phosphonate route.<sup>127</sup>  
**Reagents and conditions:** a) i) NCS, CH<sub>3</sub>CN, 50-60 °C; ii) 0.4 M mono-tetrabutylammonium phosphate in CH<sub>3</sub>CN, rt; b) i) TFAA, Et<sub>3</sub>N, CH<sub>3</sub>CN, 0 °C, 10 min; ii) 1-methylimidazole, Et<sub>3</sub>N, CH<sub>3</sub>CN, 0 °C to rt; iii) NMP (TEAHH salt) in DMF, CH<sub>3</sub>CN, rt; iv) RP<sub>18</sub> column chromatography, ion-exchange to ammonia, RP<sub>18</sub> column chromatography.

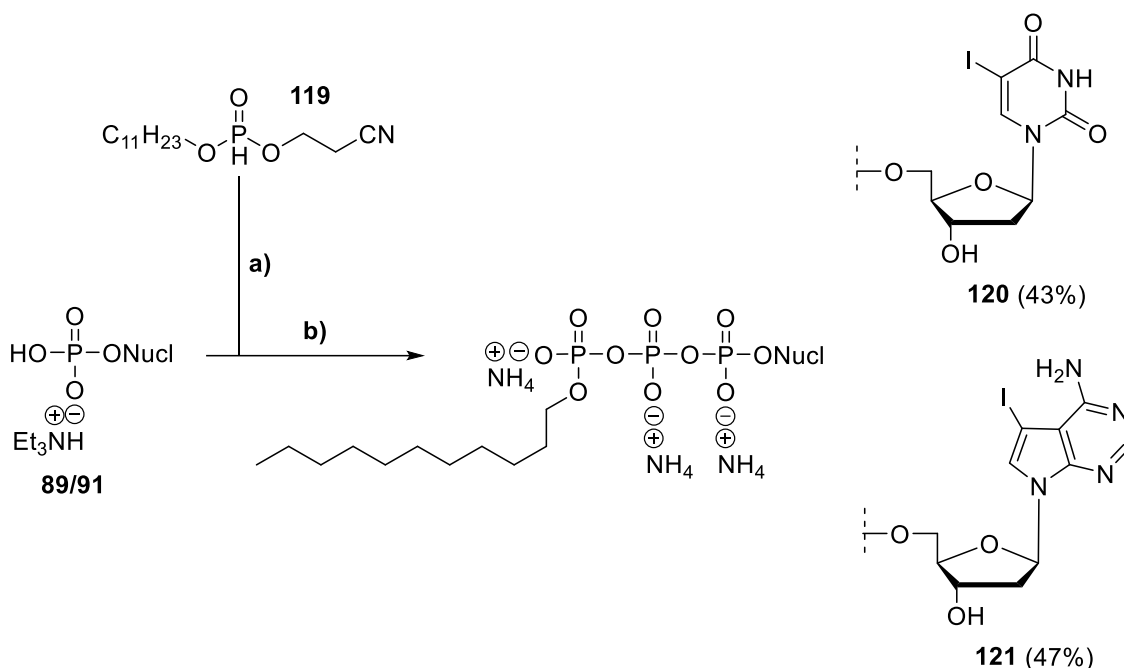
In order to synthesize  $\gamma$ -alkyl-NTPs, the  $\beta$ -cyanoethyl group was used as a protective group of the terminal phosphate moiety, which can be removed *in situ* after NMP coupling under basic conditions by  $\beta$ -elimination to acryl nitrile and the free phosphate.<sup>127</sup> Accordingly, the  $\beta$ -cyanoethyl protected  $\gamma$ -(alkyl)-*H*-phosphonate needed to be synthesized. First, diphenyl phosphonate **113** was reacted with 1-undecanol under displacement of phenol, providing intermediate **118**, followed by the addition of  $\beta$ -cyanoethanol, which resulted in  $\gamma$ -(alkyl)-*H*-phosphonate **119** in 56% yield after purification on silica gel.



Scheme 20: Preparation of (C11,  $\beta$ -cyanoethyl)-*H*-phosphonate **119**. **Reagents and conditions:** a) 1-undecanol, pyridine, 0 °C to rt, o/n; b)  $\beta$ -cyanoethanol, pyridine, rt, o/n.

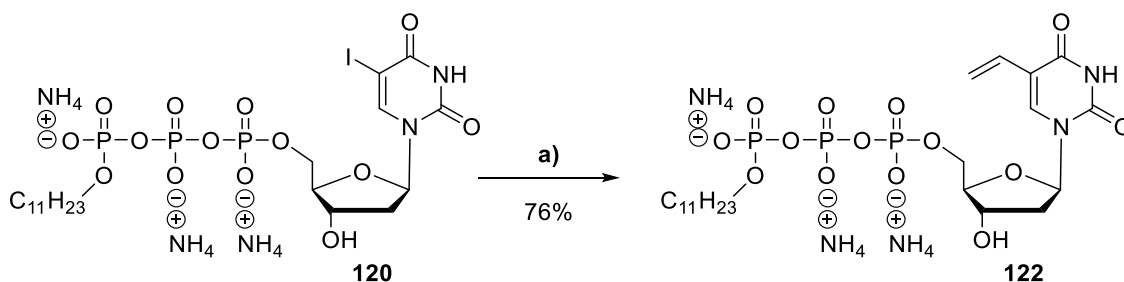
In general, the iodized nucleosides were more storage stable at -20 °C compared to their vinylated derivatives. Therefore, it seemed appropriate to prepare the iodo-substituted  $\gamma$ -C11-NTPs and employ the less elaborate STILLE cross-coupling to obtain their vinylated derivatives in the following step. After coupling the activated pyrophosphate with the

appropriate NMP, the  $\gamma$ -protected nucleoside triphosphate was formed. The *in situ* overnight treatment with  $n\text{Bu}_4\text{N}^+\text{OH}^-$  (10% in water) for  $\beta$ -cyanoethyl deprotection provided the corresponding  $\gamma$ -C11-NTPs **120** and **121** after purification on  $\text{RP}_{18}$  silica gel and ion-exchange to ammonium in good yields of 43% and 47%, respectively.

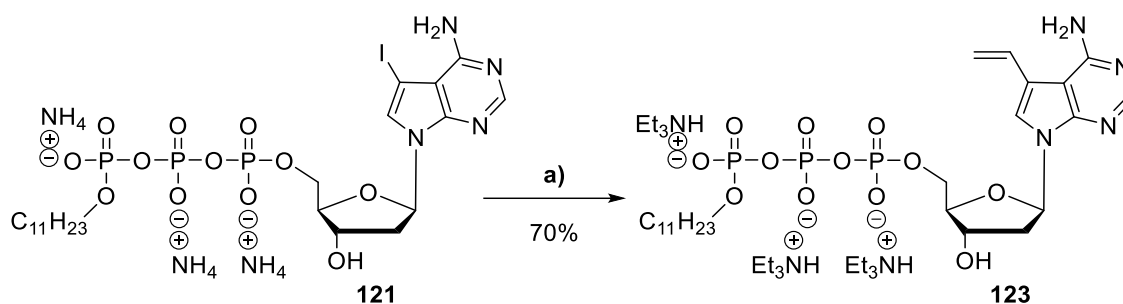


Scheme 21: Synthesis of  $\gamma$ -(C11)-NTPs **120** and **121** by *H*-phosphonate route.<sup>127</sup> **Reagents and conditions:** **a)** i) NCS,  $\text{CH}_3\text{CN}$ , 50-60 °C; ii) 0.4 M mono-tetrabutylammonium phosphate in  $\text{CH}_3\text{CN}$ , rt; **b)** i) TFAA,  $\text{Et}_3\text{N}$ ,  $\text{CH}_3\text{CN}$ , 0 °C, 10 min; ii) 1-methylimidazole,  $\text{Et}_3\text{N}$ ,  $\text{CH}_3\text{CN}$ , 0 °C to rt; iii) NMP (TEAHH salt) in DMF,  $\text{CH}_3\text{CN}$ , rt; iv) evaporation; v)  $n\text{Bu}_4\text{N}^+\text{OH}^-$ ; vi)  $\text{RP}_{18}$  column chromatography, ion-exchange to ammonia,  $\text{RP}_{18}$  column chromatography.

For the vinylation, the appropriate  $\gamma$ -C11-NTPs ( $\text{NH}_4^+$  salt) were dissolved in DMF/water (9:1 v/v). The same STILLE cross-coupling reaction conditions as for the uncapped NTPs were employed (Chapter 4.1). The compounds  $\gamma$ -C11-VdUTP **122** ( $\text{NH}_4^+$  salt) and  $\gamma$ -C11-VdATP **123** (TEAH salt) were obtained after filtration and purification on  $\text{RP}_{18}$  silica gel in good yields of 76% and 70%, respectively.



Scheme 22: STILLE cross-coupling reaction of NTPs **120**. **Reagents and conditions:** **a)**  $\text{Pd}_2(\text{dba})_3$  (5.4 mol%), tri(2-furyl) phosphine (12 mol%), tributyl(vinyl) tin, DMF/ $\text{H}_2\text{O}$  9:1 v/v, 40 °C, 16 h.

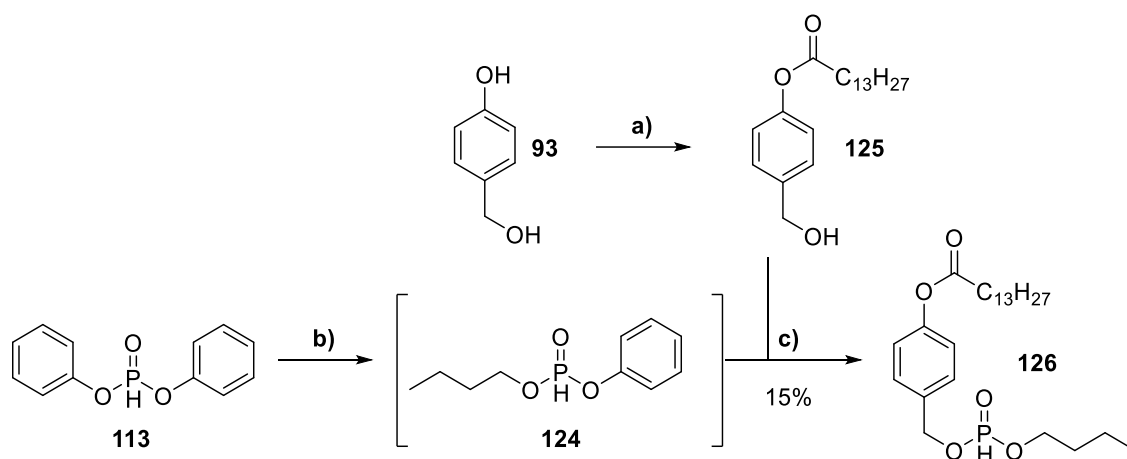


Scheme 23: STILLE cross-coupling reaction of NTPs **121**. **Reagents and conditions:** a)  $\text{Pd}_2(\text{dba})_3$  (5.4 mol%), tri(2-furyl) phosphine (12 mol%), tributyl(vinyl) tin, DMF/ $\text{H}_2\text{O}$  9:1 v/v, 40 °C, 16 h.

As described in Chapter 2.2, HIV utilizes the human RNA polymerase II to regulate its genome expression, initiated by transcription of viral genomic RNA. Naturally, labeling of newly produced viral RNA requires the bioavailability of a ribonucleotide probe. If a higher bioavailability results in more efficient labeling of viral RNA, the intracellular delivery of a stable capped ribonucleoside triphosphate probe could improve labeling efficiency. The idea was to introduce a short  $\gamma$ -C4 alkyl chain to the NTP reporter, which could improve its chemical and enzyme stability in cellular media without discriminating human RNA polymerases, to study this early steps of HIV replication.

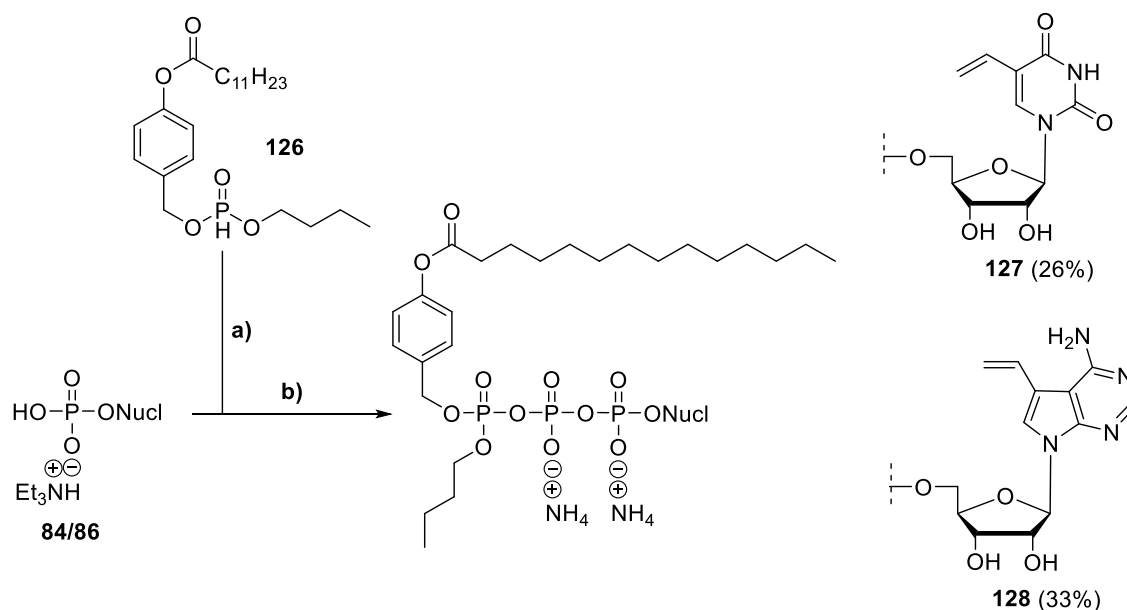
Moreover, independent of viral genome labeling, these reporters might be of benefit to the general labeling of cellular RNA in future applications. The rational design was to balance out the loss of lipophilicity caused by the shorter  $\gamma$ -C4 alkyl chain with a more extended C13 alkyl moiety in the (AB)-mask.

Accordingly, the (C4,C13AB)-*H*-phosphonate **126** was prepared by displacing a phenyl group of diphenyl phosphonate **113** with 1-butanol at 0 °C in pyridine to provide the intermediate **124**. The displacement of the second phenyl group by 4-(hydroxymethyl)phenyl tetradecanoate **125** resulted in the (C4,C13AB)-*H*-phosphonate **126** after purification on silica gel in a low yield of 15%. Noteworthy, adding 1-butanol in the second displacement step led to partial substitution of the prior introduced (AB)-mask, which resulted in an increased formation of (C4,C4)-*H*-phosphonate by-product.



Scheme 24: Preparation of (C4,C13AB)-*H*-phosphonate **126**. **Reagents and conditions:** a) tetradecanoylchloride, Et<sub>3</sub>N, THF, 0 °C to rt; b) 1-butanol, pyridine, 0 °C; c) **125**, pyridine, rt.

Following standard *H*-phosphonate route procedures,  $\gamma$ -(C4,C13AB)-NTPs of VU **127** and VA **128** were obtained in moderate yields of 26% and 33%, respectively.



Scheme 25: Synthesis of  $\gamma$ -(C4,C13AB)-TriPPPPro compounds **127** and **128** by *H*-phosphonate route.<sup>127</sup> **Reagents and conditions:** a) i) NCS, CH<sub>3</sub>CN, 50-60 °C; ii) 0.4 M mono-tetrabutylammonium phosphate in CH<sub>3</sub>CN, rt; b) i) TFAA, Et<sub>3</sub>N, CH<sub>3</sub>CN, 0 °C, 10 min; ii) 1-methylimidazole, Et<sub>3</sub>N, CH<sub>3</sub>CN, 0 °C to rt; iii) NMP (TEAHH salt) DMF, CH<sub>3</sub>CN, rt; iv) RP<sub>18</sub> column chromatography, ion-exchange to ammonia, RP<sub>18</sub> column chromatography.

In short,  $\gamma$ -capped TriPPPPro compounds were successfully synthesized. Moreover, the compounds  $\gamma$ -C11-VdUTP **129** and  $\gamma$ -C11-VdATP **130** were also prepared since they are the metabolites of interest. The description of the synthetic procedures regarding vinylated compounds is finalized at this point. The following chapters will focus on more sophisticated and “faster” bioorthogonal functionalities and aims for the overall goal of live-cell imaging.

### 4.3 Design and synthesis of 1MCP-pronucleotide reporters – finding the motif

The smallest possible dienophile used for metabolic labeling is the vinyl group.<sup>62</sup> However, reaction rates of this group in **DA<sub>INV</sub>**-reactions with tetrazines are relatively low and thus impede no-wash conditions required for live-cell imaging (Chapter 2.6). The 1-methylcyclopropene (1MCP) function is the best compromise between small size and elaborated **DA<sub>INV</sub>** rate constants.<sup>69,70</sup> Furthermore, 1MCPs show excellent stability in aqueous solution and in presence of thiols (e.g., *L*-cysteine, glutathione).<sup>70</sup> However, the linker of 1MCP has a significant impact on the stability of the strained olefin. The most frequently used motif is the 2-methylcyclopropene carbamate (e.g., the linker of **135**), which can be formed by conjugation of 1MCP alcohol to **132** primary amines by carbamate formation. The TMS-protected 1MCP alcohol **132** can be obtained by ester reduction of precursor **131**. Protected 1MCP **131** can be in turn synthesized by rhodium-catalyzed cyclopropanation from commercially available ethyl diazoacetate and trimethylsilylacetylene.<sup>157</sup> Although the carbamate linkage provides excellent stability in biological media, it is prone to degradation (polymerization by ene-reaction) during long-time storage, reaction mixture concentration, as well as multiple freeze-thaw cycles.<sup>72</sup> This drawback significantly impacts the synthetic workflow and affects the obtained yields and purity of the compounds. Nevertheless, the carbamate linkage is frequently used for biolabeling since it is synthetically accessible and readily conjugated to primary amines. Nonetheless, DEVARAJ *et al.* screened a variety of linker motifs to find a linkage with improved stability. They reported on 3-amidomethyl substituted 1MCPs (e.g., the linker of **136**) to be an excellent candidate due to its high stability in the presence of thiols as well as its excellent stability after five freeze-thaw cycles. Additionally, the motif displayed slightly improved reactions rates with tetrazines compared to the carbamate linkage.<sup>72</sup> To get synthetic access to this motif, the cyclopropene alcohol **132** can be converted to the azide **133** by treatment with diphenyl phosphoryl azide (DPPA) and DBU. Subsequent reduction with triphenylphosphine provides amine **134**, which can be activated with carboxylic acids to the appropriate methyl amide under amide bond formation.

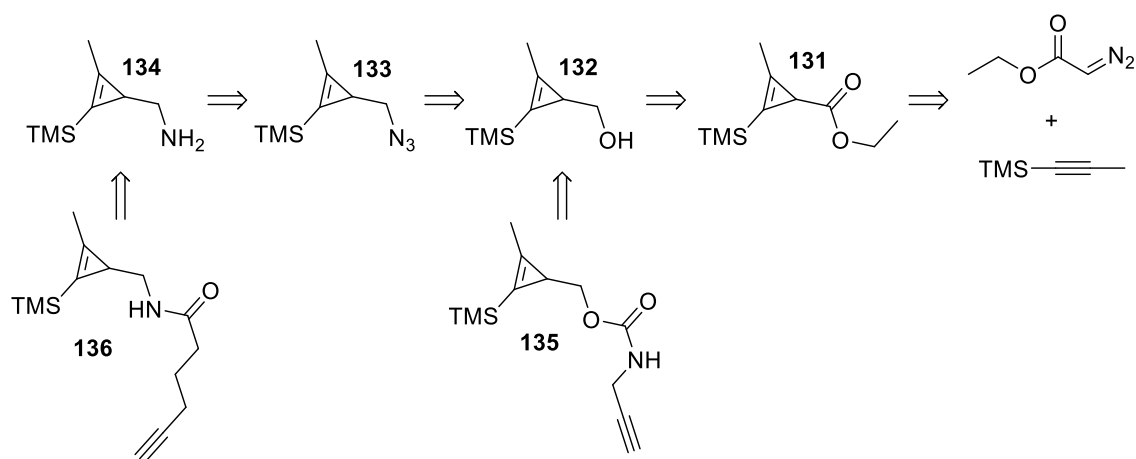


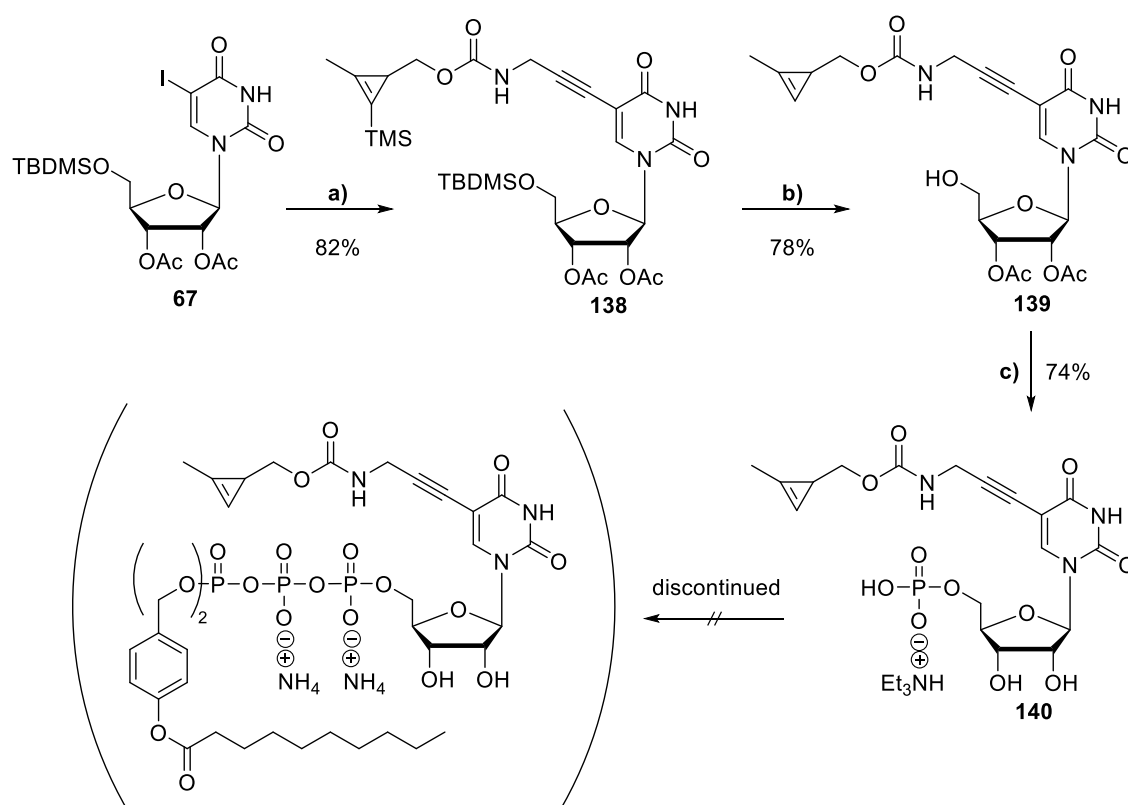
Figure 47: Retrosynthetic schema for the synthesis of 1MCP building blocks connected by carbamate **135** or amide **136** linkage.

Both linker motifs were synthesized and conjugated to terminal alkynes, which provided a functional handle for SONOGASHIRA cross-coupling reactions with iodized nucleoside derivatives. The 1MCP carbamate **135** was first synthesized by KATH-SCHORR *et al.* in 2016 for site-specific RNA labeling with a cyclopropene-modified unnatural nucleotide.<sup>77</sup> Shortly after, WAGENKNECHT *et al.* used the motif and introduced it to 2'-deoxyuridine triphosphate<sup>78</sup> and 7-deaza-2'-deoxyadenosine triphosphate<sup>76</sup> for post-synthetic labeling of oligonucleotides (Chapter 2.6.5).

In this work, the 1MCP carbamate motif should be introduced to a TriPPP compound to enable metabolic labeling of nucleic acids in living cells. Since here, the focus lay on providing tools for the visualization of viral transcription of HIV, the objective was to introduce the label to the RNA building block uridine (Scheme 26). Hence, the established method using hydroxyl protective groups for solubility improvement of the nucleoside followed by selective monophosphorylation via bis(fluorenylmethyl) phosphoramidite **87** after 5'-desilylation was employed (see Chapter 4.1). The introduction of the 1MCP carbamate **135** to protected 5-iodouridine **67** should be achieved by SONOGASHIRA cross-coupling. The desilylation of the 5'-OTBDMS group and the TMS protection of the 1MCP should be performed in one step. The deacetylation of the 2',3'-hydroxyl functions should be achieved simultaneously to Fm-group deprotection after 5'-*O*-monophosphorylation. The final 1MCP-modified  $\gamma$ -(C9C9AB)-UTP **137** should be obtained by the *H*-phosphonate route employing standard procedures.

Briefly, the 1MCP alcohol **132** was synthesized according to literature via rhodium-catalyzed cyclopropanation from commercially available ethyl diazoacetate and

trimethylsilylacetylene, and subsequent DIBAL-mediated reduction.<sup>157</sup> The 1MCP alcohol **132** was then treated with carbonyldiimidazole (CDI) and coupled with propargylamine to form the carbamate motif **135**. The C-C bond formation between **135** and protected IU **67** was carried out via SONOGASHIRA coupling. Complete conversion of the iodized nucleoside was reached after 3 h at 50 °C, and chromatography on silica gel resulted in the protected 1MCP-uridine **138** in a good yield of 82%. Simultaneous desilylation of the 1MCP and the 5'-hydroxy function was achieved by treatment of **138** with 1 M TBAF in THF (4 equiv) after 2 days at room temperature. The deprotected 1MCP-UMP **139** was isolated via normal phase chromatography in a good yield of 78%. The 5'-*O*-monophosphorylation was carried out by applying the Fm-route. The DCI-mediated coupling of **139** with bis(flourenylmethyl) phosphoramidite **87**, and subsequent oxidation with *tert*-butyl hydroperoxide provided the Fm-protected monophosphate, which was immediately deprotected: Deacetylation and Fm-group deprotection were carried out in H<sub>2</sub>O/CH<sub>3</sub>OH/Et<sub>3</sub>N (1:1:1 v/v/v) over three days. The TEAHH salt of **140** was isolated by RP<sub>18</sub> column chromatography in a good yield of 74%.



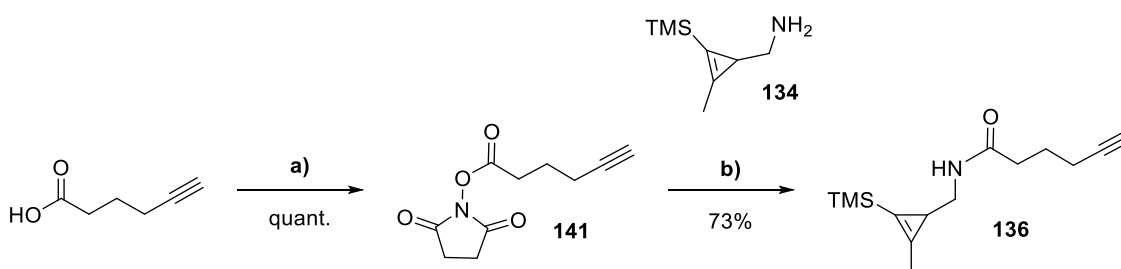
Scheme 26: Synthetic route to the 1MCP-carbamate-UMP **140**: **Reagents and conditions:** a) Pd<sub>2</sub>(dba)<sub>3</sub> (5.4 mol%), tri(2-furyl) phosphine (12 mol%), CuI (15 mol%), **135**, Et<sub>3</sub>N (7 equiv), DMF, 50 °C, 3 h; b) anhydrous 1 M TBAF in THF (4 equiv), THF, rt, 2 days; c) i) bis(flourenylmethyl)phosphoramidite **87** in CH<sub>2</sub>Cl<sub>2</sub>, 0.25 M DCI in CH<sub>3</sub>CN, CH<sub>3</sub>CN, rt; ii) 5.5 M *t*-BuOOH in decane, CH<sub>3</sub>CN, rt; iii) H<sub>2</sub>O/Me<sub>3</sub>OH/Et<sub>3</sub>N (1:1:1 v/v/v), rt, 3 days.



Unfortunately, 1MCP carbamates **139** to **140** were difficult to handle due to the instability of the reactive handle after TMS-deprotection. Insoluble material left in purged reaction flasks and high field signals in  $^1\text{H}$ -NMR spectra of the respective 1MCP compounds strongly indicated the formation of undesired polymerisate (data not shown). This instability interferes with the synthetic workflow and might disturb the later bioorthogonal labeling application since the integrity of the reporter nucleotide is not guaranteed after storage. Therefore, it was decided to abandon the synthetic route and focus on a more stable 1MCP motif.

As described above, the 3-amidomethyl substituted 1MCP motif showed improved stability and enhanced reactivity. Hence, 1MCP amine **134** was prepared from 1MCP alcohol **132** according to literature (Figure 47, not described).<sup>72</sup> 6-Heptynoic acid was selected as a functional building block to ensure sufficient flexibility and spacing between the nucleobase and the reactive bioorthogonal label. Moreover, the alkyne function provides the ability for C-C-bond formation under Sonogashira cross-coupling conditions with the respective iodized nucleobase.

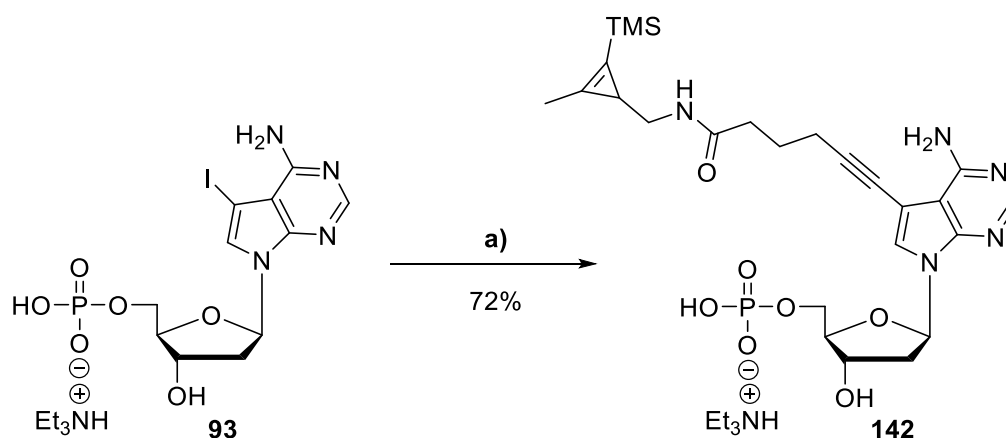
Briefly, 6-heptynoic acid was activated with disuccinimidyl carbonate in acetonitrile in the presence of pyridine, which provided the NHS ester **141** in quantitative yield. Successive amide bond formation between 1MCP amine **134** and **141** was carried out in dichloromethane at room temperature with triethylamine present. The 1MCP alkyne **136** was obtained in 73% yield after isolation on silica gel. As expected, the  $^1\text{H}$ -NMR spectra of **134** showed no degradation after long-term storage at  $-20\text{ }^\circ\text{C}$  since the stabilizing TMS function is still attached.



Scheme 27: Preparation of the methyl amide linkage of TMS-protected 1MCP **136**. **Reagents and conditions:** a) disuccinimidyl carbonate, pyridine, acetonitrile, rt; b) **134**, Et<sub>3</sub>N, CH<sub>2</sub>Cl<sub>2</sub>, rt.

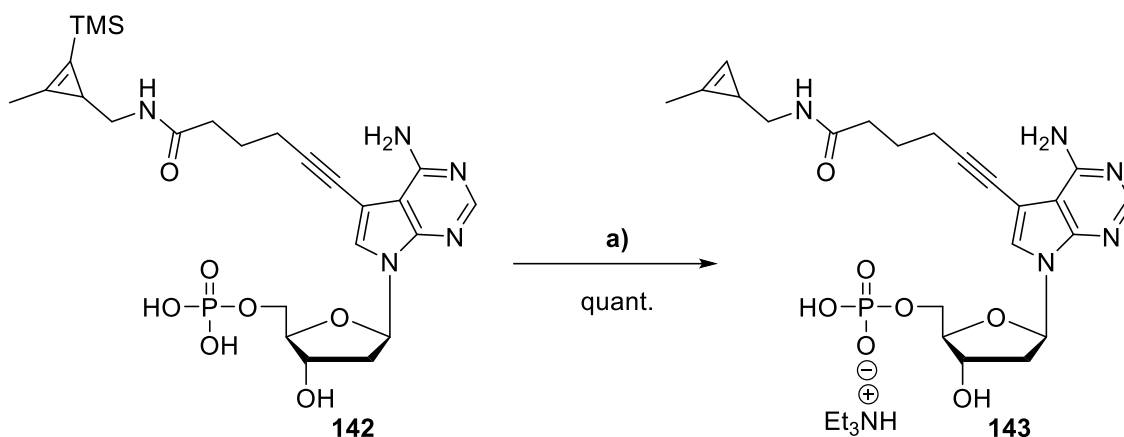
Here, the alkyne **136** was coupled directly to the appropriate iodized NMPs under SONOGASHIRA conditions with the same catalyst/ligand system (Pd<sub>2</sub>(dba)<sub>3</sub>/TFP) employed for the vinylation under STILLE cross-coupling conditions. First, the 1MCP alkyne **136** was coupled to IdAMP **91** in DMF utilizing Pd<sub>2</sub>(dba)<sub>3</sub>, TFP, copper(I) iodide, and triethylamine at  $50\text{ }^\circ\text{C}$ . Complete conversion of NMP was achieved after three hours

(TLC monitoring), and the crude product was precipitated by diethyl ether addition. Subsequent RP<sub>18</sub> column chromatography resulted in the TMS-protected 1MCP-dAMP **142** (TEAH salt) in a good yield of 72%.



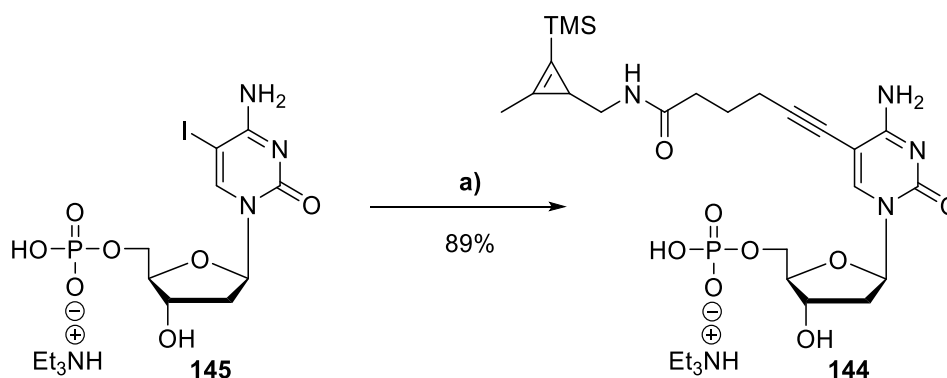
Scheme 28: Synthesis of TMS-protected 1MCP-dAMP **142** under SONOGASHIRA conditions. **Reagents and conditions:** a) Pd<sub>2</sub>(dba)<sub>3</sub> (5.4 mol%), tri(2-furyl) phosphine (12 mol%), CuI (15 mol%), **136**, Et<sub>3</sub>N (7 equiv), DMF, 50 °C, 3 h.

Desilylation of the TMS group was achieved with anhydrous TBAF. Beforehand, the NMP was transformed into its protonated form by purging the monophosphate salt through a short silica column. The appropriate fractions were pooled and filtered through a syringe filter to remove traces of SiO<sub>2</sub>. Briefly, 1.1 equivalents of TBAF monohydrate were dried by co-evaporation with THF, then dissolved again in THF. Subsequently, the TBAF solution was added to the NMP **142** (H<sup>+</sup> salt) in DMF at room temperature and stirred overnight. DMF as a co-solvent was necessary since the NMP salt was barely soluble in THF. Subsequent RP<sub>18</sub> column chromatography was buffered with 0.05 M TEAB to remove tetrabutylammonium salts and provided the desilylated TEAH salt of 1MCP-dAMP **143** in quantitative yield. Interestingly, reaction conditions comprising the TEAH salt of **143**, excessive equivalents of TBAF, or its monohydrate, gave sluggish results and should be avoided.



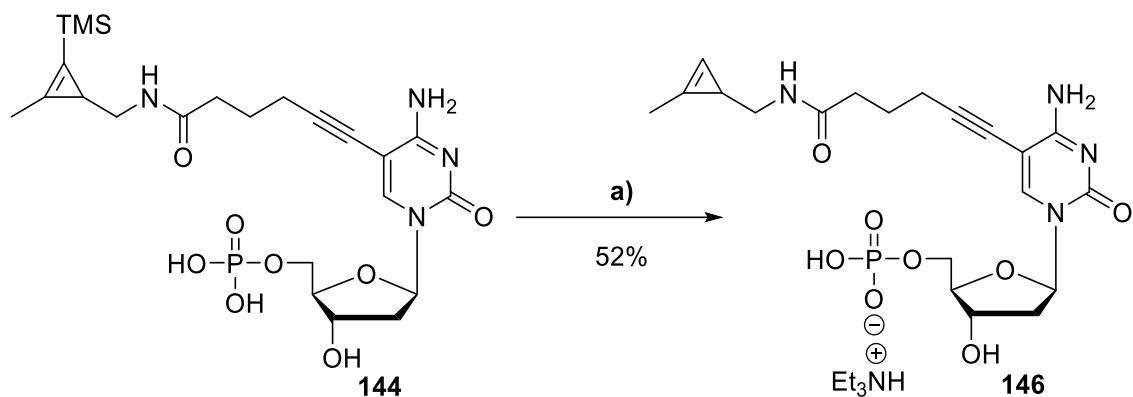
Scheme 29: TBAF-mediated deprotection of TMS-protected 1MCP-dAMP **143**. **Reagents and conditions:** a) i) Anhydrous TBAF (1.1 equiv) in THF, DMF, rt, o/n; ii) evaporation; iii) RP<sub>18</sub> column chromatography (0.05 M TEAB gradient in acetonitrile).

In addition to 1MCP-dAMP **143**, the 2'-deoxycytidine analog **144** was synthesized. Chapter 4.4.1 will discuss the synthesis and reasons for selecting the cytidine nucleoside in detail. Accordingly, IdCMP **145** (TEAH salt) was subjected to the coupling with alkyne **136** under SONOGASHIRA conditions. In contrast to the TEAH salt of IdAMP, the 2'-deoxycytidine monophosphate salt was not soluble in DMF. Thus, DMSO was used as a solvent, which enabled the complete conversion of the starting material within one hour (TLC monitoring). Precipitation of the crude product was achieved by acetone addition in the cold. Collection of the crude product and RP<sub>18</sub> column chromatography (0.05 M TEAB gradient in acetonitrile) provided TMS-protected 1MCP-dCMP **144** (TEAH salt) in an excellent yield of 89%.



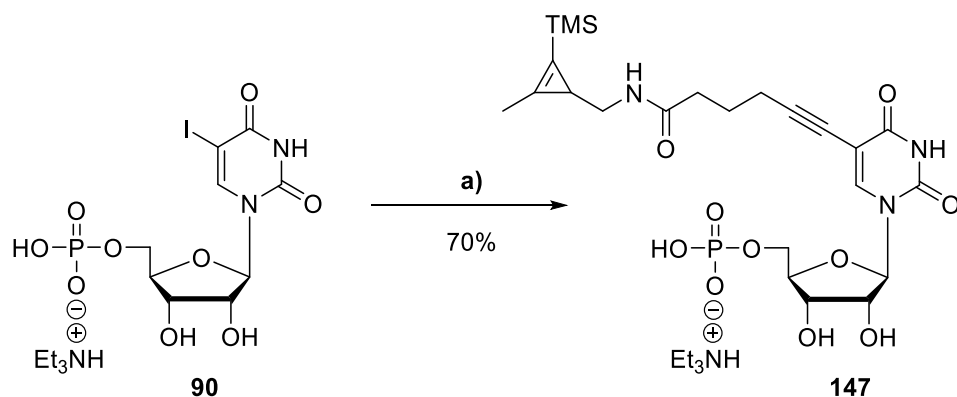
Scheme 30: Synthesis of TMS-protected 1MCP-dCMP **144** under SONOGASHIRA conditions. **Reagents and conditions:** a) Pd<sub>2</sub>(dba)<sub>3</sub> (5.4 mol%), tri(2-furyl) phosphine (12 mol%), CuI (15 mol%), **136**, Et<sub>3</sub>N (7 equiv), DMSO, 60 °C, 1 h.

The 1MCP-dCMP **144** ( $H^+$  salt) was subjected to TBAF-mediated desilylation, which provided TMS-protected 1MCP-dCMP **146** (TEAH salt) after purification by RP<sub>18</sub> column chromatography (0.05 M TEAB gradient in acetonitrile) in a moderate yield of 52%.



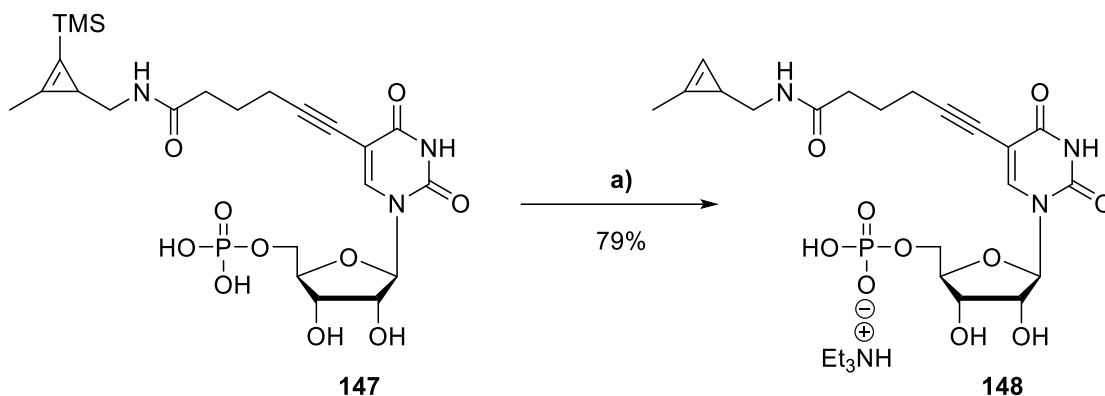
Scheme 31: TBAF-mediated deprotection of TMS-protected 1MCP-dCMP **146**. **Reagents and conditions:** a) i) Anhydrous TBAF (1.1 equiv) in THF, DMF, rt, o/n; ii) evaporation; iii) RP<sub>18</sub> column chromatography (0.05 M TEAB gradient in acetonitrile).

To synthesize an alternative to the storage-labile carbamate linked 1MCP-UMP **140**, the improved 1MCP methyl amide motif **136** was introduced to IUMP **90** via SONOGASHIRA cross-coupling. The reaction was carried out in DMSO to ensure the solubility of the TEAH salt of **90**. The complete conversion was observed after two hours. In contrast to the SONOGASHIRA couplings described above, DMSO was evaporated under an oil pump vacuum. The resulting residue was dissolved in 0.05 M TEAB and loaded onto an RP<sub>18</sub> silica gel column through a syringe filter. Automated chromatography with 0.05 M TEAB buffer in acetonitrile resulted in TMS-protected 1MCP-UMP **147** (TEAH salt) in a good yield of 70%.



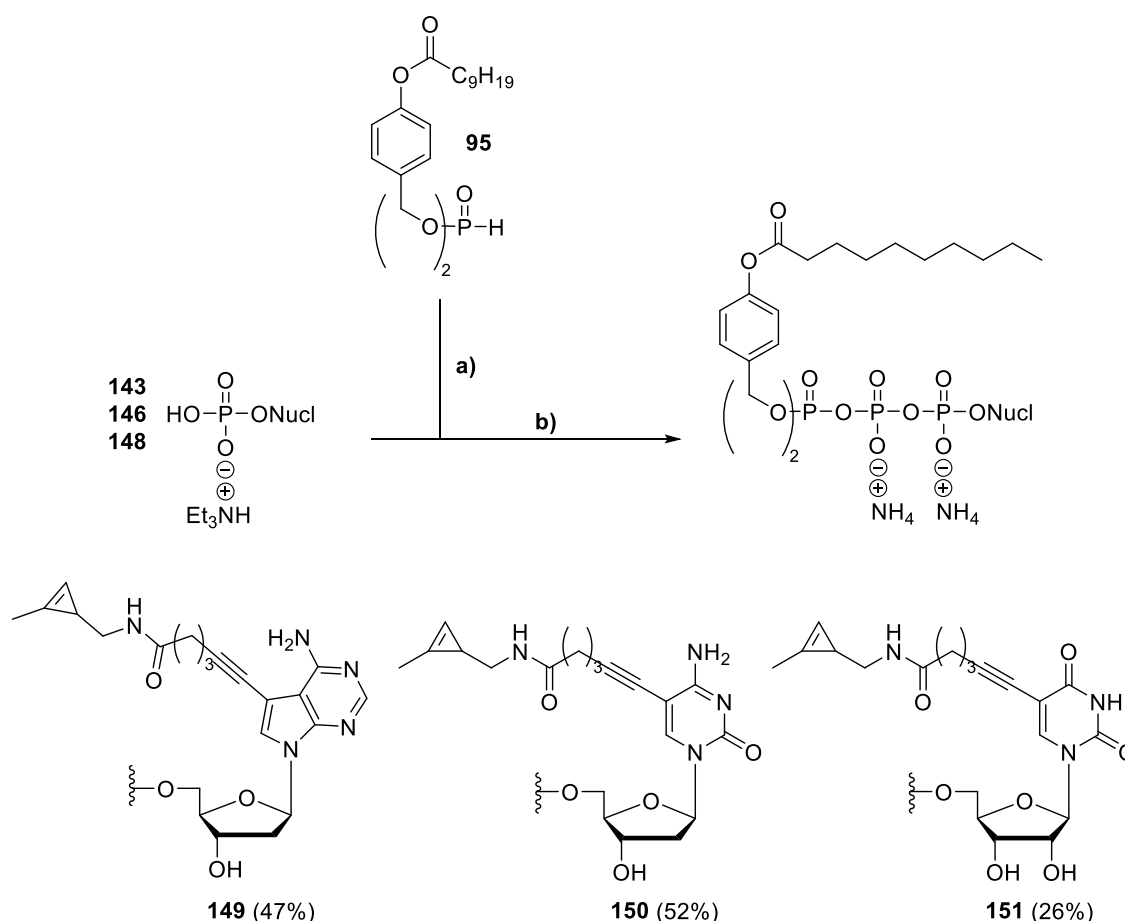
Scheme 32: Synthesis of TMS-protected 1MCP-UMP **147** under SONOGASHIRA conditions. **Reagents and conditions:** a) Pd<sub>2</sub>(dba)<sub>3</sub> (5.4 mol%), tri(2-furyl) phosphine (12 mol%), CuI (15 mol%), **136**, Et<sub>3</sub>N (7 equiv), DMSO, 50 °C, 2 h.

Subsequently, the TEAH salt of **147** was subjected to a Dowex ion-exchange chromatography ( $H^+$ ) to provide the protonated monophosphate **147**. Surprisingly, attempts to desilylate the TMS group with 1.1 equivalents of pre-dried TBAF monohydrate, resulted in no conversion of starting material. However, treatment of **147** (solved in DMF) with 3 equivalents of 1 M TBAF solution in THF resulted in full desilylation overnight. Subsequent RP<sub>18</sub> column chromatography (0.05 M TEAB gradient in acetonitrile) resulted in the TEAH salt of 1MCP-UMP **148** in a good yield of 79%.



Scheme 33: TBAF-mediated deprotection of TMS-protected 1MCP-UMP **148**. **Reagents and conditions:** a) i) Anhydrous 1 M TBAF in THF (3 equiv), DMF, rt, o/n; ii) evaporation; iii) RP<sub>18</sub> column chromatography (0.05 M TEAB gradient in acetonitrile).

All three 1MCP-modified NMPs at hand, the respective  $\gamma$ -(C9C9AB)-TriPPPPro compounds of **143**, **146**, and **148** were synthesized by the *H*-phosphonate route under standard conditions in moderate to good yields of 47%, 52%, and 26%, respectively. In our hands, the newly designed 3-amidomethyl linkage showed good stability and no sign of degradation upon concentration or extensive storage periods at -20 or -80 °C (checked by  $^1H$ -NMR spectra).

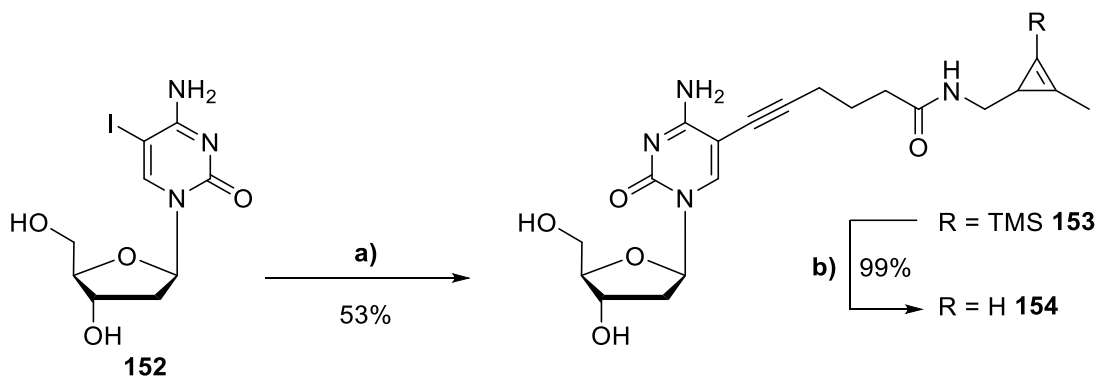


Scheme 34: Synthesis of  $\gamma$ -(C9C9AB)-1MCP-dATP **149**,  $\gamma$ -(C9C9AB)-1MCP-dCTP **150**, and  $\gamma$ -(C9C9AB)-1MCP-UTP **151** by *H*-phosphonate route.<sup>126</sup> **Reagents and conditions:** a) i) NCS, CH<sub>3</sub>CN, 50-60 °C; ii) 0.4 M mono-tetrabutylammonium phosphate in CH<sub>3</sub>CN, rt; b) TFAA, Et<sub>3</sub>N, CH<sub>3</sub>CN, 0 °C, 10 min; iii) 1-methylimidazole, Et<sub>3</sub>N, CH<sub>3</sub>CN, 0 °C to rt; iii) NMP (TEAH salt) in DMF, CH<sub>3</sub>CN, rt; iv) RP<sub>18</sub> column chromatography, ion-exchange to ammonia, RP<sub>18</sub> column chromatography.

Jumpig ahead (detailed in Chapter 4.7.3), the pronucleotide  $\gamma$ -(C9C9AB)-1MCP-dCTP **150** exhibited strong fluorescent staining of *in vitro* labeled cellular and viral DNA in HSV-1 infected Vero cells. Fluorescent staining of the introduced label was achieved in fixed and permeabilized samples. Hence, as a control, the parent 1MCP-dC **154** nucleoside reporter was synthesized to investigate the value of the TriPPPPro concept. The research question here is if the nucleoside reporter is sufficiently phosphorylated to its NTP after cellular uptake. In case of efficient phosphorylation by endogenous kinases, the application of a pronucleotide reporter would become redundant.

Hence, 1MCP-dC **154** was synthesized from IdC **152** by first introducing the alkyne **136** by SONOGASHIRA cross-coupling and subsequent desilylation of the TMS group of intermediate **153** with anhydrous TBAF. The cross-coupling reaction resulted in the intermediate **153** in a moderate yield of 53% due to incomplete conversion of starting material. The subsequent deprotection provided the desired nucleoside reporter **154** in

near quantitative yield after purification on RP<sub>18</sub> silica gel with a gradient of 0.05 M TEAB in acetonitrile.



Scheme 35: Synthesis of 1MCP-dC **154** by SONOGASHIRA-CROSS coupling from IdC **152** and subsequent desilylation of the intermediate **153**. **Reagents and conditions:** **a)** Pd<sub>2</sub>(dba)<sub>3</sub> (5.4 mol%), tri(2-furyl) phosphine (12 mol%), CuI (15 mol%), **136**, Et<sub>3</sub>N (7 equiv), DMSO, 50 °C, 2 h; **b)** i) Anhydrous TBAF (1.1 equiv) in THF, DMF, rt, o/n; ii) evaporation; iii) RP<sub>18</sub> column chromatography (0.05 M TEAB gradient in acetonitrile).

The chapter described the introduction of a stable 1MCP-motif to 2'-deoxycytidine and 2'-deoxy-7-deazaadenine monophosphates. The choice of the 3-amidomethyl substituted 1MCP motif over the carbamate linkage resulted in enhanced stability of the functionality as well as improved reaction kinetics towards tetrazines. Building up the linker unit separately with the TMS-protection still attached, and subsequent linkage to the respective monophosphates via SONOGASHIRA cross-coupling gave uncomplicated access to the respective conjugates. The following desilylation afforded the starting materials for the desired TriPPPPro preparations, which resulted in the isolation of promising pronucleotide reporters.

The following chapter introduces a different synthetic approach, in which a linker motif is first introduced to the nucleobase, enabling successive functionalization with various different building blocks.

## 4.4 Design and synthesis of rapid pronucleotide reporters

### 4.4.1 Deoxycytidine multitool precursor

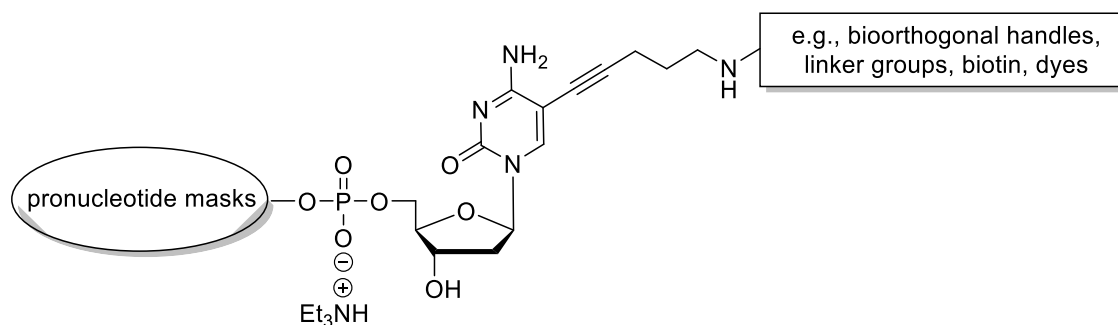


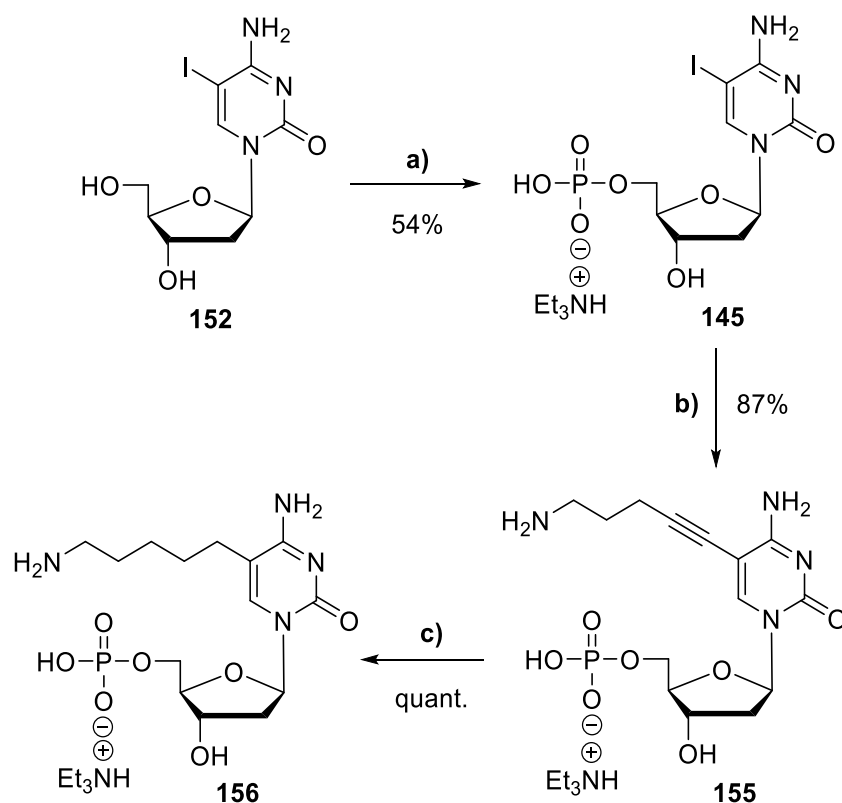
Figure 48: Illustration of the functionalization of the “multitool” precursor nucleoside monophosphate.

The objective was to synthesize a nucleoside monophosphate “multitool” precursor with a flexible linker motif, which can be used to easily attach different motifs by amide (or carbamate) bond formation (Figure 48). Subsequent TriPPPro synthesis using the *H*-phosphonate route should give simple access to “multitool”-pronucleotide reporter reporters. The focus was to develop a nucleotide reporter best suited for the metabolic labeling of herpes simplex virus genomes in host cells. Thus, 2'-deoxycytidine was selected as the starting candidate based on the G+C-rich share of the HSV genome (Chapter 2.5).<sup>25,26,46</sup> Moreover, most organisms, both prokaryotes and eukaryotes, as well as several DNA viruses (e.g., HSV-1 and HSV-2), and some retroviruses (e.g., HIV-1 and HIV-2), encode dUTPases. As mentioned in Chapter 2.5, dUTPase lowers the intracellular bioavailability of dUTP by hydrolyzing the triphosphate into dUMP and pyrophosphate. Since most DNA polymerases misincorporate dUTP instead of dTTP into DNA, thereby initiating mutations, it can be essential for the viability of these organisms or pathogens to reduce the intracellular dUTP/dTTP ratio.<sup>158</sup> Thus, choosing a 2'-deoxycytidine-based reporter molecule over a 2'-deoxyuridine derivative might benefit labeling efficiency.<sup>46</sup>

Starting with 5-iodo-2'-deoxycytidine **152** as a model nucleoside, the first step was to prepare its 5'-*O*-nucleoside monophosphate **145**. Both the SOWA & OUCHI and the YOSHIKAWA protocol were employed. The SOWA & OUCHI protocol was the more convenient method since the nucleoside showed only moderate solubility in TMP or TEP, which are utilized as solvents under YOSHIKAWA conditions. Therefore, finely crushed IdC **152** was subjected to SOWA & OUCHI reaction conditions at 0 °C (see also Chapter 4.1). Over time, the reaction mixture became clear as the solid nucleoside was consumed,



and the reaction mixture was next hydrolyzed and neutralized with ammonium bicarbonate. RP<sub>18</sub> column chromatography of the formed ammonium phosphates with pure water as eluent (preferably with a reduced flow) allowed easy separation of the 5'-*O*-monophosphate from the more polar 3',5'-*O*-bis(phosphate) by-products (Note: the separation becomes less feasible with the respective TEAH salts due to the phosphates unequal increase of lipophilicity). Treatment of the ammonium salt with an excess of triethylamine and subsequent freeze-drying provided the IdCMP **145** as its TEAH salt in 54% yield. Next, the appropriate linker was selected and introduced under SONOGASHIRA conditions. To ensure sufficient distance between the nucleoside and the bioorthogonal label, 1-amino-4-pentyne was chosen as the motif and synthesized according to literature procedures from 5-chloro-1-pentyne in two steps (data not shown).<sup>159</sup> The SONOGASHIRA cross-coupling reaction was employed in DMSO to ensure the solubility of IdCMP **145** (TEAH salt). The complete conversion was achieved within one hour at 55 °C. The crude monophosphate was precipitated by the addition of acetone in the cold, collected, and purified on RP<sub>18</sub> silica gel with a gradient of 0.05 M TEAB in acetonitrile. The TEAH salt of **155** was obtained in a good yield of 87%. To increase the flexibility of the linker unit, the alkyne group was reduced using palladium-catalyzed hydrogenation with palladium hydroxide on carbon and triethyl silane as an *in situ* hydrogen donor. The precursor multitool **156** was obtained in quantitative yield after filtration and RP<sub>18</sub> column chromatography (0.05 M TEAB buffered).



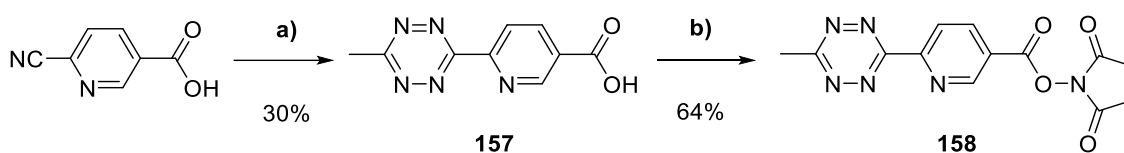
Scheme 36: Synthesis of 5-aminopent-1-yl-dCMP **156**. **Reagents and conditions:** a) i)  $\text{POCl}_3$  (4.4 equiv), pyridine (4.8 equiv),  $\text{H}_2\text{O}$  (2.8 equiv) in  $\text{CH}_3\text{CN}$  (18.9 equiv),  $0^\circ\text{C}$ , 10 min; ii) nucleoside **152**,  $0^\circ\text{C}$ ; iii) ice water,  $\text{NH}_4\text{HCO}_3$  (pH = 8); iv)  $\text{RP}_{18}$  column chromatography v) ion-exchange to TEAH; b)  $\text{Pd}_2(\text{dba})_3$  (5.4 mol%), tri(2-furyl) phosphine (12 mol%),  $\text{CuI}$  (15 mol%), 1-amino-4-pentyne,  $\text{Et}_3\text{N}$  (7 equiv),  $\text{DMSO}$ ,  $55^\circ\text{C}$ , 1 h; c)  $\text{Pd}(\text{OH})_2$ ,  $\text{Et}_3\text{SiH}$ ,  $\text{Et}_3\text{N}$ ,  $\text{MeOH}$ , pressure tube, rt, 72 h.

It is worth discussing that both **155** and **156** linker motifs can be used as the respective precursor nucleotide. The choice strongly depends on the substrate activity of the viral (or cellular) DNA polymerase of interest and might even vary from polymerase to polymerase. The more flexible linker motif was chosen as a starting point due to indications in literature that higher linker flexibility improves the post-synthetic labeling efficiency of oligonucleotides.<sup>78,160</sup> In the future, further attention should be addressed on finding the linker motif that is best suited for the cellular or viral polymerase of interest.<sup>161–163</sup> The following part details the implementation of a tetrazine bioorthogonal group via nicotinic acid conjugation.

#### 4.4.2 Nicotinic acid-conjugated TriPPPPro compound

The primary amine of the linker unit in multitool nucleotide **156** now enables the attachment of bioorthogonal handles, providing fast bioorthogonal reaction rates. The idea of the relatively long linker was to increase the distance to these “faster” and more sterically demanding labels. Nicotinic tetrazine **157** was selected as a candidate since it

exhibits a good balance between reactivity and stability.<sup>164</sup> Naturally, stability of the motif under physiological conditions is essential since the reporter pronucleotide is designed for metabolic labeling in living cells. Additionally, the carboxylic acid provides the functional group necessary for the amide bond formation with 5-(5-aminopent-1-yl)-dCMP **156**. Accordingly, the 6-(6-methyl-1,2,4,5-tetrazine-3-yl)nicotinic acid **157** was synthesized first, followed by its activation to the NHS-active ester **158**. The preparation of **157** was carried out following the report by KELE *et al.*<sup>164</sup> The asymmetric tetrazine was prepared in a pressure valve at 100 °C with 6-cyanonicotinic acid, triethyl orthoacetate, and hydrazine-hydrate.



Scheme 37: Synthesis of NHS-ester of nicotinic methyl tetrazine **158**. Reagents and conditions: a) i) triethyl orthoacetate, hydrazine-hydrate, mercapropionic acid (cat.), 100 °C, pressure tube, 2 h; ii) extraction; iii)  $\text{PhI}(\text{OAc})_2$ ,  $\text{CH}_2\text{Cl}_2/\text{MeOH}$  (10:1 v/v), rt, 16 h; b) disuccinimidyl carbonate, pyridine, DMAP (cat.), DMF, rt, 3 h.

In contrast to using sulfur as a catalyst, organosulfur mercapropionic acid was employed. After two hours, the reaction mixture was cooled to room temperature, and the pressure valve was unsealed. The reaction flask was left open overnight to reduce the concentration of cancerogenic hydrazine. Extraction provided the crude dihydrotetrazine intermediate, which was oxidized by  $\text{PhI}(\text{OAc})_2$  to provide nicotinic tetrazine **157** in 30% yield after column chromatography and washing steps using methanol. Literature procedures used *in situ* generated nitrous gases ( $\text{NO}_x$ ) as oxidation agents, resulting in **157** in 25% yield over two steps.<sup>164</sup>

Next, the NHS-active ester **158** was prepared in DMF in the presence of pyridine to ensure the solubility of nicotinic acid **157**. Almost no conversion was achieved without catalytic amounts of DMAP, but conversion was completed after three hours at room temperature with DMAP present. Extraction and isolation on silica gel resulted in **158** in a moderate yield of 64%.

The following coupling of NcTz **157** to 5-aminopent-1-yl-dCMP **156** was problematic regarding the stability of the tetrazine motif under basic conditions. First attempts to isolate the NcTz-dCMP **159** as its TEAH salt showed degradation of the product after removal of the solvents at elevated temperatures *in vacuo*, freeze-drying or storage. It was concluded that the triethylammonium counterions were responsible for the

instability of the tetrazine function. Therefore, the reaction and purification conditions were changed to circumvent basic conditions. The monophosphate **156** was dissolved in CH<sub>3</sub>OH, followed by the addition of the NcTz-NHS ester **158** dissolved in DMF. No triethylamine was added to the mixture. After three hours at room temperature, no further reaction progress was observable and the CH<sub>3</sub>OH was removed *in vacuo*.

It is possible that the absence of triethylamine (or any base) was responsible for the incomplete reaction progress. The dependency on triethylamine for reaction progress was already observed for other NHS mediated couplings conducted during this work.

To avoid full evaporation of the remaining DMF at elevated temperatures, the product was precipitated by the addition of diethyl ether. The crude monophosphate was collected and purified on silica gel with CH<sub>2</sub>Cl<sub>2</sub>/CH<sub>3</sub>OH in a 1:1 ratio. The purification provided the stable protonated form of NcTz-dCMP **159** in a low yield of 37%. No further attempts of optimization were conducted, since sufficient NcTz-dCMP **159** was available for the subsequent TriPPPPro synthesis. In future, it should be validated if the presence of triethylamine during the coupling reaction provides complete conversion of starting material without diminishing the overall yield due to the base lability of the tetrazine motif.

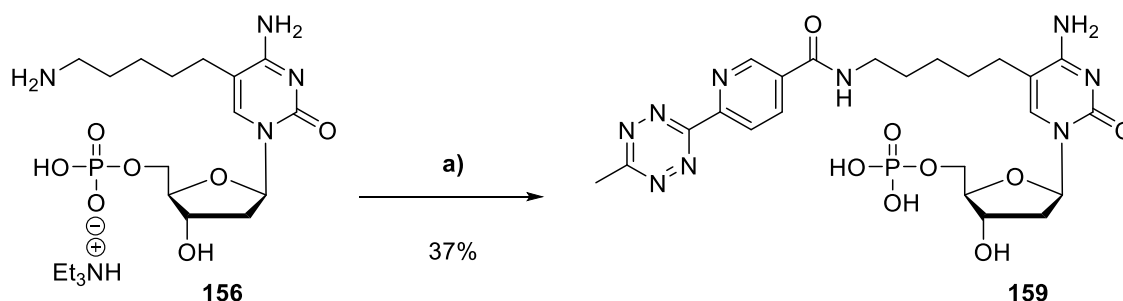
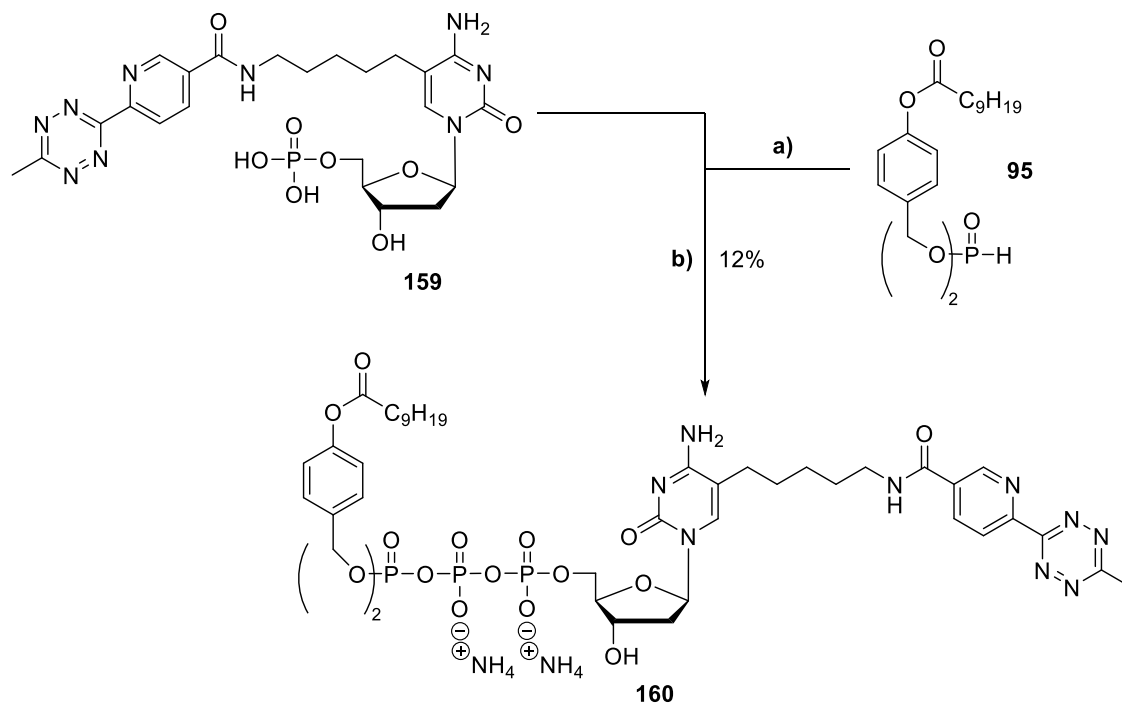


Figure 49: Synthesis of NcTz-dCMP **159**. Reagents and conditions: a) i) NcTz-NHS ester **158** in DMF, CH<sub>3</sub>OH, rt, 3 h; ii) evaporation of CH<sub>3</sub>OH; iii) precipitation by Et<sub>2</sub>O addition; iv) purification on silica gel (CH<sub>2</sub>Cl<sub>2</sub>/CH<sub>3</sub>OH, 1:1).

The  $\gamma$ -(C9C9AB)-NcTz-dCTP **160** was prepared according to *H*-phosphonate route conditions. The TEAH salt of **159** was formed *in situ* before coupling to assure the integrity of the base labile tetrazine motif. Therefore, **159** was dissolved in DMSO under addition of triethylamine (1.8 equiv). Moreover, the pyrophosphate activation with 1-methylimidazole was carried out in DMF without further addition of triethylamine. The solvent mixture of DMSO/DMF during coupling proved to be necessary in terms of solubility. The standard purification protocol resulted in the desired  $\gamma$ -(C9C9AB)-NcTz-

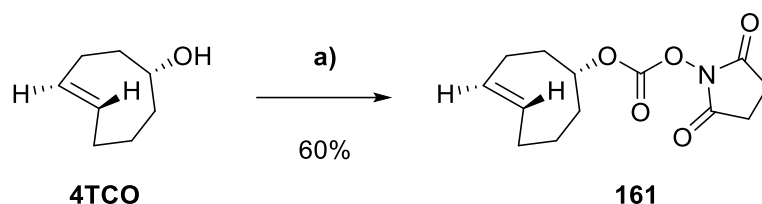
dCTP **160** in a yield of 12%. The meager yield can be explained partly due to the low conversion of monophosphate **159** during the coupling procedure. After four hours at room temperature, no further conversion was observable (RP<sub>18</sub> HPLC monitoring), and consequently, the workup procedure was initiated.



Scheme 38: Synthesis of  $\gamma$ -(C9C9AB)-NcTz-dCTP **160** by *H*-phosphonate route.<sup>126</sup> **Reagents and conditions:** **a)** i) NCS, CH<sub>3</sub>CN, 50-60 °C; ii) 0.4 M mono-tetrabutylammonium phosphate in CH<sub>3</sub>CN, rt; **b)** TFAA, Et<sub>3</sub>N, CH<sub>3</sub>CN, 0 °C, 10 min; ii) 1-methylimidazole, Et<sub>3</sub>N, DMF, 0 °C to rt; iii) NMP (TEAH salt) in DMSO, Et<sub>3</sub>N (1.8 equiv), rt; iv) RP<sub>18</sub> column chromatography, ion-exchange to ammonia, RP<sub>18</sub> column chromatography.

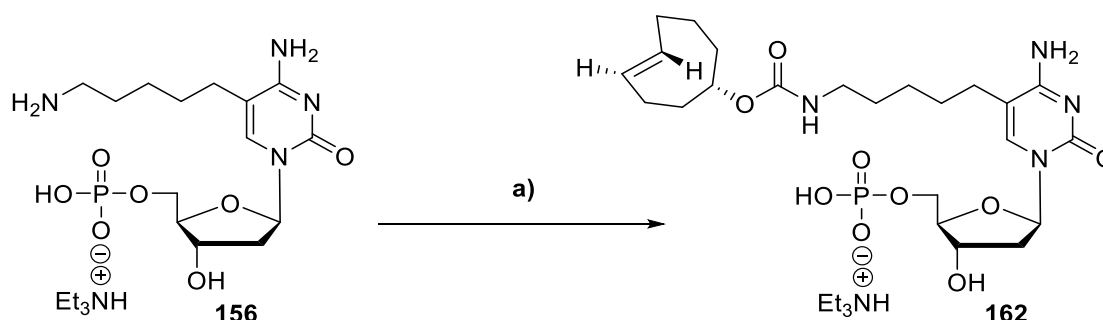
#### 4.4.3 TCO/BCN-conjugated TriPPPro compounds – finding the motif

To introduce the 4-ene TCO to 5-(5-aminopent-1-yl)-dCMP **156**, commercially available (*E*)-cyclooct-4-enol was transferred to its succinimidyl carbonate **161** with disuccinimidyl carbonate according to literature.<sup>165</sup> Extraction and isolation on silica gel resulted in 4TCO-NHS **161** in 60% yield (lit. 38%). Only traces of the *cis*-isomer were detectable in the <sup>1</sup>H-NMR spectra (≤5 mol%, data not shown).



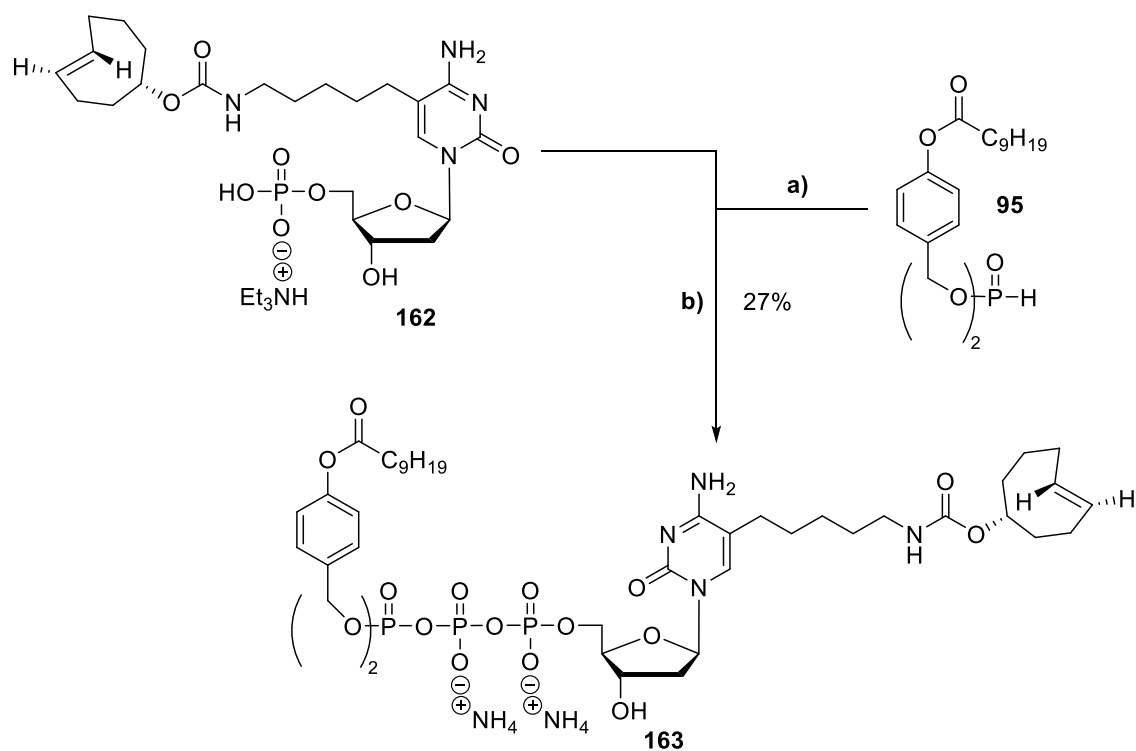
Scheme 39: Synthesis of NHS-TCO-carbonate **161**. Reagents and conditions: a) disuccinimidyl carbonate, Et<sub>3</sub>N, CH<sub>3</sub>CN, rt, o/n.

The amide bond formation between 5-(5-aminopent-1-yl)-dCMP **156** and 4TCO-NHS **161** was performed in DMSO with triethylamine present. Complete conversion of **156** was achieved after two hours at room temperature. Purification by RP<sub>18</sub> column chromatography (0.05 M TEAB gradient in acetonitrile) resulted in 4TCO-dCMP **162** (TEAH salt) in 46% yield with around 7 mol% of the *cis*-isomer (calculated via <sup>1</sup>H-NMR spectra, data not shown).



Scheme 40: Synthesis of 4TCO-dCMP **162**. Reagents and conditions: a) 4-ene TCO-NHS, Et<sub>3</sub>N, DMSO, rt, 2 h.

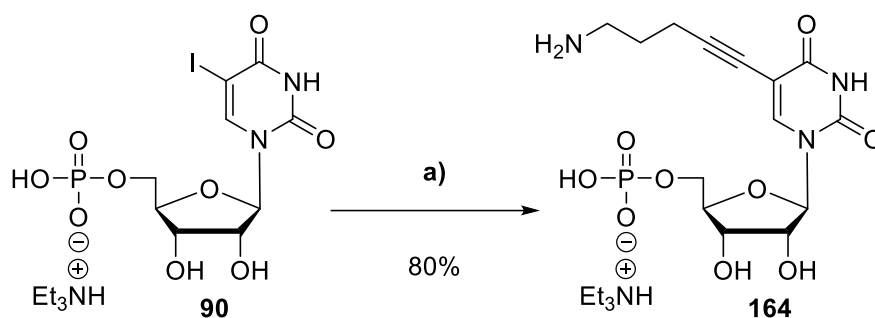
Next, the  $\gamma$ -(C9C9AB)-TriPPPro compound of **162** was synthesized by *H*-phosphonate route following standard conditions. The 1-methylimidazole-mediated activation step of the pyrophosphate was carried out in DMF to improve the solubility of the monophosphate **162**. The standard purification protocol provided the desired  $\gamma$ -(C9C9AB)-4TCO-dCTP **163** in a yield of 27% containing only traces of the *cis*-isomer (<sup>1</sup>H-NMR spectra signals of the *cis*-isomer too weak for calculations, data not shown).



Scheme 41: Synthesis of  $\gamma$ -(C9C9AB)-4TCO-dCTP **163** by *H*-phosphonate route.<sup>126</sup> **Reagents and conditions:** **a)** i) NCS, CH<sub>3</sub>CN, 50-60 °C; ii) 0.4 M mono-tetrabutylammonium phosphate in CH<sub>3</sub>CN, rt; **b)** TFAA, Et<sub>3</sub>N, CH<sub>3</sub>CN, 0 °C, 10 min; ii) 1-methylimidazole, Et<sub>3</sub>N, DMF, 0 °C to rt; iii) NMP (TEAH salt) in DMF, CH<sub>3</sub>CN, rt; iv) RP<sub>18</sub> column chromatography, ion-exchange to ammonia, RP<sub>18</sub> column chromatography.

Jumping ahead (for detailed descriptions see Chapter 0), early imaging results showed little to no staining for the TriPPPPro compounds attached via a saturated alkyl-linker motif (**160** and **163**). In contrast, the 1MCP functionalized pronucleotides (**149** and **150**, connected via an alkyne motif) exhibited excellent labeling properties in fixed and permeabilized samples. Ignoring the differences in label size of 1MCP, 4TCO, or NcTz and their potential influence on substrate affinities, these findings indicated that the respective polymerases might better tolerate the alkyne attachment at the nucleobase. The objective was hence to synthesize a new series of pronucleotide reporters, which have the potential for live-cell imaging applications and include/integrate the promising alkyne motif. Since the  $\gamma$ -(C9C9AB)-1MCP-dCTP **150** reporter showed superior imaging results in HSV-1 infected Vero cells compared to its 2'-deoxyadenosine derivative **149**, the focus was on the 2'-deoxycytidine nucleoside (Chapter 4.7.3).

From a synthetic viewpoint, the changes were easily applied by simply changing the precursor 5-(5-aminopent-1-yl)-dCMP **156** to the alkyne-linked 5-(5-aminopent-1-yn-1-yl)-dCMP **155**. Additionally to DNA metabolic reporters, this series should also obtain an RNA pronucleotide reporter with a uridine framework, comparable to the 1MCP-TriPPPPro series. The respective precursor 5-(5-aminopent-1-yn-1-yl)-UMP **164** was synthesized from IUMP **90** and 1-amino-4-pentyne via SONOGASHIRA cross-coupling in a good yield of 80%.



Scheme 42: Synthesis of 5-(5-aminopent-1-yn-1-yl)-dUMP **164**. Reagents and conditions: a) Pd<sub>2</sub>(dba)<sub>3</sub> (5.4 mol%), tri(2-furyl) phosphine (12 mol%), CuI (15 mol%), 1-amino-4-pentyne, Et<sub>3</sub>N (7 equiv), DMSO, 50 °C, 2 h.

As described before, the metabolic labeling under live-cell conditions requires exceptionally fast reaction kinetics towards tetrazines. Even though *trans*-cyclooct-4-ene (4TCO) provides such high reaction rates, it reveals sluggish stability in solutions with thiols present. Thiols are mainly responsible for the isomerization to the less reactive *cis*-cyclooct-4-ene isomer. Naturally, this concerns the overall labeling efficiency and restricts the applicability for time-demanding labeling experiments.



LEMKE and coworkers improved the stability properties by synthesizing the 3-ene (3TCO) and 2-ene (2TCO) isomers with the double bond closer to the “protective” carbamate function. Even though it was found that the 2-ene TCO showed somewhat slower reaction kinetics, the stability was significantly increased compared to the 4-ene TCO.<sup>166</sup> Later, the same group found that only one of the 2-ene TCO atropisomers – the axial 2-ene atropisomer (2TCO $\alpha$ ) - exhibits particular fast reaction kinetics and exceptional stability (Figure 50).<sup>79</sup>

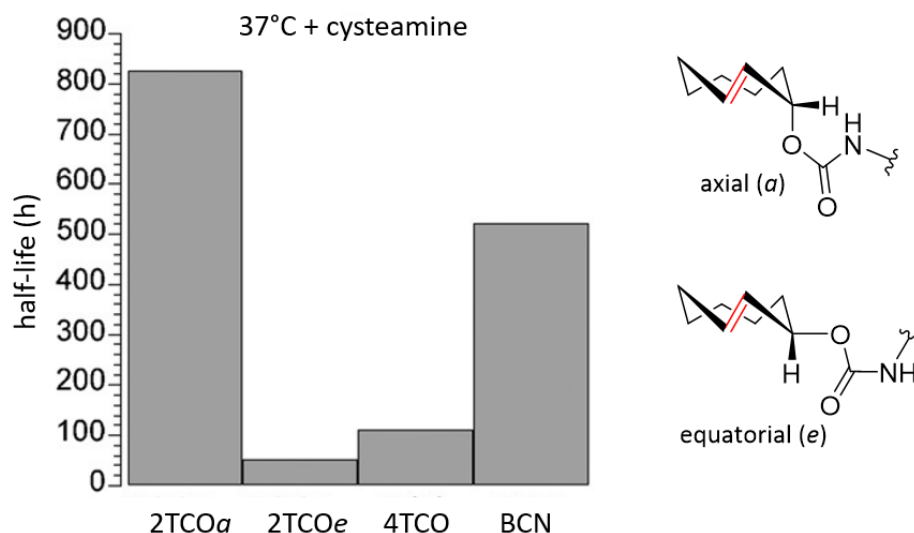


Figure 50: Comparison of the stability of the atropisomers of 2TCO $\alpha$  and 2TCO $e$  relative to 4TCO and BCN in the presence of the thiol cysteamine.<sup>79</sup>

A drawback of the 2-ene isomer is that the bicyclic product **165** of the [4+2] cycloaddition with tetrazines undergoes a  $\beta$ -elimination under the release of the respective probe **166** (Figure 51). Transferring the issue to labeling applications, the  $\beta$ -elimination of the fluorophore after staining would naturally reduce labeling efficiency, and therefore, the issue needs some consideration prior to the experiment.

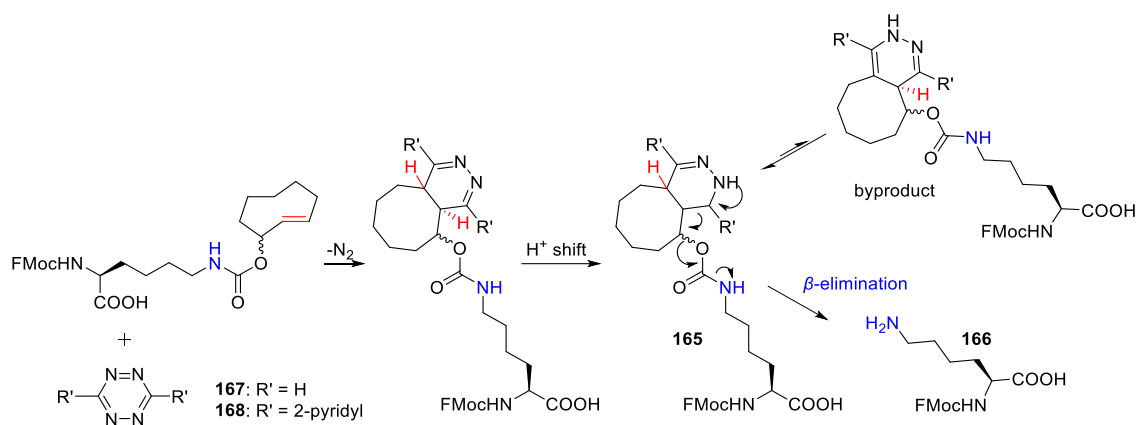


Figure 51: Potential mechanisms for the  $DA_{INV}$  mediated  $\beta$ -elimination reaction with 2TCO-conjugated lysine.<sup>167</sup>

Interestingly, CHEN *et al.* studied the  $DA_{INV}$  mediated elimination reaction in more detail to discover a reaction-triggered bioorthogonal protein decaging technique in living cells (Figure 51).<sup>167</sup> Whereas the bicyclic adduct of 3,6-dimethyl-1,2,4,5-tetrazine ( $Me_2Tz$ , **167**) and 2TCO $\alpha$  demonstrated the highest elimination efficiency (92% release of the lysine after 3 h at 37 °C, in  $H_2O/CH_3CN$ ; 8:2 v/v), the bicyclic product of 3,6-di-2-pyridyl-1,2,4,5-tetrazine ( $Py_2Tz$ , **168**) and 2TCO $\alpha$  only released 17% of the amino acid under the same conditions.<sup>167</sup> The excellent stability of the 2TCO $\alpha$ , while retaining most of its reactivity (compared to 4TCO), paired with the relatively slow  $\beta$ -elimination after the [4+2] cycloaddition with  $Py_2Tz$  **168**, make these partners an exciting labeling duo.

Fortunately, the 2TCO $\alpha$  is commercially available as its NHS carbonate **169**. Next to 2TCO $\alpha$ , an endo bicyclo[6.1.0]nonyne (BCN<sup>endo</sup>) label should be introduced to a cytidine pronucleotide to round up the labeling repertoire. The BCN is a versatile label due to its overall good stability (see Figure 51) and the ability to function as a bioorthogonal group in a SPIEDAC reaction and in a catalyst-free SPAAC with azides (Figure 52). Reactivity-wise, the BCN exhibits only moderate reaction kinetics with around  $k_2 \sim 10^{-1} M^{-1}s^{-1}$  for the SPAAC and  $k_2 \sim 10^2 M^{-1}s^{-1}$  for the SPIEDAC.<sup>168,169</sup> The BCN<sup>endo</sup> label was commercially available as its NHS carbonate **171**.

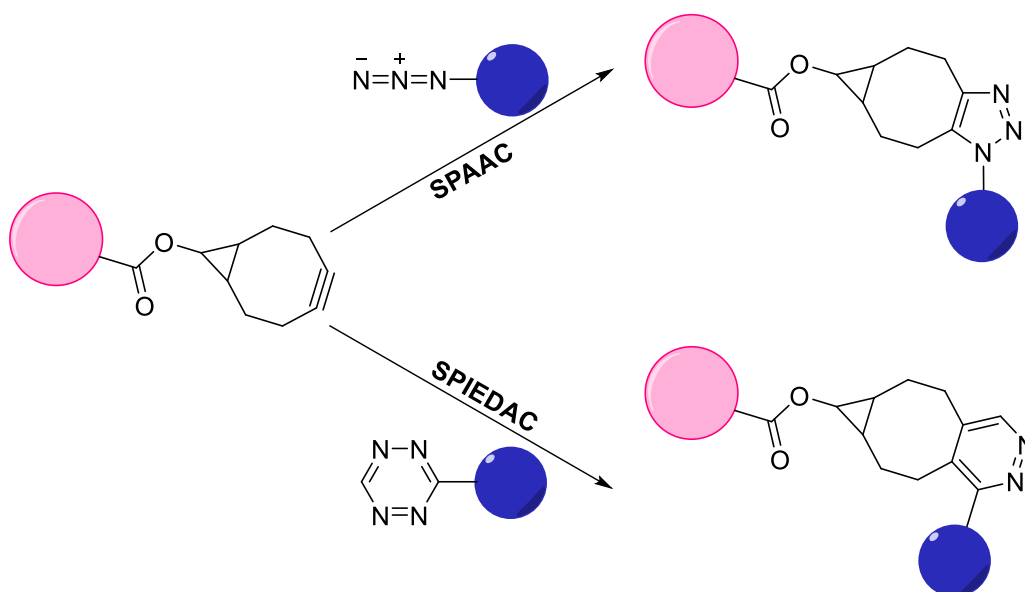
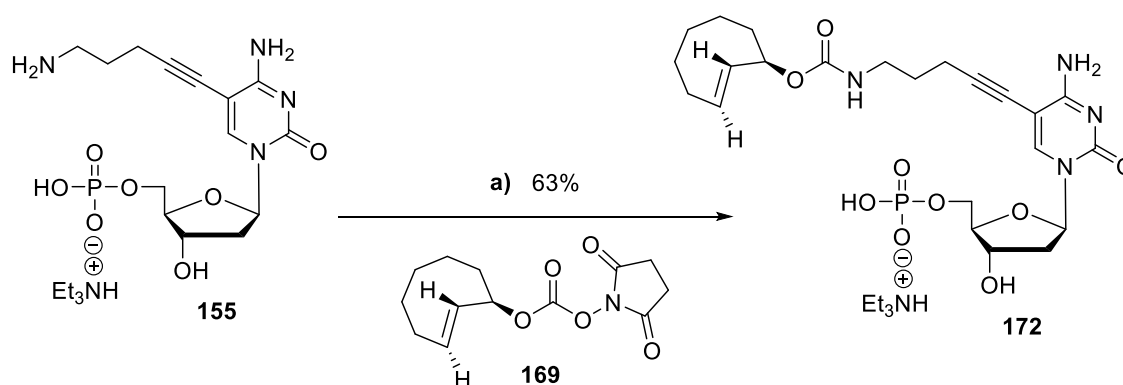
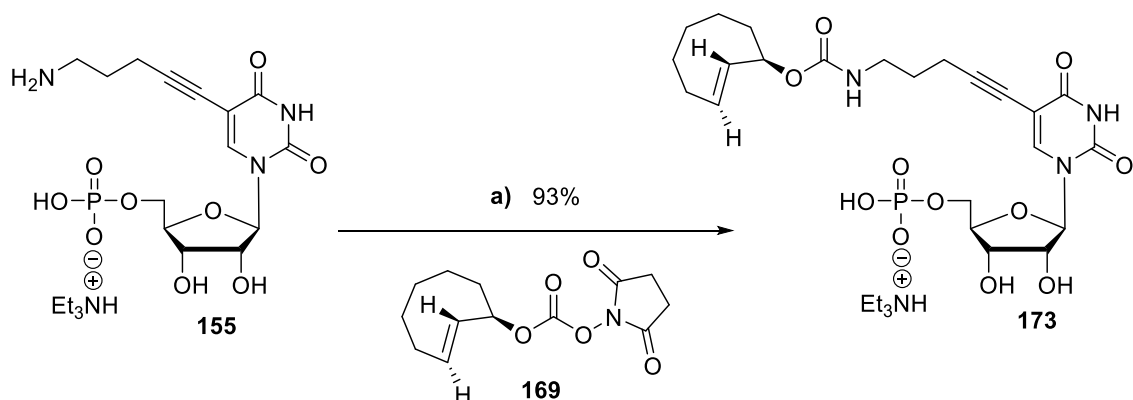


Figure 52: Reaction of BCN with an azide (SPAAC) or a tetrazine (SPIEDAC).

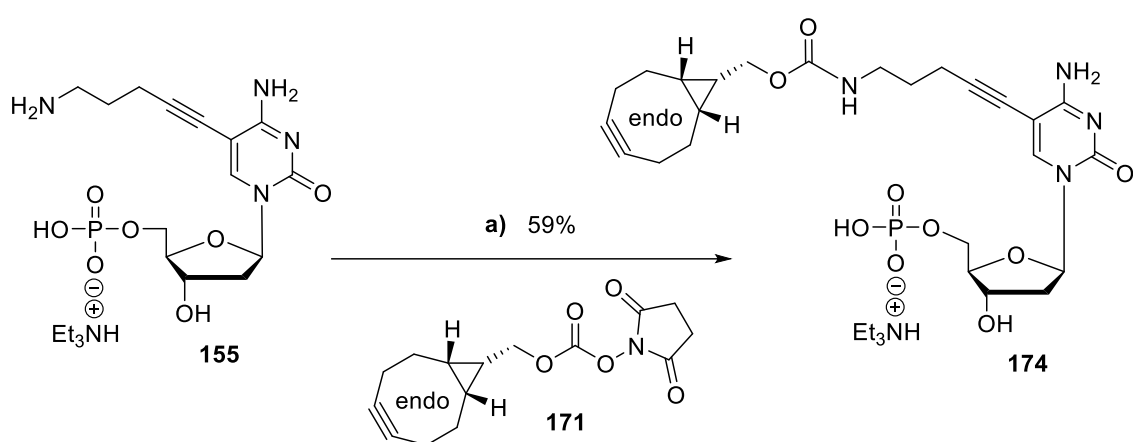
With all building blocks at hand, the first step consisted of the introduction of bioorthogonal functions to the respective linker-functionalized MP multitool precursors **155** by carbamate bond formation. In short, the respective couplings via NHS chemistry were performed in DMSO with triethylamine present. The solvent was chosen to ensure the solubility of the monophosphate. All three coupling reactions showed complete conversion of starting material within one hour at room temperature. After removing DMSO at 50 °C under an oil pump vacuum, the crude products were isolated on RP<sub>18</sub> silica gel with a gradient of 0.05 M TEAB in acetonitrile. The TEAH salts of **172**, **173**, and **174** were obtained in moderate to excellent yields of 59%, 63%, and 93%, respectively.



Scheme 43: Synthesis of 2TCO $\alpha$ -dCMP **172**. Reagents and conditions: a) 2TCO $\alpha$ -NHS **169**, Et<sub>3</sub>N, DMSO, rt, 30 min.

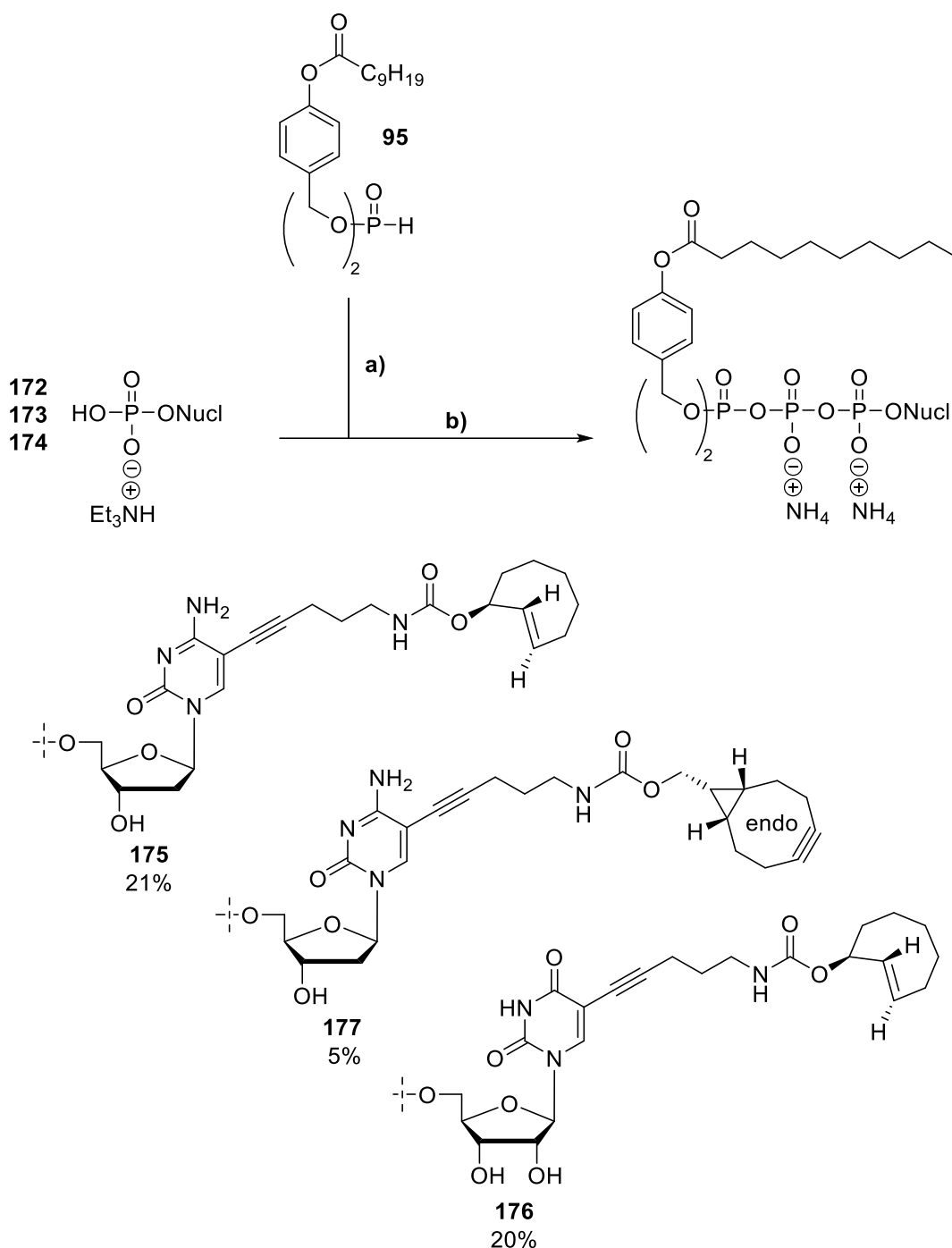


Scheme 44: Synthesis of 2TCO $\alpha$ -UMP **173**. Reagents and conditions: a) 2TCO $\alpha$ -NHS, Et<sub>3</sub>N, DMSO, rt, 1 h.



Scheme 45: Synthesis of BCN<sup>endo</sup>-dCMP **174**. Reagents and conditions: a) BCN<sup>endo</sup>-NHS carbamate **171**, Et<sub>3</sub>N, DMSO, rt, 30 min.

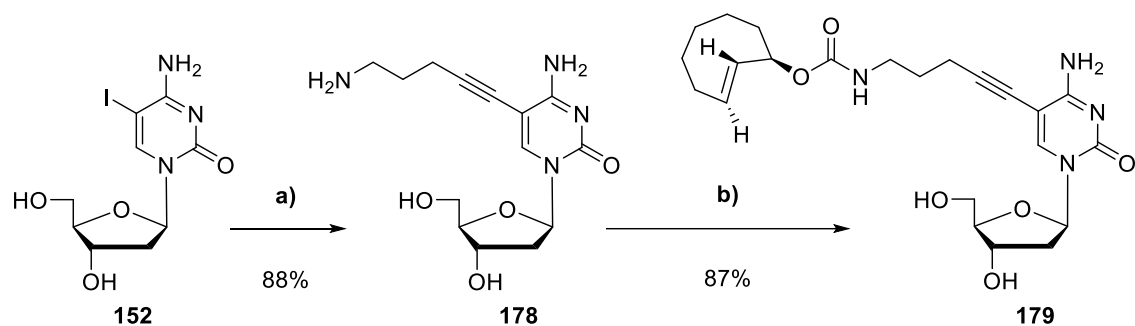
The corresponding  $\gamma$ -(C9C9AB)-TriPPPro compounds were synthesized using the *H*-phosphonate route. Deviating from standard conditions in acetonitrile only, the second pyrophosphate activation step with 1-methylimidazole was carried out in DMF to improve the solubility of the respective nucleoside monophosphate. The coupling reactions were terminated after 3 h by removing all volatiles under reduced pressure. The usual work-up procedure afforded the pronucleotide compounds **175**, **176**, and **177** in moderate to low yields of 21%, 5%, and 20%, respectively. In the case of  $\gamma$ -(C9C9AB)-BCN<sup>endo</sup>-dCTP, the meager yield could partially be explained by the relatively low solubility of the monophosphate starting material before the coupling reaction. Moreover, it became evident during the work-up procedure that larger portions of BCN<sup>endo</sup>-dCMP **177** were not consumed during the reaction. In the future, it might be reasonable to enhance the solubility of the monophosphate salt by changing the counter ions to Bu<sub>4</sub>N<sup>+</sup> and, in addition, tightly control the reaction conversion by RP<sub>18</sub> HPLC monitoring.



Scheme 46: Synthesis of  $\gamma$ -(C9C9AB)-2TCO $\alpha$ -dCTP **175**,  $\gamma$ -(C9C9AB)-BCN<sup>endo</sup>-dCTP **177**, and  $\gamma$ -(C9C9AB)-2TCO $\alpha$ -UTP **176** by *H*-phosphonate route.<sup>126</sup> **Reagents and conditions:** a) i) NCS, CH<sub>3</sub>CN, 50-60 °C; ii) 0.4 M mono-tetrabutylammonium phosphate in CH<sub>3</sub>CN, rt; b) TFAA, Et<sub>3</sub>N, CH<sub>3</sub>CN, 0 °C, 10 min; ii) 1-methylimidazole, Et<sub>3</sub>N, DMF, 0 °C to rt; iii) NMP (TEAH salt) in DMF, CH<sub>3</sub>CN, rt; iv) RP<sub>18</sub> column chromatography, ion-exchange to ammonia, RP<sub>18</sub> column chromatography.

Due to the promising imaging results provided by  $\gamma$ -(C9C9AB)-2TCO $\alpha$ -dCTP **175**, its parent nucleoside 2TCO $\alpha$ -dC **179** was synthesized to serve as a control to inform on the hypothesized “bottleneck” of endogenous kinases and the necessity of the TriPPPPro concept. Therefore, the linker-motif was introduced to IdC **152** by conducting a SONOGASHIRA cross-coupling with 1-amino-4-pentyne under the standard conditions

applied in this work. The 5-(5-aminopent-1-yn-1-yl)-2'-deoxycytidine **178** was isolated on RP<sub>18</sub> silica gel with a good yield of 88%. Subsequent functionalization by NHS chemistry was performed in DMF with a few drops of DMSO to improve the nucleoside's solubility. Reaction progress was controlled by TLC and showed full consumption of **178** after 2 h at room temperature. The nucleoside reporter 2TCO $\alpha$ -dC **179** was isolated on RP<sub>18</sub> silica gel in a good yield of 87%.



Scheme 47: Synthesis of 5-(5-aminopent-1-yn-1-yl)-dC **178** by SONOGASHIRA cross-coupling and subsequent functionalization to obtain 2TCO $\alpha$ -dC **179**. **Reagents and conditions:** a) Pd<sub>2</sub>(dba)<sub>3</sub> (5.4 mol%), tri(2-furyl) phosphine (12 mol%), CuI (15 mol%), 1-amino-4-pentyne, Et<sub>3</sub>N (7 equiv), DMSO, 60 °C, 2 h; b) 2TCO $\alpha$ -NHS, Et<sub>3</sub>N, DMF with drops of DMSO, rt, 2 h.

#### 4.4.4 $\gamma$ -(C9C9AB)-MeTz-(*E*)-dUTP synthesis

In 2014, DEVARAJ *et al.* reported on the *in situ* synthesis of (*E*)-3-substituted 6-alkenyl-1,2,4,5-tetrazine derivatives through an elimination–Heck cascade reaction.<sup>94</sup> Besides highly fluorogenic tetrazine-fluorophore conjugate probes, which provide high fluorescent “turn-on” when reacted with dienophiles (described in Chapter 2.7), DEVARAJ *et al.* also synthesized TBDMSO-protected nucleoside **180** (see Figure 54) to prove the range provided by their synthetic approach. To the best of our knowledge, no further attempts were made to study the properties of this tetrazine conjugated nucleoside for bioorthogonal labeling applications. Comparable reaction stability and kinetic studies were carried out with (*E*)-3-methyl-6-styryl-*s*-tetrazine **181**. The compound showed almost no degradation in PBS buffer throughout 48 h and overall good stability in the presence of the thiol cysteine (1 mM, 90% of **181** remaining after three hours). When reacted with an excess of (*E*)-cyclooct-4-enol **182**, second-order rate constants were specified with  $k_2 \geq 100 \text{ M}^{-1}\text{s}^{-1}$ , consistent with the general observation for this bioorthogonal duo.

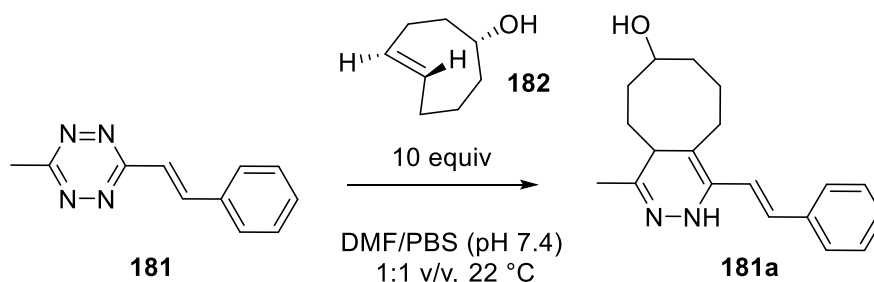


Figure 53: Reaction schema of (*E*)-3-methyl-6-styryl-*s*-tetrazine **181** with (*E*)-cyclooct-4-enol **182** for kinetic characterization.

Based on this report, the tetrazine conjugated nucleoside **180** appeared to be another suitable nucleoside reporter that provides the potential for live-cell imaging. Therefore, the objective was to develop a synthetic route to the corresponding TriPPPPro compound. Since protection of the nucleosidic OH-groups was needed for the elimination–Heck cascade reaction, TBDMSO-protected IdU **183** should be obtained from the corresponding nucleoside IdU **63** by silylation. The introduction of the tetrazine motif should be generated by the elimination–Heck cascade reaction as described by DEVARAJ *et al.* with mesylated 3-hydroxyethyl-6-methyltetrazine **190**. In the following step, the 5'-hydroxyl function should be selectively desilylated to **184** to ensure regioselective 5'-*O*-phosphorylation. The NMP **185** should be generated using phosphoramidite chemistry with bis(fluorenylmethyl)phosphoramidite **87** as described

by JESSEN *et al.* and subsequently treated with TreatHF to remove the second silyl group, providing **186**. The final  $\gamma$ -(C9C9AB)-MeTz-(*E*)-dUTP **187** should be obtained by applying the *H*-phosphonate route.

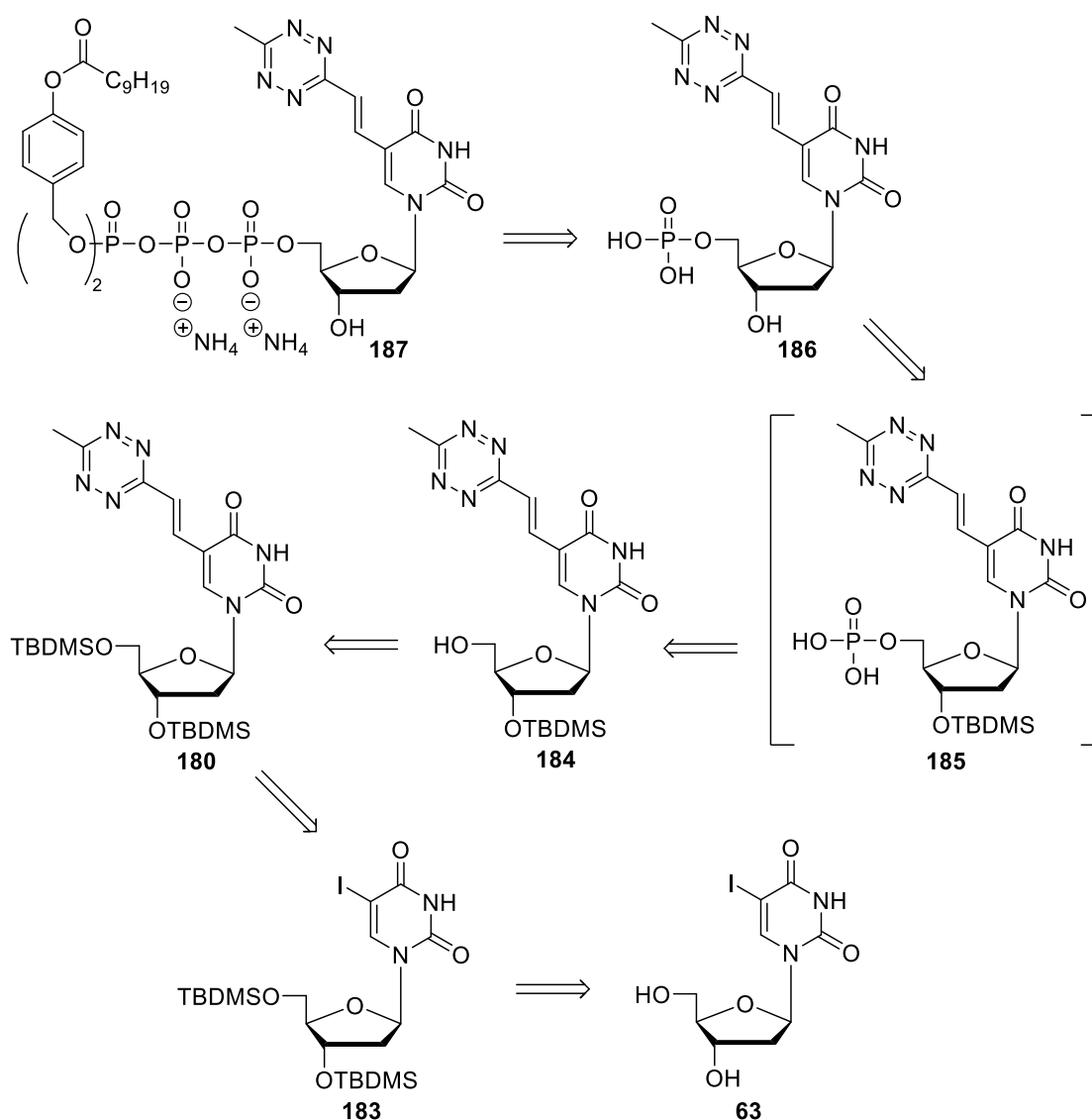


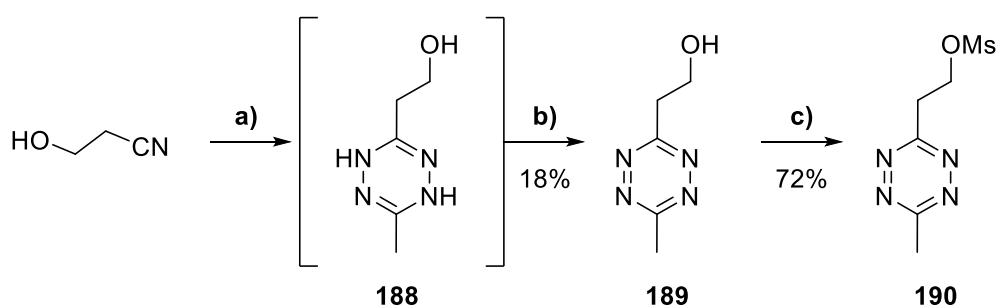
Figure S4: Retrosynthetic scheme for the synthesis of  $\gamma$ -(C9C9AB)-MeTz-(*E*)-dUTP **187**.

First, the asymmetric 6-methyl-3-hydroxyethyl-*s*-tetrazine **189** was synthesized according to literature.<sup>59</sup> Zinc triflate was used to catalyze the one-pot synthesis of 1,2,4,5-tetrazines from inactivated nitriles and hydrazine hydrate.<sup>170</sup> In short,  $\beta$ -cyanoethanol was reacted with hydrazine hydrate and acetonitrile, catalyzed by Zn(OTf)<sub>2</sub> in 1,4-dioxane at 60 °C for 16 h in a sealed pressure tube. The formed dihydrotetrazine **188** was oxidized by NaNO<sub>2</sub> under hydrochloric acid addition. The formed 6-methyl-3-hydroxyethyl-*s*-tetrazine **189** was isolated after extraction and purification on silica gel in a yield of 18%. Literature conditions with anhydrous hydrazine provided **189** in 26% yield.<sup>59</sup> Obtaining higher yields for asymmetric tetrazines



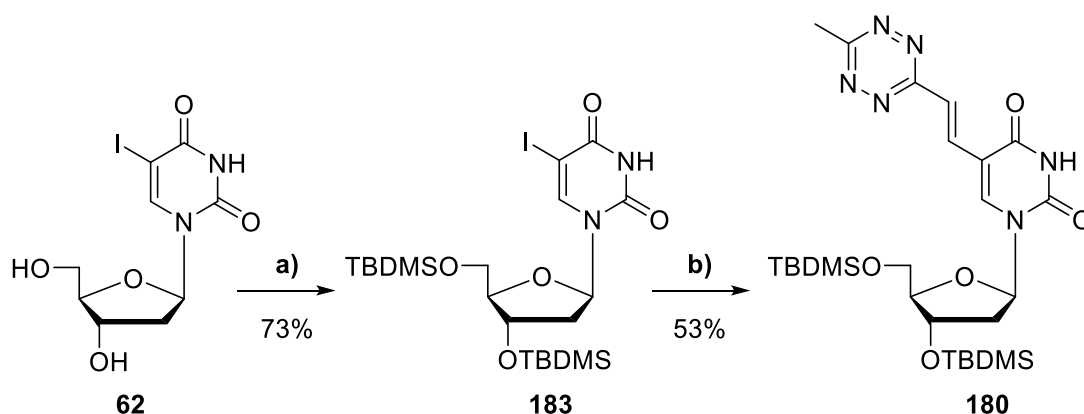
is challenging due to the simultaneous formation of the symmetric by-products (here, volatile 3,6-dimethyl-*s*-tetrazine and polar 3,6-dihydroxyethyl-*s*-tetrazine).

Next, the mesylate **190** was generated according to literature procedures by reacting **189** with methanesulfonyl chloride in dichloromethane in the presence of triethylamine.<sup>171</sup> The mesylate **190** was obtained in 72% yield after column chromatography.



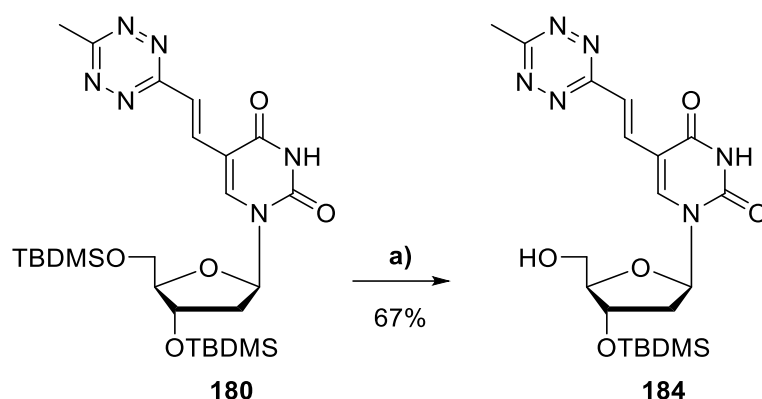
Scheme 48: Preparation of mesylate **190**. **Reagents and conditions:** a) acetonitrile, hydrazine-hydrate, Zn(OTf)<sub>2</sub>, 1,4-dioxane, 60 °C, 16 h.; b) NaNO<sub>2</sub> in water, 1M HCl, 0 °C to rt; c) MsCl, Et<sub>3</sub>N, CH<sub>2</sub>Cl<sub>2</sub>, rt.

The silylation of IdU **63** was performed under standard conditions with TBDMSCl in DMF in the presence of imidazole.<sup>172</sup> Purification on silica gel provided the protected nucleoside **183** in 73% yield. The following elimination–Heck cascade reaction was performed in analogy to the reported conditions with Pd<sub>2</sub>(dba)<sub>3</sub> as a catalyst, the ferrocene ligand QPhos, mesylate **190**, and the base *N,N*-dicyclohexylmethylamine in DMF. In contrast to the literature, no microwave irradiation was employed to reduce by-product formation. Extraction and purification on silica gel resulted in the protected MeTz-(*E*)-dU **180** in 53% yield, which is comparable to the reported yield of 47%.<sup>94</sup>



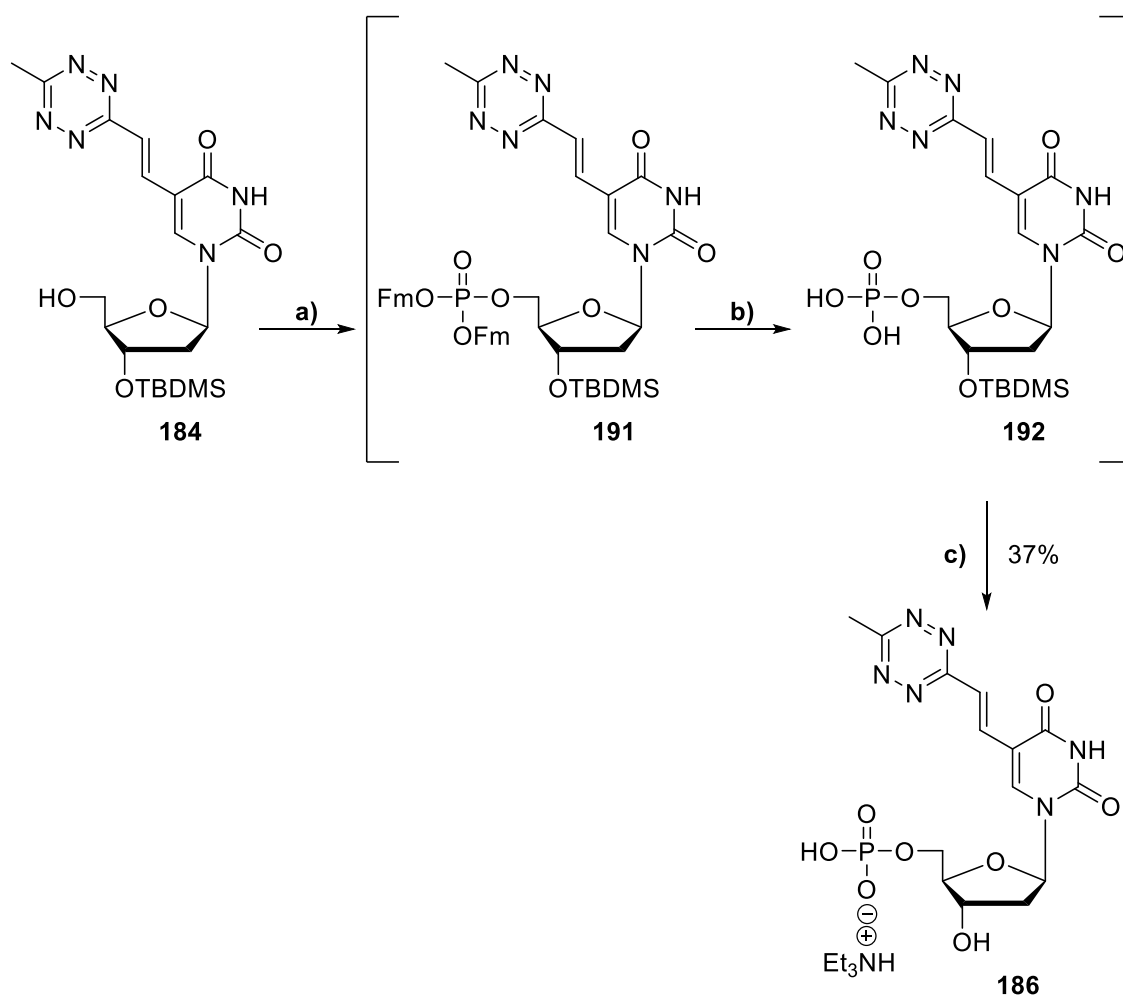
Scheme 49: Preparation of silyl-protected nucleoside **180**. **Reagents and conditions:** a) TBDMSCl, imidazole, DMF, rt; b) Pd<sub>2</sub>(dba)<sub>3</sub> (20 mol%), QPhos (40 mol%), **190**, *N,N*-dicyclohexylmethylamine, DMF, 50 °C.

The selective 5'-desilylation of **180** was achieved by applying the method described by SCOTT *et al.*<sup>173</sup> Hence, silylated nucleoside **180** was treated with aqueous TFA (TFA/H<sub>2</sub>O 1:1 v/v) in twice the volume of THF at 0 °C. Purification on silica gel resulted in the 5'-deprotected MeTz-(*E*)-dU with a moderate yield of 67%. Thin-layer chromatography monitoring revealed the additional formation of the fully deprotected nucleoside. Noteworthy, applying the orthogonal protective group strategy described in Chapter 4.1, which comprised the acetylation of the 3'-hydroxyl function, was not helpful since the deacetylation under basic conditions led to decomposition of the base-labile tetrazine motif.



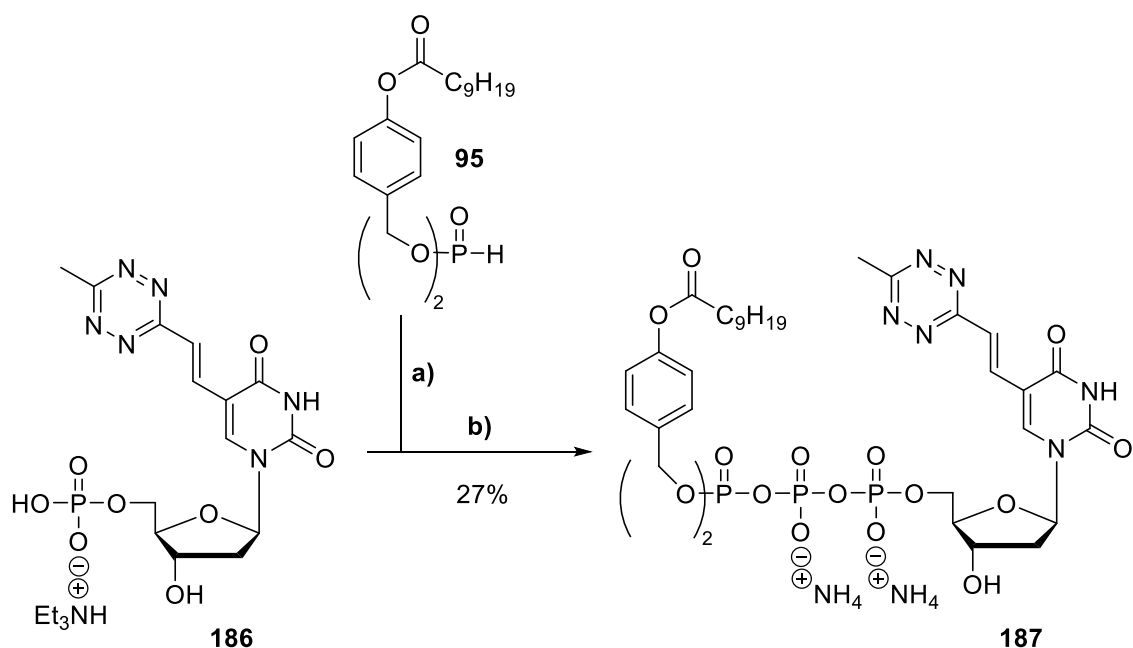
Scheme 50: Selective 5'-deprotection to nucleoside **184** according to SCORR *et al.*<sup>173</sup> **Reagents and conditions: a)** (TFA/H<sub>2</sub>O 1:1 v/v)/THF (1:2 v/v), 0 °C, 6 h.

For the monophosphorylation, the 5'-deprotected MeTz-(*E*)-dU **184** was solved in acetonitrile under the addition of dichloromethane. The reaction of bis(fluorenylmethyl) phosphoramidite **87** and **184** was mediated by DCI, followed by oxidation with *t*-BuOOH after complete conversion. The Fm-groups of **191** were deprotected under mild basic conditions with 5% piperidine in DMF. After 10 min at room temperature, full deprotection was achieved (TLC monitoring), and the piperidine salt of **192** was precipitated by the addition of diethyl ether. The crude NMP was collected and eluted through a short silica column to provide the intermediate **192** (H<sup>+</sup> salt), which was directly desilylated by TreatHF treatment in THF. The TEAH salt of monophosphate **186** was isolated by RP<sub>18</sub> column chromatography in a moderate yield of 37%.



Scheme 51: Monophosphorylation of **184** according to JESSEN *et al.*<sup>148</sup> and subsequent desilylation. **Reagents and conditions:** **a)** i) bis(fluorenylmethyl)phosphoramidite in  $\text{CH}_2\text{Cl}_2$ , 0.25 M DCI in  $\text{CH}_3\text{CN}$ ,  $\text{CH}_3\text{CN}:\text{CH}_2\text{Cl}_2$  (3:1 v/v), 40 °C; ii) 5.5 M *t*-BuOOH in decane,  $\text{CH}_3\text{CN}:\text{CH}_2\text{Cl}_2$  (3:1 v/v), rt; **b)** i) evaporation; ii) 5% piperidine in DMF, 10 min, rt; iii) precipitation by  $\text{Et}_2\text{O}$  addition; iv) short silica gel column chromatography (1:1 v/v); **c)** TreatHF in THF, rt, o/n.

In the future, the fractions collected after short silica gel column purification should be filtrated through a syringe filter for removal of  $\text{SiO}_2$  traces, which in turn might benefit the subsequent desilylation reaction with trimethylamine trihydrofluorid. Moreover, **186** should be purified on normal phase silica gel to provide the protonated monophosphate since the tetrazine motif is base-labile. The synthesis of  $\gamma$ -(C9C9AB)-MeTz-(*E*)-dUTP **187** was achieved by the *H*-phosphonate route with standard procedures in a yield of 27%. Noteworthy, no triethylamine was added to the reaction mixture during 1-methylimidazole activation to ensure the integrity of the base labile tetrazine motif.



Scheme 52: Synthesis of  $\gamma$ -(C9C9AB)-MeTz-(E)-dUTP **187** by *H*-phosphonate route.<sup>126</sup> **Reagents and conditions:** a) i) NCS, CH<sub>3</sub>CN, 50-60 °C; ii) 0.4 M mono-tetrabutylammonium phosphate in CH<sub>3</sub>CN, rt; b) TFAA, Et<sub>3</sub>N, CH<sub>3</sub>CN, 0 °C, 10 min; ii) 1-methylimidazole, CH<sub>3</sub>CN, 0 °C to rt; iii) NMP (TEAH salt) in DMF, CH<sub>3</sub>CN, rt; iv) RP<sub>18</sub> column chromatography, ion-exchange to ammonia, RP<sub>18</sub> column chromatography.

The compound  $\gamma$ -(C9C9AB)-MeTz-(E)-dUTP **187** was the last synthesized pronucleotide reporter, which bears a bioorthogonal handle, and completed the set of two tetrazine-conjugates probes. The following figure provides an overview of the synthesized TriPPPro compounds.

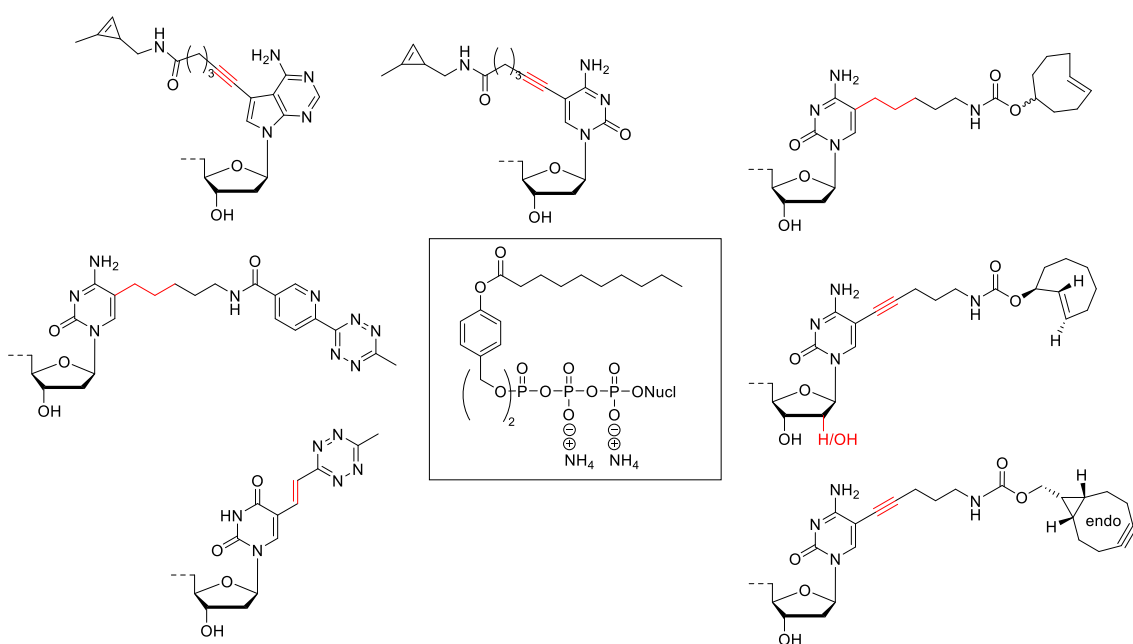


Figure 55: Overview of the bioorthogonally functionalized TriPPPro compounds.

The linkage to the nucleobase is highlighted in red. The 1MCP-functionalized pronucleotides comprise the alkyne-linker since the whole modification was introduced via SONOGASHIRA cross-coupling, not allowing subsequent hydrogenation due to the strained olefine. The pronucleotides  $\gamma$ -(C9C9AB)-NcTz-dCTP **160** and  $\gamma$ -(C9C9AB)-4TCO-dCTP **163** are bearing the saturated alkane-linkage since the hydrogenated multitool 5-aminopent-1-yl-dCMP **156** was chosen as the initial candidate. Following first imaging results, the last three probes were synthesized comprising the alkyne-motif. The BCN<sup>endo</sup> and 2TCO $\alpha$  handle were introduced to 2'-deoxycytidine. Due to the exciting properties of  $\gamma$ -(C9C9AB)-2TCO $\alpha$ -dCTP **175**, the 2TCO $\alpha$ -motif was also introduced to uridine, providing the RNA probe  $\gamma$ -(C9C9AB)-2TCO $\alpha$ -UTP **176**.

These bioorthogonal pronucleotide reporters at hand, the focus shifted to the synthesis of a pronucleotide reporter probe, which already comprises a conjugated fluorophore. The preparation of such a probe is the subject of the following chapter.

## 4.5 Synthesis of a dye-conjugated TriPPPro compound

As mentioned before, live-cell imaging is often limited due to high background staining since the elimination of unbound fluorophore signals remains challenging. The covalent attachment of a fluorophore to an appropriate nucleotide would eliminate the need for the bioorthogonal reaction, thus reducing background staining. However, the drawback of the concept is the bulkiness of the fluorophore and the related risk of interference with the nature of the biomolecule. Regarding nucleoside reporters in *in vivo* applications, it is indispensable to secure substrate activity and specificity towards the polymerase of interest as well as sufficient phosphorylation to the active triphosphates by the respective kinases. Here, the TriPPPro-concept is employed to bypass the “bottleneck” kinases and allow the direct intracellular release of the active dye-conjugated triphosphate (Chapter 2.8). Furthermore, a relatively long linker motif between the nucleobase and the bulky fluorophore was chosen to increase the reporter molecule's chance of sufficient substrate activity towards the respective polymerase. In short, this work includes the first design and synthesis of a dye-conjugated triphosphate pronucleotide for *in vitro* labeling of newly synthesized DNA (Figure 56).

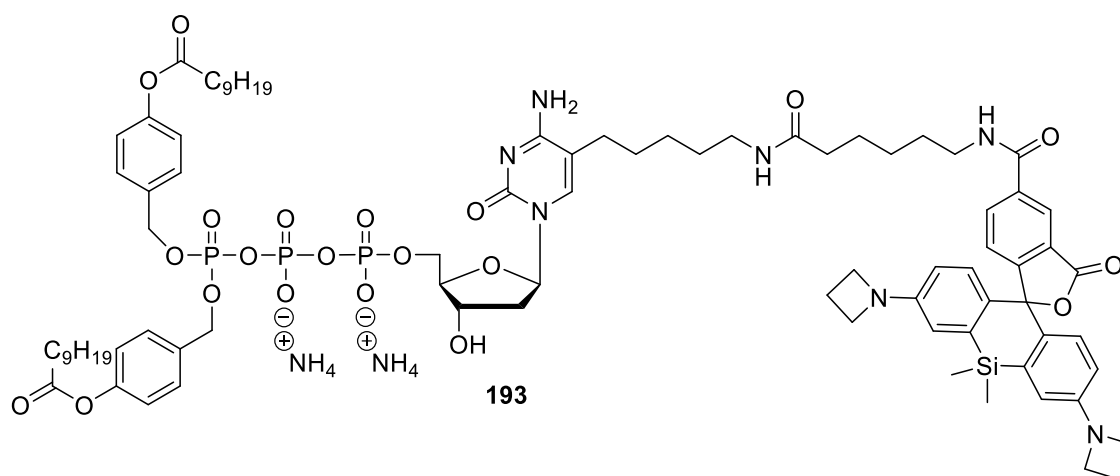
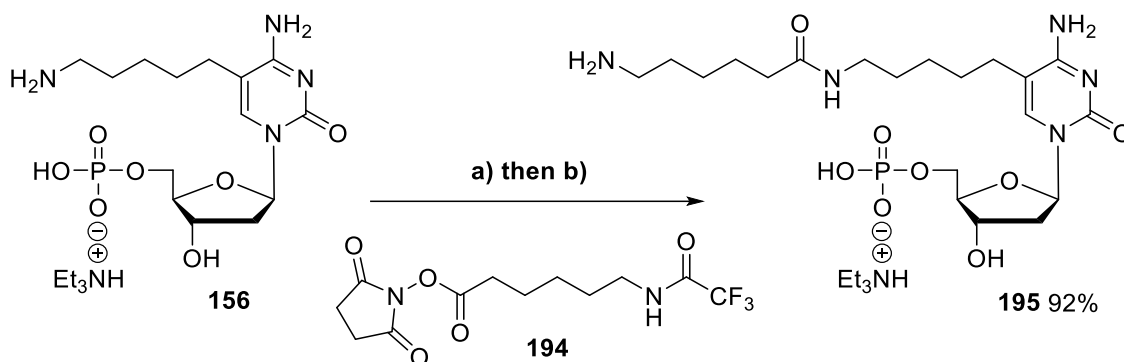


Figure 56: Design of the dye-conjugated TriPPPro compound  $\gamma$ -(C9C9AB)-SiR-dCTP **193**.

As a starting point for the design and synthesis of pronucleotide **193**, the precursor multitool nucleotide **156** was employed. The 5-aminopent-1-yl linker was elongated with a 6-aminohexanoic acid building block **194** via amide bond formation in order to increase the distance between the nucleobase of the 2'-deoxycytidine and the fluorophore. This was achieved by reacting the precursor nucleotide **156** with the trifluoroacetamide protected NHS ester (**194**, synthesized according to literature<sup>174</sup>) in the presence of triethylamine in DMSO. After complete conversion of the precursor

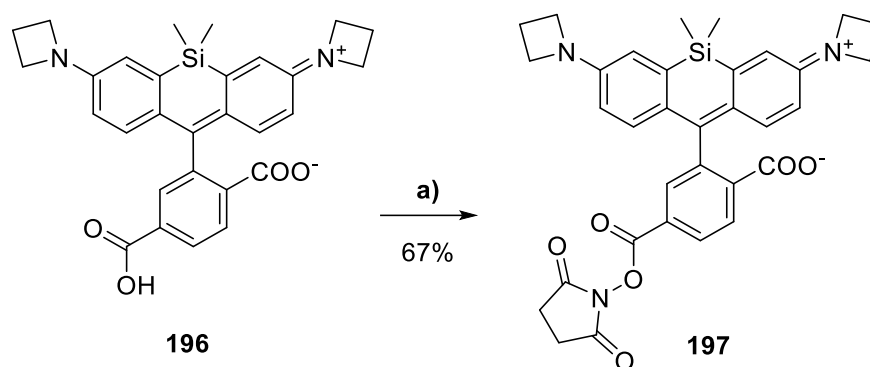
nucleotide **156**, the trifluoroacetamide protective group was cleaved *in situ* under basic conditions with an aqueous 25%  $\text{NH}_4\text{OH}$  solution at room temperature.



Scheme 53: Linker elongation resulting in 5-(6-amino-*N*-hexylhexanamide)-dCMP **195**. Reagents and conditions: a) NHS-ester **194**, Et<sub>3</sub>N, DMSO, rt, 2 h, b) 25%  $\text{NH}_4\text{OH}_{(\text{aq})}$ , rt, o/n.

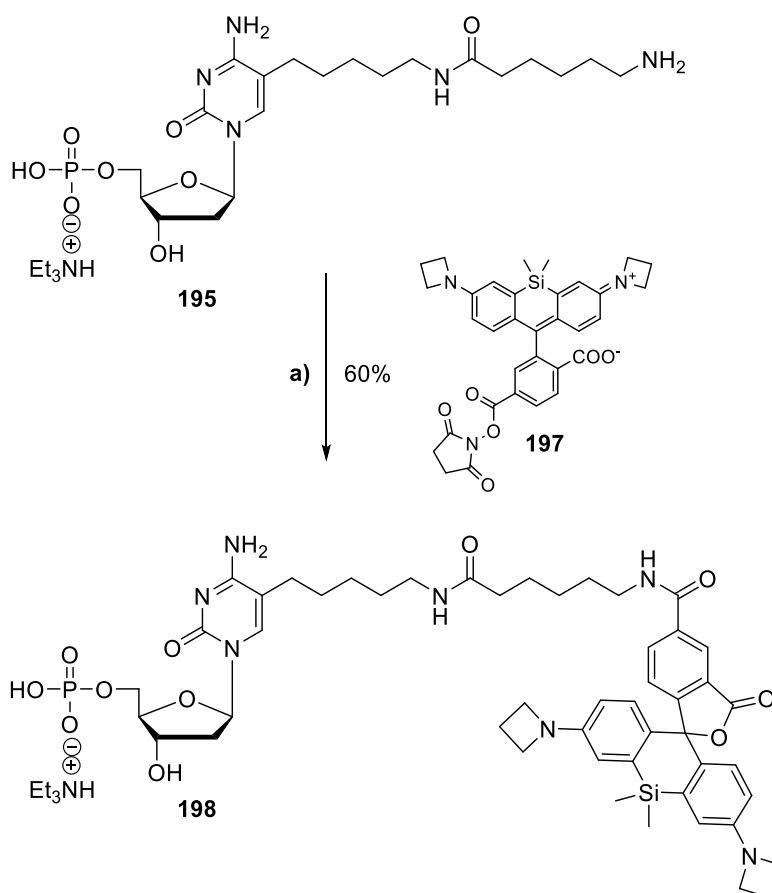
Precipitation of the crude product from DMSO and purification by RP<sub>18</sub> column chromatography (column loading via triethylamine addition) resulted in the respective TEAH salt of monophosphate **195** in an excellent yield of 92%. Next, in a second amide bond formation step, the primary amine of the linker motif can be reacted with the respective NHS-active ester of the desired fluorophore. Here, the silicon-rhodamine dye **196** was employed due to its excellent properties: As described in Chapter 2.7, silicon rhodamine dyes predominantly exist in their closed, uncharged spirolactone form, which enables improved cell-permeability of the probe. The binding to the target results in a more polar environment leading to a substantial increase in fluorescence. Additionally, nonspecific binding to hydrophobic surfaces favors the formation of the non-fluorescent spirolactone, which reduces the background signal and ultimately improves the signal-to-noise ratio of the experiment.<sup>81,87</sup>

The SiR **196** was synthesized according to literature.<sup>175</sup> The silicon-rhodamine was reacted with disuccinimidyl carbonate in DMF in the presence of triethylamine and catalytic amounts of DMAP. The formed NHS active ester **197** was isolated on silica gel in a moderate yield of 67%.



Scheme 54: Synthesis of azetidine-SiR-NHS ester **197**. Reagents and conditions: a) disuccinimidyl carbonate, Et<sub>3</sub>N, DMAP (cat.), DMF, rt, 2 h.

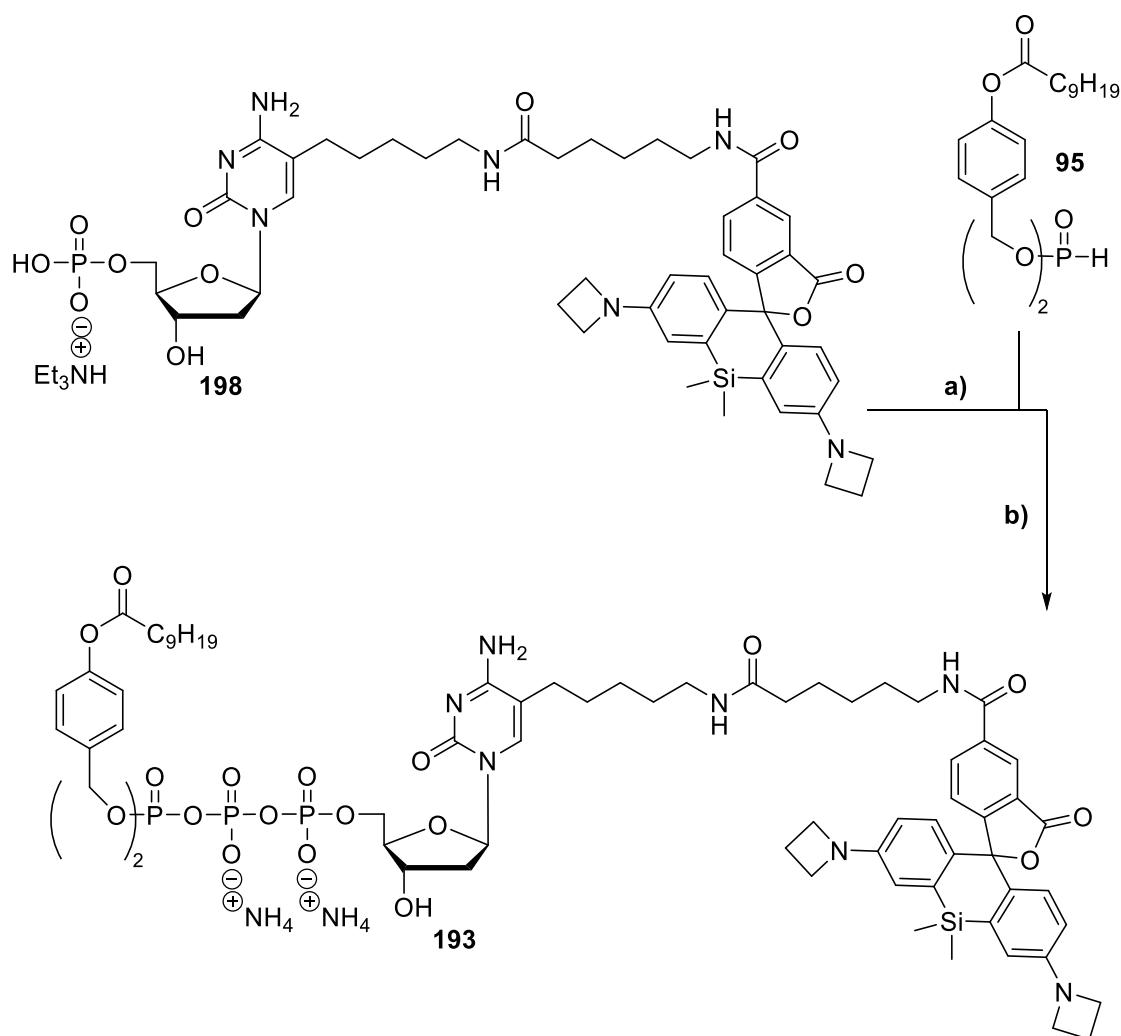
The amide bond formation between building blocks **195** and **197** was achieved in DMF in the presence of triethylamine at room temperature. After two hours and complete conversion of the monophosphate **195**, all volatiles were evaporated, and the crude product was purified on normal phase silica gel with 20% water in acetonitrile. The product containing fractions were concentrated, treated with triethylamine, filtrated through a syringe filter, and evaporated to dryness to provide the TEAH salt of the SiR-conjugated dCMP **198** in 60% yield.



Scheme 55: Synthesis of SiR-dCMP **198**. Reagents and conditions: a) 5-(6-amino-*N*-hexylhexanamide)-dCMP **195** and azetidine-SiR-NHS ester **197**, Et<sub>3</sub>N, DMF, rt, 2 h.



Next, the respective  $\gamma$ -(C9C9AB)-TriPPPro compound **193** was prepared using the *H*-phosphonate route. Here, the second activation step of the pyrophosphate with 1-methylimidazole was carried out in DMF to ensure the solubility of the monophosphate **198** in the following coupling step. Unfortunately, after performing the standard purification protocol, only around 2 mg of product were isolated; hence complete analytical data set and yield specification are not available. However, ESI mass spectrometry confirmed the formation of the desired pronucleotide **193** and HPLC chromatography showed sufficient purity to proceed to *in vitro* studies.



Scheme 56: Synthesis of  $\gamma$ -(C9C9AB)-SiR-dCTP **193** by *H*-phosphonate route.<sup>126</sup> **Reagents and conditions:** a) i) NCS, CH<sub>3</sub>CN, 50-60 °C; ii) 0.4 M mono-tetrabutylammonium phosphate in CH<sub>3</sub>CN, rt; b) TFAA, Et<sub>3</sub>N, CH<sub>3</sub>CN, 0 °C, 10 min; ii) 1-methylimidazole, DMF, 0 °C to rt; iii) NMP (TEAH salt) in DMF, CH<sub>3</sub>CN, rt; iv) RP<sub>18</sub> column chromatography, ion-exchange to ammonia, RP<sub>18</sub> column chromatography.

In part, the loss of product can be attributed to difficulties during chromatography. The zwitterionic nature of the silicon-rhodamine complicate the elution of **193** since a solvent gradient changes the polarity of the environment, which might cause compound

**193** to change its equilibrium on the column. The sudden change of the probe's polarity interferes with its consistent elution, and therefore, complicated purification. It was beneficial to apply isocratic conditions at the point the product started to move on the column (approx. after 1:1 v/v solvent ratio, blue band visible by eye).

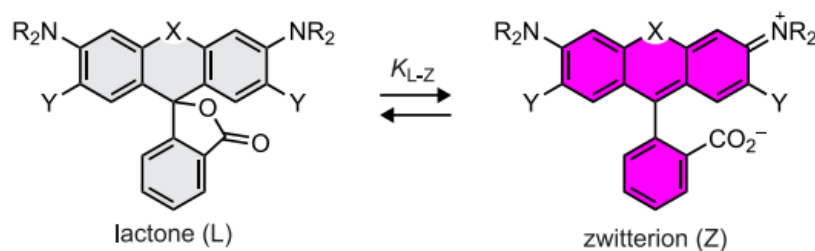
## 4.6 Building dye-tetrazine conjugates

The high demands on dye-tetrazine conjugates were described in detail in Chapter 2.7. In the case of live-cell imaging, a fundamental property of the fluorophore-conjugates must be their cell permeability and even intracellular distribution with as little unspecific binding to cellular compartments as possible.

As described before, the rhodamine-based fluorophores coexist in a lactone-zwitterion equilibrium, which can be mathematically expressed with the constant  $K_{L-z}$ . The closed nonfluorescent lactone (L) is without charge, and therefore responsible for the cell permeability of the fluorophore. Upon binding to the biomolecular targets, the equilibrium shifts to the open fluorescent zwitterionic (Z) form.

The Janelia Science Campus and their scientists synthesized various new rhodamine fluorophores to compare them to existing rhodamines by determining the  $K_{L-z}$  constant (Figure 57). Here, lower constants indicate a more dominant lipophilic lactone form, resulting in an improved diffusion-mediated cellular uptake through the lipophilic cellular membranes. As mentioned before, compared to oxygen-bearing rhodamines, the silicon-rhodamine-based fluorophores are known to show enhanced cell permeability, which is manifested in a low  $K_{L-z} = 0.0012$  for the azetidine-SiR (**entry 2**).<sup>85</sup> Due to this property, the azetidine-SiR **196** was synthesized according to literature during this work.

Furthermore, a silicon-rhodamine based on entry **1** was prepared by conjugation to a tetrazine through a double-bond, showing a high 'turn-on' value upon binding to the target molecule. In addition, the JaneliaFluor dyes JF549 (**entry 6**) and JF526 (**entry 10**) were purchased as their NHS active ester and coupled to a tetrazine motif. Here, the JF526 dye shows a low  $K_{L-z}$  of 0.005, which ranges in the same magnitude as silicon-rhodamines, making the dye an exciting candidate for live-cell imaging.<sup>85</sup>



dye	X	Y	NR <sub>2</sub>	$\lambda_{\text{abs}}$ (nm)	$\lambda_{\text{em}}$ (nm)	$\epsilon_w$ (M <sup>-1</sup> cm <sup>-1</sup> )	$\epsilon_{\text{max}}$ (M <sup>-1</sup> cm <sup>-1</sup> )	$\Phi$	$K_{L-Z}$
1	Si(CH <sub>3</sub> ) <sub>2</sub>	H		643	662	28,200	141,000	0.41	0.0034
2	Si(CH <sub>3</sub> ) <sub>2</sub>	H		646	664	5,000	152,000	0.54	0.0012
3	Si(CH <sub>3</sub> ) <sub>2</sub>	H		635	652	~400	167,000	0.56	<0.0001
4	C(CH <sub>3</sub> ) <sub>2</sub>	H		608	631	99,000	121,000	0.67	0.091
5	C(CH <sub>3</sub> ) <sub>2</sub>	H		585	609	1,500	156,000	0.78	<0.0001
6	O	H		549	571	101,000	134,000	0.88	3.5
7	O	H		525	549	94,000	122,000	0.91	0.068
8	Si(CH <sub>3</sub> ) <sub>2</sub>	H		587	609	2,200	94,000	0.53	0.0043
9	O	F		552	575	95,000	129,000	0.83	0.70
10	O	F		526	550	19,000	118,000	0.87	0.0050

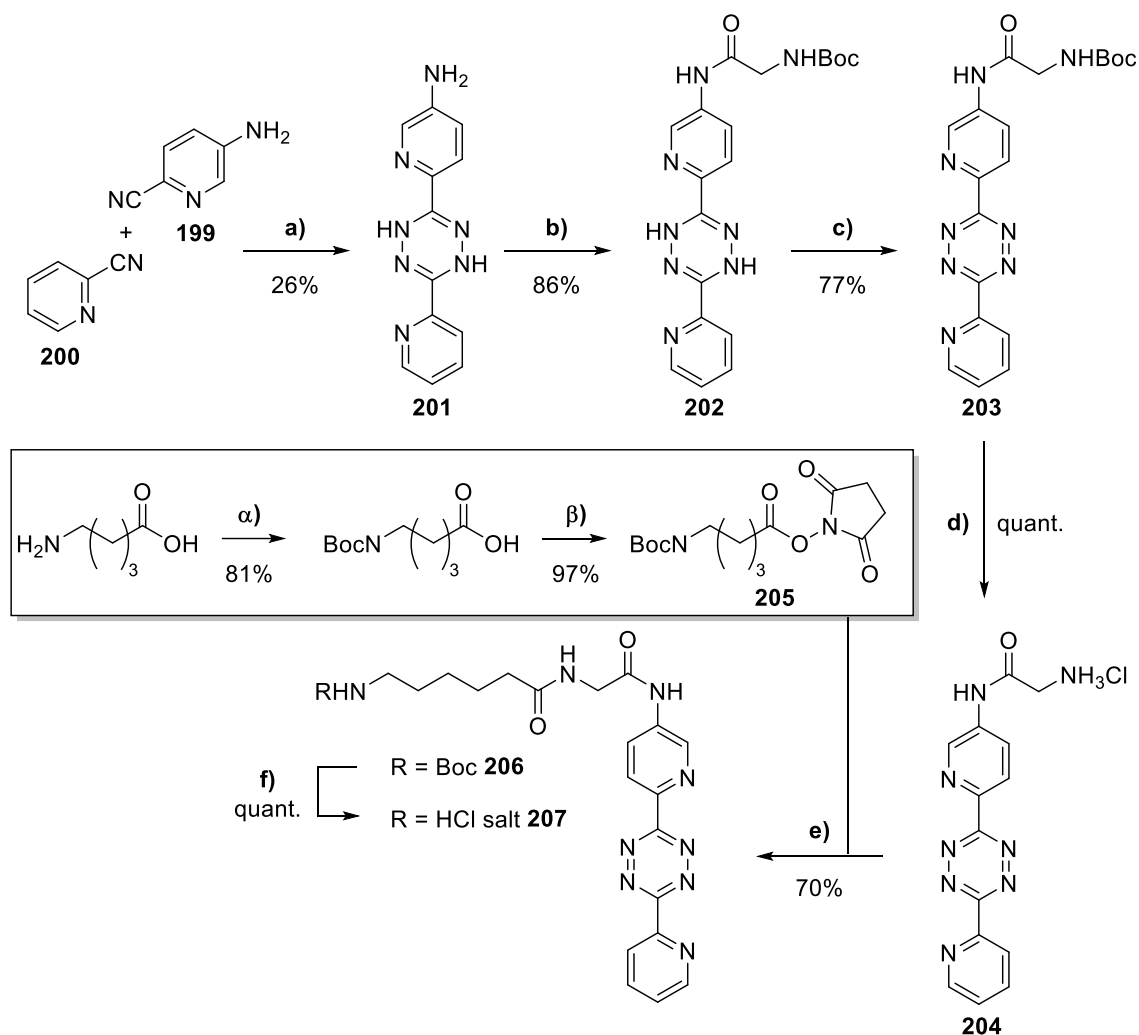
Figure 57: Various modifications (X, Y and NR<sub>2</sub>) on the rhodamine structure and their influence on the absorption maximum ( $\lambda_{\text{abs}}$ ), emission maximum ( $\lambda_{\text{em}}$ ), extinction coefficient ( $\epsilon_{\text{max}}$ ), fluorescence quantum yield ( $\Phi$ ) and the equilibrium constant ( $K_{L-Z}$ ).<sup>85</sup>

The starting point of this work was the publication of LUEDTKE and RIEDER, who labeled newly synthesized cellular DNA with VdU **16** after fixation, permeabilization, and denaturation of the samples. The staining was performed with a TAMRA-Py<sub>2</sub>Tz conjugate, which comprised a long alkyl amide spacer (see **207**).<sup>62</sup> The tetrazine-dye conjugate was provided by LANG *et al.* They used the TAMRA-Py<sub>2</sub>Tz for labeling genetically encoded cell surface proteins, which were modified with norbornene amino acids.<sup>67</sup> The Py<sub>2</sub>Tz linker motif **207** was synthesized during this work and was conjugated to the JaneliaFluor dyes JF549 and JF526 mentioned above (Figure 57, **entry 6** and **10**). As described before, the 3,6-di-2-pyridyl-1,2,4,5-tetrazine **168** is one of the fastest tetrazines due to the electron-withdrawing pyridyl groups. On the downside, the motif

exhibits a significantly lower stability compared to other tetrazines, showing a half-life of only 9 hours in PBS media at 25 °C.<sup>176</sup>

The preparation of the dihydro tetrazine **201** and the subsequent functionalization of the amine group was carried out according to LANG *et al.*<sup>67</sup> Equimolar amounts of 5-amino-2-cyanopyridine **199** and 2-cyanopyridine **200** were reacted with hydrazine hydrate at 90 °C overnight. Purification on silica gel via dry loading resulted in the asymmetric dihydrotetrazine **201** in a yield of 26% (lit. 33%). Higher yields are difficult to achieve due to the formation of both symmetric dihydrotetrazine byproducts. The dihydrotetrazine **201** was then functionalized by reacting with a mixed anhydride formed *in situ* from *N-tert*-butyloxycarbonylglycine and isobutylchloroformate. The product **202** was obtained in 86% yield after normal phase column chromatography (lit. 80%). In contrast to LANG *et al.*, who employed *in situ* generated nitrous gases  $N_xO$  to oxidize the dihydrotetrazine,  $PhI(OAc)_2$  was used as a milder oxidant.<sup>177</sup> The dihydrotetrazine **202** was stirred in dichloroethane in the presence of  $PhI(OAc)_2$  (1.5 equiv) at room temperature overnight. Isolation of the product on silica gel via dry load resulted in the tetrazine **203** in a yield of 77% (lit. 65% with  $N_xO$  gases<sup>67</sup>). According to literature, the amine's deprotection was carried out with 4 N HCl in dioxane in  $CH_2Cl_2$ .<sup>67</sup> Evaporation of all volatiles under reduced pressure resulted in the HCl salt of **204** in quantitative yield.

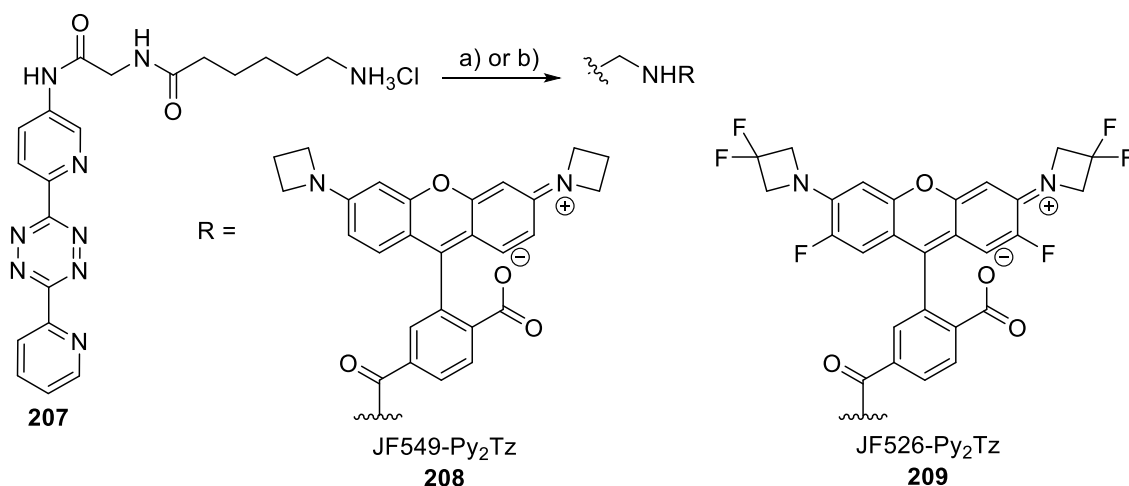
In contrast to LANG *et al.*, who coupled the HCl salt **204** to the TAMRA dye, which already comprised the NHS-active ester activated linker elongation, this work aimed to first introduce the 6-aminohexanoic acid building block to the tetrazine **204**, followed by the amide bond formation with the respective fluorophore NHS active esters. This approach is reasonable since the JaneliaFluor NHS esters are available only at high list prices. Therefore, the Boc-protected NHS-active ester of **205** was synthesized in two steps from 6-aminohexanoic acid and subsequently coupled to tetrazine **204** in the presence of triethylamine in DMF. Purification on silica gel provided compound **206** in 70% yield. Boc-deprotection with 4 N HCl in dioxane and subsequent evaporation of all volatiles resulted in the desired HCl salt **207** in quantitative yield.



Scheme 57: Synthesis of tetrazine-linker conjugate **207**. **Reagents and conditions:** **α)** NaOH, di-*tert*-butyl decarbonate, 1,4-dioxane/H<sub>2</sub>O (2:1 v/v), 0 °C – rt, 3 h; **β)** N-hydroxysuccinimide, EDC, CH<sub>2</sub>Cl<sub>2</sub>, rt, 4 h; **γ)** 64% hydrazine hydrate, 90 °C, o/n; **δ)** *N*-*tert*-butyloxycarbonylglycine, isobutylchloroformate, NMP, 0 °C, THF, 10 min, then **201**, 0 °C – rt, 3 h; **ε)** PhI(OAc)<sub>2</sub>, CH<sub>2</sub>Cl<sub>2</sub>, rt, o/n; **ζ)** 4 N HCl in dioxan, CH<sub>2</sub>Cl<sub>2</sub>, rt, 1 h; **η)** **205**, Et<sub>3</sub>N, DMF, rt, 2 h; **θ)** 4 N HCl in dioxan, CH<sub>2</sub>Cl<sub>2</sub>, rt, 1 h.

The amide bond formation between the HCl salt **207** and the commercially available JaneliaFluor NHS esters **JF549** and **JF526** were carried out in DMSO at room temperature in the presence of a base (DIPEA or Et<sub>3</sub>N). The reactions were employed directly in the purchased vials to avoid the loss of expensive dye. After complete conversion (2-4 h, TLC monitoring), the solutions were transferred to round bottom flasks, and all volatiles were removed *in vacuo* at 50 °C. The resulting residues were taken up in appropriate mixtures of CH<sub>3</sub>OH and CH<sub>2</sub>Cl<sub>2</sub> and loaded onto preparative TLC plates (1 mm thickness). Separation was achieved in constant CH<sub>2</sub>Cl<sub>2</sub>/CH<sub>3</sub>OH (95:5 v/v) and 5% acetic acid additive. The appropriate product bands were scraped from the plates, finely crushed, and transferred to glass columns. The products were washed from the silica gel using CH<sub>3</sub>OH, concentrated *in vacuo*, and filtered through a syringe filter. Evaporation of the

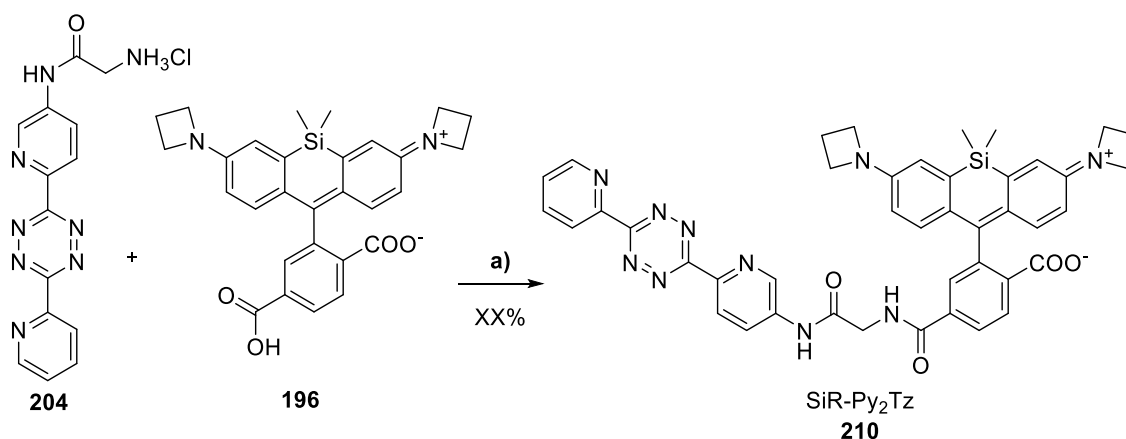
remaining CH<sub>3</sub>OH resulted in the respective JaneliaFluor-Py<sub>2</sub>Tz-conjugates **208** and **209**. The compounds were analyzed via RP<sub>18</sub> HPLC and ESI-MS.



Scheme 58: Synthesis of JF549-Py<sub>2</sub>Tz **208** and JF526-Py<sub>2</sub>Tz **209**. Reagents and conditions: **a)** JF549-NHS, DIPEA, DMSO, rt, 4 h; **b)** JF526-NHS, Et<sub>3</sub>N, DMSO, rt, 2 h.

As described above, the azetidine-SiR-NHS active ester **197** was synthesized during this work due to the property of the silicon-rhodamine to pass through biological membranes. The convergent 8-step synthesis of the azetidine-SiR-COOH **196** is described in detail in literature<sup>175</sup> and will not be described here. Reaction conditions and quantities are listed in the experimental part of this work.

The SiR-Py<sub>2</sub>Tz **210** was synthesized directly from the azetidine-SiR-COOH **196** and the HCl salt **204** by generating the active ester of **204** *in situ* with the HATU peptide coupling reagent. Hence, **204**, **196**, and HATU were added to an Eppendorf tube and dried shortly *in vacuo*. The solids were dissolved in DMF, followed by the addition of Et<sub>3</sub>N. The Eppendorf tube was first placed in a sonicator for 1 h to improve the solubility of the tetrazine **204**. It was then transferred to an incubator set to 37 °C for an additional hour. Subsequently, all volatiles were removed under reduced pressure, and the product was isolated by preparative TLC to provide SiR-Py<sub>2</sub>Tz **210** in 38% yield.



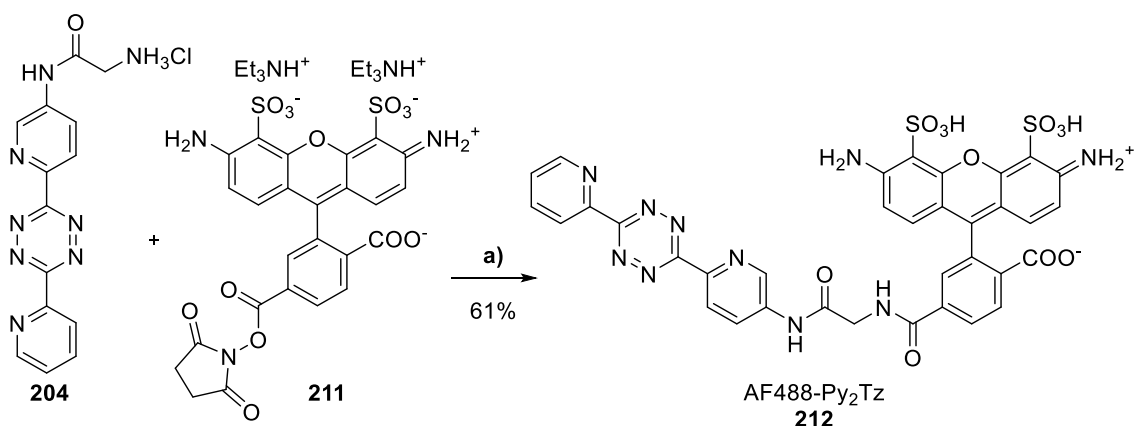
Scheme 59: Synthesis of SiR-Py<sub>2</sub>Tz **210**. Reagents and conditions: a) Azetidine-SiR-COOH **196**, tetrazine **204**, Et<sub>3</sub>N, HATU, DMF, 37 °C, 2 h.

Due to the lipophilic nature of the azetidine-SiR fluorophore, SiR-Py<sub>2</sub>Tz **210** shows relatively strong unspecific background staining of cellular compartments during imaging. It is a common concept that the sulfonation of a fluorophore decreases unspecific cellular binding due to an increase in polarity.<sup>178</sup> This positively influences the contrast in the later image. Naturally, the introduced charges impede the membrane permeability of the fluorophore, thus hindering live-cell imaging applications.

However, for fixed and permeabilized samples, it is valuable to have access to a more hydrophilic rhodamine-Py<sub>2</sub>Tz conjugate, which likely exhibits an improved signal-to-noise ratio.

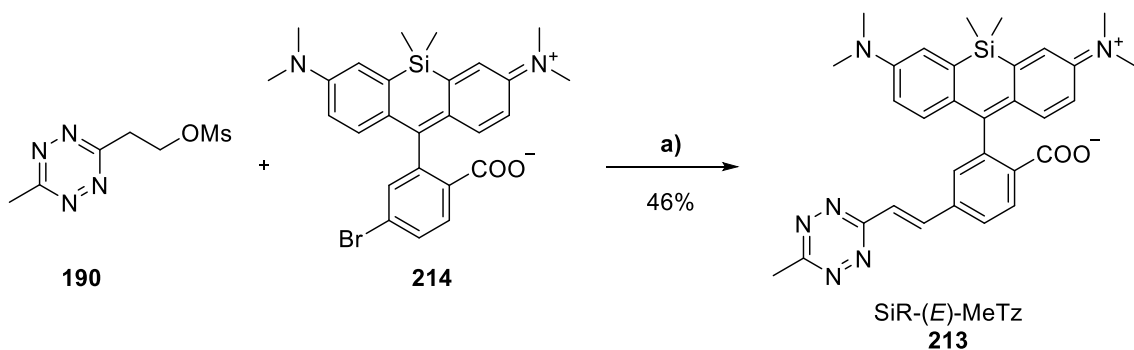
Therefore, the AlexaFlour488-NHS active ester **211** was purchased and coupled to the tetrazine **196**. The amide coupling was carried out in DMSO with triethylamine present. After complete conversion, all volatiles were removed *in vacuo*. The residue was purified on RP<sub>18</sub> silica gel with automated flash chromatography (H<sub>2</sub>O/CH<sub>3</sub>CN; 100:0 to 0:100, low flow, slow gradient, loading with as little acetonitrile in water as possible). The appropriate fractions were subjected to freeze-drying, which provided AF488-Py<sub>2</sub>Tz **212** in a yield of 61%. It should be mentioned that **212** shows poor solubility in most solvents or solvent mixtures due to its amphiphilic nature. Further, attempts to use preparative TLC as a purification method were not successful since the polarity of the sulfate groups prevents the compound from eluting (when employing reasonable solvent mixtures).





Scheme 60: Synthesis of AF488-Py<sub>2</sub>Tz **212**. Reagents and conditions: a) AF488-NHS **211**, tetrazine **196**, Et<sub>3</sub>N, DMSO, 30-40 °C, sonication, 2 h.

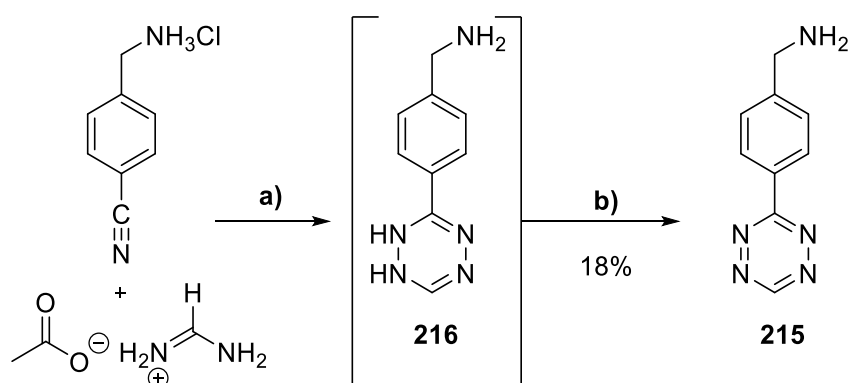
As described in Chapter 2.7, tetrazines are natural quencher moieties of various fluorophores. The quenching effect relies on either the Förster-resonance (FRET) or the through-bond energy transfer (TBET) mechanism. The FRET mechanism requires the absorption band of the tetrazine (between 520-540 nm) to overlap with the emission band of the fluorophore. In theory, TBET-systems are independent of the requirement of overlapping absorption/emission bands and rely only on a suitable covalent, conjugated linkage between the fluorophore and the tetrazine motif. KELE *et al.* described a silicon-rhodamine fluorophore attached to a methyl-substituted tetrazine motif via a double bond. After reacting with a TCO group, the fluorophore system **213** showed a 22-fold fluorescence enhancement. Furthermore, the fluorophore **213** successfully labeled the skeletal protein vimentin<sup>116TAG</sup>-mOrange, which was genetically encoded with cyclooctynylated-lysine (Lys( $\epsilon$ -N-BCN<sup>endo</sup>)). Clear live-cell imaging was possible with concentrations as low as 1.5  $\mu\text{M}$  within 10 min at 37 °C. Importantly, the labeling was specific without strong background staining.<sup>171</sup>



Scheme 61: Synthesis of SiR-(E)-MeTz **213**. Reagents and conditions Pd<sub>2</sub>(dba)<sub>3</sub> (20 mol%), QPhos (40 mol%), *N,N*-dicyclohexylmethylamine, DMF, 40 °C, MW.

Due to these exciting properties, the “turn-on” dye SiR-(*E*)-MeTz **213** was synthesized according to literature from tetrazine mesylate **190** and Br-substituted SiR **214** via an elimination–Heck cascade reaction.<sup>171</sup> As described before in Chapter 2.7, DEVARAJ *et al.* reported on the Heck-type cross-coupling reactions to connect methyl-substituted tetrazines to various fluorophores.<sup>94</sup> The reaction-type was already applied in this work to synthesize MeTz-(*E*)-dUMP **186** from IdUMP **89** and tetrazine mesylate **190** (Chapter 4.4.4). Hence, mesylate **190** was already available, and the Br-substituted SiR **214** was synthesized according to literature<sup>171</sup> in four steps (data not shown). The following elimination–Heck cascade reaction was performed according to the reported conditions with Pd<sub>2</sub>(dba)<sub>3</sub> as a catalyst, the ferrocene ligand QPhos, mesylate **190**, and the base *N,N*-dicyclohexylmethylamine in DMF under microwave irradiation. Preparative TLC provided the SiR-(*E*)-MeTz **213** in 46% yield.

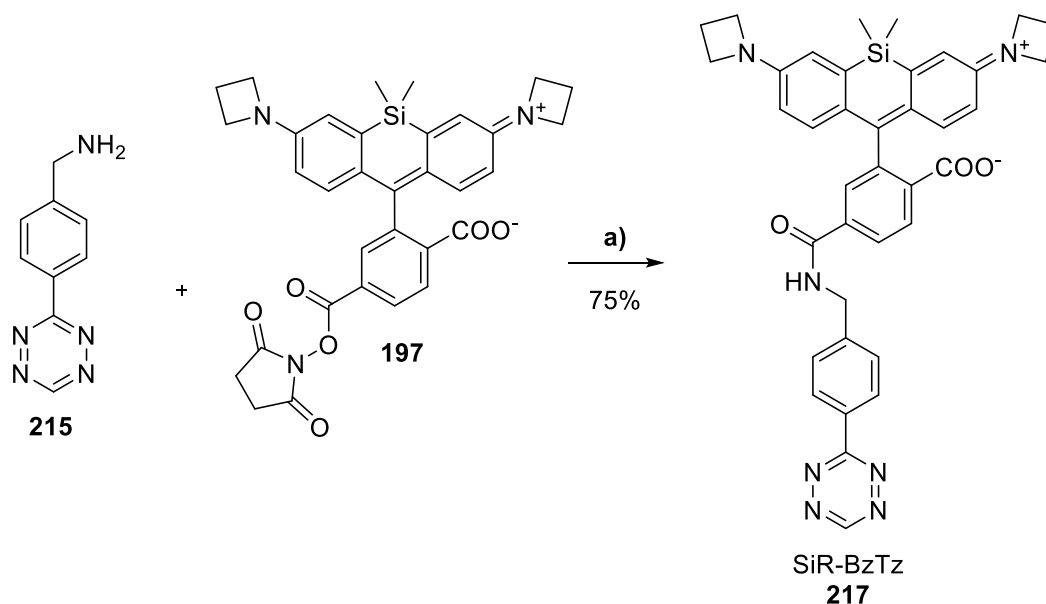
Besides the Py<sub>2</sub>Tz motif, a further tetrazine was synthesized that allowed easy excess to dye-tetrazine conjugates. Benzylamino tetrazine (**215**, BzTz) was chosen, since it provides improved stability compared to the more reactive Py<sub>2</sub>Tz motif. BzTz **215** was synthesized in a “one-pot two-steps” approach from hydrazine hydrate, 4-(aminomethyl)benzotrile hydrochloride, and formamidinium acetate. The reaction was catalyzed by Zn(OTf)<sub>2</sub> as a Lewis acid transition metal catalyst.<sup>170</sup> The oxidation of the 1,2-dihydro-tetrazine intermediate **216** was performed with *in situ* generated nitrous gases (N<sub>x</sub>O) from NaNO<sub>2</sub> under acidic conditions (Scheme 62). The tetrazine **215** was isolated after RP<sub>18</sub> column chromatography in a low yield of 18%.



Scheme 62: One-pot two-steps synthesis of the BzTz motif **215**. Reagents and conditions: a) hydrazine-hydrate (51%), 4-(aminomethyl)benzotrile hydrochloride, formamidinium acetate, ethanol, rt, 72 h; b) NaNO<sub>2</sub>, 1 N HCl, pH set to 2, 0 °C to rt, 1 h.

The amino group provides easy access to rhodamine-dye-conjugates by amide bond formation. Hence, BzTz **215** was reacted with azetidine-SiR-NHS active ester **197** in DMSO in the presence of triethylamine. Subsequently, all volatiles were removed *in*

*vacuo*, and the product was isolated by preparative TLC to provide SiR-BzTz **217** in 75% yield.



Scheme 63: Synthesis of SiR-BzTz **217**. Reagents and conditions: a) Azetidine-SiR-NHS **197**, BzTz **215**, Et<sub>3</sub>N, DMSO, 30-40 °C, sonication, 2 h.

Briefly, a variety of rhodamine-bases tetrazine-conjugates were synthesized. A selection of rhodamines were either purchased or synthesized and coupled to different tetrazine motifs. The rationale behind these fluorophore conjugates varies from improved background in live-cells (SiR-(*E*)-MeTz **213**), or in fixed cells (AF488-Py<sub>2</sub>Tz **212**), over to maximal tetrazine reactivity (SiR-Py<sub>2</sub>Tz **210**, JF549-Py<sub>2</sub>Tz **208** and JF526-Py<sub>2</sub>Tz **209**).

Together with the synthesized pronucleotide reporters, the next step was to study these bioorthogonal tools in cellular imaging experiments, which is the content of the following chapter.

## 4.7 Imaging

The functionalized TriPPP compounds were tested in HSV-1 infected Vero cells. HSV-1 was chosen as the model virus in this work since it has a relatively short replication cycle (~24 h) and a large, double-stranded genome of ~150 kbp. Furthermore, HSV-1 expresses its own herpes DNA polymerase, providing the possibility to observe whether the intracellular released nucleoside triphosphate reporters are substrates for both cellular and viral DNA polymerases. The HSV-1 VP26mCh mutant was used to infect Vero cells. This virus expresses the fluorescent protein mCherry fused to the VP26-capsid protein of the U<sub>L</sub>35 gene ( $\gamma_2$ , not essential). VP26 is a small capsomere-interacting protein, which is located at the surface of the capsid shell.<sup>179</sup> The fluorescent VP26mCh is expressed late during infection. Hence, the accumulation of fluorescent VP26mCh in the nuclear RCs provides a marker for the late stage of the replication cycle of HSV-1 in the host cell during fluorescent microscopy.

Additionally, immunofluorescence staining for the infected cell protein 8 (ICP8), a herpes simplex virus type 1 single-strand DNA-binding protein, provides further opportunity to locate viral DNA replication sites. ICP8 is a multifunctional HSV ssDNA binding protein essential for viral growth and DNA replication.<sup>180,181</sup> Thus, colocalization between immunofluorescent ICP8 signal and tagged incorporated nucleoside reporters would prove successful viral genome labeling.

The “clickable” nucleoside reporters EdU and EdC are frequently used for HSV-1 genome labeling in fixed and permeabilized host cells. DELUCA *et al.* determined the rates of viral DNA replication throughout productive HSV-1 infection.<sup>53</sup> The presented data shows the highest replication rate between 4-8 hpi with ~1919 bp/min. The replication rate decreases slightly at 8-12 hpi to ~1355 bp/min and slows down significantly after 12 hpi (Figure 58). Therefore, metabolic nucleoside reporters are usually added 4 hpi to ensure maximal incorporation rates of the metabolic reporters (not considering possible kinase bottlenecks).

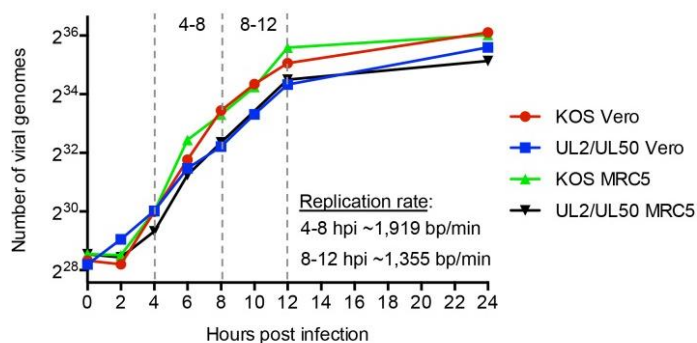


Figure 58: **Rate of viral DNA replication.** MRC5 or Vero cells were infected with KOS or UL2/UL50 HSV-1 and the number of viral genomes per hpi was determined by quantitative PCR.<sup>53</sup>

DELUCA and coworkers treated uninfected (mock-infected) or HSV-1 KOS infected Vero cells with 0 or 2.5  $\mu\text{M}$  EdU for 4-8 hpi. Cells were then fixed and permeabilized, followed by visualizing the cellular DNA by Hoechst staining (*blue*), incorporated EdU by click-chemistry with an AlexaFluor488 dye (*green*), and ICP4 (viral transcription factor 4) by immunofluorescence staining (*red*) (Figure 59).

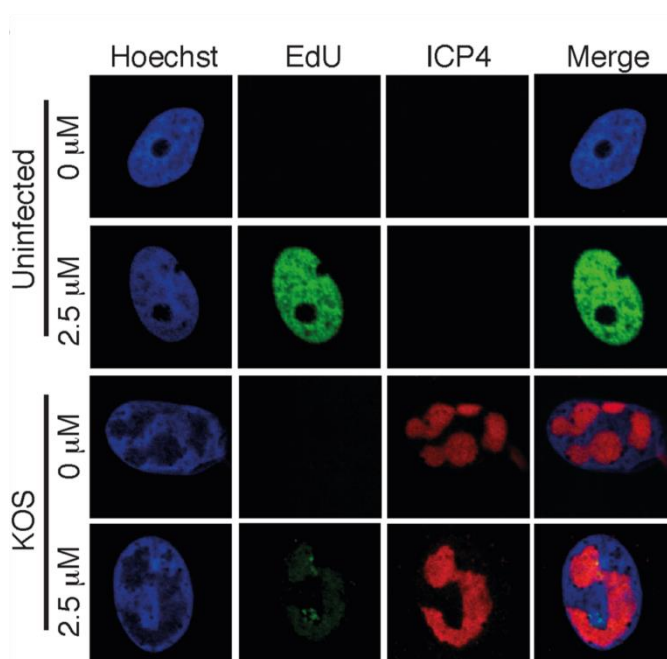


Figure 59: Vero cells were mock-infected or infected with HSV-1 KOS. After 4 hpi, cells were treated with 0 or 2.5  $\mu\text{M}$  EdU for 4 h. After fixation, cells were stained with Hoechst (*blue*) and with AlexaFluor488 azide (*green*). ICP4 was labeled by immunofluorescence. Merged panels show colocalization of viral DNA with ICP4 and the absence of dsDNA (*blue*).<sup>45</sup>

In uninfected Vero cells, EdU is incorporated into *de novo* synthesized cellular DNA, and the EdU/AF488 signal colocalizes with the Hoechst staining throughout the nucleus of the dividing cell. Without EdU present, no specific AF488-staining is observable.

In HSV-1 infected cells, the EdU/AF488 signal is locally restricted to viral RCs inside the host cell nucleus. Since HSV-1 rapidly shuts down host cell gene expression<sup>182</sup>, EdU is not incorporated into cellular DNA of infected cells. Further, the EdU/AF488 signal colocalizes with the ICP4 immunofluorescence signal and is Hoechst negative. The control without EdU present shows no DNA staining.

The same authors later used 20 min EdC pulse experiments to detect viral and cellular factors associated with viral replication. Vero cells were infected with wild-type HSV-1 and labeled with EdC 4 hpi for 20 min. The cells were then fixed, permeabilized, and stained. Cellular DNA was stained with Hoechst (*blue*), EdC labeled DNA was tagged with AlexaFluor488 (*green*), and ICP8 was stained by immunofluorescence (*red*). The *green/red* signals colocalize well, illustrated by plotting the intensities to the drawn red line in the merged channel (Figure 60). Due to the short EdC incubation time, only viral replication forks are labeled instead of whole viral genomes, resulting in a more dotted labeling pattern.<sup>53</sup>

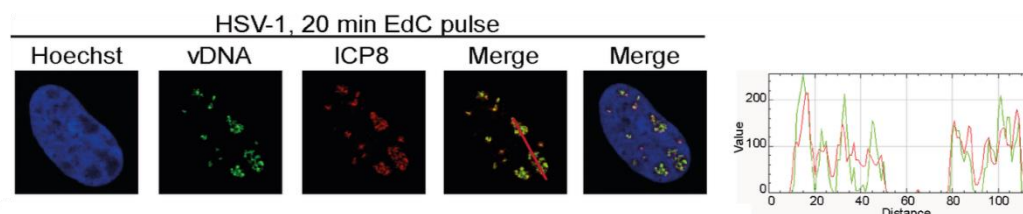


Figure 60: HSV-1 DNA synthesis was labeled with EdC for 20 min after 4 hpi with wild type HSV-1. Infected cells were fixed and stained with AlexaFluor488 azide to visualize viral replication forks (vDNA, *green*). Nuclei were stained with Hoechst (*blue*). ICP8 was labeled by immunofluorescence (*red*). An example for colocalization was generated using the RGB profiler plugin in ImageJ (corresponding to the drawn red line, *green* and *red* channel).<sup>53</sup>

#### 4.7.1 TriPPPPro stability

Due to the enzymatic cleavage mechanism of the bis(AB)-masking units of the TriPPPPro compounds, there were some initial concerns about the extracellular stability of the pronucleotides in serum-containing cell media. Fetal bovine serum (FBS) contains essential growth factors vital for cultured cells' survival, growth, and division. However, a great variety of proteins are present in the FBS media, which might cause the extracellular enzymatically triggered demasking of the TriPPPPro compounds. Early demasking would ultimately hamper the cellular uptake of the pronucleotide reporters and decrease labeling efficiency. Further, the proteins present in FBS may bind TriPPPPro-nucleotides and hence lower the concentration of "free" TriPPPPro-nucleotide that can permeate the cell membrane.

Vero cells were infected with HSV-1 VP26mCh (*red*) in 10% FBS-containing media. To test the influence of FBS, cells were incubated with 5  $\mu$ M  $\gamma$ -(C9C9AB)-1MCP-dCTP **150** either in serum-free DMEM or 10% FBS/DMEM 4 hpi. After 8 hpi, cells were fixed, permeabilized, and processed. The incorporated 1MCP-label was stained overnight with AF488-Py<sub>2</sub>Tz **212** (*green*), followed by immunofluorescence staining of ICP8 (*magenta*). To our delight,  $\gamma$ -(C9C9AB)-1MCP-dCTP **150** enabled strong fluorescence staining of the viral genome, when the TriPPPPro incubation was conducted in the serum-free media (Figure 61, top row, left cell). The 1MCP/AF488 signal colocalizes well with the VP26mCh and the ICP8 signal. Additionally, the 1MCP/AF488 signal is Hoechst negative and shows the typical pattern of viral replication compartments already known from EdU and EdC labeling experiments (e.g., Figure 58). Furthermore, intracellular 1MCP-dCTP is likely to also be a substrate of the cellular DNA polymerase. The 1MCP/AF488 signal of the top-right cell (absence of VP26mCh and ICP8 signal) shows the typical dotted fluorescence pattern deriving from cellular DNA synthesis throughout the nucleus of dividing cells. In contrast, no 1MCP/AF488 signal was detectable when incubation of  $\gamma$ -(C9C9AB)-1MCP-dCTP **150** was conducted in serum-containing media.

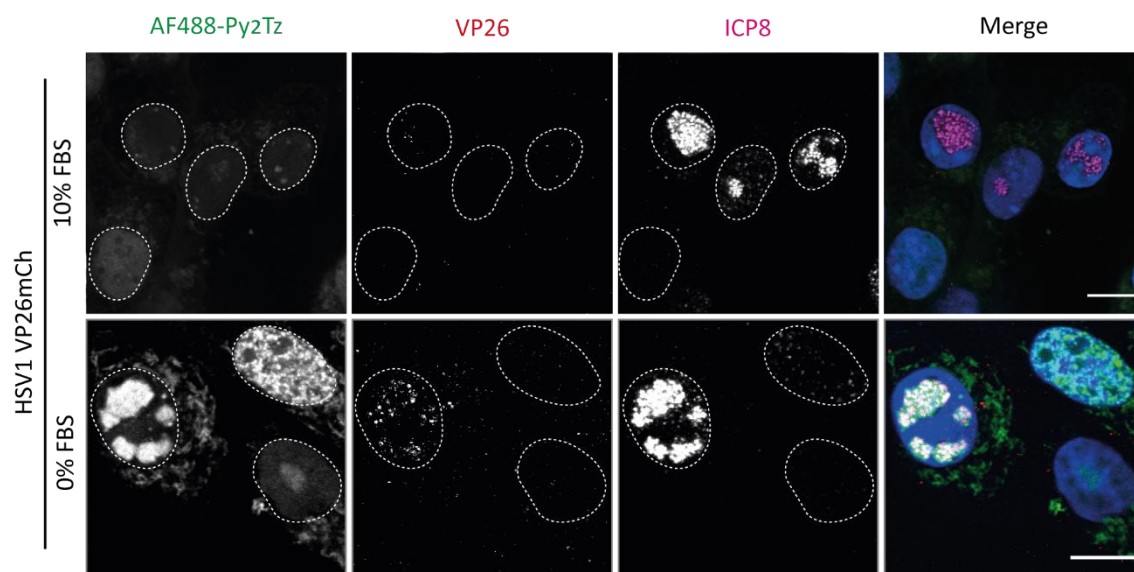


Figure 61: Vero cells were infected with HSV-1 VP26mCh (*red*) (MOI 3). 4 hpi 5  $\mu$ M C9C9AB-1MCP-dCTP **150** was added in either serum-free DMEM or 10% FBS in DMEM. 8 hpi cells were fixed in 4% PFA and permeabilized in 0.1% Triton-X100. The viral genomes containing incorporated 1MCP-dC were stained with Alexa488-Py<sub>2</sub>Tz **212** (*green*). Cells were processed with immunofluorescence for ICP8 (*magenta*), and nuclei were stained with Hoechst (*blue*). Samples were imaged using a Nikon Eclipse Ti2 Spinning disc microscope. Individual channels are shown in greyscale and the merged image is shown in color. Nuclei outlines are circled. Scalebar = 10  $\mu$ m.

These results strongly indicate that rapid extracellular demasking of one or both AB-masking groups occurs in FBS-containing media, or their binding to FBS-proteins, preventing sufficient cellular uptake of the pronucleotide reporters. The unavailability of the TriPPP compounds for membrane permeation from the extracellular medium in the presence of FBS has some consequences since cell viability is diminished without serum present. During the experiment, cells are under significant stress from HSV-1 infection itself and – in addition – from the absence of cellular growth factors. The stress increases cell death of infected cells and ultimately reduces the number of imageable cells over time.

Henceforth, the medium was changed to VP serum-free medium (VP-SFM) during infection with satisfying results. VP-SFM is a serum-free medium with an ultra-low protein concentration (5 µg/mL). The medium contains no proteins, peptides, or other components of animal or human origin. It was developed to grow Vero cells for virus production.<sup>183</sup>



### 4.7.2 TriPPPro screening

The labeling ability of the listed pronucleotide reporters (Figure 62) was studied under the conditions found to generate the best labeling results during these studies. Fluorescent staining was conducted overnight in fixed and permeabilized cells to ensure optimal staining conditions and, therefore, validate the incorporation of the respective reporters. The cyclopropene-functionalized pronucleotides  $\gamma$ -(C9C9AB)-1MCP-dATP **149** and  $\gamma$ -(C9C9AB)-1MCP-dCTP **150** will be discussed in-depth separately in Chapter 4.7.3.

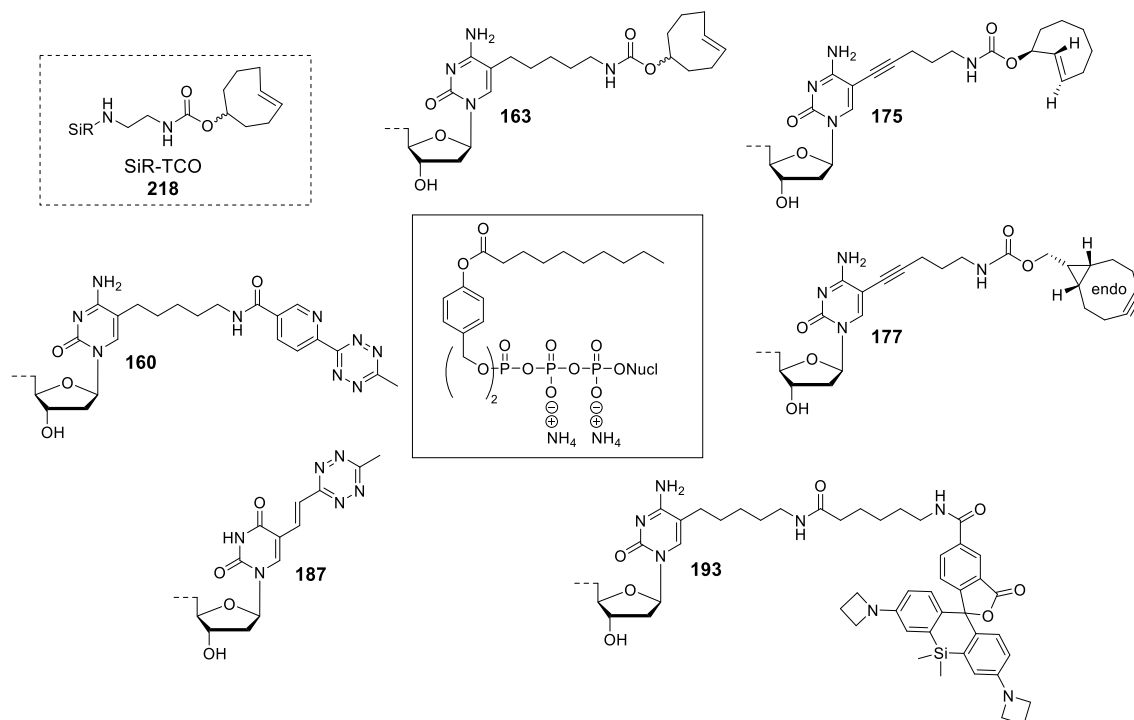


Figure 62: Structures of the pronucleotide reporters discussed in this Chapter.

Vero cells were mock-infected or infected with HSV-1 VP26mCh and treated with 0 (vehicle control) or 5  $\mu$ M of the respective pronucleotide reporter 4 hpi. The pronucleotide medium was renewed after 6 hpi to ensure sufficient availability of reporter during the incorporation phase. After 8 hpi, cells were fixed, permeabilized, and stained with 5  $\mu$ M of AF488-Py<sub>2</sub>Tz **212** (*green*) or commercially available SiR-TCO **218** (*magenta*), respectively. Naturally, no staining was performed for fluorescent pronucleotide  $\gamma$ -(C9C9AB)-SiR-dCTP **193**. The following day, the samples were washed and stained for dsDNA with Hoechst (*blue*).

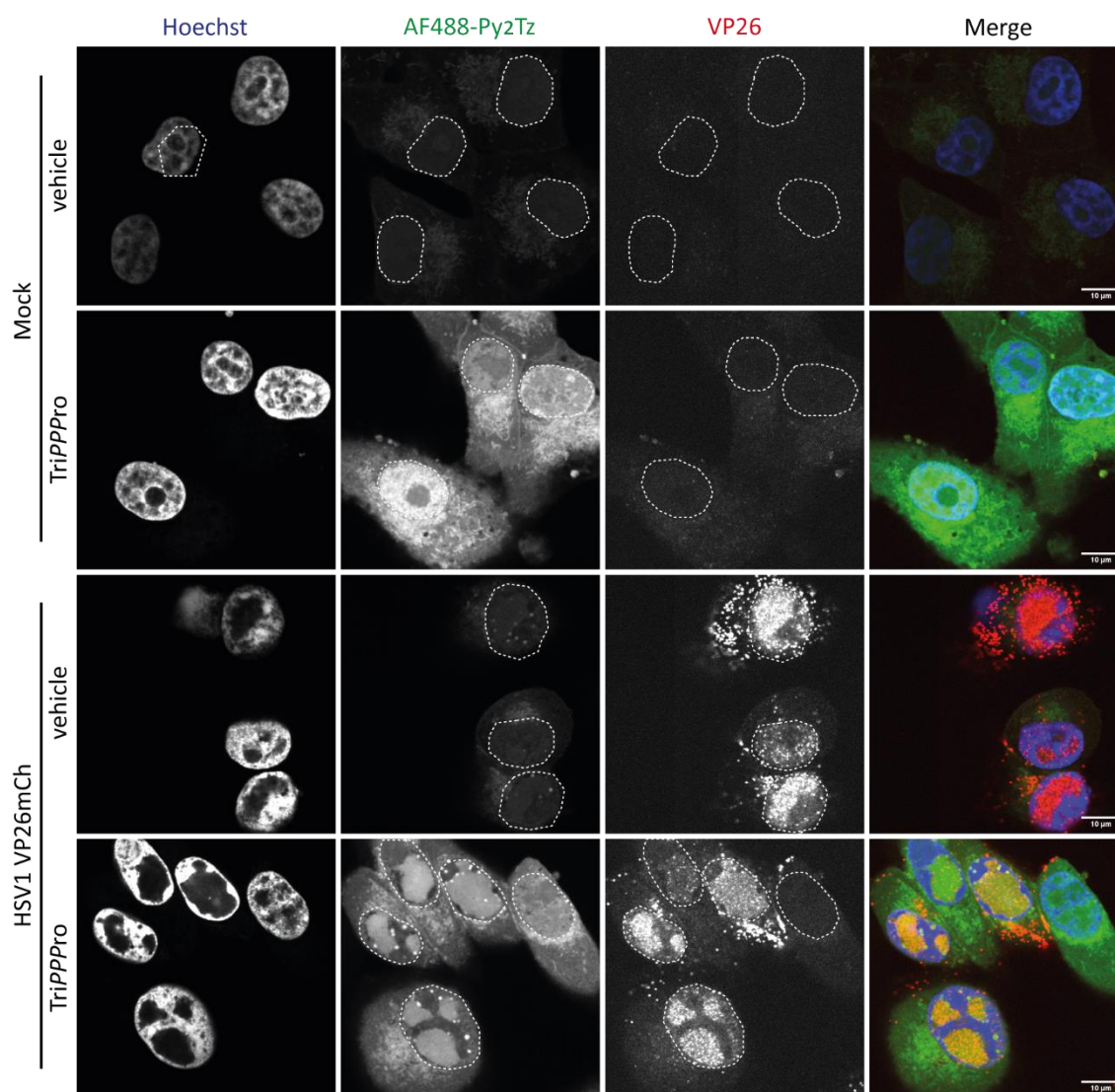


Figure 63: Confluent Vero cells were either mock- or HSV-1 VP26mCh-infected (MOI 3). The capsids of the HSV-1 are tagged with mCherry (*red*). 1 hpi medium was changed to VP-SFM and 4 hpi nascent DNA was labeled with 5  $\mu$ M  $\gamma$ -(C9C9AB)-2TCO $\alpha$ -dCTP **175** for 4 hours. The TriPPPPro medium was renewed once at 6 hpi. After 8 hpi, cells were fixed and processed: Genomes containing incorporated 2TCO $\alpha$ -dC were stained overnight with AlexaFluor488-Py<sub>2</sub>Tz **212** (*green*). Nuclei were stained with Hoechst (*blue*). Samples were imaged at x100 magnification using a Nikon Eclipse Ti2 Spinning disc microscope. Individual channels are shown in greyscale and the merged image is shown in color. Nuclei outlines are circled. Scalebar = 10  $\mu$ m.

Results will be discussed leading with the pronucleotide reporter  $\gamma$ -(C9C9AB)-2TCO $\alpha$ -dCTP **175**, which showed superior labeling qualities and serves as a reference throughout this chapter.

In uninfected Vero cells, which received treatment with **175**, a strong fluorescent signal (*green*) was observed throughout the nucleus of dividing cells. Hence, intracellularly released 2TCO $\alpha$ -dCTP was a substrate for the cellular DNA polymerase and thus modified CMP was efficiently incorporated into newly synthesized DNA. The control (mock-infected, untreated vehicle cells) exhibited no specific staining. Noteworthy, the

background is generally higher in cells treated with the respective TriPPPPro prior to staining. The increase in background signal is not surprising since unspecifically bound intracellular pronucleotide or their metabolites can react with the fluorophore-conjugate and, therefore, cause its intracellular accumulation. Moreover, possible “turn-off” properties of the 1,2,4,5-tetrazine are disrupted after the DA<sub>INV</sub> between unspecifically bound reporters – resulting in fluorescent background enhancement.

Additionally, HSV-1 VP26mCh infected and treated Vero cells showed clear staining of the viral replication compartments inside of the nucleus. These areas are knowingly Hoechst negative since the cellular DNA is pushed to the periphery of the nucleus. Here, newly synthesized viral DNA is transcribed – catalyzed by the herpes DNA polymerase. Evidently, 2TCO $\alpha$ -dCTP is also a substrate for the viral polymerase and is efficiently incorporated for sufficient fluorescent staining. The signal deriving from the viral genome colocalizes with the mCherry signal of the translated fluorescent capsid protein VP26 providing further evidence for successfully labeled viral nucleic acids.

As described in Chapter 0, the favorable stability provided by the axial 2-ene TCO comes with the drawback of a potential slow  $\beta$ -elimination of the fluorophore after successful tagging. In this work, this disadvantage caused no concerns. Overall, the motif demonstrates remarkable properties and efficient substrate activity towards cellular and viral DNA polymerases in terms of fluorescent signal output. The performance of C9C9AB-2TCO $\alpha$ -dCTP **175** in live-cell applications is the subject of Chapter 4.7.4.

In the following, the TriPPPPro compound  $\gamma$ -(C9C9AB)-4TCO-dCTP **163** will be discussed. Compared to the 2TCO $\alpha$ , the slightly more reactive 4-ene TCO is significantly less stable under physiological conditions (see Chapter 0). Additionally, the motif of **163** comprises the saturated alkyl linker instead of an alkyne bond. Polymerases evidently accept the latter motif shown in the case of  $\gamma$ -(C9C9AB)-2TCO $\alpha$ -dCTP **175** (or  $\gamma$ -(C9C9AB)-1MCP-dCTP **150**, Chapter 4.7.3).

In mock-infected Vero cells treated with **163**, no detectable signal deriving from novel cellular DNA synthesis was observable. As discussed above, the overall background is brighter than in uninfected and untreated cells. In infected cells, which were not treated with a pronucleotide (vehicle), a very weak non-specific AF488 staining is observable, which colocalizes with the VP26mCherry capsid signal. In infected cells incubated with **163**, the green signal increases with matching colocalization. Arguably, the signal could derive from the successfully incorporated reporter and subsequent

staining, or the signal could be caused by fluorescent enhancement of unspecifically bound fluorophore after the tetrazine – functioning as a quencher – reacts in the  $DA_{INV}$ .

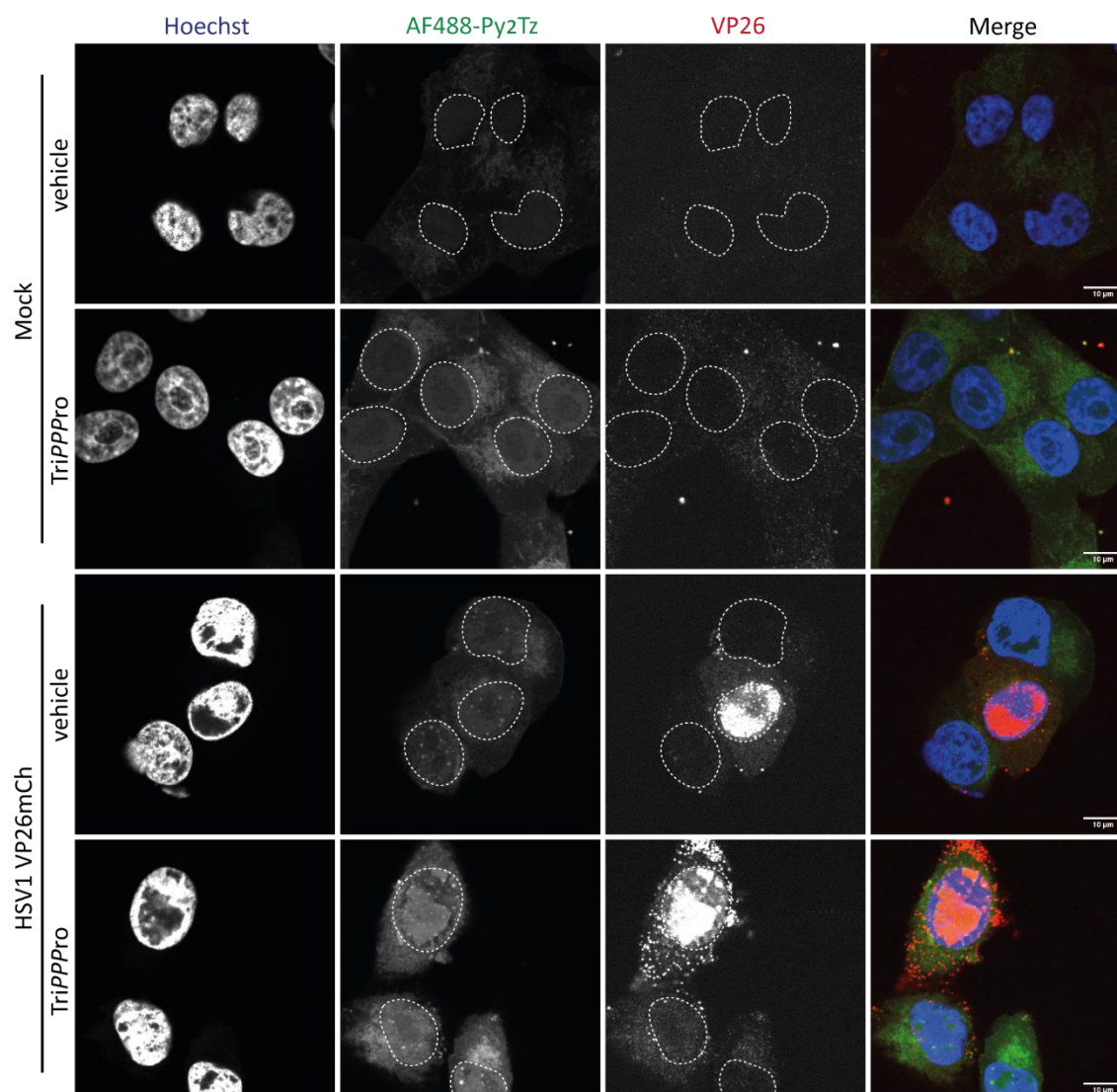


Figure 64: Confluent Vero cells were either mock- or HSV-1 VP26mCh-infected (MOI 3). The capsids of the HSV-1 are tagged with mCherry (*red*). 1 hpi medium was changed to VP-SFM and 4 hpi nascent DNA was labeled with 5  $\mu$ M  $\gamma$ -(C9C9AB)-4TCO-dCTP **163** for 4 hours. The TriPPPPro medium was renewed once at 6 hpi. After 8 hpi, cells were fixed and processed: Genomes containing incorporated 4TCO-dC were stained overnight with AlexaFluor488-Py<sub>2</sub>Tz **212** (*green*). Nuclei were stained with Hoechst (*blue*). Samples were imaged at x100 magnification using a Nikon Eclipse Ti2 Spinning disc microscope. Individual channels are shown in greyscale and the merged image is shown in color. Nuclei outlines are circled. Scalebar = 10  $\mu$ m.

By presuming the incorporation of the nucleotide reporter in the viral genome, the reasonable assumption could be made that the motif is tolerated by the herpes DNA polymerase but discriminated by cellular enzymes.

Moreover, the inferior stability of the 4-ene TCO could diminish fluorescent staining efficiency resulting in a reduced fluorescent signal. However, since there is no detectable signal for labeled cellular DNA, the overall poor performance of

$\gamma$ -(C9C9AB)-4TCO-dCTP **163** can probably mainly be attributed to the saturated alkyl linker motif.

In the case of infected Vero cell treatment with  $\gamma$ -(C9C9AB)-BCN<sup>endo</sup>-dCTP **177**, no observable cells were attached to the carrier glass after fixation and permeabilization of the samples, which can likely be attributed to cellular stress during viral infection and additional adverse effects of the TriPPPPro compound on cell viability.

However, uninfected Vero cells treated with **177** showed no staining for cellular DNA, even though **177** comprises the alkyne linker motif, which apparently is well accepted by polymerases. Hence, no attempts for optimization were performed since the reporter demonstrated no promising metabolic labeling properties. Speculatively, the bicyclo[6.1.0]nonyne function exceeds the size of modifications tolerated by the respective polymerases or – once incorporated – the “click reaction” with the Py<sub>2</sub>Tz group runs inefficiently.

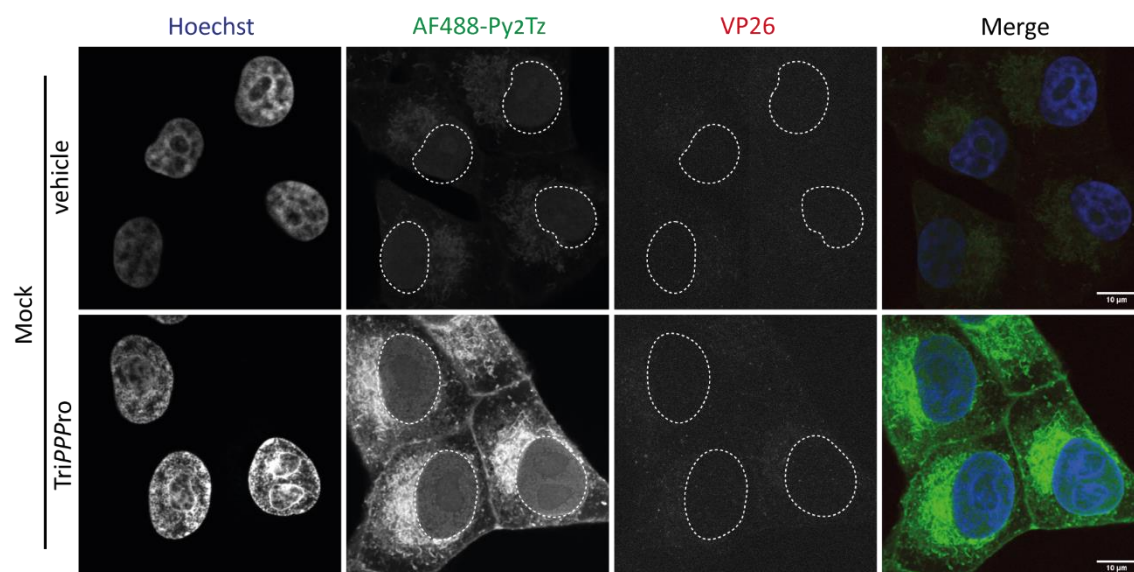


Figure 65: Confluent Vero cells were either mock- or HSV-1 VP26mCh-infected (MOI 3). The capsids of the HSV-1 are tagged with mCherry (*red*). 1 hpi medium was changed to VP-SFM and 4 hpi nascent DNA was labeled with 5  $\mu$ M  $\gamma$ -(C9C9AB)-BCN<sup>endo</sup>-dCTP **177** for 4 hours. The TriPPPPro medium was renewed once at 6 hpi. After 8 hpi, cells were fixed and processed: Genomes containing incorporated BCN<sup>endo</sup>-dC were stained overnight with AlexaFluor488-Py<sub>2</sub>Tz **212** (*green*). Nuclei were stained with Hoechst (*blue*). **No observable cells were attached to the carrier glass in case of infection with HSV-1!** Samples were imaged at x100 magnification using a Nikon Eclipse Ti2 Spinning disc microscope. Individual channels are shown in greyscale and the merged image is shown in color. Nuclei outlines are circled. Scalebar = 10  $\mu$ m.

The following pronucleotide reporters  $\gamma$ -(C9C9AB)-NcTz-dCTP **160** and the 2'-deoxyuridine pronucleotide  $\gamma$ -(C9C9AB)-MeTz-dUTP **187** carry the 1,2,4,5-tetrazine motif. The metabolic reporter **160** comprises the saturated alkyl linker motif as in the above-discussed pronucleotide C9C9AB-4TCO-dCTP **163**, which displayed poor labeling properties.

In  $\gamma$ -(C9C9AB)-MeTz-(*E*)-dUTP **187**, the methyl-substituted tetrazine is linked to the nucleobase by a short *trans*-ethylene motif.

The staining was conducted with commercially available, cell-permeable SiR-TCO **218**. The used concentration of fluorophore is unknown since the compound was not fully soluble in aqueous solutions. Insoluble material was removed by centrifugation, and the supernatant was used for cell incubation.

The uninfected and untreated control cells showed a relatively high background due to the unspecific binding of the 4TCO-fluorophore-conjugate **218**. Uninfected Vero cells treated with  $\gamma$ -(C9C9AB)-NcTz-dCTP **160** surprisingly showed a reduced background but no specific labeling of cellular DNA throughout the nucleus. In infected vehicle samples, the SiR-TCO **218** unspecifically stained viral replication compartments with low intensity. HSV-1 infected cells treated with **160** displayed no fluorescence increase compared to the control group. Hence, no detectable labeling of viral or cellular DNA was achieved.

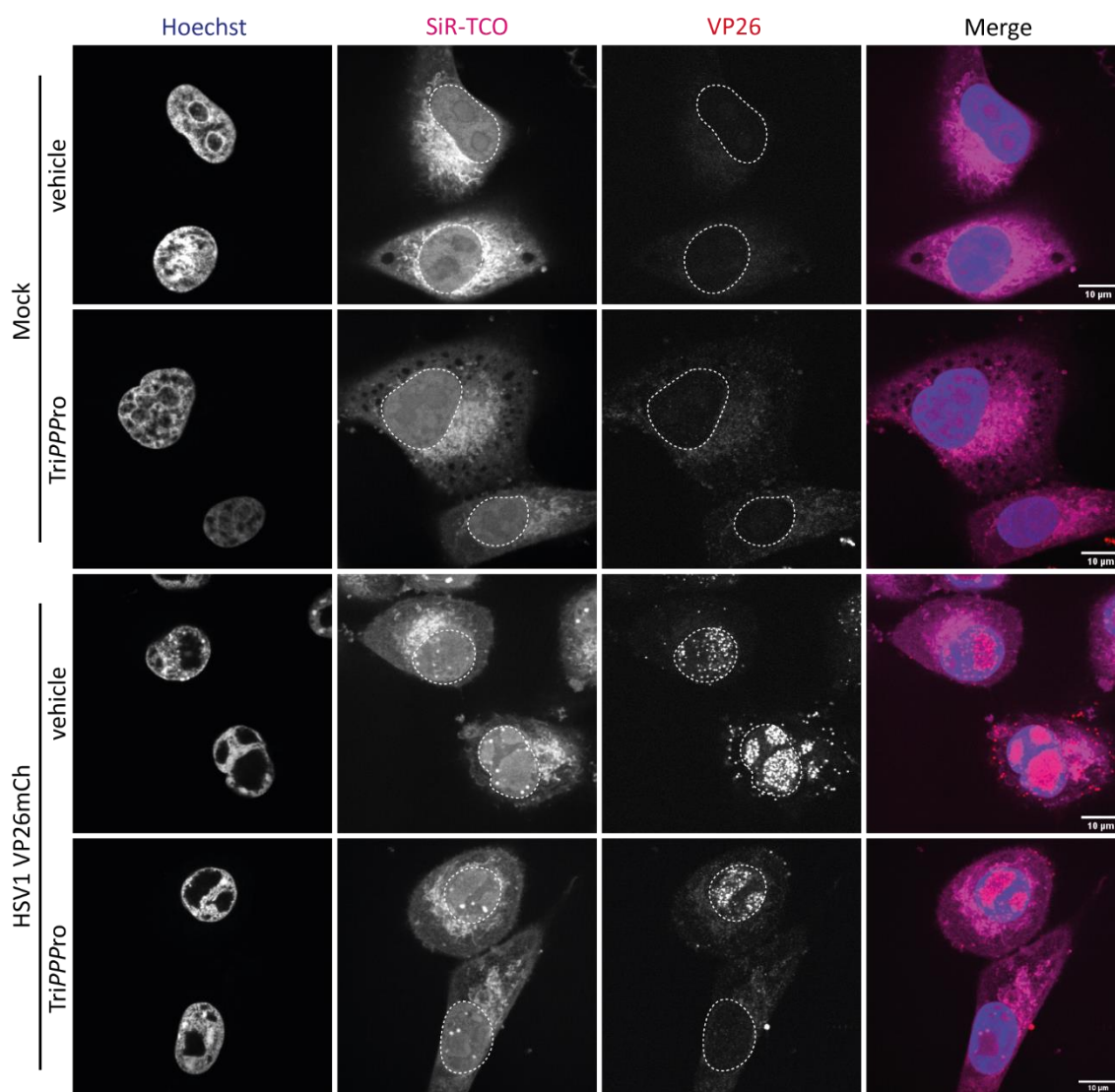


Figure 66: Confluent Vero cells were either mock- or HSV-1 VP26mCh-infected (MOI 3). The capsids of the HSV-1 are tagged with mCherry (*red*). 1 hpi medium was changed to VP-SFM and 4 hpi nascent DNA was labeled with 5  $\mu$ M  $\gamma$ -(C9C9AB)-NcTz-dCTP **160** for 4 hours. The TriPPPPro medium was renewed once at 6 hpi. After 8 hpi, cells were fixed and processed: Genomes containing incorporated NcTz-dC were stained overnight with SiR-TCO **218** (*magenta*). Nuclei were stained with Hoechst (*blue*). Samples were imaged at x100 magnification using a Nikon Eclipse Ti2 Spinning disc microscope. Individual channels are shown in greyscale and the merged image is shown in color. Nuclei outlines are circled. Scalebar = 10  $\mu$ m.

These results are not surprising compared to the labeling duo of  $\gamma$ -(C9C9AB)-4TCO-dCTP/ AF488-Py<sub>2</sub>Tz (**163/212**), which demonstrated poor DNA labeling. Beyond the shared alkyl linker motif, which is under suspicion to diminish the substrate properties towards polymerases, the 6-(6-methyl-1,2,4,5-tetrazin-3-yl)nicotinic acid group is presumably sterically more demanding than the 4TCO function. The steric demand could further impair the substrate activity of the metabolic reporter. Additionally, the 4TCO/Py<sub>2</sub>Tz duo provides an enormous reaction rate advantage compared to the discussed 4TCO/NcTz pair, which was solely designed to overcome the poor stability of 4-ene TCO under longer exposures in physiological environments.

Unfortunately, similar results were observed for  $\gamma$ -(C9C9AB)-MeTz-(E)-dUTP **187**. No specific signal beyond the intensity of the control samples was observable. It cannot finally be assessed if the metabolic reporter lacks efficient incorporation into newly synthesized cellular or viral DNA or if the inefficient “click” labeling is diminishing the successful visualization of the reporter.

Interestingly, Vero cells treated with **187** showed fluorescence signals when excited with a 561 nm laser (the VP26mCherry channel). The metabolic reporter seemingly displays fluorescent properties itself.

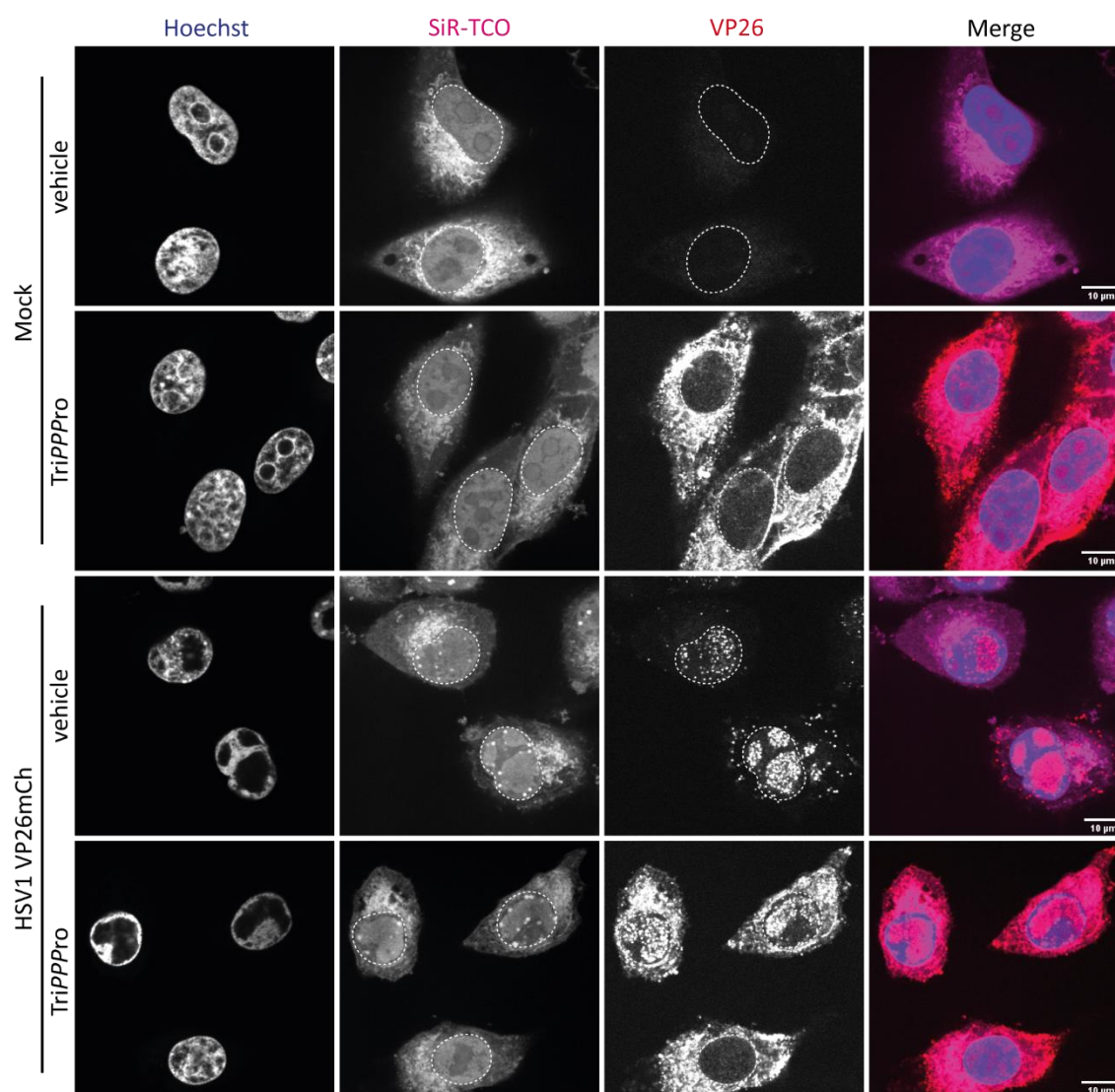


Figure 67: Confluent Vero cells were either mock- or HSV-1 VP26mCh-infected (MOI 3). The capsids of the HSV-1 are tagged with mCherry (red). 1 hpi medium was changed to VP-SFM and 4 hpi nascent DNA was labeled with 5  $\mu$ M  $\gamma$ -(C9C9AB)-MeTz-(E)-dUTP **187** for 4 hours. The TriPPPPro medium was renewed once at 6 hpi. After 8 hpi, cells were fixed and processed: Genomes containing incorporated MeTz-(E)-dU were stained overnight with SiR-TCO **218** (magenta). Nuclei were stained with Hoechst (blue). Samples were imaged at x100 magnification using a Nikon Eclipse Ti2 Spinning disc microscope. Individual channels are shown in greyscale and the merged image is shown in color. Nuclei outlines are circled. Scalebar = 10  $\mu$ m.



Lastly, mock-infected and infected Vero cells were treated with fluorescent  $\gamma$ -C9C9AB-SiR-dCTP **193**. In short, no specific labeling signal was observable. As described above, the alkyl linker motif employed here might hamper efficient incorporation by the respective polymerases. Moreover, the additional spacer and the sterically demanding silicon-rhodamine dye significantly alter the natural structure of the nucleotide, explaining the absence of a nuclear fluorescent signal.

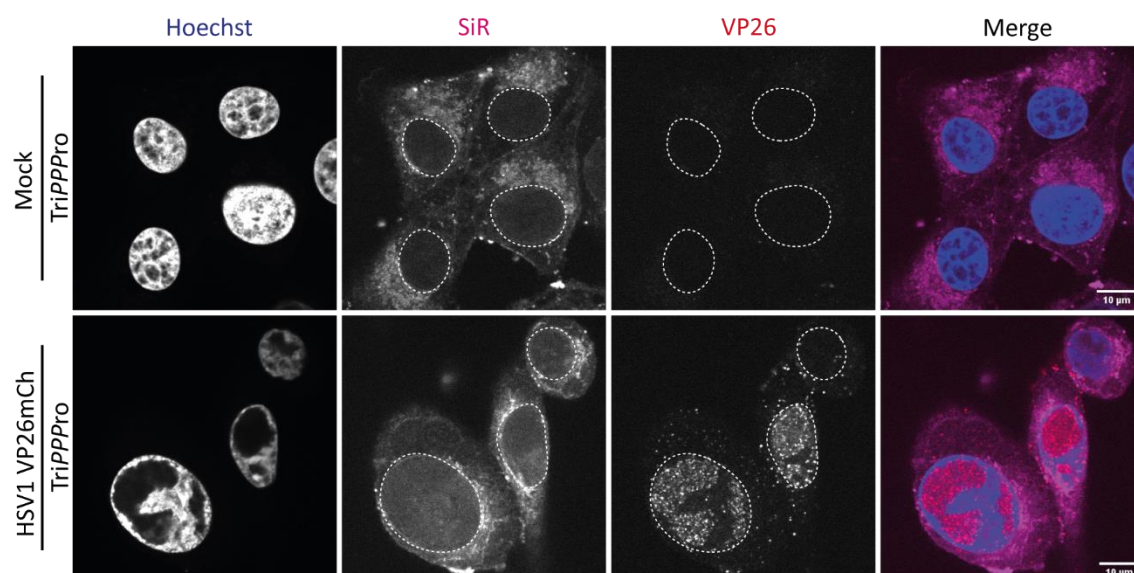


Figure 68: Confluent Vero cells were either mock- or HSV-1 VP26mCh-infected (MOI 3). The capsids of the HSV-1 are tagged with mCherry (*red*). 1 hpi medium was changed to VP-SFM and 4 hpi nascent DNA was labeled with 5  $\mu$ M  $\gamma$ -(C9C9AB)-SiR-dCTP **193** (*magenta*) for 4 hours. The TriPPPPro medium was renewed once at 6 hpi. After 8 hpi, cells were fixed and processed: Nuclei were stained with Hoechst (*blue*). Samples were imaged at x100 magnification using a Nikon Eclipse Ti2 Spinning disc microscope. Individual channels are shown in greyscale and the merged image is shown in color. Nuclei outlines are circled. Scalebar = 10  $\mu$ m.

Taken together,  $\gamma$ -(C9C9AB)-2TCO $\alpha$ -dCTP **175** displayed encouraging labeling properties in fixed and permeabilized Vero cells for cellular and viral DNA. The evaluation of the candidate's potential for application in live-cell imaging is the subject of Chapter 4.7.5.  $\gamma$ -(C9C9AB)-4TCO-dCTP **163** potentially labels viral DNA without displaying cellular DNA signals. However, the fluorescent signal is weak and might not exceed the intensity of the control. In future, 4TCO should be attached by the more promising alkyne linker and be compared to compound **175** directly.

Since the 2TCO $\alpha$  label provides exceptional stability values, the design of C9C9AB-NcTz-dCTP **160** potentially becomes redundant. However, future synthetic approaches should attach respective tetrazine motifs by an alkyne linker to explore if the exchange of the bioorthogonal reaction partners has some potential for the metabolic labeling of nucleic acids.

The  $\gamma$ -(C9C9AB)-MeTz-(E)-dUTP **187** demonstrated no cellular or herpes genome labeling. Still, it might display some value for other viral polymerases with lower fidelity, such as RNA viruses in general (except coronaviruses).<sup>184</sup>

Finally,  $\gamma$ -(C9C9AB)-SiR-dCTP **193** is the first fluorescent pronucleotide reporter described today; however, it exhibits structural flaws. As described above, the linker should be attached via an alkyne bond. Furthermore, it should be evaluated if the additional spacer is necessary or if less spacious fluorophores, e.g., coumarin dyes, can be attached in closer proximity to the nucleobase. Such a design is already underway in our laboratories.

### 4.7.3 Evaluation and comparison of the 1MCP and 2TCO $\alpha$ label

This chapter discusses the 1MCP-functionalized pronucleotides  $\gamma$ -(C9C9AB)-1MCP-dATP **149** and  $\gamma$ -(C9C9AB)-1MCP-dCTP **150** and their ability to label the HSV-1 genome and cellular DNA in fixed and permeabilized Vero cells. The signal outputs of the individual pronucleotide reporter were compared to each other and to the 2TCO $\alpha$ -functionalized pronucleotide  $\gamma$ -(C9C9AB)-2TCO $\alpha$ -dCTP **175**. Moreover, the dose-dependent labeling of herpes simplex DNA was studied with  $\gamma$ -(C9C9AB)-1MCP-dCTP **150** to determine an optimal concentration window for TriPPPPro reporters. Finally, as a control for viral genome labeling, infected cells were treated with an inhibitor of viral DNA replication during metabolic labeling.

#### Cytidine derivative provides higher viral genome signal

First, mock- or HSV-1 VP26mCh-infected Vero cells were treated with 5  $\mu$ M of  $\gamma$ -(C9C9AB)-1MCP-dCTP **150** (Figure 69) or  $\gamma$ -(C9C9AB)-1MCP-dATP **149** (Figure 70) 4 hpi. The TriPPPPro containing media were changed to VP-SFM 7 hpi. After eight hours, cells were washed, fixed, and permeabilized. Staining with AF488-Py<sub>2</sub>Tz **212** (*green*, 5  $\mu$ M) was conducted overnight at 4 °C. Afterwards, cells were washed and immunofluorescently stained against ICP8. The nucleus was colorized with Hoechst. Figure 69 shows the successful labeling of cellular and viral DNA by the cytidine-based reporter **150**. An uninfected cell displays the typical labeling pattern of dividing cells and the AF488 signal colocalizes well with the Hoechst staining. For infected cells, the AF488 signal shows the typical pattern of viral RCs, which lack a Hoechst signal. The colocalization with the immunofluorescently stained HSV-1 single-strand binding protein (ICP8) provides further proof for the successful labeling of viral genomes.

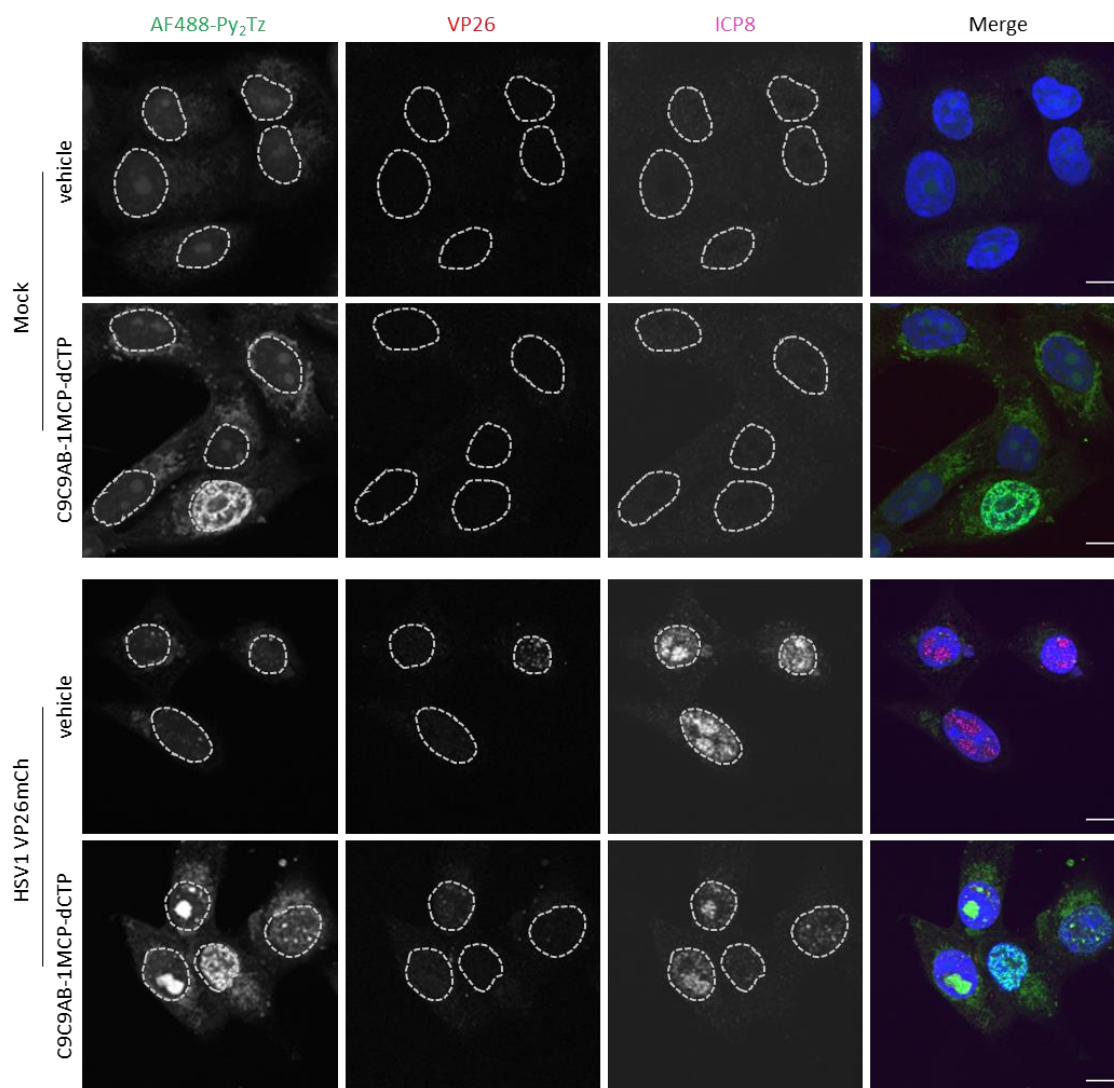


Figure 69: Confluent Vero cells were either mock- or HSV-1 VP26mCh-infected (MOI 3). The capsids of the HSV-1 are tagged with mCherry (*red*). 1 hpi medium was changed to VP-SFM and 4 hpi nascent DNA was labeled with 5  $\mu$ M  $\gamma$ -(C9C9AB)-1MCP-dCTP **150** for 3 hours. After 8 hpi, cells were fixed and processed: Genomes containing incorporated 1MCP-dC were stained overnight with AlexaFluor488-Py<sub>2</sub>Tz **212** (*green*). ICP8 was labeled by immunofluorescence (*magenta*). Nuclei were stained with Hoechst (*blue*). Samples were imaged at x100 magnification using a Nikon Eclipse Ti2 Spinning disc microscope. Individual channels are shown in greyscale and the merged image is shown in color. Nuclei outlines are circled. Scalebar = 10  $\mu$ m.<sup>185</sup>

Figure 70 shows the labeling of cellular and viral DNA by the 7-deazaadenosine-based reporter **149**. In case of metabolic labeling of cellular nucleic acid, both the C<sub>5</sub>-pyrimidine and the C<sub>7</sub>-purine modified reporter gave somewhat similar signal intensities, pleading for similar incorporation rates into the *de novo* synthesized DNA by the respective cellular DNA polymerase. In contrast, the cytidine-derivative provided higher signal intensities for viral DNA labeling than the adenosine-based reporter. The trend is illustrated in Figure 71, in which the sum intensities of the AF488 signal of viral RCs are displayed. The higher signal strength for the 2'-deoxycytidine reporter is probably

reasoned in the G+C rich HSV-1 genome. However, it cannot be excluded that the intracellularly released 1MCP-dCTP reporter also is a better substrate for the viral over the cellular DNA polymerase.

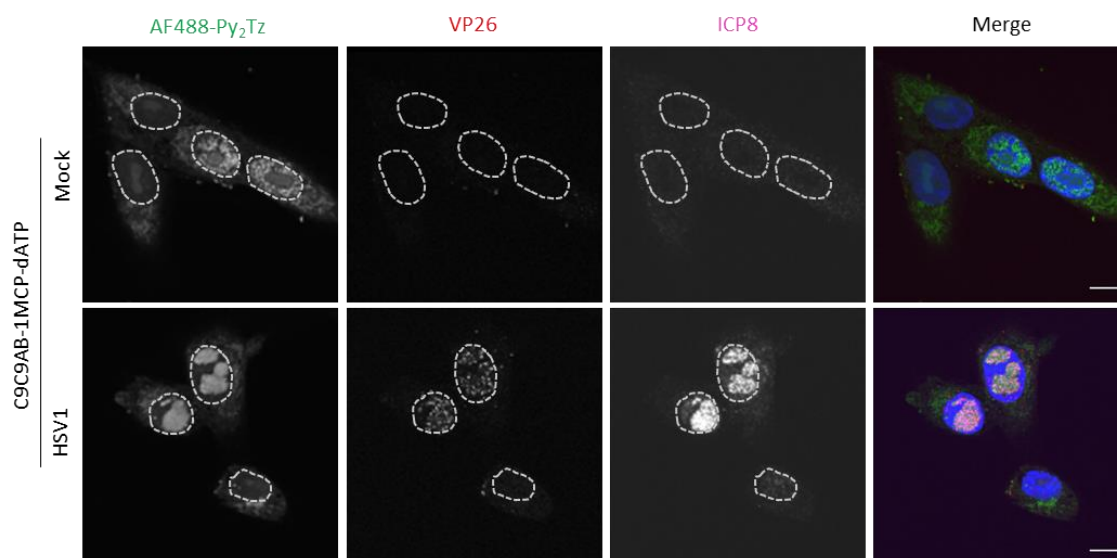


Figure 70: Confluent Vero cells were either mock- or HSV-1 VP26mCh-infected (MOI 3). The capsids of the HSV-1 are tagged with mCherry (*red*). 1 hpi medium was changed to VP-SFM and 4 hpi nascent DNA was labeled with 5  $\mu$ M  $\gamma$ -(C9C9AB)-1MCP-dATP **149** for 3 hours. After 8 hpi, cells were fixed and processed: Genomes containing incorporated 1MCP-dA were stained overnight with AlexaFluor488-Py<sub>2</sub>Tz **212** (*green*). ICP8 was labeled by immunofluorescence (*magenta*). Nuclei were stained with Hoechst (*blue*). Samples were imaged at x100 magnification using a Nikon Eclipse Ti2 Spinning disc microscope. Individual channels are shown in greyscale and the merged image is shown in color. Nuclei outlines are circled. Scalebar = 10  $\mu$ m.<sup>185</sup>

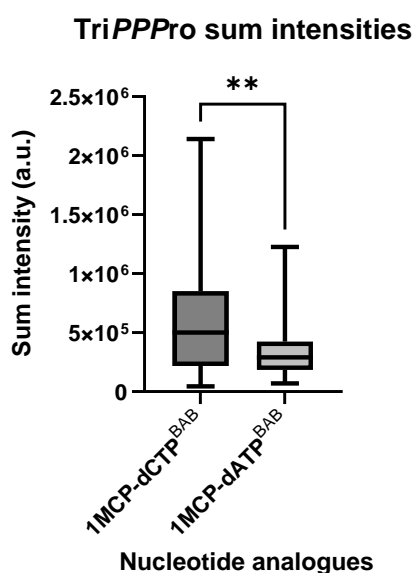


Figure 71: **Quantification of the signal intensities provided by the 1MCP pronucleotide derivatives.** Mean intensities, as well as area size of the labeled replication compartments, were measured in ImageJ. The mean intensities were multiplied by the area sizes to achieve the sum intensities of the nucleotide analogues in HSV-1 infected Vero cells. The signal intensities of at least 50 cells per sample were analyzed. Statistical analysis was performed using a t-test, \*\* $p < 0.01$ .<sup>185</sup>

**Dose-dependent fluorescent signal**

Next, different concentrations of  $\gamma$ -(C9C9AB)-1MCP-dCTP **150** were tested in HSV-1 VP26mCh infected Vero cells to study the dose-dependency of the fluorescent signal. The experimental conditions are equal to those described above with concentration between 0 and 10  $\mu$ M pronucleotide reporter and 5  $\mu$ M of the AF488 dye conjugate (Figure 72). A signal was already detectable at low concentrations of 0.5  $\mu$ M. However, it did barely exceed the background signal throughout the cell. At a concentration of 1.5  $\mu$ M clear cellular and viral DNA labeling was observed. The signal intensity increased further with a concentration of 5  $\mu$ M. Slides treated with 10  $\mu$ M of **150** also exhibited cells with strong fluorescently labeled DNA; however, a drastic increase in cell death was observed, which significantly reduced the number of imageable cells. Therefore, it was generalized that a TriPPP concentration between 1.5 to 5  $\mu$ M is the appropriate window for efficient labeling while balancing cytotoxicity in the described system (Vero cells under HSV-1 infection with a MOI of 3 PfU).

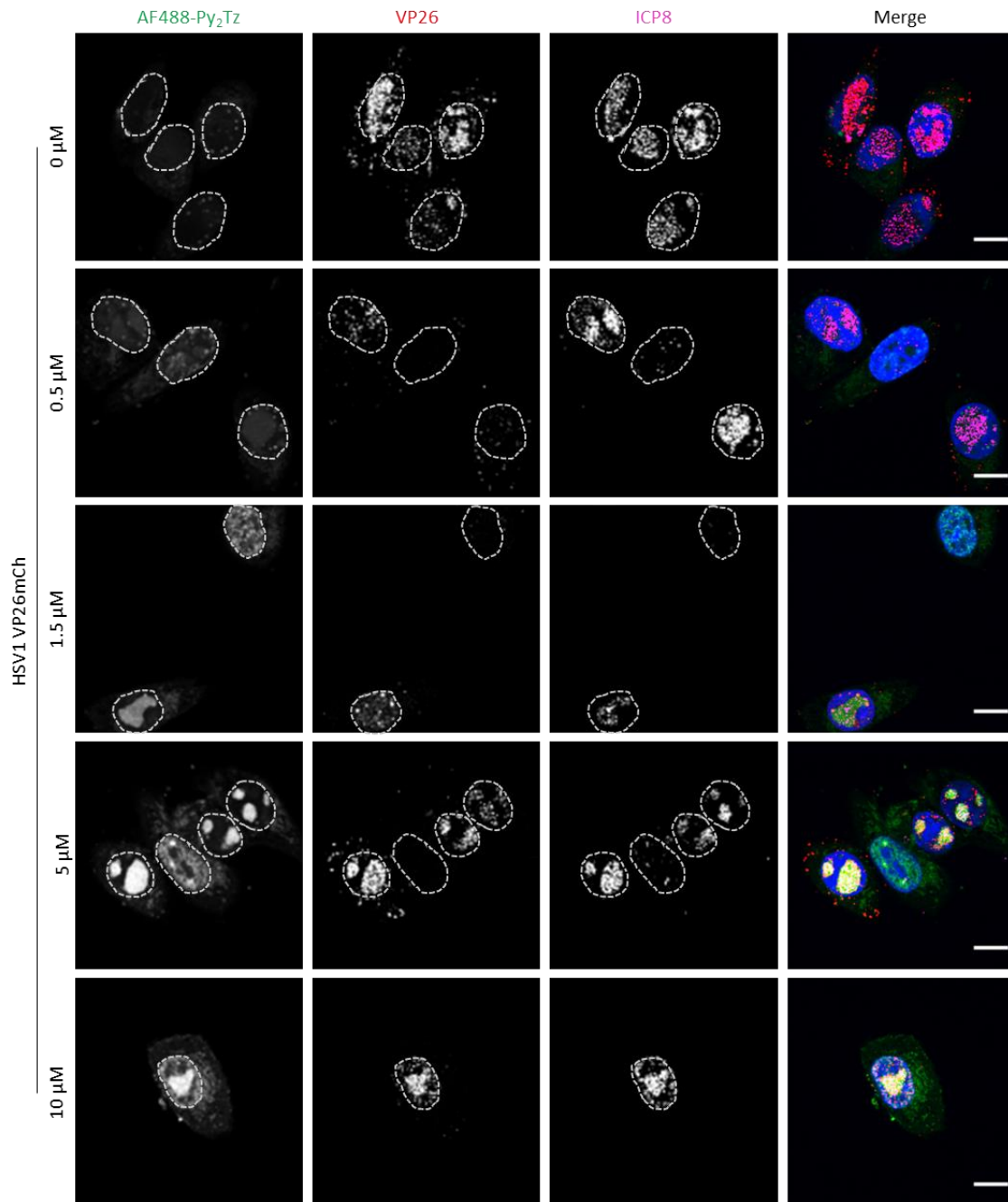


Figure 72: Confluent Vero cells were either mock- or HSV-1 VP26mCh-infected (MOI 3). The capsids of the HSV-1 are tagged with mCherry (*red*). 1 hpi medium was changed to VP-SFM and 4 hpi nascent DNA was labeled with  $\gamma$ -(C9C9AB)-1MCP-dCTP **150** for 3 hours at indicated concentrations. After 8 hpi, cells were fixed and processed: Genomes containing incorporated 1MCP-dC were stained overnight with AlexaFluor488-Py<sub>2</sub>Tz **212** (*green*). ICP8 was labeled by immunofluorescence (*magenta*). Nuclei were stained with Hoechst (*blue*). Samples were imaged at x100 magnification using a Nikon Eclipse Ti2 Spinning disc microscope. Individual channels are shown in greyscale and the merged image is shown in color. Nuclei outlines are circled. Scalebar = 10  $\mu$ m.<sup>185</sup>

### Comparison of the 1MCP and 2TCO $\alpha$ label

The 2TCO $\alpha$  label of the pronucleotide reporter  $\gamma$ -(C9C9AB)-2TCO $\alpha$ -dCTP **175** was incorporated in cellular and viral DNA under the same condition described above to enable direct comparison between the respective reporters. The imaging results for mock- and HSV-1 VP26mCh-infected Vero cells treated with **175** are displayed in Figure 73. As already shown and discussed in Chapter 0, the pronucleotide **175** enables bright labeling of cellular and viral DNA. Additionally, the AF488 signal inside of RCs colocalizes well with the ICP8 staining, providing further certainty for successful incorporation of the modified nucleotide into nascent viral genomes.

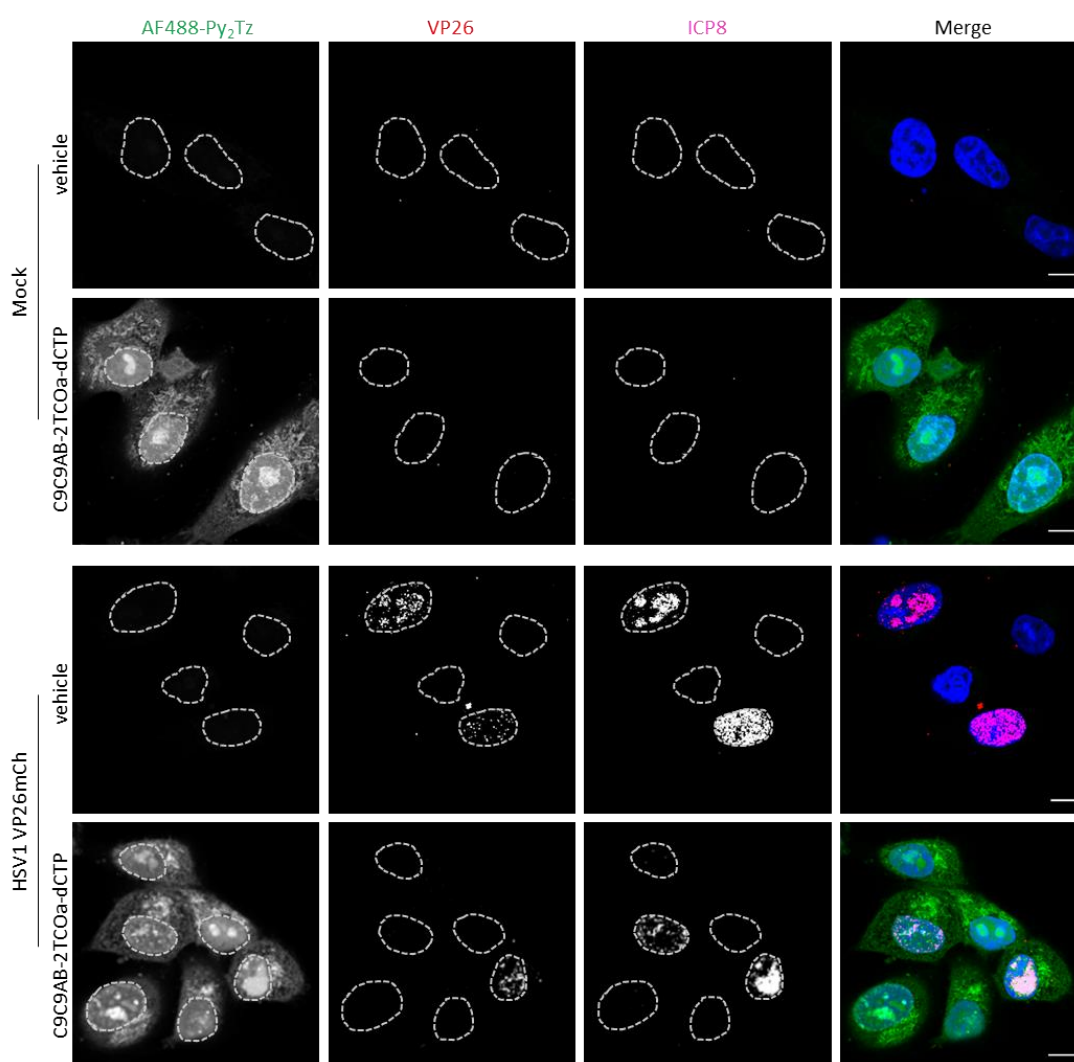


Figure 73: Confluent Vero cells were either mock- or HSV-1 VP26mCh-infected (MOI 3). The capsids of the HSV-1 are tagged with mCherry (*red*). 1 hpi medium was changed to VP-SFM and 4 hpi nascent DNA was labeled with 5  $\mu$ M  $\gamma$ -(C9C9AB)-2TCO $\alpha$ -dCTP **175** for 3 hours. After 8 hpi, cells were fixed and processed: Genomes containing incorporated 2TCO $\alpha$ -dC were stained overnight with AlexaFluor488-Py<sub>2</sub>Tz **212** (*green*). ICP8 was labeled by immunofluorescence (*magenta*). Nuclei were stained with Hoechst (*blue*). Samples were imaged at x100 magnification using a Nikon Eclipse Ti2 Spinning disc microscope. Individual channels are shown in greyscale, and the merged image is shown in color. Nuclei outlines are circled. Scalebar = 10  $\mu$ m.<sup>185</sup>

For comparability, the pronucleotide reporters' imaging results are displayed in Figure 74A. The signal deriving from  $\gamma$ -(C9C9AB)-1MCP-dATP **149** is too weak in comparison to the cytidine-based reporters and disappears due to the chosen brightness settings. The "faster" reporter  $\gamma$ -(C9C9AB)-2TCO $\alpha$ -dCTP **175** demonstrates a significantly brighter signal than its 1MCP derivative **150**. The reporters' sum intensities of labeled viral RCs are illustrated in Figure 74B.



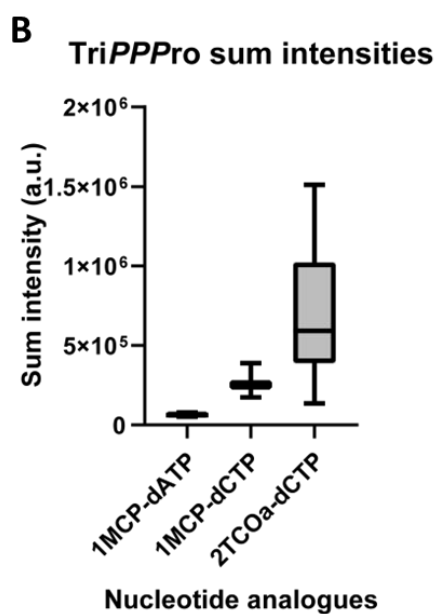
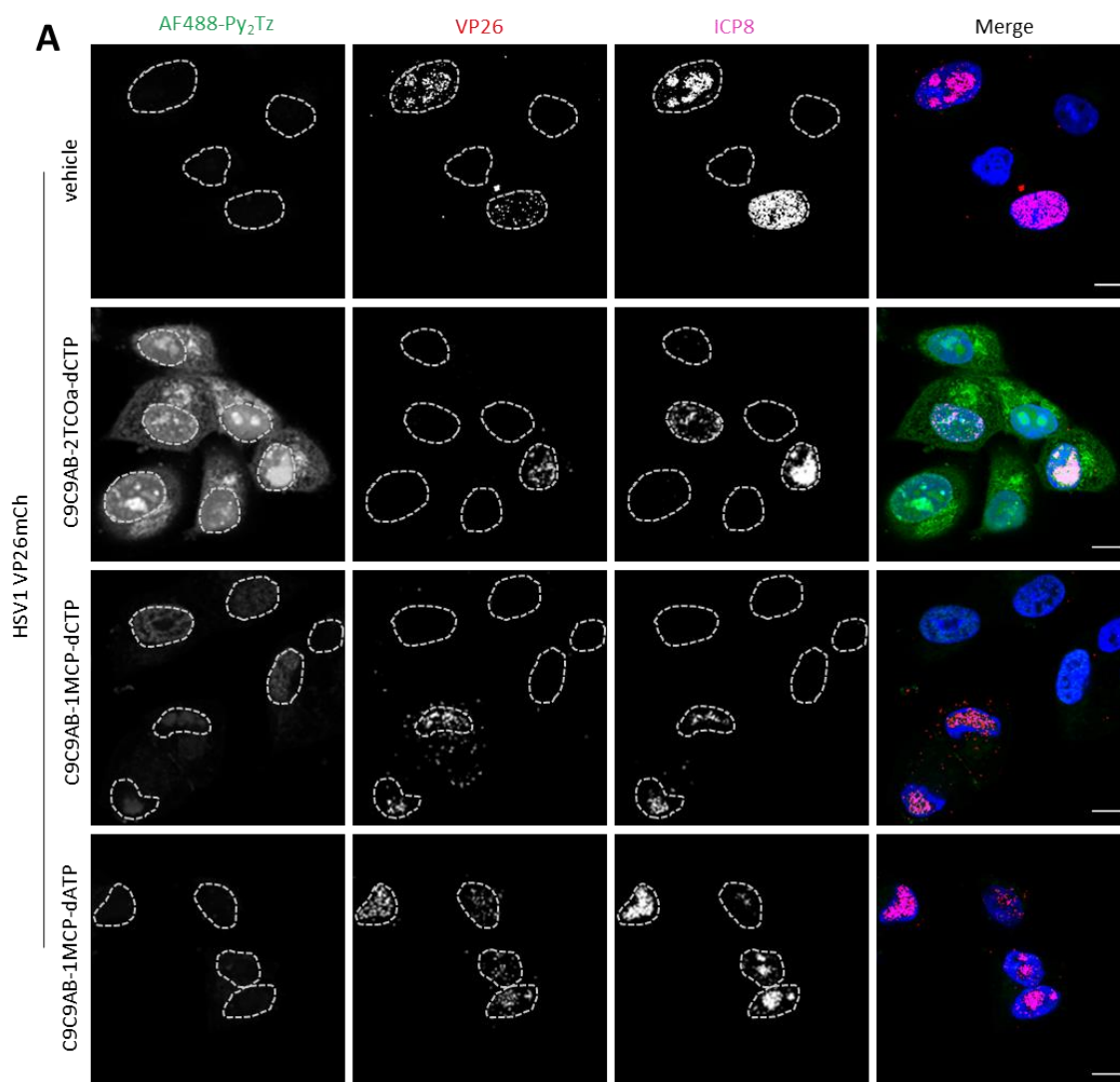


Figure 74: Comparison of signal intensities of 1MCP and 2TCOa pronucleotide probes. (A) Representative fluorescence images. Confluent Vero cells were infected with HSV-1 VP26mCh (MOI 3). The capsids of the HSV-1 are tagged with mCherry (red). 1 hpi the medium was changed to VP-SFM and 4 hpi nascent DNA was labeled with 5  $\mu$ M of the respective pronucleotide probes for 3 hours. After 7 hpi, cells were fixed and processed: Genomes containing incorporated 1MCP-dC/dA or 2TCOa-dC were stained overnight with AlexaFluor488-Py<sub>2</sub>Tz **212** (green). ICP8 was labeled by immunofluorescence (magenta). Nuclei were stained with Hoechst (blue). Samples were imaged at x100 magnification using a Nikon Eclipse Ti2 Spinning disc microscope. Individual channels are shown in greyscale and the merged image is shown in color. Nuclei outlines are circled. Scalebar = 10  $\mu$ m. (B) Quantitative comparison of signal intensities. The area size of the labeled RCs and the mean signal intensities inside of these areas were measured in ImageJ. Both factors were multiplied to calculate the sum intensities of the metabolic labeling of HSV-1 infected Vero cells. At least 50 cells per sample were analyzed.<sup>178</sup>

The significantly brighter labeling signal provided by the 2TCO $\alpha$  label led to the conclusion that its bulkiness does not observably diminish the incorporation of the reporter, but the label's reactivity considerably improves the yield of the bioorthogonal reaction.

It is striking that the label's reactivity substantially influences the signal output even under ideal staining conditions (permeabilized samples and extended reaction times). Naturally, this observation becomes especially significant for live-cell application, where the intracellular availability of the dye is reduced due to cellular compartmentalization and staining times need to be much shorter to track dynamic processes.

This observation suggests that the background signal also increases from 1MCP to 2TCO $\alpha$ . In conclusion, the reporter's metabolites might "stick" to intracellular surfaces and react with the fluorophore-conjugate, resulting in a non-specific signal, higher for faster bioorthogonal duos. Potentially the issue can be improved by fine-tuning the experiment, e.g., removing the treatment medium (containing TriPPP compound) at an earlier stage, improving the washing procedure before fluorophore addition, or synthetically altering the polarity of the pronucleotide reporter.

### **The viral DNA replication inhibitor PAA impedes metabolic labeling**

Lastly, to unequivocally demonstrate the pronucleotide reporter's ability to visualize viral DNA replication via its incorporation, HSV-1 VP26mCh infected Vero cells were treated with  $\gamma$ -(C9C9AB)-1MCP-dCTP **150** in the presence and absence of phosphonoacetic acid (PAA). PAA inhibits the synthesis of herpes simplex virus DNA and disturbs viral capsid assembly and normal egress to the cytoplasm. Depending on PAA concentrations, normal amounts of early virus proteins are translated, but late virus proteins are significantly reduced. In contrast to viral DNA synthesis, PAA shows no significant damage to synthesized host cell DNA.<sup>186</sup>

The untreated sample (vehicle, no PAA) displayed VP26 capsid signal and strong staining for ICP8 (Figure 75). The samples treated with PAA (vehicle, +PAA) showed no signal for the late viral protein VP26 and a dotted pattern for ICP8. The alteration of the ICP8 signal can be explained with the disordered formation of viral RCs caused by PAA.

Samples treated with  $\gamma$ -(C9C9AB)-1MCP-dCTP **150** in the absence of PAA showed the typical labeling results. The representative image shows labeling of viral RCs (ICP8 colocalization) and nascent cellular DNA (Hoechst colocalization). In the presence of PAA, no detectable signal of labeled viral DNA is observable. Again, the ICP8 signal is

altered and the VP26mCherry proteins were not translated. However, labeled nascent cellular DNA of dividing cells is observable since cellular DNA synthesis is not hampered by PAA. Hence, the obtained results suggested successful labeling of the herpes simplex virus genome.

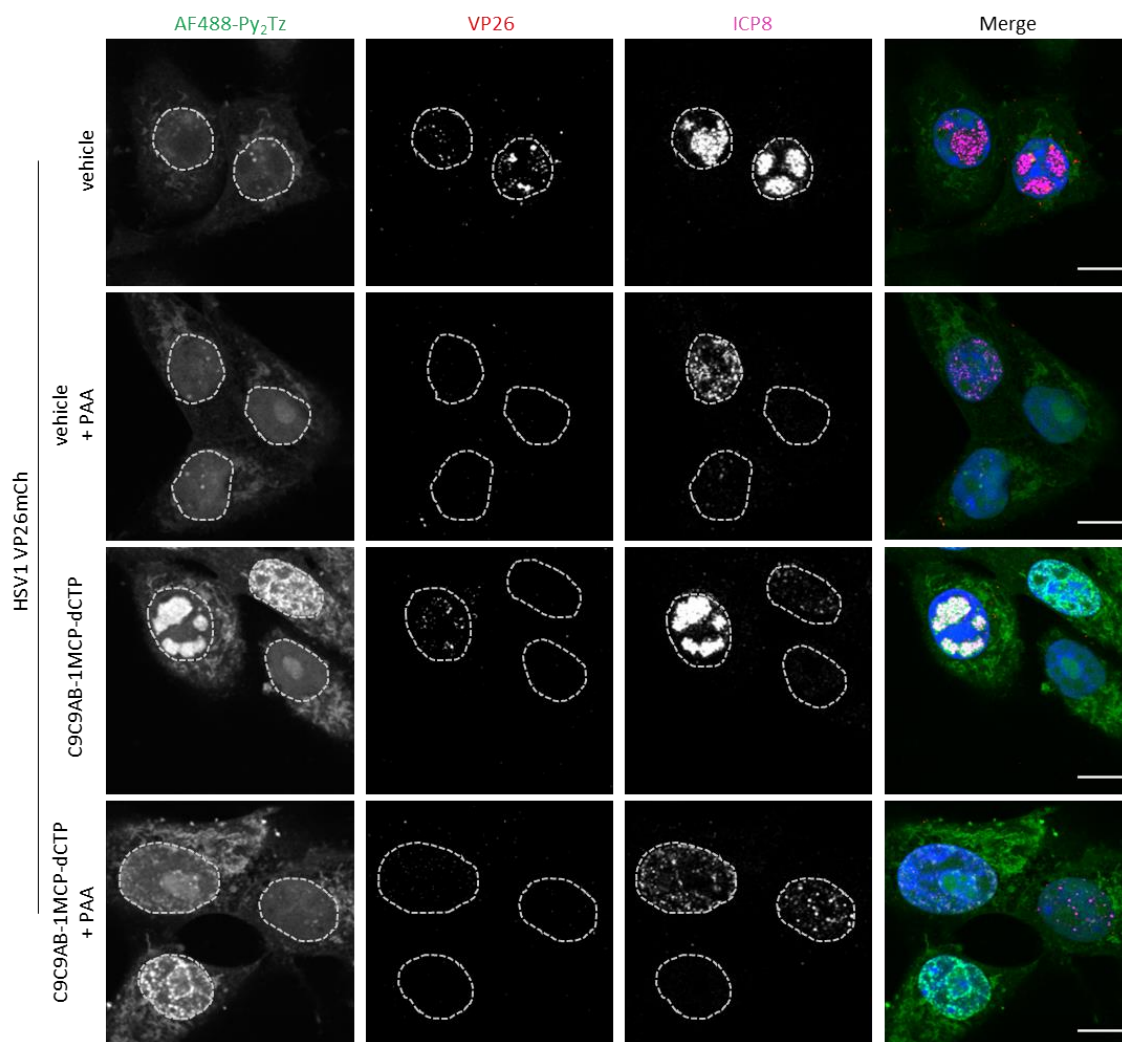


Figure 75: **Control experiment with PAA, an inhibitor of viral DNA synthesis.** Confluent Vero cells were infected with HSV-1 VP26mCh (MOI 3) in the absence or presence of PAA (400  $\mu\text{g}/\text{ml}$ , throughout the experiment). The capsids of the HSV-1 are tagged with mCherry (*red*). 1 hpi the medium was changed to VP-SFM and 4 hpi nascent DNA was labeled with 5  $\mu\text{M}$  of  $\gamma$ -(C9C9AB)-1MCP-dATP **149** for 3 hours. After 7 hpi, cells were fixed and processed: Genomes containing incorporated 1MCP-dC were stained overnight with AlexaFluor488-Py<sub>2</sub>Tz **212** (*green*). ICP8 was labeled by immunofluorescence (*magenta*). Nuclei were stained with Hoechst (*blue*). Samples were imaged at x100 magnification using a Nikon Eclipse Ti2 Spinning disc microscope. Individual channels are shown in greyscale and the merged image is shown in color. Nuclei outlines are circled. Scalebar = 10  $\mu\text{m}$ .<sup>185</sup>

### Short conclusion

Briefly, the pronucleotides  $\gamma$ -(C9C9AB)-1MCP-dATP **149** and  $\gamma$ -(C9C9AB)-1MCP-dCTP **150** provide metabolic labeling of both cellular and herpesviral DNA in fixed and permeabilized Vero cells with the Py<sub>2</sub>Tz motif as a bioorthogonal partner. Both reporters

provide similar signal intensities for the labeling of cellular DNA, whereas the cytidine-based reporter provided the superior signal for marking the herpes genome. The optimal concentration window for TriPPP compounds is between 1.5 and 5  $\mu\text{M}$  concerning signal output while retaining cellular viability. The 2TCO $\alpha$  label provides improved signal intensities compared to the 1MCP label, demonstrating the influence of superior reaction rates even under optimal staining conditions (permeabilized samples and extended reaction times). However, the 1MCP label provides a stable covalent bond with the sensor molecule, which does not undergo a  $\beta$ -elimination reaction like the 2TCO $\alpha$ -tetrazine product. Finally, the PAA inhibitor control gave further proof for successful viral DNA labeling.

#### 4.7.4 Evaluation of the TriPPP concept

Both parent nucleosides 1MCP-dC **154** and 2TCO $\alpha$ -dC **179** were synthesized (Chapters 4.3 and 0) to validate the necessity of the TriPPP concept in this context. As described before, nucleosides must be phosphorylated to their respective triphosphates before being incorporated by polymerases into *de novo* synthesized nucleic acids. Endogenous kinases, responsible for the phosphorylation cascade, often possess a narrow substrate window, limiting the efficient intracellular formation of unnatural nucleoside triphosphates (Chapter 2.8).

These nucleoside reporters were directly compared to their BAB-pronucleotides in both HSV-1 VP26mCh infected and uninfected Vero cells. Four hours after infection, the Vero cells were treated with 5  $\mu\text{M}$  of the respective pronucleotide or with 10, 20, or 30  $\mu\text{M}$  of the corresponding nucleoside. For the pronucleotides, the medium was renewed at 6 hpi to ensure the integrity of the BAB groups. The vehicle control stayed untreated. After 8 hpi, cells were washed briefly with VP-SFM, followed by fixation, permeabilization, and staining overnight at 4 °C with AF488-Py<sub>2</sub>Tz **212** (*green*). The following day, cells were washed and stained with Hoechst (*blue*).

Cells treated with  $\gamma$ -(C9C9AB)-1MCP-dCTP **150** successfully labeled viral DNA inside viral RCs. These viral factories are typically without Hoechst signal since cellular dsDNA is pushed to the periphery of the nucleus. Moreover, these locations also exhibited the VP26mCh signal (*red*) with good colocalization to the AF488 stain.

Furthermore, uninfected neighbor cells (absence of VP26mCh signal) exhibit AF488 signal throughout the nucleus with good colocalization to the Hoechst signal, thus demonstrating specific labeling of cellular DNA.

In contrast, the AF488 signal of 1MCP-dC **154** treated samples barely exceeded the signal intensity of the vehicle control. The slight increase of signal can be attributed to the higher background due to intracellular dye accumulation after the bioorthogonal reaction with the intracellularly available nucleoside reporter. Hence, the parent nucleoside 1MCP-dC **154** demonstrated no sign of DNA labeling.

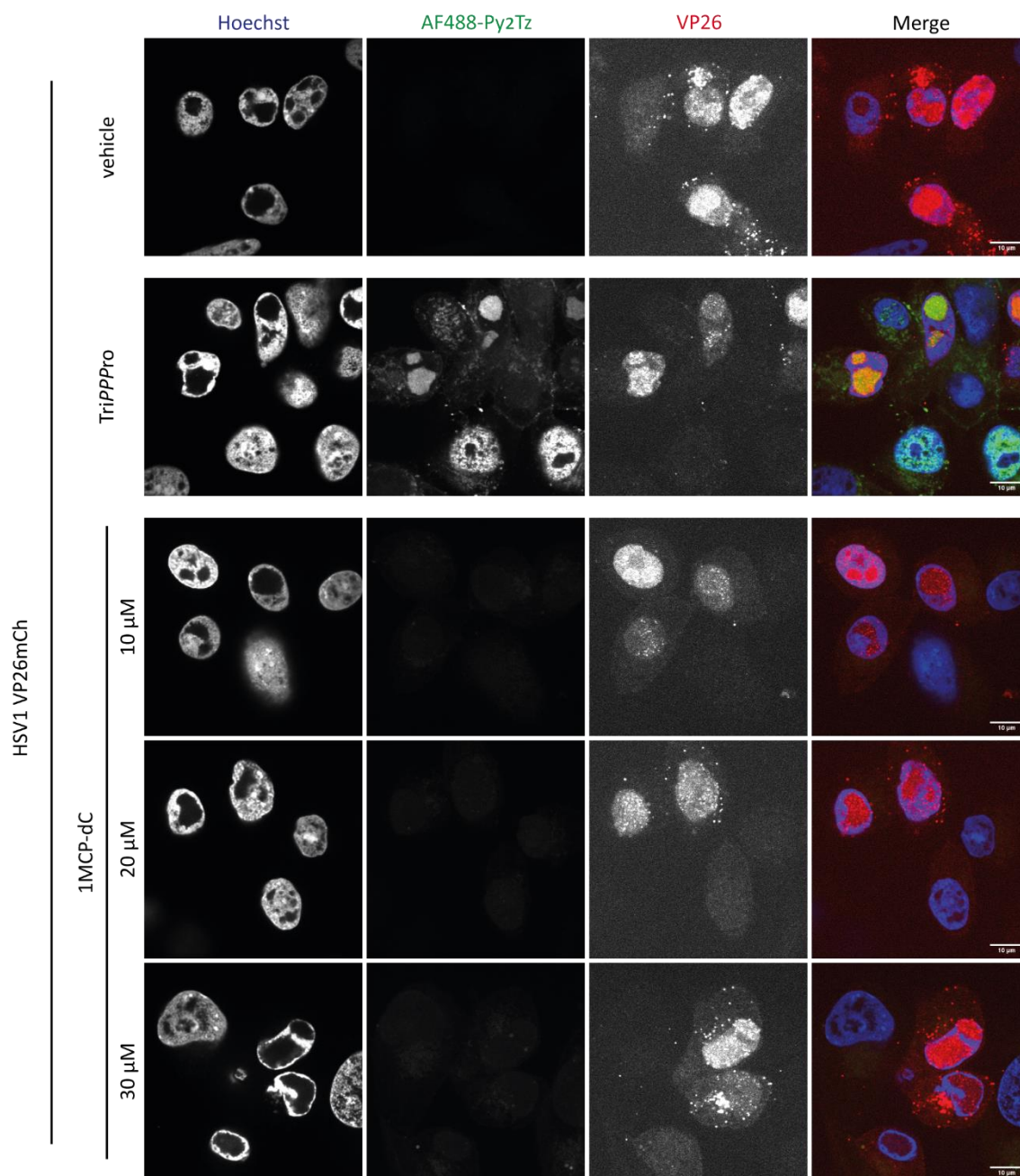


Figure 76: Confluent Vero cells were either mock- or HSV-1 VP26mCh-infected (MOI 3). The capsids of the HSV-1 are tagged with mCherry (*red*). 1 hpi medium was changed to VP-SFM and 4 hpi nascent DNA was labeled with 5  $\mu$ M of the pronucleotide  $\gamma$ -(C9C9AB)-1MCP-dCTP **150**, or 10, 20, or 30  $\mu$ M of the parent nucleoside 1MCP-dC **154** in VP-SFM. The TriPPPPro medium was renewed once at 6 hpi. After 8 hpi, cells were fixed and processed: Genomes containing incorporated 1MCP-dC were stained overnight with AlexaFluor488-Py<sub>2</sub>Tz **212** (*green*). Nuclei were stained with Hoechst (*blue*). Samples were imaged at x100 magnification using a Nikon Eclipse Ti2 Spinning disc microscope. Individual channels are shown in greyscale and the merged image is shown in color. Scalebar = 10  $\mu$ m.

The same results were found for  $\gamma$ -(C9C9AB)-2TCO $\alpha$ -dCTP **175** and its corresponding nucleoside 2TCO $\alpha$ -dC **179**. In short, both viral and cellular DNA was labeled by the pronucleotide **175**, whereas no specific signal was observed for samples treated with nucleoside **179**.

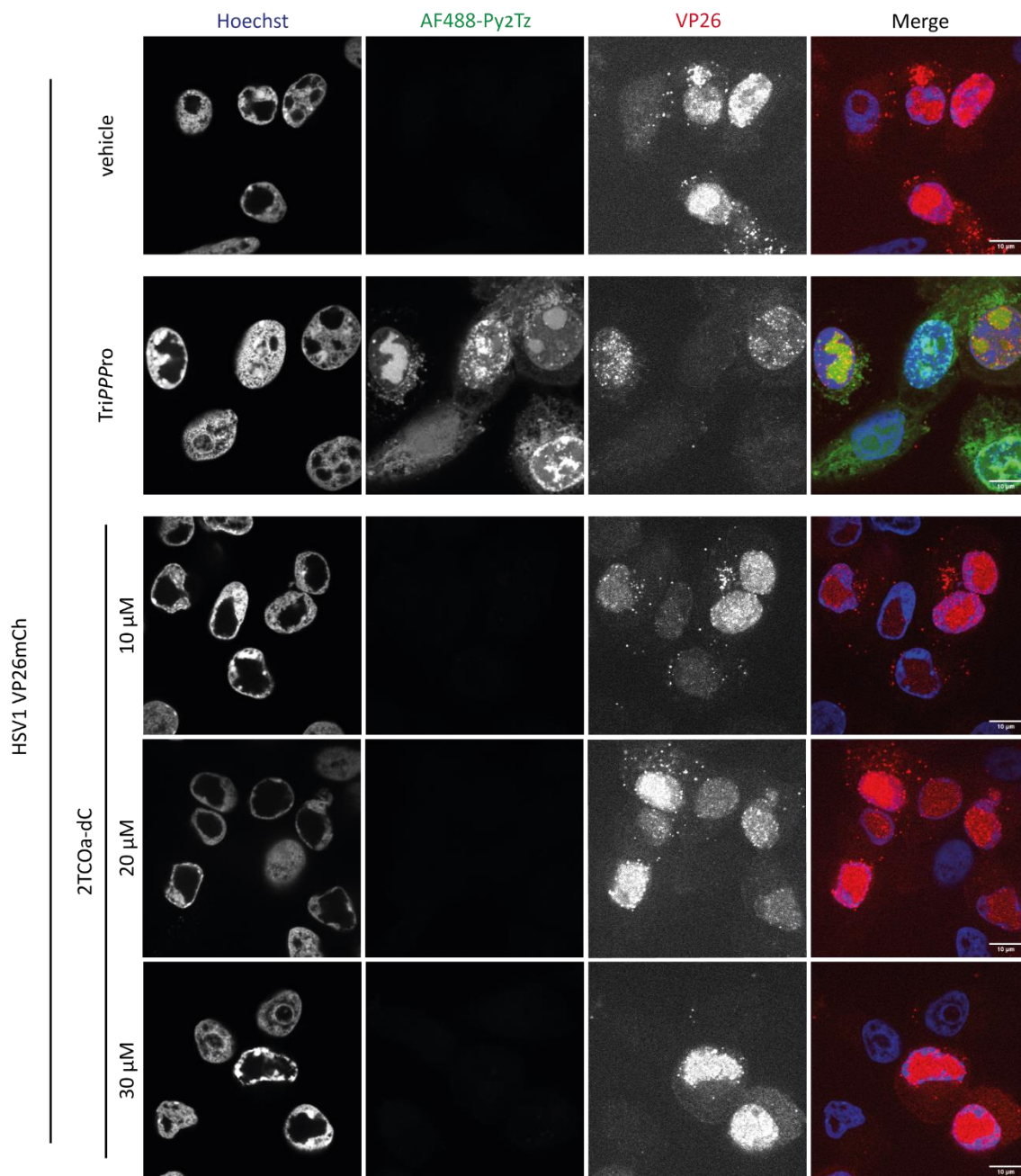


Figure 77: Confluent Vero cells were either mock- or HSV-1 VP26mCh-infected (MOI 3). The capsids of the HSV-1 are tagged with mCherry (*red*). 1 hpi medium was changed to VP-SFM and 4 hpi nascent DNA was labeled with 5  $\mu$ M of the pronucleotide  $\gamma$ -(C9C9AB)-2TCO $\alpha$ -dCTP **175**, or 10, 20, or 30  $\mu$ M of the parent nucleoside 2TCO $\alpha$ -dC **179** in VP-SFM. The TriPPPPro medium was renewed once at 6 hpi. After 8 hpi, cells were fixed and processed: Genomes containing incorporated 2TCO $\alpha$ -dC were stained overnight with AlexaFluor488-Py<sub>2</sub>Tz **212** (*green*). Nuclei were stained with Hoechst (*blue*). Samples were imaged at x100 magnification using a Nikon Eclipse Ti2 Spinning disc microscope. Individual channels are shown in greyscale and the merged image is shown in color. Scalebar = 10  $\mu$ m.

In parallel, uninfected cells were treated with pronucleotides **150** and **175** (5  $\mu\text{M}$ ) and their parent nucleosides **154** and **179** (30  $\mu\text{M}$ ).

Again, both metabolic pronucleotide reporters successfully initiate cellular DNA staining of dividing cells, confirming the results described above. In contrast, cells treated with the respective nucleosides lacked any specific AF488 signal.

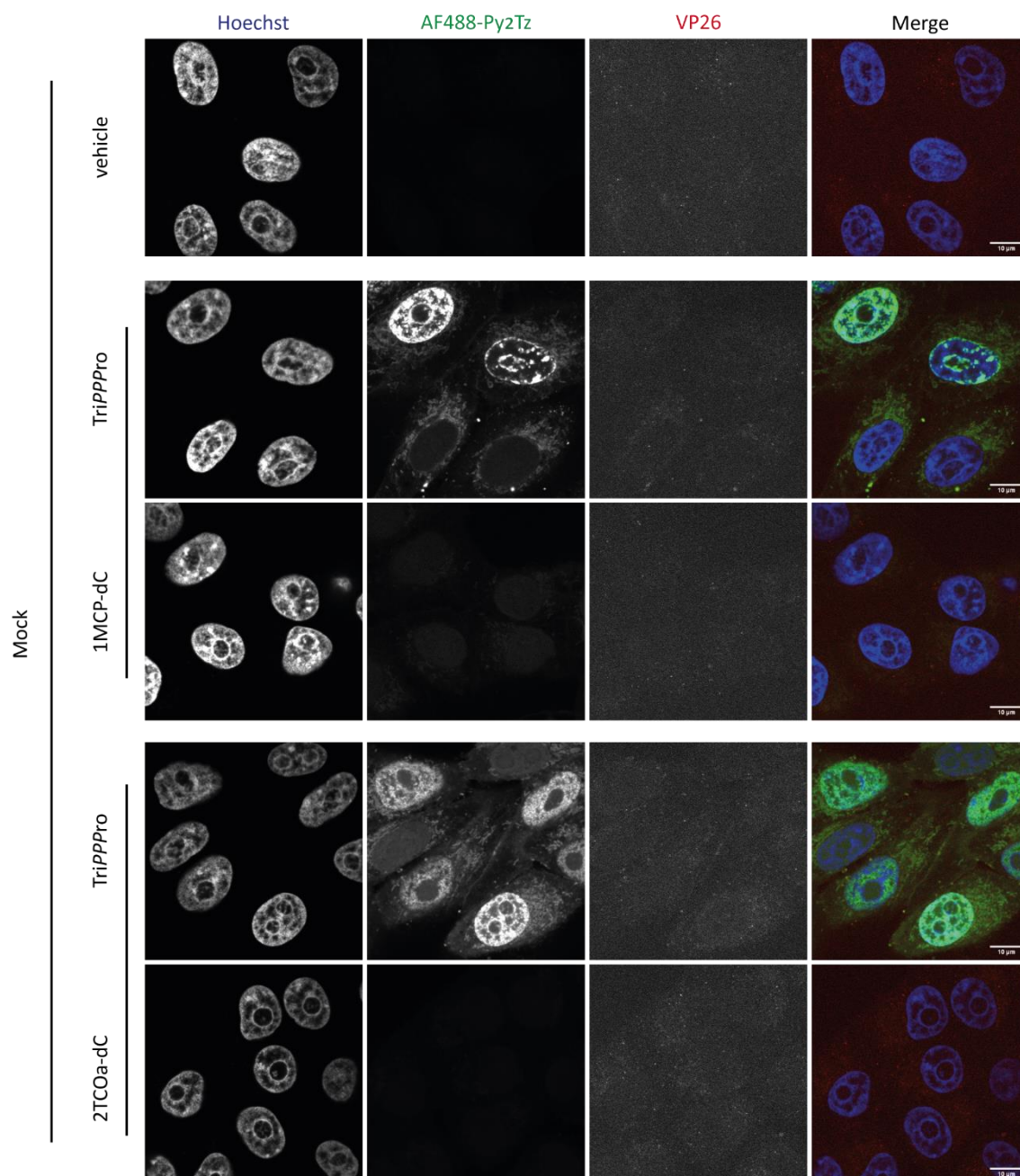


Figure 78: Confluent Vero cells were mock-infected. The capsids of the HSV-1 are tagged with mCherry (*red*). 1 hpi medium was changed to VP-SFM and 4 hpi nascent DNA was labeled with either 5  $\mu\text{M}$  of the pronucleotides **150** or **175**, or with 30  $\mu\text{M}$  of the parent nucleosides **154** or **179** in VP-SFM. The TriPPPPro medium was renewed once at 6 hpi. After 8 hpi, cells were fixed and processed: Genomes containing incorporated label were stained overnight with AlexaFluor488-Py<sub>2</sub>Tz **212** (*green*). Nuclei were stained with Hoechst (*blue*). Samples were imaged at x100 magnification using a Nikon Eclipse Ti2 Spinning disc microscope. Individual channels are shown in greyscale and the merged image is shown in color. Scalebar = 10  $\mu\text{m}$ .

These results impressively demonstrated the value of the TriPPP approach. The pronucleotide system enables the intracellular direct release of the triphosphate reporters and, thus, the incorporation of bioorthogonal labels, such as 1MCP or 2TCO $\alpha$ , into nucleic acids. This is in contrast to the respective nucleosides, which did not achieve specific staining, even at 6-fold higher treatment concentration; as explained, this may be due to the lack of phosphorylation of these nucleoside analogues by endogenous kinases. Hence, the triphosphate prodrug approach provides the potential for various exciting applications – far exceeding this work's fluorescence imaging focus.

#### 4.7.5 Evaluation of live-cell applications

To validate the applicability of live-cell imaging,  $\gamma$ -(C9C9AB)-2TCO $\alpha$ -dCTP **175** was tested as the most promising candidate since it possesses the fastest label and demonstrated the strongest labeling signal in fixed cells.

The synthesized SiR-tetrazine conjugates were chosen as the bioorthogonal partners due to their excellent cell-permeability. Initially, the conjugates SiR-Py<sub>2</sub>Tz **210**, SiR-BzTz **217**, and SiR-(*E*)-MeTz **213** (listed with decreasing reactivity) were added to Vero cells (5  $\mu$ M) and imaged without washing after around 2 h to assess the fluorophore-conjugates' background. The background signal across a single cell (*colored lines*) is plotted as signal intensity against distance (Figure 79). The SiR-Py<sub>2</sub>Tz **210** demonstrated the highest background with bright non-specific staining of cytoplasmatic organelles. Surprisingly, SiR-(*E*)-MeTz **213** showed the second-highest background, although it was solely synthesized due to its described “turn-off” properties initiated by TBET. SiR-BzTz **217** provided the lowest non-specific staining of the series. Naturally, the direct comparison of these fluorophores must be considered carefully since **210** and **217** are azetidine-SiRs, while **213** is a tetramethyl-SiR with different fluorogenic properties.



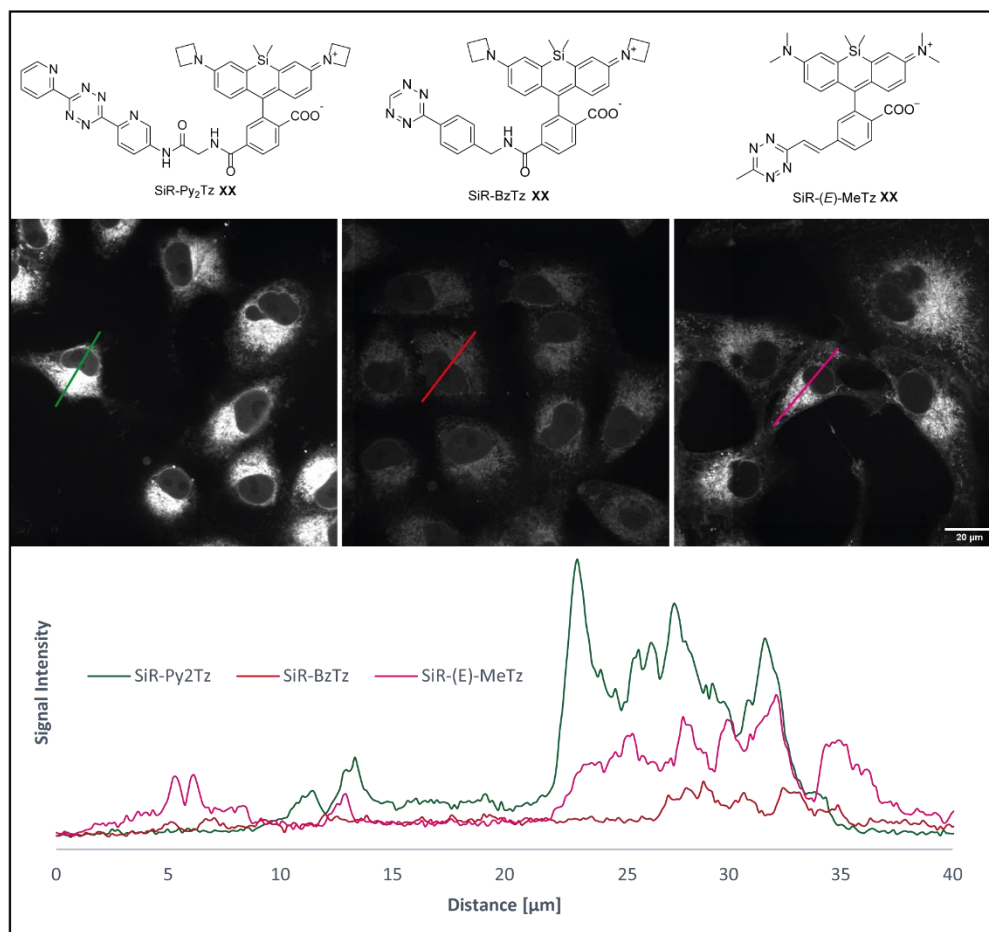


Figure 79: No-wash background signal of SiR-Py<sub>2</sub>Tz **210**, SiR-BzTz **217**, and SiR-(E)-MeTz **213** in Vero cells 2 h after addition (5 μM). The background signal intensity across a representative cell (colored lines) is plotted below.

Next, Vero cells were infected with HSV-1 VP26mCh to study the feasibility of live-cell imaging of *de novo* synthesized viral – and cellular DNA. Following the reliable protocol, 5 μM of  $\gamma$ -(C9C9AB)-2TCO $\alpha$ -dCTP **175** was added 4 hpi. After 6 hpi, the medium was renewed to improve the extracellular integrity of the AB group throughout the incorporation phase. 8 hpi, cells were washed with VP-SFM and stained with 5 μM of a SiR-tetrazine conjugate. Imaging was performed directly under no-wash conditions.

Excitingly, SiR-Py<sub>2</sub>Tz **210** provided clear staining of both cellular (top-left cell) and viral (bottom-right cells) DNA of living cells within one hour after dye addition. In contrast, SiR-BzTz **217** and SiR-(E)-MeTz **213** gave no detectable staining even after extended staining periods (Figure 80).

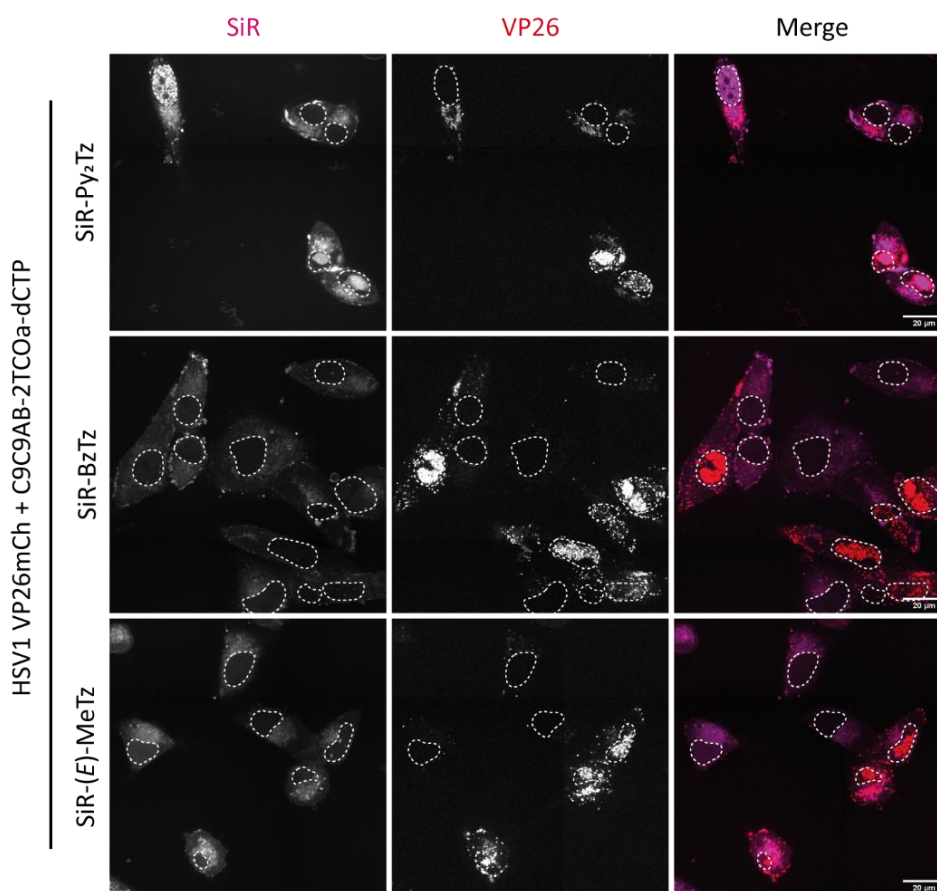


Figure 80: **Validation of live-cell application with  $\gamma$ -(C9C9AB)-2TCO $\alpha$ -dCTP **175** and selected SiR-tetrazine-conjugates.** Confluent Vero cells were infected with HSV-1 VP26mCh (MOI 3). The capsids of the HSV-1 are tagged with mCherry (red). 1 hpi medium was changed to VP-SFM and 4 hpi nascent DNA was labeled with 5  $\mu$ M  $\gamma$ -(C9C9AB)-2TCO $\alpha$ -dCTP **175** for 4 hours. The TriPPPro medium was renewed once at 6 hpi. After 8 hpi, the samples were washed in VP-SFM and stained with 5  $\mu$ M of SiR-Py<sub>2</sub>Tz **210**, SiR-BzTz **217**, or SiR-(E)-MeTz **213**. After 9 hpi, samples were imaged live at x100 magnification using a Nikon Eclipse Ti2 Spinning disc microscope. Individual channels are shown in greyscale and the merged image is shown in color. Nuclei outlines are circled. Scalebar = 10  $\mu$ m.

As described in Chapter 0, it must be considered that the 2-ene TCO/tetrazine reaction product can undergo  $\beta$ -elimination over time under the cleavage of the dye. Here, some substituted tetrazines, like Py<sub>2</sub>Tz, are less prone to an elimination reaction, thus more suited for labeling purposes. Therefore, the possibility must be considered that the BzTz or MeTz motif could react with the 2TCO $\alpha$  label followed by a rapid  $\beta$ -elimination reaction, preventing a detectable fluorescent signal formation.

However, it seemed more striking that the superior reactivity of the Py<sub>2</sub>Tz motif enabled successful staining of metabolically labeled DNA, whereas the lower reaction rates of the conjugates SiR-BzTz **217** and SiR-(E)-MeTz **213** impeded efficient staining.

Next, different concentrations between 0 and 10  $\mu$ M of  $\gamma$ -(C9C9AB)-2TCO $\alpha$ -dCTP **175** were tested to validate the optimal concentration of the pronucleotide for live-cell imaging applications. Similarly, as described above, Vero cells were infected with HSV-1

VP26mCh and treated with 0 to 10  $\mu\text{M}$  of **175** 4 hpi. The TriPPPPro medium was renewed at 5.5 hpi and changed to VP-SFM after 7 hpi. After 8 hpi, cells were briefly washed with VP-SFM and stained with 5  $\mu\text{M}$  of SiR-Py<sub>2</sub>Tz **210** in the presence of 10  $\mu\text{M}$  verapamil, a calcium channel blocker. In literature, cases are described where SiR-based sensor molecules exhibit improved staining in live cells with verapamil present.<sup>187</sup> However, in this work, live-cell experiments without verapamil treatment showed similar staining results, suggesting that the use of verapamil is redundant. The samples were imaged after 11 hpi.

The vehicle control (0  $\mu\text{M}$ ) displays the background under no-wash conditions. Samples treated with 0.5  $\mu\text{M}$  of **175** showed no visual staining of RCs, whereas 1.5  $\mu\text{M}$  of the pronucleotide displayed some labeling of viral DNA, colocalizing with the VP26mCh signal. At a concentration of 5  $\mu\text{M}$  the strongest labeling signal and clear staining of viral replication factories were observable (VP26mCh colocalization). The highest concentration of **175** (10  $\mu\text{M}$ ) led to cell death after 11 hpi. These results are in agreement with the dose-dependent labeling of viral DNA with  $\gamma$ -(C9C9AB)-1MCP-dCTP **150** in fixed Vero cells described in Chapter 4.7.3.

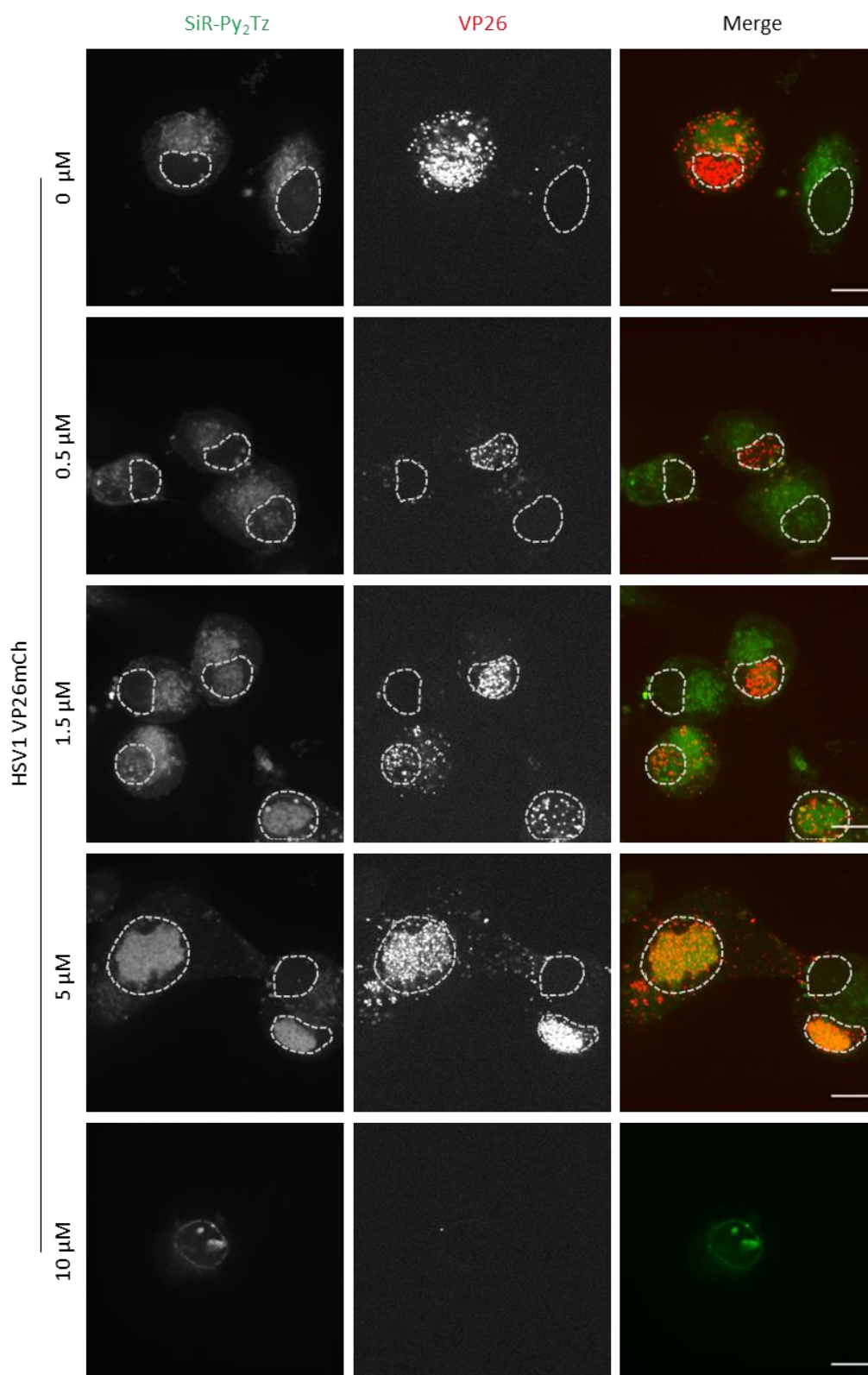


Figure 81: **Optimization of  $\gamma$ -(C9C9AB)-2TCO $\alpha$ -dCTP 175 concentration.** Confluent Vero cells were infected with HSV-1 VP26mCh (MOI 3). The capsids of the HSV-1 are tagged with mCherry (red). 1 hpi medium was changed to VP-SFM and 4 hpi nascent DNA was labeled with  $\gamma$ -(C9C9AB)-2TCO $\alpha$ -dCTP 175 for 3 hours at the indicated concentrations. The TriPPPPro medium was renewed once at 5.5 hpi and changed to VP-SFM at 7 hpi. After 8 hpi, the samples were washed in VP-SFM and stained with 5  $\mu$ M SiR-Py<sub>2</sub>Tz 210 in the presence of 10  $\mu$ M verapamil. After 11 hpi, samples were imaged live at x100 magnification using a Nikon Eclipse Ti2 Spinning disc microscope. Individual channels are shown in greyscale and the merged image is shown in color. Nuclei outlines are circled. Scalebar = 10  $\mu$ m.

Unfortunately, the SiR-Py<sub>2</sub>Tz **210** displays a relatively high background in the cytoplasm. However, the following image points out an opportunity for improvements (Figure 82). Staining was performed with 5 μM JF526-Py<sub>2</sub>Tz **209** within two hours under no-wash conditions. The conjugate provided successful staining of the viral DNA inside of RCs and novel cellular DNA. The low  $K_{L-Z}$  constant of JF526 provides the dye with the necessary membrane permeability, and the fluorophore showed an improved cellular background compared to SiR-Py<sub>2</sub>Tz **210** (compare with Figure 80). However, the JF526 dye is poorly suited for modern fluorescent microscopes since its spectral properties are unfitting to commonly built-in lasers and filters. Additionally, the fluorophore's absorption and emission spectra interfere with the simultaneous utilization of FPs, like mCherry or GFP.

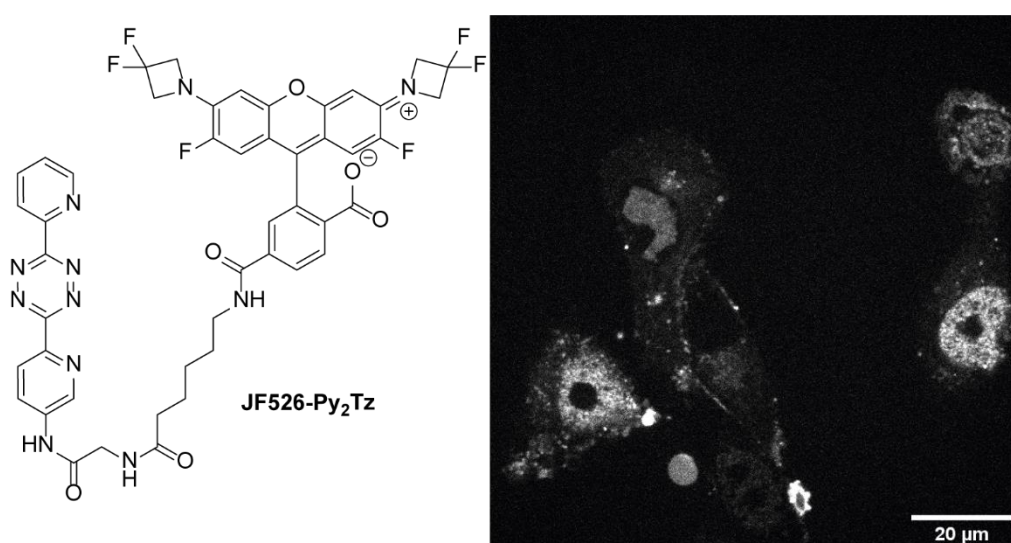


Figure 82: **Live-cell staining of incorporated 2TCO $\alpha$ -dC with JF526-Py<sub>2</sub>Tz **209**.** Confluent Vero cells were infected with HSV-1 VP26mCh (MOI 3). The capsids of the HSV-1 are tagged with mCherry (*red*). 1 hpi medium was changed to VP-SFM and 4 hpi nascent DNA was labeled with  $\gamma$ -(C9C9AB)-2TCO $\alpha$ -dCTP **175** for 4 hours at the indicated concentrations. The TriPPPPro medium was renewed once at 6 hpi. After 8 hpi, the samples were washed in VP-SFM and stained with 5 μM of JF526-Py<sub>2</sub>Tz **209**. After 10 hpi, samples were imaged live at x100 magnification using a Nikon Eclipse Ti2 Spinning disc microscope. Individual channels are shown in greyscale and the merged image is shown in color. Scalebar = 10 μm.

For the first time, these results demonstrate the successful metabolic labeling of viral and cellular DNA in living cells under no-wash conditions by combining the TriPPPPro concept with fast bioorthogonal labels of the strain-promoted DA<sub>INV</sub>. Furthermore, it was outlined that there are opportunities to improve the application further. Exciting are the options to screen different rhodamine dyes with low  $K_{L-Z}$ , to try other fluorophore classes, to change the dye-tetrazine linkage for potential “turn-off” properties (FRET or TBET) or to improved cellular distribution, and to further push the reactivity of the tetrazine by exchanging one 2-pyridyl group to a 2-pyrimidyl substitute. Such designs are already underway in our laboratories.

On the other side, exploring further improvements made for the TCO label might be exciting and worthy of the increased synthetic effort. The conformationally strained dioxolane-fused trans-cyclooctene (d-TCO, Chapter 2.6) exhibited considerably improved reaction kinetics to 4TCO or 2TCO $\alpha$ , and demonstrated exceptional stability in human serum.<sup>57</sup>

In short, the successful live-cell imaging of metabolically labeled DNA breaks the ground for future improvements and various fascinating applications yet to come.

#### 4.7.6 Evaluation of vinyl functionalized pronucleotides

Others initially tested the vinyl-modified 2'-deoxynucleotide prodrugs with poor results (data not shown). Here, the vinyl functionalized reporter series comprising VdU **16** and VdA **18** and their respective C9C9AB and  $\gamma$ -C11,C9AB pronucleotides were tested under comparable labeling conditions described for the "faster" pronucleotide reporters in the chapters above.

Mock- or HSV-1 VP26mCh-infected Vero cells were treated with the respective vinyl-modified reporters 4 hpi. The parent nucleosides were added at a concentration of 20  $\mu$ M. In contrast, the pronucleotides were added in the usual concentration of 5  $\mu$ M with the renewal of the medium after 6 hpi to improve the extracellular integrity of the AB groups throughout the incorporation phase. After 8 hpi, cells were washed with VP-SFM, fixed, permeabilized, and stained with AF488-Py<sub>2</sub>Tz **212** (*green*) overnight at room temperature. The staining was performed in an acidified mixture of PBS and 6% DMSO (pH of 5, acetic acid). The applied conditions were used by KUBOTA *et al.* for staining the incorporated RNA reporters VU **17** and VA **19** in HEK293T cells.<sup>65</sup> They found that the **DA<sub>INV</sub>** reaction rate between the tetrazine and the vinyl label increases under acidic conditions in the presence of DMSO – potentially due to lowering the HOMO of the dienophile after protonating its nucleobase.

However, even under these improved labeling conditions the vinyl functionalized nucleoside and pronucleotide reporters showed no or inconclusive viral or cellular DNA labeling in Vero cells.

Figure 83 shows HSV-1 VP26mCh (*red*) infected Vero cells treated with the indicated reporters in reference to the untreated vehicle control. Since most probe's signals did not or barely exceed the non-specific signal of the vehicle control, there was no assertion possible if successful incorporation of the reporters was achieved. However, except for the  $\gamma$ -alkylated pronucleotide reporters, where no prior knowledge is available, it is reasonable to assume that the vinyl label was incorporated due to its small size and high biocompatibility. Therefore, it was concluded that the vinyl label with reaction kinetics in the magnitude of  $10^{-2} \text{ M}^{-1}\text{s}^{-1}$  does not provide the reactivity necessary for simple staining conditions, which do not rely on heavy sample preparation, e.g., denaturation, acidification, or extensive washing steps.

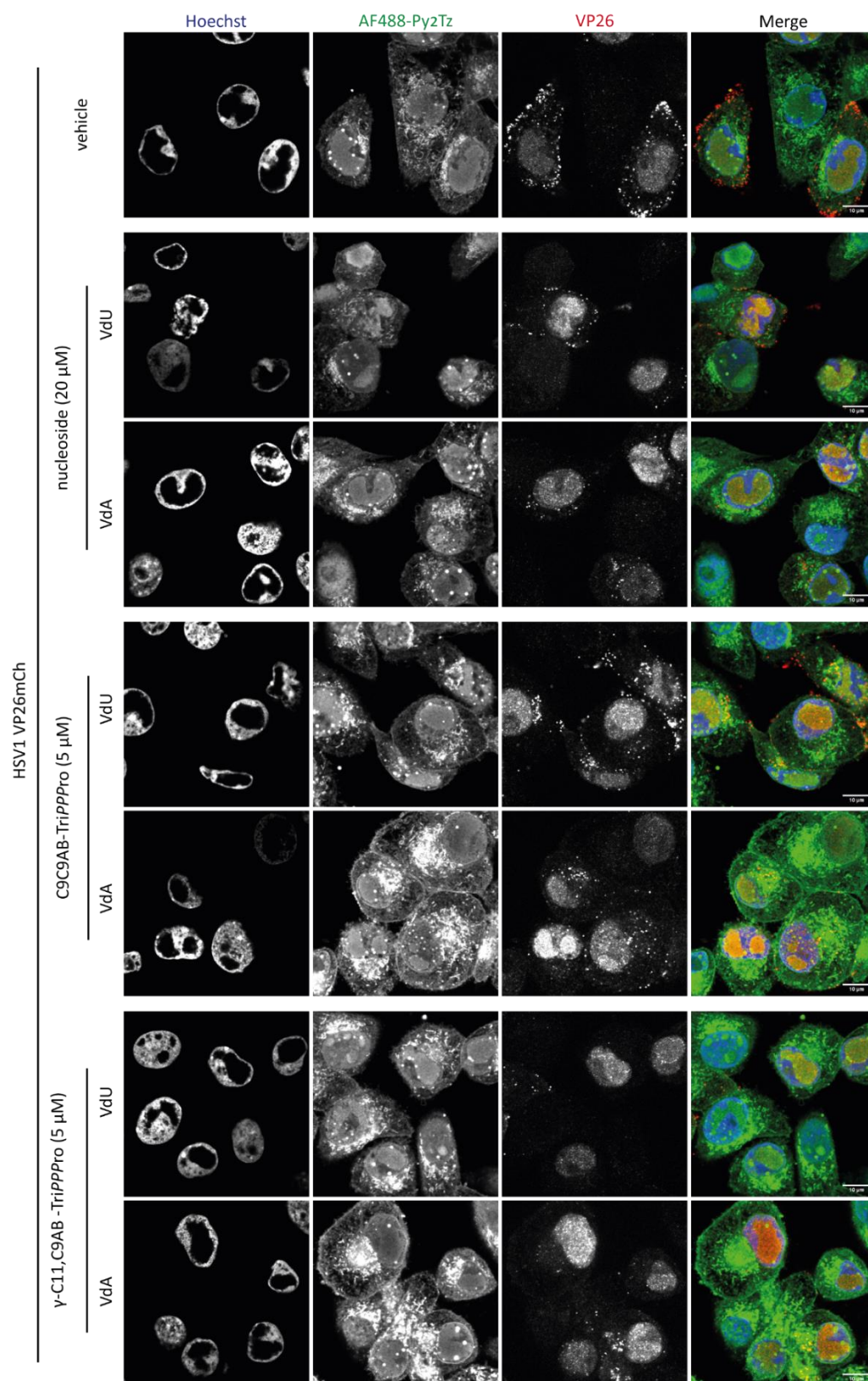


Figure 83: Confluent Vero cells were infected with HSV-1 VP26mCh (MOI 3). The capsids of the HSV-1 are tagged with mCherry (*red*). 1 hpi medium was changed to VP-SFM and 4 hpi nascent DNA were labeled for 4 hours with the respective reporters as indicated in the figure. The TriPPPPro media were renewed once at 6 hpi. After 8 hpi, cells were fixed and processed: Genomes containing incorporated label were stained overnight with AlexaFluor488-Py<sub>2</sub>Tz **212** (*green*). Nuclei were stained with Hoechst (*blue*). Samples were imaged at x100 magnification using a Nikon Eclipse Ti2 Spinning disc microscope. Individual channels are shown in greyscale and the merged image is shown in color. Scalebar = 10 μm.



Figure 84 shows uninfected Vero cells treated with the respective vinyl reporters. Again, the vehicle control was not treated with any reporter and displayed the fluorophore's background. Compared to the vehicle control, all samples showed an increase in overall background both in the cytoplasm and throughout the nucleus. Moreover, the AF488 signal in the nucleus did not colocalize with the Hoechst staining, which indicates a non-specific background signal.

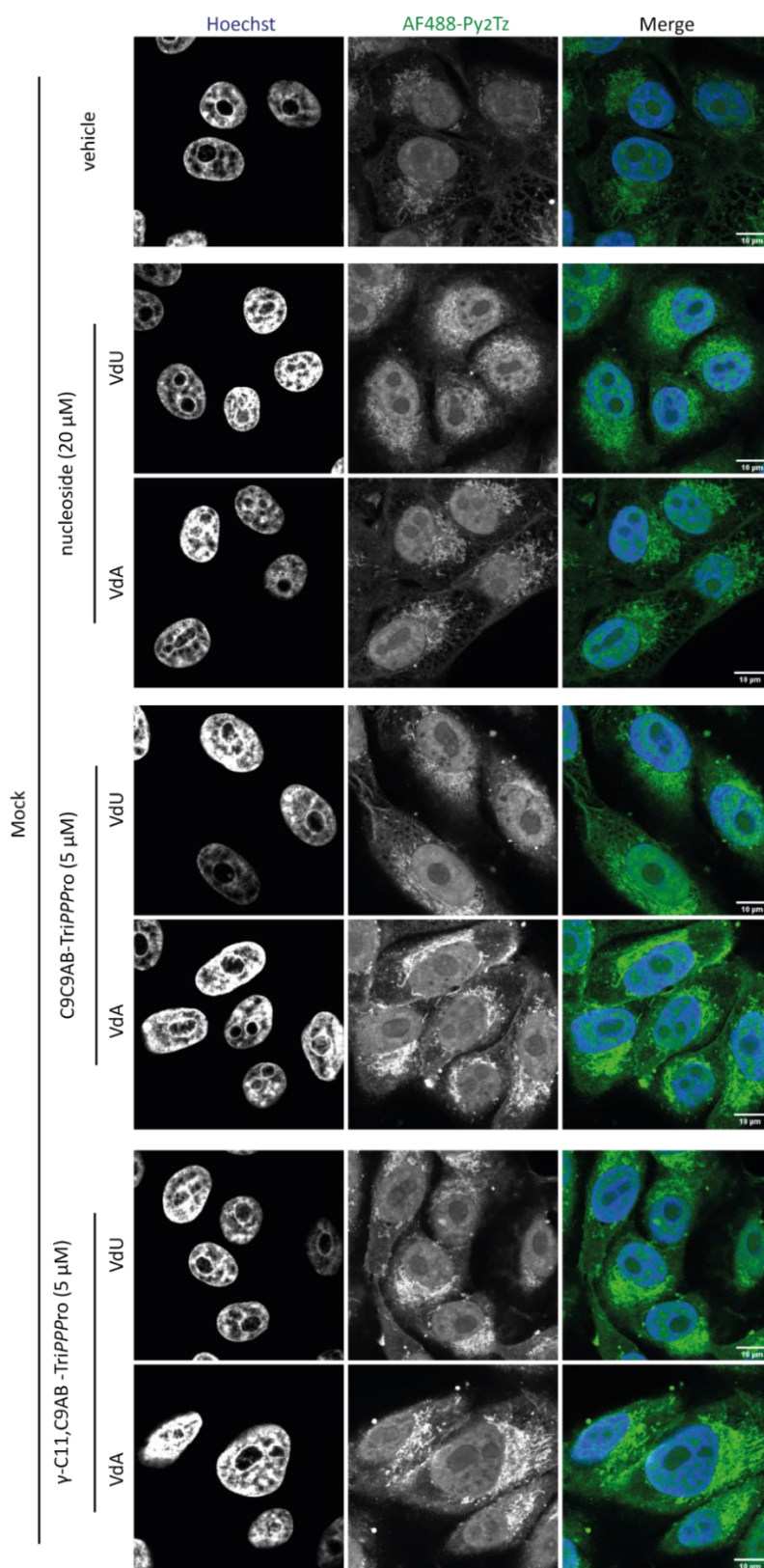


Figure 84: Confluent Vero cells were mock-infected. 1 hpi medium was changed to VP-SFM and 4 hpi nascent DNA were labeled for 4 hours with the respective reporters as indicated in the figure. The TriPPPPro media were renewed once at 6 hpi. After 8 hpi, cells were fixed and processed: Genomes containing incorporated label were stained overnight with AlexaFluor488-Py<sub>2</sub>Tz **212** (*green*). Nuclei were stained with Hoechst (*blue*). Samples were imaged at x100 magnification using a Nikon Eclipse Ti2 Spinning disc microscope. Individual channels are shown in greyscale and the merged image is shown in color. Scalebar = 10 μm.

Naturally, these findings were a setback to this work since the initial focus lay upon elevating the vinyl motif by applying different pronucleotide strategies. The objective was to improve the intracellular bioavailability of the vinyl functionalized nucleoside triphosphates and, therefore, to boost the reporter's incorporation. Furthermore, the applicability of discriminating viral polymerases over cellular targets with novel  $\gamma$ -alkylated pronucleotides should be evaluated.

The underlying assumption was that higher incorporation rates would ultimately improve the overall labeling signal. Together, the absence of any significant vinyl-deriving signal and the observation that only the fastest reaction partners, namely 1MCP/Py<sub>2</sub>Tz and 2TCO $\alpha$ /Py<sub>2</sub>Tz, provide efficient DNA labeling, consolidate the premise that high reaction kinetics must be the primary focus for successful labeling in fixed, and especially, in live cells.

Regarding pronucleotide chemistry, these findings further point to the value of the TriPPP<sub>ro</sub> concept since more demanding labels must be introduced into *de novo* synthesized nucleic acids to ensure sufficient speed for efficient staining.

Unfortunately, the evaluation of the applicability of novel  $\gamma$ -alkylated triphosphate prodrug systems is not feasible with vinyl-modified reporters due to the overall lack of detectable signal. The concept could be transferred to faster labels, e.g., to 1MCP-dC **154** or 2TCO $\alpha$ -dC **179** as initial candidates.

## 4.8 Study and production of genome labeled HSV-1

This chapter evaluates the potential to produce and isolate genome labeled HSV-1 particles. The development of such a method would allow the spatiotemporal investigation of the genome trafficking of the early infection cycle on a single-particle level. A necessary criterion is that the produced virus is still infectious, although its genome is altered by the incorporated label or even stained by the respective fluorophore. The following results are also the subject matter of the co-supervised master thesis<sup>185</sup> of Dörte Stalling.

### Incorporation of the 2TCOa label into vDNA reduces HSV-1 infectivity

The virus production protocol was adapted from the production of EdC-labeled viruses<sup>46</sup> and is illustrated in Figure 85A. In general, Vero cells were infected with a MOI of 0.01 PFU and treated with the respective TriPPP compound 2 hpi and 24 hpi. As a control, cells were treated with the same volumes of DMSO. After 72 hpi, the virus-containing supernatants were removed, and the viruses were isolated.

Here,  $\gamma$ -(C9C9AB)-2TCO $\alpha$ -dCTP **175** was selected as an initial candidate since it provided the best imaging results. Different TriPPP concentrations between 0 and 10  $\mu$ M were added to study the dose-dependency of the pronucleotide on viral infectivity, and the respective isolated virus was tested for its plaque-forming ability (viral titer) (Figure 85B).

Increasing volumes of DMSO only showed marginal effects on viral infectivity. In contrast, with increasing concentrations of **175**, the ability of the produced and labeled virus to infect cells decreased. Up to a concentration of 1.5  $\mu$ M of **175**, the virus titer decreased by around one log. The concentration of 5  $\mu$ M diminished infectivity by 2 logs. The treatment of host cells with 10  $\mu$ M of pronucleotide led to the ability of the virus to form plaques only below the detection limit. Thus, a concentration of 1.5  $\mu$ M was

selected as an initial starting point for virus production since it balances out cell health, genome labeling and viral infectivity (also see Chapter 4.7.5).

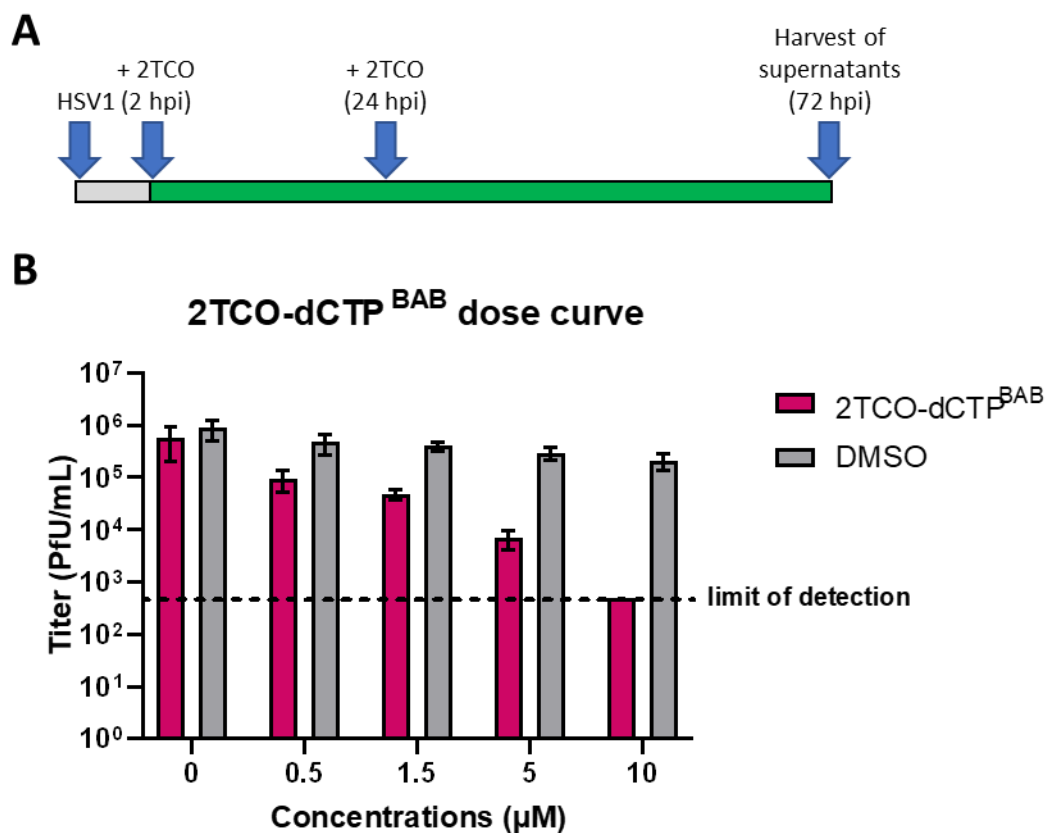


Figure 85: Dose curve of HSV-1<sup>2TCO $\alpha$</sup>  production with incorporated 2TCO $\alpha$  label. (A) Illustration of production. Cells were infected with HSV-1 VP26mCh at an MOI of 0.01 PfU. 2 hpi cells were washed, and  $\gamma$ -(C9C9AB)-2TCO $\alpha$ -dCTP (**175**, 2TCO $\alpha$ -dCTP<sup>BAB</sup>) was added in VP-SFM at concentrations as indicated. As a control, cells were treated with the same volume of DMSO. 24 hpi **175** or DMSO were added again. After 72 hpi, supernatants were harvested and removed from cell debris. The titer of the samples was assessed by plaque assay. The experiment was carried out in triplicate. (B) Quantitative analysis.<sup>185</sup>

### Production of dual-labeled HSV-1 (HSV-1<sup>1MCP</sup> and HSV-1<sup>2TCO $\alpha$</sup> )

Next, genome labeled HSV-1 VP26mCh was produced with either incorporated 1MCP or 2TCO $\alpha$ . The virus production was performed as described above with 1.5  $\mu\text{M}$  of the respective pronucleotides  $\gamma$ -(C9C9AB)-1MCP-dCTP **150** or  $\gamma$ -(C9C9AB)-2TCO $\alpha$ -dCTP **175**. The dual-labeled viruses will be referred to as HSV-1<sup>1MCP</sup> or HSV-1<sup>2TCO $\alpha$</sup> . As a control, EdC-labeled virus (HSV-1<sup>EdC</sup>) was produced in the same manner since it also comprises an artificial motif but cannot react with tetrazines.

After virus harvesting, the labeled particles were concentrated by high-speed centrifugation and purified by continuous gradient, which enabled the isolation of the virus with high titers (Table 1).

Table 1: Viral titers of the dual-labeled viruses.<sup>185</sup>

	HSV-1 <sup>EdC</sup>	HSV-1 <sup>2TCOa</sup>	HSV-1 <sup>1MCP</sup>
Titer (PFU/mL)	4.38 * 10 <sup>8</sup>	6.1 * 10 <sup>8</sup>	2.35 * 10 <sup>8</sup>

In the next step, incorporation of the labels into the genome of the produced virus was examined. The viral particles were hence adsorbed on precleaned carrier glass slides. The samples were washed with PBS and stained with 5  $\mu$ M SiR-Py<sub>2</sub>Tz **210** for 30 min (Figure 86A). Following this, the samples were imaged and processed for the VP26mCherry tag (*red*) and the silicon-rhodamine staining of the incorporated labels (*green*). Representative images for HSV-1<sup>EdC</sup>, HSV-1<sup>2TCOa</sup>, and HSV-1<sup>1MCP</sup> are displayed in Figure 86B.

An ImageJ plugin was used to detect and select VP26mCh labeled capsids. Signals were categorized as capsids with signal intensities above a threshold of 4000 units and a diameter below 0.66  $\mu$ m. At least 1000 capsids were quantified per sample to validate the colocalization of the capsids with the stained label. The signal intensity of the SiR fluorophore was analyzed and is illustrated in Figure 86D. Here, the signal of the HSV-1<sup>2TCOa</sup> samples is significantly higher compared to both the control HSV-1<sup>EdC</sup> and the HSV-1<sup>1MCP</sup> samples, giving evidence for the successful incorporation and subsequent staining with the fluorophore-dye-conjugate. It was assumed that the SiR-Py<sub>2</sub>Tz **210** unspecifically binds to viral structures due to its lipophilic nature and therefore caused high background in the HSV-1<sup>EdC</sup> control samples. Again, future novel membrane-permeable rhodamine-tetrazine-conjugates, which are less prone to unspecific binding, could improve background staining and further validate these findings.

HSV-1<sup>1MCP</sup> displayed a similar signal intensity distribution to the HSV-1<sup>EdC</sup> control samples. Since the reaction rate of the 1MCP label is three magnitudes lower than that of TCOs, it is reasonable to assume that staining times of 30 min are not sufficient for a detectable signal built-up. In future, a faster tetrazine motif or prolonged staining times could result in a detectable 1MCP-originated signal. Moreover, fluorophore-tetrazine-conjugate addition during viral replication in the producer host cells, e.g., after 48 hpi, could be an elegant way to prolong staining times and isolate fluorophore tagged viruses.

Next, the VP26mCh signals (1000 capsids) were analyzed for colocalization with the SiR signal for each dual-labelled virus. Positive colocalization of the *green* and *red* signals is indicated in *yellow* (Figure 86B and C). For calculations, the SiR threshold was set to the mean intensity of the HSV-1<sup>EdC</sup> SiR signal plus one standard deviation (Figure 86D, threshold). 2TCO $\alpha$  labeled viruses showed 85% colocalization of the VP26mCh and stained genome. The capsids of the HSV-1<sup>EdC</sup> control were 50% positive for the SiR dye. The HSV-1<sup>1MCP</sup> sample showed 30% colocalization. Also, the presumed unspecific binding of SiR-Py<sub>2</sub>Tz **210** prohibits final conclusions; however, it seemed striking that the 2TCO $\alpha$  label was successfully incorporated into the viral genome and subsequently tagged by a fluorophore. The validation of successful 1MCP incorporation must be addressed in future studies.

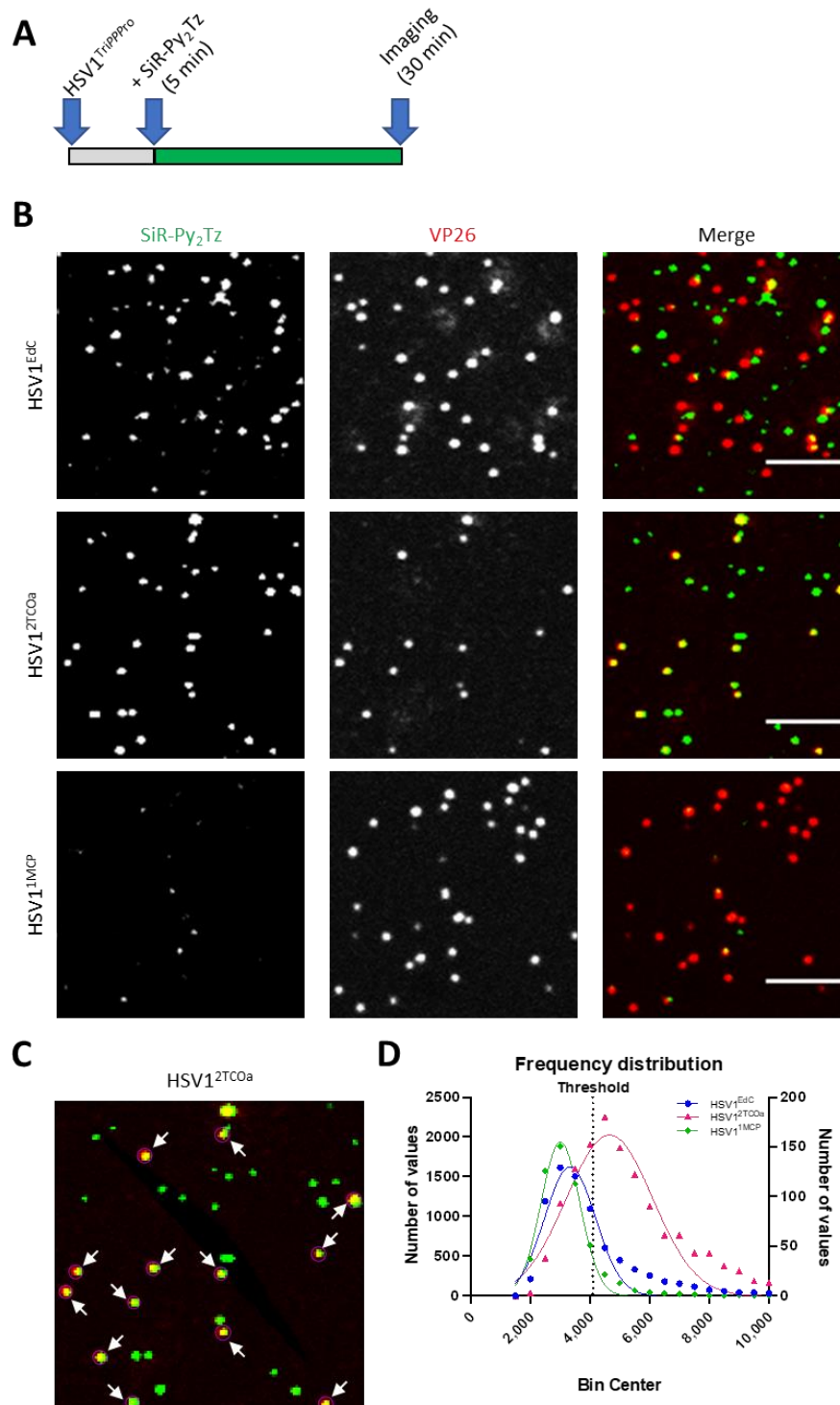


Figure 86: Validation of successful dual-labeling of HSV-1<sup>EdC</sup>, HSV-1<sup>2TCOa</sup>, and HSV-1<sup>1MCP</sup> with SiR-Py<sub>2</sub>Tz 210 staining. (A) Equivalent samples of HSV-1<sup>EdC</sup>, HSV-1<sup>2TCOa</sup>, or HSV-1<sup>1MCP</sup> were adsorbed onto precleaned Ibidi 8 well plates with a glass bottom. Capsid protein VP26 was tagged with mCherry (red). After 5 minutes, the samples were washed with PBS and stained with SiR-Py<sub>2</sub>Tz 210 (green). About 30 minutes later, the samples were imaged using a Nikon Eclipse Ti2 Spinning disk microscope. (B) Individual channels are shown in greyscales and merged images in color. A yellow signal indicates the colocalization of the red and green signals. Scale bar, 5  $\mu$ m. (C) Signal intensities were quantified using the ImageJ TrackMate plugin. Positiv capsid signals were defined, and the signal intensities of the silicon rhodamine were measured. One exemplary panel is shown for the color-coded outline overlay produced by the ImageJ plugin for particle analysis. (D) Statistical analysis was performed using one-way ANOVA, \*\*\*\* $p < 0.0001$ ; \*\*\* $p < 0.001$ .<sup>185</sup>



Moreover, the procedure was repeated with AF488-Py<sub>2</sub>Tz **212** as a further negative control. Since the rhodamine dye is not membrane permeable due to its sulfate groups, the conjugate is not able to stain the viral genome of intact particles. Again, the dual-labeled HSV-1 was adsorbed to glass slides, washed with PBS and stained for 30 min. The samples were imaged after a second washing step in both individual channels (VP26mCh in *red*, **212** in *green*). Figure 87 displays representative images of HSV-1<sup>EdC</sup>, HSV-1<sup>2TCO<sub>α</sub></sup>, and HSV-1<sup>1MCP</sup>. None of the produced viruses exhibited any green signal increase higher than the HSV-1<sup>EdC</sup> control.

It was concluded that the staining of HSV-2<sup>TCO $\alpha$</sup>  with SiR-Py<sub>2</sub>Tz **210** represents a signal from successful tagging of the incorporated 2TCO $\alpha$  of intact viral particles.

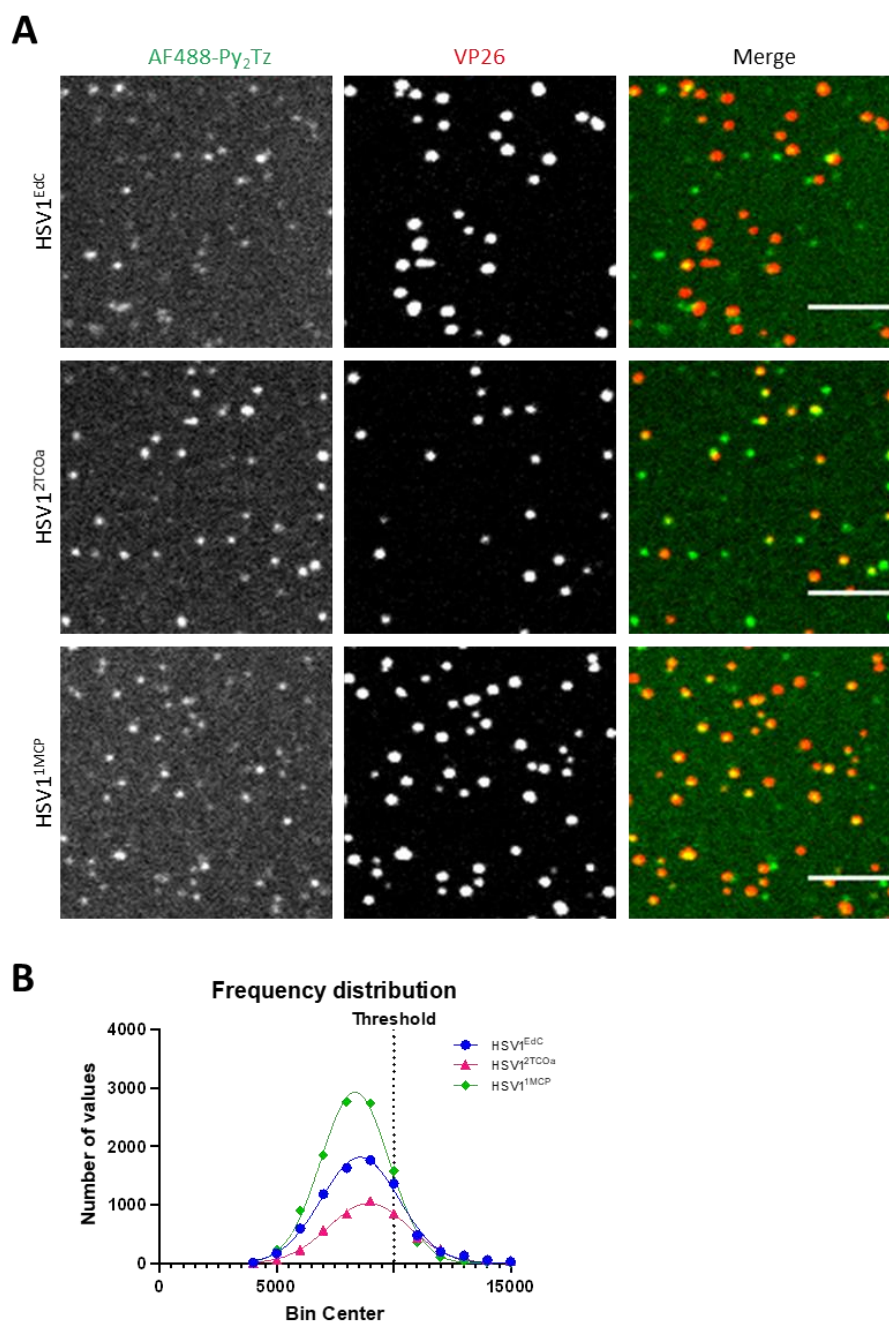


Figure 87: Validation of successful dual-labeling of HSV-1<sup>EdC</sup>, HSV-1<sup>2TCO $\alpha$</sup> , and HSV-1<sup>1MCP</sup> with AF488-Py<sub>2</sub>Tz **212** staining. (A) Equivalent samples of HSV-1<sup>EdC</sup>, HSV-1<sup>2TCO $\alpha$</sup> , or HSV-1<sup>1MCP</sup> were adsorbed onto precleaned ibidi 8 well plates with a glass bottom. Capsid protein VP26 was tagged with mCherry (red). After 5 minutes, the samples were washed with PBS and stained with AF488-Py<sub>2</sub>Tz **212** (green). About 30 minutes later, the samples were imaged using a Nikon Eclipse Ti2 Spinning disk microscope. Individual channels are shown in greyscales and merged images in color. A yellow signal indicates the colocalization of the red and green signals. Scale bar, 5  $\mu$ m. (B) Signal intensities were quantified using the TrackMate plugin in ImageJ. Positive capsid signals were defined, and the signal intensities of the silicon rhodamine were measured. Statistical analysis was performed using one-way ANOVA, \*\*p < 0.01; \*p < 0.1.<sup>185</sup>

### ***In situ* staining of HSV-1<sup>2TCO $\alpha$</sup> particles still leads to high cellular background noise**

Next, Vero cells were infected with HSV-1<sup>2TCO $\alpha$</sup>  to investigate the potential for visualizing the early infection of the virus. The SiR-Py<sub>2</sub>Tz **210** was added to the virus 30 min prior to infection to improve labeling efficiency. The mixture was then added to Vero cells with an MOI of 10 PFU. The cells were washed after 1 hpi and stained with Hoechst dye. The imaging was performed 90 min post-infection. As a control, unlabeled HSV-1 VP26mCh was processed in parallel (Figure 88). Despite washing steps, the SiR dye exhibited such a high background in the cytoplasm that the verification of successful dual labeling was not possible. Future fluorophore-conjugates, which cause less unspecific binding, will potentially help to facilitate such a simple experimental procedure.

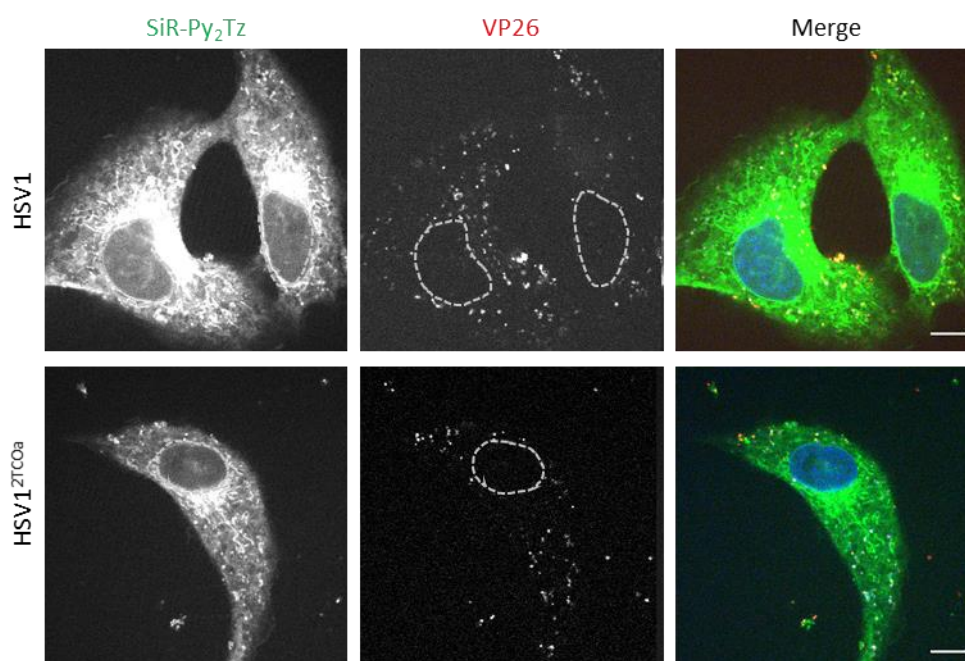


Figure 88: **Attempts to visualize HSV-1<sup>2TCO $\alpha$</sup>  cell entry.** Cells were infected with HSV-1 VP26mCh or dual-labeled HSV-1<sup>2TCO $\alpha$</sup> , which were incubated prior with SiR-Py<sub>2</sub>Tz **210** for 30 min. 1 hpi medium was changed and the samples were stained with 5  $\mu$ M SiR-Py<sub>2</sub>Tz (green) for 30 minutes. Nuclei were counterstained with Hoechst (blue). Individual channels are shown in greyscale and merged images in color. Scale bar, 10  $\mu$ m.<sup>185</sup>

### **Production of dual-labeled and prestained viruses**

To circumvent the issue of the fluorophore's background, produced HSV-1<sup>2TCO $\alpha$</sup>  was stained with 10  $\mu$ M of SiR-Py<sub>2</sub>Tz **210** for 30 min before gradient purification, causing the removal of the excessive fluorophore. The production of dual-labeled HSV-1<sup>2TCO $\alpha$ +SiR</sup> resulted in viral titers (4.43 x10<sup>8</sup> PFU) in the same magnitude than to unstained HSV-1<sup>2TCO $\alpha$</sup> .

As done previously with HSV-1<sup>2TCO $\alpha$</sup> , the HSV-1<sup>2TCO $\alpha$ +SiR</sup> was adsorbed on precleaned glass slides. After washing with PBS, the viral particles were imaged for the VP26mCh (*red*) and the SiR signal (*green*) (Figure 89A). The representative images display colocalization of almost all red and green signals, indicating successful fluorescent labeling of viral genomes. Quantification of these results is currently not possible since an appropriate HSV-1<sup>SiR</sup> control is lacking.

Next, the HSV-1<sup>2TCO $\alpha$ +SiR</sup> were tested *in vivo* (Figure 89B). Hoechst-stained Vero cells were infected with dual-labeled HSV-1<sup>2TCO $\alpha$ +SiR</sup> (MOI of 20 PFU). After 1 hpi, the medium was changed to VP-SFM, and the infected cells were fixed and imaged at 90 min post-infection. Most viral particles are attached to the cellular membrane. However, events were visible where dual-labeled particles locate in the cytosol or near the nuclear membrane (as highlighted by the image enlargement of Figure 89B).

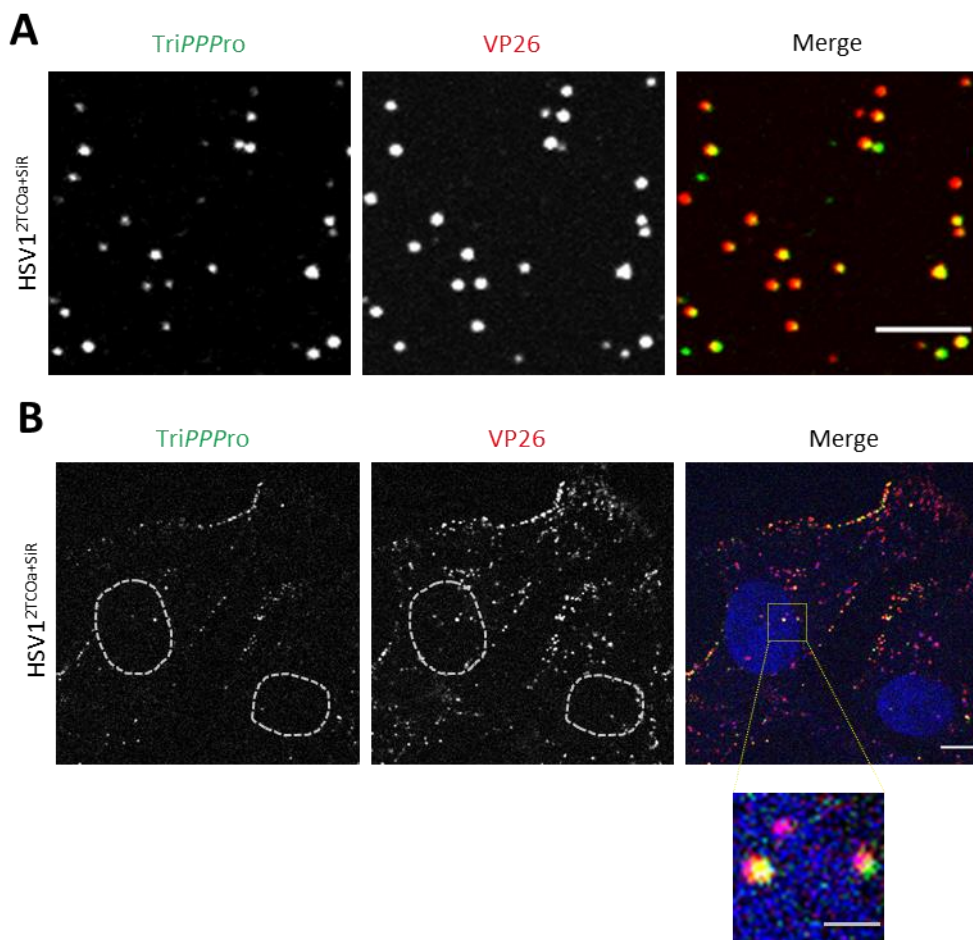


Figure 89: **Visualization of HSV-1<sup>2TCOα+SiR</sup> *in vitro* and *in vivo*.** (A) Dual-labeled HSV-1<sup>2TCOα+SiR</sup> was adsorbed on precleaned IBIDI 8 well plate with a glass bottom for 5 minutes. The samples were washed three times in PBS before imaging. The SiR-Py<sub>2</sub>Tz **210** signal (*green*) and the VP26mCh signal (*red*) are displayed in grey and merged images in color. Scale bar, 5 μm. (B) Hoechst-stained cells were infected with HSV-1<sup>2TCOα+SiR</sup> (MOI 20 PfU) and washed 1 hpi with VP-SFM. Fixation and imaging were performed 90 minutes post-infection. Nuclei are circled. Scale bar, 10 μm. Scale bar, 2 μm (magnification).<sup>185</sup>

### Investigation of HSV-1<sup>2TCOα+SiR</sup> *in vivo*

To further investigate the cell entry of HSV-1<sup>2TCOα+SiR</sup>, different time points post-infection were imaged by fixating the host cells at specific times. Hence, Vero cells were infected with the dual-labeled virus (MOI of 10 PfU), washed with VP-SFM after 1 hpi, fixed at indicated time points, and imaged (Figure 90). In all samples, colocalization events were observable inside the individual cells. Unfortunately, during data analysis, no ejection event of DNA into the nucleus was observable. Furthermore, the different time points didn't display any visible changes in the infection status of HSV-1.

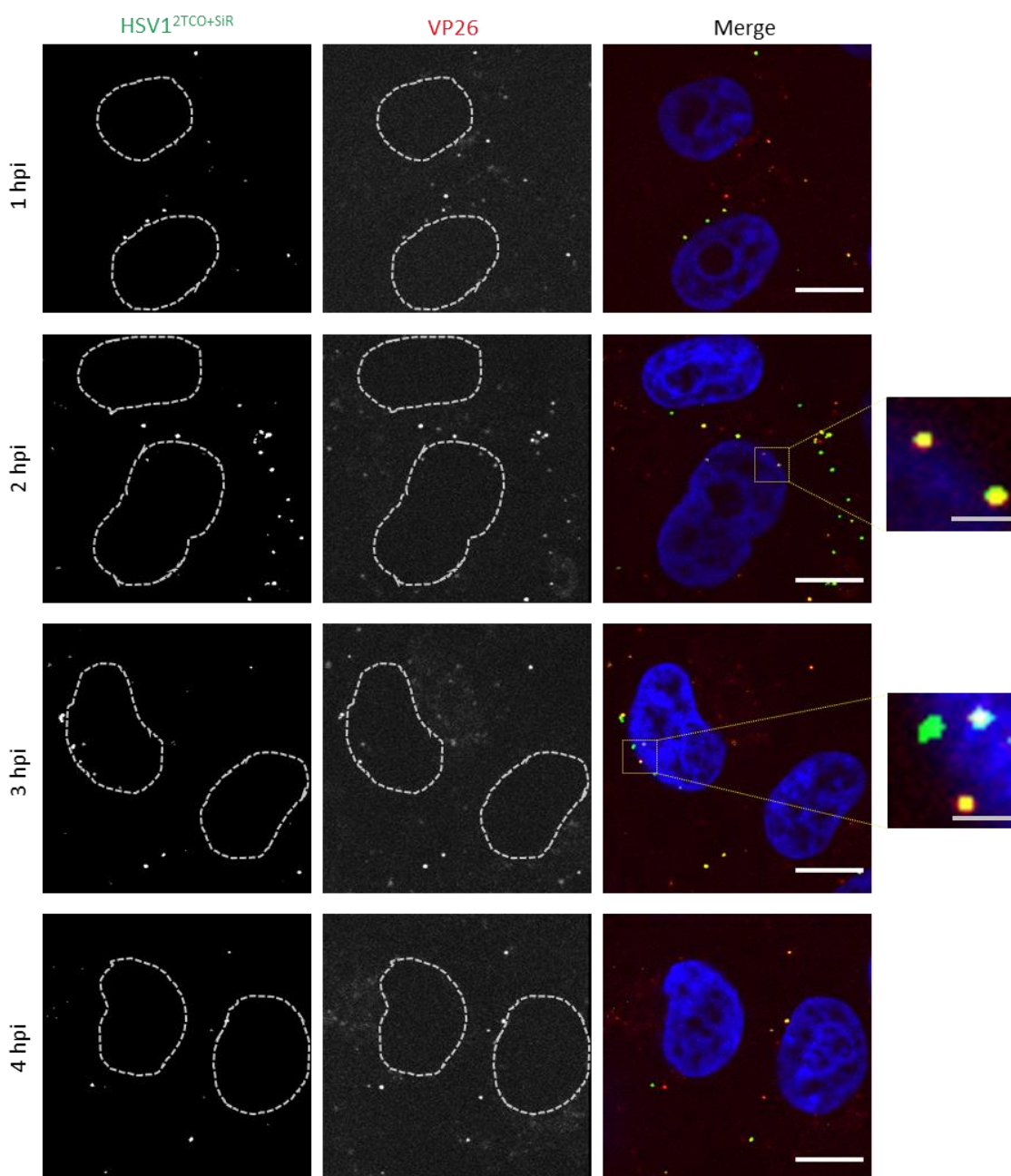


Figure 90: Investigation of HSV-1<sup>2TCO $\alpha$ +SiR</sup> cell entry *in vivo*. (B) Hoechst-stained (blue) Vero cells were infected with HSV-1<sup>2TCO $\alpha$ +SiR</sup> (MOI 10 PFU) and washed 1 hpi with VP-SFM. Fixation and imaging were performed at the indicated time points. The SiR-Py<sub>2</sub>Tz **210** (green) and the VP26mCh (red) signals are displayed in grey and merged images in color. Nuclei are circled. Scale bar, 10  $\mu$ m. Scale bar, 2  $\mu$ m (magnification).<sup>185</sup>

Summarized, the production of dual-labeled HSV-1 was feasible but still requires some future attention and concepts for final validation. Although it was shown that higher concentrations of TriPPP<sub>ro</sub> negatively influence the infectivity of the produced virus (plaque-forming ability), concentrations of 1.5  $\mu$ M of  $\gamma$ -(C9C9AB)-2TCO $\alpha$ -dCTP **175** allowed the isolation of high virus titers ( $10^8$ ) due to virus concentration by high-performance centrifugation. *In vitro* staining of HSV-1<sup>2TCO $\alpha$</sup>  with SiR-Py<sub>2</sub>Tz **210** strongly

suggests efficient labeling of the incorporated label since the signal was significantly higher than the HSV-1<sup>EdC</sup> control. Successful staining of the less reactive 1MCP function still requires some adaption, supposedly increased staining times. The *in situ* staining of HSV-1<sup>2TCO $\alpha$</sup>  before *in vivo* visualization still lacks an appropriate fluorophore-tetrazine-conjugate, which provides improved background signal. Excess fluorophore can be removed by staining the HSV-1<sup>2TCO $\alpha$</sup>  before viral purification. Importantly, the collected data suggest that the isolated HSV-1<sup>2TCO $\alpha$ +SiR</sup> possesses fluorescently labeled genome and allows the visualization of viral entry und cytoplasmatic transport. Still, further investigations are needed to achieve a final evaluation of the concept.

Even though there are questions remaining to be answered, the collected data suggests that the development of 2TCO $\alpha$  labeled virions is an enormous step towards the goal to unravel the viral genome host-cell orchestration at a single particle level with a high spatiotemporal resolution.

## 4.9 Study and production of genome labeled HIV-1

In collaboration with J. HAUBER, from the LIV in Hamburg, the vinyl-functionalized RNA pronucleotides  $\gamma$ -(C9C9AB)-VATP **102** and  $\gamma$ -(C9C9AB)-VUTP **100** were tested for the metabolic labeling of the HIV-1 genome. Maik Voges, PhD, conducted the experiments and data analysis, and illustrated the shown Figures.

The approach aimed at the production of genome labeled, infective HIV-1 particles in cell culture, followed by virus harvesting and isolation. The produced RNA-labeled virus stock could then be utilized to infect and study the early infection stages of HIV-1 in a new host cell line. The spatiotemporal visualization of HIV-1 transcription in living cells could provide exciting insights into the viral replication process, which is still not fully understood (Chapter 2.2).

For virus production in cell culture, HEK293T cells were transfected with the appropriate HIV-1 genome containing plasmids, which lack the region for the envelope (S2 classified virus). For progeny virus production, an envelope-containing plasmid was co-transfected. The separation of the viral information leads to the formation of user safe HIV-1 particles enabled for only one infection cycle (single round of infection). Additionally, a plasmid containing HIV-1 vpr-GFP (*green*) was also co-transfected and allowed dual imaging of the viral particles. The HIV-1 vpr protein regulates the import of the HIV genome into the nucleus by the PIC and is known to associate with the vRNA genome.<sup>188</sup>

In initial experiments, the pronucleotides **102** and **100** were added on the day of infection, and with some delay, the fluorophore-tetrazine conjugate JF549-Py<sub>2</sub>Tz **208** (*red*). Isolated viral particles were put on glass, and the duo VU/JF549 showed colocalization between the green and red signals. Therefore, the focus was on the  $\gamma$ -(C9C9AB)-VUTP **100** pronucleotide and the deazaadenine derivative was not investigated further.

Since intracellularly released VUTP is also a substrate for cellular RNA synthesis, different concentrations of the pronucleotide reporter **100** were tested (1, 5, or 10  $\mu$ M of **100**) and added daily to the cell culture over the course of three days, whereas the fluorophore (5  $\mu$ M of JF549-Py<sub>2</sub>Tz **208**) was added only once on the day of transfection. After three days, the virus was harvested, isolated, and coated on HCl<sub>(aq)</sub> washed microscope dishes. Imaging was performed with a Nikon A1 microscope.

Figure 91A shows a representative image from both the green (HIV vpr-GFP) and the red (JF549-Py<sub>2</sub>Tz **208**) channel for each concentration. Individual sections of the merged



images are enlarged for better visibility. The settings of all images are identical, thus comparable. The particles were tracked and analyzed via Trackmate (Fiji software). Figure 91B illustrates the percentage of colocalizing particles (red and green particles in the same location) to all particles. Figure 91C shows the percentage of the red particles compared to all individual signals. In conclusion, it was demonstrated that with increasing concentration of pronucleotide **100**, more JF549-labeled particles were found and thus significantly more colocalization events. Additionally, the mean intensity of the red signal was analyzed for each concentration, but no correlation between brightness and concentration was observable (data not shown).

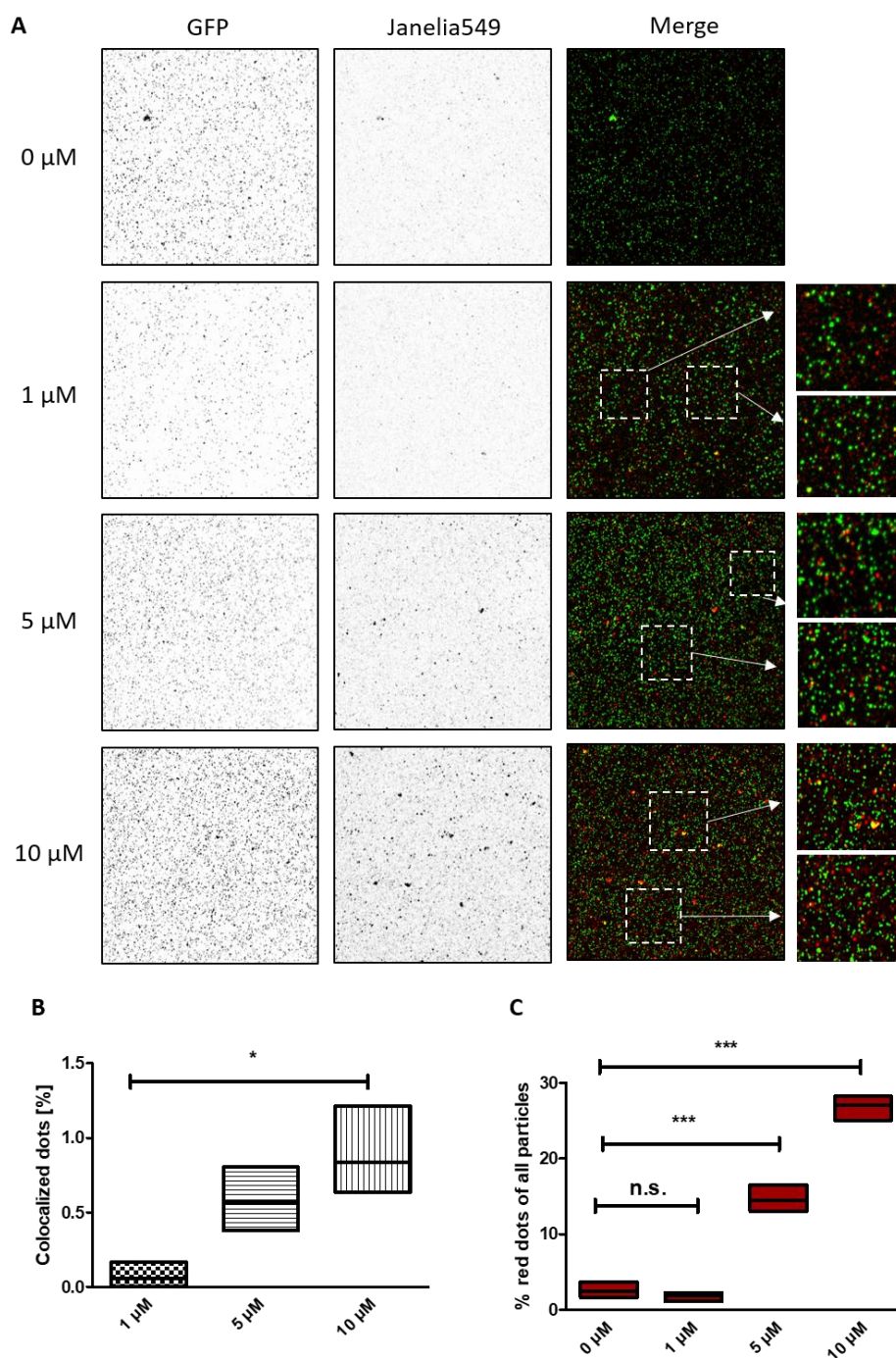


Figure 91: **Signal quantification.** Dual-labeled virus (vpr-GFP in *green*) was produced in HEK293T cells under various concentrations of  $\gamma$ -(C9C9AB)-VUTP **100** and JF549-Py<sub>2</sub>Tz **208** (*red*). Viral particles were harvested, purified, and coated on microscope dishes. Images were taken on a Nikon A1 microscope and analyzed via Trackmate in Fiji. (A) Example images for all used concentrations of **100**. All images were processed equally for comparability. (B) The percentage of colocalizing dots (green and red) compared to all signals. (C) The rate of red particles compared to all signal events.

In parallel, viral particles were produced in cell culture in the presence of parent nucleoside VU **17** (3x 5  $\mu\text{M}$ ) as described above to estimate the effect of the TriPPPPro concept. HIV-1 particles were isolated and coated on microscope dishes. The percentage

of red particles compared to all signals was analyzed and compared to the data of pronucleotide **100** (Figure 92). It was shown that cell cultures treated with the same concentration of the TriPPPro compound produced significantly more labeled viruses compared to the parent nucleoside.

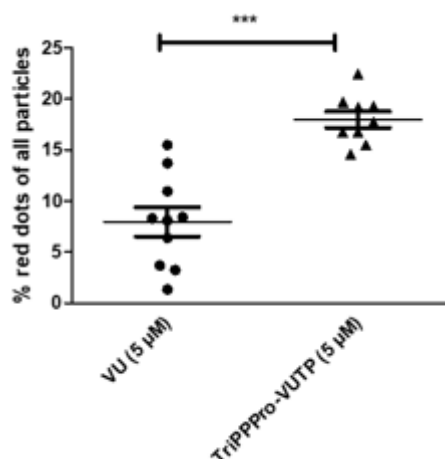


Figure 92: **Rate of genome-labeling for VU 17 compared to its TriPPPro 100 at 5 μM concentration.** Dual-labeled virus (vpr-GFP in *green*) was produced in HEK293T cells in the presence of 5 μM of VU **17** or  $\gamma$ -(C9C9AB)-VUTP **100** and JF549-Py<sub>2</sub>Tz **208** (*red*). Viral particles were harvested, purified, and coated on microscope dishes. Images were taken on a Nikon A1 microscope and analyzed via Trackmate in Fiji. The percentage of red dots compared to all events is illustrated.

It is well known that HSV-1 infection produces numerous empty capsid particles, which naturally lack the red signal but contain the green HIV-1 vpr-GFP. This circumstance explains that most particles are only green. To visualize this phenomenon, viral particles, produced in the presence of pronucleotide **100**, were imaged by electron microscopy with negative staining. Figure 93 shows representative images and enlarged areas and demonstrates that only a few functional viral particles (*blue arrows*) are attached to the carrier dish. In contrast, numerous empty structures are observable (*green arrows*). In rarer cases, capsids without an envelope are detectable (*violet arrow*), which explains single red events during fluorescence imaging.

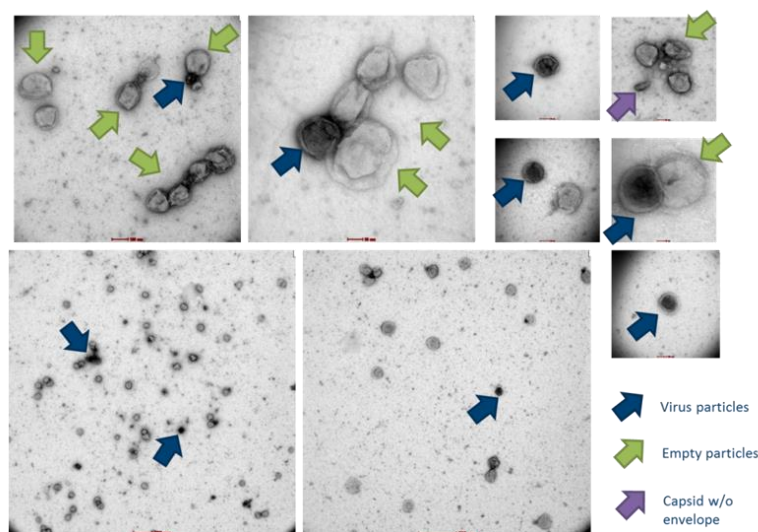


Figure 93: **Visualization of the produced virus by electron microscopy.** Dual-labeled virus was produced in HEK293T cells in the presence of  $\gamma$ -(C9C9AB)-VUTP **100** and JF549-Py<sub>2</sub>Tz **208**. Viral particles were harvested, purified and prepared for imaging. Negative staining was performed with 1% uranyl acetate. Images were taken with an OSIS Veleta CCD Camera attached to an FEI Technais G 20 Twin transmission electron microscope. Example images and enlargements show intact viral particles (*blue arrows*), empty viral particles (*green arrows*), and rare cases of capsids without a viral envelope (*violet arrow*).

Correlative light-electron microscopy (CLEM) was performed to connect the red fluorescent signal of the viral particles to intact viral structures in electron microscope images. For this, labeled viruses were fixed to carbon grids carrying gold-coated beads. First, larger overview images were taken on the Nikon A1 fluorescence microscope in the red and transmitted light channel to identify beads on the grid for later orientation. More detailed images were taken in reference to these orientation marks. The samples were then treated with 1% uranyl acetate for negative staining and visualized with an OSIS Veleta CCD Camera attached to a FEI Technais G 20 Twin transmission electron microscope.

In Figure 94, two representative sets of images are displayed. On the left side, the transmitted light image, the TEM image, and the red channel (JF549 signal) are listed from top to bottom, respectively. In the middle, the overlay of the TEM image and the red channel is displayed. Imaged enlargements of selected areas are shown as indicated. The overlaid images demonstrated clear colocalization of the red signal with intact viral structures.

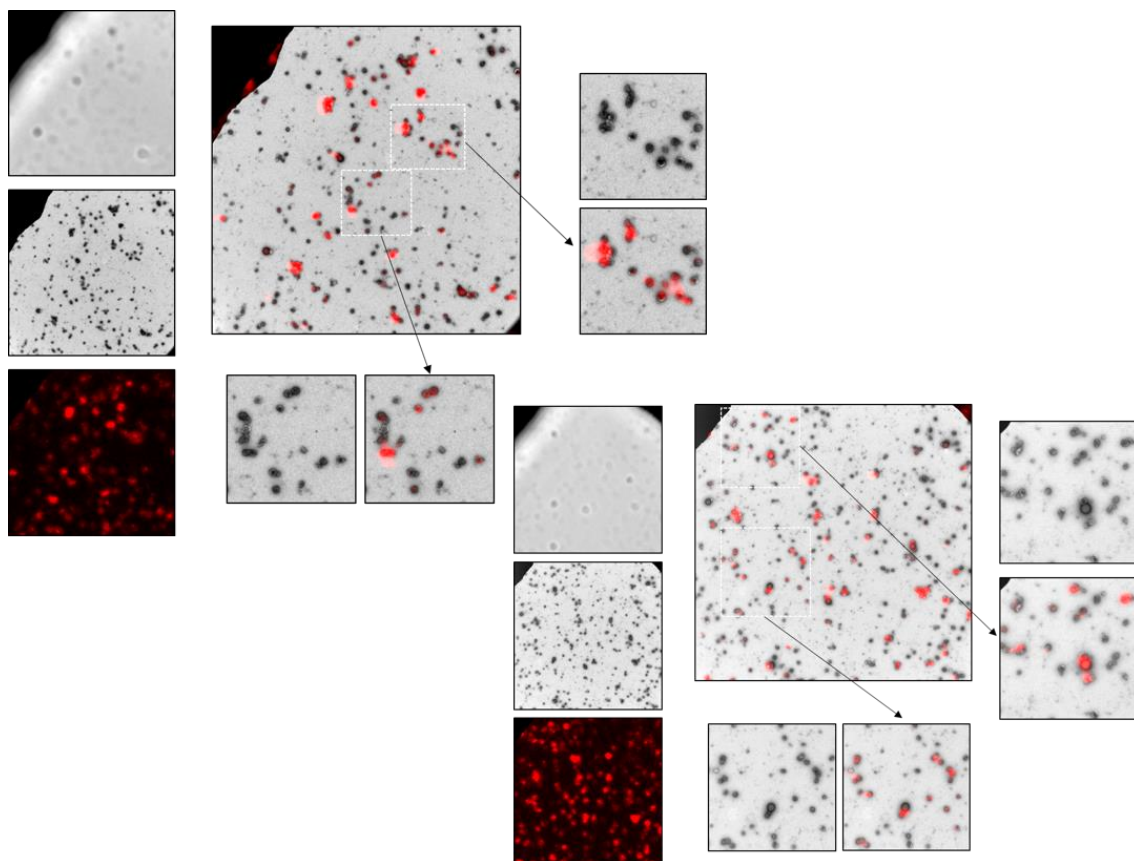


Figure 94: **Allocation of red signals to intact viral particles by CLEM.** Dual-labeled virus was produced in HEK293T cells in the presence of  $\gamma$ -(C9C9AB)-VUTP **100** and JF549-Py<sub>2</sub>Tz **208** (red). Viral particles were harvested, purified and fixed on carbon grids together with gold-coated beads. Fluorescence and transmitted light images were taken on a Nikon A1 microscope. Negative staining for electron microscopy was performed with 1% uranyl acetate. Electron microscopy images were taken with an OSIS Veleta CCD Camera attached to an FEI Technais G 20 Twin transmission electron microscope. The individual images are displayed on the left side, respectively. Correlative overlays are shown in the middle and enlargements on the right.

These observations provide further evidence for successfully viral genome labeling by utilizing the bioorthogonal duo of  $\gamma$ -(C9C9AB)-VUTP **100** and JF549-Py<sub>2</sub>Tz **208**. The ability to label the HIV-1 genome opens the opportunity to distinguish between events leading to infectious pathways (green and red particles) and events leading to no infection (green particles only).

The next step was to determine if the concept provides the opportunity to track these genome-labeled viral particles during a new infection cycle under live-cell conditions. The objective was to spatiotemporal resolve the reverse transcription of HIV-1. Since the HIV-1 vpr protein regulates the import of the HIV genome into the nucleus via the PIC, it stays associated with the genome throughout the nuclear entry. Therefore, the red signal (VU/JF549 genome taq) was expected to colocalize with the green signal (HIV-1 vpr-GFP) early during infection. While the green signal should outlast nuclear import

and reverse transcription, the red signal was expected to disappear after transcription into vDNA. Hence, the disappearance of the JF549 signal functions is a spatiotemporal marker for the reverse transcription process.

Therefore, TZM-bl cells (HeLa cell derivatives genetically modified to express more CCR5 and CD4 receptors on their surface, making them prone to HIV infection) were infected with genome-labeled HIV-1 vpr-GFP. First, by taking 3D microscope images of fixed cells, it was controlled if red-labeled particles were detectable inside of cells. The nucleus was stained with Hoechst dye and the cell membranes were stained with MAG (myelin-associated glycoprotein). Figure 95 shows an overview as a merged image of all channels on the left side. On the right side, all twelve z-stacks are displayed. Planes 6 to 8 clearly show intracellular red signal (see bottom-left) colocalizing with the vpr-GFP, thus demonstrating successful cellular uptake of the HIV-1 subviral structure.

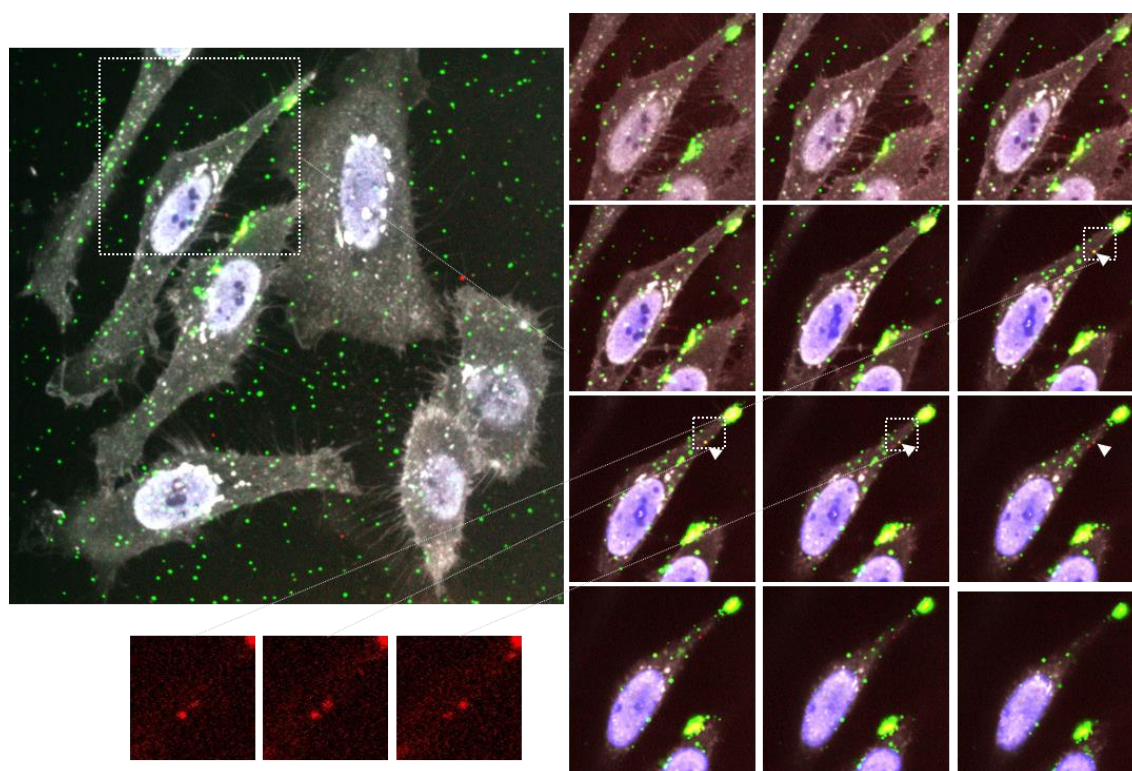


Figure 95: **Fluorescence imaging of dual-labeled viral particles of infected TZM-bl cells.** TZM-bl cells were infected with genome-labeled HIV-1 vpr-GFP (*red and green*), fixed with 4% PFA, and imaged via a Nikon A1 laser microscope. The nucleus is stained with Hoechst (*blue*) and the cell membranes are stained with MAG staining (*white*). The left representative image displays an overview of all channels (merged images). On the right, all twelve z-stacks are shown. The marked squares point out the detected intracellular red signal, and their enlargement is displayed on the bottom left (red channels, JF549 signal).

Then, live-cell imaging was performed. The nucleus was stained with Hoechst dye prior to infection, and the individual viral particles were tracked in the red and green channel. Two different events were observable: Colocalization of permanent green and red

signals without nuclear entry (i) and rapid loss of red signal directly at the nucleus while the green signal continued to be present in the nucleus (ii). Figure 96 shows both described events. Particles were tracked with Fiji Trackmate, and the green and red signal intensities were analyzed. As can be seen in Figure 96, events are displayed where both signals remain present and others where the red signal intensity drops, whereas the green signal remains steady. The sudden decrease in red signal intensity can be located at the nuclear membrane.

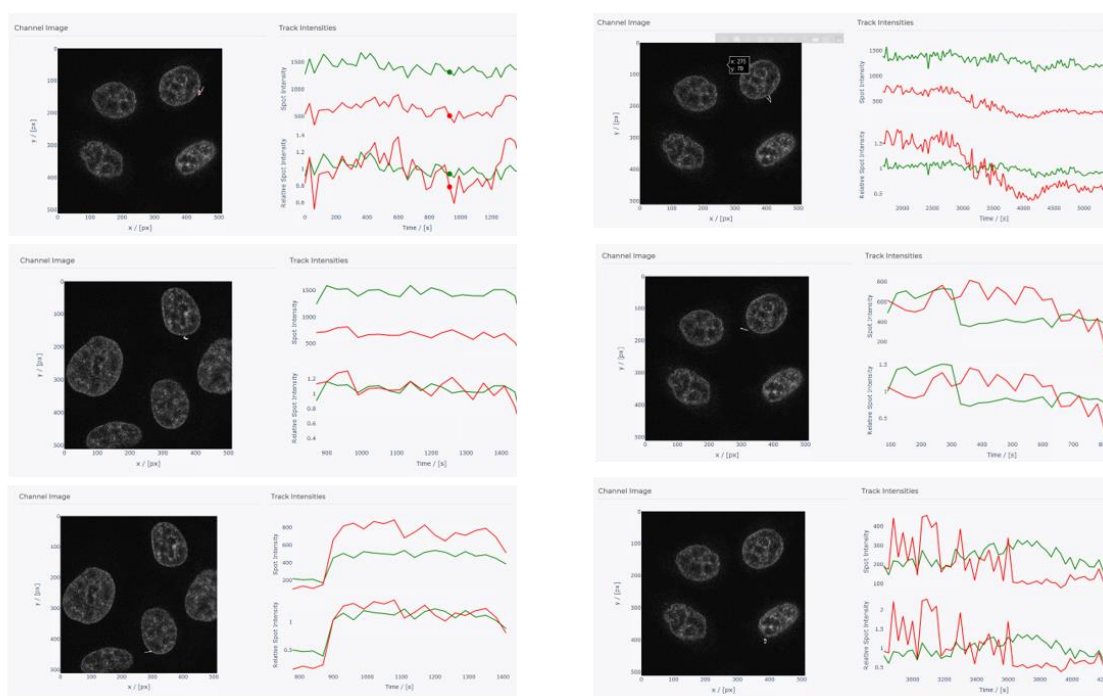


Figure 96: **Tracking of dual-labeled particles in live TZM-bl cells and loss of red signal close to the nucleus.** TZM-bl cells were infected with genome-labeled HIV-1 vpr-GFP (red and green) and imaged via a Nikon A1 laser microscope. The nucleus was stained with Hoechst shortly before infection (blue). Subviral particles were tracked with Trackmate (Fiji) and subsequently analyzed.

Since some red signals remain throughout the experiment, the disappearance of nucleus-associated signals cannot be attributed to bleaching effects but is presumably initiated by reverse transcription. The transcription process would lead to the degradation of the labeled RNA, and potentially to the diffusion of the fluorescent signal under the detection limit.

This elegant approach demonstrates the advantage of the  $DA_{INV}$  to fluorescently label biomolecules in living systems. The vinyl label is incorporated into *de novo* synthesized RNA over three days without seemingly perturbing cellular health or viral infectivity. Here, the TriPPP concept effects a significant increase in the rate of labeled viral

particles at the same reporter concentration. The disadvantage of slow reaction kinetics provided by the vinyl label was compensated by utilizing a fast tetrazine and adding the JF549-Py<sub>2</sub>Tz-conjugate early during infection, prolonging the staining time. Although the loss of red signal at the nuclear membrane is not the ultimate proof of the location of viral reverse transcription, it provides further information on the early infection of HIV-1. Furthermore, the ability to differentiate infectious viral pathways from the sheer number of uninfected events holds enormous value.

Keeping faster labels in mind (e.g., 1MCP or TCO), future applications and improvements might further impact these types of experiments and, ultimately, the understanding of viral infection.



## 5 Summary

This work provides a starting point for metabolic labeling of nucleic acids *in vivo*. The **DA<sub>INV</sub>** is highly adjustable regarding its bioorthogonal functionalities: Starting from the small vinyl function over a variety of bulkier strained olefins with increasing reaction rates but concerns for their stability under physiological conditions. On the other hand, tetrazines are also highly adjustable but also increasingly unstable with increasing reactivity. This work strived to get a sense of the complex functionalities and bring them together for the individual task in the light of nucleoside and nucleic acid labeling.

In the beginning, the vinyl function was explored, and a variety of TriPPPPro compounds were synthesized. The great advantage of the smallest label is its biocompatibility. However, this label only provides slow reaction kinetics, which impedes efficient staining in fixed and permeabilized cells without extensive sample preparation. Chapter 4.7.6 clearly showed that the DNA pronucleotide reporters  $\gamma$ -(C9C9AB)-VdA **101**,  $\gamma$ -(C9C9AB)-VdU **99**,  $\gamma$ -(C11,C9AB)-VdA **117**, and  $\gamma$ -(C11,C9AB)-VdU **116** were not suited to visualize the HIV-1 genome or cellular DNA under the same conditions compared to later, more sophisticated reporters.

Together with the LIV it was demonstrated that the RNA reporter  $\gamma$ -(C9C9AB)-VU **100** enables the preparation of dual-labeled HIV-1 particles (Chapter 4.9). The reporter was added over three days during viral infection without perturbing the infectivity or cellular health. The terminal olefins' slow reactivity was met by adding a fast rhodamine-tetrazine conjugate (JF549-Py<sub>2</sub>Tz **208**) on the first day of infection. Importantly, at the same concentration, the TriPPPPro compound was superior in producing more labeled viral particles than the parent nucleoside VU **17**.

However, it became evident that faster labels needed to be introduced to meet modern labeling experiments' requirements and finally realize the aim to fluorescently label metabolically tagged nucleic acids in living cells. Naturally, the labels became sterically more demanding, but by choosing the appropriate linker motif and bypassing the "bottleneck" kinases through the TriPPPPro concept, the awaited breakthrough was finally achieved. The development of a pronucleotide reporter moreover aimed at viral genome labeling. This allowed to study if the intracellularly released nucleoside triphosphate reporter is both a substrate for cellular as well as viral polymerases.

Since EdC showed improved incorporation compared to EdU into the viral genome of the HSV-1, the focus was laid upon the 2'-deoxycytidine as an initial candidate for the

development of nucleoside reporters for viral application together with our cooperation partner J.BOSSE, from CSSB and MHH. (Chapter 4.4.1).

Initial attempts to introduce the 1MCP label to pronucleotide reporters were complicated by the instability of the 1MCP carbamate functionality, which was prone to ene-ene dimerization upon solvent concentration. Thus, the synthetic route via protective group strategy, introduction of the 1MCP-carbamate conjugate by SONOGASHIRA cross-coupling, and subsequent phosphoramidite chemistry was abandoned. An enhanced approach was chosen where the carbamate linkage was exchanged for a methyl amide, improving the chemical stability of the label, and enhancing reaction rates. Moreover, the TMS-protected 1MCP label was introduced directly to the monophosphates by SONOGASHIRA cross-coupling via a hexanoic linker motif. After desilylation, the C9C9AB-TriPPPros of 1MCP-dATP **149** and 1MCP-dCTP **150** were prepared in good yields of 47% and 52% (Chapter 4.3).

A precursor 2'-deoxycytidine monophosphate "multitool" was prepared, which carries the linker motif at the C<sub>5</sub>-pyrimidine position and allows for the convenient introduction of different labels. Hence, 1-amino-5-pentyne was introduced by a SONOGASHIRA cross-coupling providing the primary amine for further functionalization via NHS chemistry. Initially, the alkyne attachment was hydrogenated to the more flexible alkane, resulting in the 5-aminopent-1-yl-dCMP **156** over two steps from IdCMP **145**. The pronucleotide reporters  $\gamma$ -(C9C9AB)-4TCO-dCTP **163** and  $\gamma$ -(C9C9AB)-NcTz-dCTP **160** were prepared from MP **156** in two steps. Unfortunately, labeling experiments conducted with both pronucleotide reporters provided no or inconclusive fluorescent signal (Chapter 0). In contrast, the 1MCP functionalized pronucleotides – attached via an alkyne – exhibited exciting potential as reporters in initial experiments (data not shown). Although not finally accessed, the hydrogenation to the saturated alkane was under suspicion to hamper efficient incorporation into *de novo* synthesized DNA due to an unsuitable substrate motif (Chapter 4.4).

The 5-(5-aminopent-1-yn-1-yl)-dCMP **155** was utilized as a precursor molecule since it provides the same linker motif as the 1MCP-TriPPPros. Here, BCN<sup>endo</sup> and axial 2-ene TCO (2TCO $\alpha$ ) were introduced to **155** via NHS chemistry. Both labels were commercially available as their NHS carbonates. The BCN label was selected due to its ability to react with tetrazines in a SPIEDAC as well as in a catalyst-free SPAAC with azides. The  $\gamma$ -(C9C9AB)-BCN<sup>endo</sup>-dCTP **177** was synthesized in a poor yield of 5%, mainly due to low

conversion of the monophosphate. Later during fluorescent experiments, the pronucleotide exhibited increased cytotoxicity of HSV-1 infected Vero cells, impeding their visualization. Moreover, the reporter showed no signs of metabolic labeling of cellular DNA in non-infected Vero cells (Chapter 0). Thus, no further attempts were made to improve the preparation of **177**.

The 4-ene TCO provides exceptional fast reaction rates (up to  $10^4 \text{ M}^{-1}\text{s}^{-1}$ ) but lacks stability under physiological conditions due to the isomerization to the less reactive cis-isomer. After an initial hype, the circumstance gained increasing attention in the respective literature. Thus, it was decided to introduce the vastly more stable 2TCO $\alpha$  and accept the disadvantage of the  $\beta$ -elimination reaction of the SPIEDAC product, which results in slow dissociation of the fluorophore and impedes long term visualization (Chapter 0). The pronucleotide  $\gamma$ -(C9C9AB)-2TCO $\alpha$ -dCTP **219** was prepared in 21% yield and turned out to be an exceptional metabolic reporter (Chapters 0 and 4.7.5). Therefore, the uridine RNA pronucleotide reporter  $\gamma$ -(C9C9AB)-2TCO $\alpha$ -UTP **176** (20%) was prepared over 2TCO $\alpha$ -UMP **173** (93%), and 5-(5-aminopent-1-yn-1-yl)-UMP **164** (80%) from IUMP **90** (92%).

Devaraj *et al.* introduced a methyl-tetrazine to the nucleobase of TBDMS-protected 2'-deoxyuridine via an elimination–Heck cascade reaction.<sup>94</sup> The synthesis was picked up, and the respective  $\gamma$ -(C9C9AB)-MeTz-(E)-dUTP **220** was prepared over six steps (Chapter 4.4.4). Since the TBDMS protective groups were required to introduce the *trans*-ethylene linked MeTz, the phosphoramidite route was chosen to prepare the monophosphate after selective deprotection of the 5'-hydroxy function. Unfortunately, the pronucleotide reporter produced no detectable viral or cellular DNA signal in Vero cells with the commercially available SiR-4TCO dye **218** (Chapter 4.7.2). In the future, it must be investigated if the released active triphosphate is not efficiently incorporated by the endogenous or viral polymerases or if the tetrazine label does not provide the necessary speed for efficient staining. In case of inefficient incorporation, the nucleotide reporter might still be an exciting candidate for retroviruses since the viral reverse transcriptase has a lower substrate fidelity. Considering a reporter, which is a substrate only for viral reverse transcriptase and not for higher-fidelity polymerases, and additionally, that it is still possible to push the reactivity of the TCO even further (dTCO and sTCO), makes this reporter interesting for further investigation.

Furthermore, various rhodamines were purchased or synthesized and coupled to different tetrazines (Chapter 0). The focus here was to find a fluorophore-conjugate,

which unites sufficient cell-permeability, high reaction rates, favorable cellular distribution, and low background. The novel SiR-Py<sub>2</sub>Tz **210** enabled live-cell imaging and met most of these requirements; however, it exhibited high unspecific background. Since only **210** enabled live cell applications, it should be viewed as the leading candidate for further improvements.

Regarding metabolic labeling, both 1MCP-pronucleotides efficiently label viral and cellular DNA in fixed and permeabilized samples with the fast 3,6-di(2-pyridyl)-1,2,4,5-tetrazine (Py<sub>2</sub>Tz) bioorthogonal partner. Note, there is some potential that the incorporated 1MCP label can be visualized in living cells by even faster tetrazines, making these metabolic reporters even more valuable. Moreover, it was shown that the production of HSV-1 in Vero cells under the treatment of  $\gamma$ -(C9C9AB)-1MCP-dCTP **150** still allows the isolation of high viral titers. Although labeled viral particles were not yet efficiently stained by any fluorophore-tetrazine conjugate, it is likely that 1MCP-labeled viruses can be fluorescently tagged simply by prolonging the staining times of viral particles *in vitro* or by adding the dye earlier during virus production *in vivo*.

In agreement with a high G+C share of the HSV-1 genome, the cytidine-based pronucleotide reporter displayed a stronger fluorescent signal of the viral genome in RCs compared to  $\gamma$ -(C9C9AB)-1MCP-dATP **149**. This demonstrates that labeling experiments vary from each other and have multiple parameters, which need to be addressed to get optimal results.

When ensuring the same condition in fixed and permeabilized Vero cells, the faster 2TCO $\alpha$  label provides a vastly improved signal compared to the 1MCP label (4.7.3). Considering that the TCO label is the bulkier motif, it seems striking that the limiting factor is not the efficient incorporation of the label into the viral or the cellular genome but staining efficiency. As described in Chapter 4.7.5, the focus for improvements should be laid upon increasing the reaction rates further, e.g., by introducing the dTCO label or exchanging one pyridyl (Py) to a pyrimidyl (Y) tetrazine-substituent.

Fascinating were the properties of  $\gamma$ -(C9C9AB)-2TCO $\alpha$ -dCTP **175** since this metabolic reporter, for the first time, allowed live-cell imaging of cellular and viral DNA. The ability to incorporate such a fast bioorthogonal label into *de novo* synthesized nucleic acids opens the potential for a variety of applications, far exceeding fluorescence imaging. Moreover, the concept can likely be transferred to RNA labeling. Here, the

pronucleotide reporter  $\gamma$ -(C9C9AB)-2TCO $\alpha$ -UTP **176** was already synthesized, even though not yet validated.

Next to the visualization of vDNA inside of RCs, it was shown that dual-labeled HSV-1 particles can be produced. The isolation and purification of these viruses allow for the visualization and study of viral genome trafficking in host cells on a single particle level with high spatiotemporal resolution. Even though the final assessment still misses, the obtained data indicate enormous potential (Chapter 4.8).

The bioorthogonal labeling of nucleic acids has a long history, but the final visualization of these biomolecules in living systems was not yet achieved. By combining the latest developments in the field of “click-chemistry” and pronucleotide concepts, this work successfully accomplished the highly anticipated breakthrough in live-cell imaging of nucleic acids.

Excitingly, further improvements are achievable and already underway in our laboratories. Exciting is the change of the 4TCO $\alpha$  functionality with the more reactive and stable *syn*-dTCO motif. The more reactive label would further improve fast and efficient labeling in living cells without the disadvantage of an intramolecular  $\beta$ -elimination of the **DA<sub>INV</sub>** product. Moreover, the reaction kinetics of the Py<sub>2</sub>Tz motif can further be advanced by displacing a pyridyl-substituent (Py) with a pyrimidyl-group (Y). The resulting YPyTz-motif can be coupled directly to various fluorophores, resulting in “turn-on” probes since the tetrazine would efficiently quench the attached fluorophore by a TBET mechanism. Such “fast” probes could significantly improve the dynamic of intracellular labeling and decrease overall background staining by allowing a reduction of probe concentration or efficient “turn-off” of excess fluorophore-tetrazine conjugate.

## 6 Experimental Part

### 6.1 General

Reactions with water/O<sub>2</sub>-sensitive reagents were conducted with anhydrous solvents under a dry nitrogen atmosphere.

#### Solvents

Acetonitrile	C <sub>2</sub> H <sub>3</sub> N; bp.: 81 °C; VWR chemicals, HPLC grade; anhydrous: MBraun system, molecular sieve (3 Å)
Dichloromethane	CH <sub>2</sub> Cl <sub>2</sub> ; bp.: 40 °C; distilled before use; anhydrous: MBraun system, molecular sieve (4 Å)
Diethyl ether	C <sub>4</sub> H <sub>10</sub> O; bp.: 34 °C; distilled before use
<i>N,N</i> -Dimethylformamide	C <sub>3</sub> H <sub>7</sub> NO; bp.: 153 °C; anhydrous: Acros Organics, molecular sieve (4 Å)
Dimethyl sulfoxide	C <sub>2</sub> H <sub>6</sub> OS; bp.: 190 °C; anhydrous: Acros Organics, molecular sieve (4 Å)
Ethyl acetate	C <sub>4</sub> H <sub>8</sub> O <sub>2</sub> ; bp.: 77 °C; distilled before use
Methanol	CH <sub>4</sub> O; bp.: 65 °C; distilled before use
Petroleum ether 50-70	bp.: 50-70 °C; distilled before use
<i>iso</i> -Propanol	C <sub>3</sub> H <sub>8</sub> O; bp.: 82 °C; VWR chemicals, HPLC grade
Pyridine	C <sub>5</sub> H <sub>5</sub> N; bp.: 116 °C; anhydrous: MBraun system, molecular sieve (4 Å)
Tetrahydrofuran	C <sub>4</sub> H <sub>8</sub> O; bp.: 40 °C; VWR chemicals, HPLC grade; anhydrous: MBraun system, molecular sieve (4 Å)
Water, deionized ultrapure	Sartorius Aurium <sup>®</sup> pro unit (Sartopore 0.2 μm, UV)

## Chromatography

Thin-layer chromatography was performed on pre-coated MACHERY-NAGEL TLC plates Alugram® Xtra SIL G/UV<sub>254</sub>. UV-active substances were visualized under the UV lamp at 254 nm. Furthermore, compounds were stained with Vanillin reagent (5 g vanillin, 1000 mL CH<sub>3</sub>OH/AcOH; 9:1 v/v, 35 mL H<sub>2</sub>SO<sub>4</sub>) under heating. Column chromatography on silica gel was performed using silica gel MN 60 M (0.04-0.063 mm) supplied by MECHERY-NAGEL. Automated flash chromatography on RP<sub>18</sub> silica gel was conducted with MN RS 16 g/43 g/120 g C<sub>18</sub> ec columns from MECHERY-NAGEL on Puriflash systems (430 or 5.020). High-performance liquid chromatography (HPLC) data were obtained with an Agilent 1260 Infinity II (pump G7111A, Autosampler G7129A, detector DAD G7117C) and an EC 125/3 Nucleodur 100-5 C<sub>18</sub>ec column/ EC 4/3 Nucleodur 100-5 C<sub>18</sub>ec pre-column system supplied by MECHERY-NAGEL. Method: CH<sub>3</sub>CN gradient in 2 mM tetrabutylammonium acetate buffer (pH 6); 5-80%; 0-20 min; flow 1 ml/min.

## Spectroscopy/Spectrometry

Nuclear magnetic resonance spectroscopy (NMR) spectra were measured in the institute of organic chemistry at the University of Hamburg. The NMR spectra were recorded at room temperature on 300 MHz Bruker Fourier 300, 400 MHz Bruker AMX 400 or 600 MHz Bruker AVIII 600 spectrometers. The chemical shifts ( $\delta$ ) were quoted in parts per million [ppm] and calibrated to the internal solvent signals. For further characterization, two-dimensional NMR experiments (*H,H*-COSY, HSQC, HMBC) were measured for most compounds. NMR solvents were purchased from Euroiso-Top (CDCl<sub>3</sub>, CD<sub>3</sub>OD, D<sub>2</sub>O) and Deuterio (DMSO-*d*<sub>6</sub>). Infrared spectroscopy (IR) spectra were recorded at room temperature on a Bruker Alpha IR-spectrometer. ESI mass spectrometry was performed on an Agilent 6224 ESI-TOF spectrometer in positive or negative mode. MALDI mass spectrometry was performed on a MALDI TOF-TOF Bruker UltrafleXtreme spectrometer in negative mode.

## Further Devices

Microwave reactions were conducted in a CEM discover system in closed vessel mode. For centrifugation, a Hereaus Biofuge R with 80.000 rpm was used (phase separations were conducted for 5 min at 4 °C). Freeze-drying was performed with a Christ ALPHA 2-4 LDplus.

## Preparation of buffer solutions

Preparation of 2 mM tetrabutylammonium acetate buffer: 10% aqueous tetrabutylammonium hydroxide (2.4 mL, 4.9 mmol) was added to deionized ultrapure water (2.4 L). The pH value was set to 6.0 by the addition of acetic acid (~6 mL).

Preparation of 1 M triethylammonium bicarbonate buffer (1 M TEAB): 2 Mol triethylamine (278.8 mL) were filled up to 2 L with deionized ultrapure water. Carbon dioxide deriving from dry ice was bubbled through the solution until a pH of 8 was set.

The 1 M TEAB solution was tightly capped and stored at 4 °C. Preparation of 0.05 M triethylammonium bicarbonate buffer (0.05 M TEAB): 50 mL of the 1 M TEAB solution was filled up to 1 L with deionized ultrapure water and directly used for RP<sub>18</sub> column chromatography.

## 6.2 Imaging

### 6.2.1 HSV-1 Virus

The HSV-1 VP26mCherry (Bosse lab) was utilized. The wild-type parental strain was HSV-1. The used multiplicity of infection (MOI in PfU) is stated for each imaging experiment. For virus production a MOI of 0.01 PfU was chosen. Phosphonoacetic acid (PAA Sigma Aldrich) was used as an inhibitor for viral DNA synthesis at a concentration of 400 µg/mL. PAA was added with the inoculum and at all stages of medium change.

### 6.2.2 Vero cell culture

African Green Monkey kidney fibroblast (Vero) cells were cultured in Dulbecco's Modified Eagle's Medium (DMEM, GlutaMax™, ThermoFisher Scientific) and supplemented with 10% Fetal Calf Serum (FCS, Sigma Aldrich), and 1 mM sodium pyruvate at 37°C and 5% CO<sub>2</sub>. For cell detachment for cell splitting or seeding 2 mM trypsin-EDTA (ThermoFisher Scientific, 0.25%, phenol red) was used for 2-5 min at 37°C and subsequent quenching with cell medium. Cell numbers for cell seeding were determined by a Neubauer Chamber.

### 6.2.3 Spinning-disk fluorescence microscopy

Spinning-disk microscopy was performed on a Nikon TI2-based spinning-disk system (Nikon) equipped with a Yokogawa W2, a Nikon 1.49 NA Apo-TIRF objective, and an Andor iXON888 EMCCD (Andor Technology). The resulting pixel size was 130 nm. The



image acquisition was performed with NIS-Elements. The setup was equipped with 405, 488, 561, and 640 nm laser lines and respective filter sets. For live-cell imaging the samples were humidified and heated to 37 °C at 5% CO<sub>2</sub>. Cells were grown and imaged in IBIDI 8 well plates with a glass bottom (Ibidi GmbH). Image processing and analyses were performed with ImageJ.

#### 6.2.4 Dual-labeled HSV-1 virus production

Vero cells were seeded in either 5x T500 flasks or 16x 15 cm dishes in DMEM supplemented with 10% FCS. At 80 % confluency, cells were washed once in PBS and infected with HSV-1 VP26mCh at an MOI of 0.01 PfU in VP-SFM (Virus Production serum-free medium, ThermoFisher Scientific). The infected cells were incubated at 37 °C and 5% CO<sub>2</sub>. 1 hpi, the medium was changed and 1.5 μM TriPPPPro was added in VP-SFM. 24 hpi, 1.5 μM TriPPPPro was added again. About 72 hpi, most of the infected cells showed cytopathic effects but were still attached. The virus-containing supernatants were harvested and precleared by low-speed centrifugation for 5 minutes at 3,000 xg at 4 °C. Excess cell debris was removed by filtration using a 0.45 μm cut-off filter (Filtropur BT 50). The supernatant was split in falcon tubes and underlaid by 5% OptiPrep (1 ml, Sigma Aldrich). The viruses were pelleted by centrifugation (14,000 xg, 90 min, 4°C). The virus pellets were resuspended in PBS (500 μL). Optionally, staining with the appropriate fluorophore was performed. Hence, 10 μM of SiR-Py<sub>2</sub>Tz **210** (30 min) or AF488-Py<sub>2</sub>Tz **212** (overnight) was added to the resuspended virus pellets before continuous gradient purification.

For the continuous gradient purification protocol, a ultracentrifugation tube was filled with 5% OptiPrep and underlaid with 30% OptiPrep. The gradient was adjusted with 8-25% OptiPrep using the appropriate protocol on the gradient master (BioComp Instruments) for an SW41 rotor. After virus loading, the tube was spun by ultracentrifugation (18,000 xg, 60 min, 4°C). The appropriate virus-containing band was pulled via a syringe. The samples were stored at -80°C. The virus titer was determined by Plaque Assay.

### 6.2.5 Imaging in fixed cells

$2.5 \times 10^4$  Vero cells were seeded in each well of an 8-well IBIDI plate to reach 80-90% confluency the following day. When indicated, cells were treated with 400  $\mu\text{g}/\text{ml}$  PAA 1 hpi as a control. Cells were infected with HSV-1 VP26mCh at an MOI of 3 PfU in DMEM supplemented with 10% FCS. 1 hpi, cells were washed with VP-SFM and the medium was changed to VP-SFM. After 4 hpi, 5  $\mu\text{M}$  of the respective TriPPPPro in VP-SFM was added. (Option #1) When indicated, the TriPPPPro media were renewed at 5.5 hpi and changed to VP-SFM at 7 hpi with one washing step (10 min inbetween medium change). (Option #2) When indicated, TriPPPPro media were renewed at 6 hpi and changed to VP-SFM at 8 hpi with one washing step (10 min inbetween medium change).

After 8 hpi, cells were fixed in 4% PFA for 15 minutes at room temperature and permeabilized in 0.1% Triton X-100 for 20 minutes at room temperature. The samples were blocked in 1 % FCS in PBS for 5 minutes. Incorporated labels were stained overnight with 5  $\mu\text{M}$  AF488-Py<sub>2</sub>Tz **212** in PBS.

Only Hoechst staining: Samples were washed three times with PBS and stained with Hoechst (1:1000) in PBS. Sample storage was performed at 4 °C protected from light. Images were acquired by Spinning Disc Confocal Nikon Eclipse Ti2 and processed using Image J.

ICP8 immunofluorescence protocol: The sample was washed once in PBS and stained with an ICP8 antibody (1:500, Abcam) for one hour at RT. After washing it again in PBS the second antibody (1:1000) as well as Hoechst (1:1000) was added for one hour at room temperature. The samples were washed in PBS again and stored at 4°C protected from light. Images were acquired by Spinning Disc Confocal Nikon Eclipse Ti2 and processed with ImageJ.

### 6.2.6 Live-cell imaging

$2.5 \times 10^4$  Vero cells were seeded in each well of an 8-well IBIDI plate to reach 80-90% confluency the following day. When indicated, cells were treated with 400  $\mu\text{g}/\text{ml}$  PAA 1 hpi as a control. Cells were infected with HSV-1 VP26mCh at an MOI of 3 PfU in DMEM supplemented with 10% FCS. 1 hpi, cells were washed with VP-SFM and the medium was changed to VP-SFM. After 4 hpi, 5  $\mu\text{M}$  of  $\gamma$ -(C9C9AB)-2TCO $\alpha$ -dCTP **175** in VP-SFM was added. (Option #1) The TriPPPPro media were renewed at 5.5 hpi and at 7 hpi the medium was changed to VP-SFM. (Option #2) The TriPPPPro media were renewed at 6 hpi and, shortly before 8 hpi, the cells were washed with VP-SFM and incubated for 10 min.

After 8 hpi, cells were washed again (VP-SFM) and stained with 5  $\mu\text{M}$  SiR-Py<sub>2</sub>Tz **210** in VP-SFM. Staining was performed for 1-3 h. Images were acquired by Spinning Disc Confocal Nikon Eclipse Ti2 and processed with ImageJ.

### 6.2.7 Dose curve for virus production

$2.5 \times 10^4$  Vero cells were seeded in 24 well plates to reach 80 confluency the following day. Cells were washed once in PBS and infected with HSV-1 at an MOI of 0.01 PfU in VP-SFM. 1 hpi, the inoculum was removed and cells were washed in VP-SFM. After 2 hpi, different concentrations (0, 0.5, 1.5, 5, 10  $\mu\text{M}$ ) of the respective TriPPP<sub>Pro</sub> or the corresponding volumes of DMSO were added to the infected cells. The addition was repeated after 24 hpi. After 72 hpi, most cells showed cytopathic effects but were still attached to the surface. The virus-containing supernatants were harvested and prepurified by centrifugation (3,000  $\times g$ , 5 min, 4°C). Again, the supernatants were removed and stored at -80 °C. The virus titers were determined by Plaque Assays (as described below).

### 6.2.8 Plaque Assay

The viral titer was determined by Plaque Assay with Vero cells. Therefore,  $3 \times 10^5$  Vero cells per well were seeded in a 6-well plate. The next day, a virus dilution series ( $10^{-2}$  to  $10^{-7}$ ) was prepared with DMEM supplemented with 10 % FCS. The media of the seeded cells were removed and 200  $\mu\text{L}$  of each dilution was added to the individual wells. The samples were incubated for 1 to 2 h under gentle shaking (every 15 min). After this time period, methylcellulose/DMEM (2 mL) was added, and the infected cells were incubated for about five days until visible plaques formed. The medium was removed, and the cells were fixed in 3.75% PFA/PBS for up to 20 min at room temperature. The samples were stained with crystal violet. In two countable wells, the formed plaques were counted and averaged. The counted PfU/200  $\mu\text{L}$  of the dilution was multiplied by 5 and the respective dilution factor to give the viral titer in PfU/mL.

### 6.2.9 Labeled virus genome detection in virions

An IBIDI 8 well plate was cleaned with 30% HCl<sub>aq</sub>. After around one hour, the wells were extensively washed with PBS and dried. Then, 5  $\mu\text{L}$  of the virus-containing solution (HSV-1<sup>TriPPP<sub>Pro</sub>(+dye)</sup>) was put on glass and the viral particles were adsorbed for 5 min.

Afterwards, the wells were washed three times in PBS. Unlabeled virions were stained at this stage with 5  $\mu$ M of SiR-Py<sub>2</sub>Tz **210** or AF488-Py<sub>2</sub>Tz **212** for 30 min and washed again in PBS. The samples were stored protected from light at 4 °C. Images were acquired by Spinning Disc Confocal Nikon Eclipse Ti2 and processed with ImageJ.

#### **6.2.10 Infection of cells with HSV-1<sup>2TCO</sup>**

2.5\*10<sup>4</sup> Vero cells were seeded in each well of an 8-well IBIDI plates to reach 80-90% confluency the following day. The unstained HSV-1<sup>2TCO $\alpha$</sup>  was mixed with 5  $\mu$ M SiR-Py<sub>2</sub>Tz **210** and Hoechst (1:1000) and incubated for 30 minutes. The cells were washed in VP-SFM and infected at an MOI of 10 PfU with the HSV-1<sup>2TCO $\alpha$</sup>  mixture. After 1 hpi, the inoculum was removed, and the medium was changed to VP-SFM. After 90 min post-infection, images were acquired by Spinning Disk Confocal Nikon Eclipse Ti2 and processed with ImageJ.

#### **6.2.11 Infection of cells with HSV-1<sup>TriPPP<sub>Pro</sub>+dye</sup>**

2.5\*10<sup>4</sup> Vero cells were seeded in each well of an 8-well IBIDI plates to reach 80-90% confluency the following day. The cells were washed in VP-SFM and infected at an MOI of 10 PfU with the appropriate prelabelled HSV-1<sup>TriPPP<sub>Pro</sub>+dye</sup>. Additionally, Hoechst (1:1000) was added at the same time. After 1 hpi, the inoculum was removed, and the medium was changed to VP-SFM. The samples were fixed at the indicated time points with 4% PFA for 15 min at room temperature, followed by washing in PBS. Images were acquired with the Spinning Disk Confocal Nikon Eclipse Ti2 and processed with ImageJ.

#### **6.2.12 Cell culture and production of genome labeled HIV-1 $\Delta$ env viral particles**

HEK293T cells (ATCC, CRL-3216) and TZM-bl cells (NIH AIDS Reagent Program, ARP-8129) were cultured at 37 °C and 5% CO<sub>2</sub> in DMEM (Biochrom) was supplemented with 10% FCS (Biochrom).

For virus production in HEK293T,  $\gamma$ -(C9C9AB)-VUTP **100** was added (DMEM/10%FCS) to the cell culture medium overnight approximately 16 h before transfection of the cells with replication-incompetent HIV-1 $\Delta$ env plasmid<sup>189</sup>. HIV-1 $\Delta$ env viral particles were produced by transfecting 4 $\times$  10<sup>6</sup> HEK293T cells with 8  $\mu$ g pNLT2 $\Delta$ env, 3  $\mu$ g p3env and, if indicated, with 2  $\mu$ g vpr-GFP<sup>188</sup> using TransIT LTI as a transfection reagent according to

the manufacturer's protocol (Mirus Bio LLC , USA). After 6 to 8 hpi, the medium was changed to 5  $\mu$ M JF549-Py<sub>2</sub>Tz **208** in DMEM/10%FCS. The TriPPPPro addition was repeated one and two days after transfection. At day three post transfection, virus-containing supernatants were passed through 0.2  $\mu$ m pore size filters to ensure removal of any aggregates, concentrated once or twice by ultracentrifugation (27,000 rpm for 2 h) through a sucrose cushion. The virus was stored at -80 °C. Viral titers were determined by HIV-1 p24 antigen enzyme-linked immunosorbent assay (ELISA) as previously described<sup>190</sup>.

### **6.2.13 Quantification of light signals and colocalization with confocal laser microscope**

35 mm  $\mu$ -Dishes (glass bottom, Ibidi) were cleaned with 1M HCl for 6 h, followed by washing steps with water and hot EtOH. The viral particles were fixed with 4% PFA in PBS for 1 h at 37°C and then adsorbed onto the dried dishes. Imaging was performed on an inverted confocal scanning laser microscope (Nikon A1R HD25 equipped with a Nikon 60x oil-immersion NA 1.40 objective). Images were recorded using the Nikon NIS-Elements software. Images were processed with ImageJ. Colocalization quantification of fluorescence signal was performed using Trackmate plugin and subsequent analysis.

### **6.2.14 Live-cell imaging with dual-labeled HIV-1**

10<sup>5</sup> TZM-bl cells were plated on 35 mm  $\mu$ -dishes (glass bottom, Ibidi) that were coated with 1% (v/v) fibronectin (Sigma Aldrich). The cells were stained with Hoechst (1:1000) directly before infection with dual-labeled HIV $\Delta$ env. Imaging was performed on an inverted confocal scanning laser microscope (Nikon A1R HD25 equipped with a Nikon 60x oil-immersion NA 1.40 objective and with a heating chamber at 37 °C and 5% CO<sub>2</sub>). Images were recorded using the Nikon NIS-Elements software and processing was performed with ImageJ.

### **6.2.15 Correlative light-electron microscopy**

Labeled viral particles were produced as described above. Particles were fixed with 2% PFA in vitro and coated on carbon coated grids. Imaging was performed on an inverted confocal scanning laser microscope (Nikon A1R HD25 equipped with a Nikon 60x oil-immersion NA 1.40 objective) using the Nikon NIS-Elements software. Viral particles were stained with 1% uranyl acetate (Merck, Germany) and staggered with gold beads. Images were acquired with an OSIS Veletas CCD Camera attached to a FEI Technai G 20 Twin transmission electron microscope (FEI, Netherlands) at 80 kV.

### **6.2.16 Statistical analysis for HIV-1 particle labeling**

Statistical analysis was performed with Prism version 5.03 software (Graph Pad). The statistical significance was assessed by one-way or two-way analysis of variance (ANOVA) followed by a Dunnett's Multiple Comparison Test or Bonferroni's posttest. A result of  $p < 0.05$  was considered to be statistically significant.

## 6.3 Synthesis

### General procedure I for the nucleoside monophosphate synthesis using Fm-reagent

The corresponding acetyl-protected nucleoside was solved in CH<sub>3</sub>CN. Then, a solution of bis(fluorenylmethyl)phosphoramidite in CH<sub>2</sub>Cl<sub>2</sub> was added, followed by the dropwise addition of 0.25 M DCI in CH<sub>3</sub>CN over a period of 20-30 min at room temperature. The reaction mixture was stirred under TLC monitoring (CH<sub>2</sub>Cl<sub>2</sub>/CH<sub>3</sub>OH; 30:1). A 5.5 M *t*-BuOOH in decane solution was added to the mixture and stirred for 5 min upon completion or stagnating conversion of starting material. All volatiles were removed *in vacuo*, and the residue was prepurified on silica gel (CH<sub>2</sub>Cl<sub>2</sub>/CH<sub>3</sub>OH; 29:1 or 39:1). All appropriate fractions were pooled, concentrated under reduced pressure, and the resulting residue was dissolved in a mixture of H<sub>2</sub>O/CH<sub>3</sub>CN/Et<sub>3</sub>N or H<sub>2</sub>O/MeOH/Et<sub>3</sub>N (1:1:1 v/v/v) and stirred for 1-3 days at room temperature. Colorless precipitate forms during concentration under reduced pressure, which can be removed by filtration over RP<sub>18</sub> silica gel or centrifugation. The product was purified on RP<sub>18</sub> silica gel using automated flash chromatography (H<sub>2</sub>O/CH<sub>3</sub>CN; 100:0 to 0:100) to result the monophosphate as triethylammonium salt.

### General procedure II for the nucleoside monophosphate synthesis using SOWA & OUCHI protocol

To a solution of POCl<sub>3</sub> (4.4 equiv) in CH<sub>3</sub>CN (18.9 equiv) pyridine (4.8 equiv) and H<sub>2</sub>O (2.8 equiv) were subsequently added at 0 °C. After 10 min, the corresponding nucleoside (1.0 equiv) was added, and the reaction mixture was stirred at 0 °C under RP<sub>18</sub> HPLC monitoring. Ice-cold H<sub>2</sub>O was added and stirred for 30 min upon consumption of starting material. After adjusting the pH value to 8 with solid NH<sub>4</sub>HCO<sub>3</sub>, all volatiles were removed by freeze-drying. The residue was purified on RP<sub>18</sub> silica gel using automated flash chromatography (H<sub>2</sub>O/CH<sub>3</sub>CN; 100:0 to 0:100), and subsequent freeze-drying resulted in the monophosphate as an ammonium salt. (Note, undesired diphosphates can be removed by RP<sub>18</sub> flash chromatography using H<sub>2</sub>O as eluent with reduced flow.)

**General procedure III for the nucleoside monophosphate synthesis using YOSHIKAWA protocol**

The corresponding nucleoside was solved in triethyl phosphate under gentle heating and subsequently cooled to the specified temperature (generally between -20 and 0 °C). If specified, water (0.5 equiv) was added to the mixture. Then, POCl<sub>3</sub> (1.2 to 4.0 equiv) was added, and the mixture was stirred at the same temperature under RP<sub>18</sub> HPLC monitoring. Upon consumption of starting material or the increasing formation of undesired diphosphates, ice-cold water was added to the reaction mixture, followed by the addition of solid NH<sub>4</sub>HCO<sub>3</sub>, adjusting the pH value to 8. After stirring for a further 30 min, the aqueous solution is washed three times with CH<sub>2</sub>Cl<sub>2</sub>, concentrated under reduced pressure, and freeze-dried (Note, smaller volumes of remaining triethyl phosphate can be removed by the dropwise addition of CH<sub>2</sub>Cl<sub>2</sub> until the precipitation of the monophosphate stops, followed by the decanting of the solvents). The resulting residue was purified on RP<sub>18</sub> silica gel using automated flash chromatography (0.05 M TEAB/CH<sub>3</sub>CN; 100:0 to 0:100) to provide the monophosphate as triethylammonium salt. (Note, the usage of 0.05 M TEAB as eluent removes traces of triethyl phosphate and is crucial for a successful purification. Triethylamine additive might improve MP solubility before column loading. Furthermore, diphosphate impurities can be removed after ion exchange to ammonia (Dowex-NH<sub>4</sub><sup>+</sup>) and subsequent RP<sub>18</sub> flash chromatography using H<sub>2</sub>O as eluent with reduced flow.)

**General procedure IV for the nucleoside triphosphate synthesis using modified LUDWIG & ECKSTEIN protocol**

The corresponding nucleoside was dried *in vacuo* and solved in trimethyl phosphate under gentle heating. Depending on the nucleobase, tributylamine, 1,8-bis(dimethylamino), naphthalene (proton sponge), or no base is added at this stage. After cooling to the specified temperature (between -20 and 0 °C) POCl<sub>3</sub> (1.2 to 2 equiv) was added, and the mixture was stirred at the same temperature under RP<sub>18</sub> HPLC monitoring. After consumption of starting material or the increasing formation of undesired diphosphates, a prechilled mixture containing tributyl ammonium pyrophosphate (2.5 equiv) and tributylamine (6 equiv) in CH<sub>3</sub>CN was added to the reaction mixture and kept under stirring at 0 °C or -20 °C for a specified time (15 min up to 2 h). After the slow addition of 0.05 M TEAB buffer, the reaction mixture was warmed to room temperature and washed three times with CH<sub>2</sub>Cl<sub>2</sub>. After freeze-drying the



aqueous phase, the resulting residue was dissolved in H<sub>2</sub>O and loaded onto a DEAE-Sephadex® A-25 column. The desired triphosphate was eluted using an automated flash system with a gradient of 0-1 M TEAB. The appropriate fractions were pooled, concentrated under reduced pressure, and freeze-dried. If necessary, further purification on RP<sub>18</sub> silica gel using automated flash chromatography (H<sub>2</sub>O as eluent) gives the triphosphate as triethylammonium salt.

#### **General procedure V for the vinylation of unprotected nucleosides using STILLE-cross-coupling**

The corresponding nucleoside (1 equiv), Pd<sub>2</sub>(dba)<sub>3</sub> (5.4 mol%), and tri(2-furyl) phosphine (12 mol%) were dried shortly *in vacuo* and solved in DMF. After the addition of tributyl(vinyl) tin (1.1 equiv), the reaction mixture was stirred at 60 °C until complete consumption of starting material (controlled via <sup>1</sup>H-NMR spectra). After removing the solvent under reduced pressure, the resulting residue was dissolved in CH<sub>2</sub>Cl<sub>2</sub>/CH<sub>3</sub>OH (4:1 v/v) and loaded onto Celite®. The crude product was purified on RP<sub>18</sub> silica gel using automated flash chromatography (H<sub>2</sub>O/CH<sub>3</sub>CN; 100:0 to 0:100), affording the vinylation nucleoside after freeze-drying the appropriate fractions. (Note, complete conversion of starting material is crucial for a successful purification due to similar retention times of starting material and product during chromatography. Furthermore, 5-vinyl pyrimidine nucleosides are prone to dimerization upon concentration; thus, preparing stock solutions can be beneficial.)

#### **General procedure VI for the vinylation of monophosphates using STILLE-cross-coupling**

The corresponding nucleoside monophosphate triethylammonium salt (1 equiv), Pd<sub>2</sub>(dba)<sub>3</sub> (5.4 mol%), and tri(2-furyl) phosphine (12 mol%) were dried shortly *in vacuo* and solved in DMF. After adding tributyl(vinyl) tin (1.1 equiv), the reaction mixture was stirred at 60 °C until complete consumption of starting material (controlled via <sup>1</sup>H-NMR spectra). After removing the solvent under reduced pressure, the resulting residue was dissolved in little CH<sub>3</sub>CN followed by the slow addition of H<sub>2</sub>O. A turbid suspension formed, which was filtrated over a short RP<sub>18</sub> silica plug with additional amounts of H<sub>2</sub>O. The removal of the solvent under reduced pressure and purification on RP<sub>18</sub> silica gel using automated flash chromatography (0.05 M TEAB/CH<sub>3</sub>CN; 100:0 to 0:100 or H<sub>2</sub>O/CH<sub>3</sub>CN; 100:0 to 0:100) provided the vinylation nucleoside monophosphates after

freeze-drying the appropriate fractions. (Note, complete conversion of starting material is crucial for a successful purification due to similar retention times of starting material and product during chromatography. In this work, the triethylammonium salt of nucleotides proved to be a reliable choice as starting materials in palladium-catalyzed cross-coupling reactions. Furthermore, 5-vinyl pyrimidine nucleotides are prone to dimerization upon concentration; thus, preparing stock solutions can be beneficial.)

### **General procedure VII for the vinylation of $\gamma$ -alkyl-/triphosphates using STILLE-cross-coupling**

The corresponding nucleoside triphosphate triethylammonium salt (1 equiv), Pd<sub>2</sub>(dba)<sub>3</sub> (10 mol%), and tri(2-furyl) phosphine (24 mol%) were solved in DMF or DMF/water 9:1 v/v (water was added in case of low solubility of the respective NTP). After adding tributyl(vinyl) tin (1.1 equiv), the reaction mixture was stirred at 40 °C until complete consumption of starting material (controlled via <sup>1</sup>H-NMR spectra). After removing the solvent under reduced pressure, the resulting residue was dissolved in little CH<sub>3</sub>CN followed by the slow addition of H<sub>2</sub>O. A turbid suspension formed, which was filtrated over a short RP<sub>18</sub> silica plug with additional amounts of H<sub>2</sub>O. Removal of the solvent under reduced pressure and purification on RP<sub>18</sub> silica gel using automated flash chromatography provided the vinyolated nucleoside triphosphates after freeze-drying the appropriate fractions. (Note, complete conversion of starting material is crucial for a successful purification due to similar retention times of starting material and product during chromatography. Furthermore, 5-vinyl pyrimidine nucleotides are prone to dimerization upon concentration; thus, preparing stock solutions can be beneficial.)

### **General procedure VIII for the synthesis of the $\gamma$ -modified triphosphates using the *H*-phosphonate route**

Pyrophosphate preparation: The corresponding *H*-phosphonate (1 equiv) was dissolved in CH<sub>3</sub>CN under gentle heating, and *N*-chlorosuccinimide (2.5 equiv) was added. The reaction mixture was stirred overnight at 50 °C, and the complete conversion of starting material was controlled by <sup>31</sup>P- or <sup>1</sup>H-NMR spectra. The reaction mixture was added dropwise to a diluted solution of 0.4 M tetrabutylammonium phosphate monobasic (3 equiv) in CH<sub>3</sub>CN and was subsequently stirred at room temperature for 1 h. The solvent was removed under reduced pressure, and the resulting residue was dissolved in CH<sub>2</sub>Cl<sub>2</sub>, washed with 1 M aq. NH<sub>4</sub>OAc (15 mL, 4 °C), and H<sub>2</sub>O (15 mL, 4 °C), and dried

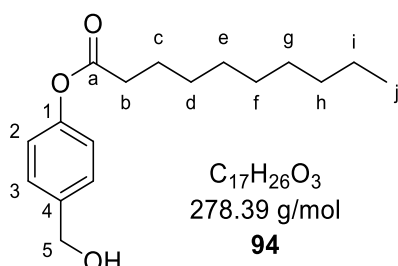
over Na<sub>2</sub>SO<sub>4</sub> (phase separation via centrifuge). Evaporation of the solvent resulted in the pyrophosphate, which was immediately carried on to the next step without further purification.

TriPPPPro preparation: The corresponding pyrophosphate (1 equiv) was solved in CH<sub>3</sub>CN and cooled to 0 °C. An ice-cold solution of TFAA (5 equiv) and Et<sub>3</sub>N (8 equiv) was added dropwise, and the resulting mixture was stirred for 10 min at room temperature. All volatiles were removed *in vacuo*, and the resulting residue was co-evaporated once with CH<sub>3</sub>CN and dissolved again in CH<sub>3</sub>CN. Et<sub>3</sub>N (5 equiv) (Note: no Et<sub>3</sub>N addition for base labile NMP-tetrazine conjugates) and 1-methylimidazole (3 equiv) were added. The reaction mixture was stirred at room temperature for 10 min, followed by the addition of the corresponding nucleoside monophosphate triethylammonium salt (0.2-0.5 equiv) dissolved in DMF. After the complete conversion of monophosphate (RP<sub>18</sub> HPLC monitoring), all volatiles were removed under reduced pressure. The resulting residue was purified on RP<sub>18</sub> silica gel using automated flash chromatography (H<sub>2</sub>O/CH<sub>3</sub>CN or THF; 100:0 to 0:100), followed by ion exchange to ammonia (Dowex-NH<sub>4</sub><sup>+</sup>), and purification on RP<sub>18</sub> silica gel using automated flash chromatography (H<sub>2</sub>O/CH<sub>3</sub>CN; 100:0 to 0:100).

*γ*-alkyl modified triphosphate preparation: The corresponding pyrophosphate (1 equiv) was solved in CH<sub>3</sub>CN and cooled to 0 °C. An ice-cold solution of TFAA (5 equiv) and Et<sub>3</sub>N (8 equiv) was added dropwise, and the resulting mixture was stirred for 10 min at room temperature. All volatiles were removed *in vacuo*, and the resulting residue was co-evaporated once with CH<sub>3</sub>CN and dissolved again in CH<sub>3</sub>CN. 1-Methylimidazole (3 equiv) was added, and the reaction mixture was stirred at room temperature for 10 min, followed by the addition of the corresponding nucleoside monophosphate triethylammonium salt (0.3-0.5 equiv) dissolved in DMF. After the complete conversion of monophosphate (RP<sub>18</sub> HPLC monitoring), the reaction mixture was concentrated under reduced pressure. An aqueous 10% tetrabutylammonium hydroxide solution (10 equiv) was added, and the resulting suspension was stirred overnight at room temperature. The solvent was removed *in vacuo*, and the crude product was purified on RP<sub>18</sub> silica gel using automated flash chromatography (H<sub>2</sub>O/CH<sub>3</sub>CN; 100:0 to 0:100) followed by ion-exchange to ammonia (Dowex-NH<sub>4</sub><sup>+</sup>) and purification on RP<sub>18</sub> silica gel using automated flash chromatography (H<sub>2</sub>O/CH<sub>3</sub>CN; 100:0 to 0:100).

### 6.3.1 Preparation of masking units

#### 4-(Hydroxymethyl)phenyl decanoate **94**



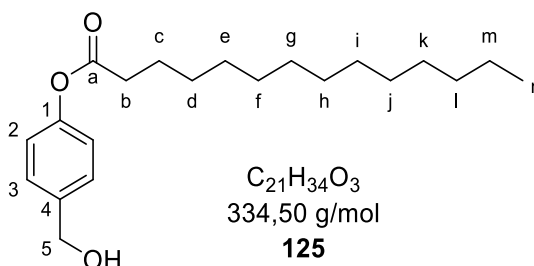
A solution of 4-hydroxybenzyl alcohol (10.0 g, 80.6 mmol) and  $Et_3N$  (10.2 mL, 73.2 mmol) in THF (75 mL) was cooled to 0 °C followed by the dropwise addition of decanoyl chloride (15.1 mL, 73.2 mmol) in THF (25 mL) throughout 1 h. The reaction was slowly warmed to room temperature and stirred overnight. The resulting suspension was filtrated, and the solvent was removed under reduced pressure. The crude product was purified with automated flash chromatography ( $CH_2Cl_2$ /ethyl acetate; 98:2 to 80:20) to provide **94** (10.2 g, 50%) as a colorless solid.  $R_f$ -value: 0.25 ( $CH_2Cl_2$ / ethyl acetate; 95:5).

$^1H$ -NMR (600 MHz,  $CDCl_3$ ):  $\delta$  [ppm] = 7.37 (d,  $^3J_{HH} = 8.5$  Hz, 2H, *H*-3), 7.06 (d,  $^3J_{HH} = 8.5$  Hz, 2H, *H*-2), 4.68 (s, 2H, *H*-5), 2.55 (t,  $^3J_{HH} = 7.5$  Hz, 2H, *H*-b), 1.75 (q,  $^3J_{HH} = 7.5$  Hz, 2H, *H*-c), 1.41 (q,  $^3J_{HH} = 7.1, 6.6$  Hz, 2H, *H*-d), 1.37-1.26 (m, 10H, *H*-e-i), 0.89 (t,  $^3J_{HH} = 7.0$  Hz, 3H, *H*-j).

$^{13}C$ -NMR (151 MHz,  $CDCl_3$ ):  $\delta$  [ppm] = 172.5 (*C*-a), 150.3 (*C*-1), 138.5 (*C*-4), 128.2 (*C*-3), 121.9 (*C*-2), 65.0 (*C*-5), 34.6 (*C*-b), 32.0 (*C*-h), 29.6, 2x 29.4, 29.3 (*C*-d-g), 25.1 (*C*-c), 22.8 (*C*-i), 14.3 (*C*-j).

IR:  $\nu$  [ $cm^{-1}$ ] = 3332, 2955, 2916, 2849, 1748, 1605, 1508, 1384, 1250, 1214, 1165, 1149, 1121, 1035, 1013, 925, 847, 819, 720.

HRMS (ESI<sup>+</sup>):  $m/z$  = calcd: 301.1774 [ $M+Na$ ]<sup>+</sup>, found: 301.1772 [ $M+Na$ ]<sup>+</sup>.

**4-(Hydroxymethyl) phenyltetradecanoate 125**

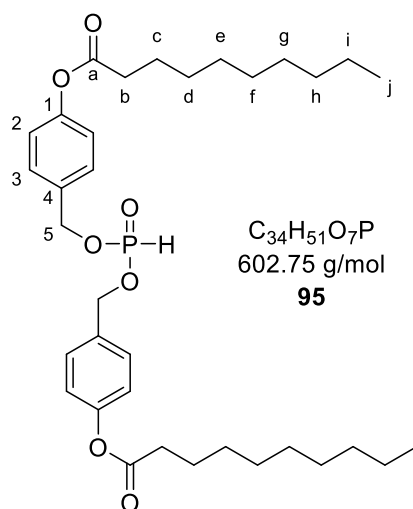
A solution of 4-hydroxybenzyl alcohol (9.93 g, 80.0 mmol) and  $Et_3N$  (10.0 mL, 72.0 mmol) in THF (75 ml) was cooled to 0 °C followed by the dropwise addition of tetradecanoyl chloride (19.6 mL, 72.0 mmol) in THF (25 mL) throughout 1 h. The reaction was slowly warmed to room temperature and stirred overnight. The resulting suspension was filtrated, and the solvent was removed under reduced pressure. The resulting crude product was purified with automated flash chromatography ( $CH_2Cl_2$ /ethyl acetate; 98:2 to 80:20) to provide **125** (10.0 g, 42%) as a colorless solid.

$^1H$ -NMR (500 MHz,  $CDCl_3$ ):  $\delta$  [ppm] = 7.36 (d,  $^3J_{HH} = 8.5$  Hz, 1H, *H*-3), 7.06 (d,  $^3J_{HH} = 8.5$  Hz, 2H, *H*-2), 4.65 (s, 2H, *H*-5), 2.55 (t,  $^3J_{HH} = 7.5$  Hz, 2H, *H*-b), 1.81 – 1.70 (m, 2H, *H*-c), 1.47 – 1.18 (m, 22H), 0.89 (t,  $^3J_{HH} = 6.9$  Hz, 3H, *H*-n).

$^{13}C$ -NMR (126 MHz,  $CDCl_3$ ):  $\delta$  [ppm] = 172.5 (*C*-a), 150.3 (*C*-1), 138.5 (*C*-4), 128.1 (*C*-3), 121.8 (*C*-2), 64.8 (*C*-5), 34.5 (*C*-b), 32.1 (*C*-l), 29.8, 29.8, 29.7, 29.6, 29.5, 29.4, 29.2 (*C*-d-k), 25.1 (*C*-c), 22.8 (*C*-m), 14.2 (*C*-n).

IR:  $\nu$  [ $cm^{-1}$ ] = 2925, 2854, 1750, 1508, 1465, 1377, 1199, 1165, 1142, 1110, 906, 729, 649.

HRMS (ESI<sup>+</sup>):  $m/z$  = calcd: 357.2406 [ $M+Na$ ]<sup>+</sup>, found: 357.2369 [ $M+Na$ ]<sup>+</sup>.

**Bis(4-decanoyloxybenzyl)-phosphonate/ (C9C9AB)-H-Phosphonate 95**

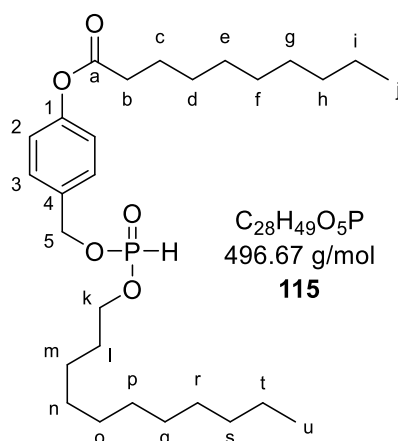
The 4-(hydroxymethyl)phenyl decanoate **94** (5.85 g, 21.0 mmol) was dried *in vacuo* and dissolved in pyridine (25 mL). Then diphenyl phosphonate (2.01 mL, 10.5 mmol) was added, and the reaction mixture was stirred for 5 h at 50 °C. The solvent was removed under reduced pressure. The residue was co-evaporated twice with toluene. The product was purified by recrystallization from *i*-PrOH to provide **95** (1.36 g, 54%) as colorless amorphous needles.

$^1H$ -NMR (400 MHz,  $CDCl_3$ ):  $\delta$  [ppm] = 7.40 – 7.32 (m, 4H, 2x *H*-2), 7.14 – 7.04 (m, 4H, 2x *H*-3), 6.93 (d,  $^1J_{HP}$  = 708.3 Hz, 1H, *P*-H), 5.11 – 4.96 (m, 4H, 2x *H*-5), 2.55 (t,  $^3J_{HH}$  = 7.5 Hz, 4H, 2x *H*-b), 1.75 (p,  $^3J_{HH}$  = 7.5 Hz, 4H, 2x *H*-c), 1.46 – 1.22 (m, 24H, *H*-alkyl), 0.88 (t,  $^3J_{HH}$  = 7.3, 6.5 Hz, 6H, 2x *H*-j).

$^{13}C$ -NMR (101 MHz,  $CDCl_3$ ):  $\delta$  [ppm] = 172.3 (2x *C*-a), 151.1 (2x *C*-1), 133.1 (d,  $^3J_{CP}$  = 6.0 Hz, 2x *C*-4), 129.4 (2x *C*-2), 122.1 (2x *C*-3), 66.8 (d,  $^2J_{CP}$  = 5.7 Hz, 2x *C*-5), 34.5 (2x *C*-b), 32.0 (2x *C*-h), 29.6, 2x 29.4, 29.2 (2x *C*-d-g), 25.0 (2x *C*-c), 22.8 (*C*-i), 14.3 (*C*-j).

$^{31}P$ -NMR (162 MHz,  $CDCl_3$ ):  $\delta$  [ppm] = 7.70 (s).

HRMS (ESI<sup>+</sup>):  $m/z$  = calcd: 625.3265 [M+Na]<sup>+</sup>, found: 625.3024 [M+Na]<sup>+</sup>.

**$\gamma$ -C11,C9AB-H-Phosphonate 115**

Diphenyl phosphonate (9.07 mL, 47.6 mmol) was solved in pyridine (60 mL) and cooled to  $-10\text{ }^{\circ}\text{C}$  followed by the dropwise addition of a solution of 4-(hydroxymethyl)phenyl decanoate **9a** (10.2 g, 36.6 mmol) dissolved in pyridine (20 mL) over a period of 30 min. The reaction mixture was warmed to room temperature and stirred for a further 10 min. Then, 1-undecanol (13.7 mL, 65.9 mmol) was added to the reaction mixture, and it was stirred for 2 h at  $40\text{ }^{\circ}\text{C}$ . The solvent was removed under reduced pressure, and the residue was co-evaporated twice with toluene and once with  $\text{CH}_2\text{Cl}_2$ . Purification on silica gel (petroleum ether/ethyl acetate; 3:2) resulted in the crude product, which was finally isolated by recrystallization from *i*-PrOH to provide **115** (2.91g, 16%) as a colorless oil.

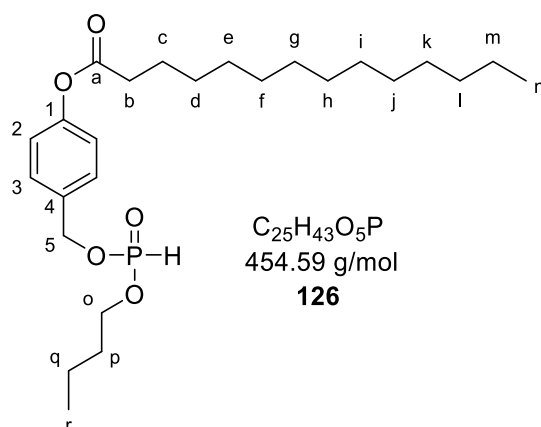
$^1\text{H-NMR}$  (400 MHz,  $\text{CDCl}_3$ ):  $\delta$  [ppm] = 7.41 (d,  $^3J_{\text{HH}} = 8.5$  Hz, 2H, *H*-2), 7.09 (d,  $^3J_{\text{HH}} = 8.5$  Hz, 2H, *H*-3), 6.88 (d,  $^1J_{\text{HP}} = 700$  Hz, 1H, *P*-H), 5.09 (d,  $^3J_{\text{HP}} = 9.5$  Hz, 2H, *H*-5), 4.09-3.96 (m, 2H, *H*-k), 2.55 (t,  $^3J_{\text{HH}} = 7.5$  Hz, 2H, *H*-b), 1.75 (q,  $^3J_{\text{HH}} = 7.5$  Hz, 2H, *H*-c), 1.68-1.62 (m, 2H, *H*-l), 1.42-1.39 (m, *H*-d), 1.37-1.25 (m, 26H, *H*-alkyl), 0.89-0.86 (m, 6H, *H*-u, *H*-j).

$^{13}\text{C-NMR}$  (101 MHz,  $\text{CDCl}_3$ ):  $\delta$  [ppm] = 172.3 (*C*-a), 151.1 (*C*-1), 133.3 (d,  $^3J_{\text{CP}} = 6.1$  Hz, *C*-4), 129.3 (*C*-3), 122.1 (*C*-2), 66.7 (d,  $^2J_{\text{CP}} = 5.4$  Hz, *C*-5), 66.2 (d,  $^2J_{\text{CP}} = 6.2$  Hz, *C*-l), 34.5 (*C*-b), 32.1, 32.0 (*C*-h', *C*-s), 30.5 (d,  $^3J_{\text{CP}} = 6.3$  Hz, *C*-k), 29.7, 29.7, 29.6, 29.6, 29.5, 2x 29.4, 2x 29.2 (*C*-d-g, *C*-n-r), 25.6 (*C*-m), 25.1 (*C*-c), 22.8, 22.8 (*C*-i, *C*-t), 14.3 (*C*-u, *C*-j).

$^{31}\text{P-NMR}$  (162 MHz,  $\text{CDCl}_3$ ):  $\delta$  [ppm] = 7.81 (s).

IR:  $\nu$  [ $\text{cm}^{-1}$ ] = 2956, 2916, 2849, 1750, 1249, 1218, 1202, 1141, 1120, 1064, 1017, 990, 957, 947, 926, 856, 551.

HRMS (ESI<sup>+</sup>):  $m/z$  calcd: 519.3210 [ $\text{M}+\text{Na}$ ]<sup>+</sup>, found: 519.3202 [ $\text{M}+\text{Na}$ ]<sup>+</sup>.

**$\gamma$ -C<sub>4</sub>,C<sub>13</sub>AB-*H*-Phosphonate **126****

Diphenyl phosphonate (2.05 mL, 10.1 mmol) was solved in pyridine (20 mL) and cooled to 0 °C. Then, 1-butanol (0.61 mL, 6.75 mmol) was added dropwise to the cooled reaction mixture, which was subsequently warmed to room temperature and stirred overnight. Then, 4-(hydroxymethyl)phenyl tetradecanoate **125** (2.71 g, 8.10 mmol) was added to the reaction mixture, and stirred overnight at room temperature. The solvent was removed under reduced pressure. The residue was co-evaporated twice with toluene and purified with automated flash chromatography (CH<sub>2</sub>Cl<sub>2</sub> + 3% acetone) to yield **126** (0.45 g, 15%) as a colorless wax.

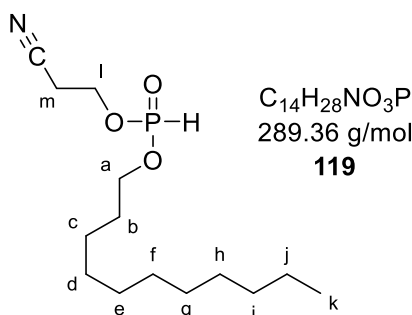
<sup>1</sup>H-NMR (400 MHz, CDCl<sub>3</sub>):  $\delta$  [ppm] = 7.41 (m, 2H, *H*-2), 7.09 (m, 2H, *H*-3), 6.88 (d, <sup>1</sup>*J*<sub>HP</sub> = 700.9 Hz, 1H, *P*-H), 5.09 (d, <sup>3</sup>*J*<sub>HH</sub> = 9.6 Hz, 2H, *H*-5), 4.15 – 3.90 (m, 2H, *H*-o), 2.55 (t, <sup>3</sup>*J*<sub>HH</sub> = 7.5 Hz, 2H, *H*-b), 1.75 (m, 2H, *H*-c), 1.68 – 1.59 (m, 2H, *H*-p), 1.45 – 1.22 (m, 22H, *H*-alkyl), 1.03 – 0.75 (m, 6H, *H*-n, *H*-r).

<sup>13</sup>C-NMR (126 MHz, CDCl<sub>3</sub>):  $\delta$  [ppm] = 172.3 (*C*-a), 151.1 (*C*-1), 133.3 (d, <sup>3</sup>*J*<sub>CP</sub> = 5.9 Hz, *C*-4), 129.3 (*C*-3), 122.1 (*C*-2), 66.7 (d, <sup>2</sup>*J*<sub>CP</sub> = 5.4 Hz, *C*-5), 65.8 (d, <sup>2</sup>*J*<sub>CP</sub> = 6.0 Hz, *C*-o), 34.5 (*C*-b), 32.5 (d, <sup>3</sup>*J*<sub>CP</sub> = 6.1 Hz, *C*-p), 32.1 (*C*-l), 29.8, 29.8, 29.8, 29.7, 29.6, 29.5, 29.4, 29.3 (*C*-d-k), 25.1 (*C*-c), 22.8 (*C*-m), 18.8 (*C*-q), 14.3 (*C*-n), 13.7 (*C*-r).

<sup>31</sup>P-NMR (162 MHz, CDCl<sub>3</sub>):  $\delta$  [ppm] = 7.83 (s).

HRMS (ESI<sup>+</sup>): *m/z* = calcd: 477.2746 [M+Na]<sup>+</sup>, found: 477.2740 [M+Na]<sup>+</sup>.



**2-Cyanoethyl undecyl phosphonate 119**

To a solution of diphenyl phosphonate (4.21 mL, 22.0 mmol) in pyridine (80 mL) a solution of 1-undecanol (4.18 mL, 20.0 mmol) in pyridine (20 mL) was slowly added at 0 °C. The solution was slowly warmed to room temperature and stirred overnight. Then, 3-hydroxypropionitrile (1.50 mL, 22.0 mmol) was added, and the reaction mixture was stirred overnight at room temperature. The solvent was removed under reduced pressure. The resulting residue was co-evaporated twice with toluene, and purified with automated flash chromatography (ethyl acetate + 0.5% Et<sub>3</sub>N) to yield **119** (3.38 g, 59%) as a colorless oil. R<sub>f</sub>-value: 0.75 (ethyl acetate + 0.5% Et<sub>3</sub>N).

<sup>1</sup>H-NMR (400 MHz, CDCl<sub>3</sub>): δ [ppm] = 6.88 (d, <sup>1</sup>J<sub>HP</sub> = 708.8 Hz, 1H, *P-H*), 4.34 – 4.21 (m, 2H, *H-l*), 4.19 – 4.01 (m, 2H, *H-a*), 2.76 (t, <sup>3</sup>J<sub>HH</sub> = 6.1 Hz, 2H, *H-m*), 1.74 – 1.65 (m, 2H, *H-b*), 1.45 – 1.13 (m, 17H, *H-alkyl*), 0.86 (t, <sup>3</sup>J<sub>HH</sub> = 6.8 Hz, 2H, *H-k*).

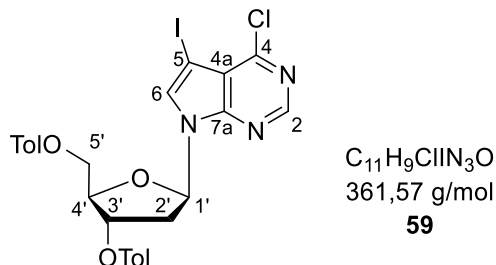
<sup>13</sup>C-NMR (101 MHz, CDCl<sub>3</sub>): δ [ppm] = 116.4 (CN), 66.6 (d, <sup>2</sup>J<sub>CP</sub> = 6.2 Hz, *C-a*), 60.0 (d, <sup>2</sup>J<sub>CP</sub> = 5.3 Hz, *C-l*), 32.0 (*C-i*), 30.4 (d, <sup>3</sup>J<sub>CP</sub> = 6.2 Hz, *C-b*), 29.7, 29.6, 29.6, 29.4, 29.2 (*C-d-h*), 25.5 (*C-c*), 22.8 (*C-j*), 20.1 (d, <sup>3</sup>J<sub>CP</sub> = 6.5 Hz, *C-m*), 14.2 (*C-k*).

<sup>31</sup>P-NMR (162 MHz, CDCl<sub>3</sub>): δ [ppm] = 7.69 (s).

HRMS (ESI<sup>+</sup>): *m/z* calcd: 290.1885 [M+H]<sup>+</sup>, found: 290.1897.

### 6.3.2 7-Deaza-7-vinyl-2'-deoxyadenosine series

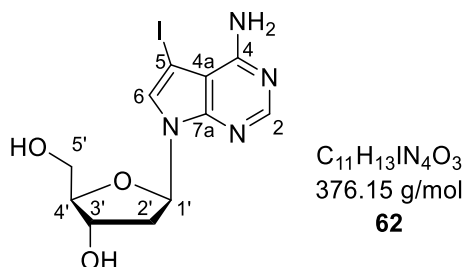
#### 4-Chloro-7-[2-deoxy-3,5-di-O-(4-toluoyl)- $\beta$ -D-erythro-pentofuranosyl]-5-iodo-7H-pyrrolo[2,3-d]pyrimidine **59**



The reaction was carried out as described in the literature with 4-Chloro-5-iodo-7H-pyrrolo[2,3-d] pyrimidine (2.90 g, 10.4 mmol), 2-deoxy-3,5-di-O-(*P*-toluoyl)- $\alpha$ -D-erythro-pentofuranosyl chloride (4.85 g, 12.5 mmol), KOH (1.46 g, 26.0 mmol) and TDA-1 (233  $\mu$ L, 728  $\mu$ mol) in CH<sub>3</sub>CN (180 mL). The product **59** (4.99 g, 76%) was obtained as colorless crystals after recrystallization from *i*-PrOH.

The analytical data was in accordance with those described.<sup>139</sup>

#### 7-Deaza-7-iodo-2'-deoxyadenosine **62**



The reaction was carried out as described in the literature with compound  $\beta$ -nucleoside (1.44 g, 2.23 mmol) in 1,4-dioxane (40 mL) and 25% NH<sub>4</sub>OH (80 mL). The product **62** (792 mg, 94%) was obtained as brownish solid after recrystallization from methanol.

The analytical data was in accordance with those described.<sup>140</sup>

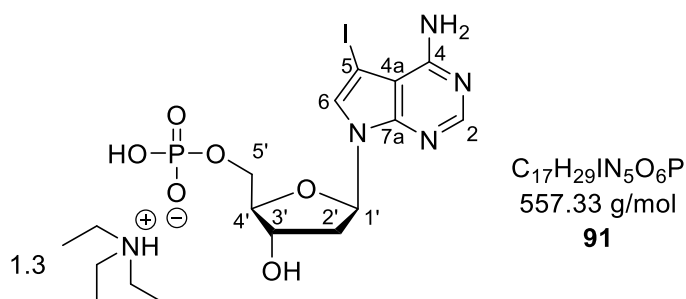
<sup>1</sup>H-NMR (600 MHz, DMSO-*d*<sub>6</sub>)  $\delta$  8.10 (s, 1H, *H*-2), 7.65 (s, 1H, *H*-6), 6.66 (s, 2H, NH<sub>2</sub>), 6.48 (dd, <sup>3</sup>*J*<sub>HH</sub> = 8.2, 5.9 Hz, 1H, *H*-1'), 5.24 (d, <sup>3</sup>*J*<sub>HH</sub> = 4.0 Hz, 1H, 3'-OH), 5.02 (t, <sup>3</sup>*J*<sub>HH</sub> = 5.5 Hz, 1H, 5'-OH), 4.32 (m, 1H, *H*-3'), 3.81 (td, <sup>3</sup>*J*<sub>HH</sub> = 4.4, 2.5 Hz, 1H, *H*-4'), 3.56 (dt, <sup>2</sup>*J*<sub>HH</sub> = 11.6 Hz, <sup>3</sup>*J*<sub>HH</sub> = 4.9 Hz, 1H, *H*-5'a), 3.50 (ddd, <sup>2</sup>*J*<sub>HH</sub> = 11.7 Hz, <sup>3</sup>*J*<sub>HH</sub> = 5.7, 4.3 Hz, 1H, *H*-5'b), 2.45 (ddd, <sup>2</sup>*J*<sub>HH</sub> = 13.8 Hz, <sup>3</sup>*J*<sub>HH</sub> = 8.2, 5.8 Hz, 1H, *H*-2'a), 2.15 (ddd, <sup>2</sup>*J*<sub>HH</sub> = 13.1 Hz, <sup>3</sup>*J*<sub>HH</sub> = 6.0, 2.7 Hz, 1H, *H*-2'b).

$^{13}\text{C}$ -NMR (151 MHz, DMSO):  $\delta$  [ppm] = 157.2 (C-4), 151.9 (C-2), 149.7 (C-7a), 126.7 (C-6), 103.1 (C-4a), 87.4 (C-4'), 82.9 (C-1'), 70.9 (C-3'), 61.9 (C-5'), 51.8 (C-5).

IR:  $\nu$  [ $\text{cm}^{-1}$ ] = 3461, 3331, 3202, 3129, 2929, 2856, 1632, 1584, 1553, 1477, 1309, 1094, 1055, 985, 950, 928, 714, 562, 421.

HRMS (ESI<sup>+</sup>):  $m/z$  calcd: 377.0111 [M+H]<sup>+</sup>, found: 377.0139.

### 7-Deaza-7-iodo-2'-deoxyadenosine monophosphate **91**



The reaction was carried out according to the general procedure III with IdA **62** (1.16 g, 3.10 mmol) and  $\text{POCl}_3$  (347  $\mu\text{L}$ , 3.72 mmol) in triethyl phosphate (25 mL) at  $-20^\circ\text{C}$  in an overnight reaction. Purification on RP<sub>18</sub> silica gel using automated flash chromatography (0.05 M TEAB/ $\text{CH}_3\text{CN}$ ; 100:0 to 0:100) provided the TEAH salt of **91** (1.20 g, 66%) as a colorless solid.

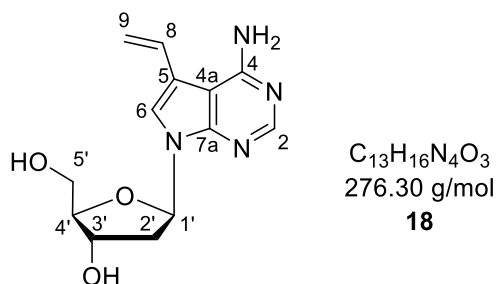
$^1\text{H}$ -NMR (600 MHz,  $\text{D}_2\text{O}$ )  $\delta$  [ppm] = 8.03 (s, 1H, H-2), 7.59 (s, 1H, H-6), 6.53 (dd,  $^3J_{\text{HH}} = 7.8$ , 6.2 Hz, 1H, H-1'), 4.68 – 4.65 (m, 1H, H-3'), 4.21 – 4.19 (m, 1H, H-4'), 4.01 – 3.97 (m, 2H, H-5'), 3.19 (q,  $^3J_{\text{HH}} = 7.3$  Hz, 6H, H-a), 2.67 – 2.59 (m, 1H, H-2'a), 2.54 – 2.47 (m, 1H, H-2'b), 1.27 (t,  $^3J_{\text{HH}} = 7.3$  Hz, 10H, H-b).

$^{13}\text{C}$ -NMR (151 MHz,  $\text{D}_2\text{O}$ )  $\delta$  [ppm] = 156.2 (C-4), 150.7 (C-2), 148.6 (C-7a), 127.0 (C-6), 103.5 (C-4a), 85.3 (d,  $^3J_{\text{CP}} = 8.6$  Hz, C-4'), 82.9 (C-1'), 71.4 (C-3'), 64.6 (d,  $^2J_{\text{CP}} = 4.8$  Hz, C-5'), 51.8 (C-5), 46.6 (C-a), 38.7 (H-2'), 8.2 (C-b).

$^{31}\text{P}$ -NMR (162 MHz,  $\text{D}_2\text{O}$ ):  $\delta$  [ppm] = 1.09 (s).

IR:  $\nu$  [ $\text{cm}^{-1}$ ] = 3445, 3291, 3115, 2981, 2939, 2683, 2379, 1630, 1580, 1551, 1470, 1445, 1166, 1029, 973, 917, 836, 806, 789, 712, 498.

HRMS (ESI<sup>-</sup>):  $m/z$  calcd: 454,9623 [M-H]<sup>-</sup>, found: 454.9580.

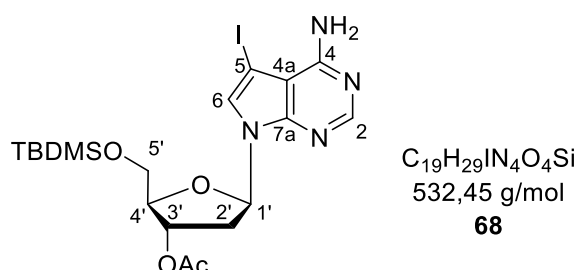
**7-Deaza-7-vinyl-2'-deoxyadenosine 18**

The reaction was carried out according to the general procedure V with IdA **62** (113 mg, 0.30 mmol), Pd<sub>2</sub>(dba)<sub>3</sub> (15 mg, 16 μmol, 5.4 mol%), tri(2-furyl) phosphine (8.4 mg, 36 μmol, 12 mol%) and tributyl(vinyl) tin (96 μL, 0.33 mmol) in DMF (3 mL). Purification on RP<sub>18</sub> silica gel with automated flash chromatography (H<sub>2</sub>O/CH<sub>3</sub>CN; 100:0 to 0:100) provided **18** (68 mg, 83%) as a colorless solid.

<sup>1</sup>H-NMR (400 MHz, DMSO-*d*<sub>6</sub>): δ [ppm] = 8.04 (s, 1H, *H*-2), 7.61 (s, 1H, *H*-6), 7.09 (dd, <sup>3</sup>*J*<sub>HH</sub> = 17.2, 10.9, 1.9 Hz, 1H, *H*-8), 6.66 (s, 2H, NH<sub>2</sub>), 6.51 (dd, <sup>3</sup>*J*<sub>HH</sub> = 8.3 Hz, 5.9 Hz, 1H, *H*-1'), 5.55 (dd, <sup>3</sup>*J*<sub>HH</sub> = 17.2 Hz, <sup>2</sup>*J*<sub>HH</sub> = 1.7 Hz, 1H, *trans*-*H*-9), 5.24 – 5.19 (m, 1H, 3'-OH), 5.12 (dd, <sup>3</sup>*J*<sub>HH</sub> = 10.8 Hz, <sup>2</sup>*J*<sub>HH</sub> = 1.8 Hz, 1H, *cis*-*H*-9), 5.10 – 5.05 (m, 1H, 5'-OH), 4.41 – 4.31 (m, 1H, *H*-3'), 3.87 – 3.80 (m, 1H, *H*-4'), 3.66 – 3.47 (m, 2H, *H*-5'), 2.57 – 2.41 (m, 7H, *H*-2'a, DMSO-*d*<sub>6</sub>), 2.22 – 2.11 (m, 1H, *H*-2'b).

<sup>13</sup>C-NMR (151 MHz, DMSO-*d*<sub>6</sub>): δ [ppm] = 157.6 (*C*-4), 151.4 (*C*-2), 150.3 (*C*-7a), 129.0 (*C*-8), 118.6 (*C*-6), 114.1 (*C*-5), 113.0 (*C*-9), 100.7 (*C*-4a), 87.3 (*C*-4'), 83.0 (*C*-1'), 71.0 (*C*-3'), 62.0 (*C*-5'), 40.2 - 38.9 (m, *C*-2', DMSO-*d*<sub>6</sub>).

HRMS (ESI<sup>+</sup>): *m/z* calcd: 276.1222 [M+H]<sup>+</sup>, found: 277.1302.

**3'-O-Acetyl-5'-O-*tert*-butyldimethylsilyl-7-deaza-7-iodo-2'-deoxyadenosine 68**

The nucleoside **62** (800 mg, 2.18 mmol) was dried *in vacuo* and solved in pyridine (16 mL). Then, TBDMSCl (353 mg, 2.34 mmol) was added, and the resulting solution was stirred overnight at room temperature. The solvent was removed under reduced pressure and the resulting residue was co-evaporated twice with toluene. The residue

was resuspended in CH<sub>3</sub>CN (16 mL) followed by the stepwise addition of DMAP (21 mg, 175 μmol), Et<sub>3</sub>N (389 μL, 2.81 mmol), and Ac<sub>2</sub>O (241 μL, 2.55 mmol). The resulting solution was stirred for 1 h at room temperature. Upon completion, methanol was added to the reaction mixture, and stirring was continued for 10 min. All volatiles were removed under reduced pressure, and the resulting residue was dissolved in H<sub>2</sub>O/ ethyl acetate. The organic layer was washed with H<sub>2</sub>O and brine once and was dried over Na<sub>2</sub>SO<sub>4</sub>. The solvent was removed under reduced pressure, and the crude product was recrystallized from *i*-PrOH to yield **68** (951 mg, 79%) as a colorless solid.

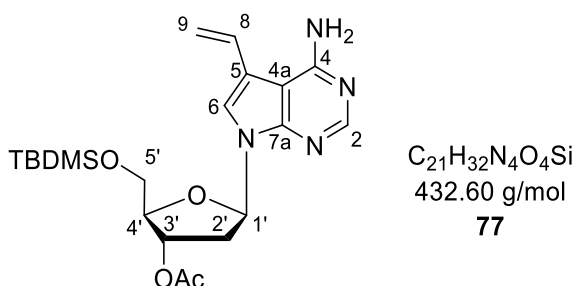
<sup>1</sup>H-NMR (400 MHz, DMSO-*d*<sub>6</sub>) δ [ppm] = 8.11 (s, 1H, *H*-2), 7.58 (s, 1H, *H*-6), 6.68 (s, 2H, NH<sub>2</sub>), 6.52 (dd, <sup>3</sup>J<sub>HH</sub> = 8.7, 5.8 Hz, 1H, *H*-1'), 5.32 – 5.22 (m, 1H, *H*-3'), 4.11 – 4.02 (m, 1H, *H*-4'), 3.86 – 3.71 (m, 2H, *H*-5'), 2.70 – 2.56 (m, 1H, *H*-2'a), 2.46 – 2.34 (m, 1H, *H*-2'b), 2.08 (s, 3H, Ac-CH<sub>3</sub>), 0.90 (s, 9H, *t*Bu-C(CH<sub>3</sub>)<sub>3</sub>), 0.10 (s, 3H, Si-CH<sub>3</sub>), 0.08 (s, 3H, Si-CH<sub>3</sub>).

<sup>13</sup>C-NMR (101 MHz, DMSO): δ [ppm] = 169.9 (CH<sub>3</sub>-CO), 157.2 (*C*-4), 152.1 (*C*-2), 149.9 (*C*-7a), 125.7 (*C*-6), 103.0 (*C*-4a), 84.0 (*C*-4'), 82.6 (*C*-1'), 74.6 (*C*-3'), 63.3 (*C*-5'), 52.4 (*C*-5), 37.1 (*C*-2'), 25.8 (*t*Bu-CH<sub>3</sub>), 20.8 (Ac-CH<sub>3</sub>), 18.0 (*t*Bu-C(CH<sub>3</sub>)<sub>3</sub>), -5.5 (Si-CH<sub>3</sub>), -5.6 (Si-CH<sub>3</sub>).

IR: ν [cm<sup>-1</sup>] = 3456, 3283, 3125, 2927, 2857, 1732, 1632, 1582, 1471, 1445, 1245, 1123, 945, 7, 834, 776, 571, 416.

HRMS (ESI<sup>+</sup>): *m/z* calcd: 533.1081 [M+H]<sup>+</sup>, found: 533.1070.

### 3'-O-Acetyl-5'-O-*tert*-butyldimethylsilyl-7-deaza-7-vinyl-2'-deoxyadenosine **77**



The protected nucleoside **68** (730 mg, 1.37 mmol), Pd<sub>2</sub>(dba)<sub>3</sub> (68 mg, 74 μmol, 5.4 mol%) and tri(2-furyl) phosphine (38 mg, 0.16 mmol, 12 mol%) were dried *in vacuo* and solved in DMF (2 mL). After adding tributyl(vinyl) tin (440 μL, 1.51 mmol), the reaction was stirred for 2 h at 60 °C. The reaction was monitored by TLC (petroleum ether/ethyl acetate; 4:6), and after complete conversion of starting material, the solvent was removed under reduced pressure. The crude product was purified on silica gel

(petroleum ether/ethyl acetate; 3:7 to 2:8), providing **77** (593 mg, 91%) as a light-yellow foam.  $R_f$ -value: 0.15 (petroleum ether/ethyl acetate; 4:6).

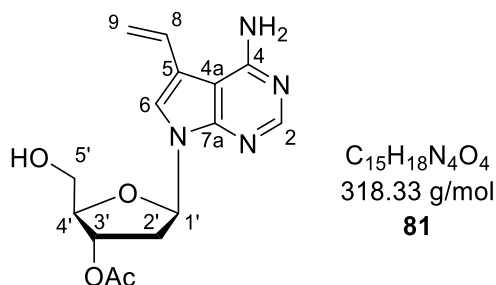
$^1\text{H-NMR}$  (400 MHz,  $\text{CDCl}_3$ ):  $\delta$  [ppm] = 8.17 (s, 1H,  $H$ -2), 7.15 (s, 1H,  $H$ -6), 6.73 (dd,  $^3J_{\text{HH}} = 17.4$ , 11.0, 1H,  $H$ -8), 6.63 (dd,  $^3J_{\text{HH}} = 9.1$ , 5.5 Hz, 1H,  $H$ -1'), 5.46 – 5.31 (m, 3H,  $\text{trans-}H$ -8,  $\text{NH}_2$ ), 5.29 – 5.24 (m, 1H,  $H$ -3'), 5.22 (dd,  $^3J_{\text{HH}} = 11.0$  Hz,  $^2J_{\text{HH}} = 1.5$  Hz, 1H,  $\text{cis-}H$ -9), 4.09 – 3.97 (m, 1H,  $H$ -4'), 3.86 – 3.67 (m, 2H,  $H$ -5'), 2.48 – 2.29 (m, 2H,  $H$ -2'), 1.99 (s, 3H,  $\text{Ac-CH}_3$ ), 0.83 (s, 9H,  $t\text{Bu-C}(\text{CH}_3)_3$ ), 0.01 (s, 3H,  $\text{Si-CH}_3$ ), 0.01 (s, 3H,  $\text{Si-CH}_3$ ).

$^{13}\text{C-NMR}$  (101 MHz,  $\text{CDCl}_3$ ):  $\delta$  [ppm] = 170.8 ( $\text{CH}_3\text{-CO}$ ), 157.0 ( $C$ -4), 151.6 ( $C$ -2), 151.1 ( $C$ -7a), 129.3 ( $C$ -8), 119.7 ( $C$ -6), 116.7 ( $C$ -5), 115.6 ( $C$ -9), 101.6 ( $C$ -4a), 85.0 ( $C$ -4'), 83.3 ( $C$ -1'), 75.8 ( $C$ -3'), 63.9 ( $C$ -5'), 38.7 ( $C$ -2'), 26.1 ( $t\text{Bu-CH}_3$ ), 21.2 ( $\text{Ac-CH}_3$ ), 18.5 ( $t\text{Bu-C}(\text{CH}_3)_3$ ), -5.2 ( $\text{Si-CH}_3$ ), -5.4 ( $\text{Si-CH}_3$ ).

IR:  $\nu$  [ $\text{cm}^{-1}$ ] = 3318, 3120, 2953, 2928, 2856, 1738, 1622, 1577, 1461, 1235, 1193, 1123, 1101, 1068, 1017, 1005, 832, 776. 566.

HRMS (ESI<sup>+</sup>):  $m/z$  calcd: 433.2271 [ $\text{M}+\text{H}$ ]<sup>+</sup>, found: 433.2260.

### 3'-O-Acetyl-7-deaza-7-vinyl-2'-deoxyadenosine **81**



The nucleoside **77** (476 mg, 1.10 mmol) was solved in 40 mL THF followed by the addition of TreatHF (359  $\mu\text{L}$ , 2.20 mmol). After stirring overnight at room temperature, all volatiles were removed under reduced pressure, and the residue was purified on silica gel ( $\text{CH}_2\text{Cl}_2/\text{CH}_3\text{OH}$ ; 19:1) to yield **81** (289 mg, 83%) as a colorless foam.  $R_f$ -value: 0.27 ( $\text{CH}_2\text{Cl}_2/\text{CH}_3\text{OH}$ ; 19:1).

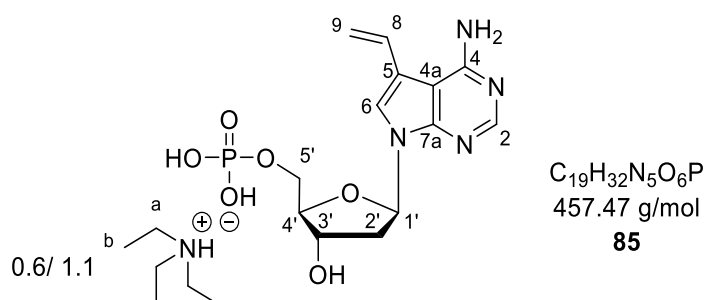
$^1\text{H-NMR}$  (400 MHz,  $\text{DMSO-}d_6$ )  $\delta$  [ppm] = 8.06 (s, 1H,  $H$ -2), 7.70 (s, 1H,  $H$ -6), 7.11 (dd,  $^3J_{\text{HH}} = 17.2$ , 10.9 Hz, 1H,  $H$ -8), 6.77 (s, 2H,  $\text{NH}_2$ ), 6.50 (dd,  $^3J_{\text{HH}} = 9.3$ , 5.5 Hz, 1H,  $H$ -1'), 5.57 (dd,  $^3J_{\text{HH}} = 17.3$  Hz,  $^2J_{\text{HH}} = 1.8$  Hz, 1H,  $\text{trans-}H$ -8), 5.36 – 5.24 (m, 2H,  $H$ -3',  $\text{OH}$ ), 5.14 (dd,  $^3J_{\text{HH}} = 10.8$  Hz,  $^2J_{\text{HH}} = 1.8$  Hz, 1H,  $\text{cis-}H$ -9), 4.05 – 3.95 (m, 1H,  $H$ -4'), 3.72 – 3.56 (m, 2H,  $H$ -5'), 2.81 – 2.65 (m, 1H,  $H$ -2'a), 2.42 – 2.30 (m, 1H,  $H$ -2'b), 2.09 (s, 3H,  $\text{Ac-CH}_3$ ).

$^{13}\text{C}$ -NMR (101 MHz, DMSO):  $\delta$  [ppm] = 170.0 (CH<sub>3</sub>-CO), 157.7 (C-4), 151.6 (C-2), 150.5 (C-7a), 129.0 (C-8), 118.5 (C-6), 114.4 (C-5), 113.3 (C-9), 100.7 (C-4a), 84.5 (C-4'), 83.0 (C-1'), 75.1 (C-3'), 61.7 (C-5'), 36.7 (C-2'), 20.9 (Ac-CH<sub>3</sub>).

IR:  $\nu$  [cm<sup>-1</sup>] = 3472, 3334, 3117, 2915, 1732, 1623, 1575, 1531, 1461, 1369, 1232, 1196, 1098, 1060, 985, 922, 799, 565.

HRMS (ESI<sup>+</sup>):  $m/z$  calcd: 319.1406 [M+H]<sup>+</sup>, found: 319.1431.

### 7-Deaza-7-vinyl-2'-deoxyadenosine monophosphate **85**



**STILLE-coupling:** The reaction was carried out according to the general procedure V with IdAMP **91** (1.1 TEAH, 72 mg, 0.13 mmol), Pd<sub>2</sub>(dba)<sub>3</sub> (6.3 mg, 6.9  $\mu$ mol, 5.4 mol%), tri(2-furyl) phosphine (3.5 mg, 15  $\mu$ mol, 12 mol%) and tributyl(vinyl) tin (41  $\mu$ L, 0.14 mmol) in DMF (4 mL) for 2 h. Purification on RP<sub>18</sub> silica gel with automated flash chromatography (H<sub>2</sub>O/CH<sub>3</sub>CN; 100:0 to 0:100) provided the TEAH salt of **85** (0.6 TEAH, 33 mg, 62%) as a colorless solid.

**Fm-route:** The reaction was carried out according to the general procedure I with protected 7-deaza-7-vinyl-2'-deoxyadenosine **81** (223 mg, 0.700 mmol) in CH<sub>3</sub>CN (10 mL), bis(fluorenylmethyl)phosphoramidite (657 mg, 1.26 mmol) in CH<sub>2</sub>Cl<sub>2</sub> (2 mL), and 0.25 M DCI in CH<sub>3</sub>CN (5.04 mL, 1.26 mmol). The reaction was stirred for 15 min, followed by the addition of a 5.5 M *t*-BuOOH in decane solution (255  $\mu$ L, 1.40 mmol). Deprotection was carried out in H<sub>2</sub>O/MeOH/Et<sub>3</sub>N (1:1:1 v/v/v) overnight, after prepurification of the intermediate on silica gel (CH<sub>2</sub>Cl<sub>2</sub>/CH<sub>3</sub>OH; 39:1). The product was purified on RP<sub>18</sub> silica gel using automated flash chromatography (H<sub>2</sub>O/CH<sub>3</sub>CN; 100:0 to 0:100) to provide the monophosphate **85** (1.1 TEAH, 181 mg, 55%) as triethylammonium salt.

$^1\text{H}$ -NMR (400 MHz, D<sub>2</sub>O)  $\delta$  [ppm] = 8.04 (s, 1H, H-2), 7.59 (s, 1H, H-6), 6.71 (ddd,  $^3J_{\text{HH}} = 17.4, 11.0, 0.9$  Hz, 1H, H-9), 6.54 (dd,  $^3J_{\text{HH}} = 7.8, 6.2$  Hz, 1H, H-1'), 5.63 (dd,  $^3J_{\text{HH}} = 17.4, ^2J_{\text{HH}} = 1.2$  Hz, 1H, *trans*-H-9), 5.33 (dd,  $^3J_{\text{HH}} = 11.0, ^2J_{\text{HH}} = 1.3$  Hz, 1H, *cis*-H-9), 4.73 – 4.65

(m, 1H, *H*-3'), 4.29 – 4.18 (m, 1H, *H*-4'), 4.10 – 4.00 (m, 2H, *H*-5'), 3.19 (q,  $^3J_{\text{HH}} = 7.3$  Hz, 6H, *H*-a), 2.72 – 2.8 (m, 1H, *H*-2'a), 2.57 – 2.41 (m, 1H, *H*-2'b), 1.27 (t,  $^3J_{\text{HH}} = 7.3$  Hz, 10H, *H*-b).

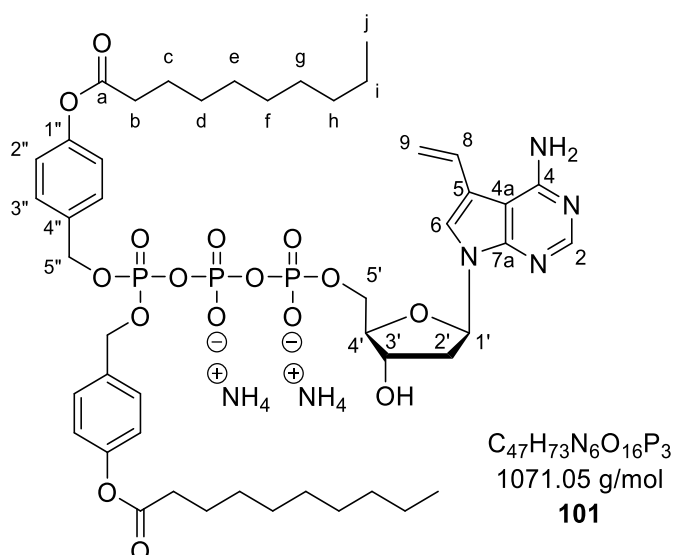
$^{13}\text{C}$ -NMR (101 MHz,  $\text{D}_2\text{O}$ )  $\delta$  [ppm] = 154.1 (*C*-4), 148.2 (*C*-7a), 147.0 (*C*-2), 126.8 (*C*-8), 119.9 (*C*-6), 116.9 (*C*-5), 116.6 (*C*-9), 100.2 (*C*-4a), 85.3 (d,  $^3J_{\text{CP}} = 8.6$  Hz, *C*-4'), 83.0 (*C*-1'), 71.3 (*C*-3'), 64.7 (d,  $^2J_{\text{CP}} = 5.0$  Hz, *C*-5'), 46.6 (*C*-a), 38.9 (*C*-2'), 8.2 (*C*-b).

$^{31}\text{P}$ -NMR (162 MHz,  $\text{D}_2\text{O}$ ):  $\delta$  [ppm] = 0.76 (s).

IR:  $\nu$  [ $\text{cm}^{-1}$ ] = 3345, 3324, 3200, 2939, 1666, 1630, 1583, 1464, 1347, 1307, 1187, 1163, 1057, 1000, 925, 800, 720, 511.

HRMS (ESI<sup>-</sup>): *m/z* calcd: 355.0813 [*M*-H]<sup>-</sup>, found: 355.0801.

### $\gamma$ -(**C9C9AB**)-VdATP **101**



The reaction was carried out with the general procedure VIII with the pyrophosphate of **95** (382 mg, 406  $\mu\text{mol}$ ), TFAA (282  $\mu\text{L}$ , 2.03 mmol), and  $\text{Et}_3\text{N}$  (453  $\mu\text{L}$ , 3.25 mmol) in  $\text{CH}_3\text{CN}$  (3 ml). The subsequent activation step was performed with  $\text{Et}_3\text{N}$  (283  $\mu\text{L}$ , 2.03 mmol) and 1-methylimidazole (81  $\mu\text{L}$ , 1.02 mmol) in  $\text{CH}_3\text{CN}$  (2 ml), followed by the coupling with monophosphate **85** (1.1 TEAH, 38 mg, 81  $\mu\text{mol}$ ) solved in DMF (3 mL). Purification on  $\text{RP}_{18}$  silica gel with automated flash chromatography ( $\text{H}_2\text{O}/\text{THF}$ ; 100:0 to 0:100), Dowex ion-exchange ( $\text{NH}_4^+$ ), and  $\text{RP}_{18}$  silica gel with automated flash chromatography ( $\text{H}_2\text{O}/\text{CH}_3\text{CN}$ ; 100:0 to 0:100) as well as subsequent freeze-drying provided **101** (38 mg, 43%) as colorless cotton.



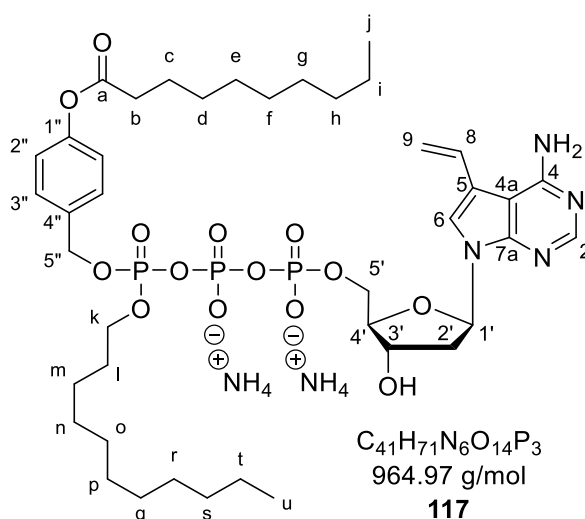
$^1\text{H-NMR}$  (400 MHz, MeOD):  $\delta$  [ppm] = 8.02 (s, 1H, *H*-2), 7.76 (s, 1H, *H*-6), 7.36 (dd,  $^3J_{\text{HH}} = 8.6, 2.0$  Hz, 4H, 4x *H*-2''), 6.98 (dd,  $^3J_{\text{HH}} = 8.5, 1.9$  Hz, 4H, 4x *H*-3''), 6.67 (dd,  $^3J_{\text{HH}} = 17.3, 11.0$  Hz, 1H, *H*-8), 6.57 – 6.47 (m, 1H, *H*-1'), 5.77 (dd,  $^3J_{\text{HH}} = 17.3$  Hz,  $^2J_{\text{HH}} = 1.1$  Hz, 1H, *trans-H*-9), 5.24 (dd,  $^3J_{\text{HH}} = 11.0$  Hz,  $^2J_{\text{HH}} = 1.2$  Hz, 1H, *cis-H*-9), 5.15 (m, 4H, 2x *H*-5''), 4.62 – 4.54 (m, 1H, *H*-3'), 4.43 – 4.19 (m, 2H, *H*-5'), 4.17 – 4.10 (m, 1H, *H*-4'), 2.54 (t,  $^3J_{\text{HH}} = 7.4$  Hz, 4H, 2x *H*-b), 2.49 – 2.27 (m, 2H, *H*-2'), 1.70 (p,  $^3J_{\text{HH}} = 7.3$  Hz, 4H, 2x *H*-c), 1.51 – 1.21 (m, 24H, 2x *H*-d-i), 0.89 (t,  $^3J_{\text{HH}} = 6.6$  Hz, 6H, 2x *H*-j).

$^{13}\text{C-NMR}$  (101 MHz, MeOD):  $\delta$  [ppm] = 173.7 (2x *C*-a), 152.3 (2x *C*-1''), 148.4 (*C*-4), 144.0 (*C*-7a), 134.8 (d,  $^3J_{\text{CP}} = 7.6$  Hz, 2x *C*-4''), 130.4 (4x *C*-3''), 127.4 (*C*-8), 122.8 (4x *C*-2''), 122.3 (*C*-6), 118.5 (*C*-5), 118.0 (*C*-9), 100.1 (*C*-4a), 87.6 (*C*-4'), 84.9 (*C*-1'), 72.3 (*C*-3'), 70.4 (d,  $^2J_{\text{CP}} = 5.9$  Hz, 2x *C*-5''), 67.0 (d,  $^2J_{\text{CP}} = 4.2$  Hz, *C*-5'), 41.8 (*C*-2'), 35.0 (2x *C*-b), 33.1 (2x *C*-h), 30.6, 30.4, 30.4, 30.2 (2x *C*-d-g), 26.0 (2x *C*-c), 23.8 (2x *C*-i), 14.5 (2x *C*-j).

$^{31}\text{P-NMR}$  (162 MHz, MeOD):  $\delta$  [ppm] = -11.18 (d,  $^2J_{\text{PP}} = 19.3$  Hz, *P*- $\alpha$ ), -13.10 (d,  $^2J_{\text{PP}} = 16.2$  Hz, *P*- $\gamma$ ), -23.60 (t,  $^2J_{\text{PP}} = 18.1$  Hz, *P*- $\beta$ ).

HRMS (ESI<sup>-</sup>): *m/z* calcd: 1035.3692 [*M*-H]<sup>-</sup>, found: 1035.3558.

#### VS204: $\gamma$ -(*C*11,*C*9AB)-VdATP 117



The reaction was carried out with the general procedure VIII with the pyrophosphate of **115** (177 mg, 212  $\mu\text{mol}$ ), TFAA (147  $\mu\text{L}$ , 1.06 mmol), and  $\text{Et}_3\text{N}$  (236  $\mu\text{L}$ , 1.70 mmol) in  $\text{CH}_3\text{CN}$  (6 ml). The subsequent activation step was performed with  $\text{Et}_3\text{N}$  (148  $\mu\text{L}$ , 1.06 mmol) and 1-methylimidazole (42  $\mu\text{L}$ , 530  $\mu\text{mol}$ ) in  $\text{CH}_3\text{CN}$  (6 ml) followed by the coupling with monophosphate **85** (1.1 TEAH, 50 mg, 106  $\mu\text{mol}$ ) solved in DMF (4 mL). Purification on RP<sub>18</sub> silica gel with automated flash chromatography ( $\text{H}_2\text{O}/\text{THF}$ ; 100:0 to

0:100), Dowex ion-exchange ( $\text{NH}_4^+$ ), and RP<sub>18</sub> silica gel with automated flash chromatography ( $\text{H}_2\text{O}/\text{CH}_3\text{CN}$ ; 100:0 to 0:100) as well as subsequent freeze-drying provided **117** (72 mg, 65%) as colorless cotton.

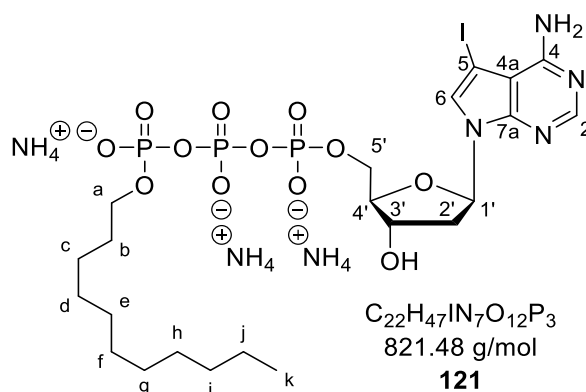
$^1\text{H-NMR}$  (400 MHz, MeOD):  $\delta$  [ppm] = 8.07 (s, 1H, *H-2*), 7.80 (s, 1H, *H-6*), 7.45 (d,  $^3J_{\text{HH}} = 7.9$  Hz, 2H, 2x *H-2''*), 7.01 (d,  $^3J_{\text{HH}} = 8.5$  Hz, 2H, 2x *H-3''*), 6.70 (dd,  $^3J_{\text{HH}} = 17.3, 11.0$  Hz, 1H, *H-8*), 6.54 (t,  $^3J_{\text{HH}} = 6.7$  Hz, 1H, *H-1'*), 5.80 (d,  $^3J_{\text{HH}} = 17.3$  Hz, 1H, *trans-H-9*), 5.27 (d,  $^3J_{\text{HH}} = 11.2$  Hz, 1H, *cis-H-9*), 5.24 – 5.18 (m, 2H, *H-5''*), 4.63 – 4.56 (m, 1H, *H-3'*), 4.45 – 4.34 (m, 1H, *H-5'a*), 4.33 – 4.22 (m, 1H, *H-5'b*), 4.20 – 4.05 (m, 3H, *H-4'*, *H-k*), 2.55 (t,  $^3J_{\text{HH}} = 7.4$  Hz, 2H, *H-b*), 2.49 – 2.24 (m, 2H, *H-2'*), 1.81 – 1.52 (m, 4H, *H-c*, *H-l*), 1.52 – 1.12 (m, 28H, *H-d-l*, *H-m-t*), 0.94 – 0.82 (m, 6H, *H-j*, *H-u*).

$^{13}\text{C-NMR}$  (151 MHz, MeOD):  $\delta$  [ppm] = 173.6 (*C-a*), 152.4 (*C-4*), 152.3 (*C-1''*), 148.5 (*C-2*), 144.1 (*C-7a*), 135.0 (d,  $^3J_{\text{CP}} = 7.3$  Hz, *C-4''*), 130.2 (2x *C-3''*), 127.4 (*C-8*), 122.8 (2x *C-2''*), 122.4 (*C-6*), 118.6 (*C-5*), 118.0 (*C-9*), 100.2 (*C-4a*), 87.6 (d,  $^3J_{\text{CP}} = 7.9$  Hz, *C-4'*), 84.9 (*C-1'*), 72.3 (*C-3'*), 70.2 (d,  $^2J_{\text{CP}} = 5.4$  Hz, *C-5''*), 69.9 (d,  $^2J_{\text{CP}} = 6.3$  Hz, *C-5'*), 66.9 (*C-k*), 41.9 (*C-2'*), 35.0 (*C-b*), 33.1, 33.0 (*C-h*, *C-s*), 31.2 (d,  $^3J_{\text{CP}} = 7.2$  Hz, *C-l*), 30.7, 30.7, 30.6, 30.6, 30.5, 30.4, 30.4, 30.3, 30.2 (*C-d-g*, *C-n-r*), 26.5 (*C-m*), 26.0 (*C-c*), 23.7, 23.7 (*C-i*, *C-t*), 14.5, 14.4 (*C-j*, *C-u*).

$^{31}\text{P-NMR}$  (162 MHz, MeOD):  $\delta$  [ppm] = -11.29 (d,  $^2J_{\text{PP}} = 19.4$  Hz, *P- $\alpha$* ), -13.02 (dd,  $^2J_{\text{PP}} = 16.2, 2.5$  Hz, *P- $\gamma$* ), -23.68 – -23.98 (m, *P- $\beta$* ).

MALDI-MS:  $m/z$  calcd: 929.8988 [ $\text{M-H}$ ]<sup>-</sup>, found: 929.710.

### $\gamma$ -C11-IdATP **121**



The reaction was carried out with the general procedure VIII with the pyrophosphate of **119** (313 mg, 500  $\mu\text{mol}$ ), TFAA (348  $\mu\text{L}$ , 2.50 mmol), and  $\text{Et}_3\text{N}$  (558  $\mu\text{L}$ , 4.00 mmol) in  $\text{CH}_3\text{CN}$  (10 ml). The subsequent activation step was performed with  $\text{Et}_3\text{N}$  (349  $\mu\text{L}$ ,

2.50 mmol) and 1-methylimidazole (100  $\mu$ L, 1.25 mmol) in  $\text{CH}_3\text{CN}$  (10 ml) followed by the coupling with monophosphate **91** (1.3 TEAH, 147 mg, 250  $\mu$ mol) solved in DMF (2.5 mL). Deprotection was carried out with 10% aq. tetrabutylammonium hydroxide (13.0 mL, 5.00 mmol). Purification on  $\text{RP}_{18}$  silica gel with automated flash chromatography ( $\text{H}_2\text{O}/\text{CH}_3\text{CN}$ ; 100:0 to 0:100), Dowex ion-exchange ( $\text{NH}_4^+$ ) and  $\text{RP}_{18}$  silica gel with automated flash chromatography ( $\text{H}_2\text{O}/\text{CH}_3\text{CN}$ ; 100:0 to 0:100) as well as subsequent freeze-drying provided **121** (92 mg, 45%) as colorless cotton.

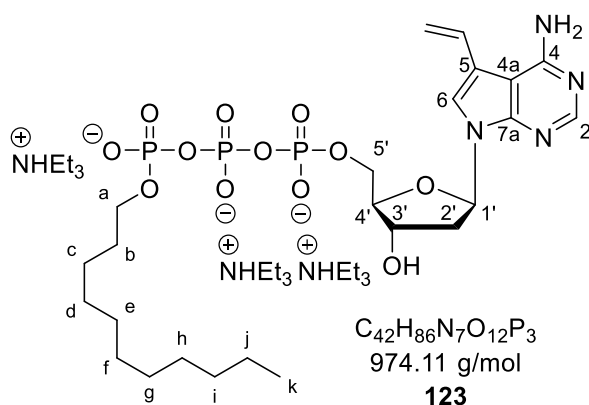
$^1\text{H-NMR}$  (400 MHz,  $\text{D}_2\text{O}$ ):  $\delta$  [ppm] = 8.30 (s, 1H, *H*-2), 7.72 (s, 1H, *H*-6), 6.53 (t,  $^3J_{\text{HH}} = 6.6$  Hz, 1H, *H*-1'), 4.72 – 4.58 (m, 1H, *H*-3'), 4.32 – 4.14 (m, 3H, *H*-4', *H*-a), 4.05 – 3.88 (m, 2H, *H*-5'), 2.56 – 2.34 (m, 2H, *H*-2'), 1.70 – 1.50 (m, 2H, *H*-b), 1.38 – 1.15 (m, 5H), 1.12 – 0.85 (m, 13H), 0.62 (t,  $^3J_{\text{HH}} = 7.0$  Hz, 3H, *H*-k).

$^{13}\text{C-NMR}$  (101 MHz,  $\text{D}_2\text{O}$ ):  $\delta$  [ppm] = 152.0, 147.3, 139.9, 129.4, 102.7, 85.7 (d,  $^3J_{\text{CP}} = 8.8$  Hz), 85.6, 83.9, 71.0, 66.7 (d,  $^2J_{\text{CP}} = 6.6$  Hz), 66.7, 61.2, 53.1, 39.9, 31.6, 31.2, 30.3, 30.2, 29.3, 29.1, 29.0, 28.9, 28.6, 25.4, 22.3, 13.8 (low intensity spectra, not all signals included).

$^{31}\text{P-NMR}$  (162 MHz,  $\text{D}_2\text{O}$ ):  $\delta$  [ppm] = -10.52 – -11.01 (m), -11.28 (d,  $^2J_{\text{PP}} = 18.1$  Hz, *P*- $\gamma$ ), -22.67 (t,  $^2J_{\text{PP}} = 18.0$  Hz, *P*- $\beta$ ).

MALDI-MS:  $m/z$  calcd: 769.0671 [ $\text{M-H}$ ] $^-$ , found: 768.900.

### $\gamma$ -C11-VdATP **123**



The reaction was carried out according to the general procedure VII with  $\gamma$ -C11-IdATP **121** (4  $\text{NH}_4^+$ , 23 mg, 28  $\mu$ mol),  $\text{Pd}_2(\text{dba})_3$  (2.6 mg, 2.8  $\mu$ mol, 10 mol%), tri(2-furyl) phosphine (1.6 mg, 6.7  $\mu$ mol, 24 mol%) and tributyl(vinyl) tin (9.0  $\mu$ L, 31 mmol) in DMF/water 1:1 v/v (3 mL) for 5 h at 40  $^\circ\text{C}$ . Purification on  $\text{RP}_{18}$  silica gel with automated

flash chromatography (0.05 M TEAB/CH<sub>3</sub>CN; 100:0 to 0:100) provided the TEAH salt of **123** (19 mg, 70%) as a colorless solid.

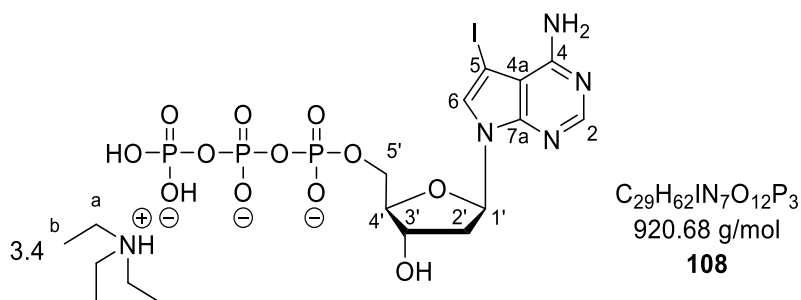
<sup>1</sup>H-NMR (600 MHz, D<sub>2</sub>O):  $\delta$  [ppm] = 8.18 (s, 1H, *H*-2), 7.63 (s, 1H, *H*-6), 6.70 (dd, <sup>3</sup>*J*<sub>HH</sub> = 17.3, 11.1 Hz, 1H, *H*-8), 6.53 – 6.41 (m, 1H, *H*-1'), 5.67 (d, <sup>3</sup>*J*<sub>HH</sub> = 17.4 Hz, 1H, *trans*-*H*-9), 5.35 (d, <sup>3</sup>*J*<sub>HH</sub> = 11.1 Hz, 1H, *cis*-*H*-9), 4.66 – 4.55 (m, 1H, *H*-3'), 4.28 – 4.22 (m, 1H, *H*-4'), 4.22 – 4.15 (m, 2H, *H*-5'), 3.93 – 3.86 (m, 2H, *H*-a), 2.46 – 2.33 (m, 2H, *H*-2'), 1.50 – 1.42 (m, 2H, *H*-b), 1.15 – 1.05 (m, 2H, *H*-c), 1.03 – 0.75 (m, 14H, *H*-d-j), 0.58 (t, <sup>3</sup>*J*<sub>HH</sub> = 7.2 Hz, 3H, *H*-k).

<sup>13</sup>C-NMR (151 MHz, D<sub>2</sub>O):  $\delta$  [ppm] = 150.9 (*C*-4), 146.7 (*C*-2), 142.8 (*C*-7a), 125.8 (*C*-8), 121.0 (*C*-6), 118.1 (*C*-5), 117.8 (*C*-9), 99.4 (*C*-4a), 85.54 (d, <sup>3</sup>*J*<sub>CP</sub> = 7.9 Hz, *C*-4'), 83.6 (*C*-1'), 70.9 (*C*-3'), 66.7 (d, <sup>2</sup>*J*<sub>CP</sub> = 6.2 Hz, *C*-5'), 65.6 (d, <sup>2</sup>*J*<sub>CP</sub> = 4.2 Hz, *C*-a), 40.0 (*C*-2'), 31.4 (*C*-i), 30.1 (d, <sup>3</sup>*J*<sub>CP</sub> = 7.3 Hz, *C*-b), 29.2, 2x 29.1, 28.9, 28.8 (*C*-d-h), 25.3 (*C*-c), 22.2 (*C*-j), 13.6 (*C*-k).

<sup>31</sup>P-NMR (243 MHz, D<sub>2</sub>O):  $\delta$  [ppm] = -10.77 (d, <sup>2</sup>*J*<sub>PP</sub> = 18.4 Hz, *P*- $\alpha$ ), -11.21 (d, <sup>2</sup>*J*<sub>PP</sub> = 18.2 Hz, *P*- $\gamma$ ), -22.80 (t, <sup>2</sup>*J*<sub>PP</sub> = 17.9 Hz, *P*- $\beta$ ).

MALDI-MS: *m/z* calcd: 671.2012 [M+H]<sup>+</sup>, found: 671.202.

### 7-Deaza-7-iodo-2'-deoxyadenosine triphosphate **108**



The reaction was carried out according to the general procedure IV with IdA **62** (301 mg, 0.80 mmol) and POCl<sub>3</sub> (90  $\mu$ L, 0.96 mmol) in triethyl phosphate (10 mL) at -20 °C in an overnight reaction followed by the addition of tributyl ammonium pyrophosphate (1.10 g, 2.00 mmol) and tributylamine (1.14 mL, 4.80 mmol) in CH<sub>3</sub>CN (4 mL). The reaction mixture was stirred for 2 h at -15 °C. Purification by ion-exchange chromatography through a DEAE-Sephadex<sup>®</sup> A-25 column (0-1 M TEAB) provided the TEAH salt of **108** (634 mg, 87%) as a colorless solid.

<sup>1</sup>H-NMR (400 MHz, D<sub>2</sub>O):  $\delta$  [ppm] = 8.01 (s, 1H, *H*-2), 7.59 (s, 1H, *H*-6), 6.46 (dd, <sup>3</sup>*J*<sub>HH</sub> = 7.8, 6.2 Hz, 1H, *H*-1'), 4.64 – 4.59 (m, 1H, *H*-3'), 4.16 – 4.10 (m, 1H, *H*-4'), 4.09 – 3.99 (m,

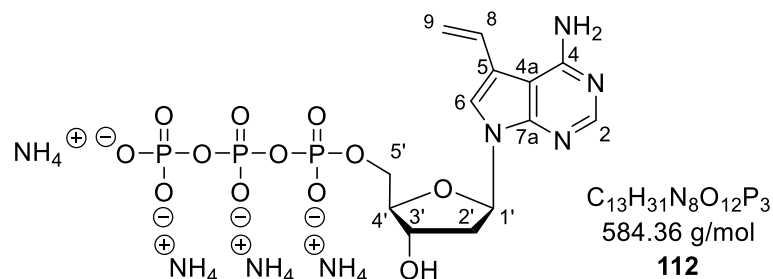
2H, *H*-5'), 3.07 (q,  $^3J_{\text{HH}} = 7.3$  Hz, 18H, *H*-a), 2.58 – 2.47 (m, 1H, *H*-2'a), 2.44 – 2.31 (m, 1H, *H*-2'b), 1.15 (t,  $^3J_{\text{HH}} = 7.3$  Hz, 28H, *H*-b).

$^{13}\text{C}$ -NMR (126 MHz,  $\text{D}_2\text{O}$ ):  $\delta$  [ppm] = 155.7 (*C*-4), 149.8 (*C*-2), 148.8 (*C*-7a), 128.0 (*C*-6), 103.7 (*C*-4a), 85.6 (d,  $^3J_{\text{CP}} = 9.1$  Hz, *C*-4'), 83.4 (*C*-1'), 71.5 (*C*-3'), 66.0 (d,  $^2J_{\text{CP}} = 5.6$  Hz, *C*-5'), 52.4 (*C*-5), 47.0 (*C*-a), 39.2 (*C*-2'), 8.6 (*C*-b).

$^{31}\text{P}$ -NMR (162 MHz,  $\text{D}_2\text{O}$ ):  $\delta$  [ppm] = -10.8 (d,  $^2J_{\text{PP}} = 19.8$  Hz, *P*- $\alpha$ ), -11.4 (d,  $^2J_{\text{PP}} = 20.0$  Hz, *P*- $\gamma$ ), -23.3 (t,  $^2J_{\text{PP}} = 19.9$  Hz, *P*- $\beta$ ).

MALDI-MS: *m/z* calcd: 614.8949 [*M*-H] $^-$ , found: 614.663.

### 7-Deaza-7-vinyl-2'-deoxyadenosine triphosphate **112**



The reaction was carried out according to the general procedure VII with IdATP **108** (3.4 TEAH, 58 mg, 60  $\mu\text{mol}$ ),  $\text{Pd}_2(\text{dba})_3$  (5.5 mg, 6.0  $\mu\text{mol}$ , 10 mol%), tri(2-furyl) phosphine (3.3 mg, 14  $\mu\text{mol}$ , 24 mol%) and tributyl(vinyl) tin (19  $\mu\text{L}$ , 66 mmol) in DMF/water 1:1 v/v (3 mL) for 5 h at 40  $^\circ\text{C}$ . Purification on RP $_{18}$  silica gel with automated flash chromatography (100%  $\text{H}_2\text{O}$ ) provided the TEAH salt of **112**. Ion-exchange to ammonium resulted in the  $\text{NH}_4^+$  salt (19 mg, 54%) as a colorless solid.

$^1\text{H}$ -NMR (500 MHz,  $\text{D}_2\text{O}$ ):  $\delta$  [ppm] = 8.23 (s, 1H, *H*-2), 7.74 (s, 1H, *H*-6), 6.83 (dd,  $^3J_{\text{HH}} = 17.4$ , 11.1 Hz, 1H, *H*-8), 6.63 (t,  $^3J_{\text{HH}} = 6.9$  Hz, 1H, *H*-1'), 5.75 (dd,  $^3J_{\text{HH}} = 17.4$ ,  $^2J_{\text{HH}} = 1.1$  Hz, 1H, *trans*-*H*-9), 5.42 (dd,  $^3J_{\text{HH}} = 11.0$ ,  $^2J_{\text{HH}} = 1.1$  Hz, 1H, *cis*-*H*-9), 4.78 – 4.75 (m, 1H, *H*-3'), 4.32 – 4.24 (m, 3H, *H*-4', *H*-5'), 2.69 – 2.60 (m, 1H, *H*-2'a), 2.53 – 2.44 (m, 1H, *H*-2'b).

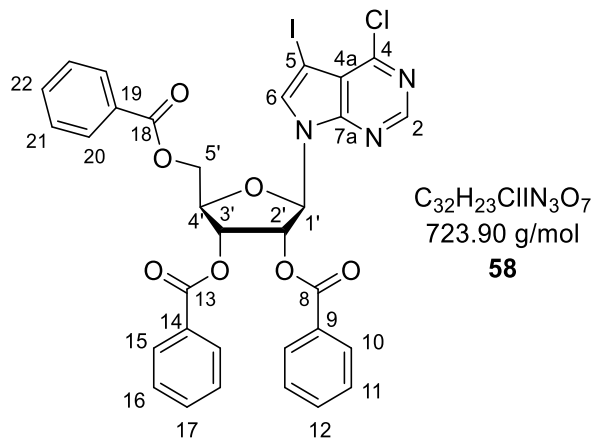
$^{13}\text{C}$ -NMR (126 MHz,  $\text{D}_2\text{O}$ ):  $\delta$  [ppm] = 151.7 (*C*-4), 147.4 (*C*-2), 144.3 (*C*-7a), 126.3 (*C*-8), 121.0 (*C*-6), 118.1 (*C*-5), 117.8 (*C*-9), 99.9, 85.7 (d,  $^3J_{\text{CP}} = 8.7$  Hz, *C*-4'), 83.7 (*C*-1'), 71.4 (*C*-3'), 66.1 (d,  $^2J_{\text{CP}} = 5.3$  Hz, *C*-5'), 40.0 (*C*-2').

$^{31}\text{P}$ -NMR (202 MHz,  $\text{D}_2\text{O}$ ):  $\delta$  [ppm] = -9.5 (d,  $^2J_{\text{PP}} = 19.3$  Hz, *P*- $\alpha$ ), -10.0 (d,  $^2J_{\text{PP}} = 19.9$  Hz, *P*- $\gamma$ ), -21.9 (t,  $^2J_{\text{PP}} = 19.7$  Hz, *P*- $\beta$ ).

MALDI-MS: *m/z* calcd: 515.0140 [*M*-H] $^-$ , found: 515.040.

### 6.3.3 7-Deaza-7-vinyladenosine series

#### 1'-(4-Chloro-5-iodo-7*H*-pyrrolo[2,3-*d*]pyrimidine)- $\beta$ -D-ribofuranose-2',3',4'-tri-*O*-benzoate **58**



4-Chloro-5-iodo-7*H*-pyrrolo[2,3-*d*]pyrimidine (1.96 g, 7.00 mmol) was suspended in  $CH_3CN$  (100 mL) followed by the addition of BSA (1.94 mL, 7.70 mmol) at 0 °C to form a solution. The reaction mixture was stirred for 15 min at room temperature, followed by the addition of 1-*O*-acetyl-2,3,5-*tri-O*-benzoyl- $\beta$ -D-ribofuranose (3.89 g, 7.70 mmol). Subsequently trimethylsilyl trifluoromethanesulfonate (1.40 mL, 7.70 mmol) was added dropwise over 10 min. Then, the reaction mixture was slowly heated to 80 °C and stirred for 1.5 h. The reaction mixture was cooled to room temperature and diluted with ethyl acetate (200 mL). The organic phase was sequentially washed with sat. aq.  $NaHCO_3$  and brine, dried over  $Na_2SO_4$  and concentrated under reduced pressure. The crude product was purified on silica gel (petroleum ether/ethyl acetate; 8:2) to yield **58** (2.70 mg, 53%) as a yellow foam.  $R_f$ -value: 0.58 (petroleum ether/ethyl acetate; 4:6).

$^1H$ -NMR (500 MHz,  $CDCl_3$ ):  $\delta$  [ppm] = 8.85 (s, 1H, *H*-2), 8.15 – 8.08, 8.02 – 7.98, 7.95 – 7.89 (3x m, 3x 2H, 2x *H*-10, 2x *H*-15, 2x *H*-20), 7.64 – 7.52 (m, 4H, *H*-6, *H*-12, *H*-17, *H*-22), 7.52 – 7.49, 7.42 – 7.39, 7.39 – 7.34 (3xm, 3x 2H, 2x *H*-11, 2x *H*-16, 2x *H*-20), 6.67 (d,  $^3J_{HH}$  = 5.4 Hz, 1H, *H*-1'), 6.15 (t,  $^3J_{HH}$  = 5.6 Hz, 1H, *H*-2'), 6.11 (dd,  $^3J_{HH}$  = 5.8, 4.4 Hz, 1H, *H*-3'), 4.90 (dd,  $^2J_{HH}$  = 12.2,  $^3J_{HH}$  = 3.1 Hz, 1H, *H*-5'a), 4.80 (m, 1H, *H*-4'), 4.69 (dd,  $^2J_{HH}$  = 12.3,  $^3J_{HH}$  = 3.7 Hz, 1H, *H*-5'b).

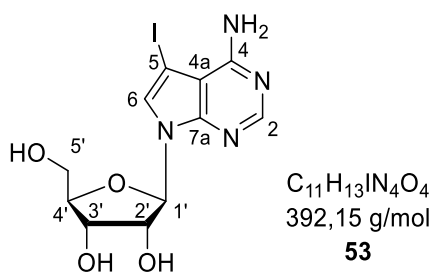
$^{13}C$ -NMR (126 MHz,  $CDCl_3$ ):  $\delta$  [ppm] = 166.2, 165.5, 165.2 (*C*-8, *C*-13, *C*-18), 153.3 (*C*-4), 151.4 (*C*-2), 151.1 (*C*-7a), 133.9, 133.9, 133.7 (*C*-12, *C*-17, *C*-22), 132.2 (*C*-6), 130.0, 130.0, 129.8 (2x *C*-10, 2x *C*-15, 2x *C*-20), **129.4, 128.8, 128.5** (*C*-9, *C*-14, *C*-19), **129.0, 128.7**,

**128.7** (2x C-11, 2x C-16, 2x C-22), 117.9 (C-4a), 86.9 (C-1'), 80.8 (C-4'), 74.3 (C-2'), 71.6 (C-3'), 63.6 (C-5'), 53.8 (C-5).

IR:  $\nu$  [ $\text{cm}^{-1}$ ] = 1722, 1576, 1538, 1449, 1315, 1260, 1207, 1177, 1119, 1091, 1068, 1025, 950, 905, 728, 705, 686, 647, 598.

HRMS (ESI<sup>+</sup>):  $m/z$  calcd: 724.0347 [M+H]<sup>+</sup>, found: 724.0342.

### 7-Deaza-7-iodoadenosine **53**



The reaction was carried out according to the literature with modifications. Compound **58** (2.32 g, 3.21 mmol) was dissolved in 1,4-dioxane (20 mL) and 25% NH<sub>4</sub>OH (40 mL) and placed in an autoclave. The reaction mixture was heated overnight at 120 °C. After cooling to room temperature, all volatiles were removed under reduced pressure, and the crude product was recrystallized from CH<sub>3</sub>OH to provide **53** (911 mg, 72%) as a colorless solid.

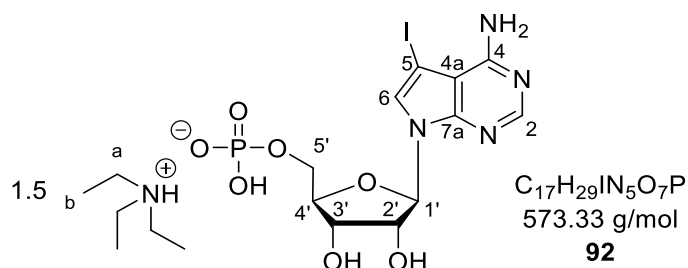
The analytical data was in accordance with those described.<sup>135</sup>

<sup>1</sup>H-NMR (400 MHz, DMSO-*d*<sub>6</sub>):  $\delta$  [ppm] = 8.10 (s, 1H, H-2), 7.67 (s, 1H, H-6), 6.67 (s, 2H, NH<sub>2</sub>), 6.03 (d, <sup>3</sup>J<sub>HH</sub> = 6.2 Hz, 1H, H-1'), 5.31 (d, <sup>3</sup>J<sub>HH</sub> = 6.3 Hz, 1H, 2'-OH), 5.15 (m, 1H, 5'-OH), 5.11 (d, <sup>3</sup>J<sub>HH</sub> = 4.6 Hz, 1H, 3'-OH), 4.35 (m, 1H, H-2'), 4.07 (m, 1H, H-3'), 3.89 (m, 1H, H-4'), 3.61 (m, 1H, H-5'a), 3.53 (m, 1H, H-5'b).

<sup>13</sup>C-NMR (101 MHz, DMSO-*d*<sub>6</sub>):  $\delta$  [ppm] = 157.2 (C-4), 151.9 (C-2), 150.1 (C-7a), 127.1 (C-6), 103.2 (C-4a), 86.8 (C-1'), 85.2 (C-4'), 73.9 (C-2'), 70.5 (C-3'), 61.6 (C-5'), 51.8 (C-5).

IR:  $\nu$  [ $\text{cm}^{-1}$ ] = 3200, 1630, 1588, 1552, 1475, 1342, 1197, 1129, 1085, 1062, 1034, 996, 950, 912, 897, 871, 767, 706, 681, 640, 601, 587, 434, 393.

HRMS (ESI<sup>+</sup>):  $m/z$  calcd: 393.0060 [M+H]<sup>+</sup>, found: 393.0074.

**7-Deaza-7-iodoadenosine monophosphate 92**

The reaction was carried out according to the general procedure VI with IA **53** (784 mg, 2.00 mmol), water (18  $\mu$ L, 1.0 mmol), and POCl<sub>3</sub> (746  $\mu$ L, 8.00 mmol) in triethyl phosphate (75 mL) at -20 °C for 3 days. Purification on RP<sub>18</sub> silica gel using automated flash chromatography (0.05 M TEAB/CH<sub>3</sub>CN; 100:0 to 0:100) provided the TEAH salt of **92** (1.5 TEAH, 1.00 g, 80%) as a colorless solid.

<sup>1</sup>H-NMR (500 MHz, D<sub>2</sub>O):  $\delta$  [ppm] = 7.95 (s, 1H, *H*-2), 7.58 (s, 1H, *H*-6), 6.10 (dd, <sup>3</sup>*J*<sub>HH</sub> = 6.3, 1.7 Hz, 1H, *H*-1), 4.58 – 4.48 (m, 1H, *H*-2'), 4.41 – 4.33 (m, 1H, *H*-3'), 4.27 – 4.17 (m, 1H, *H*-4'), 4.02 – 3.93 (m, 2H, *H*-5'), 3.10 (q, <sup>3</sup>*J*<sub>HH</sub> = 7.3 Hz, 9H, *H*-a), 1.18 (t, <sup>3</sup>*J*<sub>HH</sub> = 7.3 Hz, 14H, *H*-b).

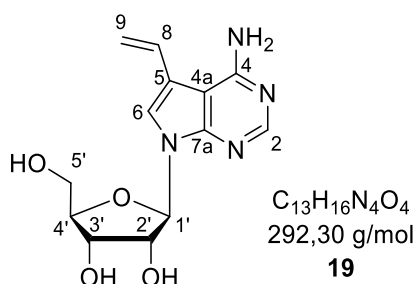
<sup>13</sup>C-NMR (126 MHz, D<sub>2</sub>O):  $\delta$  [ppm] = 156.9 (*C*-4), 149.8 (*C*-2), 149.8 (*C*-7a), 127.5 (*C*-6), 104.1 (*C*-4a), 86.4 (*C*-1'), 84.1 (d, <sup>3</sup>*J*<sub>CP</sub> = 8.5 Hz, *C*-4'), 74.4 (*C*-2'), 71.0 (*C*-3'), 64.7 (d, <sup>2</sup>*J*<sub>CP</sub> = 5.0 Hz, *C*-5'), 52.7 (*C*-5), 47.0 (*C*-a), 8.6 (*C*-b).

<sup>31</sup>P-NMR (202 MHz, D<sub>2</sub>O):  $\delta$  [ppm] = 2.97 (s).

IR:  $\nu$  [cm<sup>-1</sup>] = 3410, 3114, 2945, 2885, 1664, 1617, 1553, 1542, 1450, 1134, 1049, 951, 933, 819, 493.

HRMS (ESI<sup>+</sup>): *m/z* calcd: 470.9572 [M-H]<sup>+</sup>, found: 470.9549.



**7-Deaza-7-vinyladenosine 19**

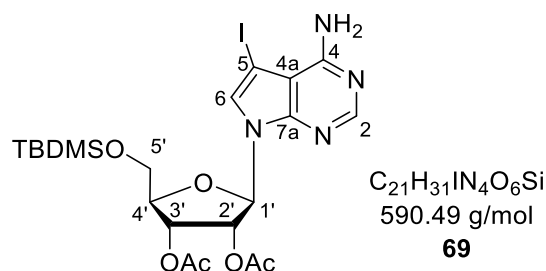
The reaction was carried out according to the general procedure V with IA **53** (118 mg, 0.30 mmol),  $Pd_2(dba)_3$  (15 mg, 16  $\mu$ mol, 5.4 mol%), tri(2-furyl) phosphine (8.4 mg, 36  $\mu$ mol, 12 mol%) and tributyl(vinyl) tin (96  $\mu$ L, 0.33 mmol) in DMF (3 mL). Purification on RP<sub>18</sub> silica gel with automated flash chromatography ( $H_2O/CH_3CN$ ; 100:0 to 0:100) provided **19** (76 mg, 87%) as a colorless solid.

$^1H$ -NMR (600 MHz,  $DMSO-d_6$ ):  $\delta$  [ppm] = 8.06 (s, 1H, *H*-2), 7.67 (s, 1H, *H*-6), 7.11 (dd,  $^3J_{HH}$  = 17.2, 10.9 Hz, 1H, *H*-8), 6.76 (s, 2H, NH), 6.04 (d,  $^3J_{HH}$  = 6.2 Hz, 1H, *H*-1'), 5.57 (dd,  $^3J_{HH}$  = 17.2 Hz,  $^2J_{HH}$  = 1.7 Hz, 1H, *trans*-*H*-9), 5.28 (d,  $^3J_{HH}$  = 6.4 Hz, 1H, 2'-OH), 5.22 (s, 1H, 5'-OH), 5.13 (dd,  $^2J_{HH}$  = 10.9 Hz,  $^3J_{HH}$  = 1.7 Hz, 1H, *cis*-*H*-9), 5.09 (d,  $^3J_{HH}$  = 4.7 Hz, 1H, 3'-OH), 4.40 (dd,  $^3J_{HH}$  = 5.8 Hz, 1H, *H*-2'), 4.09 (dd,  $^3J_{HH}$  = 4.1 Hz, 1H, *H*-3'), 3.93 – 3.86 (m, 1H, *H*-4'), 3.63 (dd,  $^2J_{HH}$  = 11.9 Hz,  $^3J_{HH}$  = 3.8 Hz, 1H, *H*-5'a), 3.54 (dd,  $^2J_{HH}$  = 11.9 Hz,  $^3J_{HH}$  = 3.9 Hz, 1H, *H*-5'a).

$^{13}C$ -NMR (151 MHz,  $DMSO-d_6$ ):  $\delta$  [ppm] = 156.2 (*C*-4), 150.1 (*C*-2), 149.6 (*C*-7a), 128.6 (*C*-8), 119.6 (*C*-6), 114.6 (*C*-4a), 113.6 (*C*-9), 100.5 (*C*-5), 87.0 (*C*-1'), 85.2 (*C*-4'), 73.8 (*C*-2'), 70.5 (*C*-3'), 61.6 (*C*-5').

IR:  $\nu$  [ $cm^{-1}$ ] = 3334 (m), 1625 (vs), 1584 (vs), 1463 (s), 1347 (m), 1287 (m), 1204 (w), 1111 (m), 1080 (s), 1039 (s), 895 (w), 798 (w), 573 (w).

HRMS (ESI<sup>+</sup>):  $m/z$  calcd: 293.1250 [ $M+H$ ]<sup>+</sup>, found: 293.1254.

**3',5'-Di-O-acetyl-5'-O-tert-butyl-dimethylsilyl-7-deaza-7-iodoadenosine 69**

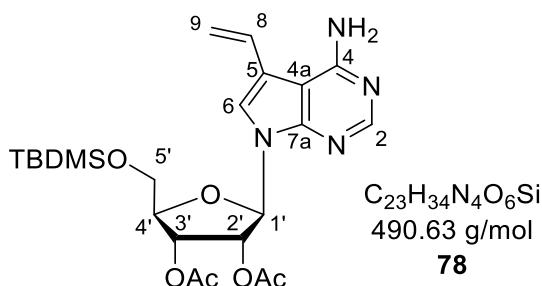
The nucleoside **53** (1.00 g, 2.55 mmol) was dried *in vacuo* and solved in pyridine (30 mL). Then, TBDMSCI (461 mg, 3.06 mmol) was added, and the resulting solution stirred overnight at room temperature. The solvent was removed under reduced pressure and the resulting residue co-evaporated twice with toluene. The residue is resuspended in CH<sub>3</sub>CN (40 mL) followed by the stepwise addition of DMAP (23 mg, 191 μmol), Et<sub>3</sub>N (933 μL, 6.73 mmol), and Ac<sub>2</sub>O (579 μL, 6.12 mmol). The resulting solution was stirred for 1 h at room temperature. Upon completion, methanol was added to the reaction mixture, and stirring was continued for 10 min. All volatiles were removed under reduced pressure, and the resulting residue was dissolved in H<sub>2</sub>O/ ethyl acetate. The organic layer was washed with H<sub>2</sub>O and brine once and was dried over Na<sub>2</sub>SO<sub>4</sub>. The solvent was removed under reduced pressure, and the crude product was purified with automated flash chromatography (petroleum ether/ethyl acetate; 7:3) to yield **69** (1.38 g, 91%) as a light-yellow foam. *R<sub>f</sub>*-value: 0.20 (petroleum ether/ ethyl acetate; 6:4).

<sup>1</sup>H-NMR (400 MHz, DMSO-*d*<sub>6</sub>) δ [ppm] = 8.12 (s, 1H, *H*-2), 7.57 (s, 1H, *H*-6), 6.74 (s, 2H, NH<sub>2</sub>), 6.35 (d, <sup>3</sup>*J*<sub>HH</sub> = 7.1 Hz, 1H, *H*-1'), 5.63 (dd, <sup>3</sup>*J*<sub>HH</sub> = 7.1, 5.3 Hz, 1H, *H*-2'), 5.41 (dd, <sup>3</sup>*J*<sub>HH</sub> = 5.3, 2.3 Hz, 1H, *H*-3'), 4.30 – 4.14 (m, 1H, *H*-4'), 3.94 – 3.78 (m, 2H, *H*-5'), 2.13 (s, 3H, Ac-CH<sub>3</sub>), 1.96 (s, 3H, Ac-CH<sub>3</sub>), 0.93 (s, 9H, *t*Bu-C(CH<sub>3</sub>)<sub>3</sub>), 0.13 (s, 3H, Si-CH<sub>3</sub>), 0.12 (s, 3H, Si-CH<sub>3</sub>).

<sup>13</sup>C-NMR (101 MHz, DMSO): δ [ppm] = 169.6 (Ac-CO), 169.2 (Ac-CO), 157.3 (C-4), 152.4 (C-2), 150.4 (C-7a), 125.5 (C-6), 103.1 (C-4a), 83.4 (C-1'), 82.6 (C-4'), 73.1 (C-2'), 71.2 (C-3'), 63.0 (C-5'), 53.5 (C-5), 25.8 (*t*Bu-CH<sub>3</sub>), 20.5 (Ac-CH<sub>3</sub>), 20.1 (Ac-CH<sub>3</sub>), 18.0 (*t*Bu-C(CH<sub>3</sub>)<sub>3</sub>), -5.5 (Si-CH<sub>3</sub>), -5.6 (Si-CH<sub>3</sub>).

IR:  $\nu$  [cm<sup>-1</sup>] = 2953, 2929, 2857, 1746, 1618, 1578, 1556, 1464, 1441, 1237, 1212, 1089, 830, 778, 598.

HRMS (ESI<sup>+</sup>): *m/z* calcd: 591.1136 [M+H]<sup>+</sup>, found: 591.1137.

**3',5'-Di-O-acetyl-5'-O-tert-butyldimethylsilyl-7-deaza-7-vinyladenosine 78**

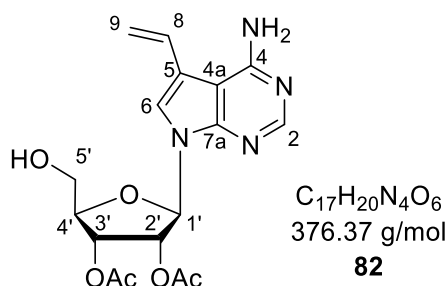
The protected nucleoside **69** (1.00 g, 1.70 mmol),  $Pd_2(dba)_3$  (84 mg, 92  $\mu$ mol, 5.4 mol%) and tri(2-furyl) phosphine (47 mg, 0.20 mmol, 12 mol%) were dried *in vacuo* and solved in DMF (10 mL). After the addition of tributyl(vinyl) tin (547  $\mu$ L, 1.87 mmol) the reaction was stirred for 2 h at 60 °C. The reaction was monitored by TLC (petroleum ether/ethyl acetate; 4:6) and after complete conversion of starting material, the solvent was removed under reduced pressure. The crude product was purified on silica gel (petroleum ether/ethyl acetate; 3:7 to 2:8) affording **78** (765 mg, 92%) as a light-yellow foam.  $R_f$ -value: 0.15 (petroleum ether/ethyl acetate; 4:6)

$^1H$ -NMR (500 MHz,  $CDCl_3$ ):  $\delta$  [ppm] = 8.30 (s, 1H, *H*-2), 7.37 (s, 1H, *H*-6), 6.83 (dd,  $^3J_{HH}$  = 17.4, 11.0 Hz, 1H, *H*-8), 6.61 (d,  $^3J_{HH}$  = 7.6 Hz, 1H, *H*-1'), 5.63 (dd,  $^3J_{HH}$  = 7.6, 5.3 Hz, 1H, *H*-2'), 5.53 (dd,  $^3J_{HH}$  = 17.5 Hz,  $^2J_{HH}$  = 1.5 Hz, 1H, *trans*-*H*-9), 5.50 (s, 2H,  $NH_2$ ), 5.48 (dd,  $^3J_{HH}$  = 5.2, 1.9 Hz, 1H, *H*-3'), 5.35 (dd,  $^3J_{HH}$  = 11.0,  $^2J_{HH}$  = 1.4 Hz, 1H, *cis*-*H*-9), 4.30 – 4.19 (m, 1H, *H*-4'), 3.96 – 3.79 (m, 2H, *H*-5'), 2.14 (s, 3H, Ac- $CH_3$ ), 1.99 (s, 3H, Ac- $CH_3$ ), 0.97 (s, 9H, *t*Bu- $C(CH_3)_3$ ), 0.16 (s, 3H, Si- $CH_3$ ), 0.15 (s, 3H, Si- $CH_3$ ).

$^{13}C$ -NMR (126 MHz,  $CDCl_3$ ):  $\delta$  [ppm] = 170.2 ( $CH_3$ -CO), 169.7 ( $CH_3$ -CO), 157.1 (*C*-4), 2x 151.9 (*C*-2, *C*-7a), 129.1 (*C*-8), 119.5 (*C*-6), 117.1 (*C*-9), 116.1 (*C*-4a), 101.8 (*C*-5), 83.7, 83.6 (*C*-4', *C*-1'), 73.8 (*C*-2'), 72.3 (*C*-3'), 63.5 (*C*-5'), 26.1 (*t*Bu- $CH_3$ ), 20.9 (Ac- $CH_3$ ), 20.6 (Ac- $CH_3$ ), 18.5 (*t*Bu- $C(CH_3)_3$ ), -5.3 (Si- $CH_3$ ), -5.4 (Si- $CH_3$ ).

IR:  $\nu$  [ $cm^{-1}$ ] = 3372, 3129, 2954, 2929, 2857, 1746, 1621, 1576, 1461, 1238, 1210, 1088, 830, 777, 570.

HRMS (ESI<sup>+</sup>):  $m/z$  calcd: 491.2326 [ $M+H$ ]<sup>+</sup>, found: 491.2326.

**3',5'-Di-O-acetyl-7-deaza-7-vinyladenosine **82****

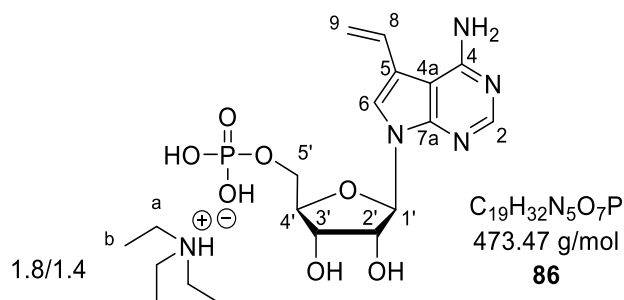
The nucleoside **78** (707 mg, 1.44 mmol) was solved in 40 mL THF followed by the addition of TreatHF (939  $\mu$ L, 5.76 mmol). After stirring overnight at room temperature, all volatiles were removed under reduced pressure, and the residue was purified on silica gel ( $CH_2Cl_2/CH_3OH$ ; 19: 1) to yield **82** (489 mg, 90%) as a colorless foam.  $R_f$ -value: 0.27 ( $CH_2Cl_2/CH_3OH$ ; 19:1).

$^1H$ -NMR (400 MHz,  $DMSO-d_6$ )  $\delta$  [ppm] = 8.07 (s, 1H, *H*-2), 7.73 (s, 1H, *H*-6), 7.11 (dd,  $^3J_{HH}$  = 17.2, 10.9 Hz, 1H, *H*-8), 6.83 (s, 2H,  $NH_2$ ), 6.33 (d,  $^3J_{HH}$  = 7.4 Hz, 1H, *H*-1'), 5.73 (dd,  $^3J_{HH}$  = 13.4, 6.0 Hz, 1H, *H*-2'), 5.61 – 5.51 (m, 2H, *trans*-*H*-9, *OH*), 5.45 (dd,  $^3J_{HH}$  = 5.5, 2.3 Hz, 1H, *H*-3'), 5.16 (dd,  $^3J_{HH}$  = 10.8,  $^2J_{HH}$  = 1.7 Hz, 1H, *cis*-*H*-9), 4.21 – 4.13 (m, 1H, *H*-4'), 3.77 – 3.58 (m, 2H, *H*-5'), 2.14 (s, 3H, Ac- $CH_3$ ), 1.96 (s, 3H, Ac- $CH_3$ ).

$^{13}C$ -NMR (101 MHz,  $DMSO$ ):  $\delta$  [ppm] = 169.6 (Ac-CO), 169.3 (Ac-CO), 157.7 (*C*-4), 151.8 (*C*-2), 150.9 (*C*-7a), 128.8 (*C*-8), 118.5 (*C*-6), 114.9 (*C*-9), 113.7 (*C*-4a), 100.8 (*C*-5), 84.0 (*C*-1'), 83.1 (*C*-4'), 72.6 (*C*-2'), 71.3 (*C*-3'), 61.2 (*C*-5'), 20.5 (Ac- $CH_3$ ), 20.2 (Ac- $CH_3$ ).

IR:  $\nu$  [ $cm^{-1}$ ] = 3477, 3357, 3124, 2987, 2931, 1741, 1623, 1574, 1532, 1462, 1428, 1370, 1238, 1209, 1078, 1042, 902, 800, 571.

HRMS (ESI<sup>+</sup>):  $m/z$  calcd: 377.1461 [ $M+H$ ]<sup>+</sup>, found: 377.1482.

**7-Deaza-7-vinyladenosine monophosphate 86**

**STILLE-coupling:** The reaction was carried out according to the general procedure VI with IAMP **92** (1.5 TEAH, 250 mg, 0.40 mmol), Pd<sub>2</sub>(dba)<sub>3</sub> (20 mg, 22 μmol, 5.4 mol%), tri(2-furyl) phosphine (11 mg, 48 μmol, 12 mol%) and tributyl(vinyl) tin (129 μL, 0.14 mmol) in DMF (6 mL) for 2 h. Purification on RP<sub>18</sub> silica gel with automated flash chromatography (1. RP<sub>18</sub> flash chromatography: 0.05 M TEAB/CH<sub>3</sub>CN; 100:0 to 0:100, 2. RP<sub>18</sub> flash chromatography: H<sub>2</sub>O/CH<sub>3</sub>CN; 100:0 to 0:100) provided the TEAH salt of **86** (1.8 TEAH, 202 mg, 91%) as a light-yellow solid.

**Fm-route:** The reaction was carried out according to the general procedure I with protected 7-deaza-7-vinyladenosine **82** (395 mg, 1.05 mmol) in CH<sub>3</sub>CN (15 mL), bis(fluorenylmethyl)phosphoramidite (986 mg, 1.89 mmol) in CH<sub>2</sub>Cl<sub>2</sub> (2 mL), and 0.25 M DCl in CH<sub>3</sub>CN (7.56 mL, 1.89 mmol). The reaction was stirred for 15 min, followed by the addition of a 5.5 M *t*-BuOOH in decane solution (382 μL, 2.10 mmol). Deprotection was carried out in H<sub>2</sub>O/MeOH/Et<sub>3</sub>N (1:1:1 v/v/v) overnight, after prepurification of the intermediate on silica gel (CH<sub>2</sub>Cl<sub>2</sub>/CH<sub>3</sub>OH; 39:1). The product was purified on RP<sub>18</sub> silica gel using automated flash chromatography (H<sub>2</sub>O/CH<sub>3</sub>CN; 100:0 to 0:100) to provide the monophosphate **86** (1.4 TEAH, 433 mg, 80%) as triethylammonium salt.

<sup>1</sup>H-NMR (400 MHz, D<sub>2</sub>O): δ [ppm] = 8.05 (s, 1H, *H*-2), 7.61 (s, 1H, *H*-6), 6.79 (ddd, <sup>2</sup>*J*<sub>HH</sub> = 17.5, <sup>3</sup>*J*<sub>HH</sub> = 11.0, 1.0 Hz, 1H, *H*-8), 6.20 (d, <sup>3</sup>*J*<sub>HH</sub> = 6.4 Hz, 1H, *H*-1'), 5.64 (dd, <sup>2</sup>*J*<sub>HH</sub> = 17.5 Hz, <sup>3</sup>*J*<sub>HH</sub> = 1.3 Hz, 1H, *trans*-*H*-9), 5.33 (dd, <sup>3</sup>*J*<sub>HH</sub> = 11.0 Hz, <sup>3</sup>*J*<sub>HH</sub> = 1.3 Hz, 1H, *cis*-9-*H*), 4.64 (dd, <sup>3</sup>*J*<sub>HH</sub> = 6.4, 5.3 Hz, 1H, *H*-2'), 4.46 (dd, <sup>3</sup>*J*<sub>HH</sub> = 5.3, 3.2 Hz, 1H, *H*-3'), 4.40 – 4.27 (m, 1H, *H*-4'), 4.05 (dd, <sup>3</sup>*J*<sub>HH</sub> = 5.1, 3.5 Hz, 2H, *H*-5'), 3.17 (q, <sup>3</sup>*J*<sub>HH</sub> = 7.3 Hz, 8H, *H*-a), 1.26 (t, <sup>3</sup>*J*<sub>HH</sub> = 7.3 Hz, 12H, *H*-b).

<sup>13</sup>C-NMR (101 MHz, D<sub>2</sub>O): δ [ppm] = 156.2 (*C*-4), 149.9 (*C*-2), 149.7 (*C*-7a), 127.3 (*C*-8), 119.3 (*C*-6), 116.7 (*C*-4a), 116.4 (*C*-9), 100.8 (*C*-5), 85.9 (*C*-1'), 83.7 (d, <sup>3</sup>*J*<sub>CP</sub> = 8.7 Hz, *C*-4'), 73.9 (*C*-2'), 70.7 (*C*-3'), 64.2 (d, <sup>2</sup>*J*<sub>CP</sub> = 4.4 Hz, *C*-5'), 46.6 (*C*-a), 8.2 (*C*-b).

<sup>31</sup>P-NMR (162 MHz, DMSO-*d*6): δ [ppm] = 1.26 (s).





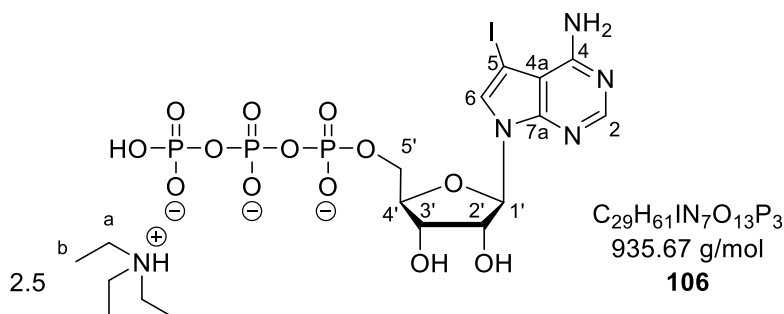
4.34 – 4.28 (m, 1H, *H*-5'b), 4.28 – 4.24 (m, 1H, *H*-4'), 4.22 – 4.13 (m, 2H, *H*-o), 2.62 – 2.55 (m, 2H, *H*-b), 1.79 – 1.69 (m, 2H, *H*-c), 1.70 – 1.61 (m, 2H, *H*-p), 1.49 – 1.23 (m, 22H, *H*-d-k, *H*-q), 0.95 – 0.88 (m, 6H, *H*-n, *H*-r).

$^{13}\text{C}$ -NMR (151 MHz, MeOD):  $\delta$  [ppm] = 173.7 (*C*-a), 152.3 (*C*-4), 152.3 (*C*-1''), 149.1 (*C*-2), 144.2 (*C*-7a), 135.1 (d,  $^3J_{\text{CP}} = 7.0$  Hz, *C*-4''), 130.3 (d,  $^4J_{\text{CP}} = 4.6$  Hz, 2x *C*-3''), 127.3 (*C*-8), 122.8 (d,  $^5J_{\text{CP}} = 2.0$  Hz, 2x *C*-2''), 122.5 (*C*-6), 118.7, 118.1 (*C*-9, 4-a), 101.4 (*C*-5), 88.7 (*C*-1'), 85.1 (d,  $^3J_{\text{CP}} = 8.1$  Hz, *C*-4'), 76.6 (*C*-2'), 71.6 (*C*-3'), 70.3 (d,  $^2J_{\text{CP}} = 5.2$  Hz, *C*-5''), 69.6 (d,  $^2J_{\text{CP}} = 6.4$  Hz, *C*-5'), 66.6 (*C*-o), 35.0 (*C*-b), 33.3 (d,  $^3J_{\text{CP}} = 7.4$  Hz, *C*-p), 33.1 (*C*-l), 30.8, 2x 30.8, 30.7, 30.6, 30.5, 30.4, 30.2 (*C*-d-k), 26.0 (*C*-c), 23.7 (*C*-m), 19.7 (*C*-q), 14.4 (*C*-n), 13.9 (*C*-r).

$^{31}\text{P}$ -NMR (243 MHz, MeOD):  $\delta$  [ppm] = -11.25 (d,  $^2J_{\text{PP}} = 18.8$  Hz, *P*- $\alpha$ ), -12.78 – -13.04 (m, *P*- $\gamma$ ), -23.61 (t,  $^2J_{\text{PP}} = 15.4$  Hz, *P*- $\beta$ ).

MALDI-MS:  $m/z$  calcd: 903.3117 [*M*-H] $^-$ , found: 903.330.

### 7-Deaza-7-iodoadenosine triphosphate 106



The reaction was carried out according to the general procedure IV with IA **53** (227 mg, 0.58 mmol), proton sponge (249 mg, 1.16 mmol), and  $\text{POCl}_3$  (108  $\mu\text{L}$ , 1.16 mmol) in triethyl phosphate (10 mL) at 0 °C for 3 h followed by the addition of tributyl ammonium pyrophosphate (796 mg, 1.45 mmol) and tributylamine (827  $\mu\text{L}$ , 3.48 mmol) in  $\text{CH}_3\text{CN}$  (2.9 mL). The reaction mixture was stirred for 45 min at 0 °C. Purification by ion-exchange chromatography through a DEAE-Sephadex<sup>®</sup> A-25 column (0-1 M TEAB) and RP<sub>18</sub> flash column chromatography ( $\text{H}_2\text{O}/\text{CH}_3\text{CN}$ ; 100:0 to 50:50) provided the TEAH salt of **106** (137 mg, 27%) as a colorless solid.

$^1\text{H}$ -NMR (400 MHz,  $\text{D}_2\text{O}$ ):  $\delta$  [ppm] = 8.24 (s, 1H, *H*-2), 7.75 (s, 1H, *H*-6), 6.11 (d,  $^3J_{\text{HH}} = 5.2$  Hz, 1H, *H*-1'), 4.51 – 4.31 (m, 4H, *H*-2', *H*-3', *H*-4', *H*-5'a), 4.31 – 4.19 (m, 1H, *H*-5'b), 3.18 (q,  $^3J_{\text{HH}} = 7.3$  Hz, 15H, *H*-a), 1.25 (t,  $^3J_{\text{HH}} = 7.3$  Hz, 23H, *H*-b).

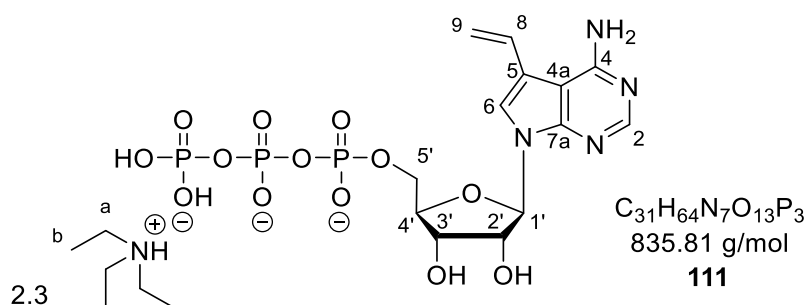


$^{13}\text{C}$ -NMR (101 MHz,  $\text{D}_2\text{O}$ ):  $\delta$  [ppm] = 151.0 (C-4), 147.3 (C-2), 144.0 (C-7a), 129.2 (C-6), 102.4 (C-4a), 86.9 (C-1'), 83.4 (d,  $^3J_{\text{CP}} = 9.2$  Hz, C-4'), 75.0 (C-2'), 70.0 (C-3'), 65.2 (d,  $^2J_{\text{CP}} = 5.8$  Hz, C-5'), 53.4 (C-5), 46.6 (C-a), 8.2 (C-b).

$^{31}\text{P}$ -NMR (162 MHz,  $\text{D}_2\text{O}$ ):  $\delta$  [ppm] = -10.69 (d,  $^2J_{\text{PP}} = 18.8$  Hz, P- $\alpha$ ), -11.34 (d,  $^2J_{\text{PP}} = 19.8$  Hz, P- $\gamma$ ), -23.10 (t,  $^2J_{\text{PP}} = 19.2$  Hz, P- $\beta$ ).

MALDI-MS:  $m/z$  calcd: 630.8899 [M-H] $^-$ , found: 630.476.

### 7-Deaza-7-vinyladenosine triphosphate **111**



The reaction was carried out according to the general procedure VII with IUTP **106** (2.5 TEAH, 20 mg, 22  $\mu\text{mol}$ ),  $\text{Pd}_2(\text{dba})_3$  (2.0 mg, 2.2  $\mu\text{mol}$ , 10 mol%), tri(2-furyl) phosphine (1.2 mg, 5.3  $\mu\text{mol}$ , 24 mol%) and tributyl(vinyl) tin (7  $\mu\text{L}$ , 24 mmol) in DMF (1 mL) for 5 h at 40  $^\circ\text{C}$ . Purification on  $\text{RP}_{18}$  silica gel with automated flash chromatography (100%  $\text{H}_2\text{O}$ ) provided the TEAH salt of **111** (11 mg, 67%) as a colorless solid.

$^1\text{H}$ -NMR (400 MHz,  $\text{D}_2\text{O}$ ):  $\delta$  [ppm] = 8.23 (s, 1H, H-2), 7.72 (s, 1H, H-6), 6.72 (dd,  $^3J_{\text{HH}} = 17.4, 11.0$  Hz, 1H, H-8), 6.17 (d,  $^3J_{\text{HH}} = 5.1$  Hz, 1H, H-1'), 5.77 (d,  $^3J_{\text{HH}} = 17.4$  Hz, 1H, trans-H-9), 5.40 (d,  $^3J_{\text{HH}} = 11.1$  Hz, 1H, cis-H-9), 4.52 – 4.43 (m, 2H, H-2', H-3'), 4.43 – 4.37 (m, 1H, H-5'a), 4.34 – 4.26 (m, 1H, H-5'b), 3.22 (q,  $^3J_{\text{HH}} = 7.3$  Hz, 14H, H-a), 1.30 (t,  $^3J_{\text{HH}} = 7.3$  Hz, 22H, H-b).

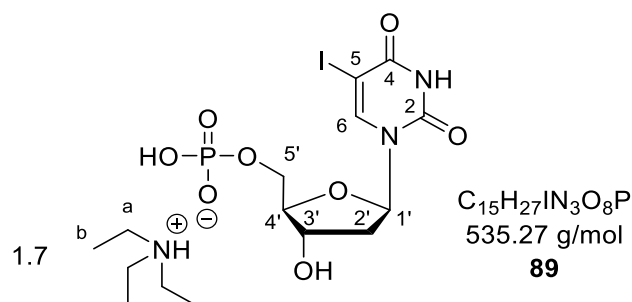
$^{13}\text{C}$ -NMR (101 MHz,  $\text{D}_2\text{O}$ ):  $\delta$  [ppm] = 153.5 (C-4), 149.8 (C-2), 145.7 (C-7a), 128.2 (C-8), 123.1 (C-6), 120.6, 120.4 (C-9, C-4a), 102.0 (C-5), 89.2 (C-1'), 86.0 (d,  $^3J_{\text{CP}} = 9.1$  Hz, C-4'), 77.5 (C-2'), 72.7 (C-3'), 67.9 (d,  $^2J_{\text{CP}} = 5.3$  Hz, C-5'), 49.2 (C-a), 10.7 (C-b).

$^{31}\text{P}$ -NMR (162 MHz,  $\text{D}_2\text{O}$ ):  $\delta$  [ppm] = -10.68 (d,  $^2J_{\text{PP}} = 19.1$  Hz, P- $\alpha$ ), -11.31 (d,  $^2J_{\text{PP}} = 19.7$  Hz, P- $\gamma$ ), -23.05 (t,  $^2J_{\text{PP}} = 19.5$  Hz, P- $\beta$ ).

MALDI-MS:  $m/z$  calcd: 531.0089 [M-H] $^-$ , found: 531.158.

### 6.3.4 5-Vinyl-2'-deoxyuridine series

#### 5-Iodo-2'-deoxyuridine monophosphate **89**



The reaction was carried out according to the general procedure II with  $POCl_3$  (1.65 mL, 17.7 mmol) in  $CH_3CN$  (3.96 mL, 75.8 mmol), pyridine (1.56 mL, 19.3 mmol),  $H_2O$  (202  $\mu$ L, 11.2 mmol), and nucleoside IdU **63** (1.42 g, 40.1 mmol) for 3 h. Purification on  $RP_{18}$  silica gel with automated flash chromatography (100%  $H_2O$ , reduced flow, then  $H_2O/CH_3CN$ ; 100:0 to 0:100) provided the ammonium salt of **89**. Ion-exchange to TEAH resulted in the TEAH salt of **89** (1.7 TEAH, 1.27 g, 52%) as a colorless solid.

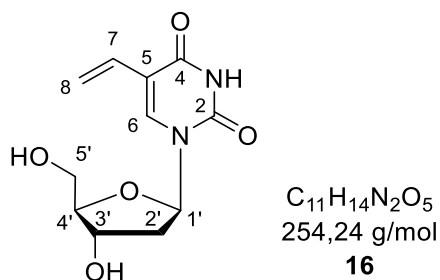
$^1H$ -NMR (400 MHz,  $DMSO-d_6$ ):  $\delta$  [ppm] = 8.27 (s, 1H,  $H-6$ ), 6.28 (t,  $^3J_{HH} = 6.9$  Hz, 1H,  $H-1'$ ), 4.62 – 4.51 (m, 1H,  $H-3'$ ), 4.24 – 4.13 (m, 1H,  $H-4'$ ), 4.04 – 3.95 (m, 2H,  $H-5'$ ), 3.22 (q,  $^3J_{HH} = 7.3$  Hz, 12H,  $H-a$ ), 2.44 – 2.33 (m, 2H,  $H-2'$ ), 1.30 (t,  $^3J_{HH} = 7.3$  Hz, 18H,  $H-b$ ).

$^{13}C$ -NMR (101 MHz,  $DMSO-d_6$ ):  $\delta$  [ppm] = 163.4 ( $C-4$ ), 151.6 ( $C-2$ ), 146.3 ( $C-6$ ), 86.0 (d,  $^3J_{CP} = 8.4$  Hz,  $C-4'$ ), 85.5 ( $C-1'$ ), 71.1 ( $C-3'$ ), 68.3 ( $C-5$ ), 64.0 (d,  $^2J_{CP} = 4.7$  Hz,  $C-5'$ ), 46.7 ( $C-a$ ), 38.6 ( $C-2'$ ), 8.2 ( $C-b$ ).

$^{31}P$ -NMR (162 MHz,  $DMSO-d_6$ ):  $\delta$  [ppm] = 2.81 (s).

IR:  $\nu$  [ $cm^{-1}$ ] = 3174, 2983, 2944, 2809, 2433, 1679, 1607, 1522, 1430, 1392, 1272, 1662, 1041, 964, 935, 837, 794, 776, 596, 515.

HRMS (ESI $^-$ ):  $m/z$  calcd: 432.9303 [ $M-H$ ] $^-$ , found: 432.9280.

**5-Vinyl-2'-deoxyuridine 16**

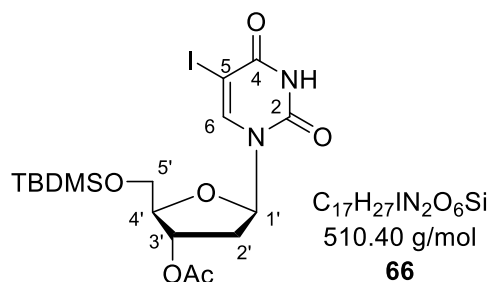
The reaction was carried out according to the general procedure V with IdU **63** (202 mg, 0.57 mmol),  $Pd_2(dba)_3$  (28 mg, 31  $\mu$ mol, 5.4 mol%), tri(2-furyl) phosphine (16 mg, 68  $\mu$ mol, 12 mol%) and tributyl(vinyl) tin (183  $\mu$ L, 0.63 mmol) in DMF (5 mL). Purification on RP<sub>18</sub> silica gel with automated flash chromatography (H<sub>2</sub>O/CH<sub>3</sub>CN; 100:0 to 0:100) provided **16** (122 mg, 84%) as a colorless solid.

<sup>1</sup>H-NMR (600 MHz, DMSO-*d*<sub>6</sub>):  $\delta$  [ppm] = 11.40 (s, 1H, NH), 8.12 (s, 1H, H-6), 6.37 (dd, <sup>3</sup>J<sub>HH</sub> = 17.7, <sup>2</sup>J<sub>HH</sub> = 11.5 Hz, 1H, H-7), 6.16 (t, <sup>3</sup>J<sub>HH</sub> = 6.6 Hz, 1H, H-1'), 5.92 (dd, <sup>3</sup>J<sub>HH</sub> = 17.7, <sup>2</sup>J<sub>HH</sub> = 2.0 Hz, 1H, *trans*-H-8), 5.24 (d, <sup>3</sup>J<sub>HH</sub> = 4.3 Hz, 1H, 3'-OH), 5.14 – 5.09 (m, 2H, *cis*-H-8, 5'-OH), 4.30 – 4.22 (m, 1H, H-3'), 3.79 (m, 1H, H-4'), 3.64 (ddd, <sup>2</sup>J<sub>HH</sub> = 11.8 Hz, <sup>3</sup>J<sub>HH</sub> = 5.0, 3.5 Hz, 1H, H-5'b), 3.58 (ddd, <sup>2</sup>J<sub>HH</sub> = 11.9 Hz, <sup>3</sup>J<sub>HH</sub> = 4.7, 3.5 Hz, 1H, H-5'b), 2.20 – 2.08 (m, 2H, H-2').

<sup>13</sup>C-NMR (101 MHz, DMSO-*d*<sub>6</sub>):  $\delta$  [ppm] = 162.1 (C-4), 149.6 (C-2), 137.9 (C-6), 128.8 (C-7), 113.9 (C-8), 110.8 (C-5), 87.5 (C-4'), 84.4 (C-1'), 70.0 (C-3'), 61.0 (C-5'), 40.0 (C-2').

IR:  $\nu$  [cm<sup>-1</sup>] = 3246, 3025, 2966, 2833, 1693, 1651, 1472, 1420, 1274, 1186, 1100, 1052, 1015, 989, 912, 852, 571.

HRMS (ESI<sup>+</sup>): *m/z* calcd: 277.0800 [M+Na]<sup>+</sup>, found: 277.0834.

**3'-O-Acetyl-5'-O-tert-butyltrimethylsilyl-5-iodo-2'-deoxyuridine 66**

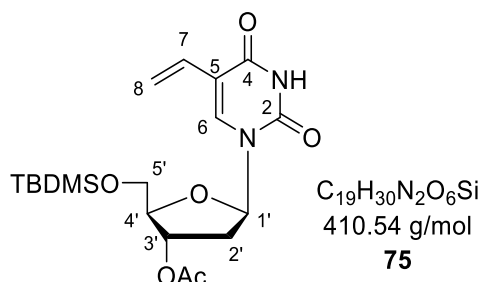
5-Iodo-2'-deoxyuridine **63** (710 mg, 2.01 mmol) was co-evaporated with pyridine once and suspended in 15 mL pyridine. Then, TBDMSO (363 mg, 2.41 mmol) was added, and the forming solution was stirred overnight at room temperature, followed by the addition of Ac<sub>2</sub>O (0.95 mL, 10.0 mmol). After stirring overnight at room temperature, all volatiles were removed under reduced pressure, and the resulting residue was co-evaporated with toluene twice. The crude product was purified on silica gel (petroleum ether/ethyl acetate; 7:3 to 1:1) to provide **66** (829 mg, 81%) as a colorless foam. *R<sub>f</sub>*-value: 0.23 (petroleum ether/ethyl acetate; 7:3).

<sup>1</sup>H-NMR (400 MHz, DMSO-*d*<sub>6</sub>): δ [ppm] = 11.76 (bs, 1H, NH), 8.00 (s, 1H, H-6), 6.09 (dd, <sup>3</sup>*J*<sub>HH</sub> = 8.6, 5.7 Hz, 1H, H-1'), 5.21 – 5.07 (m, 1H, H-3'), 4.14 – 4.05 (m, 1H, H-4'), 3.89 – 3.76 (m, 2H, H-5'), 2.32 (ddd, <sup>2</sup>*J*<sub>HH</sub> = 14.1 Hz, <sup>3</sup>*J*<sub>HH</sub> = 5.7, 1.6 Hz, 1H, H-2'a), 2.21 (ddd, <sup>2</sup>*J*<sub>HH</sub> = 14.3 Hz, <sup>3</sup>*J*<sub>HH</sub> = 8.7, 6.2 Hz, 1H, H-2'b) 2.06 (s, 3H, Ac-CH<sub>3</sub>), 0.90 (s, 9H, tBu-C(CH<sub>3</sub>)<sub>3</sub>), 0.13 (s, 3H, Si-CH<sub>3</sub>), 0.12 (s, 3H, Si-CH<sub>3</sub>).

<sup>13</sup>C-NMR (101 MHz, DMSO-*d*<sub>6</sub>): δ [ppm] = 170.0 (Ac-CO), 160.4 (C-4), 150.1 (C-2), 143.7 (C-6), 84.6, 84.6 (C-1', C-4'), 74.5 (C-3'), 70.3 (C-5), 63.2 (C-5'), 37.3 (C-2'), 25.9 (tBu-CH<sub>3</sub>), 20.8 (Ac-CH<sub>3</sub>), 18.1 (tBu-C(CH<sub>3</sub>)<sub>3</sub>), -5.3 (Si-(CH<sub>3</sub>)<sub>2</sub>).

IR: ν [cm<sup>-1</sup>] = 3203, 3085, 2927, 2853, 1719, 1685, 1250, 1145, 829, 781, 673, 541, 417.

HRMS (ESI<sup>+</sup>): *m/z* calcd: 533.0581 [M+Na]<sup>+</sup>, found: 533.0589.

**3'-O-Acetyl-5'-O-tert-butylidimethylsilyl-5-vinyl-2'-deoxyuridine 75**

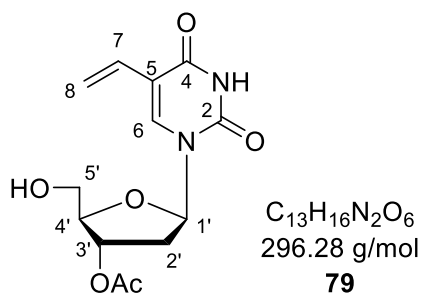
The protected nucleoside **66** (510 mg, 1.00 mmol),  $Pd_2(dba)_3$  (49 mg, 54  $\mu$ mol, 5.4 mol%) and tri(2-furyl) phosphine (28 mg, 120  $\mu$ mol, 12 mol%) were dried *in vacuo* and solved in 7 mL DMF. After the addition of tributyl(vinyl) tin (32  $\mu$ L, 0.11 mmol), the reaction was stirred for 2 h at 60 °C. The reaction was monitored by  $^1H$ -NMR spectra and after complete conversion 7 mL ethyl acetate was added. The reaction mixture was filtrated over Celite® and the solvents were removed under reduced pressure. The crude product was purified on silica gel (petroleum ether/ethyl acetate; 7:3 to 6:4, column loaded using  $CH_2Cl_2$ ) affording **75** (381 mg, 93%) as a colorless foam.  $R_f$ -value: 0.67 ( $CH_2Cl_2/CH_3OH$ ; 19:1)

$^1H$ -NMR (500 MHz, MeOD):  $\delta$  [ppm] = 7.83 (s, 1H, H-6), 6.40 (dd,  $^3J_{HH} = 17.8, 11.7$  Hz, 1H, H-7), 6.22 (dd,  $^3J_{HH} = 8.6, 5.6$  Hz, 1H, H-1'), 5.96 (dd,  $^3J_{HH} = 17.6$  Hz,  $^4J_{HH} = 1.7$  Hz, 1H, *trans*-H-8), 5.32 – 5.24 (m, 1H, H-3'), 5.20 (dd,  $^3J_{HH} = 11.5$  Hz,  $^4J_{HH} = 1.7$  Hz, 1H, *cis*-H-8), 4.21 – 4.13 (m, 1H, H-4'), 4.00 – 3.88 (m, 2H, H-5'), 2.48 (ddd,  $^2J_{HH} = 14.1$  Hz,  $^3J_{HH} = 5.6, 1.5$  Hz, 1H, H-2'a), 2.25 (ddd,  $^2J_{HH} = 14.0$  Hz,  $^3J_{HH} = 8.6, 6.3$  Hz, 1H, H-2'b), 2.09 (s, 3H, Ac- $CH_3$ ), 0.93 (s, 9H, *t*Bu- $C(CH_3)_3$ ), 0.14 (s, 3H, Si- $CH_3$ ), 0.13 (s, 3H, Si- $CH_3$ ).

$^{13}C$ -NMR (126 MHz, MeOD):  $\delta$  [ppm] = 172.2 (Ac-CO), 164.3 (C-4), 151.4 (C-2), 138.1 (C-6), 129.5 (C-7), 116.1 (C-8), 113.5 (C-5), 87.1, 87.0 (C-1', C-4'), 76.5 (C-3'), 64.7 (H-5'), 39.2 (C-2'), 26.5 (*t*Bu- $CH_3$ ), 20.8 (Ac- $CH_3$ ), 19.3 (*t*Bu- $C(CH_3)_3$ ), -5.3 (Si- $CH_3$ ), -5.3 (Si- $CH_3$ ).

IR:  $\nu$  [ $cm^{-1}$ ] = 3227, 3061, 3017, 2949, 2929, 2884, 2855, 2396, 1716, 1669, 1513, 1317, 1282, 1122, 1003, 829, 781, 626, 552, 406.

HRMS (ESI<sup>+</sup>):  $m/z$  calcd: 433.1765 [ $M+Na$ ]<sup>+</sup>, found: 433.1778.

**3'-O-Acetyl-5-vinyl-2'-deoxyuridine 79**

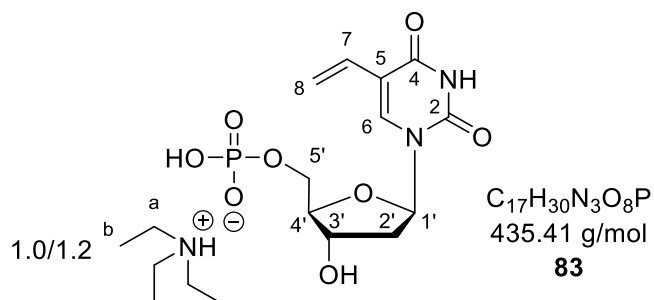
The nucleoside **75** (370 mg, 900  $\mu$ mol) was solved in 10 mL THF followed by the addition of TreatHF (440  $\mu$ L, 2.70 mmol). After stirring overnight at room temperature, all volatiles were removed under reduced pressure, and the residue was purified on silica gel ( $CH_2Cl_2/CH_3OH$ ; 19: 1) to yield **79** (267 mg, 100%) as a colorless foam.  $R_f$ -value: 0.40 ( $CH_2Cl_2/CH_3OH$ ; 19:1).

$^1H$ -NMR (400 MHz, MeOD):  $\delta$  [ppm] = 8.23 (s, 1H, *H*-6), 6.45 (dd,  $^3J_{HH} = 17.7$ , 11.4 Hz, 1H, *H*-7), 6.36 – 6.25 (m, 1H, *H*-1'), 5.94 (dd,  $^3J_{HH} = 17.7$  Hz,  $^4J_{HH} = 1.7$  Hz, 1H, *trans*-*H*-8), 5.37 – 5.28 (m, 1H, *H*-3'), 5.17 (dd,  $^3J_{HH} = 11.5$  Hz,  $^4J_{HH} = 1.6$  Hz, 1H, *cis*-*H*-8), 4.16 – 4.07 (m, 1H, *H*-4'), 3.87 – 3.79 (m, 2H, *H*-5'), 2.47 – 2.30 (m, 2H, *H*-2'), 2.09 (s, 3H, Ac- $CH_3$ ).

$^{13}C$ -NMR (126 MHz, MeOD):  $\delta$  [ppm] = 172.2 (Ac-CO), 164.4 (*C*-4), 151.6 (*C*-2), 138.7 (*C*-6), 129.2 (*C*-7), 115.4 (*C*-8), 113.7 (*C*-5), 87.0, 86.6 (*C*-1', *C*-4'), 76.5 (*C*-3'), 62.9 (*H*-5'), 38.9 (*C*-2'), 20.9 (Ac- $CH_3$ ).

IR:  $\nu$  [ $cm^{-1}$ ] = 3500, 3189, 3063, 2932, 2857, 1706, 1668, 1470, 1402, 1372, 1236, 1204, 1128, 1097, 1063, 833, 572, 508, 452, 412.

HRMS (ESI<sup>+</sup>):  $m/z$  calcd: 319.0906 [ $M+Na$ ]<sup>+</sup>, found: 319.0912.

**5-Vinyl-2'-deoxyuridine monophosphate 83**

**STILLE-coupling:** The reaction was carried out according to the general procedure VI with IdUMP **89** (1.7 TEAH, 424 mg, 0.70 mmol),  $Pd_2(dba)_3$  (35 mg, 38  $\mu$ mol, 5.4 mol%), tri(2-furyl) phosphine (20 mg, 84  $\mu$ mol, 12 mol%) and tributyl(vinyl) tin (225  $\mu$ L, 0.77 mmol) in DMF (10 mL). Purification on RP<sub>18</sub> silica gel with automated flash chromatography (H<sub>2</sub>O/CH<sub>3</sub>CN; 100:0 to 0:100) provided the TEAH salt of **83** (1.0 TEAH, 255 mg, 84%) as a light-yellow solid.

**Fm-route:** The reaction was carried out according to the general procedure I with protected 5-vinyl-2'-deoxyuridine **79** (148 mg, 0.500 mmol) in CH<sub>3</sub>CN (6 mL), bis(fluorenylmethyl)phosphoramidite (470 mg, 0.900 mmol) in CH<sub>2</sub>Cl<sub>2</sub> (3 mL), and 0.25 M DCI in CH<sub>3</sub>CN (3.60 mL, 0.900 mmol). The reaction was stirred for 10 min, followed by the addition of a 5.5 M *t*-BuOOH in decane solution (182  $\mu$ L, 1.00 mmol). Deprotection was carried out in H<sub>2</sub>O/MeOH/Et<sub>3</sub>N (5:5:3 v/v/v) for 2 day, after prepurification of the intermediate on silica gel (CH<sub>2</sub>Cl<sub>2</sub>/CH<sub>3</sub>OH; 29:1). The product was purified on RP<sub>18</sub> silica gel using automated flash chromatography (H<sub>2</sub>O/CH<sub>3</sub>CN; 100:0 to 0:100) to provide the monophosphate **83** (1.2 TEAH, 164 mg, 72%) as triethylammonium salt.

<sup>1</sup>H-NMR (600 MHz, D<sub>2</sub>O):  $\delta$  [ppm] = 7.98 (s, 1H, *H*-6), 6.50 (dd, <sup>3</sup>*J*<sub>HH</sub> = 17.7, 11.5 Hz, 1H, *H*-7), 6.35 (m, 1H, *H*-1'), 5.96 (dd, <sup>3</sup>*J*<sub>HH</sub> = 17.7 Hz, <sup>2</sup>*J*<sub>HH</sub> = 1.3 Hz, 1H, *trans*-*H*-8), 5.31 (dd, <sup>3</sup>*J*<sub>HH</sub> = 11.5 Hz, <sup>2</sup>*J*<sub>HH</sub> = 1.3 Hz, 1H, *cis*-*H*-8), 4.61 – 4.56 (m, 1H, *H*-3'), 4.22 – 4.18 (m, 1H, *H*-4'), 4.14 – 4.03 (m, 2H, *H*-5'), 3.20 (q, <sup>3</sup>*J*<sub>HH</sub> = 7.3 Hz, 8H, *H*-a), 2.44 – 2.37 (m, 2H, *H*-2'), 1.28 (t, <sup>3</sup>*J*<sub>HH</sub> = 7.3 Hz, 12H, *H*-b).

<sup>13</sup>C-NMR (151 MHz, D<sub>2</sub>O):  $\delta$  [ppm] = 164.5 (C-4), 150.9 (C-2), 138.3 (C-6), 127.6 (C-7), 116.5 (C-8), 113.0 (C-5), 85.8 (d, <sup>3</sup>*J*<sub>CP</sub> = 8.7 Hz, C-4'), 85.5 (C-1'), 71.1 (C-3'), 64.7 (d, <sup>2</sup>*J*<sub>CP</sub> = 5.1 Hz, C-5'), 46.6 (C-a), 39.0 (C-2'), 8.2 (C-b).

<sup>31</sup>P-NMR (162 MHz, D<sub>2</sub>O):  $\delta$  [ppm] = 0.15 (s).



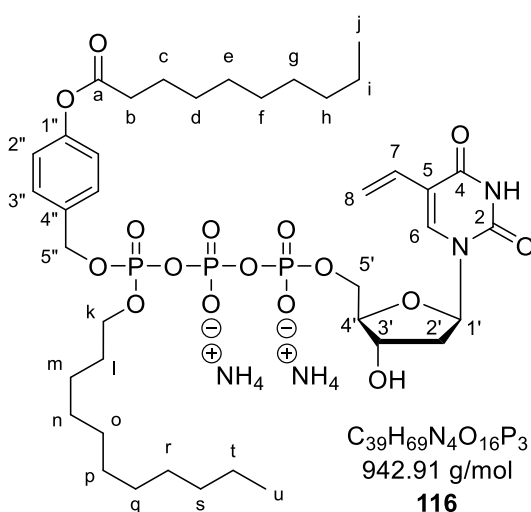


(C-7), 122.8 (4x C-2''), 116.2 (C-8), 113.6 (C-5), 87.6 (d,  $^3J_{CP} = 9.3$  Hz, C-4'), 86.3 (C-1'), 72.3 (C-3'), 70.4 (d,  $^2J_{CP} = 5.0$  Hz, 2x C-5''), 66.8 (d,  $^2J_{CP} = 5.8$  Hz, C-5'), 40.8 (C-2'), 35.0 (2x C-b), 33.0 (2x C-h), 30.6, 30.4, 30.4, 30.2 (2x C-d-g), 26.0 (2x C-c), 23.7 (2x C-i), 14.4 (2x C-j).

$^{31}P$ -NMR (202 MHz, MeOD):  $\delta$  [ppm] = -10.48 (d,  $^2J_{PP} = 20.2$  Hz, P- $\alpha$ ), -12.07 (d,  $^2J_{PP} = 17.5$  Hz, P- $\gamma$ ), -22.51 (dd,  $^2J_{PP} = 20.2, 17.2$  Hz, P- $\beta$ ).

HRMS (ESI<sup>-</sup>):  $m/z$  calcd: 1013.3372 [M-H]<sup>-</sup>, found: 1013.3315.

### $\gamma$ -(C11,C9AB)-VdUTP **116**



The reaction was carried out with the general procedure VIII with the pyrophosphate of **115** (334 mg, 400  $\mu$ mol), TFAA (278  $\mu$ L, 2.00 mmol), and Et<sub>3</sub>N (446  $\mu$ L, 3.20 mmol) in CH<sub>3</sub>CN (5 ml). The subsequent activation step was performed with Et<sub>3</sub>N (279  $\mu$ L, 2.00 mmol) and 1-methylimidazole (80  $\mu$ L, 1.00 mmol) in CH<sub>3</sub>CN (6 ml) followed by the coupling with monophosphate **83** (1.0 TEAH, 87 mg, 200  $\mu$ mol) solved in DMF (3 mL). Purification on RP<sub>18</sub> silica gel with automated flash chromatography (H<sub>2</sub>O/THF; 100:0 to 0:100), Dowex ion-exchange (NH<sub>4</sub><sup>+</sup>), and RP<sub>18</sub> silica gel with automated flash chromatography (H<sub>2</sub>O/CH<sub>3</sub>CN; 100:0 to 0:100) as well as subsequent freeze-drying provided **116** (49 mg, 26%) as colorless cotton.

$^1H$ -NMR (600 MHz, MeOD):  $\delta$  [ppm] = 8.01 (d,  $^5J_{HH} = 2.0$  Hz, 1H, H-6), 7.50 (d,  $^3J_{HH} = 8.1$  Hz, 2H, 2x H-2''), 7.10 (d,  $^3J_{HH} = 8.5$  Hz, 2H, 2x H-3''), 6.58 (ddd,  $^3J_{HH} = 17.6, 11.7$  Hz,  $^4J_{HH} = 2.4$  Hz, 1H, H-7), 6.34 (dd,  $^3J_{HH} = 7.6, 6.0$  Hz, 1H, H-1'), 6.15 (ddd,  $^3J_{HH} = 17.7$  Hz,  $^2J_{HH} = 2.1$  Hz,  $^5J_{HH} = 2.1$  Hz, 1H, trans-H-8), 5.22 (m, 2H, H-5''), 5.19 (ddd,  $^3J_{HH} = 11.6$  Hz,  $^2J_{HH} = 4.3$  Hz,  $^5J_{HH} = 1.9$  Hz, 1H, trans-H-8), 4.64 – 4.59 (m, 1H, H-3'), 4.30 (ddd,  $^2J_{HH} =$

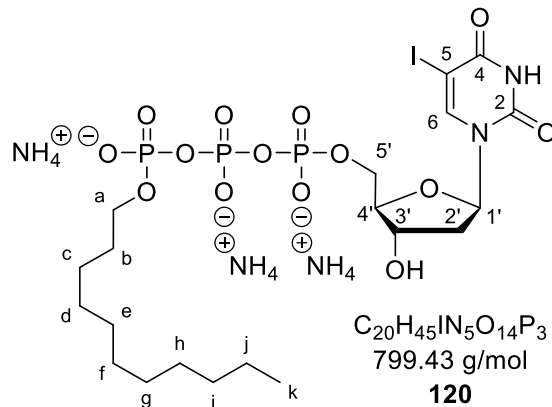
10.0 Hz,  $^3J_{\text{HH}} = 6.1, 3.0$  Hz, 1H, *H-5'a*), 4.26 – 4.20 (m, 1H, *H-5'b*), 4.16 – 4.09 (m, 2H, *H-k*), 4.08 – 4.03 (m, 1H, *H-4'*), 2.59 (t,  $^3J_{\text{HH}} = 7.4$  Hz, 2H, *H-b*), 2.36 – 2.20 (m, 2H, *H-2'*), 1.81 – 1.71 (m, 2H, *H-c*), 1.67 – 1.59 (m, 2H, *H-l*), 1.50 – 1.23 (m, 28H, *H-d-i, H-m-t*), 0.99 – 0.87 (m, 6H, *H-j, H-u*).

$^{13}\text{C-NMR}$  (151 MHz, MeOD):  $\delta$  [ppm] = 173.7 (*C-a*), 164.4 (*C-4*), 152.3 (*C-1''*), 151.5 (*C-2*), 139.5 (*C-6*), 135.2 (d,  $^3J_{\text{CP}} = 7.0$  Hz, *C-4''*), 130.4 (d,  $^4J_{\text{CP}} = 3.0$  Hz, 2x *C-3''*), 129.9 (*C-7*), 122.8 (2x *C-2''*), 116.2 (*C-5*), 113.6 (*C-8*), 87.6 (d,  $^3J_{\text{CP}} = 9.3$  Hz, *C-4'*), 86.3 (*C-1'*), 72.3 (d,  $^4J_{\text{CP}} = 3.9$  Hz, *C-3'*), 70.3 (d,  $^2J_{\text{CP}} = 5.7$  Hz, *C-5''*), 69.9 (d,  $^2J_{\text{CP}} = 6.3$  Hz, *C-5'*), 66.9 – 66.7 (m, *C-k*), 40.9 (*C-2'*), 35.0 (*C-b*), 33.1, 33.0 (*C-h, C-s*), 31.2 (d,  $^3J_{\text{CP}} = 7.2$  Hz, *C-l*), 30.8, 30.7, 30.7, 30.6, 30.5, 30.4, 30.4, 30.3, 30.2 (*C-d-g, C-n-r*), 26.6 (*C-m*), 26.0 (*C-c*), 23.8, 23.7 (*C-i, C-t*), 14.5, 14.4 (*C-j, C-u*).

$^{31}\text{P-NMR}$  (243 MHz, MeOD):  $\delta$  [ppm] = -11.75 (d,  $^2J_{\text{PP}} = 19.2$  Hz, *P- $\alpha$* ), -13.04 (dd,  $^2J_{\text{PP}} = 17.0, 3.1$  Hz, *P- $\gamma$* ), -23.69 (t,  $^2J_{\text{PP}} = 18.1$  Hz, *P- $\beta$* ).

MALDI-MS:  $m/z = \text{calc: } 907.3318$  [*M-H*] $^-$ , found: 907.181.

### $\gamma$ -C11-IdUTP **120**



The reaction was carried out with the general procedure VIII with the pyrophosphate of **119** (313 mg, 500  $\mu\text{mol}$ ), TFAA (348  $\mu\text{L}$ , 2.50 mmol), and  $\text{Et}_3\text{N}$  (558  $\mu\text{L}$ , 4.00 mmol) in  $\text{CH}_3\text{CN}$  (10 ml). The subsequent activation step was performed with  $\text{Et}_3\text{N}$  (349  $\mu\text{L}$ , 2.50 mmol) and 1-methylimidazole (100  $\mu\text{L}$ , 1.25 mmol) in  $\text{CH}_3\text{CN}$  (10 ml) followed by the coupling with monophosphate **89** (1.7 TEAH, 152 mg, 250  $\mu\text{mol}$ ) solved in DMF (2.5 mL). Deprotection was carried out with 10% aq. tetrabutylammonium hydroxide (13.0 mL, 5.00 mmol). Purification on  $\text{RP}_{18}$  silica gel with automated flash chromatography ( $\text{H}_2\text{O}/\text{CH}_3\text{CN}$ ; 100:0 to 0:100), Dowex ion-exchange ( $\text{NH}_4^+$ ) and  $\text{RP}_{18}$

silica gel with automated flash chromatography (H<sub>2</sub>O/CH<sub>3</sub>CN; 100:0 to 0:100) as well as subsequent freeze-drying provided **120** (84 mg, 42%) as colorless cotton.

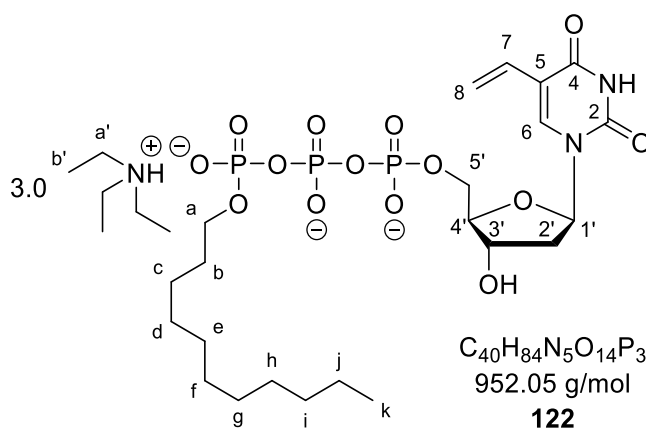
<sup>1</sup>H-NMR (400 MHz, D<sub>2</sub>O): δ [ppm] = 8.26 (s, 1H, *H*-6), 6.26 (t, <sup>3</sup>*J*<sub>HH</sub> = 6.8 Hz, 1H, *H*-1'), 4.63 – 4.54 (m, 1H, *H*-3'), 4.25 – 4.12 (m, 3H, *H*-5', *H*-4'), 3.96 (q, <sup>3</sup>*J*<sub>HH</sub> = 6.8 Hz, 2H, *H*-a), 2.46 – 2.26 (m, 2H, *H*-2'), 1.63 (p, <sup>3</sup>*J*<sub>HH</sub> = 7.0 Hz, 2H, *H*-b), 1.40 – 1.15 (m, 16H, *H*-C-j), 0.84 (t, <sup>3</sup>*J*<sub>HH</sub> = 6.5 Hz, 3H, *H*-k).

<sup>13</sup>C-NMR (101 MHz, D<sub>2</sub>O): δ [ppm] = 163.0 (*C*-4), 151.2 (*C*-2), 146.1 (*C*-6), 85.7 – 85.5 (m, *C*-4', *C*-1'), 70.7 (*C*-3'), 68.4 (*C*-5), 67.1 (d, <sup>2</sup>*J*<sub>CP</sub> = 6.2 Hz, *C*-a), 65.4 (d, <sup>2</sup>*J*<sub>CP</sub> = 6.0 Hz, *C*-5'), 38.9 (*C*-2'), 31.2 (*C*-i), 29.9 (d, <sup>2</sup>*J*<sub>CP</sub> = 7.3 Hz, *C*-b), 3x 28.8, 28.6, 28.6 (*C*-d-h), 25.0 (*C*-c), 22.1 (*C*-j), 13.4 (*C*-k).

<sup>31</sup>P-NMR (162 MHz, D<sub>2</sub>O): δ [ppm] = -10.98 (d, <sup>2</sup>*J*<sub>PP</sub> = 20.0 Hz, *P*-α), -11.73 (d, <sup>2</sup>*J*<sub>PP</sub> = 18.5 Hz, *P*-γ), -23.20 (t, <sup>2</sup>*J*<sub>PP</sub> = 18.8 Hz, *P*-β).

MALDI-MS: *m/z* calcd: 747.0351 [*M*-H]<sup>-</sup>, found: 746.855.

### γ-C11-VdUTP **122**



The reaction was carried out according to the general procedure VII with γ-C11-IdUTP **120** (4 NH<sub>4</sub><sup>+</sup>, 24 mg, 30 μmol), Pd<sub>2</sub>(dba)<sub>3</sub> (2.7 mg, 3.0 μmol, 10 mol%), tri(2-furyl) phosphine (1.7 mg, 7.2 μmol, 24 mol%) and tributyl(vinyl) tin (10 μL, 33 mmol) in DMF/water 1:1 v/v (3 mL) for 5 h at 40 °C. Purification on RP<sub>18</sub> silica gel with automated flash chromatography (0.05 M TEAB/CH<sub>3</sub>CN; 100:0 to 0:100) provided the TEAH salt of **122** (22 mg, 76%) as a colorless solid.

<sup>1</sup>H-NMR (400 MHz, MeOD): δ [ppm] = 8.05 (s, 1H, *H*-6), 6.60 (dd, <sup>3</sup>*J*<sub>HH</sub> = 17.6, 11.7 Hz, 1H, *H*-7), 6.32 (t, <sup>3</sup>*J*<sub>HH</sub> = 6.6 Hz, 1H, *H*-1'), 6.16 (dd, <sup>3</sup>*J*<sub>HH</sub> = 17.6 Hz, <sup>2</sup>*J*<sub>HH</sub> = 1.9 Hz, 1H, *trans*-

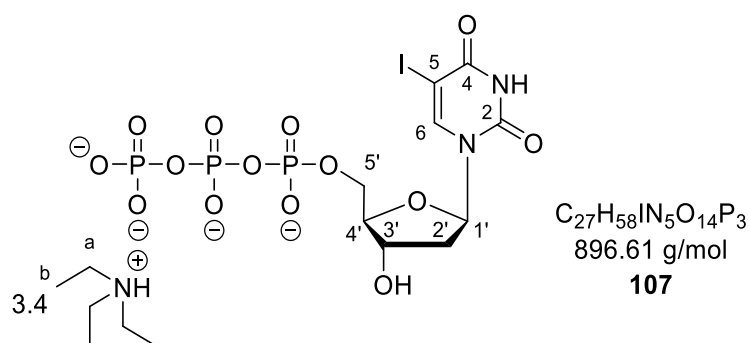
$H_8$ ), 5.20 (dd,  $^3J_{\text{HH}} = 11.6$  Hz,  $^2J_{\text{HH}} = 2.0$  Hz, 1H, *cis-H-8*), 4.69 (dt,  $^3J_{\text{HH}} = 6.0, 3.8$  Hz, 1H, *H-3'*), 4.38 (ddd,  $^2J_{\text{HH}} = 11.4$  Hz,  $^3J_{\text{HH}} = 6.4, 3.2$  Hz, 1H, *H-5'a*), 4.27 – 4.20 (m, 1H, *H-5'b*), 4.10 – 3.99 (m, 3H, *H-4'*, *H-a*), 3.21 (q,  $^3J_{\text{HH}} = 7.3$  Hz, 18H, *H-a'*), 2.38 – 2.21 (m, 2H, *H-b*), 1.65 (p,  $^3J_{\text{HH}} = 6.8$  Hz, 2H, *H-c*), 1.45 – 1.24 (m, 43H, *H-d-j*, *H-b'*), 0.91 (t,  $^3J_{\text{HH}} = 7.0$  Hz, 3H, *H-k*).

$^{13}\text{C-NMR}$  (101 MHz, MeOD):  $\delta$  [ppm] = 164.4 (*C-4*), 151.5 (*C-2*), 139.7 (*C-6*), 130.1 (*C-7*), 116.1 (*C-8*), 113.4 (*C-5*), 87.8 (d,  $^3J_{\text{CP}} = 9.1$  Hz, *C-4'*), 86.3 (*C-1'*), 71.7 (*C-3'*), 67.3 (d,  $^2J_{\text{CP}} = 6.3$  Hz, *C-a*), 66.4 (d,  $^2J_{\text{CP}} = 5.8$  Hz, *C-5'*), 47.3 (*C-a'*), 40.8 (*C-2'*), 33.1 (*C-i*), 31.9 (d,  $^3J_{\text{CP}} = 8.1$  Hz, *C-b*), 30.8, 2x 30.8, 30.6, 30.5, 27.0 (*C-c*), 23.7 (*C-j*), 14.4 (*C-k*), 9.1 (*C-b'*).

$^{31}\text{P-NMR}$  (162 MHz, MeOD):  $\delta$  [ppm] = -11.22 (d,  $^2J_{\text{PP}} = 18.8$  Hz, *P- $\alpha$* ), -11.82 (d,  $^2J_{\text{PP}} = 19.0$  Hz, *P- $\gamma$* ), -23.39 (t,  $^2J_{\text{PP}} = 18.9$  Hz, *P- $\beta$* ).

**MALDI-MS:**  $m/z$  calcd: 671.151 [ $\text{M}+\text{Na}$ ] $^+$ , found: 671.082.

### 5-Iodo-2'-deoxyuridine triphosphate **107**



The reaction was carried out according to the general procedure IV with IdU **63** (1.06 g, 0.58 mmol), tributylamine (1.43 mL, 6.00 mmol) and  $\text{POCl}_3$  (336  $\mu\text{L}$ , 3.60 mmol) in triethyl phosphate (15 mL) at  $-20$   $^\circ\text{C}$  for 2 days followed by the addition of tributyl ammonium pyrophosphate (4.12 g, 7.50 mmol) and tributylamine (4.28 mL, 18.0 mmol) in  $\text{CH}_3\text{CN}$  (15 mL). The reaction mixture was stirred for 2 h at  $-15$   $^\circ\text{C}$ . Purification by ion-exchange chromatography through a DEAE-Sephadex<sup>®</sup> A-25 column (0-1 M TEAB) and RP<sub>18</sub> flash column chromatography (100%  $\text{H}_2\text{O}$ , reduced flow) provided the TEAH salt of **107** (855 mg, 31%) as a colorless solid.

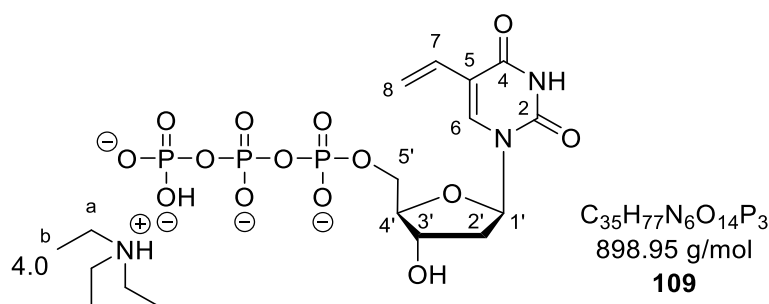
$^1\text{H-NMR}$  (400 MHz,  $\text{D}_2\text{O}$ ):  $\delta$  [ppm] = 8.22 (s, 1H, *H-6*), 6.22 (dd,  $^3J_{\text{HH}} = 7.4, 6.2$  Hz, 1H, *H-1'*), 4.68 – 4.57 (m, 1H, *H-3'*), 4.33 (ddd,  $^2J_{\text{HH}} = 11.3$  Hz,  $^3J_{\text{HH}} = 7.3, 3.9$  Hz, 1H, *H-5'a*), 4.20 (ddd,  $^2J_{\text{HH}} = 11.3$  Hz,  $^3J_{\text{HH}} = 5.7, 4.3$  Hz, 1H, *H-5'b*), 4.13 – 4.07 (m, 1H, *H-4'*), 3.20 (q,  $^3J_{\text{HH}} = 7.3$  Hz, 19H, *H-a*), 2.37 – 2.22 (m, 2H, *H-2'*), 1.33 (t,  $^3J_{\text{HH}} = 7.3$  Hz, 28H, *H-b*).

$^{13}\text{C}$ -NMR (101 MHz,  $\text{D}_2\text{O}$ ):  $\delta$  [ppm] = 162.3 (C-4), 150.5 (C-2), 145.3 (C-6), 84.8 (m, C-4', C-1'), 70.0 (C-3'), 67.3 (C-5), 64.6 (d,  $^2J_{\text{CP}} = 5.6$  Hz, C-5'), 45.8 (C-a), 38.0 (C-2'), 7.4 (C-b).

$^{31}\text{P}$ -NMR (162 MHz, MeOD):  $\delta$  [ppm] = -10.32 (d,  $^2J_{\text{PP}} = 21.5$  Hz, P- $\alpha$ ), -11.34 (d,  $^2J_{\text{PP}} = 21.6$  Hz, P- $\gamma$ ), -23.75 (t,  $^2J_{\text{PP}} = 21.5$  Hz, P- $\beta$ ).

MALDI-MS:  $m/z$  calcd: 592.8630  $[\text{M-H}]^-$ , found: 592.614.

### 5-Vinyl-2'-deoxyuridine triphosphate **109**



The reaction was carried out according to the general procedure VII with IdUTP **107** (3.3 TEAH, 56 mg, 60  $\mu\text{mol}$ ),  $\text{Pd}_2(\text{dba})_3$  (5.5 mg, 6.0  $\mu\text{mol}$ , 10 mol%), tri(2-furyl) phosphine (3.3 mg, 1.4  $\mu\text{mol}$ , 24 mol%) and tributyl(vinyl) tin (19  $\mu\text{L}$ , 66 mmol) in DMF/water 9:1 v/v (3 mL) for 5 h at 40  $^\circ\text{C}$ . Purification on RP<sub>18</sub> silica gel with automated flash chromatography (100%  $\text{H}_2\text{O}$ ) provided the TEAH salt of **109** (48 mg, 89%) as a colorless solid.

$^1\text{H}$ -NMR (600 MHz,  $\text{D}_2\text{O}$ ):  $\delta$  [ppm] = 7.88 (s, 1H, H-6), 6.43 (dd,  $^3J_{\text{HH}} = 17.9$ , 11.6 Hz, 1H, H-7), 6.27 (dd,  $^3J_{\text{HH}} = 7.5$ , 6.4 Hz, 1H, H-1'), 5.89 (dd,  $^3J_{\text{HH}} = 17.7$ ,  $^2J_{\text{HH}} = 1.4$  Hz, 1H, *trans*-H-8), 5.24 (dd,  $^3J_{\text{HH}} = 11.5$ ,  $^2J_{\text{HH}} = 1.4$  Hz, 1H, *cis*-H-8), 4.60 – 4.57 (m, 1H, H-3'), 4.21 – 4.04 (m, 3H, H-5', H-4'), 3.11 (q,  $^3J_{\text{HH}} = 7.3$  Hz, 26H, H-a), 2.39 – 2.24 (m, 2H, H-2'), 1.19 (t,  $^3J_{\text{HH}} = 7.3$  Hz, 36H, H-b).

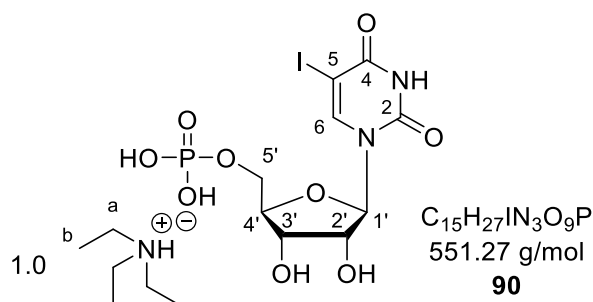
$^{13}\text{C}$ -NMR (151 MHz,  $\text{D}_2\text{O}$ ):  $\delta$  [ppm] = 164.5 (C-4), 151.0 (C-2), 138.3 (C-6), 127.6 (C-7), 116.6 (C-8), 113.0 (C-5), 85.6 (d,  $^3J_{\text{CP}} = 9.1$  Hz, C-4'), 85.3 (C-1'), 70.8 (C-3'), 65.4 (d,  $^2J_{\text{CP}} = 5.6$  Hz, C-5'), 46.6 (C-a), 38.8 (C-2'), 8.2 (C-b).

$^{31}\text{P}$ -NMR (162 MHz, MeOD):  $\delta$  [ppm] = -10.26 (d,  $^2J_{\text{PP}} = 21.2$  Hz, P- $\alpha$ ), -11.37 (d,  $^2J_{\text{PP}} = 21.5$  Hz, P- $\gamma$ ), -23.69 (t,  $^2J_{\text{PP}} = 21.7$  Hz, P- $\beta$ ).

MALDI-MS:  $m/z$  calcd: 492.9820  $[\text{M-H}]^-$ , found: 493.027.

### 6.3.5 5-Vinyluridine series

#### 5-Iodouridine monophosphate **90**



The reaction was carried out according to the general procedure II with  $POCl_3$  (221  $\mu$ L, 2.38 mmol) in  $CH_3CN$  (533  $\mu$ L, 10.2 mmol), pyridine (210  $\mu$ L, 2.60 mmol),  $H_2O$  (27  $\mu$ L, 1.51 mmol), and nucleoside IU **64** (199 mg, 0.54 mmol) for 5 h. Purification on  $RP_{18}$  silica gel with automated flash chromatography (100%  $H_2O$ , reduced flow, then  $H_2O/CH_3CN$ ; 100:0 to 0:100) provided the ammonium salt of **90**. Ion-exchange to TEAH resulted in the TEAH salt of **90** (1.0 TEAH, 195 mg, 65%) as a colorless solid.

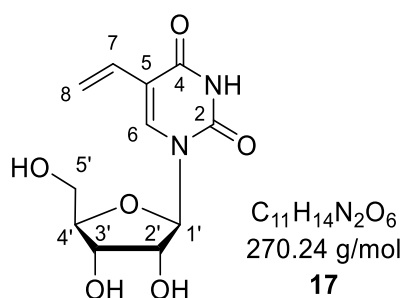
$^1H$ -NMR (400 MHz,  $D_2O$ ):  $\delta$  [ppm] = 8.27 (s, 1H,  $H$ -6), 5.94 (d,  $^3J_{HH}$  = 5.1 Hz, 1H,  $H$ -1'), 4.39 – 4.35 (m, 1H,  $H$ -2'), 4.34 – 4.31 (m, 1H,  $H$ -3'), 4.29 – 4.25 (m, 1H,  $H$ -4'), 4.15 (ddd,  $^2J_{HH}$  = 11.8 Hz,  $^3J_{HH}$  = 4.4, 2.6 Hz, 1H,  $H$ -5'a), 4.09 (ddd,  $^2J_{HH}$  = 11.7 Hz,  $^3J_{HH}$  = 5.5, 3.2 Hz, 1H,  $H$ -5'b), 3.21 (q,  $^3J_{HH}$  = 7.3 Hz, 6H,  $H$ -a), 1.28 (t,  $^3J_{HH}$  = 7.3 Hz, 9H,  $H$ -b).

$^{13}C$ -NMR (101 MHz,  $D_2O$ ):  $\delta$  [ppm] = 163.0 ( $C$ -4), 151.5 ( $C$ -2), 145.9 ( $C$ -6), 88.7 ( $C$ -1'), 83.5 (d,  $^3J_{CP}$  = 8.8 Hz,  $C$ -4'), 73.9 ( $C$ -2'), 69.7 ( $C$ -3'), 68.5 ( $C$ -5), 64.2 (d,  $^2J_{CP}$  = 4.9 Hz,  $C$ -5'), 46.6 ( $C$ -a), 8.2 ( $C$ -b).

$^{31}P$ -NMR (162 MHz,  $D_2O$ ):  $\delta$  [ppm] = 0.11 (s).

IR:  $\nu$  [ $cm^{-1}$ ] = 3174, 3063, 2986, 2944, 2815, 2691, 2494, 1674, 1609, 1444, 1261, 1153, 1036, 914, 803, 755, 605, 500, 432.

HRMS (ESI $^-$ ):  $m/z$  calcd: 448.9252 [ $M-H$ ] $^-$ , found: 448.9251.

5-Vinyluridine **17**

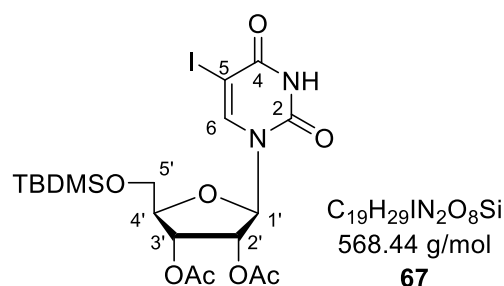
The reaction was carried out according to the general procedure V with IU **64** (185 mg, 0.50 mmol), Pd<sub>2</sub>(dba)<sub>3</sub> (25 mg, 27 μmol, 5.4 mol%), tri(2-furyl) phosphine (14 mg, 60 μmol, 12 mol%) and tributyl(vinyl) tin (161 μL, 0.55 mmol) in DMF (4 mL). Purification on RP<sub>18</sub> silica gel with automated flash chromatography (H<sub>2</sub>O/CH<sub>3</sub>CN; 100:0 to 0:100) provided **17** (125 mg, 85%) as a colorless solid.

<sup>1</sup>H-NMR (400 MHz, DMSO-*d*<sub>6</sub>): δ [ppm] = 11.45 (s, 1H, NH), 8.21 (s, 1H, H-6), 6.37 (dd, <sup>3</sup>J<sub>HH</sub> = 17.7, <sup>2</sup>J<sub>HH</sub> = 11.5 Hz, 1H, H-7), 5.92 (dd, <sup>3</sup>J<sub>HH</sub> = 17.7 Hz, <sup>2</sup>J<sub>HH</sub> = 2.0 Hz, 1H, *trans*-H-8), 5.79 (d, <sup>3</sup>J<sub>HH</sub> = 4.7 Hz, 1H, H-1'), 5.43 (d, <sup>3</sup>J<sub>HH</sub> = 5.4 Hz, 1H, 2'-OH), 5.25 (t, <sup>3</sup>J<sub>HH</sub> = 4.8 Hz, 1H, 5'-OH), 5.13 (dd, <sup>3</sup>J<sub>HH</sub> = 11.4 Hz, <sup>2</sup>J<sub>HH</sub> = 2.0 Hz, 1H, *cis*-H-8), 5.09 (d, <sup>3</sup>J<sub>HH</sub> = 5.3 Hz, 1H, 3'-OH), 4.10 – 4.05 (m, 1H, H-2'), 4.04 – 3.98 (m, 1H, H-3'), 3.89 – 3.84 (m, 1H, 4'), 3.75 – 3.54 (m, 2H, H-5').

<sup>13</sup>C-NMR (101 MHz, DMSO-*d*<sub>6</sub>): δ [ppm] = 162.1 (C-4), 149.8 (C-2), 138.0 (C-6), 128.6 (C-7), 114.0 (C-8), 110.8 (C-5), 88.2 (C-1'), 84.6 (C-4'), 73.9 (C-2'), 69.4 (C-3'), 60.4 (C-5').

IR: ν [cm<sup>-1</sup>] = 3367, 3197, 3057, 2931, 1668, 1468, 1414, 1361, 1270, 1100, 1077, 1047, 994, 915, 756, 578, 410.

HRMS (ESI): *m/z* calcd: 269.0779 [M-H]<sup>-</sup>, found: 269.0790.

**2',3'-Di-O-acetyl-5'-O-tert-butylidimethylsilyl-5-iodouridine 67**

5-Iodouridine **64** (1.11 g, 3.00 mmol) was dried *in vacuo* and solved in 15 mL pyridine. Then, TBDMSCl (542 mg, 3.60 mmol) was added, and the reaction mixture was stirred overnight at room temperature, followed by the addition of Ac<sub>2</sub>O (1.99 mL, 21.0 mmol). After stirring overnight at room temperature, all volatiles were removed under reduced pressure and the resulting residue dissolved in a mixture of ethyl acetate/water (100 mL, 1:1 v/v). The aqueous phase was extracted with ethyl acetate twice, the combined organic layers were dried over Na<sub>2</sub>SO<sub>4</sub>, and the solvent was removed *in vacuo*. The resulting residue was purified on silica gel (petroleum ether/ethyl acetate; 7:3) to yield **67** (1.51 g, 88%) as a colorless foam. *R<sub>f</sub>*-value: 0.23 (petroleum ether/ethyl acetate; 7:3)

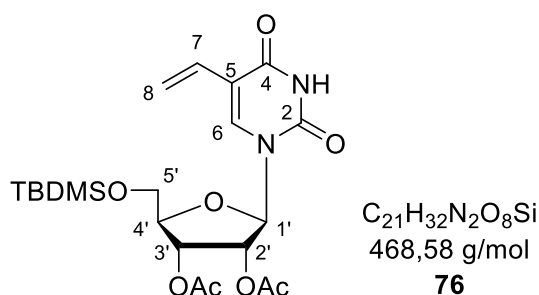
<sup>1</sup>H-NMR (400 MHz, DMSO-*d*<sub>6</sub>): δ [ppm] = 11.82 (s, 1H, NH), 8.04 (s, 1H, H-6), 6.06 – 5.97 (m, 1H, H-1'), 5.34 – 5.25 (m, 2H, H-2', H-3'), 4.24 – 4.17 (m, 1H, H-4'), 3.91 – 3.78 (m, 2H, H-5'), 2.10 (s, 3H, Ac-CH<sub>3</sub>), 2.01 (s, 3H, Ac-CH<sub>3</sub>), 0.93 (s, 9H, *t*Bu-C(CH<sub>3</sub>)<sub>3</sub>), 0.15 (s, 3H, Si-CH<sub>3</sub>), 0.14 (s, 3H, Si-CH<sub>3</sub>).

<sup>13</sup>C-NMR (101 MHz, DMSO-*d*<sub>6</sub>): δ [ppm] = 169.5 (Ac-CO), 169.4 (Ac-CO), 160.3 (C-4), 150.2 (C-2), 143.6 (C-6), 85.2 (C-1'), 82.8 (C-4'), 72.4 (C-2'), 71.1 (C-3'), 70.8 (C-5), 62.9 (C-5'), 25.9 (*t*Bu-CH<sub>3</sub>), 20.4 (Ac-CH<sub>3</sub>), 20.2 (Ac-CH<sub>3</sub>), 18.1 (*t*Bu-C(CH<sub>3</sub>)<sub>3</sub>), -5.4 (Si-(CH<sub>3</sub>)<sub>2</sub>), -5.4 (Si-(CH<sub>3</sub>)<sub>2</sub>).

IR:  $\nu$  [cm<sup>-1</sup>] = 3187, 3066, 2954, 2930, 2857, 1688, 1612, 1439, 1397, 1364, 1231, 1211, 1164, 1118, 1045, 829, 777, 604, 430.

HRMS (ESI<sup>+</sup>): *m/z* calcd: 569.0816 [M+H]<sup>+</sup>, found: 569.0830.



**2',3'-Di-O-acetyl-5'-O-tert-butyldimethylsilyl-5-vinyluridine 76**

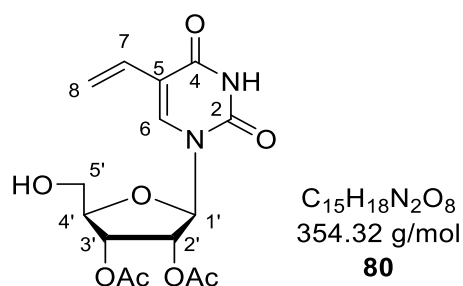
The protected nucleoside **67** (57 mg, 0.10 mmol),  $Pd_2(dba)_3$  (4.9 mg, 5.4  $\mu$ mol, 5.4 mol%) and tri(2-furyl) phosphine (2.8 mg, 12  $\mu$ mol, 12 mol%) were dried *in vacuo* and solved in 1 mL DMF. After the addition of tributyl(vinyl) tin (32  $\mu$ L, 0.11 mmol) the reaction was stirred for 2 h at 60 °C. The reaction was monitored by  $^1H$ -NMR spectra and after complete conversion, 1 mL ethyl acetate was added. The reaction mixture was filtrated over Celite® and the solvents were removed under reduced pressure. The crude product was purified on silica gel (petroleum ether/ethyl acetate; 7:3 to 6:4, column loaded using  $CH_2Cl_2$ ) affording **76** (42 mg, 90%) as a light-yellow foam.  $R_f$ -value: 0.23 (petroleum ether/ethyl acetate; 7:3)

$^1H$ -NMR (400 MHz, DMSO-*d*6):  $\delta$  [ppm] = 11.57 (s, 1H, NH), 7.77 (s, 1H, H-6), 6.33 (dd,  $^3J_{HH} = 17.6$  Hz, 11.5 Hz, 1H, H-7), 6.01 (d,  $^3J_{HH} = 6.5$  Hz, 1H, H-1'), 5.98 (dd,  $^3J_{HH} = 17.7$  Hz,  $^2J_{HH} = 2.1$  Hz, 1H, *trans*-H-7), 5.39 (t,  $^3J_{HH} = 6.2$  Hz, 1H, H-2'), 5.31 (dd,  $^3J_{HH} = 5.9$ , 3.3 Hz, 1H, H-3'), 5.19 (dd,  $^3J_{HH} = 11.5$ ,  $^2J_{HH} = 2.1$  Hz, 1H, *cis*-H-8), 4.18 (q,  $^3J_{HH} = 3.4$  Hz, 1H, H-4'), 3.86 (m, 2H, H-5'), 2.10 (s, 3H, Ac- $CH_3$ ), 2.02 (s, 3H, Ac- $CH_3$ ), 0.88 (s, 9H, *t*Bu- $C(CH_3)_3$ ), 0.08 (s, 6H, Si- $(CH_3)_2$ ).

$^{13}C$ -NMR (101 MHz, DMSO-*d*6):  $\delta$  [ppm] = 169.4 (Ac-CO), 169.3 (Ac-CO), 161.9 (C-4), 149.6 (C-2), 137.4 (C-6), 128.4 (C-7), 115.3 (C-8), 111.7 (C-5), 86.0 (C-1'), 82.5 (C-4'), 72.2 (C-2'), 70.5 (C-3'), 62.8 (C-5'), 25.7 (*t*Bu- $CH_3$ ), 20.4 (Ac- $CH_3$ ), 20.2 (Ac- $CH_3$ ), 18.0 (*t*Bu- $C(CH_3)_3$ ), -5.5 (Si- $CH_3$ ), -5.6 (Si- $CH_3$ ).

IR:  $\nu$  [ $cm^{-1}$ ] = 3202, 3067, 2953, 2929, 2883, 2857, 1746, 1713, 1685, 1461, 1363, 1231, 1090, 830, 779, 667, 572, 407.

HRMS (ESI<sup>+</sup>):  $m/z$  calcd: 491.1826 [M+Na]<sup>+</sup>, found: 491.1838.

**2',3'-Di-O-acetyl-5-vinyluridine 80**

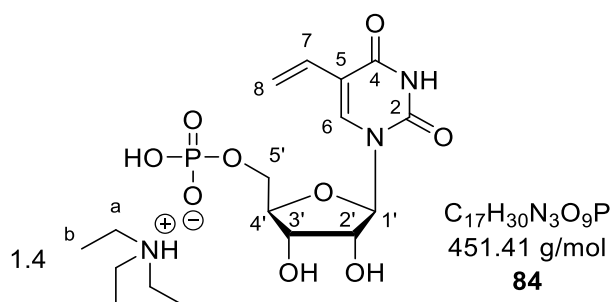
The nucleoside **76** (590 mg, 1.26 mmol) was solved in 10 mL THF followed by the addition of TreatHF (616  $\mu$ L, 3.78 mmol). After stirring overnight at room temperature, all volatiles were removed under reduced pressure, and the residue was purified on silica gel ( $CH_2Cl_2/CH_3OH$ ; 19: 1) to yield **80** (446 mg, 100%) as a colorless foam.  $R_f$ -value: 0.48 ( $CH_2Cl_2/CH_3OH$ ; 19:1)

$^1H$ -NMR (400 MHz,  $DMSO-d_6$ ):  $\delta$  [ppm] = 11.54 (s, 1H, NH), 8.16 (s, 1H, H-6), 6.37 (dd,  $^3J_{HH}$  17.7, 11.5 Hz, 1H, H-7), 6.04 (d,  $^3J_{HH}$  = 6.3 Hz, 1H, H-1'), 5.93 (dd,  $^3J_{HH}$  = 17.7 Hz,  $^2J_{HH}$  = 1.9 Hz, 1H, *trans*-H-8), 5.51 (t,  $^3J_{HH}$  = 4.8 Hz, 1H, OH), 5.43 – 5.37 (m, 1H, H-2'), 5.36 – 5.33 (m, 1H, H-3'), 5.17 (dd,  $^3J_{HH}$  = 11.5 Hz,  $^2J_{HH}$  = 2.0 Hz, 1H, *cis*-H-8), 4.19 – 4.13 (m, 1H, H-4'), 3.75 – 3.60 (m, 2H, H-5'), 2.10 (s, 3H, Ac-CH<sub>3</sub>), 2.02 (s, 3H, Ac -CH<sub>3</sub>).

$^{13}C$ -NMR (101 MHz,  $DMSO-d_6$ ):  $\delta$  [ppm] = 169.5 (Ac-CO), 169.4 (Ac-CO), 162.0 (C-4), 149.7 (C-2), 137.5 (H-6), 128.4 (H-7), 114.6 (H-8), 111.6 (H-5), 85.7 (C-1'), 83.2 (C-4'), 72.6 (C-2'), 70.9 (C-3'), 60.7 (C-5'), 20.5 (Ac -CH<sub>3</sub>), 20.3 (Ac -CH<sub>3</sub>).

IR:  $\nu$  [ $cm^{-1}$ ] = 3499, 3198, 3063, 2938, 1705, 1667, 1469, 1372, 1236, 1202, 1098, 1063, 1022, 572, 412.

HRMS (ESI<sup>+</sup>):  $m/z$  calcd: 319.0906 [M+Na]<sup>+</sup>, found: 319.0912.

**5-Vinyluridine monophosphate 84**

**Still-coupling:** The reaction was carried out according to the general procedure VI with IUMP **90** (1.0 TEAH, 165 mg, 0.30 mmol),  $Pd_2(dba)_3$  (15 mg, 16  $\mu$ mol, 5.4 mol%), tri(2-furyl) phosphine (8.4 mg, 36  $\mu$ mol, 12 mol%), and tributyl(vinyl) tin (96  $\mu$ L, 0.33 mmol) in DMF (4 mL) for 2 h. Purification on RP<sub>18</sub> silica gel with automated flash chromatography (H<sub>2</sub>O/CH<sub>3</sub>CN; 100:0 to 0:100) provided the TEAH salt of **84** (1.0 TEAH, 115 mg, 85%) as a light-yellow solid.

**Fm-route:** The reaction was carried out according to the general procedure I with protected 5-vinyluridine **80** (213 mg, 0.600 mmol) in CH<sub>3</sub>CN (10 mL), bis(fluorenylmethyl)phosphoramidite (563 mg, 1.08 mmol) in CH<sub>2</sub>Cl<sub>2</sub> (4 mL), and 0.25 M DCI in CH<sub>3</sub>CN (4.32 mL, 1.08 mmol). The reaction was stirred for 15 min, followed by the addition of a 5.5 M *t*-BuOOH in decane solution (218  $\mu$ L, 1.20 mmol). Deprotection was carried out in H<sub>2</sub>O/CH<sub>3</sub>CN/Et<sub>3</sub>N (1:1:1 v/v/v) overnight, after prepurification of the intermediate on silica gel (CH<sub>2</sub>Cl<sub>2</sub>/CH<sub>3</sub>OH; 39:1). The product was purified on RP<sub>18</sub> silica gel using automated flash chromatography (H<sub>2</sub>O/CH<sub>3</sub>CN; 100:0 to 0:100) to provide the monophosphate **84** (1.2 TEAH, 209 mg, 74%) as triethylammonium salt.

<sup>1</sup>H-NMR (400 MHz, D<sub>2</sub>O):  $\delta$  [ppm] = 7.99 (s, 1H, *H*-6), 6.52 (dd, <sup>3</sup>*J*<sub>HH</sub> = 17.7, 11.5 Hz, 1H, *H*-7), 6.08 – 5.92 (m, 2H, *H*-1', *trans*-*H*-8), 5.33 (dd, <sup>3</sup>*J*<sub>HH</sub> = 11.5 Hz, <sup>2</sup>*J*<sub>HH</sub> = 1.4 Hz, 1H, *cis*-*H*-8), 4.42 (t, <sup>3</sup>*J*<sub>HH</sub> = 5.3 Hz, 1H, *H*-2'), 4.36 (t, <sup>3</sup>*J*<sub>HH</sub> = 4.7 Hz, 1H, *H*-3'), 4.31 – 4.26 (m, 1H, *H*-4'), 4.14 (ddd, <sup>2</sup>*J*<sub>HH</sub> = 11.8 Hz, <sup>3</sup>*J*<sub>HH</sub> = 4.0, 2.5 Hz, 1H, *H*-5'a), 4.08 (ddd, <sup>2</sup>*J*<sub>HH</sub> = 11.8 Hz, <sup>3</sup>*J*<sub>HH</sub> = 5.3, 2.9 Hz, 1H, *H*-5'b), 3.21 (q, <sup>3</sup>*J*<sub>HH</sub> = 7.3 Hz, 9H, *H*-a), 1.29 (t, <sup>3</sup>*J*<sub>HH</sub> = 7.3 Hz, 13H, *H*-b).

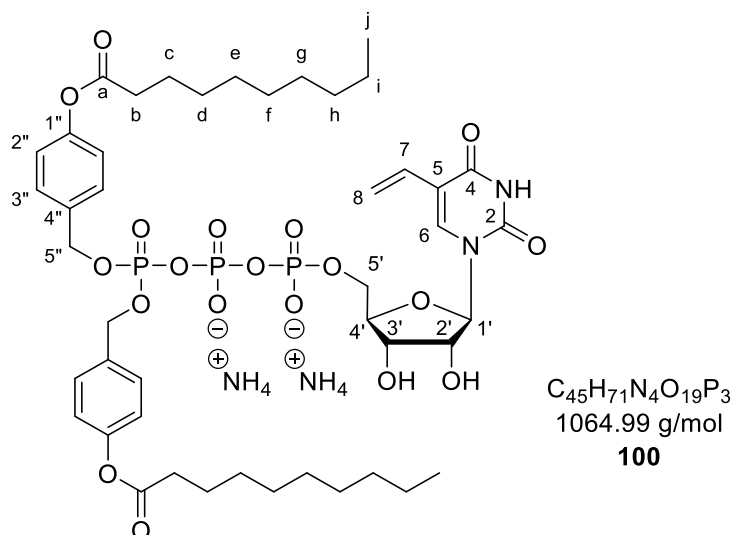
<sup>13</sup>C-NMR (101 MHz, D<sub>2</sub>O):  $\delta$  [ppm] = 164.4 (C-4), 151.1 (C-2), 138.1 (C-6), 127.6 (C-7), 116.6 (C-8), 113.0 (C-5), 88.5 (C-1'), 83.6 (d, <sup>3</sup>*J*<sub>CP</sub> = 8.9 Hz, C-4'), 73.9 (C-2'), 69.9 (C-3'), 64.1 (d, <sup>2</sup>*J*<sub>CP</sub> = 4.8 Hz, C-5'), 46.7 (C-a), 8.2 (C-b).

<sup>31</sup>P-NMR (162 MHz, D<sub>2</sub>O):  $\delta$  [ppm] = 0.54 (s).

IR:  $\nu$  [ $\text{cm}^{-1}$ ] = 3501, 3192, 3063, 2943, 1705, 1667, 1470, 1237, 1129, 1097, 1063, 1022, 803, 572, 508, 408.

HRMS (ESI<sup>-</sup>):  $m/z$  calcd: 349.0442 [M-H]<sup>-</sup>, found: 349.0403.

### $\gamma$ -(C9C9AB)-VUTP **100**



The reaction was carried out with the general procedure VIII with the pyrophosphate of **95** (250 mg, 266  $\mu\text{mol}$ ), TFAA (185  $\mu\text{L}$ , 1.33 mmol), and  $\text{Et}_3\text{N}$  (297  $\mu\text{L}$ , 2.13 mmol) in  $\text{CH}_3\text{CN}$  (3 ml). The subsequent activation step was performed with  $\text{Et}_3\text{N}$  (185  $\mu\text{L}$ , 1.33 mmol) and 1-methylimidazole (53  $\mu\text{L}$ , 665  $\mu\text{mol}$ ) in  $\text{CH}_3\text{CN}$  (3 ml) followed by the coupling with monophosphate **84** (1.5 TEAH, 67 mg, 133  $\mu\text{mol}$ ) solved in DMF (3 mL). Purification on  $\text{RP}_{18}$  silica gel with automated flash chromatography ( $\text{H}_2\text{O}/\text{CH}_3\text{CN}$ ; 100:0 to 0:100), Dowex ion-exchange ( $\text{NH}_4^+$ ) and  $\text{RP}_{18}$  silica gel with automated flash chromatography ( $\text{H}_2\text{O}/\text{CH}_3\text{CN}$ ; 100:0 to 0:100) as well as subsequent freeze-drying provided **100** (60 mg, 43%) as colorless cotton.

$^1\text{H-NMR}$  (600 MHz, MeOD):  $\delta$  [ppm] = 8.02 (s, 1H,  $H$ -6), 7.40 (d,  $^3J_{\text{HH}}$  = 8.6 Hz, 4H, 2x  $H$ -2''), 7.06 (d,  $^3J_{\text{HH}}$  = 8.4 Hz, 4H, 2x  $H$ -3''), 6.59 (dd,  $^3J_{\text{HH}}$  = 17.6, 11.7 Hz, 1H,  $H$ -7), 6.16 (dd,  $^3J_{\text{HH}}$  = 17.6 Hz,  $^2J_{\text{HH}}$  = 1.9 Hz, 1H, *trans*- $H$ -8), 6.00 (d,  $^3J_{\text{HH}}$  = 5.4 Hz, 1H,  $H$ -1'), 5.24 – 5.11 (m, 5H, *cis*- $H$ -8, 2x  $H$ -5''), 4.39 – 4.34 (m, 1H,  $H$ -2'), 4.32 – 4.27 (m, 3H,  $H$ -3',  $H$ -5'), 4.16 – 4.13 (m, 1H,  $H$ -4'), 2.59 (t,  $^3J_{\text{HH}}$  = 7.4 Hz, 4H, 2x  $H$ -b), 1.79 – 1.71 (m, 4H, 2x  $H$ -c), 1.50 – 1.28 (m, 24H, 2x  $H$ -d-i), 0.93 (t,  $^3J_{\text{HH}}$  = 6.8 Hz, 6H, 2x  $H$ -j).

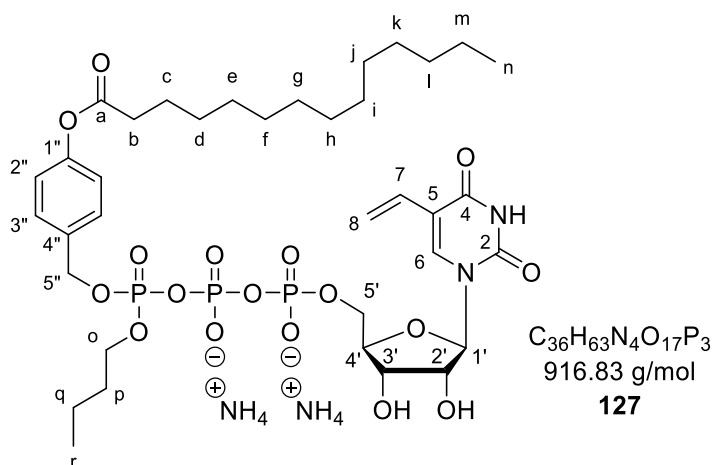
$^{13}\text{C-NMR}$  (151 MHz, MeOD):  $\delta$  [ppm] = 173.8 (2x  $C$ -a), 164.3 ( $C$ -4), 152.3 (2x  $C$ -1''), 151.8 ( $C$ -2), 139.6 ( $C$ -6), 135.0 (d,  $^3J_{\text{CP}}$  = 7.5 Hz, 2x  $C$ -4''), 130.6 (2x  $C$ -3''), 130.5 (d,  $^4J_{\text{CP}}$  = 2.0 Hz, 2x  $C$ -3''), 129.9 ( $C$ -7), 122.8 (4x  $C$ -2''), 116.4 ( $C$ -8), 113.6 ( $C$ -5), 89.8 ( $C$ -1'), 85.2 (d,  $^3J_{\text{CP}}$  =

9.3 Hz, C-4'), 75.5 (C-2'), 71.4 (C-3'), 70.4 (d,  $^2J_{CP} = 5.7$  Hz, C-5''), 66.5 (d,  $^2J_{CP} = 5.6$  Hz, C-5'), 35.0 (2x C-b), 33.0 (2x C-h), 30.6, 30.4, 30.4, 30.2 (2x C-d-g), 26.0 (2x C-c), 23.7 (2x C-i), 14.4 (2x C-j).

$^{31}\text{P}$ -NMR (243 MHz, MeOD):  $\delta$  [ppm] = -10.3 (d,  $^2J_{PP} = 19.2$  Hz, P- $\alpha$ ), -11.8 (d,  $^2J_{PP} = 16.5$  Hz, P- $\gamma$ ), -22.21 (t,  $^2J_{PP} = 18.4$  Hz, P- $\beta$ ).

HRMS (ESI<sup>-</sup>):  $m/z$  calcd: 1029.3322 [M-H]<sup>-</sup>, found: 1029.3122.

### $\gamma$ -(C4,C13AB)-VUTP **127**



The reaction was carried out with the general procedure VIII with the pyrophosphate of **126** (317 mg, 400  $\mu\text{mol}$ ), TFAA (278  $\mu\text{L}$ , 2.00 mmol), and Et<sub>3</sub>N (446  $\mu\text{L}$ , 3.20 mmol) in CH<sub>3</sub>CN (12 ml). The subsequent activation step was performed with Et<sub>3</sub>N (279  $\mu\text{L}$ , 2.00 mmol) and 1-methylimidazole (80  $\mu\text{L}$ , 1.00  $\mu\text{mol}$ ) in CH<sub>3</sub>CN (12 ml) followed by the coupling with monophosphate **84** (1.1 TEAH, 92 mg, 200  $\mu\text{mol}$ ) solved in DMF (4 mL). Purification on RP<sub>18</sub> silica gel with automated flash chromatography (H<sub>2</sub>O/CH<sub>3</sub>CN; 100:0 to 0:100), Dowex ion-exchange (NH<sub>4</sub><sup>+</sup>) and RP<sub>18</sub> silica gel with automated flash chromatography (H<sub>2</sub>O/CH<sub>3</sub>CN; 100:0 to 0:100) as well as subsequent freeze-drying provided **127** (47 mg, 26%) as colorless cotton.

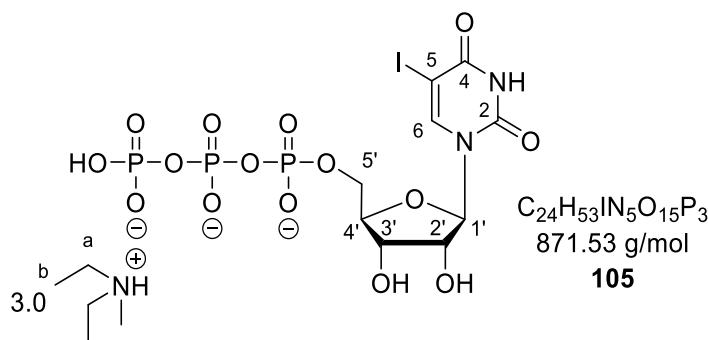
$^1\text{H}$ -NMR (600 MHz, MeOD):  $\delta$  [ppm] = 8.00 (s, 1H, H-6), 7.51 – 7.42 (m, 2H, H, 2x H-2'), 7.12 – 7.03 (m, 2H, 2x H-3'), 6.56 (ddd,  $^3J_{HH} = 17.7, 11.7$  Hz,  $^4J_{HH} = 2.6$  Hz, 1H, H-7), 6.14 (ddd,  $^3J_{HH} = 17.6, 3.1$  Hz,  $^5J_{HH} = 1.9$  Hz, 1H, *trans*-H-8), 5.97 (d,  $^3J_{HH} = 5.4$  Hz, 1H, H-1'), 5.24 – 5.12 (m, 3H, H-5'', *cis*-H-8), 4.35 – 4.32 (m, 1H, H-2'), 4.30 – 4.21 (m, 3H, H-5', H-3'), 4.16 – 4.07 (m, 3H, H-4', H-o), 2.56 (t,  $^3J_{HH} = 7.4$  Hz, 2H, H-b), 1.76 – 1.68 (m, 2H, H-c), 1.64 – 1.56 (m, 2H, H-l), 1.45 – 1.21 (m, 22H, H-d-m, H-q), 0.92 – 0.86 (m, 6H, H-n, H-r).

$^{13}\text{C}$ -NMR (151 MHz, MeOD):  $\delta$  [ppm] = 173.8 (C-a), 164.4 (C-4), 152.3 (C-1''), 151.9 (C-2), 139.6 (C-6), 135.2 (d,  $^3J_{\text{CP}} = 7.4$  Hz, C-4''), 130.4 (d,  $^4J_{\text{CP}} = 2.3$  Hz, 2x C-3''), 129.9 (C-7), 122.8 (C-2''), 116.3 (C-5), 113.6 (C-8), 89.8 (C-1'), 85.2 (d,  $^3J_{\text{CP}} = 9.2$  Hz, C-4'), 75.5 (C-2'), 71.4 (d,  $J_{\text{CP}} = 3.8$  Hz, C-3'), 70.3 (d,  $^2J_{\text{CP}} = 5.6$  Hz, C-5''), 69.6 (d,  $^2J_{\text{CP}} = 6.4$  Hz, C-5'), 66.5 (C-o), 35.0 (C-b), 33.3 (d,  $^3J_{\text{CP}} = 7.3$  Hz, C-p), 33.1 (C-l), 30.8 (d,  $^4J_{\text{CP}} = 4.9$  Hz), 30.8, 2x 30.8, 30.7, 30.6, 30.5, 30.4, 30.1, (C-d-k), 26.0 (C-c), 23.7 (C-m), 19.7 (C-q), 14.4 (C-n), 14.0 (C-r).

$^{31}\text{P}$ -NMR (243 MHz, MeOD):  $\delta$  [ppm] = -11.66 (d,  $^2J_{\text{PP}} = 18.9$  Hz, P- $\alpha$ ), -12.93 (d,  $^2J_{\text{PP}} = 16.5$  Hz, P- $\gamma$ ), -23.47 (t,  $^2J_{\text{PP}} = 17.9$  Hz, P- $\beta$ ).

MALDI-MS:  $m/z$  calcd: 881.2797 [M-H] $^-$ , found: 881.296.

### 5-Iodouridine triphosphate **105**



The reaction was carried out according to the general procedure IV with IU **64** (740 mg, 2.00 mmol), proton sponge (857 mg, 4.00 mmol), and  $\text{POCl}_3$  (373  $\mu\text{L}$ , 4.00 mmol) in triethyl phosphate (15 mL) at 2 °C for 3 days followed by the addition of tributyl ammonium pyrophosphate (2.74 g, 5.00 mmol) and tributylamine (2.85 mL, 12.0 mmol) in  $\text{CH}_3\text{CN}$  (10 mL). The reaction mixture was stirred for 15 min at 0 °C. Purification by ion-exchange chromatography through a DEAE-Sephadex<sup>®</sup> A-25 column (0-1 M TEAB) and RP<sub>18</sub> flash column chromatography ( $\text{H}_2\text{O}/\text{CH}_3\text{CN}$ ; 100:0 to 95:5) provided the TEAH salt of **105** (539 mg, 29%) as a colorless solid.

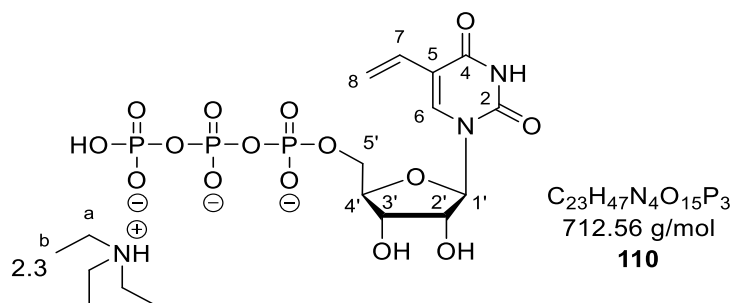
$^1\text{H}$ -NMR (400 MHz,  $\text{D}_2\text{O}$ ):  $\delta$  [ppm] = 8.23 (s, 1H, H-6), 5.90 (d,  $^3J_{\text{HH}} = 4.7$  Hz, 1H, H-1'), 4.43 – 4.32 (m, 2H, H-2', H-3'), 4.26 – 4.23 (m, 1H, H-5'a), 4.22 – 4.17 (m, 2H, H-5'b, H-4'), 3.16 (q,  $^3J_{\text{HH}} = 7.3$  Hz, 19H, H-a), 1.24 (t,  $^3J_{\text{HH}} = 7.4$  Hz, 27H, H-b).

$^{13}\text{C}$ -NMR (101 MHz,  $\text{D}_2\text{O}$ ):  $\delta$  [ppm] = 163.1 (C-4), 151.6 (C-2), 145.9 (C-6), 88.3 (C-1'), 83.5 (d,  $^3J_{\text{CP}} = 9.3$  Hz, C-4'), 73.7 (C-2'), 69.6 (C-3'), 68.5 (C-5), 65.1 (d,  $^2J_{\text{CP}} = 5.5$  Hz, C-5'), 46.6 (C-a), 8.2 (C-b).

$^{31}\text{P}$ -NMR (162 MHz,  $\text{D}_2\text{O}$ ):  $\delta$  [ppm] = -11.04 (d,  $^2J_{\text{PP}}$  = 19.7 Hz,  $P$ - $\alpha$ ), -11.87 (d,  $^2J_{\text{PP}}$  = 20.5 Hz,  $P$ - $\gamma$ ), -23.45 (t,  $^2J_{\text{PP}}$  = 20.9 Hz,  $P$ - $\beta$ ).

MALDI-MS:  $m/z$  calcd: 608.8579  $[\text{M}-\text{H}]^-$ , found: 608.461.

### 5-Vinyluridine triphosphate **110**



The reaction was carried out according to the general procedure VII with IUTP **105** (3.0 TEAH, 20 mg, 22  $\mu\text{mol}$ ),  $\text{Pd}_2(\text{dba})_3$  (2.0 mg, 2.2  $\mu\text{mol}$ , 10 mol%), tri(2-furyl) phosphine (1.2 mg, 5.3  $\mu\text{mol}$ , 24 mol%), and tributyl(vinyl) tin (7  $\mu\text{L}$ , 24 mmol) in DMF (1 mL) for 5 h at 40  $^\circ\text{C}$ . Purification on RP<sub>18</sub> silica gel with automated flash chromatography (100%  $\text{H}_2\text{O}$ ) provided the TEAH salt of **110** (14 mg, 86%) as a colorless solid.

$^1\text{H}$ -NMR (400 MHz,  $\text{D}_2\text{O}$ ):  $\delta$  [ppm] = 7.96 (s, 1H,  $H$ -6), 6.51 (dd,  $^3J_{\text{HH}}$  = 17.7, 11.5 Hz, 1H,  $H$ -7), 6.03 – 5.94 (m, 2H,  $H$ -1', *trans*- $H$ -8), 5.32 (dd,  $^3J_{\text{HH}}$  = 11.5 Hz,  $^2J_{\text{HH}}$  = 1.4 Hz, 1H, *cis*- $H$ -8), 4.46 – 4.39 (m, 2H,  $H$ -2',  $H$ -3'), 4.32 – 4.27 (m, 1H,  $H$ -5'a), 4.27 – 4.21 (m, 2H,  $H$ -5'b,  $H$ -4'), 3.18 (q,  $^3J_{\text{HH}}$  = 7.3 Hz, 13H,  $H$ -a), 1.26 (t,  $^3J_{\text{HH}}$  = 7.3 Hz, 21H,  $H$ -b).

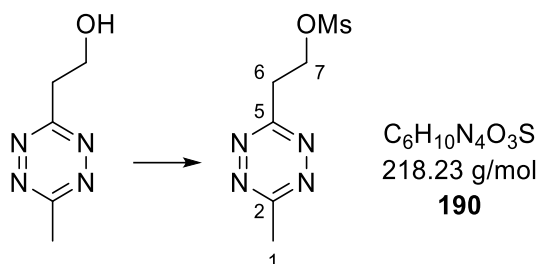
$^{13}\text{C}$ -NMR (101 MHz,  $\text{D}_2\text{O}$ ):  $\delta$  [ppm] = 164.5 ( $C$ -4), 151.2 ( $C$ -2), 138.0 ( $C$ -6), 127.5 ( $C$ -7), 116.7 ( $C$ -8), 113.1 ( $C$ -5), 88.1 ( $C$ -1'), 83.5 (d,  $^3J_{\text{CP}}$  = 9.1 Hz,  $C$ -4'), 73.7 ( $C$ -2'), 69.7 ( $C$ -3'), 65.1 (d,  $^2J_{\text{CP}}$  = 5.5 Hz,  $C$ -5'), 46.6 ( $C$ -a), 8.2 ( $C$ -b).

$^{31}\text{P}$ -NMR (162 MHz,  $\text{D}_2\text{O}$ ):  $\delta$  [ppm] = -10.32 – -11.06 (m,  $P$ - $\alpha$ ), -11.74 (d,  $^2J_{\text{PP}}$  = 19.8 Hz,  $P$ - $\gamma$ ), -23.12 (t,  $^2J_{\text{PP}}$  = 21.6 Hz,  $P$ - $\beta$ ).

MALDI-MS:  $m/z$  calcd: 508.9769  $[\text{M}-\text{H}]^-$ , found: 509.137.

### 6.3.6 Preparation of $\gamma$ -(C9C9AB)-MeTz-(E)-dUTP

#### 2-(6-methyl-1,2,4,5-tetrazin-3-yl)ethyl methanesulfonate **190**



The reaction was carried out as described in the literature with 3-hydroxypropionitrile (1.34 mL, 20.0 mmol),  $CH_3CN$  (3.16 mL, 60.0 mmol), hydrazine hydrate (9.73 mL, 200 mmol), and  $Zn(OTf)_2$  (1.45 g, 4.00 mmol, 20 mol%) in dioxane (8 mL) in a pressure tube. After stirring overnight at 60 °C,  $NaNO_2$  (11.0 g, 160 mmol) solved in water (80 mL) was added. The product **189** (510 mg, 18%) was obtained as a pink oil after purification on silica gel ( $CH_2Cl_2/CH_3OH$ ; 60:40 to 40:60).

$^1H$ -NMR (300 MHz,  $CDCl_3$ ):  $\delta$  [ppm] = 4.26 (t,  $^3J_{HH}$  = 5.8 Hz, 2H, *H*-7), 3.57 (t,  $^3J_{HH}$  = 5.9 Hz, 2H, *H*-6), 3.06 (s, 3H, *H*-1).

The analytical data was in accordance with those described.<sup>59</sup>

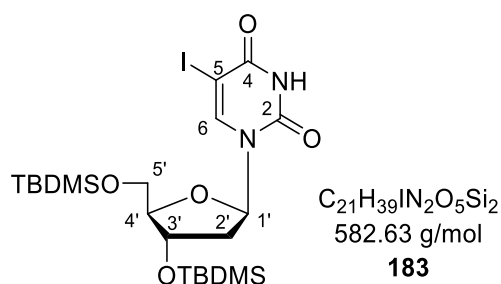
The subsequent reaction was carried out as described in the literature with OH-tetrazine **189** (266 mg, 1.90 mmol), methanesulfonyl chloride (294  $\mu$ L, 3.80 mmol), and  $Et_3N$  (530  $\mu$ L, 3.80 mmol) in  $CH_2Cl_2$  (5 mL). The product **190** (300 mg, 72%) was obtained as a pink solid after extraction and purification on silica gel ( $CH_2Cl_2/CH_3OH$ ; 95:5 to 50:50).

$^1H$ -NMR (600 MHz,  $CDCl_3$ ):  $\delta$  [ppm] = 4.87 (t,  $^3J_{HH}$  = 6.2 Hz, 2H, *H*-7), 3.76 (t,  $^3J_{HH}$  = 6.2 Hz, 2H, *H*-6), 3.08 (s, 3H, *H*-1), 3.02 (s, 3H,  $CH_3$ -Ms).

$^{13}C$ -NMR (151 MHz,  $CDCl_3$ ):  $\delta$  [ppm] = 168.3 (*C*-2), 166.2 (*C*-5), 66.1 (*C*-7), 37.7 ( $CH_3$ -Ms), 34.7 (*C*-6), 21.3 (*C*-1).

The analytical data was in accordance with those described.<sup>171</sup>



**3',5'-Di-*O*-*tert*-butyldimethylsilyl-5-iodo-2'-deoxyuridine 183**

The reaction was carried out as described in the literature with IdU **63** (1.00 g, 2.82 mmol), TBDMSCl (1.28 g, 8.47 mmol), imidazole (1.36 g, 19.8 mmol) in DMF (10 mL). The product **183** (1.20 g, 73%) was obtained after extraction and purification on silica gel.

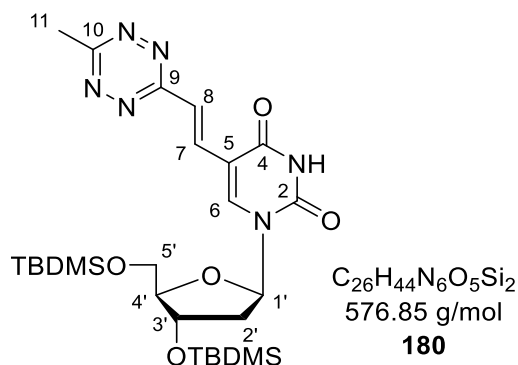
The analytical data was in accordance with those described.<sup>172</sup>

<sup>1</sup>H-NMR (400 MHz, CDCl<sub>3</sub>): δ [ppm] = 8.41 (bs, 1H, NH), 8.08 (s, 1H, H-6), 6.27 (dd, <sup>3</sup>J<sub>HH</sub> = 8.0, 5.6 Hz, 1H, H-1'), 4.45 – 4.31 (m, 1H, H-3'), 4.02 – 3.95 (m, 1H, H-4'), 3.89 (dd, <sup>2</sup>J<sub>HH</sub> = 11.5, <sup>3</sup>J<sub>HH</sub> = 2.4 Hz, 1H, H-5'a), 3.76 (dd, <sup>2</sup>J<sub>HH</sub> = 11.5, <sup>3</sup>J<sub>HH</sub> = 2.4 Hz, 1H, H-5'b), 2.31 (ddd, <sup>2</sup>J<sub>HH</sub> = 13.1, <sup>3</sup>J<sub>HH</sub> = 5.6, 2.2 Hz, 1H, H-2'a), 2.07 – 1.94 (m, 1H, H-2'b), 0.95 (s, 9H, tBu-C(CH<sub>3</sub>)<sub>3</sub>), 0.89 (s, 9H, tBu-C(CH<sub>3</sub>)<sub>3</sub>), 0.16 – 0.08 (4s, 12H, 2x Si-(CH<sub>3</sub>)<sub>2</sub>).

<sup>13</sup>C-NMR (101 MHz, CDCl<sub>3</sub>): δ [ppm] = 159.9 (C-4), 149.8 (C-2), 144.6 (C-6), 88.6 (C-4'), 86.0 (C-1'), 72.8 (C-3'), 68.4 (C-5), 63.3 (C-5'), 42.2 (C-2'), 26.3 (tBu-CH<sub>3</sub>), 25.9 (tBu-CH<sub>3</sub>), 18.7 (tBu-C(CH<sub>3</sub>)<sub>3</sub>), 18.2 (tBu-C(CH<sub>3</sub>)<sub>3</sub>), -4.5 (Si-CH<sub>3</sub>), -4.7 (Si-CH<sub>3</sub>), -4.9 (Si-CH<sub>3</sub>), -5.1 (Si-CH<sub>3</sub>).

HRMS (ESI<sup>+</sup>): *m/z* calcd: 583.1520 [M+Na]<sup>+</sup>, found: 583.1534.

**3',5'-Di-*O*-*tert*-butyldimethylsilyl-((*E*)-2-(6-methyl-1,2,4,5-tetrazin-3-yl)vinyl)-2'-deoxyuridine **180****



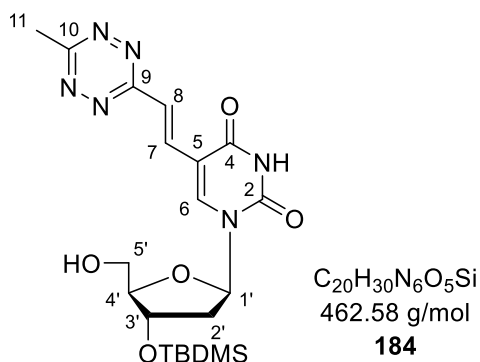
Nucleoside **183** (350 mg, 600  $\mu$ mol), tetrazine **190** (144 mg, 660  $\mu$ mol),  $Pd_2(dba)_3$  (28 mg, 30  $\mu$ mol) and QPhos (85 mg, 120  $\mu$ mol) were dried *in vacuo* shortly and solved in DMF (15 mL). After adding *N,N*-dicyclohexylmethylamine (386  $\mu$ L, 1.80 mmol), the reaction mixture was stirred for 3 h at 50 °C. The reaction mixture was diluted with ethyl acetate, washed with brine (3x), and dried over  $Na_2SO_4$ . The solvent was removed under reduced pressure, and the residue was purified on silica gel (petroleum ether/ethyl acetate; 8:2 to 7:3), giving **180** (183 mg, 53%) as a red solid.

$^1H$ -NMR (400 MHz,  $CDCl_3$ ):  $\delta$  [ppm] = 8.98 (s, 1H, NH), 8.15 – 8.06 (m, 2H, *H*-7, *H*-6), 7.89 (d,  $^3J_{HH}$  = 16.0 Hz, 1H, *H*-8), 6.32 (dd,  $^3J_{HH}$  = 7.5, 5.8 Hz, 1H, *H*-1'), 4.42 (dt,  $^3J_{HH}$  = 5.5, 2.5 Hz, 1H, *H*-3'), 4.03 (q,  $^3J_{HH}$  = 2.6 Hz, 1H, *H*-4'), 3.92 (dd,  $^3J_{HH}$  = 11.5,  $^2J_{HH}$  = 2.8 Hz, 1H, *H*-5'a), 3.80 (dd,  $^3J_{HH}$  = 11.5,  $^2J_{HH}$  = 2.5 Hz, 1H, *H*-5'b), 3.02 (s, 3H, *H*-11), 2.41 (ddd,  $^2J_{HH}$  = 13.2,  $^3J_{HH}$  = 2.6 Hz, 5.8, 1H, *H*-2'a), 2.07 (ddd,  $^2J_{HH}$  = 13.4,  $^3J_{HH}$  = 7.6, 5.8, 1H, *H*-2'b), 0.92 (s, 9H, *t*Bu- $C(CH_3)_3$ ), 0.90 (s, 9H, *t*Bu- $C(CH_3)_3$ ), 0.09 - 0.14 (4s, 12H, 2x Si- $(CH_3)_2$ ).

$^{13}C$ -NMR (151 MHz,  $CDCl_3$ ):  $\delta$  [ppm] = 166.3 (*C*-10), 165.1 (*C*-9), 161.3 (*C*-4), 149.1 (*C*-2), 142.1 (*C*-6), 132.7 (*C*-7), 122.4 (*C*-8), 110.7 (*C*-5), 88.7 (*C*-4'), 86.3 (*C*-1'), 72.6 (*C*-3'), 63.2 (*C*-5'), 42.3 (*C*-2'), 26.1 (*t*Bu- $CH_3$ ), 25.9 (*t*Bu- $CH_3$ ), 21.3 (*C*-11), 18.6 (*t*Bu- $C(CH_3)_3$ ), 18.1 (*t*Bu- $C(CH_3)_3$ ), -4.5 (Si- $CH_3$ ), -4.7 (Si- $CH_3$ ), -5.2 (Si- $CH_3$ ), -5.2 (Si- $CH_3$ ).

HRMS (ESI $^-$ ): *m/z* calcd: 577.2990 [ $M+H$ ] $^-$ , found: 577.2967.

**3'-O-*Tert*-butyldimethylsilyl-((*E*)-2-(6-methyl-1,2,4,5-tetrazin-3-yl)vinyl)-2'-deoxyuridine **184****

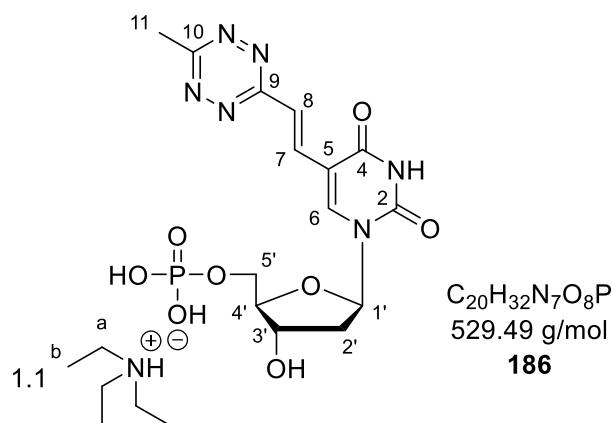


Nucleoside **180** (156 mg, 270  $\mu$ mol) was solved in THF (4 mL) followed by the addition of 2 mL aqueous TFA (TFA/H<sub>2</sub>O, 1:1 v/v) at 0 °C. After stirring for 6 h at 0 °C, the reaction mixture was neutralized with sat. aq. NaHCO<sub>3</sub> and diluted with ethyl acetate. The organic layer was washed with H<sub>2</sub>O and brine and was dried over Na<sub>2</sub>SO<sub>4</sub>. The solvent was removed under reduced pressure, and the crude product was isolated on silica gel (CH<sub>2</sub>Cl<sub>2</sub>/CH<sub>3</sub>OH; 19:1), affording **184** (84 mg, 67%) as a red solid.

<sup>1</sup>H-NMR (500 MHz, DMSO-*d*<sub>6</sub>):  $\delta$  [ppm] = 11.73 (s, 1H, NH), 8.49 (s, 1H, H-6), 7.95 (d, <sup>3</sup>J<sub>HH</sub> = 16.1 Hz, 1H, H-7), 7.91 (d, <sup>3</sup>J<sub>HH</sub> = 16.1 Hz, 1H, H-8), 6.15 (t, <sup>3</sup>J<sub>HH</sub> = 6.5 Hz, 1H, H-1'), 5.26 (t, <sup>3</sup>J<sub>HH</sub> = 5.2 Hz, 1H, 5'-OH), 4.49 – 4.43 (m, 1H, H-3'), 3.81 (q, <sup>3</sup>J<sub>HH</sub> = 3.8 Hz, 1H, H-4'), 3.69 (ddd, <sup>2</sup>J<sub>HH</sub> = 11.9, <sup>3</sup>J<sub>HH</sub> = 5.2, 3.9 Hz, 1H, H-5'a), 3.59 (ddd, <sup>2</sup>J<sub>HH</sub> = 12.0, <sup>3</sup>J<sub>HH</sub> = 5.1, 3.7 Hz, 1H, H-5'b), 2.92 (s, 3H, H-11), 2.39 – 2.30 (m, 1H, H-2'a), 2.16 (ddd, <sup>2</sup>J<sub>HH</sub> = 13.3, <sup>3</sup>J<sub>HH</sub> = 6.3, 4.1 Hz, 1H, H-2'b), 0.88 (s, 9H, *t*Bu-C(CH<sub>3</sub>)<sub>3</sub>), -0.09 (s, 6H, Si-CH<sub>3</sub>).

<sup>13</sup>C-NMR (126 MHz, DMSO-*d*<sub>6</sub>):  $\delta$  [ppm] = 165.9 (C-10), 164.4 (C-9), 162.0 (C-4), 149.2 (C-2), 143.6 (C-6), 133.5 (C-7), 119.6 (C-8), 109.1 (C-5), 87.6 (C-4'), 84.7 (C-1'), 71.3 (C-3'), 60.4 (C-5'), 25.7 (*t*Bu-CH<sub>3</sub>), 20.8 (C-11), 17.7 (*t*Bu-C(CH<sub>3</sub>)<sub>3</sub>), -4.8 (Si-CH<sub>3</sub>), -4.9 (Si-CH<sub>3</sub>).

HRMS (ESI<sup>+</sup>): *m/z* calcd: 461.1974 [M-H]<sup>+</sup>, found: 461.1942.

**((E)-2-(6-methyl-1,2,4,5-tetrazin-3-yl)vinyl)-2'-deoxyuridine monophosphate 186**

The nucleoside **184** (83 mg, 0.18 mmol) was dried *in vacuo* shortly and solved in 6 mL CH<sub>3</sub>CN/DCM (3:1 v/v). Then, a solution of bis(fluorenylmethyl)phosphoramidite (140 mg, 0.27 mmol) in 1.5 mL CH<sub>2</sub>Cl<sub>2</sub> and 0.25 M DCI in CH<sub>3</sub>CN were added simultaneously over a period of 30 min at 40 °C. After further 10 min, TLC indicated complete conversion of starting material (CH<sub>2</sub>Cl<sub>2</sub>/CH<sub>3</sub>OH; 30:1). A 5.5 M *t*-BuOOH in decane (56 μL, 0.31 mmol) solution was added to the reaction mixture followed by the evaporation of all volatiles under reduced pressure. The resulting residue was solved in 5% piperidine in DMF (3 mL) and stirred for 10 min at room temperature. The crude monophosphate was precipitated by the slow addition of Et<sub>2</sub>O (40 mL) and collected via centrifugation. The resulting residue was solved in CH<sub>3</sub>OH and passed through a short silica column (CH<sub>2</sub>Cl<sub>2</sub>/CH<sub>3</sub>OH; 1:1). After removing the solvents under reduced pressure, the resulting residue was solved in THF (5 mL) followed by the addition of TreatHF (88 μL, 0.54 mmol). The reaction mixture was stirred for 14 h at room temperature. All volatiles were removed under reduced pressure, and the residue was purified on RP<sub>18</sub> silica gel using automated flash chromatography (H<sub>2</sub>O/CH<sub>3</sub>CN; 100:0 to 0:100), affording **186** (36 mg, 37%) as a red solid.

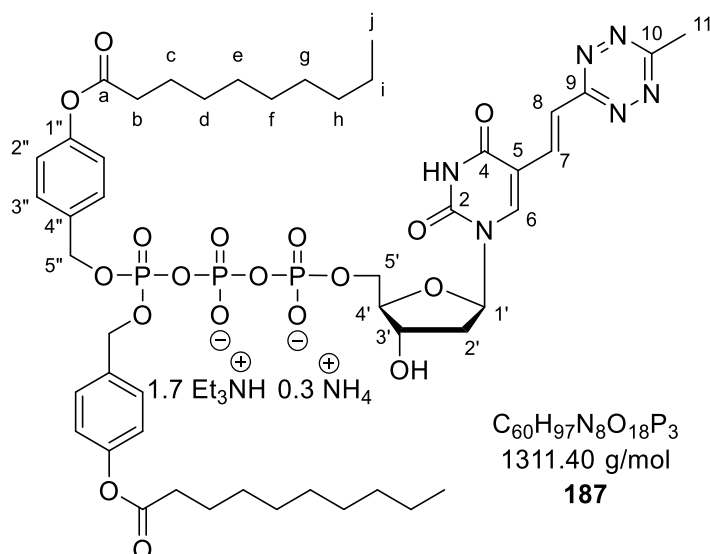
<sup>1</sup>H-NMR (500 MHz, MeOD): δ [ppm] = 8.37 (s, 1H, *H*-6), 8.07 (2x s, 2H, *H*-7, *H*-8), 6.34 (dd, <sup>3</sup>*J*<sub>HH</sub> = 7.7, 6.1 Hz, 1H, *H*-1'), 4.55 (dt, <sup>3</sup>*J*<sub>HH</sub> = 5.3, 2.5 Hz, 1H, *H*-3'), 4.15 – 4.05 (m, 3H, *H*-4', *H*-5'), 3.18 (q, <sup>3</sup>*J*<sub>HH</sub> = 7.3 Hz, 7H, *H*-a), 2.96 (s, 3H, *H*-11), 2.43 – 2.27 (m, 2H, *H*-2'), 1.30 (t, <sup>3</sup>*J*<sub>HH</sub> = 7.3 Hz, 10H, *H*-b).

<sup>13</sup>C-NMR (126 MHz, MeOD): δ [ppm] = 167.4 (*C*-10), 166.4 (*C*-9), 163.9 (*C*-4), 151.2 (*C*-2), 144.5 (*C*-6), 135.1 (*C*-7), 122.1 (*C*-8), 111.6 (*C*-5), 88.2 (d, <sup>3</sup>*J*<sub>CP</sub> = 8.3 Hz, *C*-4'), 87.2 (*C*-1'), 73.0 (*C*-3'), 66.0 (d, <sup>2</sup>*J*<sub>CP</sub> = 5.1 Hz, *C*-5'), 47.7 (*C*-a), 41.3 (*C*-2'), 21.0 (*C*-11), 9.3 (*C*-b).

<sup>31</sup>P-NMR (162 MHz, MeOD): δ [ppm] = 1.04 (s).

HRMS (ESI<sup>-</sup>):  $m/z$  calcd: 427.0773 [M-H]<sup>-</sup>, found: 427.0771.

**$\gamma$ -(C9C9AB)-MeTz-(E)-dUTP **187****



The reaction was carried out with the general procedure VIII with the pyrophosphate of **95** (122 mg, 130  $\mu$ mol), TFAA (90  $\mu$ L, 650  $\mu$ mol), and Et<sub>3</sub>N (145  $\mu$ L, 1.04 mmol) in CH<sub>3</sub>CN (5 ml). The subsequent activation step was performed with 1-methylimidazole (26  $\mu$ L, 325  $\mu$ mol) in DMF (3 ml), followed by the coupling with monophosphate **186** (1.1 TEAH, 35 mg, 65  $\mu$ mol) solved in DMF (2 mL). Purification on RP<sub>18</sub> silica gel with automated flash chromatography (H<sub>2</sub>O/CH<sub>3</sub>CN; 100:0 to 0:100), Dowex ion-exchange (NH<sub>4</sub><sup>+</sup>), and RP<sub>18</sub> silica gel with automated flash chromatography (H<sub>2</sub>O/CH<sub>3</sub>CN; 100:0 to 0:100) as well as subsequent freeze-drying provided **187** (20 mg, 27%) as red cotton.

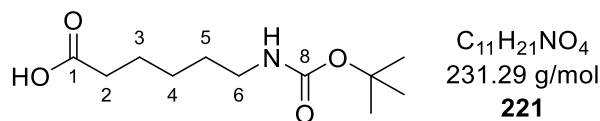
<sup>1</sup>H-NMR (400 MHz, MeOD):  $\delta$  [ppm] = 8.29 (s, 1H, H-6), 8.10 (s, 2H, H-6, H-7), 7.48 – 7.37 (m, 4H, 4x H-2''), 7.03 (m, 4H, 4x H-3''), 6.34 (m, 1H, H-1'), 5.20 (m, 4H, 2x H-5''), 4.68 – 4.60 (m, 1H, H-3'), 4.36 – 4.21 (m, 2H, H-5'), 4.14 – 4.08 (m, 1H, H-4'), 3.21 (q, <sup>3</sup>J<sub>HH</sub> = 7.3 Hz, 10H, HEt<sub>3</sub>N<sup>+</sup>), 2.93 (s, 3H, H-11), 2.59 (t, <sup>3</sup>J<sub>HH</sub> = 7.4 Hz, 4H, 2x H-b), 2.40 – 2.26 (m, 2H, H-2'), 1.81 – 1.69 (m, 4H, 2x H-c), 1.53 – 1.23 (m, 42H, 2x H-d-l, HEt<sub>3</sub>N<sup>+</sup>), 0.97 – 0.86 (m, 6H, 2x H-j).

<sup>31</sup>P-NMR (162 MHz, MeOD):  $\delta$  [ppm] = -11.67 (d, <sup>2</sup>J<sub>PP</sub> = 20.4 Hz, P- $\alpha$ ), -13.34 (d, <sup>2</sup>J<sub>PP</sub> = 17.7 Hz, P- $\gamma$ ), -23.95 (dd, <sup>2</sup>J<sub>PP</sub> = 20.5, 17.7 Hz, P- $\beta$ ).

HRMS (ESI<sup>-</sup>):  $m/z$  calcd: 1107.3652 [M-H]<sup>-</sup>, found: 1107.3271.

### 6.3.7 Preparation of the 3,6-di-2-pyridyl-1,2,4,5-tetrazine motifs

#### 6-((*Tert*-butoxycarbonyl)amino)hexanoic acid **221**



To an ice-cold solution of 6-aminohexanoic acid (787 mg, 6.00 mmol) and NaOH (240 mg, 6.00 mmol) in 1,4-dioxane and H<sub>2</sub>O (25 mL; 2:1 v/v) was added di-*tert*-butyl dicarbonate (1.44 g, 6.60 mmol). The reaction mixture was slowly warmed to room temperature and stirred for 3 h. After removing all volatiles under reduced pressure, the residue was solved in H<sub>2</sub>O, and the pH was adjusted to 4-5 with 1 N HCl. The aqueous solution was extracted twice with ethyl acetate. The combined organic layers were washed with brine, dried over Na<sub>2</sub>SO<sub>4</sub>, and concentrated under reduced pressure. The crude product was purified with automated flash chromatography (CH<sub>2</sub>Cl<sub>2</sub>/CH<sub>3</sub>OH; 99:1 to 96:4) to yield **221** (1.12 g, 81%) as a colorless solid. R<sub>f</sub>-value: 0.50 (CH<sub>2</sub>Cl<sub>2</sub>/CH<sub>3</sub>OH; 95:5).

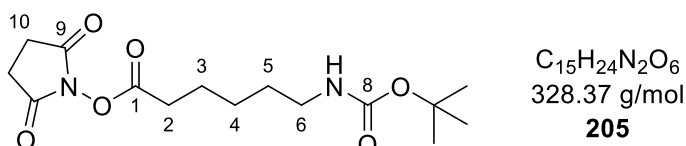
<sup>1</sup>H-NMR (600 MHz, CDCl<sub>3</sub>): δ [ppm] = 4.55 (s, 1H, NH), 3.13 – 3.09 (m, 2H, H-6), 2.35 (t, <sup>3</sup>J<sub>HH</sub> = 7.4 Hz, 2H, H-2), 1.69 – 1.60 (m, 2H, H-3), 1.53 – 1.46 (m, 2H, H-5), 1.44 (s, 9H, *t*Bu-CH<sub>3</sub>), 1.41 – 1.34 (m, 2H, H-4).

<sup>13</sup>C-NMR (151 MHz, CDCl<sub>3</sub>): δ [ppm] = 178.7 (COOH), 156.2 (C-8), 79.3 (C-(CH<sub>3</sub>)<sub>3</sub>), 40.5 (C-6), 33.9 (C-2), 29.9 (C-5), 28.6 (*t*Bu-CH<sub>3</sub>), 26.3 (C-4), 24.5 (C-3).

IR: ν [cm<sup>-1</sup>] = 3364, 2984, 2944, 2871, 1684, 1516, 1364, 1248, 1164, 995, 869, 636, 585, 484.

HRMS (ESI<sup>+</sup>): m/z = calcd for 254.1368 [M+Na]<sup>+</sup>, found: 254.1381.

#### 6-((*Tert*-butoxycarbonyl)amino)hexanoic acid *N*-hydroxysuccinimide ester **205**



To a solution of 6-((*tert*-butoxycarbonyl)amino)hexanoic acid **221** (231 mg, 1.00 mmol) and *N*-hydroxysuccinimide (115 mg, 1.00 mmol) in CH<sub>2</sub>Cl<sub>2</sub> (10 mL) was added EDC (288 mg, 1.50 mmol) at room temperature. After 4 h, the reaction mixture was diluted

with CH<sub>2</sub>Cl<sub>2</sub> (40 mL), washed twice with brine, and dried over Na<sub>2</sub>SO<sub>4</sub>. The removal of the solvent provided **205** (317 mg, 97%) as a colorless solid.

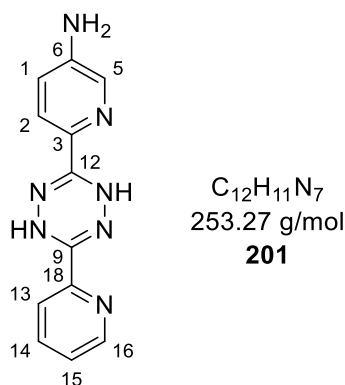
<sup>1</sup>H-NMR (400 MHz, CDCl<sub>3</sub>): δ [ppm] = 4.59 (s, 1H, NH), 3.11 (t, <sup>3</sup>J<sub>HH</sub> = 6.8 Hz, 2H, H-6), 2.85 – 2.77 (m, 4H, H-10), 2.60 (t, <sup>3</sup>J<sub>HH</sub> = 7.4 Hz, 2H, H-2), 1.80 – 1.70 (m, 2H, H-3), 1.57 – 1.34 (m, 13H, H-5, H-4, (tBu-(CH<sub>3</sub>)<sub>3</sub>).

<sup>13</sup>C-NMR (101 MHz, CDCl<sub>3</sub>): δ [ppm] = 169.3 (C-9), 168.6 (C-1), 156.1 (C-7), 79.2 (C-(CH<sub>3</sub>)<sub>3</sub>), 40.4 (C-6), 31.0 (C-2), 29.7 (C-5), 28.5 (tBu-CH<sub>3</sub>), 26.0 (C-4), 25.7 (C-10), 24.4 (C-3).

IR: ν [cm<sup>-1</sup>] = 3389, 2980, 2937, 2871, 1820, 1788, 1728, 1691, 1513.1363, 1249, 1211, 1169, 1059, 990, 864, 652, 407.

HRMS (ESI<sup>+</sup>): *m/z* = calcd: 351.1532 [M+Na]<sup>+</sup>, found: 351.1539.

#### 6-(6-(Pyridin-2-yl)-1,4-dihydro-1,2,4,5-tetrazin-3-yl)pyridin-3-amine **201**



The reaction was carried out as described in the literature with 5-amino-2-cyanopyridine (2.73 g, 22.9 mmol) and 2-cyanopyridine (2.38 g, 22.9 mmol) in 50% hydrazine hydrate (5.7 mL). The product **201** (1.50 g, 26%) was obtained as an orange solid after purification on silica gel (CH<sub>2</sub>Cl<sub>2</sub>/CH<sub>3</sub>OH; 98:2 to 95:5, dry load).

The analytical data was in accordance with those described.<sup>67</sup>

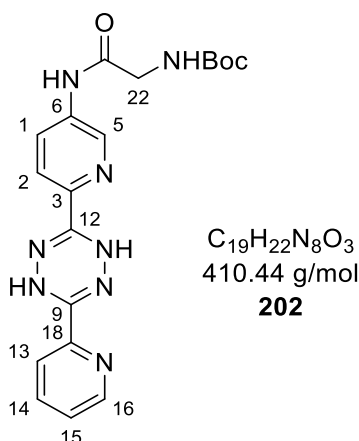
<sup>1</sup>H-NMR (400 MHz, DMSO-*d*<sub>6</sub>): δ [ppm] = 8.71 (s, 1H, dihydro-NH), 8.65 (s, 1H, dihydro-NH), 8.62 (ddd, <sup>3</sup>J<sub>HH</sub> = 4.9, <sup>4</sup>J<sub>HH</sub> = 1.7, <sup>5</sup>J<sub>HH</sub> = 1.0 Hz, 1H, H-16), 8.02 – 7.86 (m, 3H, H-5, H-13, H-15), 7.66 (dd, <sup>3</sup>J<sub>HH</sub> = 8.6, <sup>5</sup>J<sub>HH</sub> = 0.7 Hz, 1H, H-2), 7.51 (ddd, <sup>3</sup>J<sub>HH</sub> = 7.3, <sup>3</sup>J<sub>HH</sub> = 4.9, <sup>4</sup>J<sub>HH</sub> = 1.4 Hz, 1H, H-14), 7.00 (dd, <sup>3</sup>J<sub>HH</sub> = 8.6, <sup>4</sup>J<sub>HH</sub> = 2.7 Hz, 1H, H-1), 5.87 (s, 2H, NH<sub>2</sub>).

$^{13}\text{C}$ -NMR (101 MHz,  $\text{DMSO-}d_6$ ):  $\delta$  [ppm] = 148.5 (C-16), 147.5, 146.6, 146.6, 146.6 (C-6, C-9, C-12, C-18), 137.3 (C-15), 134.1, 134.1 (C-3, C-5), 125.1 (C-14), 121.8 (C-2), 120.8 (C-13), 120.3 (C-1).

HRMS (ESI<sup>+</sup>):  $m/z$  calcd: 254.1154 [M+H]<sup>+</sup>, found: 254.1053.

IR:  $\nu$  [cm<sup>-1</sup>] = 3459, 3325, 3051, 3011, 1565, 1423, 878, 838, 740, 667, 404.

**2-(Boc-amino)-N-(6-(6-(pyridin-2-yl)-1,4-dihydro-1,2,4,5-tetrazin-3-yl)pyridin-3-yl)acetamid **202****



The reaction was carried out as described in the literature with *N*-(*tert*-butoxycarbonyl)glycine (0.886 g, 5.06 mmol), *N*-methyl pyrrolidone (1.11 ml, 11.0 mmol), *isobutyl* chloroformate (571  $\mu\text{l}$ , 4.44 mmol) in THF (25 mL), and dihydrotetrazine **201** (557 mg, 2.20 mmol) solved in THF (15 mL). The product **202** (780 mg, 86%) was obtained as an orange solid after purification on silica gel ( $\text{CH}_2\text{Cl}_2/\text{CH}_3\text{OH}$ ; 99:1 to 95:5, dry load).

The analytical data was in accordance with those described.<sup>67</sup>

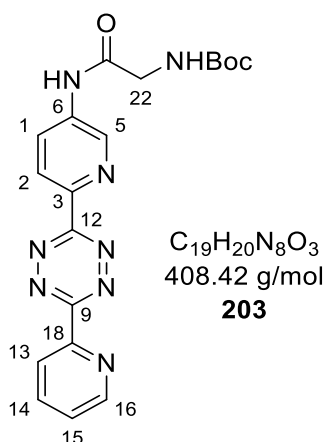
$^1\text{H}$ -NMR (400 MHz,  $\text{DMSO-}d_6$ ):  $\delta$  [ppm] = 10.40 (s, 1H, Tz-NH), 8.93 (s, 1H, H<sub>2</sub>Tz), 8.87 (s, 1H, H<sub>2</sub>Tz), 8.82 (d,  $^4J_{\text{HH}} = 2.4$  Hz, 1H, H-5), 8.63 (m, H-16), 8.15 (dd,  $^3J_{\text{HH}} = 8.7$  Hz,  $^4J_{\text{HH}} = 2.5$  Hz, 1H, H-1), 8.01 – 7.88 (m, 3H, H-2, H-13, H-15), 7.52 (ddd,  $^3J_{\text{HH}} = 7.3$ , 4.8 Hz,  $^4J_{\text{HH}} = 1.5$  Hz, 1H, H-14), 7.12 (t,  $^3J_{\text{HH}} = 6.1$  Hz, 1H, NHBoc), 3.78 (d,  $^3J_{\text{HH}} = 6.1$  Hz, 2H, H-22), 1.40 (s, 9H, BoC-CH<sub>3</sub>).

$^{13}\text{C}$ -NMR (101 MHz,  $\text{DMSO-}d_6$ ):  $\delta$  [ppm] = 169.1 (C-21), 155.9 (BoC-CO), 148.6 (C-16), 147.3 (C-9), 146.3 (C-12), 146.0 (C-18), 141.6 (C-3), 138.9 (C-5), 137.4 (C-15), 137.0 (C-6), 126.8 (C-1), 125.3 (C-14), 121.4 (C-13), 120.9 (C-2), 78.2 (BoC-C(CH<sub>3</sub>)<sub>3</sub>), 43.8 (C-22), 28.2 (BoC-CH<sub>3</sub>).



HRMS (ESI<sup>+</sup>):  $m/z$  calcd: 411.1888 [M+H]<sup>+</sup>, found: 411.1885.

**2-(Boc-amino)-N-(6-(6-(pyridin-2-yl)-1,2,4,5-tetrazin-3-yl)pyridin-3-yl)acetamide 203**



The reaction was carried out as described in the literature with dihydrotetrazine **202** (739 mg, 1.80 mmol) and phenyl iodonium diacetate (870 mg, 2.70 mmol) in  $CH_2Cl_2$  (25 mL) at room temperature overnight. The product **203** (566 mg, 77%) was obtained as an orange solid after purification on silica gel ( $CH_2Cl_2/CH_3OH$ ; 98:2 to 94:6, dry load).

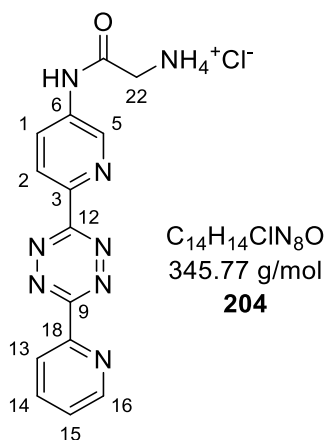
The analytical data was in accordance with those described.<sup>177</sup>

<sup>1</sup>H-NMR (400 MHz,  $DMSO-d_6$ ):  $\delta$  [ppm] = 10.62 (s, 1H, Tz-NH), 9.06 (d, <sup>4</sup> $J_{HH}$  = 2.7 Hz, 1H, H-5), 8.94 (ddd, <sup>3</sup> $J_{HH}$  = 4.7 Hz, <sup>4</sup> $J_{HH}$  = 1.8 Hz, <sup>5</sup> $J_{HH}$  = 0.9 Hz, 1H, H-16), 8.64 (d, <sup>3</sup> $J_{HH}$  = 8.7 Hz, 1H, H-2), 8.60 (dt, <sup>3</sup> $J_{HH}$  = 7.9 Hz, <sup>4</sup> $J_{HH}$  = 1.1 Hz, 1H, H-13), 8.43 (dd,  $J$  = 8.7 Hz, <sup>4</sup> $J_{HH}$  = 2.6 Hz, 1H, H-1), 8.16 (td, <sup>3</sup> $J_{HH}$  = 7.8 Hz, <sup>4</sup> $J_{HH}$  = 1.8 Hz, 1H, H-14), 7.73 (ddd, <sup>3</sup> $J_{HH}$  = 7.7, 4.7, <sup>4</sup> $J_{HH}$  = 1.2 Hz, 1H, H-15), 7.18 (t, <sup>3</sup> $J_{HH}$  = 6.1 Hz, 1H, NHBoc), 3.85 (d, <sup>3</sup> $J_{HH}$  = 6.1 Hz, 2H), 1.42 (s, 9H, BoC-CH<sub>3</sub>).

<sup>13</sup>C-NMR (101 MHz,  $DMSO-d_6$ ):  $\delta$  [ppm] = 170.0 (C-21), 163.5 (C-9), 163.2 (C-12), 156.4 (BoC-CO), 151.1 (C-16), 150.6 (C-18), 144.5 (C-6), 141.8 (C-5), 138.7 (C-3), 138.3 (C-14), 127.0 (C-15), 126.7 (C-1), 125.4 (C-2), 124.7 (C-13), 78.7 (BoC-C(CH<sub>3</sub>)<sub>3</sub>), 44.4 (C-22), 28.7 (BoC-CH<sub>3</sub>).

HRMS (ESI<sup>+</sup>):  $m/z$  calcd: 409.1737 [M+H]<sup>+</sup>, found: 409.1728.

IR:  $\nu$  [cm<sup>-1</sup>] = 3285, 3099, 2976, 2934, 1709, 1691, 1532, 1395, 1364, 1249, 1168.1050, 779, 590, 405.

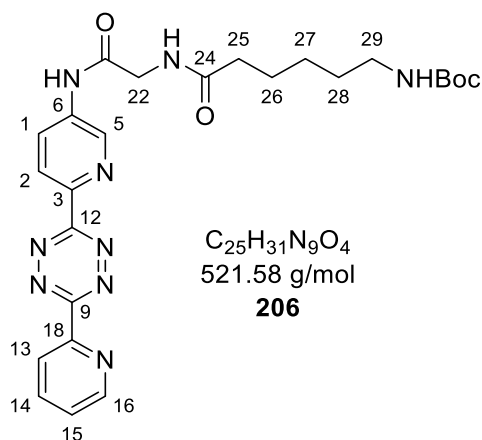
**2-Oxo-2-((6-(6-(pyridin-2-yl)-1,2,4,5-tetrazin-3-yl)pyridin-3-yl)amino)ethan-1-aminium chloride **204****

The reaction was carried out according to the literature with modifications. The tetrazine **203** (566 mg, 1.38 mmol) was solved in  $CH_2Cl_2$  (30 mL) and  $CH_3OH$  (10 mL) followed by the addition of 4 N HCl in 1,4-dioxane (13 mL). The reaction was stirred for 1 h at room temperature, and subsequent removal of all volatiles provided the compound **204** (476 mg, 100%) as HCl salt. The product was deemed pure enough for the next step.

The analytical data was in accordance with those described.<sup>67</sup>

$^1H$ -NMR (400 MHz,  $DMSO-d_6$ ):  $\delta$  [ppm] = 11.52 (s, 1H, Tz-NH), 9.15 (d,  $^4J_{HH} = 2.4$  Hz, 1H, H-5) 8.94 (ddd,  $^3J_{HH} = 4.8$  Hz,  $^4J_{HH} = 1.6$  Hz,  $^5J_{HH} = 0.9$  Hz, 1H, H-16), 8.69 (d,  $^3J_{HH} = 8.7$  Hz, 1H, H-2), 8.61 (dt,  $^3J_{HH} = 8.0$  Hz,  $^4J_{HH} = 1.1$  Hz, 1H, H-13), 8.44 (dd,  $J = 8.7$  Hz,  $^4J_{HH} = 2.5$  Hz, 1H, H-1), 8.33 (bs, 3H,  $NH_3$ ), 8.18 (td,  $^3J_{HH} = 7.8$  Hz,  $^4J_{HH} = 1.8$  Hz, 1H, H-14), 7.75 (ddd,  $^3J_{HH} = 7.7$ , 4.7,  $^4J_{HH} = 1.2$  Hz, 1H, H-15), 3.94 (q,  $^3J_{HH} = 5.4$  Hz, 2H, H-22).

**Tert-butyl(6-oxo-6-((2-oxo-2-((6-(6-(pyridin-2-yl)-1,2,4,5-tetrazin-3-yl)pyridin-3-yl)amino)ethyl)amino)hexyl)carbamate **206****



The tetrazine **204** (69 mg, 200  $\mu$ mol) and the NHS-ester **205** (72 mg, 220  $\mu$ mol) were dried *in vacuo* and suspended in DMF (5 mL) followed by the addition of Et<sub>3</sub>N (143  $\mu$ L, 880  $\mu$ mol). The reaction mixture was stirred for 2 h at room temperature. Upon consumption of starting material, the solvent was removed under reduced pressure, and the residue was purified on silica gel (CH<sub>2</sub>Cl<sub>2</sub>/CH<sub>3</sub>OH; 95:5) to yield **206** (73 mg, 70%) as a red solid. *R<sub>f</sub>*-value: 0.44 (CH<sub>2</sub>Cl<sub>2</sub>/CH<sub>3</sub>OH; 95:5).

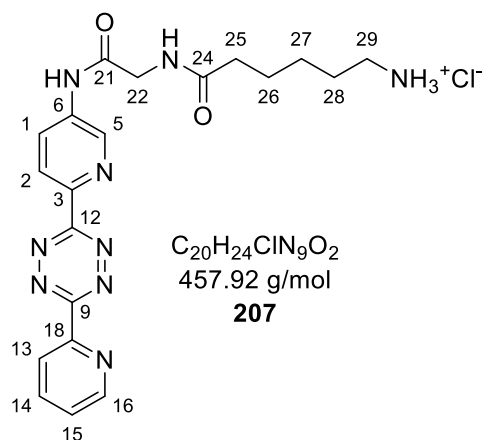
<sup>1</sup>H-NMR (500 MHz, DMSO-*d*<sub>6</sub>):  $\delta$  [ppm] = 10.65 (s, 1H, Tz-NH), 9.06 (d, <sup>4</sup>*J*<sub>HH</sub> = 2.5 Hz, 1H, H-5), 8.93 (ddd, <sup>3</sup>*J*<sub>HH</sub> = 4.8, <sup>4</sup>*J*<sub>HH</sub> = 1.7, <sup>5</sup>*J*<sub>HH</sub> = 0.9 Hz, 1H, H-16), 8.64 (d, <sup>3</sup>*J*<sub>HH</sub> = 8.6 Hz, 1H, H-2), 8.59 (dd, *J* = 7.9, <sup>4</sup>*J*<sub>HH</sub> = 1.1 Hz, 1H, H-13), 8.41 (dd, <sup>3</sup>*J*<sub>HH</sub> = 8.7, <sup>4</sup>*J*<sub>HH</sub> = 2.6 Hz, 1H, H-1), 8.24 (t, <sup>3</sup>*J*<sub>HH</sub> = 5.8 Hz, 1H, NH-23), 8.15 (td, <sup>3</sup>*J*<sub>HH</sub> = 7.7, <sup>4</sup>*J*<sub>HH</sub> = 1.8 Hz, 1H, H-14), 7.73 (ddd, <sup>3</sup>*J*<sub>HH</sub> = 7.6, <sup>3</sup>*J*<sub>HH</sub> = 4.7, <sup>4</sup>*J*<sub>HH</sub> = 1.2 Hz, 1H, H-15), 6.76 (t, <sup>3</sup>*J*<sub>HH</sub> = 5.8 Hz, 1H, NH-Boc), 3.97 (d, <sup>3</sup>*J*<sub>HH</sub> = 5.9 Hz, 2H, H-22), 2.90 (q, <sup>3</sup>*J*<sub>HH</sub> = 6.7 Hz, 2H, H-29), 2.17 (t, <sup>3</sup>*J*<sub>HH</sub> = 7.5 Hz, 2H, H-25), 1.52 (p, <sup>3</sup>*J*<sub>HH</sub> = 7.6 Hz, 2H, H-26), 1.42 – 1.33 (m, 11H, H-28, BoC-CH<sub>3</sub>), 1.25 (m, 2H, H-27).

<sup>13</sup>C-NMR (126 MHz, DMSO-*d*<sub>6</sub>):  $\delta$  [ppm] = 172.7 (C-21), 169.2 (C-24), 163.0 (C-9), 162.7 (C-12), 155.5 (CO-Boc), 150.6 (C-16), 150.2 (C-18), 144.0 (C-6), 141.3 (C-5), 138.2 (C-3), 137.7 (C-14), 126.5 (C-15), 126.3 (C-1), 124.9 (C-2), 124.2, 77.3, 42.7 (C-22), 35.0 (C-25), 29.3 (C-28), 28.3 (BoC-CH<sub>3</sub>), 26.0 (C-27), 24.9 (C-26).

HRMS (ESI<sup>+</sup>): *m/z* calcd: 522.2577 [M+H]<sup>+</sup>, found: 522.2560.

IR:  $\nu$  [cm<sup>-1</sup>] = 3311, 3102, 3067, 2932, 2862, 1716, 1683, 1642, 1521, 1394, 1250, 1171, 591, 401.

**6-oxo-6-((2-oxo-2-((6-(6-(pyridin-2-yl)-1,2,4,5-tetrazin-3-yl)pyridin-3-yl)amino)ethyl)amino)hexan-1-aminium chloride **207****



The tetrazine **206** (566 mg, 1.38 mmol) was suspended in  $CH_2Cl_2$  (6 mL) followed by the addition of 4 N HCl in 1,4-dioxane (900  $\mu$ L). The reaction was stirred for 1 h at room temperature, and subsequent removal of all volatiles and subsequent freeze-drying resulted in the HCl salt **207** (55 mg, 100%). The product was deemed pure enough for the next step.

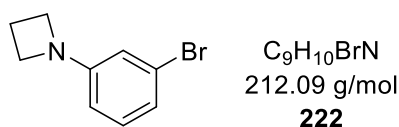
$^1H$ -NMR (600 MHz,  $DMSO-d_6$ ):  $\delta$  [ppm] = 10.90 (s, 1H, Tz-NH), 9.13 (d,  $^4J_{HH} = 2.5$  Hz, 1H, H-5), 8.94 (dt,  $^3J_{HH} = 4.6$  Hz,  $^4J_{HH} = 1.4$  Hz, 1H, H-16), 8.64 (d,  $^3J_{HH} = 8.6$  Hz, 1H, H-2), 8.61 (dt,  $^3J_{HH} = 7.9$  Hz,  $^4J_{HH} = 1.1$  Hz, 1H, H-13), 8.43 (dd,  $^3J_{HH} = 8.7$  Hz,  $^4J_{HH} = 2.5$  Hz, 1H, H-1), 8.32 (t,  $^3J_{HH} = 5.9$  Hz, 1H, NH-23), 8.18 (td,  $^3J_{HH} = 7.7$  Hz,  $^4J_{HH} = 1.8$  Hz, 1H, H-14), 7.93 (m, 2H,  $NH_2$ ), 7.75 (ddd,  $^3J_{HH} = 7.6$  Hz,  $^3J_{HH} = 4.7$  Hz,  $^4J_{HH} = 1.2$  Hz, 1H, H-15), 4.00 (d,  $^3J_{HH} = 5.1$  Hz, 2H, H-22), 2.82 – 2.71 (m, 2H, H-29), 2.20 (,  $^3J_{HH} = 7.4$  Hz, 2H, H-25), 1.61 – 1.51 (m, 4H, H-26, H-28), 1.34 (m, 2H, H-27).

$^{13}C$ -NMR (126 MHz,  $DMSO-d_6$ ):  $\delta$  [ppm] = 172.6 (C-21), 169.2 (C-24), 163.0 (C-9), 162.7 (C-12), 150.6 (C-16), 150.2 (C-18), 144.0 (C-6), 141.3 (C-5), 138.2 (C-3), 137.8 (C-14), 126.6 (C-15), 126.3 (C-1), 124.9 (C-2), 124.2 (C-3), 42.8 (C-22), 38.7 (C-29), 34.8 (C-25), 26.7 (C-28), 25.4 (C-27), 24.6 (C-26).

HRMS (ESI<sup>+</sup>):  $m/z$  calcd: 422.2047 [M+H]<sup>+</sup>, found: 422.2283.

### 6.3.8 Preparation of rhodamine-tetrazine-conjugates

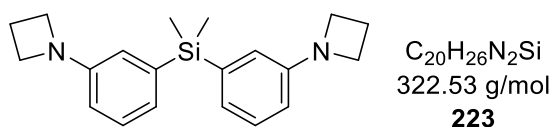
#### 1-(3-Bromophenyl)azetidide **222**



The reaction was carried out as described in the literature with 3-bromoiodobenzene (2.68 mL, 21.0 mmol), ethylene glycol (2.82 mL, 50.4 mmol), azetidide (1.69 mL, 25.2 mmol), copper(I) iodide (400 mg, 2.10 mmol) and  $K_3PO_4$  (13.4 g, 63.0 mmol) in 1-butanol (30 mL) at 100 °C overnight. The aniline **222** (3.40 g, 76%) was obtained as a colorless oil after purification on silica gel (petroleum ether/diethyl ether; 100:0 to 90:10).

The analytical data was in accordance with those described.<sup>175</sup>

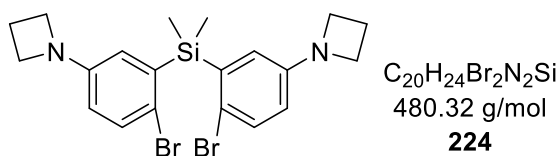
#### Bis(3-(azetidide-1-yl)phenyl)dimethylsilane **223**



The reaction was carried out as described in the literature with aniline **222** (5.51 g, 26.0 mmol), *n*-BuLi (1.6 M in hexanes, 16.3 mL, 26.0 mmol), and dichlorodimethylsilane (1.31 mL, 10.8 mmol) in THF (55 mL). The silane **223** (3.50 g, 100%) was obtained as a colorless oil after purification on silica gel (petroleum ether/diethyl ether; 100:0 to 70:30).

The analytical data was in accordance with those described.<sup>175</sup>

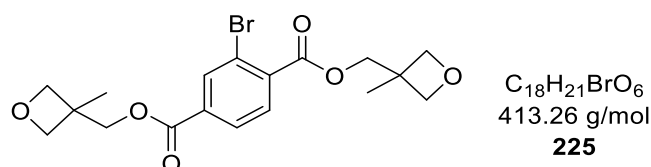
#### Bis(5-(azetidide-1-yl)-2-bromophenyl)dimethylsilane **224**



The reaction was carried out as described in the literature with silane **223** (3.77 g, 11.7 mmol) and *N*-bromosuccinimide (4.17 g, 23.4 mmol) in DMF (50 mL) at room temperature for 3 days. The silane **224** (5.62 g, 100%) was obtained as a colorless oil after purification on silica gel (petroleum ether/diethyl ether; 100:0 to 70:30).

The analytical data was in accordance with those described.<sup>175</sup>

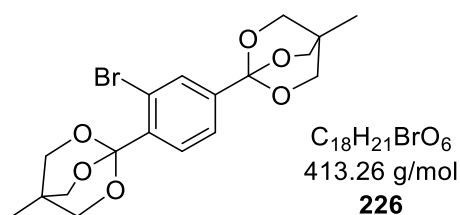
### Bis((3-methyloxetan-3-yl)methyl) 2-bromoterephthalate **225**



The reaction was carried out as described in the literature with 2-bromoterephthalic acid (4.17 g, 17.0 mmol), thionyl chloride (4.94 mL, 68.0 mmol), DMF (1 drop), and in the following step with 3-methyl-3-oxetanemethanol (6.78 mL, 68.0 mmol) and pyridine (10.96 mL, 136.0 mmol) in  $CH_2Cl_2$  (40 mL). The terephthalate **225** (6.60 g, 94%) was obtained as a colorless oil after purification on silica gel (petroleum ether/ethyl acetate; 50:50).

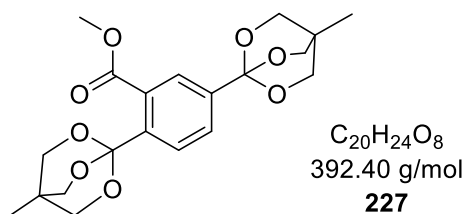
The analytical data was in accordance with those described.<sup>175</sup>

### 1,1'-(2-Bromo-1,4-phenylene)bis(4-methyl-2,6,7-trioxabicyclo[2.2.2]octane) **226**



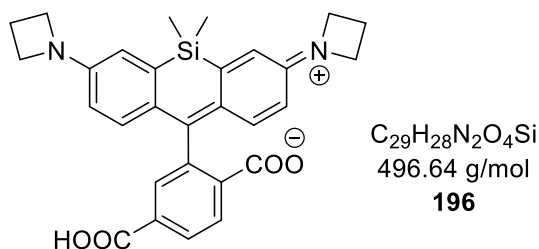
The reaction was carried out as described in the literature with terephthalate **225** (3.97 g, 9.60 mmol),  $BF_3 \cdot OEt_2$  (592  $\mu$ L, 4.80 mmol) and  $Et_3N$  (4 mL) in  $CH_2Cl_2$  (40 mL). The bromide **226** (2.00 g, 50%) was obtained as a colorless solid after purification on silica gel (petroleum ether/ethyl acetate; 100:0 to 80:20 with constant 40% ( $CH_2Cl_2$  + 1%  $Et_3N$ )).

The analytical data was in accordance with those described.<sup>175</sup>

**Methyl 2,5-bis(4-methyl-2,6,7-trioxabicyclo[2.2.2]octan-1-yl)benzoate **227****

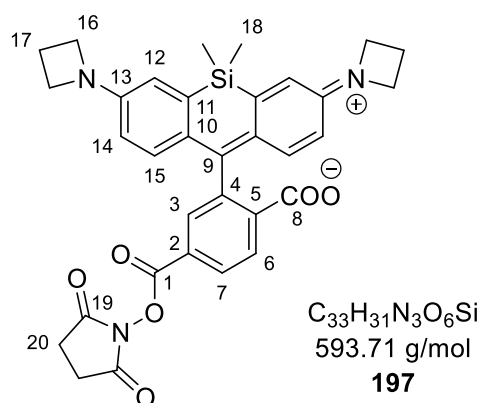
The reaction was carried out as described in the literature with bromide **226** (909 mg, 2.20 mmol), *n*-BuLi (1.6 M in hexanes, 2.06 mL, 3.30 mmol), and methyl chloroformate (340  $\mu$ L, 4.40 mmol) in THF (25 mL). The methyl benzoate **227** (709 mg, 82%) was obtained as a colorless solid after purification on silica gel (petroleum ether/ethyl acetate; 100:0 to 50:50 with constant 40% ( $CH_2Cl_2$  + 1%  $Et_3N$ )).

The analytical data was in accordance with those described.<sup>175</sup>

**Azetidine-SiR-COOH **196****

The reaction was carried out as described in the literature with dibromide **224** (600 mg, 1.25 mmol) in THF (30 mL), *tert*-butyllithium (1.6 M in hexanes, 3.12 mL, 5.00 mmol) and a solution of ester **227** (327 mg, 0.833 mmol) in THF (15 mL). The intermediate product (502 mg, 680  $\mu$ mol, 82%) was purified on silica gel ( $CH_2Cl_2/CH_3OH$ ; 99:1 to 80:20 + 1% AcOH). The diester was treated with 25% w/v NaOH (1.5 mL) in 2,2,2-trifluoroethanol (4.5 mL). The silicon rhodamine **196** was (200 mg, 48% over both steps) was obtained as a blue solid after purification on silica gel (petroleum ether/ethyl acetate; 90:10 to 40:60 + 1% AcOH).

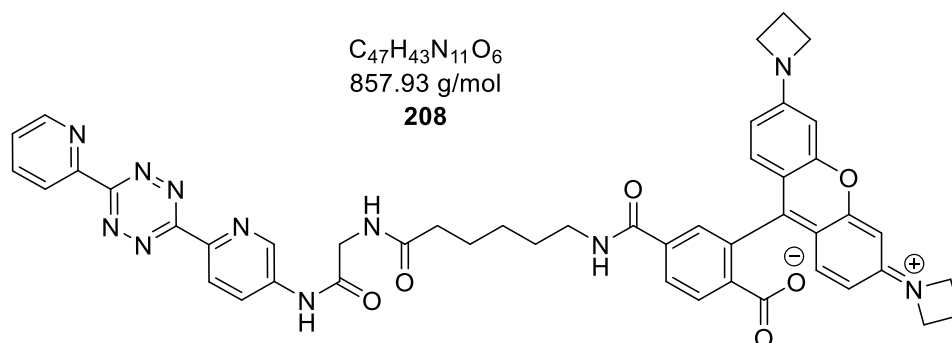
The analytical data was in accordance with those described.<sup>175</sup>

Azetidine-SiR-NHS ester **197**

Azetidine-SiR-COOH **196** (99 mg, 200  $\mu$ mol) and DMAP (4.9 mg, 40  $\mu$ mol) were dried *in vacuo* shortly and solved in DMF (3 mL). After adding  $Et_3N$  (84  $\mu$ L, 600  $\mu$ mol) and disuccinimidyl carbonate (62 mg, 240  $\mu$ mol), the reaction mixture was stirred at room temperature for 2 h. Subsequently, all volatiles were removed under reduced pressure, and the resulting residue was purified on silica gel ( $CH_2Cl_2/CH_3OH$ ; 95:5 + 1% AcOH), affording NHS ester **197** (80 mg, 67%) as a blue solid.

$^1H$ -NMR (300 MHz,  $CDCl_3$ ):  $\delta$  [ppm] = 8.28 (dd,  $^3J_{HH} = 8.0$  Hz,  $^4J_{HH} = 1.4$  Hz, 1H, *H*-7), 8.07 (dd,  $^3J_{HH} = 8.0$  Hz,  $^4J_{HH} = 0.8$  Hz, 1H, *H*-6), 8.00 (d,  $^4J_{HH} = 1.1$  Hz, 1H, *H*-3), 6.74 (d,  $^3J_{HH} = 8.7$  Hz, 2H, *H*-15), 6.66 (d,  $^4J_{HH} = 2.6$  Hz, 2H, *H*-12), 6.30 (dd,  $^3J_{HH} = 8.7$  Hz,  $^4J_{HH} = 2.6$  Hz, 2H, *H*-14), 3.91 (t,  $^3J_{HH} = 7.3$  Hz, 8H, *H*-16), 2.90 (s, 4H, *H*-20), 2.37 (m, 4H, *H*-17), 0.62 (s, 3H, *H*-18), 0.56 (s, 3H, *H*-18).

HRMS (ESI<sup>+</sup>): *m/z* calcd: 594.2060 [M+H]<sup>+</sup>, found: 594.2064.

JaneliaFluor549-Py<sub>2</sub>Tz **208**

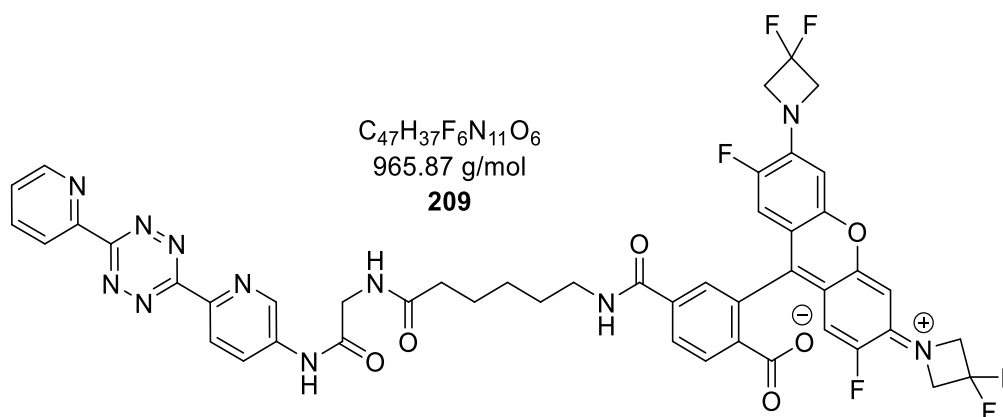
The HCl salt **207** (3.4 mg, 7.4  $\mu$ mol) was solved in DMSO (0.3 mL) followed by the addition of DIPEA (4.0  $\mu$ L, 22  $\mu$ mol). The resulting solution was added to the vial of the commercially available JF549-NHS ester (2.0 mg, 3.7  $\mu$ mol) and was shaken for 4 h at



room temperature until the complete conversion of starting material was achieved (TLC monitoring, CH<sub>2</sub>Cl<sub>2</sub>:CH<sub>3</sub>OH; 8:2 v/v + 5% AcOH). The solvent was removed under reduced pressure at 50 °C, and the crude product was purified by preparative TLC (CH<sub>2</sub>Cl<sub>2</sub>/CH<sub>3</sub>OH; 95:5 + 5% AcOH, thickness: 1 mm). After scraping the appropriate fraction from the pTLC, the product was flushed from the silica gel using CH<sub>3</sub>OH, and the resulting solution was filtered through a syringe filter. The removal of the solvent under reduced pressure resulted in JF549-Py<sub>2</sub>Tz **208** (2.0 mg, 63%) as a dark pink solid.

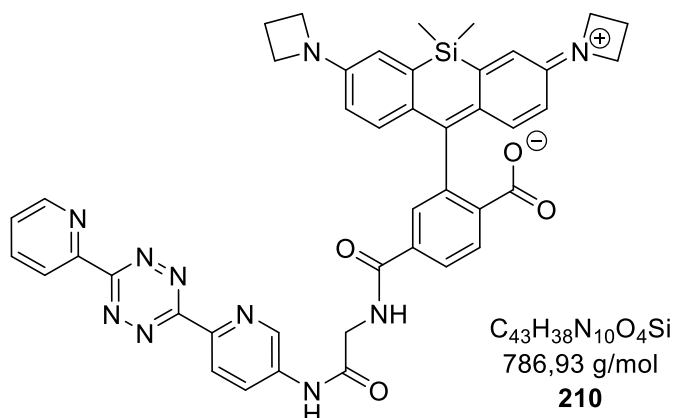
HRMS (ESI<sup>-</sup>):  $m/z$  = calcd: 856.3325 [M-H]<sup>-</sup>, found: 856.3254 [M-H]<sup>-</sup>.

### JaneliaFluor526-Py<sub>2</sub>Tz **209**



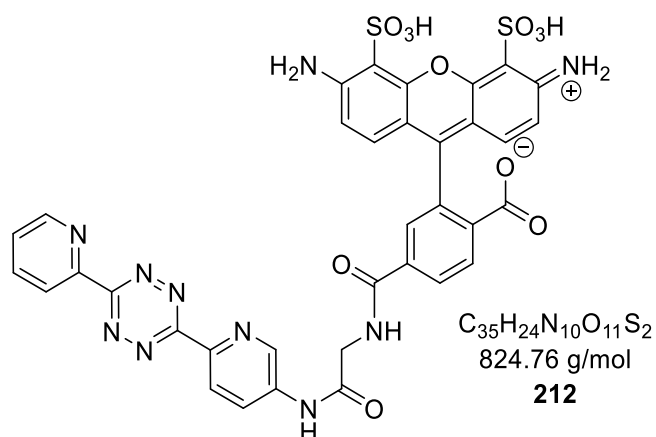
The HCl salt **207** (0.8 mg, 2.3 μmol) was solved in DMSO (0.5 mL) followed by the addition of Et<sub>3</sub>N (1.0 μL, 7.5 μmol). The resulting solution was added to the vial of the commercially available JF526-NHS ester (1.0 mg, 1.5 μmol) and was shaken for 2 h at room temperature. The solvent was removed under reduced pressure at 50 °C, and the crude product was purified by preparative TLC (CH<sub>2</sub>Cl<sub>2</sub>/CH<sub>3</sub>OH; 95:5 + 5% AcOH, thickness: 1 mm). After scraping the appropriate fraction from the pTLC, the product was flushed from the silica gel using CH<sub>3</sub>OH, and the resulting solution was filtered through a syringe filter. The removal of the solvent under reduced pressure resulted in JF526-Py<sub>2</sub>Tz **209** (1.0 mg, 78%) as a pink solid.

HRMS (ESI<sup>-</sup>):  $m/z$  = calcd: 851.1919 [M-H]<sup>-</sup>, found: 851.1907 [M-H]<sup>-</sup>.

**Siliconrhodamine-Py<sub>2</sub>Tz 210**

In an Eppendorf Tube, siliconrhodamine **196** (12.4 mg, 25  $\mu$ mol), the HCl salt **204** (12.9 mg, 38  $\mu$ mol) and HATU (12.4 mg, 33  $\mu$ mol) were dissolved in DMF (0.5 mL). After adding Et<sub>3</sub>N (17  $\mu$ L, 125  $\mu$ mol), the tube was sealed and placed in a sonicator for 1 h to improve the solubility. Subsequently, the tube was transferred to an incubator set to 37 °C for an additional hour. The solvent was removed under reduced pressure at 50 °C, and the crude product was purified by preparative TLC (CH<sub>2</sub>Cl<sub>2</sub>/CH<sub>3</sub>OH; 95:5 to 80:20 + 5% AcOH, thickness: 1 mm). After scraping the appropriate fraction from the pTLC, the product was flushed from the silica gel using CH<sub>3</sub>OH, and the resulting solution was filtered through a syringe filter. The removal of the solvent under reduced pressure resulted in the SiR-Py<sub>2</sub>Tz **210** (7.4 mg, 38%) as a blue solid.

**HRMS (ESI<sup>-</sup>):**  $m/z$  = calcd: 785.2774 [M-H]<sup>-</sup>; found: 785.2633 [M-H]<sup>-</sup>.

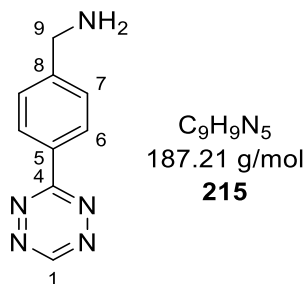
**AlexaFluor488-Py<sub>2</sub>Tz 212**

AlexaFluor488-NHS ester **211** (5.0 mg, 6.0  $\mu$ mol) and the HCl salt **204** (4.1 mg, 12  $\mu$ mol) were combined in a vial and solved in DMSO (0.5 mL). After adding Et<sub>3</sub>N (4.1  $\mu$ L, 30  $\mu$ mol), the vial was sealed and sonicated for 2 h at 30-40 °C. All volatiles were

removed *in vacuo* at 50 °C and the crude product was purified on RP<sub>18</sub> silica gel using automated flash chromatography (H<sub>2</sub>O/CH<sub>3</sub>CN; 100:0 to 0:100) to yield the AF488-Py<sub>2</sub>Tz **212** (3.0 mg, 61%) as a colorless solid

**HRMS (ESI):**  $m/z$  = calcd: 823.0995 [M-H]<sup>-</sup>, found: 823.0768 [M-H]<sup>-</sup>.

#### (4-(1,2,4,5-Tetrazin-3-yl)phenyl)methanamine **215**

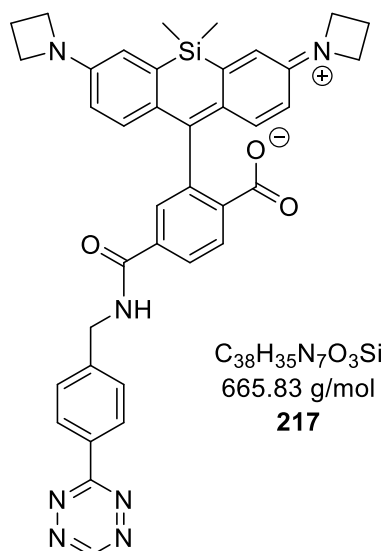


4-(Aminomethyl)benzotrile hydrochloride (0.506 g, 3.00 mmol), formamidinium acetate (3.12 g, 30.0 mmol), and Zn(OTf)<sub>2</sub> (654 mg, 1.80 mmol) were suspended in ethanol (9 ml). Hydrazine-hydrate (51%, 8 mL) was added slowly, and the reaction mixture was stirred for 72 hours at room temperature. Then, 1 N HCl (120 mL) was added slowly under ice bath cooling, followed by the addition of NaNO<sub>2</sub> (2.07 g, 30.0 mmol). Under cooling, the pH value was set to 2 with 1 N HCl. The solution was stirred for 1 h and then concentrated *in vacuo*. The resulting residue was taken up in water, filtrated over cotton to remove excess of salt, and purified on RP<sub>18</sub> silica gel with automated flash chromatography (H<sub>2</sub>O/CH<sub>3</sub>CN; 100:0 to 0:100) to provide **215** (99 mg, 18%) as a pink solid.

<sup>1</sup>H-NMR (400 MHz, D<sub>2</sub>O):  $\delta$  [ppm] = 10.42 (s, 1H, H-1), 8.56 – 8.49 (m, 2H, H-6), 7.78 – 7.70 (m, 2H, H-7), 4.35 (s, 2H, H-9).

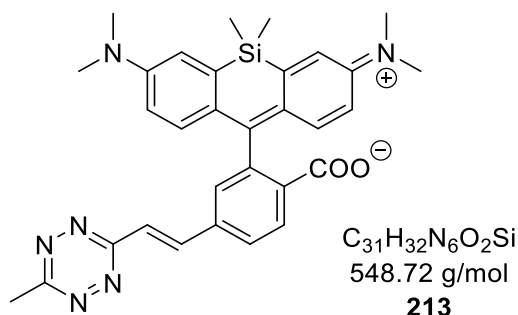
<sup>13</sup>C-NMR (101 MHz, D<sub>2</sub>O):  $\delta$  [ppm] = 166.2 (C-4), 157.5 (C-1), 137.5 (C-8), 132.0 (C-5), 129.7 (C-7), 128.9 (C-6), 42.7 (C-9).

MS (EI<sup>+</sup>):  $m/z$  calcd: 187.09 [M+H]<sup>+</sup>, found: 187.12.

**Siliconrhodamine-BzTz 217**

Azetidine-SiR-NHS **197** (5.9 mg, 10  $\mu$ mol) and (4-(1,2,4,5-tetrazin-3-yl)phenyl)methanamine **215** (2.9 mg, 13  $\mu$ mol) were added to a vial and solved in DMSO (0.3 mL). After adding Et<sub>3</sub>N (4.2  $\mu$ L, 30  $\mu$ mol), the vial was sealed and sonicated for 2 h at 30-40 °C. All volatiles were removed *in vacuo* at 50 °C and the crude product was purified by preparative TLC (CH<sub>2</sub>Cl<sub>2</sub>/CH<sub>3</sub>OH; 95:5 + 5% AcOH, thickness: 1 mm). After scraping the appropriate fraction from the pTLC, the product was flushed from the silica gel using CH<sub>3</sub>OH, and the resulting solution was filtered through a syringe filter. The removal of the solvent under reduced pressure resulted in the SiR-BzTz **217** (5.0 mg, 75%) as a light-blue solid.

HRMS (ESI<sup>+</sup>): *m/z* calcd: 666.2664 [M+H]<sup>+</sup>, found: 666.2643.

**Siliconrhodamine-(E)-MeTz 213**

The reaction was carried out according to the literature with minor modifications: 6'-bromo-3,7-bis(dimethylamino)-5,5-dimethyl-3'*H*,5*H*-spiro[dibenzo[b,e]siline-10,1'-isobenzofuran]-3'-one **214** (31 mg, 60  $\mu$ mol), 2-(6-methyl-1,2,4,5-tetrazin-3-yl)ethyl methanesulfonate **190** (16 mg, 72  $\mu$ mol), *N,N*-dicyclohexylmethylamine (51  $\mu$ L,

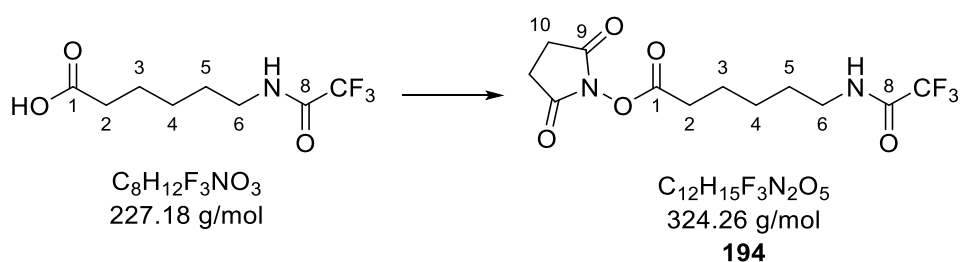
240  $\mu\text{mol}$ ),  $\text{Pd}_2(\text{dba})_3$  (5.5 mg, 6  $\mu\text{mol}$ , 10 mol%), and QPhos (17 mg, 24  $\mu\text{mol}$ , 40 mol%) in DMF (3 mL). The SiR **213** (13 mg, 44%) was obtained as a blue solid after purification by preparative TLC (petroleum ether/ethyl acetate; 50:50).

HRMS (ESI<sup>+</sup>):  $m/z$  calcd: 549.2429 [M+H]<sup>+</sup>, found: 549.2434.

The analytical data was in accordance with those described.<sup>171</sup>

### 6.3.9 Preparation of $\gamma$ -(C9C9AB)-SiR-dCTP

#### 6-(Trifluoroacetamido)hexanoic acid *N*-hydroxysuccinimide ester **194**



6-Aminohexanoic acid (6.56 g, 5.00 mmol) was suspended in  $\text{CH}_3\text{OH}$  (65 mL) under gentle heating, followed by the addition of  $\text{Et}_3\text{N}$  (34.9 mL, 25.0 mmol). Then, ethyl trifluoroacetate (8.92 mL, 7.50 mmol) was added dropwise to the suspension at room temperature, and the resulting solution was stirred overnight. After removing all volatiles under reduced pressure, the resulting residue was dissolved in ethyl acetate, washed three times with 1 N HCl, and dried over  $\text{Na}_2\text{SO}_4$ . After removing the solvent *in vacuo*, the crude product was purified by recrystallization from  $\text{Et}_2\text{O}$  to yield **228** (8.60 g, 76%) as a colorless solid.

<sup>1</sup>H-NMR (500 MHz,  $\text{DMSO}-d_6$ ):  $\delta$  [ppm] = 11.98 (s, 1H, COOH), 9.38 (t, <sup>3</sup> $J_{\text{HH}}$  = 5.7 Hz, 1H, NH), 3.16 (q, <sup>3</sup> $J_{\text{HH}}$  = 6.7 Hz, 2H, H-6), 2.19 (t, <sup>3</sup> $J_{\text{HH}}$  = 7.4 Hz, 2H, H-2), 1.56 – 1.43 (m, 4H, H-3, H-5), 1.30 – 1.22 (m, 2H, H-4).

<sup>13</sup>C-NMR (126 MHz,  $\text{DMSO}-d_6$ ):  $\delta$  [ppm] = 174.4 (C-1), 156.1 (q, <sup>2</sup> $J_{\text{CF}}$  = 35.9 Hz, C-8), 116.0 (q, <sup>1</sup> $J_{\text{CF}}$  = 288.4 Hz,  $\text{CF}_3$ ), 33.5 (C-2), 27.9 (C-5), 25.7 (C-4), 24.1 (C-3).

To a solution of acid **228** (1.14 g, 5.00 mmol) and pyridine (807  $\mu\text{L}$ , 10.0 mmol) in  $\text{CH}_3\text{CN}$  (7 mL) was added disuccinimidyl carbonate (1.54 g, 6.00 mmol). The resulting suspension was stirred overnight at room temperature, during which time a solution formed, which was diluted with ethyl acetate, washed twice with 1 N HCl, twice with

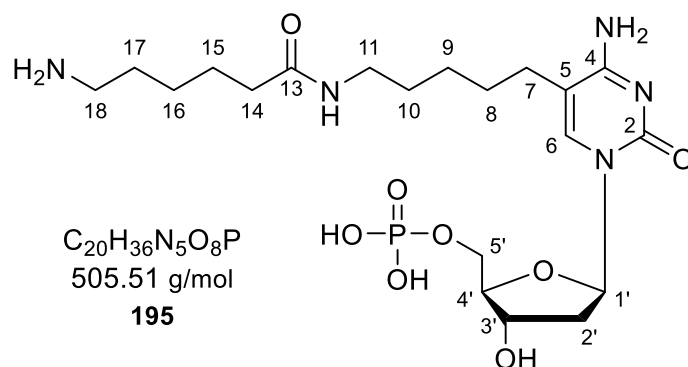
sat. aq. NaHCO<sub>3</sub> and dried over Na<sub>2</sub>SO<sub>4</sub>. The removal of the solvent *in vacuo* provided **194** (1.62 g, 100%) as a colorless solid.

<sup>1</sup>H-NMR (500 MHz, DMSO-*d*<sub>6</sub>): δ [ppm] = 9.39 (t, <sup>3</sup>J<sub>HH</sub> = 5.8 Hz, 1H, NH), 3.17 (q, <sup>3</sup>J<sub>HH</sub> = 6.7 Hz, 2H, H-6), 2.81 (s, 4H, H-10), 2.67 (t, <sup>3</sup>J<sub>HH</sub> = 7.3 Hz, 2H, H-2), 1.63 (p, <sup>3</sup>J<sub>HH</sub> = 7.4 Hz, 2H, H-3), 1.56 – 1.46 (m, 2H, H-5), 1.40 – 1.31 (m, 2H, H-4).

<sup>13</sup>C-NMR (126 MHz, DMSO-*d*<sub>6</sub>): δ [ppm] = 170.2 (C-9), 168.9 (C-1), 156.1 (q, <sup>2</sup>J<sub>CF</sub> = 36.1 Hz, C-8), 117.3 – 114.5 (m, CF<sub>3</sub>), 30.0 (C-2), 27.7 (C-5), 25.4 (C-10), 25.2 (C-4), 23.8 (C-3).

HRMS (ESI<sup>+</sup>): *m/z* = calcd: 347.0825 [M+Na]<sup>+</sup>, found: 347.0850.

### 5-(4-Amino-5-(5-(6-aminohexanamido)pentyl)-2'-deoxycytidine monophosphate **195**



The monophosphate triethylammonium salt **156** (1.0 TEAH, 148 mg, 300 μmol) and the NHS-ester **194** (127 mg, 390 μmol) were dried *in vacuo* and suspended in DMSO (3 mL) followed by the addition of Et<sub>3</sub>N (84 μL, 600 μmol). The resulting solution was stirred at 50 °C. After 2 h TLC (H<sub>2</sub>O/CH<sub>3</sub>CN; 3:7) showed complete conversion of starting material, and the excess of Et<sub>3</sub>N was removed *in vacuo*. Then, 25% aq. ammonia hydroxide solution (10 mL) was added, and the reaction mixture was stirred overnight at room temperature. The ammonia hydroxide solution was removed under reduced pressure, followed by the slow addition of acetone to the remaining DMSO solution. The precipitate was dissolved in DMF (1 mL) and precipitated again with diethyl ether. The crude product was collected by centrifugation, dissolved in 0.05 M TEAB, and purified on RP<sub>18</sub> silica gel using automated flash chromatography (0.05 M TEAB/CH<sub>3</sub>CN; 100:0 to 0:100) to yield the TEAH salt of **195** (178 mg, 92%) as a colorless solid. Note: Extensive co-evaporation after column chromatography leads to the loss of all TEAH counter ions potentially due to the intracellular primary amine function.

<sup>1</sup>H-NMR (500 MHz, D<sub>2</sub>O): δ [ppm] = 7.66 (s, 1H, H-6), 6.32 (dd, <sup>3</sup>J<sub>HH</sub> = 7.6, 6.2 Hz, 1H, H-1'), 4.59 – 4.49 (m, 1H, H-3'), 4.18 – 4.09 (m, 1H, H-4'), 3.99 – 3.88 (m, 2H, H-5'), 3.28

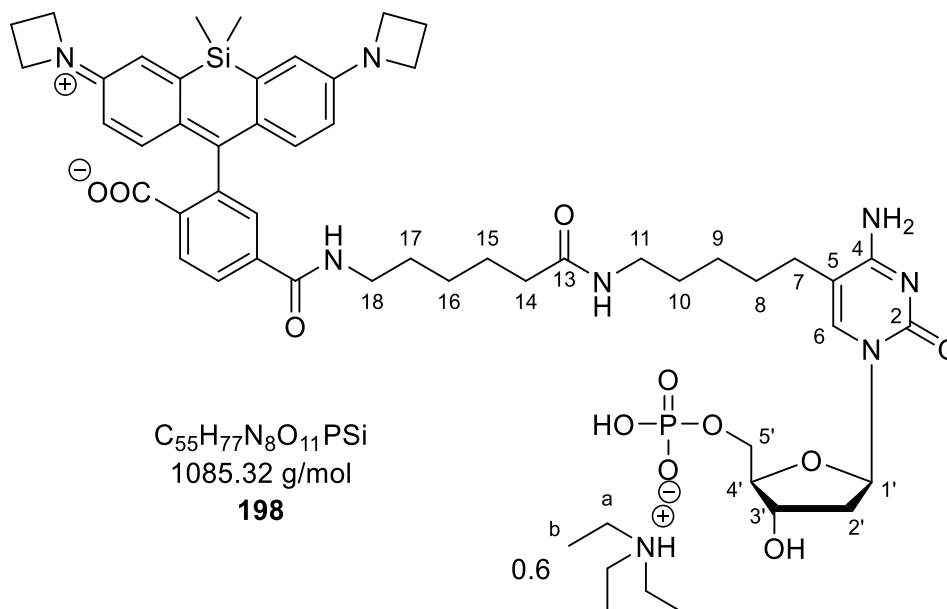
– 3.08 (m, 2H, *H*-11), 3.01 – 2.93 (m, 2H, *H*-18), 2.43 (t,  $^3J_{\text{HH}} = 7.3$  Hz, 2H, *H*-7), 2.42 – 2.28 (m, 2H, *H*-2'), 2.23 (t,  $^3J_{\text{HH}} = 7.4$  Hz, 2H, *H*-14), 1.71 – 1.60 (m, 2H, *H*-15), 1.63 – 1.49 (m, 6H, *H*-8, *H*-10, *H*-17), 1.40 – 1.26 (m, 4H, *H*-9, *H*-16).

$^{13}\text{C}$ -NMR (126 MHz,  $\text{D}_2\text{O}$ ):  $\delta$  [ppm] = 176.9 (*C*-13), 165.8 (*C*-4), 157.6 (*C*-2), 139.2 (*C*-6), 109.1 (*C*-5), 86.2 (d,  $^3J_{\text{CP}} = 8.1$  Hz, *C*-4'), 86.0 (*C*-1'), 71.6 (*C*-3'), 64.1 (d,  $^2J_{\text{CP}} = 4.5$  Hz, *C*-5'), 39.6 (*C*-18), 39.4 (*C*-11), 39.1 (*C*-2'), 35.8 (*C*-14), 28.3 (*C*-10), 27.1 (*C*-7), 26.9 (*C*-15), 26.8 (*C*-8), 25.6 (*C*-9), 25.4 (*C*-16), 25.3 (*C*-17).

$^{31}\text{P}$ -NMR (202 MHz,  $\text{D}_2\text{O}$ ):  $\delta$  [ppm] = 5.19 (s).

HRMS (ESI $^-$ ):  $m/z$  = calcd: 504.2229 [*M*-H] $^-$ , found: 504.2066 [*M*-H] $^-$ .

### (SiR)-2'-deoxycytidine monophosphate **198**



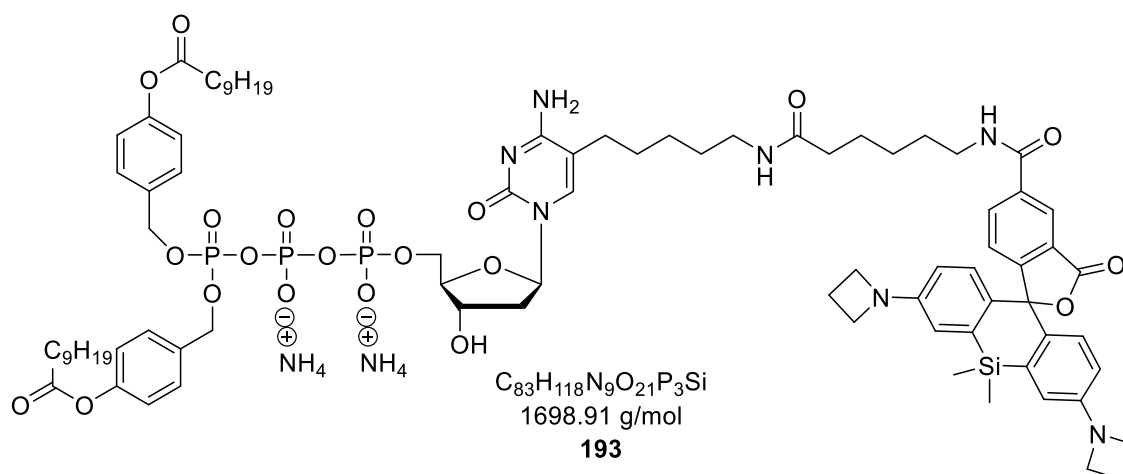
The TEAH salt of **195** (1.4 TEAH, 19 mg, 30  $\mu\text{mol}$ ) and the SiR-NHS active ester **197** (20 mg, 33  $\mu\text{mol}$ ) were solved in DMF (2 mL) under the addition of a few drops of triethylamine. The reaction mixture was stirred for 2 h at room temperature (complete conversion was controlled by TLC ( $\text{H}_2\text{O}/\text{CH}_3\text{CN}$ ; 3:7)). All volatiles were removed under reduced pressure, and the crude product was purified on normal phase silica gel ( $\text{H}_2\text{O}/\text{CH}_3\text{CN}$ ; 5:95 to 20:80). The appropriate fractions were collected, treated with triethylamine (1 mL), and filtered through a syringe filter to remove traces of silica. The removal of all volatiles provided the TEAH salt of SiR-dCMP **198** (17 mg, 60%) as a blue solid.

$^1\text{H-NMR}$  (500 MHz,  $\text{D}_2\text{O}$ ):  $\delta$  [ppm] = 7.95 – 7.86 (m, 2H, SiR-arom.), 7.51 (d,  $^3J_{\text{HH}} = 5.2$  Hz, 2H, SiR-arom.), 7.01 – 6.83 (m, 4H, SiR-arom.), 6.29 (dd,  $^3J_{\text{HH}} = 9.1$  Hz,  $^4J_{\text{HH}} = 1.9$  Hz, 1H, SiR-arom.), 6.22 (dd,  $^3J_{\text{HH}} = 9.2$  Hz,  $^4J_{\text{HH}} = 2.5$  Hz, 1H, SiR), 6.09 (t,  $^3J_{\text{HH}} = 7.0$  Hz, 1H,  $H-1'$ ), 4.51 – 4.46 (m, 1H,  $H-3'$ ), 4.32 – 4.21 (m, 8H, SiR-azetidine), 4.05 – 4.01 (m, 1H,  $H-4'$ ), 3.99 – 3.93 (m, 2H,  $H-5'$ ), 3.48 – 3.33 (m, 1H,  $H$ -alkyl), 3.21 (q,  $^3J_{\text{HH}} = 7.3$  Hz, 5H, H-a), 3.03 – 2.96 (m, 2H,  $H$ -alkyl), 2.53 – 2.46 (m, 4H, SiR-azetidine), 2.24 – 2.16 (m, 4H,  $H$ -alkyl), 2.12 – 2.07 (m, 2H,  $H$ -alkyl), 1.65 – 1.54 (m, 4H,  $H$ -alkyl), 1.29 (t,  $^3J_{\text{HH}} = 7.3$  Hz, 8H, H-b), 1.26 – 1.14 (m, 6H,  $H$ -alkyl), 1.13 – 1.03 (m, 2H,  $H$ -alkyl), 0.63 (s, 3H, Si- $\text{CH}_3$ ), 0.42 (s, 3H, Si- $\text{CH}_3$ ).

$^{31}\text{P-NMR}$  (202 MHz,  $\text{D}_2\text{O}$ ):  $\delta$  [ppm] = 2.28 (s).

HRMS (ESI $^-$ ):  $m/z$  = calcd: 983.3974 [ $\text{M}^{\text{isotope}}\text{-H}$ ] $^-$ , found: 983.3635 [ $\text{M}^{\text{isotope}}\text{-H}$ ] $^-$ .

### $\gamma$ -(C9C9AB)-SiR-dCTP **193**



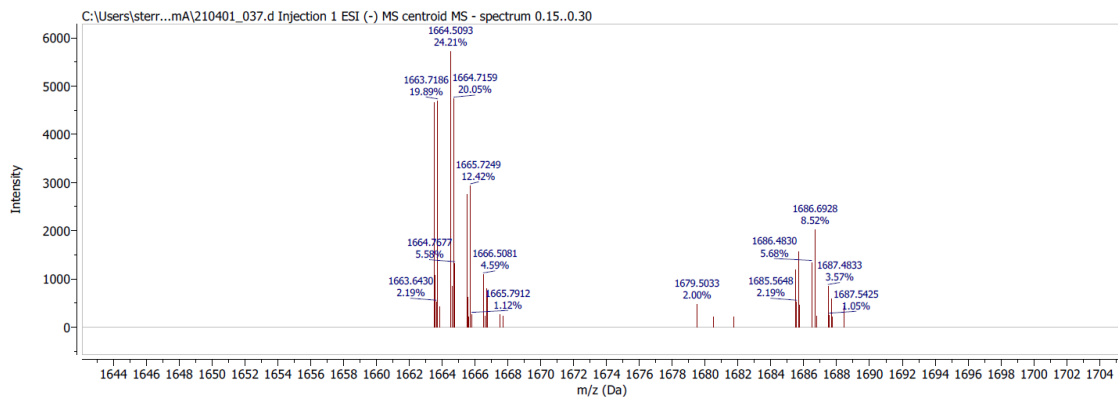
The reaction was carried out with the general procedure VIII with the pyrophosphate of **95** (28 mg, 30  $\mu\text{mol}$ ), TFAA (21  $\mu\text{L}$ , 150  $\mu\text{mol}$ ), and  $\text{Et}_3\text{N}$  (34  $\mu\text{L}$ , 240  $\mu\text{mol}$ ) in  $\text{CH}_3\text{CN}$  (3 ml). The subsequent activation step was performed with 1-methylimidazole (6  $\mu\text{L}$ , 75  $\mu\text{mol}$ ) in DMF (3 ml) followed by the coupling with monophosphate **198** (0.6 TEA, 16 mg, 15  $\mu\text{mol}$ ) solved in DMF (2 mL). Purification on  $\text{RP}_{18}$  silica gel with automated flash chromatography ( $\text{H}_2\text{O}/\text{CH}_3\text{CN}$ ; 100:0 to 0:100), Dowex ion-exchange ( $\text{NH}_4^+$ ) and  $\text{RP}_{18}$  silica gel with automated flash chromatography ( $\text{H}_2\text{O}/\text{CH}_3\text{CN}$ ; 100:0 to 40:60) as well as subsequent freeze-drying provided **193** (around 2 mg, 8%) as blue cotton.

Nuclear magnetic resonance spectroscopy was not performed, due to the isolated quantity of product. Mass spectrometry detected an isotopic mass peak. Performed HPLC



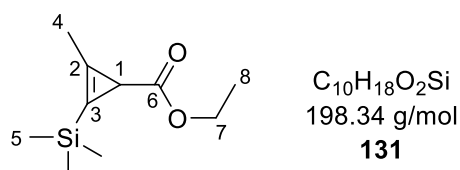
analytic exhibited a peak with a retention time typical for *bis*(C9AB)-pronucleotides. The product was deemed pure enough for subsequent cell experiments.

HRMS (ESI<sup>-</sup>):  $m/z$  = calcd: 1663.6854 [ $M^{\text{isotope-H}}$ ]<sup>-</sup>, found: 1663.6430 [ $M^{\text{isotope-H}}$ ]<sup>-</sup>.



### 6.3.10 Preparation of 1MCP-modified pronucleotides

#### 2-Methyl-3-(trimethylsilyl)cycloprop-2-ene-1-carbonsäureethylester **131**



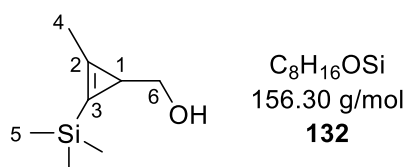
The reaction was carried out as described in the literature with 1-(trimethylsilyl)-1-propyne (1.80 g, 16.0 mmol) and dirhodium tetraacetate (42 mg, 96  $\mu$ mol) in CH<sub>2</sub>Cl<sub>2</sub> (2 mL) followed by the addition of ethyl diazoacetate (0.91 g, 8.0 mmol) solved in CH<sub>2</sub>Cl<sub>2</sub> (5.5 mL). The 1MCP ester **131** (1.21 g, 76%) was obtained as a colorless liquid after purification on silica gel (CH<sub>2</sub>Cl<sub>2</sub>/hexane; 10:90 to 30:70).

The analytical data was in accordance with those described.<sup>69</sup>

<sup>1</sup>H-NMR (400 MHz, CDCl<sub>3</sub>):  $\delta$  [ppm] = 4.16 – 4.04 (m, 2H, H-7), 2.18 (s, 3H, H-4), 1.97 (s, 1H, H-1), 1.23 (t, <sup>3</sup>J = 7.1 Hz, 3H, H-4), 0.18 (s, 9H, H-5).

<sup>13</sup>C-NMR (101 MHz, CDCl<sub>3</sub>):  $\delta$  [ppm] = 177.2 (C-6), 122.7 (C-2), 104.25 (C-3), 60.0 (C-7), 21.4 (C-1), 14.6 (C-8), 12.0 (C-4), -1.4 (C-5).

#### (2-Methyl-3-(trimethylsilyl)cyclopro-2-en-1-yl)methanol **132**



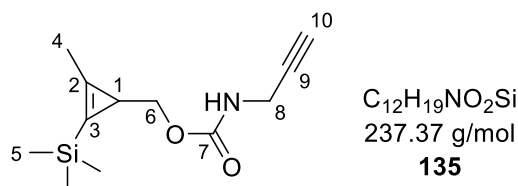
The reaction was carried out according to the literature with modifications. Diisobutylaluminum hydride (9.2 mL, 16 mmol, 25-wt% in Toluol) was solved in diethyl ether (25 mL) and cooled to 0 °C followed by the dropwise addition of 1MCP ester **131** (1.21 g, 6.08 mmol) solved in diethyl ether (5 mL). The reaction mixture was stirred at 0 °C for 3 h and subsequently quenched with 0.25 M Rochelle's salt (60 mL). After extraction with diethyl ether (4x50 mL), the organic layers were dried over NaSO<sub>4</sub> and concentrated carefully under reduced pressure. The 1MCP alcohol **132** (0.749 g, 79%) was obtained as a colorless liquid after purification on silica gel (ethyl acetate/petroleum ether; 1:15 to 1:9 v/v).

The analytical data was in accordance with those described.<sup>69</sup>

$^1\text{H-NMR}$  (500 MHz,  $\text{CDCl}_3$ ):  $\delta$  [ppm] = 3.49 (dd,  $^3J = 4.6$ ,  $^2J = 1.0$  Hz, 2H, *H*-6), 2.22 (s, 3H, *H*-4), 1.56 (t,  $^3J = 4.6$  Hz, 1H, *H*-1), 0.17 (s, 9H, *H*-5).

$^{13}\text{C-NMR}$  (126 MHz,  $\text{CDCl}_3$ ):  $\delta$  [ppm] = 135.6 (*C*-2), 111.4 (*C*-3), 69.4 (*C*-6), 22.3 (*C*-1), 13.6 (*C*-4), -1.0 (*C*-5).

***O*-(2-Methyl-3-(trimethylsilyl)cycloprop-2-en-1-yl)methyl-*N*-prop-2-yn-1-ylcarbamate **135****



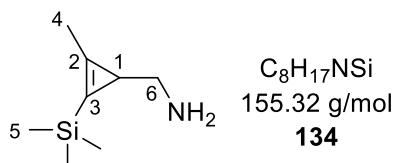
The reaction was carried out as described in the literature with 1,1'-carbonylimidazole (0.917 g, 5.65 mmol) in THF (9 mL) and 1MCP alcohol **132** (0.736 g, 4.71 mmol) in THF (6 mL), followed by DIPEA (8.2 mL, 47 mmol) and propargylamine (0.62 mL, 9.4 mmol). The 1MCP alkyne **135** (0.761 g, 68%) was obtained as a colorless liquid after purification on silica gel (ethyl acetate/petroleum ether; 1:12 to 1:9 v/v).

The analytical data was in accordance with those described.<sup>78</sup>

$^1\text{H-NMR}$  (400 MHz,  $\text{CDCl}_3$ ):  $\delta$  [ppm] = 4.79 (s, 1H, N-H), 4.04 – 3.81 (m, 4H, *H*-6, *H*-8), 2.23 (t,  $^3J = 2.5$  Hz, 1H, *H*-10), 2.19 (s, 3H, *H*-4), 1.54 (t,  $^3J = 5.5$  Hz, 1H, *H*-1), 0.15 (s, 9H, *H*-5).

$^{13}\text{C-NMR}$  (101 MHz,  $\text{CDCl}_3$ ):  $\delta$  [ppm] = 166.3 (*C*-7), 134.6 (*C*-2), 111.2 (*C*-3), 80.2 (*C*-9), 74.1 (*C*-6), 71.5 (*C*-10), 31.0 (*C*-8), 18.7 (*C*-1), 13.4 (*C*-4), -1.1 (*C*-5).

**(2-Methyl-3-(trimethylsilyl)cycloprop-2-en-1-yl)methanamine **134****

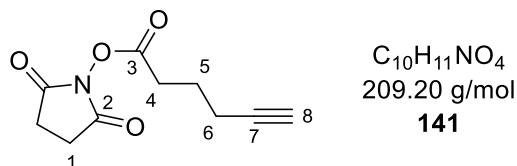


The reaction was carried out as described in the literature<sup>72</sup> with (2-Methyl-3-(trimethylsilyl)cycloprop-2-en-1-yl)methanol **132** (3.30 g, 21.1 mmol), DBU (4.10 mL, 2.74 mmol), and DPPA (5.91 mL, 2.74 mmol) in THF (50 mL) at room temperature overnight.  $\text{PPh}_3$  (7.20 g, 2.47 mmol) was used for the Staudinger reduction of the cyclopropane azide. After extraction, the product **134** (2.42 g, 73%) was obtained as a colorless oil.

The analytical data was in accordance with those described.<sup>72</sup>

<sup>1</sup>H-NMR (400 MHz, CDCl<sub>3</sub>): δ [ppm] = 2.69 – 2.49 (m, 2H, *H*-6), 2.20 (s, 3H, *H*-4), 1.45 (t, <sup>3</sup>*J* = 4.4, 1H, *H*-1), 0.16 (s, 9H, *H*-5).

### 2,5-Dioxopyrrolidin-1-yl hex-5-ynoate **141**

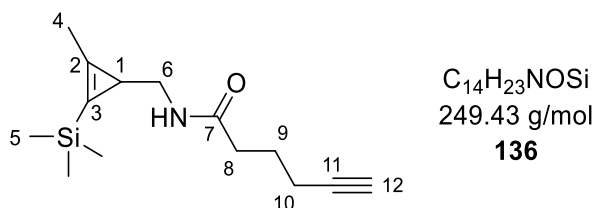


Disuccinimidyl carbonate (2.25 g, 8.80 mmol) was added to a solution of hexynoic acid (882 μL, 8.00 mmol) and pyridine (1.29 mL, 16.0 mmol) in acetonitrile (7 mL). The reaction mixture was stirred overnight at room temperature. The solution was added to ethyl acetate (50 mL), washed twice with 1 N HCl and sat. aq. NaHCO<sub>3</sub>, and dried over NaSO<sub>4</sub>. The removal of the organic solvent under reduced pressure resulted in the NHS active ester **141** (1.67 g, quant.) as a colorless wax.

<sup>1</sup>H-NMR (600 MHz, CDCl<sub>3</sub>): δ [ppm] = 2.82 (d, <sup>3</sup>*J* = 6.8 Hz, 4H, *H*-1), 2.76 (t, <sup>3</sup>*J* = 7.4 Hz, 2H, *H*-4), 2.33 (td, <sup>3</sup>*J* = 6.9, 2.7 Hz, 2H, *H*-6), 2.01 (t, <sup>3</sup>*J* = 2.6 Hz, 1H, *H*-8), 1.95 (p, <sup>3</sup>*J* = 7.1 Hz, 2H, *H*-5).

<sup>13</sup>C-NMR (151 MHz, CDCl<sub>3</sub>): δ [ppm] = 169.2 (C-1), 168.3 (C-3), 82.5 (C-7), 69.9 (C-8), 29.8 (C-4), 25.7 (C-1), 23.4 (C-5), 17.7 (C-6).

### *N*-((2-Methyl-3-(trimethylsilyl)cycloprop-2-en-1-yl)methyl)hex-5-ynamide **136**



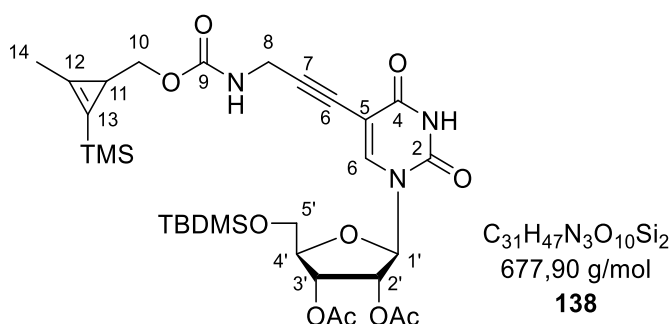
The NHS-active ester **141** (1.09 g, 5.20 mmol) was solved in CH<sub>2</sub>Cl<sub>2</sub> (10 mL) followed by the addition of triethylamine (762 μL, 5.72 mmol) and 1MCP amine **134** (0.808 g, 5.70 mmol). After stirring for 3 h at room temperature, the reaction mixture was directly loaded onto a silica column. The isolation of the product on silica gel (CH<sub>2</sub>Cl<sub>2</sub>/CH<sub>3</sub>OH; 90:10 to 80:20) provided **136** (0.950 g, 73%) as a colorless wax.

$^1\text{H-NMR}$  (500 MHz,  $\text{CDCl}_3$ ):  $\delta$  [ppm] = 5.33 (bs, NH), 3.23 – 3.06 (m, 2H, H-6), 2.29 (t,  $^3J$  = 7.3 Hz, 2H, H-8), 2.26 (td,  $^3J$  = 6.8 Hz,  $^4J$  = 2.7 Hz, 2H, H-10), 2.18 (s, 3H, H-4), 1.97 (t,  $^4J$  = 2.6 Hz, 1H, H-12), 1.86 (m, 2H, H-9), 1.44 (t,  $^3J$  = 4.6 Hz, 1H, H-1), 0.16 (s, 9H, H-5).

$^{13}\text{C-NMR}$  (126 MHz,  $\text{CDCl}_3$ ):  $\delta$  [ppm] = 171.9 (C-7), 136.0 (C-2), 111.8 (C-3), 83.8 (C-11), 69.2 (C-12), 46.2 (C-6), 35.4 (C-8), 24.4 (C-9), 19.4 (C-1), 18.0 (C-10), 13.3 (C-4), -0.9 (C-5).

HRMS (ESI $^-$ ):  $m/z$  = calcd: 250.1627 [M-H] $^-$ , found: 250.1639 [M-H] $^-$ .

**2',3'-Di-O-acetyl-5'-O-tert-butylidimethylsilyl-5-(5-(3-(((2-methyl-3-(trimethylsilyl)cycloprop-2-en-1-yl)methoxy)carbonyl)amino)prop-1-yn-1-yl) uridine **138****



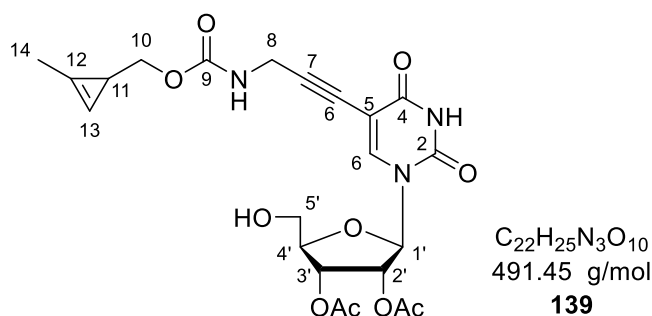
The protected IU **67** (227 mg, 400  $\mu\text{mol}$ ),  $\text{Pd}_2(\text{dba})_3$  (20 mg, 22  $\mu\text{mol}$ , 5.4 mol%), tri(2-furyl) phosphine (11 mg, 48  $\mu\text{mol}$ , 12 mol%) and copper(I) iodide (11 mg, 60  $\mu\text{mol}$ , 15 mol%) were dissolved in DMF (6 mL). The reaction flask was then evaporated and flushed with nitrogen (3x) followed by the addition of triethylamine (388  $\mu\text{L}$ , 2.80 mmol) and alkyne **135** (114 mg, 480  $\mu\text{mol}$ ). The reaction mixture was stirred for 3 h at 50  $^\circ\text{C}$  and was then concentrated *in vacuo* until 3-4 mL DMF remained. The reaction mixture was diluted with ethyl acetate and filtrated over Celite $^\circ$  to remove the precipitated catalyst system. After removing all volatiles under reduced pressure, the product was purified on silica gel (petroleum ether/ethyl acetate; 80:20) to provide nucleoside **138** (222 mg, 82%) as a light-yellow foam.

$^1\text{H-NMR}$  (400 MHz, MeOD):  $\delta$  [ppm] = 8.07 (s, 1H, H-6), 6.18 (d,  $^3J$  = 6.1 Hz, 1H, H-1'), 5.42 – 5.37 (m, 2H, H-2', H-3'), 4.34 – 4.28 (m, 1H, H-4'), 4.12 – 4.07 (m, 2H, H-8), 4.02 – 3.80 (m, 4H, H-5', H-10), 2.21 (s, 3H, H-14), 2.14 (s, 3H, Ac-CH $_3$ ), 2.05 (s, 3H, Ac-CH $_3$ ), 1.55 (t,  $^3J$  = 5.4 Hz, 1H, H-11), 1.00 (s, 9H, TMS-C(CH $_3$ ) $_3$ ), 0.23 (s, 3H, Si-CH $_3$ ), 0.21 (s, 3H, Si-CH $_3$ ), 0.18 (s, 9H, tBu-C(CH $_3$ ) $_3$ ).

$^{13}\text{C-NMR}$  (101 MHz, MeOD):  $\delta$  [ppm] = 171.5 (Ac-CO), 171.3 (Ac-CO), 164.1 (C-9), 158.9 (C-4), 151.3 (C-2), 143.5 (C-6), 136.1 (C-12), 112.2 (C-13), 101.2 (C-5), 91.8 (C-7), 87.2 (C-

1'), 85.5 (C-4'), 75.0 (C-2'), 74.7 (C-10), 74.6 (C-10), 73.2 (C-3'), 64.4 (C-5'), 31.9 (C-8), 26.6 (tBu-CH<sub>3</sub>), 20.5 (Ac-CH<sub>3</sub>), 20.2 (Ac-CH<sub>3</sub>), 19.8 (C-11), 19.3 (tBu-C(CH<sub>3</sub>)<sub>3</sub>), 13.2 (C-14), -1.1 (TMS-CH<sub>3</sub>), -5.2 (TBDMSi-CH<sub>3</sub>), -5.3 (TBDMSi-CH<sub>3</sub>).

**2',3'-Di-O-acetyl-5-(5-(3-(((2-methylcycloprop-2-en-1-yl)methoxy)carbonyl)amino)prop-1-yn-1-yl) uridine **139****



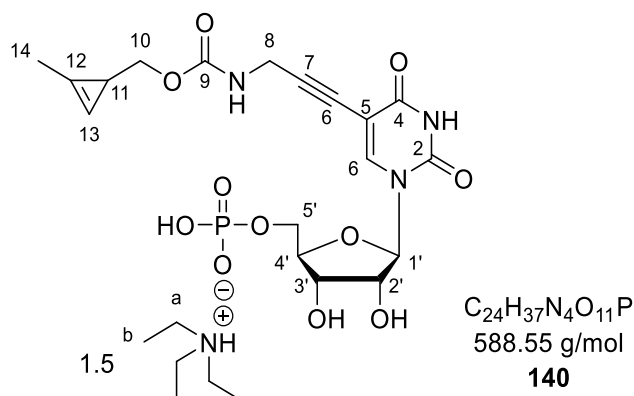
The silylated nucleoside **138** (212 mg, 313 μmol) was dissolved in THF (5 mL) followed by the addition of 1 M TBAF in THF (903 μL, 1.25 mmol). The reaction mixture was stirred at room temperature for 2 days. The solvent was removed under reduced pressure, and the residue was prepurified on silica gel (CH<sub>2</sub>Cl<sub>2</sub>/CH<sub>3</sub>OH; 95:5), followed by the isolation of the product on RP<sub>18</sub> silica gel using automated flash chromatography (H<sub>2</sub>O/CH<sub>3</sub>CN; 70:30 to 0:100). The appropriate fractions were freeze-dried to yield the deprotected nucleoside **139** (120 mg, 78%) as a light-yellow solid.

<sup>1</sup>H-NMR (400 MHz, CDCl<sub>3</sub>): δ [ppm] = 8.77 (s, 1H, NH), 8.17 (s, 1H, H-6), 6.56 (s, 1H, H-13), 6.09 (d, <sup>3</sup>J = 6.1 Hz, 1H, H-1'), 5.52 – 5.41 (m, 2H, H-2', H-3'), 5.37 – 5.29 (m, 1H, NH), 4.23 (m, 1H, H-4'), 4.15 (d, <sup>3</sup>J = 5.7 Hz, 2H, H-8), 4.02 – 3.84 (m, 4H, H-5', H-10), 2.14 – 2.12 (m, 6H, Ac-CH<sub>3</sub>, H-14), 2.08 (s, 3H, Ac-CH<sub>3</sub>), 1.68 – 1.60 (m, 1H, H-11).

<sup>13</sup>C-NMR (101 MHz, CDCl<sub>3</sub>): δ [ppm] = 170.1 (Ac-CO), 169.8 (Ac-CO), 161.2 (C-9, HMBC), 156.7 (C-4, HMBC), 149.5 (C-2), 144.0 (C-6, HMBC), 120.6 (C-12, HMBC), 102.3 (C-13), 100.4 (C-5), 87.5 (C-1'), 83.9 (C-4'), 73.6 (C-2'), 73.1 (C-10), 71.5 (C-3'), 61.8 (C-5'), 31.8 (C-8, HMBC), 20.8 (Ac-CH<sub>3</sub>), 20.6 (Ac-CH<sub>3</sub>), 17.3 (C-11), 11.8 (C-14).

HRMS (ESI<sup>-</sup>): *m/z* = calcd: 492.1618 [M+H]<sup>+</sup>, found: 492.1636 [M+H]<sup>+</sup>.

**5-(5-(3-(((2-Methylcycloprop-2-en-1-yl)methoxy)carbonyl)amino)prop-1-yn-1-yl)uridine monophosphate **140****

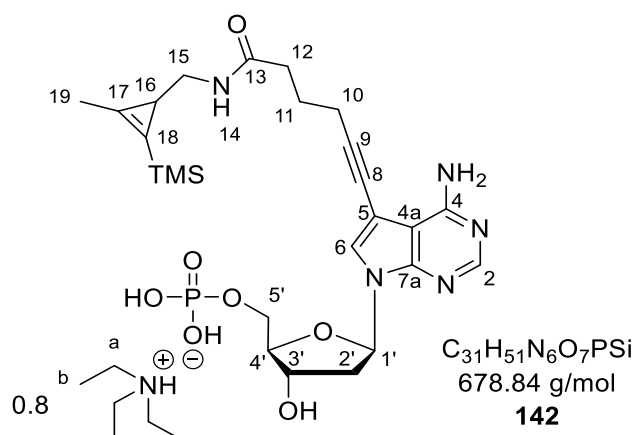


The reaction was carried out with the general procedure I with acetylated nucleoside **139** (79 mg, 160  $\mu$ mol) solved in acetonitrile (5 mL), bis(fluorenylmethyl)phosphoramidite (150 mg, 288  $\mu$ mol) solved in  $CH_2Cl_2$  (2 mL) and DCI (1.15 mL, 288  $\mu$ mol). After adding the DCI over a period of 30 min, the reaction mixture was stirred for a further 15 min. The oxidation was performed with *t*-BuOOH (58  $\mu$ L, 320  $\mu$ mol). The deprotection was carried out in a mixture of  $H_2O/CH_3OH/Et_3N$  (30 mL, 1:1:1 v/v/v) for 3 days. The product was purified on RP<sub>18</sub> silica gel using automated flash chromatography ( $H_2O/CH_3CN$ ; 100:0 to 0:100) to yield the TEAH salt of **140** (76 mg, 74%) as a colorless solid.

$^1H$ -NMR (600 MHz,  $D_2O$ ):  $\delta$  [ppm] = 8.18 (s, 1H, *H*-6), 6.67 (s, 1H, *H*-13), 5.97 (d,  $^3J_{HH}$  = 4.8 Hz, 1H, *H*-1'), 4.38 (t,  $^3J_{HH}$  = 5.0 Hz, 1H, *H*-2'), 4.34 (t,  $^3J_{HH}$  = 5.0 Hz, 1H, *H*-3'), 4.31 – 4.26 (m, 1H, *H*-4'), 4.19 – 4.03 (m, 5H, *H*-5', *H*-10a, *H*-8), 4.02 – 3.93 (m, 1H, *H*-10b), 3.23 (q,  $^3J_{HH}$  = 7.3 Hz, 10H, *H*-a), 2.14 (d,  $^3J_{HH}$  = 1.2 Hz, 3H, *H*-14), 1.68 – 1.65 (m, 1H, *H*-11), 1.30 (t,  $^3J_{HH}$  = 7.3 Hz, 15H, *H*-b).

$^{13}C$ -NMR (151 MHz,  $D_2O$ ):  $\delta$  [ppm] = 164.5 (*C*-9), 158.5 (*C*-4, HMBC), 150.7 (*C*-2), 144.5 (*C*-6), 120.5 (*C*-12), 101.1 (*C*-13), 99.4 (*C*-5), 89.0 (*C*-1'), 83.4 (d,  $^3J_{CP}$  = 8.8 Hz, *C*-4'), 73.9 (*C*-2'), 73.2 (*C*-10), 73.0 (*C*-10), 69.6 (*C*-3'), 63.9 (d,  $^2J_{CP}$  = 4.5 Hz, *C*-5'), 46.7 (*C*-b), 30.9 (*C*-8, HSQC), 16.5 (*C*-11), 10.7 (*C*-14), 8.2 (*C*-a).

$^{31}P$ -NMR (162 MHz,  $D_2O$ ):  $\delta$  [ppm] = 0.99 (s).

**(TMS-1MCP)-7-deaza-2'-deoxyadenosine monophosphate 142**

The TEAH salt of IdAMP **91** (1.3 TEAH, 118 mg, 200  $\mu$ mol), Pd<sub>2</sub>(dba)<sub>3</sub> (10 mg, 11  $\mu$ mol, 5.4 mol%), tri(2-furyl) phosphine (5.6 mg, 24  $\mu$ mol, 12 mol%) and copper(I) iodide (5.7 mg, 30  $\mu$ mol, 15 mol%) were suspended in DMF (8 mL). The reaction flask was then evaporated and flushed with nitrogen (3x) followed by the addition of triethylamine (194  $\mu$ L, 1.40 mmol) and alkyne **136** (60 mg, 240  $\mu$ mol). The reaction mixture was stirred for 3 h at 50 °C and was then concentrated *in vacuo* until 3-4 mL DMF remained. Slow addition of diethyl ether led to precipitation of the crude monophosphate, which was collected, dissolved in 0.05 M TEAB, and purified on RP<sub>18</sub> silica gel using automated flash chromatography (0.05 M TEAB/CH<sub>3</sub>CN; 100:0 to 0:100). The resulting monophosphate was solved in CH<sub>3</sub>OH, filtered through a syringe filter, and concentrated *in vacuo* to yield the TEAH salt of **142** (95 mg, 72%) as a light-yellow solid.

<sup>1</sup>H-NMR (300 MHz, MeOD):  $\delta$  [ppm] = 8.10 (s, 1H, H-2), 7.69 (s, 1H, H-6), 6.62 (dd, <sup>3</sup>J<sub>HH</sub> = 8.1, 5.9 Hz, 1H, H-1'), 4.63 – 4.54 (m, 1H, H-3'), 4.12 – 4.00 (m, 3H, H-4', H-5'), 3.25 (dd, <sup>2</sup>J<sub>HH</sub> = 13.5 Hz, <sup>3</sup>J<sub>HH</sub> = 4.1 Hz, 1H, H-15a), 3.16 (q, <sup>3</sup>J<sub>HH</sub> = 7.3 Hz, 5H, H-a), 2.81 (dd, <sup>2</sup>J<sub>HH</sub> = 13.5 Hz, <sup>3</sup>J<sub>HH</sub> = 5.6 Hz, 1H, H-15b), 2.64 – 2.45 (m, 3H, H-2'a, H-10), 2.42 – 2.26 (m, 3H, H-2'b, H-12), 2.18 (s, 3H, H-19), 2.00 – 1.82 (m, 2H, H-11), 1.43 (dd, <sup>3</sup>J<sub>HH</sub> = 5.6, 4.1 Hz, 1H, H-16), 1.28 (t, <sup>3</sup>J<sub>HH</sub> = 7.3 Hz, 8H, H-b), 0.14 (s, 9H, Si-(CH<sub>3</sub>)<sub>3</sub>).

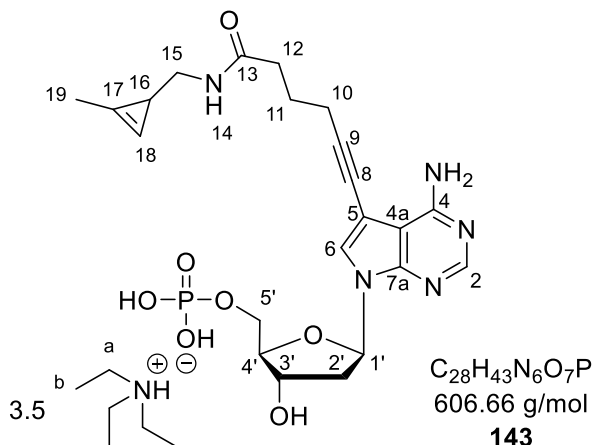
<sup>13</sup>C-NMR (75 MHz, MeOD):  $\delta$  [ppm] = 174.9 (C-13), 158.1 (C-4), 152.0 (C-2), 149.9 (C-7a), 137.9 (C-17), 127.2 (C-6), 112.9 (C-18), 98.7 (C-5), 93.2 (C-9), 87.5 (d, <sup>3</sup>J<sub>CP</sub> = 8.4 Hz, C-4'), 84.7 (C-1'), 74.7 (C-8), 73.1 (C-3'), 66.3 (d, J<sub>CP</sub> = 4.1 Hz, C-5'), 47.9 (C-15), 47.7 (C-a), 41.4 (C-2'), 36.1 (C-12), 26.2 (C-11), 20.7 (C-16), 19.9 (C-10), 13.1 (C-19), 9.1 (C-b), -1.0 (Si-(CH<sub>3</sub>)<sub>3</sub>).

<sup>31</sup>P-NMR (162 MHz, MeOD):  $\delta$  [ppm] = 1.01 (s).



HRMS (ESI<sup>-</sup>):  $m/z$  = calcd: 576.2049 [M-H]<sup>-</sup>, found: 576.2135 [M-H]<sup>-</sup>.

**(1MCP)-7-deaza-2'-deoxyadenosine monophosphate 143**



An appropriate amount of TMS-1MCP-dAMP triethylammonium salt **142** was solved in CH<sub>3</sub>OH and passed through a short silica column to remove triethylammonium counter ions. The appropriate fractions were concentrated *in vacuo*, filtered through a syringe filter, and evaporated to dryness to provide protonated TMS-1MCP-dAMP (92 mg, 160 μmol). In parallel, TBAF monohydrate (49 mg, 176 μmol) was co-evaporated with THF (1 mL) and solved again in THF (0.5 mL). Then, the monophosphate was dissolved in DMF (300 μL) followed by the addition of the prepared TBAF solution in THF, and the reaction mixture was stirred at room temperature overnight. The solvents were removed under reduced pressure, and the residue was purified on RP<sub>18</sub> silica gel using automated flash chromatography (0.05 M TEAB/CH<sub>3</sub>CN; 100:0 to 0:100). The resulting monophosphate was solved in water, filtered through a syringe filter, and concentrated *in vacuo* to yield the TEAH salt of **143** (136 mg, 100%) as a light-yellow solid.

<sup>1</sup>H-NMR (600 MHz, D<sub>2</sub>O): δ [ppm] = 8.07 (s, 1H, H-2), 7.54 (s, 1H, H-6), 6.58 – 6.52 (m, 2H, H-18, H-1'), 4.68 – 4.63 (m, 1H, H-3'), 4.22 – 4.17 (m, 1H, H-4'), 4.02 – 3.94 (m, 2H, H-5'), 3.19 (q, <sup>3</sup>J<sub>HH</sub> = 7.3 Hz, 9H, H-a), 3.11 – 3.03 (m, 2H, H-15), 2.63 (dddd, <sup>2</sup>J<sub>HH</sub> = 14.0 Hz, <sup>3</sup>J<sub>HH</sub> = 8.0, 6.1 Hz, <sup>4</sup>J<sub>HH</sub> = 1.8 Hz, 1H, H-2'a), 2.54 – 2.44 (m, 3H, H-10, H-2'b), 2.39 (t, <sup>3</sup>J<sub>HH</sub> = 7.2 Hz, 2H, H-12), 2.01 (2x s, 3H, H-19), 1.93 – 1.86 (m, 2H, H-11), 1.48 – 1.43 (m, 1H, H-16), 1.27 (t, <sup>3</sup>J<sub>HH</sub> = 7.3 Hz, 13H, H-b).

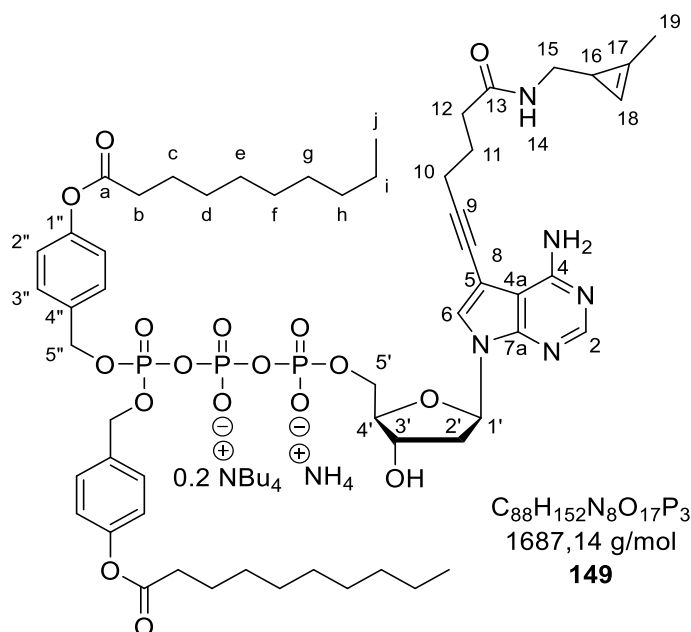
<sup>13</sup>C-NMR (151 MHz, D<sub>2</sub>O): δ [ppm] = 175.7 (C-13), 156.8 (C-4), 151.5 (C-2), 148.1 (C-7a), 125.4 (C-6), 121.1 (C-17), 102.7 (C-4a), 101.9 (C-18), 97.1 (C-5), 92.9 (C-9), 85.4 (d, <sup>3</sup>J<sub>CP</sub> = 8.7 Hz, C-4'), 82.9 (C-1'), 73.2 (C-8), 71.5 (C-3'), 64.5 (d, <sup>2</sup>J<sub>CP</sub> = 5.1 Hz, C-5'), 46.6 (C-a),

44.8 (C-15), 38.8 (C-2'), 34.9 (C-12), 24.2 (C-11), 18.4 (C-10), 16.8 (C-16), 10.6 (C-19), 8.2 (C-a).

$^{31}\text{P}$ -NMR (243 MHz,  $\text{D}_2\text{O}$ ):  $\delta$  [ppm] = 1.37 (s).

HRMS (ESI):  $m/z$  = calcd: 504.1648[M-H] $^-$ , found: 504.1652 [M-H] $^-$ .

### $\gamma$ -(C9C9AB)-1MCP-dATP **149**



The reaction was carried out with the general procedure VIII with the pyrophosphate of **95** (99 mg, 105  $\mu\text{mol}$ ), TFAA (73  $\mu\text{L}$ , 525  $\mu\text{mol}$ ), and  $\text{Et}_3\text{N}$  (117  $\mu\text{L}$ , 840  $\mu\text{mol}$ ) in  $\text{CH}_3\text{CN}$  (6 ml). The subsequent activation step was performed with 1-methylimidazole (21  $\mu\text{L}$ , 263  $\mu\text{mol}$ ) in  $\text{CH}_3\text{CN}$  (6 ml) followed by the coupling with monophosphate **143** (3.4 TEAH, 45 mg, 53  $\mu\text{mol}$ ) solved in DMF (3 mL). Purification on  $\text{RP}_{18}$  silica gel with automated flash chromatography ( $\text{H}_2\text{O}/\text{CH}_3\text{CN}$ ; 100:0 to 0:100), Dowex ion-exchange ( $\text{NH}_4^+$ ) and  $\text{RP}_{18}$  silica gel with automated flash chromatography ( $\text{H}_2\text{O}/\text{CH}_3\text{CN}$ ; 100:0 to 0:100) as well as subsequent freeze-drying provided **149** (30 mg, 47%) as colorless cotton.

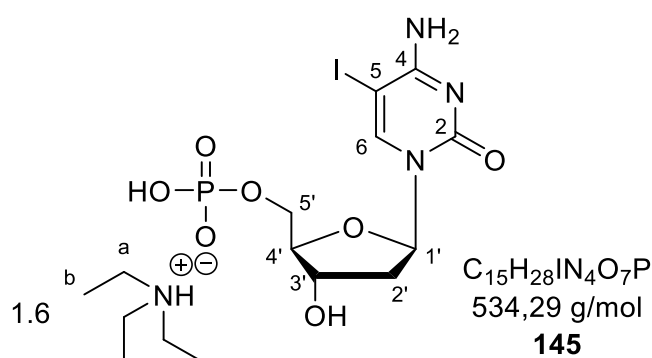
$^1\text{H}$ -NMR (600 MHz, MeOD):  $\delta$  [ppm] = 8.11 (s, 1H, H-2), 7.75 (s, 1H, H-6), 7.40 – 7.35 (m, 4H, 4x H-2''), 7.03 – 6.97 (m, 4H, 4x H-3''), 6.66 (s, 1H, H-18), 6.60 – 6.56 (m, 1H, H-1'), 5.22 – 5.12 (m, 4H, 4x H-5''), 4.70 – 4.62 (m, 1H, H-3'), 4.32 – 4.23 (m, 2H, H-5'), 4.16 – 4.12 (m, 1H, H-4'), 3.27 – 3.22 (m, 2H,  $\text{NBU}_4$ ), 3.13 – 3.09 (m, 2H, H-15), 2.56 (t,  $^3J_{\text{HH}} = 7.5$  Hz, 4H, 2x H-b), 2.54 – 2.49 (m, 1H, H-2'a), 2.47 (t,  $^3J_{\text{HH}} = 6.9$  Hz, 2H, H-10), 2.37 (m, 3H, H-12, H-2'b), 2.10 (2x s, 3H, H-19), 1.92 – 1.84 (m, 2H, H-11), 1.78 – 1.63 (m, 7H, 2x

$H$ -c,  $\text{NBu}_4$ ), 1.52 (td,  $^3J_{\text{HH}} = 4.3, 1.7$  Hz, 1H,  $H$ -16), 1.47 – 1.26 (m, 26H, 2x  $H$ -d-l,  $\text{NBu}_4$ ), 1.03 (t,  $^3J_{\text{HH}} = 7.4$  Hz, 3H,  $\text{NBu}_4$ ), 0.94 – 0.88 (m, 6H, 2x  $H$ -j).

$^{31}\text{P}$ -NMR (243 MHz, MeOD):  $\delta$  [ppm] = -11.40 (d,  $^2J_{\text{PP}} = 20.2$ ,  $P$ - $\alpha$ ), -13.21 (d,  $^2J_{\text{PP}} = 16.5$ ,  $P$ - $\gamma$ ), -23.75 (t,  $^2J_{\text{PP}} = 18.0$ ,  $P$ - $\beta$ ).

HRMS (ESI $^-$ ):  $m/z = \text{calcd: } 1184.4533$  [ $\text{M-H}$ ] $^-$ , found: 1184.3984 [ $\text{M-H}$ ] $^-$ .

### 5-Iodo-2'-deoxycytidine monophosphate **145**



The reaction was carried out according to the general procedure II with  $\text{POCl}_3$  (648  $\mu\text{L}$ , 6.95 mmol) in  $\text{CH}_3\text{CN}$  (1.56 mL, 7.58 mmol), pyridine (613  $\mu\text{L}$ , 19.3 mmol),  $\text{H}_2\text{O}$  (80  $\mu\text{L}$ , 4.42 mmol), and nucleoside IdC **152** (558 mg, 1.58 mmol) for 3 h. Purification on RP $_{18}$  ica gel with automated flash chromatography (100%  $\text{H}_2\text{O}$ , reduced flow, then  $\text{H}_2\text{O}/\text{CH}_3\text{CN}$ ; 100:0 to 0:100) provided the ammonium salt of **145**. Ion-exchange to TEAH resulted in the TEAH salt of **145** (1.6 TEAH, 510 mg, 54%) as a colorless solid.

$^1\text{H}$ -NMR (300 MHz,  $\text{D}_2\text{O}$ ):  $\delta$  [ppm] = 8.24 (s, 1H,  $H$ -6), 6.26 (t,  $^3J_{\text{HH}} = 6.7$  Hz,  $H$ -1'), 4.54 (m, 1H,  $H$ -3'), 4.19 (q,  $^3J_{\text{HH}} = 3.7$  Hz, 1H,  $H$ -4'), 4.04-4.01 (m, 2H,  $H$ -5'), 3.21 (q,  $^3J_{\text{HH}} = 7.3$  Hz, 8 H,  $H$ -a), 2.43 (ddd,  $^2J_{\text{HH}} = 13.9$  Hz,  $^3J_{\text{HH}} = 6.3, 3.6$  Hz, 1H,  $H$ -2'), 2.31 (dt,  $^2J_{\text{HH}} = 14.1$  Hz,  $^3J_{\text{HH}} = 6.5$  Hz, 1H,  $H$ -2'), 1.29 (t,  $^3J_{\text{HH}} = 7.3$  Hz, 12 H,  $H$ -b).

$^{13}\text{C}$ -NMR (101 MHz,  $\text{D}_2\text{O}$ ):  $\delta$  [ppm] = 164.6 ( $C$ -4), 156.6 ( $C$ -2), 147.6 ( $C$ -6), 86.3 ( $C$ -1'), 85.8 (d,  $^3J_{\text{CP}} = 8.6$  Hz,  $C$ -4'), 70.9 ( $C$ -3'), 64.3 (d,  $^2J_{\text{CP}} = 4.7$  Hz,  $C$ -5'), 57.9 ( $C$ -5), 46.6 ( $C$ -a), 39.5 ( $C$ -2'), 8.2 ( $C$ -b).

$^{31}\text{P}$ -NMR (162 MHz,  $\text{D}_2\text{O}$ ):  $\delta$  [ppm] = 1.00 (s).

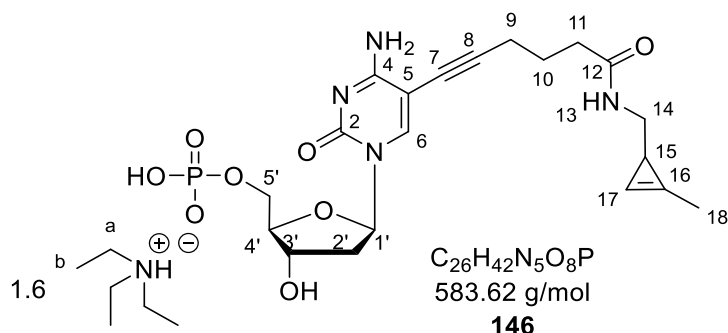
IR:  $\nu$  [ $\text{cm}^{-1}$ ] = 3187, 2985, 2944, 2683, 2483, 1620, 1476, 1285, 1158, 1043, 916, 778, 504.

HRMS (ESI $^-$ ):  $m/z = \text{calcd: } 431.9463$  [ $\text{M-H}$ ] $^-$ , found: 431.9462 [ $\text{M-H}$ ] $^-$ .



HRMS (ESI<sup>-</sup>):  $m/z$  = calcd: 553.1884 [M-H]<sup>-</sup>, found: 533.1550 [M-H]<sup>-</sup>.

**(1MCP)-2'-deoxycytidine monophosphate 146**



An appropriate amount of TMS-1MCP-dCMP triethylammonium salt **144** was solved in CH<sub>3</sub>OH and passed through a short silica column to remove triethylammonium counter ions. The appropriate fractions were concentrated *in vacuo*, filtered through a syringe filter, and evaporated to dryness to provide protonated TMS-1MCP-dCMP (161 mg, 290 μmol). In parallel, TBAF monohydrate (89 mg, 319 μmol) was co-evaporated with THF (1 mL) and solved again in THF (3 mL). Then, the monophosphate was dissolved in DMF (2 mL) followed by the addition of the prepared TBAF solution in THF, and the reaction mixture was stirred at 30 °C overnight. The solvents were removed under reduced pressure, and the residue was purified on RP<sub>18</sub> silica gel using automated flash chromatography (0.05 M TEAB/CH<sub>3</sub>CN; 100:0 to 0:100). The resulting monophosphate was solved in water, filtered through a syringe filter, and concentrated *in vacuo* to yield the TEAH salt of **146** (131 mg, 70%) as a light-yellow solid.

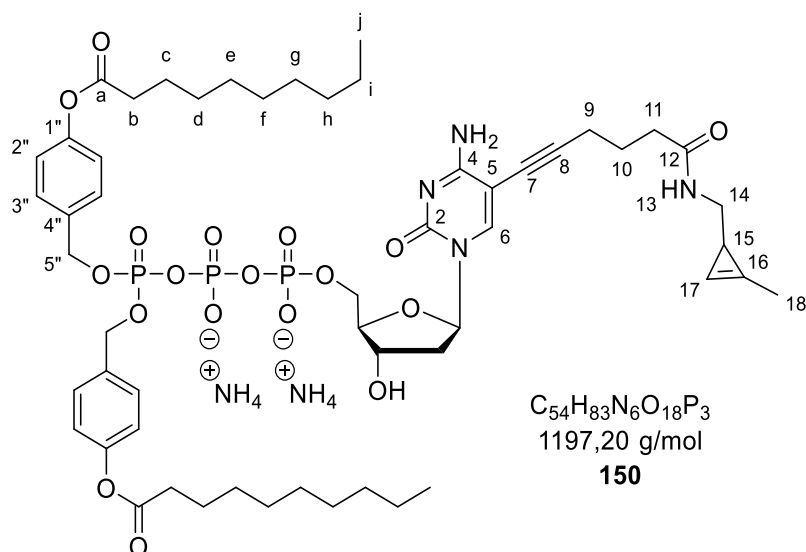
<sup>1</sup>H-NMR (600 MHz, MeOD): δ [ppm] = 8.01 (s, 1H, H-6), 6.59 – 6.55 (m, 1H, H-17), 6.19 (dd, <sup>3</sup>J<sub>HH</sub> = 7.7, 5.8 Hz, 1H, H-1'), 4.39 (dt, <sup>3</sup>J<sub>HH</sub> = 5.7, 2.7 Hz, 1H, H-3'), 4.02 – 3.92 (m, 3H, H-4', H-5'), 3.02 (d, <sup>3</sup>J<sub>HH</sub> = 4.3 Hz, 2H, H-14), 2.94 (q, <sup>3</sup>J<sub>HH</sub> = 7.3 Hz, 10H, H-a), 2.40 (t, <sup>3</sup>J<sub>HH</sub> = 6.8, 2H, H-9), 2.32 – 2.27 (m, 2H, H-11), 2.27 – 2.23 (m, 1H, H-2'a), 2.08 (ddd, <sup>2</sup>J<sub>HH</sub> = 13.7 Hz, <sup>3</sup>J = 7.8, 6.0 Hz, 1H, H-2'b), 2.03 – 2.02 (m, 3H, H-18), 1.82 – 1.76 (m, 2H, H-10), 1.43 (m, H-15), 1.16 (t, <sup>3</sup>J<sub>HH</sub> = 7.3 Hz, 14H, H-b).

<sup>13</sup>C-NMR (151 MHz, MeOD): δ [ppm] = 175.4 (C-12), 166.6 (C-4), 156.9 (C-2), 144.8 (C-6), 122.8 (C-16), 103.9 (C-17), 96.7 (C-8), 93.8 (C-5), 88.0 (d, <sup>2</sup>J<sub>CP</sub> = 8.6 Hz, C-4'), 87.7 (C-1'), 72.7 (C-7), 72.7 (C-3'), 65.8 (d, <sup>3</sup>J<sub>CP</sub> = 5.1 Hz, C-5'), 47.4 (C-a), 46.4 (C-14), 41.8 (C-2'), 36.0 (C-11), 25.7 (C-10), 19.9 (C-15), 19.0 (C-9), 11.5 (C-18), 9.6 (C-b).

<sup>31</sup>P-NMR (202 MHz, MeOD): δ [ppm] = 2.46 (s).

HRMS (ESI<sup>-</sup>):  $m/z$  = calcd: 481.1494 [M-H]<sup>-</sup>, found: 481.1244 [M-H]<sup>-</sup>.

### $\gamma$ -(C9C9AB)-1MCP-dCTP **150**



The reaction was carried out with the general procedure VIII with the pyrophosphate of **95** (132 mg, 140  $\mu$ mol), TFAA (97  $\mu$ L, 700  $\mu$ mol), and Et<sub>3</sub>N (156  $\mu$ L, 1.12 mmol) in CH<sub>3</sub>CN (6 ml). The subsequent activation step was performed with 1-methylimidazole (28  $\mu$ L, 350  $\mu$ mol) in CH<sub>3</sub>CN (6 ml) followed by the coupling with monophosphate **146** (1.6 TEAH, 45 mg, 70  $\mu$ mol) solved in DMF (3 mL). Purification on RP<sub>18</sub> silica gel with automated flash chromatography (H<sub>2</sub>O/CH<sub>3</sub>CN; 100:0 to 0:100), Dowex ion-exchange (NH<sub>4</sub><sup>+</sup>) and RP<sub>18</sub> silica gel with automated flash chromatography (H<sub>2</sub>O/CH<sub>3</sub>CN; 100:0 to 0:100) as well as subsequent freeze-drying provided **150** (43 mg, 52%) as colorless cotton.

<sup>1</sup>H-NMR (400 MHz, MeOD):  $\delta$  [ppm] = 8.17 (s, 1H, H-6), 7.46 – 7.38 (m, 4H, 4x H-2''), 7.10 – 7.02 (m, 4H, 4x H-3''), 6.70 – 6.66 (m, 1H, H-17), 6.21 (t, <sup>3</sup>J<sub>HH</sub> = 6.5 Hz, 1H, H-1'), 5.23 – 5.16 (m, 4H, 4x H-5''), 4.64 – 4.56 (m, 1H, H-3'), 4.36 – 4.14 (m, 2H, H-5'), 4.14 – 4.07 (m, 1H, H-4'), 3.15 – 3.09 (m, 2H, H-14), 2.60 (t, <sup>3</sup>J<sub>HH</sub> = 7.4 Hz, 4H, 2x H-b), 2.49 (t, <sup>3</sup>J<sub>HH</sub> = 6.8 Hz, 2H, H-9), 2.44 – 2.32 (m, 3H, H-11, H-2'a), 2.29 – 2.18 (m, 1H, H-2'b), 2.12 (m, 3H, H-18), 1.94 – 1.82 (m, 2H, H-10), 1.81 – 1.69 (m, 4H, 2x H-c), 1.49 – 1.26 (m, 24H, 2x H-d-i), 0.96 – 0.89 (m, 6H, 2x H-j).

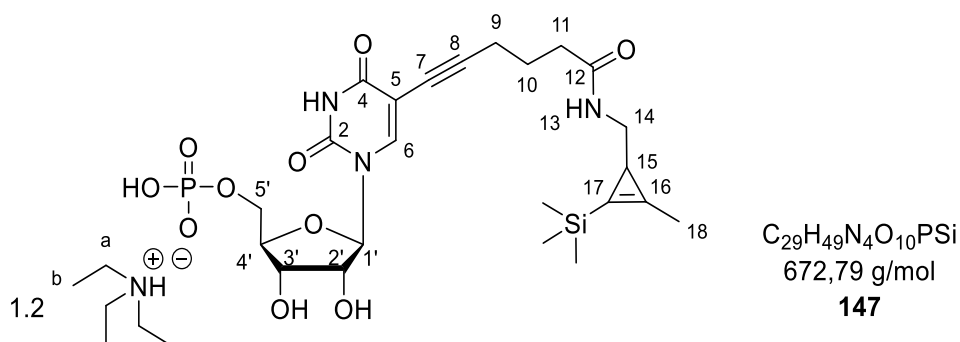
<sup>13</sup>C-NMR (151 MHz, MeOD):  $\delta$  [ppm] = 175.4 (C-12), 173.7 (2x C-a), 152.3 (2x C-1''), 146.3 (C-6), 135.0 (d, <sup>3</sup>J<sub>CP</sub> = 9.6 Hz, 2x C-4''), 130.5 (d, <sup>4</sup>J<sub>CP</sub> = 1.6 Hz, 4x C-3''), 122.8 (4x C-2''), 122.7 (C-16), 98.7 (C-8), 93.1 (C-5), 104.0 (C-17), 88.5 (C-1'), 88.2 (d, <sup>2</sup>J<sub>CP</sub> = 10.6 Hz, C-4'), 72.2 (C-7), 70.4 (C-3'), 70.4 (2x C-5''), 66.5 (m, C-5'), 2x 46.4 (C-14, diaster.), 41.6 (C-2'),

35.9 (C-11), 35.0 (2x C-b), 33.1 (2x C-h), 30.6, 30.4, 30.4, 30.2 (2x C-d-g), 26.0 (C- C-c), 25.5 (C-10), 23.7 (2x i), 20.0 (C-15), 19.1 (C-9), 14.5 (C-j), 11.6 (C-18).

$^{31}\text{P}$ -NMR (162 MHz, MeOD):  $\delta$  [ppm] = -11.483(d,  $^2J_{\text{PP}} = 20.2$ , P- $\alpha$ ), -13.23 (d,  $^2J_{\text{PP}} = 17.1$ , P- $\gamma$ ), -23.80 (dd,  $^2J_{\text{PP}} = 19.9$ , 17.3, P- $\beta$ ).

HRMS (ESI $^-$ ):  $m/z$  = calcd: 1161.4373 [M-H] $^-$ , found: 1161.754 [M-H] $^-$ .

### (TMS-1MCP)-uridine monophosphate **147**



The TEAH salt of IUMP **90** (1.55 TEAH, 121 mg, 200  $\mu\text{mol}$ ),  $\text{Pd}_2(\text{dba})_3$  (11 mg, 11  $\mu\text{mol}$ , 5.4 mol%), tri(2-furyl) phosphine (5.6 mg, 24  $\mu\text{mol}$ , 12 mol%) and copper(I) iodide (5.7 mg, 30  $\mu\text{mol}$ , 15 mol%) were suspended in DMSO (3 mL). The reaction flask was then evaporated and flushed with nitrogen (3x) followed by the addition of triethylamine (194  $\mu\text{L}$ , 1.40 mmol) and alkyne **136** (60 mg, 240  $\mu\text{mol}$ ). The reaction mixture was stirred for 2 h at 50  $^\circ\text{C}$  and was then concentrated *in vacuo* at the same temperature to remove all volatiles. The remaining solids were dissolved in 0.05 M TEAB and purified on RP $_{18}$  silica gel using automated flash chromatography (0.05 M TEAB/ $\text{CH}_3\text{CN}$ ; 100:0 to 0:100). The resulting monophosphate was solved in  $\text{CH}_3\text{OH}$ , filtered through a syringe filter, and concentrated *in vacuo* to yield the TEAH salt of **147** (97 mg, 70%) as a light-yellow solid.

$^1\text{H}$ -NMR (500 MHz, MeOD):  $\delta$  [ppm] = 9.08 (s, 1H, H-6), 6.01 (s, 1H, H-1'), 4.40 – 4.09 (m, 5H, H-2', H-3', H-5'), 3.23 (dd,  $^3J_{\text{HH}} = 13.6$ , 4.2 Hz, 1H, H-14a), 3.16 (q,  $^3J_{\text{HH}} = 7.3$  Hz, 7H), 2.84 (dd,  $^3J_{\text{HH}} = 13.5$ , 5.5 Hz, 1H, H-14a), 2.73 (t,  $^3J_{\text{HH}} = 7.3$  Hz, 2H, H-9), 2.28 (t,  $^3J_{\text{HH}} = 7.5$  Hz, 2H, H-11), 2.19 (s, 3H, H-18), 2.00 (p,  $^3J_{\text{HH}} = 7.4$  Hz, 2H, H-10), 1.43 (dd,  $^3J_{\text{HH}} = 5.5$ , 4.1 Hz, 1H, H-15), 1.29 (t,  $^3J_{\text{HH}} = 7.3$  Hz, 10H, H-b), 0.15 (s, 9H, Si-( $\text{CH}_3$ ) $_3$ ).

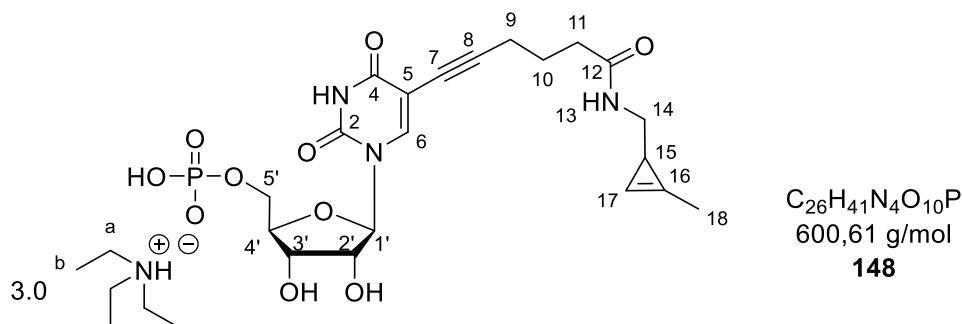
$^{13}\text{C}$ -NMR (126 MHz, MeOD):  $\delta$  [ppm] = 174.7 (C-12), 159.8 (C-4), 157.2 (C-2), 139.4 (C-6), 137.8 (C-16), 112.9 (C-17), 109.8 (C-5), 102.2 (HMBC, C-8), 93.6 (C-1'), 84.7 (d,  $^2J_{\text{CP}} =$

8.2 Hz, C-4'), 77.1 (C-2'), 69.5 (C-3'), 63.9 (m, C-5'), 47.8 (C-14), 47.7 (C-a), 36.1 (C-11), 28.4 (C-9), 24.4 (C-10), 20.7 (C-15), 13.0 (C-18), 9.3 (C-b), -1.0 (Si-(CH<sub>3</sub>)<sub>3</sub>).

<sup>31</sup>P-NMR (202 MHz, MeOD): δ [ppm] = 2.13 (s).

HRMS (ESI<sup>-</sup>): *m/z* = calcd: 570.1673 [M-H]<sup>-</sup>, found: 570.1610 [M-H]<sup>-</sup>.

### (1MCP)-uridine monophosphate **148**



An appropriate amount of TMS-1MCP-UMP triethylammonium salt **147** was subjected to a Dowex ion-exchange chromatography to provide protonated TMS-1MCP-dCMP (50 mg, 90 μmol). The monophosphate was dissolved in a DMF/ THF mixture (1:2 v/v, 3 mL) followed by the addition of 1 M TBAF in THF (270 μl, 270 μmol). The reaction mixture was stirred at room temperature overnight. The solvents were removed under reduced pressure, and the residue was purified on RP<sub>18</sub> silica gel using automated flash chromatography (0.05 M TEAB/CH<sub>3</sub>CN; 100:0 to 0:100). The appropriate fractions were freeze-dried to yield the TEAH salt of **148** (57 mg, 79%) as a light-yellow solid.

It is suspected that the two diastereomeric products exist in *syn*- and *anti*-rotamers during NMR spectroscopy. Hence, no signal assignment was carried out.

<sup>1</sup>H-NMR (500 MHz, MeOD): δ [ppm] = 9.13 (s, 0.4H), 8.02 (s, 0.6H), 6.67 – 6.60 (m, 1H), 6.04 – 5.92 (m, 1H), 4.34 – 4.00 (m, 5H), 3.14 – 3.04 (m, 2H), 2.86 (q, <sup>3</sup>J<sub>HH</sub> = 7.3 Hz, 21H), 2.77 – 2.68 (m, 1H), 2.46 – 2.36 (m, 2H), 2.26 (t, <sup>3</sup>J<sub>HH</sub> = 7.5 Hz, 1H), 1.99 (p, <sup>3</sup>J<sub>HH</sub> = 7.4 Hz, 1H), 1.92 – 1.79 (m, 1H), 1.55 – 1.48 (m, 1H), 1.17 (t, <sup>3</sup>J<sub>HH</sub> = 7.3 Hz, 32H).

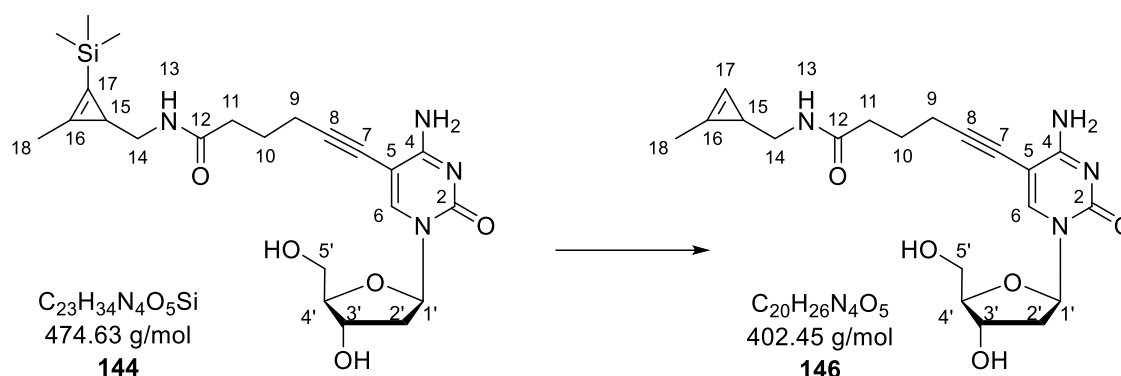
<sup>13</sup>C-NMR (126 MHz, MeOD): δ [ppm] = 175.4, 175.0, 151.8, 144.1, 139.6, 122.8, 103.9, 103.8, 102.3, 101.7, 94.8, 93.6, 89.7, 85.8, 84.8, 77.2, 75.2, 72.0, 69.6, 65.6, 49.5, 49.3, 49.2, 49.0, 48.8, 48.7, 48.5, 47.2, 46.4, 46.3, 36.1, 35.9, 28.4, 25.7, 24.4, 19.6, 19.0, 19.0, 11.5, 11.5, 10.1.

<sup>31</sup>P-NMR (202 MHz, MeOD): δ [ppm] = 3.18 (s), 3.00 (s).

HRMS (ESI<sup>-</sup>): *m/z* = 498.1283 [M-H]<sup>-</sup>, found: 498.1131 [M-H]<sup>-</sup>.





**(1MCP)-2'-deoxycytidine 146**

IdC **152** (53 mg, 150  $\mu$ mol),  $Pd_2(dba)_3$  (7.4 mg, 8.0  $\mu$ mol, 5.4 mol%), tri(2-furyl) phosphine (4.2 mg, 18  $\mu$ mol, 12 mol%) and copper(I) iodide (4.3 mg, 23  $\mu$ mol, 15 mol%) were suspended in DMSO (1 mL). The reaction flask was then evaporated and flushed with nitrogen (3x) followed by the addition of triethylamine (146  $\mu$ L, 1.05 mmol) and alkyne **136** (45 mg, 180  $\mu$ mol). The reaction mixture was stirred for 2 h at 50  $^{\circ}C$  and then concentrated *in vacuo*. The residue was dissolved in water, filtered through a syringe filter, and purified on RP<sub>18</sub> silica gel using automated flash chromatography (H<sub>2</sub>O/CH<sub>3</sub>CN; 100:0 to 0:100) to yield the TMS-protected intermediate **144** (38 mg, 53%) as a light-yellow solid.

<sup>1</sup>H-NMR (300 MHz, DMSO-*d*<sub>6</sub>):  $\delta$  [ppm] = 8.07 (s, 1H), 7.75 – 7.62 (m, 2H), 6.77 (s, 1H), 6.11 (t, <sup>3</sup>J<sub>HH</sub> = 6.6 Hz, 1H), 5.19 (d, <sup>3</sup>J<sub>HH</sub> = 4.2 Hz, 1H), 5.05 (t, <sup>3</sup>J<sub>HH</sub> = 5.0 Hz, 1H), 4.24 – 4.13 (m, 1H), 3.78 (q, <sup>3</sup>J<sub>HH</sub> = 3.4 Hz, 1H), 3.66 – 3.49 (m, 2H), 3.15 – 3.01 (m, 1H), 2.77 – 2.65 (m, 1H), 2.39 (t, <sup>3</sup>J<sub>HH</sub> = 7.0 Hz, 2H), 2.23 – 2.08 (m, 5H), 2.04 – 1.89 (m, 1H), 1.83 – 1.68 (m, 2H), 1.32 (dd, <sup>3</sup>J<sub>HH</sub> = 5.3, 4.2 Hz, 1H), 0.13 (s, 8H).

The nucleoside **144** (38 mg, 80  $\mu$ mol) was solved in DMF (1 mL). In parallel, TBAF monohydrate (25 mg, 88  $\mu$ mol) was co-evaporated with THF (1 mL) and solved again in THF (3 mL). The TBAF in THF solution was added to the solved nucleoside and the reaction mixture was stirred overnight at room temperature. The solvents were removed under reduced pressure, and the residue was purified on RP<sub>18</sub> silica gel using automated flash chromatography (0.05 M TEAB/CH<sub>3</sub>CN; 100:0 to 0:100) to provide 1MCP-dC **146** (32 mg, 99%) as a light-yellow solid.

<sup>1</sup>H-NMR (400 MHz, MeOD):  $\delta$  [ppm] = 8.26 (s, 1H, *H*-6), 6.66 – 6.60 (m, 1H, *H*-17), 6.20 (t, <sup>3</sup>J<sub>HH</sub> = 6.3 Hz, 1H, *H*-1'), 5.48 (s, 1H, NH), 4.39 – 4.31 (m, 1H, *H*-3'), 3.96 – 3.89 (m, 1H, *H*-4'), 3.82 (dd, <sup>2</sup>J<sub>HH</sub> = 12.1, <sup>3</sup>J<sub>HH</sub> = 3.1 Hz, 1H, *H*-5'a), 3.72 (dd, <sup>2</sup>J<sub>HH</sub> = 12.1 Hz, <sup>3</sup>J<sub>HH</sub> = 3.6 Hz,

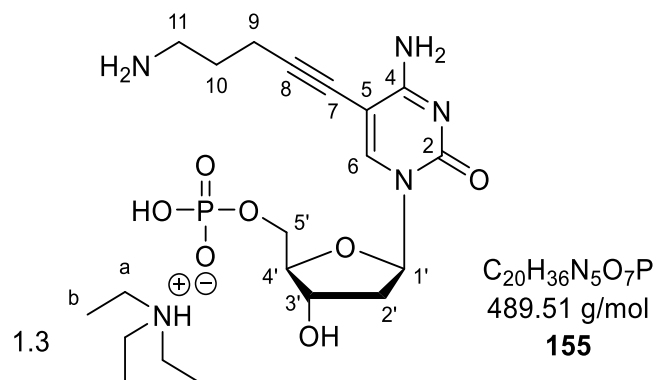
$^1\text{H}$ ,  $H-5'b$ ), 3.09 (d,  $^3J_{\text{HH}} = 4.3$  Hz, 2H,  $H-14$ ), 2.47 (t,  $^3J_{\text{HH}} = 6.9$  Hz, 2H,  $H-9$ ), 2.41 – 2.27 (m, 3H,  $H-2'a$ ,  $H-11$ ), 2.17 – 2.06 (m, 4H,  $H-2'b$ ,  $H-18$ ), 1.92 – 1.81 (m, 2H,  $H-10$ ), 1.50 (td,  $^3J_{\text{HH}} = 4.3, 1.7$  Hz, 1H,  $H-15$ ).

$^{13}\text{C}$ -NMR (101 MHz, MeOD):  $\delta$  [ppm] = 175.2 (C-12), 166.5 (C-4), 156.8 (C-2), 145.2 (C-6), 122.8 (C-16), 103.8 (C-13), 96.3 (C-8), 93.4 (C-5), 89.0 (C-4'), 87.8 (C-1'), 72.8 (C-7), 71.7 (C-3'), 62.5 (C-5'), 46.4 (C-14), 42.4 (C-2'), 36.1 (C-11), 25.9 (C-10), 19.8 (C-15), 18.9 (C-18), 11.4 (C-18).

HRMS (ESI<sup>-</sup>):  $m/z$  = calcd: 403.1981 [M+H]<sup>+</sup>, found: 403.1994 [M+H]<sup>+</sup>.

### 6.3.11 Preparation of rapid pronucleotide reporters

#### 5-(5-Aminopent-1-yn-1-yl)-2'-deoxycytidine monophosphate **155**



The TEAH salt of IdCMP **145** (1.4 TEAH, 862 mg, 1.50 mmol),  $\text{Pd}_2(\text{dba})_3$  (74 mg, 81  $\mu\text{mol}$ , 5.4 mol%) and tri(2-furyl) phosphine (42 mg, 180  $\mu\text{mol}$ , 12 mol%) were dried *in vacuo* shortly and solved in DMSO (10 mL). The reaction flask was evaporated and flushed with nitrogen three times. After the addition of  $\text{Et}_3\text{N}$  (624  $\mu\text{L}$ , 4.50 mmol) and 4-pentyne-1-amine (203  $\mu\text{L}$ , 2.10 mmol), the reaction mixture was stirred at 55 °C for 1.5 h (complete conversion was controlled by TLC ( $\text{H}_2\text{O}/\text{CH}_3\text{CN}$ ; 3:7)). After adding  $\text{H}_2\text{O}$  (30 mL) to the turbid suspension, the reaction mixture was filtrated over a short  $\text{RP}_{18}$  silica plug with additional amounts of  $\text{H}_2\text{O}$ . Then, the  $\text{H}_2\text{O}$  was removed under reduced pressure, followed by the slow addition of acetone to the DMSO solution. The precipitated crude product was collected by centrifugation, dissolved in 0.05 M TEAB, and purified on  $\text{RP}_{18}$  silica gel using automated flash chromatography (0.05 M TEAB/ $\text{CH}_3\text{CN}$ ; 100:0 to 0:100) to yield the TEAH salt **155** (676 mg, 87%) as a light-yellow solid.

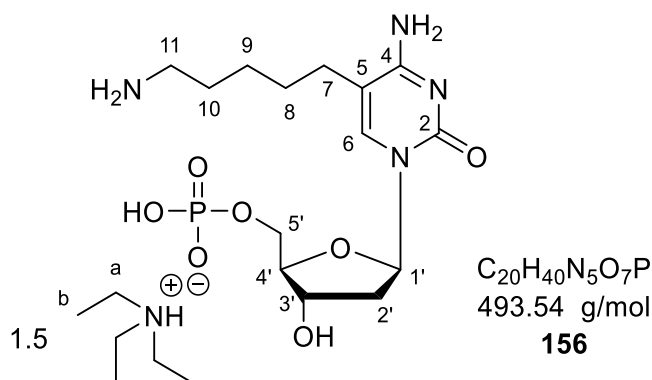
$^1\text{H-NMR}$  (600 MHz,  $\text{D}_2\text{O}$ ):  $\delta$  [ppm] = 8.03 (s, 1H,  $H-6$ ), 6.17 (dd,  $^3J_{\text{HH}} = 7.4, 6.2$ , 1H,  $H-1'$ ), 4.44 (dt,  $^3J_{\text{HH}} = 6.3, 3.2$  Hz, 1H,  $H-3'$ ), 4.04 (qd,  $^3J_{\text{HH}} = 3.7, 1.1$  Hz, 1H,  $H-4'$ ), 3.83 (dd,  $^3J_{\text{HH}} = 5.1, 3.7$  Hz, 2H,  $H-5'$ ), 3.10 – 3.02 (m, 11H,  $H-a, H-11$ ), 2.45 (t,  $^3J_{\text{HH}} = 6.6$  Hz, 2H,  $H-9$ ), 2.30 – 2.18 (m, 2H,  $H-2'$ ), 1.82 (p,  $^3J_{\text{HH}} = 6.9$  Hz, 2H,  $H-10$ ), 1.14 (t,  $^3J_{\text{HH}} = 7.3$  Hz, 13H,  $H-b$ ).

$^{13}\text{C-NMR}$  (151 MHz,  $\text{D}_2\text{O}$ ):  $\delta$  [ppm] = 165.7 ( $C-4$ ), 151.3 ( $C-2$ ), 144.0 ( $C-6$ ), 99.8 ( $C-5$ ), 93.6 ( $C-8$ ), 86.5 (d,  $^3J_{\text{CP}} = 8.5$  Hz,  $C-4'$ ), 85.5 ( $C-1'$ ), 72.8 ( $C-7$ ), 71.0 ( $C-3'$ ), 63.5 (d,  $^2J_{\text{CP}} = 4.5$  Hz,  $H-5'$ ), 46.6 ( $C-a$ ), 39.1 ( $C-2'$ ), 38.7 ( $C-11$ ), 25.2 ( $C-10$ ), 16.1 ( $C-9$ ), 8.2 ( $C-b$ ).

$^{31}\text{P-NMR}$  (202 MHz,  $\text{D}_2\text{O}$ ):  $\delta$  [ppm] = 0.52 (s).

HRMS (ESI $^-$ ):  $m/z$  = calcd: 387.1075 [ $\text{M-H}$ ] $^-$ , found: 387.1003 [ $\text{M-H}$ ] $^-$ .

### 5-(5-Aminopent-1-yl)-2'-deoxycytidine monophosphate **156**



5-(5-Aminopent-1-yl)-dCMP triethylammonium salt **155** (450 mg, 920  $\mu\text{mol}$ ) and 20%  $\text{Pd}(\text{OH})_2/\text{C}$  (129 mg, 184  $\mu\text{mol}$ ) were dried *in vacuo*, co-evaporated with  $\text{CH}_3\text{OH}$  once and suspended in 30 mL  $\text{CH}_3\text{OH}$ . After the stepwise addition of  $\text{Et}_3\text{N}$  (641  $\mu\text{L}$ , 4.60 mmol) and triethylsilane (1.47 mL, 9.20 mmol), the pressure tube was closed tightly, and the reaction mixture was stirred at room temperature for 36 h. The reaction mixture was diluted with  $\text{H}_2\text{O}$  and filtered through a short silica column using  $\text{H}_2\text{O}/\text{CH}_3\text{CN}$  1:1 v/v (TLC controlled). All volatiles were removed under reduced pressure. The residue was purified on  $\text{RP}_{18}$  silica gel using automated flash chromatography (0.05 M TEAB/ $\text{CH}_3\text{CN}$ ; 100:0 to 0:100) to yield the TEAH salt of **156** (497 mg, 81%) as a colorless solid.

$^1\text{H-NMR}$  (600 MHz,  $\text{D}_2\text{O}$ ):  $\delta$  [ppm] = 7.77 (s, 1H,  $H-6$ ), 6.34 (dd,  $^3J_{\text{HH}} = 7.5, 6.2$  Hz, 1H,  $H-1'$ ), 4.57 – 4.54 (m, 1H,  $H-3'$ ), 4.17 – 4.12 (m, 1H,  $H-4'$ ), 3.98 – 3.91 (m, 2H,  $H-5'$ ), 3.18 (q,  $^3J_{\text{HH}} = 7.3$  Hz, 9H,  $H-a$ ), 2.99 – 2.93 (m, 2H,  $H-11$ ), 2.50 – 2.40 (m, 2H,  $H-7$ ), 2.40 – 2.27

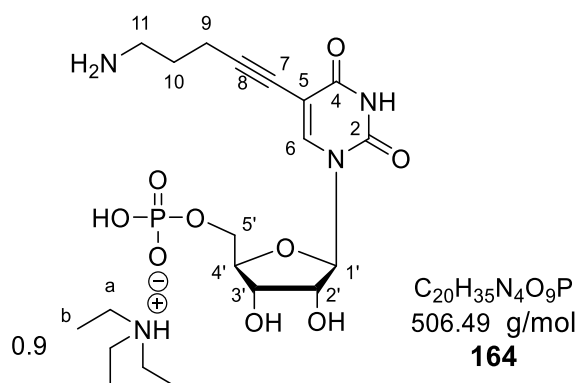
(m, 2H, *H*-2'), 1.77 – 1.63 (m, 2H, *H*-10), 1.63 – 1.55 (m, 2H, *H*-8), 1.43 – 1.32 (m, 2H, *H*-9), 1.27 (t,  $^3J_{\text{HH}} = 7.3$  Hz, 13H, *H*-b).

$^{13}\text{C}$ -NMR (151 MHz,  $\text{D}_2\text{O}$ ):  $\delta$  [ppm] = 165.3 (*C*-4), 157.3 (*C*-2), 138.9 (*C*-6), 108.2 (*C*-5), 86.1 (d,  $^3J_{\text{CP}} = 8.2$  Hz, *C*-4'), 85.5 (*C*-1'), 71.0 (*C*-3'), 63.6 (d,  $^2J_{\text{CP}} = 4.5$  Hz, *C*-5'), 46.6 (*C*-a), 39.2 (*C*-11), 39.1 (*C*-2'), 26.0 (*C*-10), 25.6, 25.6 (*C*-7, *C*-8), 24.1 (*C*-9), 8.2 (*C*-b).

$^{31}\text{P}$ -NMR (243 MHz,  $\text{D}_2\text{O}$ ):  $\delta$  [ppm] = 3.77 (s).

HRMS (ESI<sup>-</sup>):  $m/z$  = calcd: 391.1388 [*M*-H]<sup>-</sup>, found: 391.1252 [*M*-H]<sup>-</sup>.

### 5-(5-Aminopent-1-yn-1-yl)-uridine monophosphate **164**



The TEAH salt of IUMP **90** (1.55 TEAH, 304 mg, 0.500 mmol),  $\text{Pd}_2(\text{dba})_3$  (25 mg, 27  $\mu\text{mol}$ , 5.4 mol%) and tri(2-furyl) phosphine (14 mg, 60  $\mu\text{mol}$ , 12 mol%) were dried *in vacuo* shortly and dissolved in DMSO (3 mL). The reaction flask was evaporated and flushed with nitrogen three times. After the addition of  $\text{Et}_3\text{N}$  (693  $\mu\text{L}$ , 5.00 mmol) and 4-pentyne-1-amine (68  $\mu\text{L}$ , 0.70 mmol), the reaction mixture was stirred at 50 °C for 2 h (complete conversion was controlled by TLC ( $\text{H}_2\text{O}/\text{CH}_3\text{CN}$ ; 3:7)). All volatiles were removed under reduced pressure at 50 °C. The remaining residue was dissolved in 0.05 M TEAB and purified on  $\text{RP}_{18}$  silica gel using automated flash chromatography (0.05 M TEAB/ $\text{CH}_3\text{CN}$ ; 100:0 to 0:100, loading through a syringe filter to remove the catalyst) to yield the TEAH salt **164** (200 mg, 80%) as a light-yellow solid.

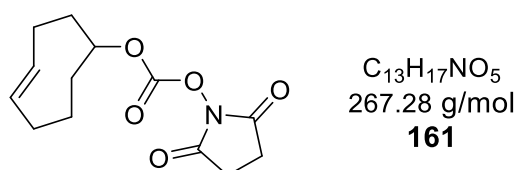
$^1\text{H}$ -NMR (400 MHz,  $\text{D}_2\text{O}$ ):  $\delta$  [ppm] = 8.21 (s, 1H, *H*-6), 6.01 (d,  $^3J_{\text{HH}} = 5.0$  Hz, 1H, *H*-1'), 4.40 (t,  $^3J_{\text{HH}} = 5.1$  Hz, 1H, *H*-2'), 4.36 (t,  $^3J_{\text{HH}} = 4.6$  Hz, 1H, *H*-3'), 4.32 – 4.26 (m, 1H, *H*-4'), 4.14 – 4.01 (m, 2H, *H*-5'), 3.27 – 3.16 (m, 8H, *H*-b, *H*-11), 2.61 (t,  $^3J_{\text{HH}} = 6.5$  Hz, 2H, *H*-9), 1.98 (p,  $^3J_{\text{HH}} = 6.9$  Hz, 2H, *H*-10), 1.30 (t,  $^3J_{\text{HH}} = 7.3$  Hz, 9H, *H*-a).

$^{13}\text{C}$ -NMR (101 MHz,  $\text{D}_2\text{O}$ ):  $\delta$  [ppm] = 164.8 (C-4), 150.8 (C-2), 143.7 (C-6), 100.0 (C-5), 93.9 (C-8), 88.4 (C-1'), 84.1 (d,  $^3J_{\text{CP}} = 8.7$  Hz, C-4'), 74.2 (C-2'), 72.5 (C-7), 69.8 (C-3'), 63.4 (d,  $^2J_{\text{CP}} = 4.2$  Hz, C-5'), 46.7 (C-a), 38.6 (C-11), 25.2 (C-10), 16.1 (C-9), 8.2 (C-b).

$^{31}\text{P}$ -NMR (162 MHz,  $\text{D}_2\text{O}$ ):  $\delta$  [ppm] = 2.85 (s).

HRMS (ESI $^-$ ):  $m/z$  = calcd: 404.0864 [M-H] $^-$ , found: 404.0719 [M-H] $^-$ .

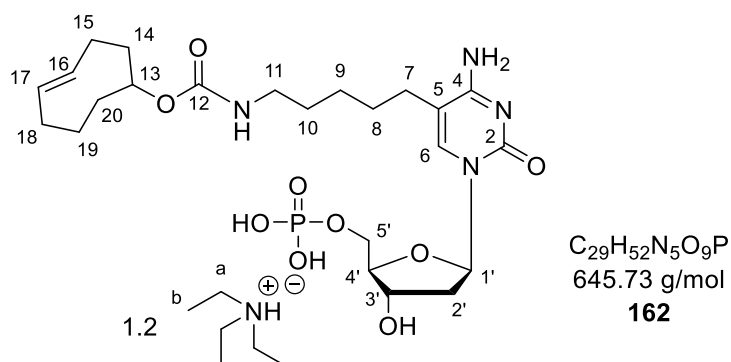
### (*E*)-Cyclooct-4-en-1-yl (2,5-dioxopyrrolidin-1-yl) carbonate **161**



The reaction was carried out as described in the literature with (*E*)-cyclooct-4-enol (189 mg, 1.50 mmol), disuccinimidyl ester (961 mg, 3.75 mmol), and triethylamine (627  $\mu\text{L}$ , 4.50 mmol) in  $\text{CH}_3\text{CN}$  (2 mL) at room temperature overnight. The product **161** (566 mg, 77%) was obtained as a colorless solid after purification on silica gel (petroleum ether/ethyl acetate; 6:4).

The analytical data was in accordance with those described.<sup>165</sup>

### (4TCO)-2'-deoxycytidine monophosphate **162**



The TEAH salt of 5-(5-aminopent-1-yl)-dCMP **156** (1.0 TEAH, 49 mg, 0.10 mmol) was solved in DMSO (2 mL) under the addition of  $\text{Et}_3\text{N}$  (42  $\mu\text{L}$ , 0.30 mmol). After adding 4TCO-NHS active ester **161** (37 mg, 0.14 mmol) to the reaction mixture, it was stirred for 60 min at room temperature (complete conversion was controlled by TLC ( $\text{H}_2\text{O}/\text{CH}_3\text{CN}$ ; 3:7)). All volatiles were removed under reduced pressure at 60  $^\circ\text{C}$ . The resulting residue was dissolved in 0.05 M TEAB and purified on RP $_{18}$  silica gel using automated flash chromatography (0.05 M TEAB/ $\text{CH}_3\text{CN}$ ; 100:0 to 0:100) to yield the TEAH salt **162** (31 mg, 46%) as a light-yellow solid.

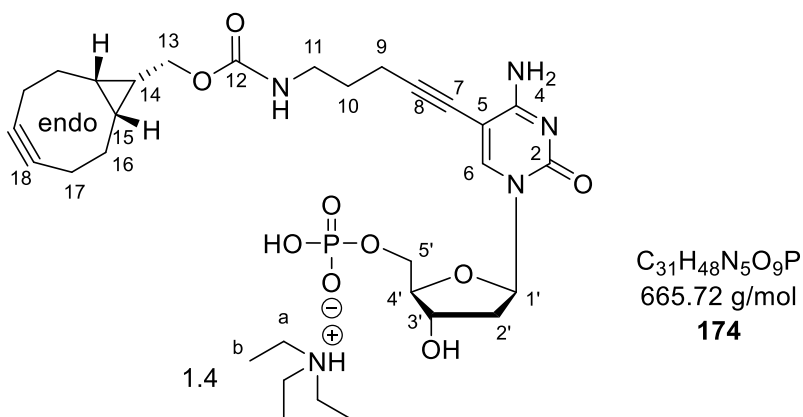


*H*-17), 5.10 – 5.04 (m, 4H, 4x *H*-5''), 4.58 – 4.45 (m, 2H, *H*-13, *H*-3'), 4.21 – 4.05 (m, 2H, *H*-5'), 3.95 – 3.90 (m, 1H, *H*-4'), 3.13 – 3.03 (m, 2H, *H*-11), 2.94 (m, 2H, *H*-alkyl), 2.47 (t,  $^3J_{\text{HH}} = 7.4$  Hz, 4H, 2x *H*-b), 2.28 – 2.20 (m, 2H, *H*-alkyl), 2.19 – 2.12 (m, 1H, *H*-alkyl), 2.10 – 2.02 (m, 2H, *H*-alkyl), 2.02 – 1.91 (m, 1H, *H*-alkyl), 1.83 – 1.69 (m, 1H, *H*-alkyl), 1.69 – 1.57 (m, 4H, *H*-alkyl), 1.56 – 1.08 (m, 40H, *H*-alkyl), 0.85 – 0.74 (m, 6H, 2x *H*-j).

$^{31}\text{P}$ -NMR (162 MHz, MeOD):  $\delta$  [ppm] = -11.68 (d,  $^2J_{\text{PP}} = 19.9$  Hz, *P*- $\alpha$ ), -13.18 (d,  $^2J_{\text{PP}} = 16.8$  Hz, *P*- $\gamma$ ), -23.38 – -24.00 (m, *P*- $\beta$ ).

HRMS (ESI<sup>-</sup>):  $m/z = \text{calcd: } 1224.5138 [\text{M}^{\text{isotope}}\text{-H}]^-$ , found: 1224.4977  $[\text{M}^{\text{isotope}}\text{-H}]^-$ .

### (BCN<sup>endo</sup>)-2'-deoxycytidine monophosphate **174**



The TEAH salt of 5-(5-aminopent-1-yl-1-yn)-dCMP **155** (0.4 TEAH, 51 mg, 0.12 mmol) was solved in DMSO (2 mL) under the addition of Et<sub>3</sub>N (60  $\mu\text{L}$ , 0.43 mmol). The commercially available BCN-NHS active ester (42 mg, 0.14 mmol) was added to the reaction mixture, which was stirred for 30 min at 40 °C (complete conversion was controlled by TLC (H<sub>2</sub>O/CH<sub>3</sub>CN; 3:7)). All volatiles were removed under reduced pressure at 60 °C, and the resulting residue was dissolved in 0.05 M TEAB and purified on RP<sub>18</sub> silica gel using automated flash chromatography (0.05 M TEAB/CH<sub>3</sub>CN; 100:0 to 0:100) to yield the TEAH salt **174** (50 mg, 59%) as a light-yellow solid.

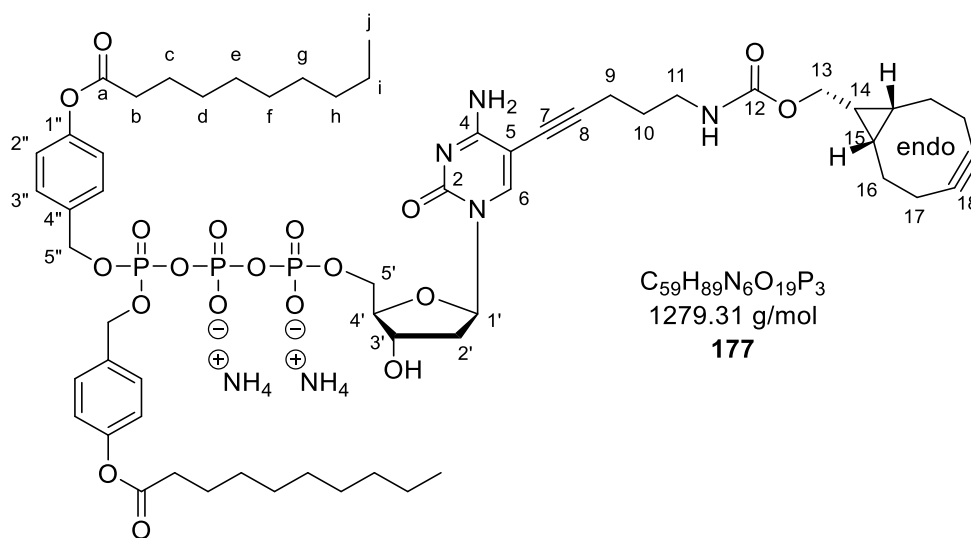
$^1\text{H}$ -NMR (400 MHz, MeOD):  $\delta$  [ppm] = 8.11 (s, 1H, H-6), 6.28 (dd,  $^3J_{\text{HH}} = 7.7, 5.7$  Hz, 1H, H-1'), 4.50 (t,  $^3J_{\text{HH}} = 3.7$  Hz, 1H, H-3'), 4.16 (d,  $^3J_{\text{HH}} = 8.1$  Hz, 1H, H-4'), 4.13 – 4.00 (m, 5H, H-4', H-5', H-13), 3.29 (t,  $^3J_{\text{HH}} = 6.6$  Hz, 2H, H-11), 3.21 (q,  $^3J_{\text{HH}} = 7.3$  Hz, 7H, H-b), 2.50 (t,  $^3J_{\text{HH}} = 6.7$  Hz, 2H, H-alkyl), 2.37 (ddd,  $^2J_{\text{HH}} = 13.5$  Hz,  $^3J_{\text{HH}} = 5.8, 2.9$  Hz, 1H, H-5'a), 2.33 – 2.13 (m, 6H, H-alkyl), 1.82 – 1.74 (m, 2H, H-alkyl), 1.68 – 1.55 (m, 2H, H-alkyl), 1.33 (t,  $^3J_{\text{HH}} = 7.3$  Hz, 11H, H-b), 0.99 – 0.88 (m, 2H, H-15).

$^{31}\text{P}$ -NMR (162 MHz, MeOD):  $\delta$  [ppm] = 1.02 (s).



HRMS (ESI<sup>-</sup>):  $m/z$  = calcd: 563.1912 [M-H]<sup>-</sup>, found: 563.1910 [M-H]<sup>-</sup>.

**$\gamma$ -(C9C9AB)-BCN<sup>endo</sup>-dCTP **177****

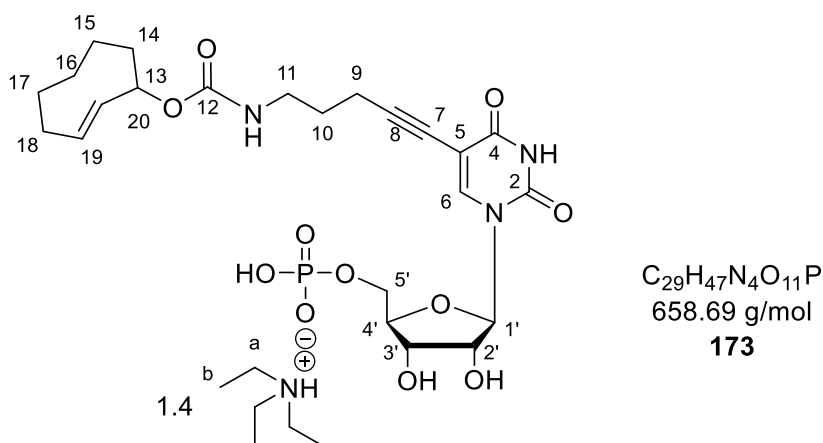


The reaction was carried out with the general procedure VIII with the pyrophosphate of **95** (145 mg, 154  $\mu$ mol), TFAA (107  $\mu$ L, 771  $\mu$ mol), and Et<sub>3</sub>N (172  $\mu$ L, 1.23 mmol) in CH<sub>3</sub>CN (6 ml). The subsequent activation step was performed with 1-methylimidazole (31  $\mu$ L, 386  $\mu$ mol) in DMF (3 ml) followed by the coupling with monophosphate **174** (1.4 TEAH, 54 mg, 77  $\mu$ mol) solved in DMF (3 mL) under the addition of Et<sub>3</sub>N (22  $\mu$ L, 154  $\mu$ mol). Purification on RP<sub>18</sub> silica gel with automated flash chromatography (H<sub>2</sub>O/CH<sub>3</sub>CN; 100:0 to 0:100), Dowex ion-exchange (NH<sub>4</sub><sup>+</sup>), and RP<sub>18</sub> silica gel with automated flash chromatography (H<sub>2</sub>O/CH<sub>3</sub>CN; 100:0 to 0:100) as well as subsequent freeze-drying provided **177** (5 mg, 5%) as colorless cotton.

<sup>1</sup>H-NMR (600 MHz, MeOD):  $\delta$  [ppm] = 8.21 (s, 1H), 7.42 – 7.39 (m, 4H), 7.07 – 7.02 (m, 4H), 6.17 – 6.08 (m, 1H), 5.22 – 5.13 (m, 4H), 4.63 – 4.58 (m, 1H), 4.30 – 4.22 (m, 2H), 4.13 – 4.09 (m, 3H), 3.24 (t, <sup>3</sup>J<sub>HH</sub> = 6.5 Hz, 2H), 2.61 – 2.55 (m, 6H), 2.47 (t, <sup>3</sup>J<sub>HH</sub> = 6.7 Hz, 2H), 2.38 (ddd, <sup>2</sup>J<sub>HH</sub> = 13.6 Hz, <sup>3</sup>J<sub>HH</sub> = 6.0, 3.4 Hz, 1H), 2.30 – 2.11 (m, 8H), 1.80 – 1.69 (m, 8H), 1.66 – 1.52 (m, 2H), 1.47 – 1.27 (m, 37H), 0.91 (t, <sup>3</sup>J<sub>HH</sub> = 6.9 Hz, 2H).

<sup>31</sup>P-NMR (243 MHz, MeOD):  $\delta$  [ppm] = -11.85 (d, <sup>2</sup>J<sub>PP</sub> = 20.2 Hz, P- $\alpha$ ), -13.29 (d, <sup>2</sup>J<sub>PP</sub> = 16.5 Hz, P- $\gamma$ ), -23.96 (t, <sup>2</sup>J<sub>PP</sub> = 18.0 Hz, P- $\beta$ ).

HRMS (ESI<sup>-</sup>):  $m/z$  = calcd: 1243.4795 [M-H]<sup>-</sup>, found: 1243.4315 [M-H]<sup>-</sup>.

**(2TCO $\alpha$ )-uridine monophosphate **173****

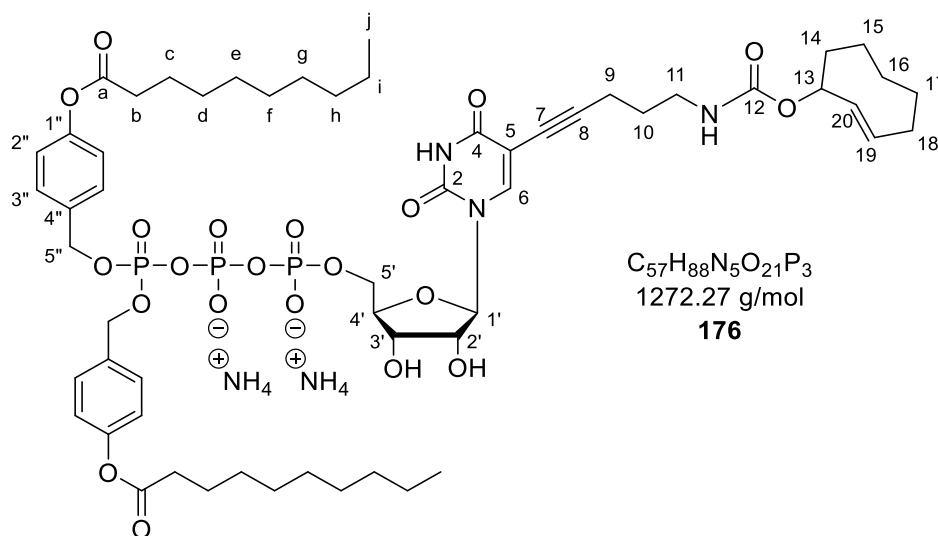
The TEAH salt of 5-(5-aminopent-1-yn-1-yl)-UMP **164** (0.9 TEAH, 46 mg, 90  $\mu$ mol) was solved in DMSO (2 mL) under the addition of Et<sub>3</sub>N (60  $\mu$ L, 0.43 mmol). The commercially available 2TCO $\alpha$ -NHS active ester (39 mg, 0.14 mmol) was added to the reaction mixture, which was stirred for 60 min at room temperature (complete conversion was controlled by TLC (H<sub>2</sub>O/CH<sub>3</sub>CN; 3:7)). All volatiles were removed under reduced pressure at 60 °C, and the resulting residue was dissolved in 0.05 M TEAB and purified on RP<sub>18</sub> silica gel using automated flash chromatography (0.05 M TEAB/CH<sub>3</sub>CN; 100:0 to 0:100) to yield the TEAH salt **173** (59 mg, 93%) as a light-yellow solid.

<sup>1</sup>H-NMR (400 MHz, MeOD):  $\delta$  [ppm] = 8.05 (s, 1H, *H*-6), 5.97 (d, <sup>3</sup>J<sub>HH</sub> = 5.7 Hz, 1H, *H*-1'), 5.92 – 5.79 (m, 1H, *H*-19), 5.59 – 5.51 (m, 1H, *H*-20), 5.24 (s, 1H, *H*-13), 4.30 – 4.22 (m, 2H, *H*-2', *H*-3'), 4.16 – 4.10 (m, 1H, *H*-4'), 4.10 – 4.06 (m, 2H, *H*-5'), 3.29 – 3.23 (m, 2H, *H*-11), 3.18 (q, <sup>3</sup>J<sub>HH</sub> = 7.3 Hz, 9H, *H*-a), 2.55 – 2.40 (m, 2H, *H*-alkyl), 2.11 – 1.43 (m, 5H, *H*-alkyl), 1.31 (t, <sup>3</sup>J<sub>HH</sub> = 7.3 Hz, 13H, *H*-b), 1.23 – 1.11 (m, 1H, *H*-alkyl), 0.95 – 0.80 (m, 1H, *H*-alkyl).

<sup>13</sup>C-NMR (101 MHz, MeOD):  $\delta$  [ppm] = 164.7 (*C*-4), 158.5 (*C*-12), 151.7 (*C*-2), 144.2 (*C*-6), 132.9 (*C*-20), 132.6 (*C*-19), 101.7 (*C*-5), 95.0 (*C*-8), 89.7 (*C*-1'), 85.6 (d, <sup>3</sup>J<sub>CP</sub> = 8.1 Hz, *C*-4'), 75.2 (*C*-3'), 75.0 (*C*-13), 71.8 (*C*-7), 65.7 (d, <sup>2</sup>J<sub>CP</sub> = 4.9 Hz, *C*-5'), 47.7 (*C*-a), 41.7 (*C*-2'), 40.9 (*C*-11), **37.0, 36.8, 30.1, 29.5, 25.2, 17.8** (*C*-alkyl), 9.3 (*C*-b).

<sup>31</sup>P-NMR (162 MHz, MeOD):  $\delta$  [ppm] = 1.02 (s).

HRMS (ESI<sup>-</sup>): *m/z* = calcd: 556.1702 [M-H]<sup>-</sup>, found: 556.1639 [M-H]<sup>-</sup>.

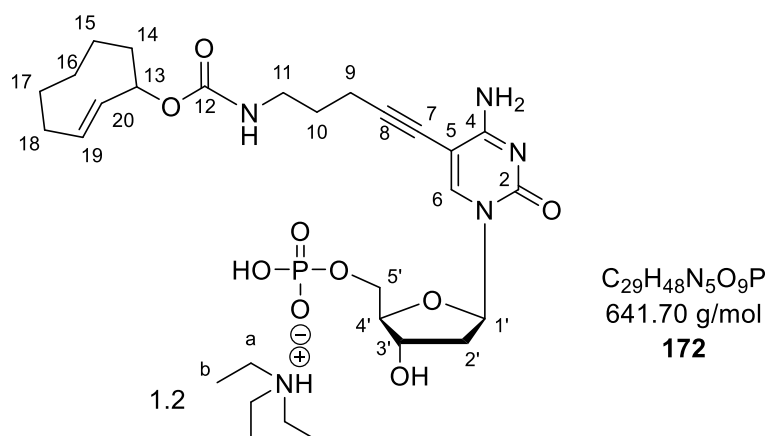
**$\gamma$ -(C9C9AB)-2TCO $\alpha$ -UTP **176****

The reaction was carried out with the general procedure VIII with the pyrophosphate of **95** (160 mg, 170  $\mu$ mol), TFAA (118  $\mu$ L, 850  $\mu$ mol), and  $Et_3N$  (190  $\mu$ L, 1.36 mmol) in  $CH_3CN$  (6 ml). The subsequent activation step was performed with 1-methylimidazole (34  $\mu$ L, 425  $\mu$ mol) in DMF (3 ml) followed by the coupling with monophosphate **173** (1.4 TEAH, 59 mg, 85  $\mu$ mol) solved in DMF (3 mL). Purification on  $RP_{18}$  silica gel with automated flash chromatography ( $H_2O/CH_3CN$ ; 100:0 to 0:100), Dowex ion-exchange ( $NH_4^+$ ) and  $RP_{18}$  silica gel with automated flash chromatography ( $H_2O/CH_3CN$ ; 100:0 to 0:100) as well as subsequent freeze-drying provided **176** (22 mg, 20%) as colorless cotton.

$^1H$ -NMR (600 MHz, MeOD):  $\delta$  [ppm] = 7.97 (s, 1H), 7.41 (dd,  $^3J_{HH}$  = 8.5, 3.4 Hz, 4H), 7.09 – 6.99 (m, 4H), 5.92 (d,  $^3J_{HH}$  = 5.8 Hz, 1H), 5.87 – 5.80 (m, 1H), 5.65 – 5.59 (m, 1H), 5.56 – 5.51 (m, 1H), 5.21 – 5.16 (m, 4H), 4.34 – 4.31 (m, 1H), 4.29 – 4.20 (m, 3H), 4.16 – 4.09 (m, 1H), 3.27 – 3.18 (m, 1H), 2.58 (t,  $^3J_{HH}$  = 7.4 Hz, 5H), 2.46 – 2.37 (m, 1H), 2.30 – 1.55 (m, 16H), 1.54 – 1.24 (m, 30H), 1.19 – 1.11 (m, 1H), 1.03 (t,  $^3J_{HH}$  = 7.4 Hz, 1H), 0.97 – 0.88 (m, 6H).

$^{31}P$ -NMR (243 MHz, MeOD):  $\delta$  [ppm] = -11.52 (d,  $^2J_{PP}$  = 19.8 Hz,  $P$ - $\alpha$ ), -13.23 (d,  $^2J_{PP}$  = 17.3 Hz,  $P$ - $\gamma$ ), -23.64 (t,  $^2J_{PP}$  = 18.2 Hz,  $P$ - $\beta$ ).

HRMS (ESI $^-$ ):  $m/z$  = calcd: 1236.4581 [ $M-H$ ] $^-$ , found: 1236.4267 [ $M-H$ ] $^-$ .

**(2TCO $\alpha$ )-2'-deoxycytidine monophosphate **172****

The TEAH salt of 5-(5-aminopent-1-yn-1-yl)-dCMP **155** (0.4 TEAH, 51 mg, 0.12 mmol) was solved in DMSO (2 mL) under the addition of Et<sub>3</sub>N (60  $\mu$ L, 0.43 mmol). The commercially available 2TCO $\alpha$ -NHS active ester (39 mg, 0.14 mmol) was added to the reaction mixture, which was stirred for 30 min at 40 °C (complete conversion was controlled by TLC (H<sub>2</sub>O/CH<sub>3</sub>CN; 3:7)). All volatiles were removed under reduced pressure at 60 °C, and the resulting residue was dissolved in 0.05 M TEAB and purified on RP<sub>18</sub> silica gel using automated flash chromatography (0.05 M TEAB/CH<sub>3</sub>CN; 100:0 to 0:100) to yield the TEAH salt **172** (50 mg, 63%) as a light-yellow solid.

<sup>1</sup>H-NMR (500 MHz, MeOD):  $\delta$  [ppm] = 8.08 (s, 1H, *H*-6), 6.26 (dd, <sup>3</sup>*J*<sub>HH</sub> = 7.7, 5.8 Hz, 1H, *H*-1'), 5.89 – 5.78 (m, 1H, *H*-19), 5.54 (dd, <sup>3</sup>*J*<sub>HH</sub> = 16.4, 2.4 Hz, 1H, *H*-20), 5.24 (s, 1H, *H*-13), 4.47 (m, 1H, *H*-3'), 4.12 – 4.00 (m, 3H, *H*-5', *H*-4'), 3.27 (m, 2H, *H*-11), 3.18 (q, <sup>3</sup>*J*<sub>HH</sub> = 7.3 Hz, 7H, *H*-a), 2.54 – 2.40 (m, 3H, *H*-alkyl), 2.35 (ddd, <sup>2</sup>*J*<sub>HH</sub> = 13.5 Hz, <sup>3</sup>*J*<sub>HH</sub> = 5.8, 2.9 Hz, 1H, *H*-2'a), 2.16 (ddd, <sup>2</sup>*J*<sub>HH</sub> = 13.6 Hz, <sup>3</sup>*J*<sub>HH</sub> = 7.7, 6.1 Hz, 1H, *H*-2'b), 2.03 – 1.44 (m, 9H, *H*-alkyl), 1.30 (t, <sup>3</sup>*J*<sub>HH</sub> = 7.3 Hz, 10H, *H*-b), 1.21 – 1.10 (m, 1H, *H*-alkyl), 0.91 – 0.81 (m, 1H, *H*-alkyl).

<sup>13</sup>C-NMR (126 MHz, MeOD):  $\delta$  [ppm] = 166.6 (*C*-4), 158.5 (*C*-12), 156.8 (*C*-2), 144.7 (*C*-6), 132.9 (*C*-20), 132.6 (*C*-19), 96.9 (*C*-5), 93.8 (*C*-8), 87.8 (d, <sup>3</sup>*J*<sub>CP</sub> = 8.69 Hz, *C*-4'), 87.7 (*C*-1'), 75.1 (*C*-13), 72.6 (*C*-3'), 72.4 (*C*-7), 65.8 (d, <sup>2</sup>*J*<sub>CP</sub> = 5.12 Hz, *C*-5'), 47.7 (*C*-a), 41.7 (*C*-alkyl), 41.7 (*C*-2'), 40.6 (*C*-11), **37.0, 36.8, 30.1, 29.7, 25.2, 17.6** (*C*-alkyl), 9.2 (*C*-b).

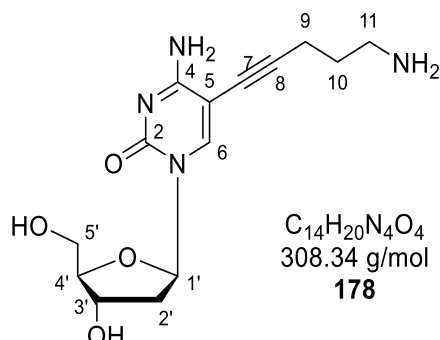
<sup>31</sup>P-NMR (202 MHz, D<sub>2</sub>O):  $\delta$  [ppm] = 2.27 (s).

HRMS (ESI<sup>-</sup>): *m/z* = calcd: 539.1912 [M-H]<sup>-</sup>, found: 539.1908 [M-H]<sup>-</sup>.



HRMS (ESI<sup>-</sup>):  $m/z$  = calcd: 1219.4792 [M-H]<sup>-</sup>, found: 1219.4329 [M-H]<sup>-</sup>.

### 5-(5-Aminopent-1-yn-1-yl)-2'-deoxycytidine **178**

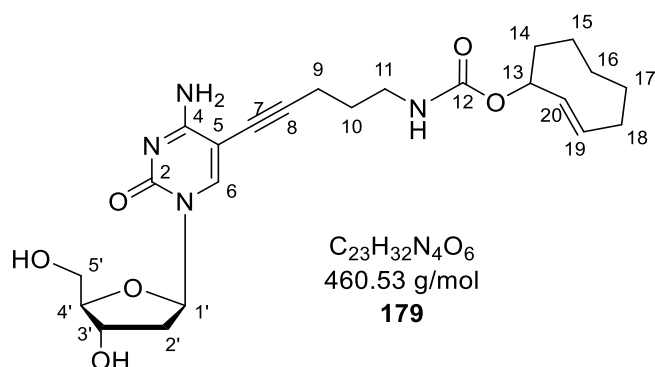


IdC **152** (212 mg, 600  $\mu$ mol), Pd<sub>2</sub>(dba)<sub>3</sub> (30 mg, 32  $\mu$ mol, 5.4 mol%) and tri(2-furyl) phosphine (17 mg, 72  $\mu$ mol, 12 mol%) were dried *in vacuo* shortly and solved in DMSO (2 mL). The reaction flask was evaporated and flushed with nitrogen three times. After the addition of Et<sub>3</sub>N (582  $\mu$ L, 4.20 mmol) and 4-pentyne-1-amine (75  $\mu$ L, 780  $\mu$ mol), the reaction mixture was stirred at 60 °C for 1 h (complete conversion was controlled by TLC (CH<sub>2</sub>Cl<sub>2</sub>:CH<sub>3</sub>OH; 9:1)). All volatiles were removed *in vacuo* and the crude product was purified on RP<sub>18</sub> silica gel using automated flash chromatography (H<sub>2</sub>O/CH<sub>3</sub>CN; 100:0 to 0:100, loading through syringe filter) to yield **178** (163 mg, 88%) as a light-yellow solid.

<sup>1</sup>H-NMR (400 MHz, DMSO-*d*<sub>6</sub>):  $\delta$  [ppm] = 8.06 (s, 1H, H-6), 7.65 (s, 1H, NH), 6.74 (s, 1H, NH), 6.11 (dd, <sup>3</sup>J<sub>HH</sub> = 7.1, 6.0 Hz, 1H, H-1'), 5.18 (s, 2H, NH), 4.26 – 4.16 (m, 1H, H-3'), 3.81 – 3.74 (m, 1H, H-4'), 3.69 – 3.50 (m, 2H, H-5'), 3.27 (s, 2H, 2x OH), 2.62 (t, <sup>3</sup>J<sub>HH</sub> = 6.6 Hz, 2H, H-11), 2.43 (t, <sup>3</sup>J<sub>HH</sub> = 7.1 Hz, 2H, H-9), 2.17 – 2.05 (m, 1H, H-2'a), 2.03 – 1.92 (m, 1H, H-2'b), 1.62 – 1.53 (m, 2H, H-10).

<sup>13</sup>C-NMR (101 MHz, MSO-*d*<sub>6</sub>):  $\delta$  [ppm] = 164.5 (C-4), 153.5 (C-2), 143.4 (C-6), 95.7 (C-8), 90.5 (C-5), 87.4 (C-4'), 85.2 (C-1'), 72.0 (C-7), 70.1 (C-3'), 61.0 (C-5), 40.7 (C-2'), 40.7 (C-11), 31.7 (C-10), 16.6 (C-9).

HRMS (ESI<sup>+</sup>):  $m/z$  = calcd: 331.1396 [M+Na]<sup>+</sup>, found: 331.1396 [M+Na]<sup>+</sup>.

**(2TCO $\alpha$ )-2'-deoxycytidine **179****

5-(5-aminopent-1-yn-1-yl)-dC **178** (25 mg, 80  $\mu$ mol) was solved in DMF (2 mL) under the addition of 4-5 drops of DMSO, followed by the addition of Et<sub>3</sub>N (40  $\mu$ L, 288  $\mu$ mol). The commercially available 2TCO $\alpha$ -NHS active ester (26 mg, 96  $\mu$ mol) was added to the reaction mixture, which was stirred for 2 h at 40 °C (complete conversion was controlled by TLC (CH<sub>2</sub>Cl<sub>2</sub>:CH<sub>3</sub>OH; 19:1)). All volatiles were removed under reduced pressure at 50 °C, and the resulting residue was purified on RP<sub>18</sub> silica gel using automated flash chromatography (H<sub>2</sub>O/CH<sub>3</sub>CN; 100:0 to 0:100) to yield **179** (32 mg, 87%) as a white solid after freeze-drying the appropriate fractions.

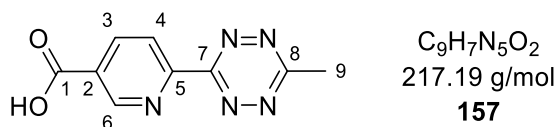
<sup>1</sup>H-NMR (500 MHz, MeOD):  $\delta$  [ppm] = 8.29 (s, 1H, *H*-6), 6.23 (t, <sup>3</sup>*J*<sub>HH</sub> = 6.3 Hz, 1H), 5.90 – 5.80 (m, 1H, *H*-19), 5.57 (dd, <sup>3</sup>*J*<sub>HH</sub> = 16.3, 2.4 Hz, 1H, *H*-20), 5.26 (s, 1H, *H*-13), 4.42 – 4.36 (m, 1H, *H*-3'), 3.97 – 3.94 (m, 1H, *H*-4'), 3.85 (dd, <sup>2</sup>*J*<sub>HH</sub> = 12.1 Hz, <sup>3</sup>*J*<sub>HH</sub> = 3.1 Hz, 1H, *H*-5'a), 3.76 (dd, <sup>2</sup>*J*<sub>HH</sub> = 12.0 Hz, <sup>3</sup>*J*<sub>HH</sub> = 3.6 Hz, 1H, *H*-5'b), 3.32 – 3.27 (m, 2H, *H*-11), 2.59 – 2.43 (m, 2H, *H*-alkyl), 2.39 (ddd, <sup>2</sup>*J*<sub>HH</sub> = 13.6 Hz, <sup>3</sup>*J*<sub>HH</sub> = 6.1, 4.0 Hz, 1H, *H*-2'a), 2.19 – 2.12 (m, 1H, *H*-alkyl), 2.10 – 1.96 (m, 3H, *H*-alkyl), 1.93 – 1.83 (m, 1H, *H*-alkyl), 1.82 – 1.70 (m, 3H, *H*-alkyl), 1.70 – 1.60 (m, 1H, *H*-alkyl), 1.56 – 1.45 (m, 1H, *H*-alkyl), 1.24 – 1.10 (m, 1H, *H*-alkyl), 0.94 – 0.82 (m, 1H, *H*-alkyl).

<sup>13</sup>C-NMR (126 MHz, MeOD):  $\delta$  [ppm] = 166.6 (*C*-4), 158.5 (*C*-12), 156.8 (*C*-2), 145.1 (*C*-6), 132.8 (*C*-20), 132.4 (*C*-19), 96.4 (*C*-5), 93.4 (*C*-8), 89.0 (*C*-4'), 87.8 (*C*-1'), 75.1 (*C*-13), 72.6 (*C*-7), 71.7 (*C*-3'), 62.5 (*C*-5'), 42.4 (*C*-alkyl), 41.6 (*C*-2'), **40.5, 37.0, 36.8, 30.1, 29.8, 25.2, 17.5** (*C*-alkyl).

HRMS (ESI<sup>+</sup>): *m/z* = calcd: 461.2400 [M+H]<sup>+</sup>, found: 461.2395 [M+H]<sup>+</sup>.

### 6.3.12 Preparation of the $\gamma$ -(C9C9AB)-NcTz-dCTP

#### 6-(6-Methyl-1,2,4,5-tetrazin-3-yl)nicotinic acid **157**



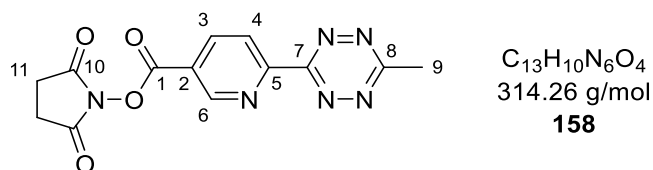
To a nitrogen flushed pressure tube was added 6-cyanoic acid (474 mg, 3.20 mmol), triethylorthoacetate (14.6 mL, 80.0 mmol), mercaptopropionic acid (139  $\mu$ L, 1.60 mmol), and hydrazine hydrate (14.0 mL, 224 mmol). The pressure tube was sealed tightly, and the emulsion was stirred for 2 h at 100 °C. The reaction mixture was cooled to room temperature and opened carefully. The opened flask was left until the following day to reduce toxic hydrazine levels. The reaction mixture was diluted with ethyl acetate and acidified with aq. citric acid (10%). The aqueous phase was extracted with ethyl acetate several times until color change indicated sufficient extraction. The organic phase was washed with aq. citric acid (10%) and brine and was dried over  $Na_2SO_4$ . The removal of the solvent provided the crude dihydrotetrazine intermediate, which was solved in 20 mL  $CH_2Cl_2/CH_3OH$  (10:1 v/v) followed by the addition of  $PhI(OAc)_2$  (2.06 g, 6.40 mmol). The reaction mixture was stirred overnight at room temperature and was directly loaded onto a silica column ( $CH_2Cl_2/CH_3OH$ ; 9:1 + 1% AcOH). Collecting the appropriate fractions and removing the solvents provided the crude tetrazine, which was purified by washing the solid in  $CH_3OH$  twice. Collection of the product via centrifugation provided tetrazine **157** (210 mg, 30%) as a violet solid.

$^1H$ -NMR (400 MHz,  $DMSO-d_6$ )  $\delta$  [ppm] = 9.34 (dd,  $^4J_{HH} = 2.1$ ,  $^5J_{HH} = 0.9$ , 1H, H-6), 8.64 (dd,  $^3J_{HH} = 8.2$ ,  $^5J_{HH} = 0.9$ , 1H, H-4), 8.57 (dd,  $^3J_{HH} = 8.2$ ,  $^4J_{HH} = 2.1$ , 1H, H-3), 3.06 (s, 3H, H-9).

$^{13}C$ -NMR (101 MHz,  $DMSO-d_6$ )  $\delta$  [ppm] = 167.7 (C-8), 165.8 (C-1), 162.8 (C-7), 153.4 (C-5), 150.9 (C-6), 138.6 (C-3), 128.5 (C-2), 123.6 (C-4), 21.0 (C-9).

HRMS (ESI):  $m/z$  = calcd: 216.0527  $[M-H]^-$ , found: 216.0481  $[M-H]^-$ .



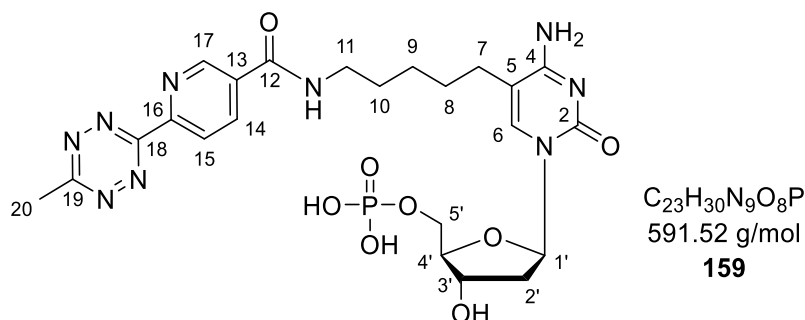
**6-(6-Methyl-1,2,4,5-tetrazin-3-yl)nicotinic acid active ester **158****

Tetrazine **157** (120 mg, 550  $\mu$ mol) and disuccinimidyl carbonate (211 mg, 825  $\mu$ mol) were dried *in vacuo* shortly and solved in DMF (3 mL). After adding pyridine (89  $\mu$ L, 1.10 mmol) and DMAP (6.7 mg, 55  $\mu$ mol), the reaction mixture was stirred at room temperature for 3 h. Then, the reaction mixture was diluted with ethyl acetate and washed twice with aq. 1 N HCl, twice with sat. aq. NaHCO<sub>3</sub>, dried over Na<sub>2</sub>SO<sub>4</sub> and concentrated *in vacuo*. The crude product was isolated on silica gel (CH<sub>2</sub>Cl<sub>2</sub>/CH<sub>3</sub>OH; 98:2 + 1% AcOH), affording **158** (110 mg, 64%) as a red solid.

<sup>1</sup>H-NMR (400 MHz, DMSO-*d*<sub>6</sub>):  $\delta$  [ppm] = 9.51 (dd, <sup>4</sup>J<sub>HH</sub> = 2.0, <sup>5</sup>J<sub>HH</sub> = 1.2, 1H, H-6), 8.83 – 8.73 (m, 2H, H-3, H-4), 3.08 (s, 3H, H-9), 2.94 (s, 4H, 2x H-11).

<sup>13</sup>C-NMR (101 MHz, DMSO-*d*<sub>6</sub>):  $\delta$  [ppm] = 170.1 (2x C-10), 167.8 (C-8), 162.6 (C-1), 160.6 (C-7), 155.4 (C-5), 151.1 (C-6), 139.6 (C-3), 124.1 (C-4), 122.8 (C-2), 25.6 (2x C-11), 21.1 (C-9).

HRMS (ESI<sup>+</sup>): *m/z* = calcd: 315.0842 [M+Na]<sup>+</sup>, found: 315.0842.

**(NcTz)-2'-deoxycytidine monophosphate **159****

The TEAH salt of 5-(5-aminopent-1-yn-1-yl)-dCMP **155** (1.4 TEAH, 107 mg, 200  $\mu$ mol) was solved in CH<sub>3</sub>OH (8 mL) followed by the addition of NcTz-NHS active ester (69 mg, 220  $\mu$ mol) solved in DMF (2 mL). The reaction was stirred for 3 h at room temperature, after which the CH<sub>3</sub>OH was removed under reduced pressure. The monophosphate was precipitated from the remaining DMF solution by the addition of Et<sub>2</sub>O. The precipitate was collected and purified on a short silica gel column (CH<sub>2</sub>Cl<sub>2</sub>/CH<sub>3</sub>OH; 1:1). The appropriate fractions were concentrated *in vacuo* and filtered through a syringe filter.



(H<sub>2</sub>O/CH<sub>3</sub>CN; 100:0 to 0:100), Dowex ion-exchange (NH<sub>4</sub><sup>+</sup>) and RP<sub>18</sub> silica gel with automated flash chromatography (H<sub>2</sub>O/CH<sub>3</sub>CN; 100:0 to 0:100) as well as subsequent freeze-drying provided 160 (8 mg, 12%) as red cotton.

<sup>1</sup>H-NMR (400 MHz, MeOD):  $\delta$  [ppm] = 9.20 – 9.18 (m, 2H, *H*-17), 8.83 – 8.45 (m, 2H, *H*-14, *H*-15), 8.01 (s, 1H, *H*-1'), 7.27 – 7.22 (m, 4H, 2x *H*-2''), 6.88 (d, <sup>3</sup>*J*<sub>HH</sub> = 8.5 Hz, 4H, 2x *H*-3''), 6.12 (t, <sup>3</sup>*J*<sub>HH</sub> = 6.4 Hz, 1H, *H*-1'), 5.05 (d, <sup>3</sup>*J*<sub>HH</sub> = 8.2 Hz, 4H, 2x *H*-5''), 4.56 – 4.47 (m, 1H, *H*-3'), 4.28 – 4.15 (m, 2H, *H*-5'), 3.98 – 3.92 (m, 1H, *H*-4'), 3.40 – 3.33 (m, 2H, *H*-11), 3.00 (s, 3H, *H*-20), 2.45 (t, <sup>3</sup>*J*<sub>HH</sub> = 7.4 Hz, 4H, *H*-b), 2.43 – 2.26 (m, 2H, *H*-2'), 2.23 – 2.16 (m, 2H, *H*-alkyl), 1.68 – 1.57 (m, 6H, *H*-alkyl), 1.54 – 1.46 (m, 2H, *H*-alkyl), 1.44 – 1.36 (m, 2H, *H*-alkyl), 1.34 – 1.12 (m, 24H, *H*-alkyl), 0.83 – 0.75 (m, 6H, *H*-j).

<sup>31</sup>P-NMR (162 MHz, Methanol-*d*<sub>4</sub>)  $\delta$  -11.88 (d, <sup>2</sup>*J*<sub>PP</sub> = 20.3 Hz, *P*- $\alpha$ ), -13.14 (d, <sup>2</sup>*J*<sub>PP</sub> = 16.8 Hz, *P*- $\gamma$ ), -23.77 (dd, <sup>2</sup>*J*<sub>PP</sub> = 20.2, 17.4 Hz, *P*- $\beta$ ).

HRMS (ESI<sup>-</sup>): *m/z* = calcd: 1270.4761 [M-H]<sup>-</sup>, found: 1270.4168 [M-H]<sup>-</sup>.

## 7 References

- (1) Clemente, J. C., Ursell, L. K., Parfrey, L. W., Knight, R. The impact of the gut microbiota on human health: an integrative view. *Cell* **2012**, *148*, 1258–1270.
- (2) O'Hara, A. M., Shanahan, F. The gut flora as a forgotten organ. *EMBO Rep.* **2006**, *7*, 688–693.
- (3) Bandea, C. The Origin and Evolution of Viruses as Molecular Organisms. *Nat Prec* **2009**.
- (4) Müller, T. G., Sakin, V., Müller, B. A Spotlight on Viruses-Application of Click Chemistry to Visualize Virus-Cell Interactions. *Molecules* **2019**, *24*.
- (5) Schermelleh, L., Ferrand, A., Huser, T., Eggeling, C., Sauer, M., Biehlmaier, O., Drummen, G. P. C. Super-resolution microscopy demystified. *Nat. Cell Biol.* **2019**, *21*, 72–84.
- (6) Turner, B. G., Summers, M. F. Structural biology of HIV. *J. Mol. Biol.* **1999**, *285*, 1–32.
- (7) Campbell, E. M., Hope, T. J. HIV-1 capsid: the multifaceted key player in HIV-1 infection. *Nat. Rev. Microbiol.* **2015**, *13*, 471–483.
- (8) Doitsh, G., Galloway, N. L. K., Geng, X., Yang, Z., Monroe, K. M., Zepeda, O., Hunt, P. W., Hatano, H., Sowinski, S., Muñoz-Arias, I., Greene, W. C. Cell death by pyroptosis drives CD4 T-cell depletion in HIV-1 infection. *Nature* **2014**, *505*, 509–514.
- (9) Monroe, K. M., Yang, Z., Johnson, J. R., Geng, X., Doitsh, G., Krogan, N. J., Greene, W. C. IFI16 DNA sensor is required for death of lymphoid CD4 T cells abortively infected with HIV. *Science* **2014**, *343*, 428–432.
- (10) Müller, T. G., Zila, V., Peters, K., Schifferdecker, S., Stanic, M., Lucic, B., Laketa, V., Lusic, M., Müller, B., Kräusslich, H.-G. HIV-1 uncoating by release of viral cDNA from capsid-like structures in the nucleus of infected cells. *eLife* **2021**, *10*.
- (11) Briggs, J. A. G., Wilk, T., Welker, R., Kräusslich, H.-G., Fuller, S. D. Structural organization of authentic, mature HIV-1 virions and cores. *EMBO J.* **2003**, *22*, 1707–1715.
- (12) Francis, A. C., Melikyan, G. B. Live-Cell Imaging of Early Steps of Single HIV-1 Infection. *Viruses* **2018**, *10*.

- (13) Burdick, R. C., Li, C., Munshi, M., Rawson, J. M. O., Nagashima, K., Hu, W.-S., Pathak, V. K. HIV-1 uncoats in the nucleus near sites of integration. *PNAS USA* **2020**, *117*, 5486–5493.
- (14) Selyutina, A., Persaud, M., Lee, K., KewalRamani, V., Diaz-Griffero, F. Nuclear Import of the HIV-1 Core Precedes Reverse Transcription and Uncoating. *Cell Rep.* **2020**, *32*, 108201.
- (15) Dharan, A., Bachmann, N., Talley, S., Zwickelmaier, V., Campbell, E. M. Nuclear pore blockade reveals that HIV-1 completes reverse transcription and uncoating in the nucleus. *Nat. Microbiol.* **2020**, *5*, 1088–1095.
- (16) Appen, A. von, Kosinski, J., Sparks, L., Ori, A., DiGuilio, A. L., Vollmer, B., Mackmull, M.-T., Banterle, N., Parca, L., Kastritis, P., Buczak, K., Mosalaganti, S., Hagen, W., Andres-Pons, A., Lemke, E. A., Bork, P., Antonin, W., Glavy, J. S., Bui, K. H., Beck, M. In situ structural analysis of the human nuclear pore complex. *Nature* **2015**, *526*, 140–143.
- (17) Zila, V., Margiotta, E., Turoňová, B., Müller, T. G., Zimmerli, C. E., Mattei, S., Allegretti, M., Börner, K., Rada, J., Müller, B., Lusic, M., Kräusslich, H.-G., Beck, M. Cone-shaped HIV-1 capsids are transported through intact nuclear pores. *Cell* **2021**, *184*, 1032-1046.e18.
- (18) Beck, M., Baumeister, W. Cryo-Electron Tomography: Can it Reveal the Molecular Sociology of Cells in Atomic Detail? *Trends Cell Biol.* **2016**, *26*, 825–837.
- (19) Mahamid, J., Pfeffer, S., Schaffer, M., Villa, E., Danev, R., Cuellar, L. K., Förster, F., Hyman, A. A., Plitzko, J. M., Baumeister, W. Visualizing the molecular sociology at the HeLa cell nuclear periphery. *Science* **2016**, *351*, 969–972.
- (20) Engelman, A. N., Singh, P. K. Cellular and molecular mechanisms of HIV-1 integration targeting. *Cell. Mol. Life Sci.* **2018**, *75*, 2491–2507.
- (21) Freed, E. O. HIV-1 replication. *Somat. Cell Mol. Genet.* **2001**, *26*, 13–33.
- (22) Schröder, A. R., Shinn, P., Chen, H., Berry, C., Ecker, J. R., Bushman, F. HIV-1 Integration in the Human Genome Favors Active Genes and Local Hotspots. *Cell* **2002**, *110*, 521–529.
- (23) Scherer, K. M., Manton, J. D., Soh, T. K., Mascheroni, L., Connor, V., Crump, C. M., Kaminski, C. F. A fluorescent reporter system enables spatiotemporal analysis of

- host cell modification during herpes simplex virus-1 replication. *J. Biol. Chem.* **2020**.
- (24) Kukhanova, M. K., Korovina, A. N., Kochetkov, S. N. Human herpes simplex virus: life cycle and development of inhibitors. *Biochem. (Mosc.)* **2014**, *79*, 1635–1652.
- (25) Kieff, E. D., Bachenheimer, S. L., Roizman, B. Size, composition, and structure of the deoxyribonucleic acid of herpes simplex virus subtypes 1 and 2. *J. Virol.* **1971**, *8*, 125–132.
- (26) Ibáñez, F. J., Farías, M. A., Gonzalez-Troncoso, M. P., Corrales, N., Duarte, L. F., Retamal-Díaz, A., González, P. A. Experimental Dissection of the Lytic Replication Cycles of Herpes Simplex Viruses in vitro. *Front. microbiol.* **2018**, *9*, 2406.
- (27) Sodeik, B., Ebersold, M. W., Helenius, A. Microtubule-mediated transport of incoming herpes simplex virus 1 capsids to the nucleus. *The Journal of cell biology* **1997**, *136*, 1007–1021.
- (28) Monier, K., Armas, J. C., Etteldorf, S., Ghazal, P., Sullivan, K. F. Annexation of the interchromosomal space during viral infection. *Nat. Cell Biol.* **2000**, *2*, 661–665.
- (29) Kobiler, O., Weitzman, M. D. Herpes simplex virus replication compartments: From naked release to recombining together. *PLoS Pathog.* **2019**, *15*, e1007714.
- (30) Roller, R. J., Johnson, D. C. Herpesvirus Nuclear Egress across the Outer Nuclear Membrane. *Viruses* **2021**, *13*.
- (31) Giepmans, B. N. G., Adams, S. R., Ellisman, M. H., Tsien, R. Y. The fluorescent toolbox for assessing protein location and function. *Science* **2006**, *312*, 217–224.
- (32) Prendergast, F. G., Mann, K. G. Chemical and physical properties of aequorin and the green fluorescent protein isolated from *Aequorea forskålea*. *Biochemistry* **1978**, *17*, 3448–3453.
- (33) Tsien, R. Y. The green fluorescent protein. *Annu. Rev. Biochem.* **1998**, *67*, 509–544.
- (34) Shaner, N. C., Patterson, G. H., Davidson, M. W. Advances in fluorescent protein technology. *J. Cell Sci.* **2007**, *120*, 4247–4260.
- (35) Specht, E. A., Braselmann, E., Palmer, A. E. A Critical and Comparative Review of Fluorescent Tools for Live-Cell Imaging. *Annu. Rev. Physiol.* **2017**, *79*, 93–117.
- (36) Beliu, G., Kurz, A. J., Kuhlemann, A. C., Behringer-Pliess, L., Meub, M., Wolf, N., Seibel, J., Shi, Z.-D., Schnermann, M., Grimm, J. B., Lavis, L. D., Doose, S., Sauer, M.

- Bioorthogonal labeling with tetrazine-dyes for super-resolution microscopy. *Commun. Biol.* **2019**, *2*, 261.
- (37) Rust, M. J., Lakadamyali, M., Zhang, F., Zhuang, X. Assembly of endocytic machinery around individual influenza viruses during viral entry. *Nat. Struct. Mol. Biol.* **2004**, *11*, 567–573.
- (38) Piccinotti, S., Kirchhausen, T., Whelan, S. P. J. Uptake of rabies virus into epithelial cells by clathrin-mediated endocytosis depends upon actin. *J. Virol.* **2013**, *87*, 11637–11647.
- (39) Lakadamyali, M., Rust, M. J., Babcock, H. P., Zhuang, X. Visualizing infection of individual influenza viruses. *PNAS* **2003**, *100*, 9280–9285.
- (40) Kops, A. d. B., Knipe, D. M. Formation of DNA replication structures in herpes virus-infected cells requires a viral DNA binding protein. *Cell* **1988**, *55*, 857–868.
- (41) Gratzner, H. G. Monoclonal antibody to 5-bromo- and 5-iododeoxyuridine: A new reagent for detection of DNA replication. *Science* **1982**, *218*, 474–475.
- (42) Salic, A., Mitchison, T. J. A chemical method for fast and sensitive detection of DNA synthesis in vivo. *PNAS* **2008**, *105*, 2415–2420.
- (43) Qu, D., Wang, G., Wang, Z., Zhou, L., Chi, W., Cong, S., Ren, X., Liang, P., Zhang, B. 5-Ethynyl-2'-deoxycytidine as a new agent for DNA labeling: detection of proliferating cells. *Anal. Biochem.* **2011**, *417*, 112–121.
- (44) Neef, A. B., Samain, F., Luedtke, N. W. Metabolic labeling of DNA by purine analogues in vivo. *Chembiochem* **2012**, *13*, 1750–1753.
- (45) Dembowski, J. A., DeLuca, N. A. Selective recruitment of nuclear factors to productively replicating herpes simplex virus genomes. *PLoS Pathog.* **2015**, *11*, e1004939.
- (46) Sekine, E., Schmidt, N., Gaboriau, D., O'Hare, P. Spatiotemporal dynamics of HSV genome nuclear entry and compaction state transitions using bioorthogonal chemistry and super-resolution microscopy. *PLoS Pathog.* **2017**, *13*, e1006721.
- (47) Jao, C. Y., Salic, A. Exploring RNA transcription and turnover in vivo by using click chemistry. *PNAS* **2008**, *105*, 15779–15784.
- (48) Xu, H., Franks, T., Gibson, G., Huber, K., Rahm, N., Strambio De Castillia, C., Luban, J., Aiken, C., Watkins, S., Sluis-Cremer, N., Ambrose, Z. Evidence for biphasic

- uncoating during HIV-1 infection from a novel imaging assay. *Retrovirology* **2013**, *10*, 70.
- (49) Bejarano, D. A., Puertas, M. C., Börner, K., Martinez-Picado, J., Müller, B., Kräusslich, H.-G. Detailed Characterization of Early HIV-1 Replication Dynamics in Primary Human Macrophages. *Viruses* **2018**, *10*.
- (50) Wang, I.-H., Suomalainen, M., Andriasyan, V., Kilcher, S., Mercer, J., Neef, A., Luedtke, N. W., Greber, U. F. Tracking viral genomes in host cells at single-molecule resolution. *Cell Host Microbe* **2013**, *14*, 468–480.
- (51) Peng, K., Muranyi, W., Glass, B., Laketa, V., Yant, S. R., Tsai, L., Cihlar, T., Müller, B., Kräusslich, H.-G. Quantitative microscopy of functional HIV post-entry complexes reveals association of replication with the viral capsid. *eLife* **2014**, *3*, e04114.
- (52) Stultz, R. D., Cenker, J. J., McDonald, D. Imaging HIV-1 Genomic DNA from Entry through Productive Infection. *J. Virol.* **2017**, *91*.
- (53) Dembowski, J. A., Dremel, S. E., DeLuca, N. A. Replication-Coupled Recruitment of Viral and Cellular Factors to Herpes Simplex Virus Type 1 Replication Forks for the Maintenance and Expression of Viral Genomes. *PLoS Pathog.* **2017**, *13*, e1006166.
- (54) Sletten, E. M., Bertozzi, C. R. Bioorthogonal chemistry: fishing for selectivity in a sea of functionality. *Angew. Chem. Int. Ed.* **2009**, *48*, 6974–6998.
- (55) Knall, A.-C., Slugovc, C. Inverse electron demand Diels-Alder (IEDDA)-initiated conjugation: a (high) potential click chemistry scheme. *Chem. Soc. Rev.* **2013**, *42*, 5131–5142.
- (56) Oliveira, B. L., Guo, Z., Bernardes, G. J. L. Inverse electron demand Diels-Alder reactions in chemical biology. *Chem. Soc. Rev.* **2017**, *46*, 4895–4950.
- (57) Darko, A., Wallace, S., Dmitrenko, O., Machovina, M. M., Mehl, R. A., Chin, J. W., Fox, J. M. Conformationally Strained trans-Cyclooctene with Improved Stability and Excellent Reactivity in Tetrazine Ligation. *Chem. Sci.* **2014**, *5*, 3770–3776.
- (58) Karver, M. R., Weissleder, R., Hilderbrand, S. A. Synthesis and evaluation of a series of 1,2,4,5-tetrazines for bioorthogonal conjugation. *Bioconjug. Chem.* **2011**, *22*, 2263–2270.



- (59) Eising, S., Engwerda, A. H. J., Riedijk, X., Bickelhaupt, F. M., Bongers, K. M. Highly Stable and Selective Tetrazines for the Coordination-Assisted Bioorthogonal Ligation with Vinylboronic Acids. *Bioconjug. Chem.* **2018**, *29*, 3054–3059.
- (60) Sauer, J. Structure-reactivity problem in cycloaddition reactions to form heterocyclic compounds. *Chem. heterocycl. compounds* **1995**, *31*, 1140–1154.
- (61) Taylor, M. T., Blackman, M. L., Dmitrenko, O., Fox, J. M. Design and synthesis of highly reactive dienophiles for the tetrazine-trans-cyclooctene ligation. *J. Am. Chem. Soc.* **2011**, *133*, 9646–9649.
- (62) Rieder, U., Luedtke, N. W. Alkene-tetrazine ligation for imaging cellular DNA. *Angew. Chem. Int. Ed.* **2014**, *53*, 9168–9172.
- (63) Huang, L.-L., Liu, K., Zhang, Q., Xu, J., Zhao, D., Zhu, H., Xie, H.-Y. Integrating Two Efficient and Specific Bioorthogonal Ligation Reactions with Natural Metabolic Incorporation in One Cell for Virus Dual Labeling. *Anal. Chem.* **2017**, *89*, 11620–11627.
- (64) Busskamp, H., Batroff, E., Niederwieser, A., Abdel-Rahman, O. S., Winter, R. F., Wittmann, V., Marx, A. Efficient labelling of enzymatically synthesized vinyl-modified DNA by an inverse-electron-demand Diels-Alder reaction. *Chem. Commun.* **2014**, *50*, 10827–10829.
- (65) Kubota, M., Nainar, S., Parker, S. M., England, W., Furche, F., Spitale, R. C. Expanding the Scope of RNA Metabolic Labeling with Vinyl Nucleosides and Inverse Electron-Demand Diels-Alder Chemistry. *ACS Chem. Biol.* **2019**, *14*, 1698–1707.
- (66) Devaraj, N. K., Weissleder, R., Hilderbrand, S. A. Tetrazine-based cycloadditions: application to pretargeted live cell imaging. *Bioconjug. Chem.* **2008**, *19*, 2297–2299.
- (67) Lang, K., Davis, L., Torres-Kolbus, J., Chou, C., Deiters, A., Chin, J. W. Genetically encoded norbornene directs site-specific cellular protein labelling via a rapid bioorthogonal reaction. *Nat. Chem.* **2012**, *4*, 298–304.
- (68) Schoch, J., Jäschke, A. Synthesis and enzymatic incorporation of norbornene-modified nucleoside triphosphates for Diels-Alder bioconjugation. *RSC Adv.* **2013**, *3*, 4181.

- (69) Patterson, D. M., Nazarova, L. A., Xie, B., Kamber, D. N., Prescher, J. A. Functionalized cyclopropenes as bioorthogonal chemical reporters. *J. Am. Chem. Soc.* **2012**, *134*, 18638–18643.
- (70) Yang, J., Šečkutè, J., Cole, C. M., Devaraj, N. K. Live-cell imaging of cyclopropene tags with fluorogenic tetrazine cycloadditions. *Angew. Chem. Int. Ed.* **2012**, *51*, 7476–7479.
- (71) Dowd, P., Gold, A. The thermal dimerization of cyclopropene. *Tetrahedron Lett.* **1969**, *10*, 85–86.
- (72) Yang, J., Liang, Y., Šečkutè, J., Houk, K. N., Devaraj, N. K. Synthesis and reactivity comparisons of 1-methyl-3-substituted cyclopropene mini-tags for tetrazine bioorthogonal reactions. *Chemistry* **2014**, *20*, 3365–3375.
- (73) Wu, H., Devaraj, N. K. Advances in Tetrazine Bioorthogonal Chemistry Driven by the Synthesis of Novel Tetrazines and Dienophiles. *Acc. Chem. Res.* **2018**, *51*, 1249–1259.
- (74) Späte, A.-K., Bußkamp, H., Niederwieser, A., Schart, V. F., Marx, A., Wittmann, V. Rapid labeling of metabolically engineered cell-surface glycoconjugates with a carbamate-linked cyclopropene reporter. *Bioconjug. Chem.* **2014**, *25*, 147–154.
- (75) Elliott, T. S., Townsley, F. M., Bianco, A., Ernst, R. J., Sachdeva, A., Elsässer, S. J., Davis, L., Lang, K., Pisa, R., Greiss, S., Lilley, K. S., Chin, J. W. Proteome labeling and protein identification in specific tissues and at specific developmental stages in an animal. *Nat. Biotechnol.* **2014**, *32*, 465–472.
- (76) Ploschik, D., Röncke, F., Beike, H., Strasser, R., Wagenknecht, H.-A. DNA Primer Extension with Cyclopropenylated 7-Deaza-2'-deoxyadenosine and Efficient Bioorthogonal Labeling in Vitro and in Living Cells. *Chembiochem* **2018**, *19*, 1949–1953.
- (77) Eggert, F., Kath-Schorr, S. A cyclopropene-modified nucleotide for site-specific RNA labeling using genetic alphabet expansion transcription. *Chem. Commun.* **2016**, *52*, 7284–7287.
- (78) Merkel, M., Arndt, S., Ploschik, D., Cserép, G. B., Wenge, U., Kele, P., Wagenknecht, H.-A. Scope and Limitations of Typical Copper-Free Bioorthogonal Reactions with DNA: Reactive 2'-Deoxyuridine Triphosphates for Postsynthetic Labeling. *J. Org. Chem.* **2016**, *81*, 7527–7538.

- (79) Hoffmann, J.-E., Plass, T., Nikić, I., Aramburu, I. V., Koehler, C., Gillandt, H., Lemke, E. A., Schultz, C. Highly Stable trans-Cyclooctene Amino Acids for Live-Cell Labeling. *Chemistry* **2015**, *21*, 12266–12270.
- (80) Royzen, M., Yee, N., Mejia Oneto, J. M. In Vivo Bioconjugation Using Bio-orthogonal Chemistry. In *Handbook of in vivo chemistry in mice: From lab to living system*; Tanaka, K., Vong, K., Eds.; Wiley-VCH: Weinheim, 2020; Vols. 27, pp. 249–279.
- (81) Peng, T., Hang, H. C. Site-Specific Bioorthogonal Labeling for Fluorescence Imaging of Intracellular Proteins in Living Cells. *J. Am. Chem. Soc.* **2016**, *138*, 14423–14433.
- (82) Wang, K., Wang, D., Ji, K., Chen, W., Zheng, Y., Dai, C., Wang, B. Post-synthesis DNA modifications using a trans-cyclooctene click handle. *Org. Biomol. Chem.* **2015**, *13*, 909–915.
- (83) Asare-Okai, P. N., Agustin, E., Fabris, D., Royzen, M. Site-specific fluorescence labelling of RNA using bio-orthogonal reaction of trans-cyclooctene and tetrazine. *Chem. Commun.* **2014**, *50*, 7844–7847.
- (84) Blizzard, R. J., Backus, D. R., Brown, W., Bazewicz, C. G., Li, Y., Mehl, R. A. Ideal Bioorthogonal Reactions Using A Site-Specifically Encoded Tetrazine Amino Acid. *J. Am. Chem. Soc.* **2015**, *137*, 10044–10047.
- (85) Zheng, Q., Ayala, A. X., Chung, I., Weigel, A. V., Ranjan, A., Falco, N., Grimm, J. B., Tkachuk, A. N., Wu, C., Lippincott-Schwartz, J., Singer, R. H., Lavis, L. D. Rational Design of Fluorogenic and Spontaneously Blinking Labels for Super-Resolution Imaging. *ACS Cent. Sci.* **2019**, *5*, 1602–1613.
- (86) Wang, L., Tran, M., D'Este, E., Roberti, J., Koch, B., Xue, L., Johnsson, K. A general strategy to develop cell permeable and fluorogenic probes for multicolour nanoscopy. *Nat. Chem.* **2020**, *12*, 165–172.
- (87) Lukinavičius, G., Umezawa, K., Olivier, N., Honigmann, A., Yang, G., Plass, T., Mueller, V., Reymond, L., Corrêa, I. R., Luo, Z.-G., Schultz, C., Lemke, E. A., Heppenstall, P., Eggeling, C., Manley, S., Johnsson, K. A near-infrared fluorophore for live-cell super-resolution microscopy of cellular proteins. *Nat. Chem.* **2013**, *5*, 132–139.

- (88) Wirth, R., Gao, P., Nienhaus, G. U., Sunbul, M., Jäschke, A. SiRA: A Silicon Rhodamine-Binding Aptamer for Live-Cell Super-Resolution RNA Imaging. *J. Am. Chem. Soc.* **2019**, *141*, 7562–7571.
- (89) Lukinavičius, G., Blaukopf, C., Pershagen, E., Schena, A., Reymond, L., Derivery, E., Gonzalez-Gaitan, M., D'Este, E., Hell, S. W., Wolfram Gerlich, D., Johnsson, K. SiR-Hoechst is a far-red DNA stain for live-cell nanoscopy. *Nat. Commun.* **2015**, *6*, 8497.
- (90) Schvartz, T., Aloush, N., Goliand, I., Segal, I., Nachmias, D., Arbely, E., Elia, N. Direct fluorescent-dye labeling of  $\alpha$ -tubulin in mammalian cells for live cell and superresolution imaging. *Mol. Biol. Cell* **2017**, *28*, 2747–2756.
- (91) Devaraj, N. K., Hilderbrand, S., Upadhyay, R., Mazitschek, R., Weissleder, R. Bioorthogonal turn-on probes for imaging small molecules inside living cells. *Angew. Chem. Int. Ed.* **2010**, *49*, 2869–2872.
- (92) Carlson, J. C. T., Meimetis, L. G., Hilderbrand, S. A., Weissleder, R. BODIPY-tetrazine derivatives as superbright bioorthogonal turn-on probes. *Angew. Chem. Int. Ed.* **2013**, *52*, 6917–6920.
- (93) Kim, T. G., Castro, J. C., Loudet, A., Jiao, J. G.-S., Hochstrasser, R. M., Burgess, K., Topp, M. R. Correlations of structure and rates of energy transfer for through-bond energy-transfer cassettes. *J. Phys. Chem. A.* **2006**, *110*, 20–27.
- (94) Wu, H., Yang, J., Šečkutė, J., Devaraj, N. K. In situ synthesis of alkenyl tetrazines for highly fluorogenic bioorthogonal live-cell imaging probes. *Angew. Chem. Int. Ed.* **2014**, *53*, 5805–5809.
- (95) Stella, V. J. Prodrugs as therapeutics. *Expert Opin. Ther. Pat.* **2004**, *14*, 277–280.
- (96) Dahan, A., Khamis, M., Agbaria, R., Karaman, R. Targeted prodrugs in oral drug delivery: the modern molecular biopharmaceutical approach. *Expert Opin. Ther. Pat.* **2012**, *9*, 1001–1013.
- (97) Markovic, M., Ben-Shabat, S., Dahan, A. Prodrugs for Improved Drug Delivery: Lessons Learned from Recently Developed and Marketed Products. *Pharmaceutics* **2020**, *12*.
- (98) Farquhar, D., Srivastva, D. N., Kattesch, N. J., Saunders, P. P. Biologically reversible phosphate-protective groups. *J. Pharm. Sci.* **1983**, *72*, 324–325.

- (99) Freed, J. J., Farquhar, D., Hampton, A. Evidence for acyloxymethyl esters of pyrimidine 5'-deoxyribonucleotides as extracellular sources of active 5'-deoxyribonucleotides in cultured cells. *Biochem. Pharmacol.* **1989**, *38*, 3193–3198.
- (100) Arimilli, M., Kim, C., Dougherty, J., Mulato, A., Oliyai, R., Shaw, J., Cundy, K., Bischofberger, N. Synthesis, in Vitro Biological Evaluation and Oral Bioavailability of 9-[2-(Phosphonomethoxy)Propyl]Adenine (PMPA) Prodrugs. *Antivir. Chem. Chemother.* **1997**, *8*, 557–564.
- (101) Clercq, E. de, Holý, A. Acyclic nucleoside phosphonates: a key class of antiviral drugs. *Nat. Rev. Drug Discov.* **2005**, *4*, 928–940.
- (102) Périgaud, C., Gosselin, G., Lefebvre, I., Girardet, J.-L., Benzaria, S., Barber, I., Imbach, J.-L. Rational design for cytosolic delivery of nucleoside monphosphates “SATE” and “DTE” as enzyme-labile transient phosphate protecting groups. *Bioorganic Med. Chem. Lett.* **1993**, *3*, 2521–2526.
- (103) Pradere, U., Garnier-Amblard, E. C., Coats, S. J., Amblard, F., Schinazi, R. F. Synthesis of nucleoside phosphate and phosphonate prodrugs. *Chem. Rev.* **2014**, *114*, 9154–9218.
- (104) Wiemer, A. J., Wiemer, D. F. Prodrugs of phosphonates and phosphates: crossing the membrane barrier. *Top. Curr. Chem.* **2015**, *360*, 115–160.
- (105) Hostetler, K. Y., Beadle, J. R., Kini, G. D., Gardner, M. F., Wright, K. N., Wu, T.-H., Korba, B. A. Enhanced oral absorption and antiviral activity of 1-O-octadecyl-sn-glycero-3-phospho-acyclovir and related compounds in hepatitis b virus infection, in vitro. *Biochem. Pharmacol.* **1997**, *53*, 1815–1822.
- (106) Marty, F. M., Winston, D. J., Rowley, S. D., Vance, E., Papanicolaou, G. A., Mullane, K. M., Brundage, T. M., Robertson, A. T., Godkin, S., Momméja-Marin, H., Boeckh, M. CMX001 to prevent cytomegalovirus disease in hematopoietic-cell transplantation. *N. Engl. J. Med.* **2013**, *369*, 1227–1236.
- (107) Valiaeva, N., Wyles, D. L., Schooley, R. T., Hwu, J. B., Beadle, J. R., Prichard, M. N., Hostetler, K. Y. Synthesis and antiviral evaluation of 9-(S)-3-alkoxy-2-(phosphonomethoxy)propyl nucleoside alkoxyalkyl esters: inhibitors of hepatitis C virus and HIV-1 replication. *Bioorg. Med. Chem.* **2011**, *19*, 4616–4625.

- (108) McGuigan, C., Pathirana, R. N., Mahmood, N., Devine, K. G., Hay, A. J. Aryl phosphate derivatives of AZT retain activity against HIV1 in cell lines which are resistant to the action of AZT. *Antivir. Res.* **1992**, *17*, 311–321.
- (109) Mehellou, Y., Balzarini, J., McGuigan, C. Aryloxy phosphoramidate triesters: a technology for delivering monophosphorylated nucleosides and sugars into cells. *ChemMedChem* **2009**, *4*, 1779–1791.
- (110) Gibson, A. K., Shah, B. M., Nambiar, P. H., Schafer, J. J. Tenofovir Alafenamide. *Ann Pharmacother* **2016**, *50*, 942–952.
- (111) eEML - *Electronic Essential Medicines List*, 2021.  
<https://list.essentialmeds.org/?query=sofosbuvir>. Accessed 21 January 2021.
- (112) Wu, K., He, M., Khan, I., Asare Okai, P. N., Lin, Q., Fuchs, G., Royzen, M. Bio-orthogonal chemistry-based method for fluorescent labelling of ribosomal RNA in live mammalian cells. *Chem. Commun.* **2019**, *55*, 10456–10459.
- (113) Meier, C., Lorey, M., Clercq, E. de, Balzarini, J. Cyclic saligenyl phosphotriesters of 2',3'-dideoxy-2',3'-didehydrothymidine (d4T) — a new pro-nucleotide approach. *Bioorganic Med. Chem. Lett.* **1997**, *7*, 99–104.
- (114) Meier, C., Habel, L., Haller-Meier, F., Lomp, A., Herderich, M., Klöcking, R., Meerbach, A., Wutzler, P. Chemistry and anti-herpes simplex virus type 1 evaluation of cycloSal-nucleotides of acyclic nucleoside analogues. *Antivir. Chem. Chemother.* **1998**, *9*, 389–402.
- (115) Meier, C. cycloSal-pronucleotides design of chemical trojan horses. *Mini-Rev. Med. Chem.* **2002**, *2*, 219–234.
- (116) Meier, C., Balzarini, J. Application of the cycloSal-prodrug approach for improving the biological potential of phosphorylated biomolecules. *Antivir. Res.* **2006**, *71*, 282–292.
- (117) Meier, C. cycloSal Phosphates as Chemical Trojan Horses for Intracellular Nucleotide and Glycosylmonophosphate Delivery — Chemistry Meets Biology. *Eur. J. Org. Chem.* **2006**, *2006*, 1081–1102.
- (118) Thomson, W., Nicholls, D., Irwin, W. J., Al-Mushadani, J. S., Freeman, S., Karpas, A., Petrik, J., Mahmood, N., Hay, A. J. Synthesis, bioactivation and anti-HIV activity

- of the bis(4-acyloxybenzyl) and mono(4-acyloxybenzyl) esters of the 5'-monophosphate of AZT. *J. Chem. Soc.* **1993**, 1239–1245.
- (119) Jessen, H. J., Schulz, T., Balzarini, J., Meier, C. Bioreversible Maskierung von Nucleosiddiphosphaten. *Angew. Chem. Int. Ed.* **2008**, *120*, 8847–8850.
- (120) Meier, C., Jessen, H. J., Schulz, T., Weinschenk, L., Pertenbreiter, F., Balzarini, J. Rational Development of Nucleoside Diphosphate Prodrugs: DiPPro-Compounds. *Curr. Med. Chem.* **2015**, *22*, 3933–3950.
- (121) Schulz, T., Balzarini, J., Meier, C. The DiPPro approach: synthesis, hydrolysis, and antiviral activity of lipophilic d4T diphosphate prodrugs. *ChemMedChem* **2014**, *9*, 762–775.
- (122) Pertenbreiter, F., Balzarini, J., Meier, C. Nucleoside mono- and diphosphate prodrugs of 2',3'-dideoxyuridine and 2',3'-dideoxy-2',3'-didehydrouridine. *ChemMedChem* **2015**, *10*, 94–106.
- (123) Weinschenk, L., Gollnest, T., Schols, D., Balzarini, J., Meier, C. Bis(benzoyloxybenzyl)-DiPPro nucleoside diphosphates of anti-HIV active nucleoside analogues. *ChemMedChem* **2015**, *10*, 891–900.
- (124) Weinschenk, L., Schols, D., Balzarini, J., Meier, C. Nucleoside Diphosphate Prodrugs: Nonsymmetric DiPPro-Nucleotides. *J. Med. Chem.* **2015**, *58*, 6114–6130.
- (125) Gollnest, T., Oliveira, T. D. de, Schols, D., Balzarini, J., Meier, C. Lipophilic prodrugs of nucleoside triphosphates as biochemical probes and potential antivirals. *Nat. Commun.* **2015**, *6*, 8716.
- (126) Gollnest, T., Dinis de Oliveira, T., Rath, A., Hauber, I., Schols, D., Balzarini, J., Meier, C. Membrane-permeable Triphosphate Prodrugs of Nucleoside Analogues. *Angew. Chem. Int. Ed.* **2016**, *55*, 5255–5258.
- (127) Zhao, C., Weber, S., Schols, D., Balzarini, J., Meier, C. Prodrugs of  $\gamma$ -Alkyl-Modified Nucleoside Triphosphates: Improved Inhibition of HIV Reverse Transcriptase. *Angew. Chem. Int. Ed.* **2020**, *59*, 22063–22071.
- (128) Jia, X., Weber, S., Schols, D., Meier, C. Membrane Permeable, Bioreversibly Modified Prodrugs of Nucleoside Diphosphate- $\gamma$ -Phosphonates. *J. Med. Chem.* **2020**, *63*, 11990–12007.

- (129) Capek, P., Cahová, H., Pohl, R., Hocek, M., Gloeckner, C., Marx, A. An efficient method for the construction of functionalized DNA bearing amino acid groups through cross-coupling reactions of nucleoside triphosphates followed by primer extension or PCR. *Chemistry* **2007**, *13*, 6196–6203.
- (130) Hocek, M. Synthesis of base-modified 2'-deoxyribonucleoside triphosphates and their use in enzymatic synthesis of modified DNA for applications in bioanalysis and chemical biology. *J. Org. Chem.* **2014**, *79*, 9914–9921.
- (131) Hocek, M., Fojta, M. Cross-coupling reactions of nucleoside triphosphates followed by polymerase incorporation. Construction and applications of base-functionalized nucleic acids. *Org. Biomol. Chem.* **2008**, *6*, 2233–2241.
- (132) Hollenstein, M. Nucleoside triphosphates--building blocks for the modification of nucleic acids. *Molecules (Basel, Switzerland)* **2012**, *17*, 13569–13591.
- (133) Jäger, S., Rasched, G., Kornreich-Leshem, H., Engeser, M., Thum, O., Famulok, M. A versatile toolbox for variable DNA functionalization at high density. *J. Am. Chem. Soc.* **2005**, *127*, 15071–15082.
- (134) Kuwahara, M., Nagashima, J., Hasegawa, M., Tamura, T., Kitagata, R., Hanawa, K., Hososhima, S., Kasamatsu, T., Ozaki, H., Sawai, H. Systematic characterization of 2'-deoxynucleoside- 5'-triphosphate analogs as substrates for DNA polymerases by polymerase chain reaction and kinetic studies on enzymatic production of modified DNA. *Nucleic Acids Res.* **2006**, *34*, 5383–5394.
- (135) Seela, F., Ming, X. 7-Functionalized 7-deazapurine  $\beta$ -d and  $\beta$ -l-ribonucleosides related to tubercidin and 7-deazainosine: glycosylation of pyrrolo[2,3-d]pyrimidines with 1-O-acetyl-2,3,5-tri-O-benzoyl- $\beta$ -d or  $\beta$ -l-ribofuranose. *Tetrahedron* **2007**, *63*, 9850–9861.
- (136) Vorbrüggen, H., Ruh-Pohlenz, C. Synthesis Of Nucleosides. In *Organic reactions*; Wiley Online Library: [Hoboken, N.J.], 2004-, pp. 1–630.
- (137) Seela, F., Xu, K. 7-Halogenated 7-Deazapurine 2'-Deoxyribonucleosides Related to 2'-Deoxyadenosine, 2'-Deoxyxanthosine, and 2'-Deoxyisoguanosine: Syntheses and Properties. *Helv. Chim. Acta* **2008**, *91*, 1083–1105.
- (138) Seela, F., Westermann, B., Bindig, U. Liquid–liquid and solid–liquid phase-transfer glycosylation of pyrrolo[2,3-d]pyrimidines: stereospecific synthesis of 2-



- deoxy- $\beta$ -D-ribofuranosides related to 2'-deoxy-7-carbaguanosine. *J. Chem. Soc., Perkin Trans. 1* **1988**, 697–702.
- (139) Seela, F., Peng, X. Pyrrolo[2,3-d]pyrimidine  $\beta$ -L-Nucleosides Containing 7-Deazaadenine, 2-Amino-7-deazaadenine, 7-Deazaguanine, 7-Deazaisoguanine, and 7-Deazaxanthine. *Collect. Czech. Chem. Commun.* **2006**, *71*, 956–977.
- (140) Seela, F., Peng, X. Synthesis and properties of 7-substituted 7-deazapurine (pyrrolo2,3-dpyrimidine) 2'-deoxyribonucleosides. *Curr. Protoc. Nucleic Acid Chem.* **2005**, Chapter 1, Unit 1.10.
- (141) Matsuda, A., Shinozaki, M., Suzuki, M., Watanabe, K., Miyasaka, T. A Convenient Method for the Selective Acylation of Guanine Nucleosides. *Synthesis* **1986**, 1986, 385–386.
- (142) Rahim, S. G., Duggan, M. J., Walker, R. T., Jones, A. S., Dyer, R. L., Balzarini, J., Clercq, E. de. Synthesis and biological properties of 2'-deoxy-5-vinyluridine and 2'-deoxy-5-vinylcytidine. *Nucleic Acids Res.* **1982**, *10*, 5285–5295.
- (143) Ogino, M., Taya, Y., Fujimoto, K. Detection of methylcytosine by DNA photoligation via hydrophobic interaction of the alkyl group. *Org. Biomol. Chem.* **2009**, *7*, 3163.
- (144) Nakamura, S., Ogasawara, S., Matuda, S., Saito, I., Fujimoto, K. Template directed reversible photochemical ligation of oligodeoxynucleotides. *Molecules* **2011**, *17*, 163–178.
- (145) Farina, V., Krishnan, B. Large rate accelerations in the stille reaction with tri-2-furylphosphine and triphenylarsine as palladium ligands: mechanistic and synthetic implications. *J. Am. Chem. Soc.* **1991**, *113*, 9585–9595.
- (146) Andersen, N. G., Keay, B. A. 2-furyl phosphines as ligands for transition-metal-mediated organic synthesis. *Chem. Rev.* **2001**, *101*, 997–1030.
- (147) Wicke, L., Engels, J. W. Postsynthetic on column RNA labeling via Stille coupling. *Bioconjug. Chem.* **2012**, *23*, 627–642.
- (148) Cremosnik, G. S., Hofer, A., Jessen, H. J. Iterative synthesis of nucleoside oligophosphates with phosphoramidites. *Angew. Chem. Int. Ed.* **2014**, *53*, 286–289.

- (149) Caron, J., Lepeltier, E., Reddy, L. H., Lepêtre-Mouelhi, S., Wack, S., Bourgaux, C., Couvreur, P., Desmaële, D. Squalenoyl Gemcitabine Monophosphate: Synthesis, Characterisation of Nanoassemblies and Biological Evaluation. *Eur. J. Org. Chem.* **2011**, *2011*, 2615–2628.
- (150) Sowa, T., Ouchi, S. The Facile Synthesis of 5'-Nucleotides by the Selective Phosphorylation of a Primary Hydroxyl Group of Nucleosides with Phosphoryl Chloride. *Bull. Chem. Soc. Jpn.* **1975**, *48*, 2084–2090.
- (151) Yoshikawa, M., Kato, T., Takenishi, T. Studies of Phosphorylation. III. Selective Phosphorylation of Unprotected Nucleosides. *BCSJ* **1969**, *42*, 3505–3508.
- (152) Weising, S., Sterrenberg, V., Schols, D., Meier, C. Synthesis and Antiviral Evaluation of TriPPPro-AbacavirTP, TriPPPro-CarbovirTP, and Their 1',2'-cis-Disubstituted Analogues. *ChemMedChem* **2018**, *13*, 1771–1778.
- (153) Mohamady, S., Jakeman, D. L. An improved method for the synthesis of nucleoside triphosphate analogues. *J. Org. Chem.* **2005**, *70*, 10588–10591.
- (154) Ludwig, J. A new route to nucleoside 5'-triphosphates. *Acta Biochim Biophys Acad Sci Hung.* **1981**, *16*, 131–133.
- (155) Gillerman, I., Fischer, B. An improved one-pot synthesis of nucleoside 5'-triphosphate analogues. *Nucleosides Nucleotides Nucleic Acids* **2010**, *29*, 245–256.
- (156) Kore, A. R., Shanmugasundaram, M., Senthilvelan, A., Srinivasan, B. An improved protection-free one-pot chemical synthesis of 2'-deoxynucleoside-5'-triphosphates. *Nucleosides Nucleotides Nucleic Acids* **2012**, *31*, 423–431.
- (157) Patterson, D. M., Nazarova, L. A., Xie, B., Kamber, D. N., Prescher, J. A. Functionalized cyclopropenes as bioorthogonal chemical reporters. *J. Am. Chem. Soc.* **2012**, *134*, 18638–18643.
- (158) Hizi, A., Herzig, E. dUTPase: the frequently overlooked enzyme encoded by many retroviruses. *Retrovirology* **2015**, *12*, 70.
- (159) Yu, T.-B., Bai, J. Z., Guan, Z. Cycloaddition-promoted self-assembly of a polymer into well-defined beta sheets and hierarchical nanofibrils. *Angew. Chem. Int. Ed.* **2009**, *48*, 1097–1101.
- (160) Eördögh, Á., Steinmeyer, J., Peewasan, K., Schepers, U., Wagenknecht, H.-A., Kele, P. Polarity Sensitive Bioorthogonally Applicable Far-Red Emitting Labels for






- Postsynthetic Nucleic Acid Labeling by Copper-Catalyzed and Copper-Free Cycloaddition. *Bioconjug. Chem.* **2016**, *27*, 457–464.
- (161) Lee, S. E., Sidorov, A., Goullain, T., Mignet, N., Thorpe, S. J., Brazier, J. A., Dickman, M. J., Hornby, D. P., Grasby, J. A., Williams, D. M. Enhancing the catalytic repertoire of nucleic acids: a systematic study of linker length and rigidity. *Nucleic Acids Res.* **2001**, *29*, 1565–1573.
- (162) Goullain, T., Sidorov, A., Mignet, N., Thorpe, S. J., Lee, S. E., Grasby, J. A., Williams, D. M. Enhancing the catalytic repertoire of nucleic acids. II. Simultaneous incorporation of amino and imidazolyl functionalities by two modified triphosphates during PCR. *Nucleic Acids Res.* **2001**, *29*, 1898–1905.
- (163) Bergen, K., Steck, A.-L., Strütt, S., Baccaro, A., Welte, W., Diederichs, K., Marx, A. Structures of KlenTaq DNA polymerase caught while incorporating C5-modified pyrimidine and C7-modified 7-deazapurine nucleoside triphosphates. *J. Am. Chem. Soc.* **2012**, *134*, 11840–11843.
- (164) Cserép, G., Demeter, O., Bätzner, E., Kállay, M., Wagenknecht, H.-A., Kele, P. Synthesis and Evaluation of Nicotinic Acid Derived Tetrazines for Bioorthogonal Labeling. *Synthesis* **2015**, *47*, 2738–2744.
- (165) Kara, S. S., Ateş, M. Y., Deveci, G., Cetinkaya, A., Kahveci, M. U. Direct synthesis of tetrazine functionalities on polymer backbones. *J. Polym. Sci. Part A: Polym. Chem.* **2019**, *57*, 673–680.
- (166) Nikić, I., Plass, T., Schraidt, O., Szymański, J., Briggs, J. A. G., Schultz, C., Lemke, E. A. Minimal tags for rapid dual-color live-cell labeling and super-resolution microscopy. *Angew. Chem. Int. Ed.* **2014**, *53*, 2245–2249.
- (167) Li, J., Jia, S., Chen, P. R. Diels-Alder reaction-triggered bioorthogonal protein decaging in living cells. *Nat. Chem. Biol.* **2014**, *10*, 1003–1005.
- (168) Dommerholt, J., Rutjes, F. P. J. T., van Delft, F. L. Strain-Promoted 1,3-Dipolar Cycloaddition of Cycloalkynes and Organic Azides. *Top. Curr. Chem.* **2016**, *374*, 16.
- (169) Wang, D., Chen, W., Zheng, Y., Dai, C., Wang, K., Ke, B., Wang, B. 3,6-Substituted-1,2,4,5-tetrazines: tuning reaction rates for staged labeling applications. *Org. Biomol. Chem.* **2014**, *12*, 3950–3955.









- (170) Yang, J., Karver, M. R., Li, W., Sahu, S., Devaraj, N. K. Metal-catalyzed one-pot synthesis of tetrazines directly from aliphatic nitriles and hydrazine. *Angew. Chem. Int. Ed.* **2012**, *51*, 5222–5225.
- (171) Kozma, E., Estrada Girona, G., Paci, G., Lemke, E. A., Kele, P. Bioorthogonal double-fluorogenic siliconrhodamine probes for intracellular super-resolution microscopy. *Chem. Commun.* **2017**, *53*, 6696–6699.
- (172) Sheng, J., Hassan, A. E. A., Zhang, W., Zhou, J., Xu, B., Soares, A. S., Huang, Z. Synthesis, structure and imaging of oligodeoxyribonucleotides with tellurium-nucleobase derivatization. *Nucleic Acids Res.* **2011**, *39*, 3962–3971.
- (173) Zhu, X.-F., Williams, H. J., Scott, A. I. Facile and highly selective 5'-desilylation of multisilylated nucleosides. *J. Chem. Soc.* **2000**, 2305–2306.
- (174) McKeen, C. M., Brown, L. J., Nicol, J. T. G., Mellor, J. M., Brown, T. Synthesis of fluorophore and quencher monomers for use in scorpion primers and nucleic acid structural probes. *Org. Biomol. Chem.* **2003**, *1*, 2267–2275.
- (175) Grimm, J. B., Brown, T. A., Tkachuk, A. N., Lavis, L. D. General Synthetic Method for Si-Fluoresceins and Si-Rhodamines. *ACS Cent. Sci.* **2017**, *3*, 975–985.
- (176) Maggi, A., Ruivo, E., Fissers, J., Vangestel, C., Chatterjee, S., Joossens, J., Sobott, F., Staelens, S., Stroobants, S., van der Veken, P., Wyffels, L., Augustyns, K. Development of a novel antibody-tetrazine conjugate for bioorthogonal pretargeting. *Org. Biomol. Chem.* **2016**, *14*, 7544–7551.
- (177) Selvaraj, R., Fox, J. M. An efficient and mild oxidant for the synthesis of s-tetrazines. *Tetrahedron Lett.* **2014**, *55*, 4795–4797.
- (178) Grimm, J. B., Lavis, L. D. Caveat fluorophore: an insiders' guide to small-molecule fluorescent labels. *Nat. Methods* **2021**.
- (179) Kobayashi, R., Kato, A., Sagara, H., Watanabe, M., Maruzuru, Y., Koyanagi, N., Aii, J., Kawaguchi, Y. Herpes Simplex Virus 1 Small Capsomere-Interacting Protein VP26 Regulates Nucleocapsid Maturation. *J. Virol.* **2017**, *91*.
- (180) Weerasooriya, S., DiScipio, K. A., Darwish, A. S., Bai, P., Weller, S. K. Herpes simplex virus 1 ICP8 mutant lacking annealing activity is deficient for viral DNA replication. *PNAS* **2019**, *116*, 1033–1042.

- (181) Weller, S. K., Lee, K. J., Sabourin, D. J., Schaffer, P. A. Genetic analysis of temperature-sensitive mutants which define the gene for the major herpes simplex virus type 1 DNA-binding protein. *J Virol* **1983**, *45*, 354–366.
- (182) Rutkowski, A. J., Erhard, F., L'Hernault, A., Bonfert, T., Schilhabel, M., Crump, C., Rosenstiel, P., Efstathiou, S., Zimmer, R., Friedel, C. C., Dölken, L. Widespread disruption of host transcription termination in HSV-1 infection. *Nat. Commun.* **2015**, *6*, 7126.
- (183) Frazzati-Gallina, N. M., Paoli, R. L., Mourão-Fuches, R. M., Jorge, S. A., Pereira, C. A. Higher production of rabies virus in serum-free medium cell cultures on microcarriers. *J. Biotechnol.* **2001**, *92*, 67–72.
- (184) Kautz, T. F., Forrester, N. L. RNA Virus Fidelity Mutants: A Useful Tool for Evolutionary Biology or a Complex Challenge? *Viruses* **2018**, *10*.
- (185) Dörte Stalling. *Characterization of novel iEDDA nucleosides for bioorthogonal herpesvirus genome labeling*. master thesis: Hannover, 2022.
- (186) Honess, R. W., Watson, D. H. Herpes simplex virus resistance and sensitivity to phosphonoacetic acid. *J. Virol.* **1977**, *21*, 584–600.
- (187) Gerasimaitė, R., Seikowski, J., Schimpfhauser, J., Kostiuik, G., Gilat, T., D'Este, E., Schnorrenberg, S., Lukinavičius, G. Efflux pump insensitive rhodamine-jasplakinolide conjugates for G- and F-actin imaging in living cells. *Org. Biomol. Chem.* **2020**, *18*, 2929–2937.
- (188) McDonald, D., Vodicka, M. A., Lucero, G., Svitkina, T. M., Borisy, G. G., Emerman, M., Hope, T. J. Visualization of the intracellular behavior of HIV in living cells. *J. Cell Biol.* **2002**, *159*, 441–452.
- (189) Sarkar, I., Hauber, I., Hauber, J., Buchholz, F. HIV-1 proviral DNA excision using an evolved recombinase. *Science* **2007**, *316*, 1912–1915.
- (190) Schäfer, B., Hauber, I., Bunk, A., Heukeshoven, J., Düsedau, A., Bevec, D., Hauber, J. Inhibition of multidrug-resistant HIV-1 by interference with cellular S-adenosylmethionine decarboxylase activity. *J. Infect. Dis.* **2006**, *194*, 740–750.







## 8 Hazardous substance register

All hazardous and CMR substances used are listed in the following tables. The GHS pictograms and the H- and P-statements were taken from the Sigma Aldrich and Alfa Aesar catalogues.







Substance	GHS pictograms	H-statements	P-statements
(1,1'-Bis(diphenylphosphino)-ferrocene)palladium(II) dichloride	This substance is not classified as dangerous according to directive 67/548/EWG.		
(1S,2E)-Cyclooct-2-en-1-yl succinimidylcarbonate	This substance is not classified as dangerous according to directive 67/548/EWG.		
1,1'-Carbonylimidazole	 Danger	302-314	280-305+351+338-310
1,2-Dichloroethane	 Danger	225-302-304-315-319-331-335-350	210-301+310-303+361+353-304+340+311-305+351+338-331
1,4-Dioxane	 Danger	225-319-335-351-EUH019-EUH066	202-210-233-240-305+351+338-308+313
1-Butanol	 Danger	226-302-318-315-335-336	210-280-302+352-305+351+338-313
1-Ethyl-3-(3-dimethylaminopropyl) carbodiimide hydrochloride	 Danger	302-311-315-317-373-410	260-273-280-301+312-302+352+312-314

1- <i>O</i> -acetyl-2,3,5- <i>tri-O</i> -benzoyl- $\beta$ - <i>D</i> -ribofuranose	This substance is not classified as dangerous according to directive 67/548/EWG.		
1-Undecanol	 Warning	319-410	273- 305+351+338
2,2,2-Trifluoroethanol	  Danger	226-301+331- 318-360F-373	201-210-280- 304+340- 305+351+338- 308+310
2'-Deoxy-5-iodocytidine	 Warning	302	-
2-Bromoterephthalic acid	 Warning	315-319-335	261-280- 302+352- 304+340- 305+351+338
2-Cyanopyridine	 Warning	302-315-319-335	261- 305+351+338
2-deoxy-3,5-di- <i>O</i> -( <i>P</i> -toluoyl)- $\alpha$ - <i>D</i> - <i>erythro</i> -pentofuranosyl chloride	This substance is not classified as dangerous according to directive 67/548/EWG.		
3-Bromiodobenzene	 Warning	315-319-335	261-264-271- 280-302+352- 305+351+338
3-Bromo- <i>N,N</i> -dimethylaniline	 Danger	301+311+331- 319-351-373-410	201-273-280- 301+310+330- 302+352+312- 304+340+311
3-Hydroxypropionitrile	This substance is not classified as dangerous according to directive 67/548/EWG.		









## Hazardous substance register








3-Mercaptopropionic acid	 Danger	301+314	270-280-301- 330+331- 303+361+353- 304+340+310- 305+351+338
3-Methyl-3-oxetanemethanol	This substance is not classified as dangerous according to directive 67/548/EWG.		
4-(Diethylamino)salicylaldehyde	 Warning	315-319-335	261- 305+351+338
4-(Dimethylamino)pyridine	 Danger	310-301-315-319	302+352- 305+351+338
4-Chloro-5-iodo-7H-pyrrolo[2,3-d]-pyrimidine	This substance is not classified as dangerous according to directive 67/548/EWG.		
4-Dimethylaminopyridine	 Danger	301+331-310- 315-318-370-411	262-273-280- 301+310- 302+352+310- 305+351+338
4-Hydroxybenzyl alcohol	 Warning	319-412	264-273-280- 305+351+338- 337+313-501
5-Amino-2-cyanopyridine	 Warning	302+312+332- 315-319-335	261-280- 301+312- 302+352+312- 304+340+312- 305+351+338
5-Bromophthalide	This substance is not classified as dangerous according to directive 67/548/EWG.		









5-Iodocytidine	This substance is not classified as dangerous according to directive 67/548/EWG.		
6-Aminohexanoic acid	This substance is not classified as dangerous according to directive 67/548/EWG.		
9-Fluorenylmethanole	This substance is not classified as dangerous according to directive 67/548/EWG.		
Acetic acid	 Danger	226-314	210-233-240-280-303+361+353-305+351+338
Acetic anhydride	 Danger	226-302-331-314-335	210-260-280-303+361+353-305+351+338-312
Acetone	 Danger	225-319-336-EUH066	210-233-240-241-242-305+351+338
Acetonitrile	 Danger	225-302+312+332-319	210-280-301+312-302+352-304+340-305+351+338
Amino-4-pentyne	 Danger	225-314	210-280-305+351+338-310
Ammonium acetate	This substance is not classified as dangerous according to directive 67/548/EWG.		
Ammonium bicarbonate	 Warning	302	264-301+330+331-312










## Hazardous substance register

Ammonium chloride	 Warning	319-302	270-280- 305+351+338
Azetidine	 Danger	225-314	210-280- 305+351+338- 310
Bis(trimethylsilyl)acetamide	 Warning	315-319-335	261-280- 305+351+338- 304+340-405- 501
Bis(triphenylphosphine)palladium(II) dichloride	 Warning	317-413	261-272-273- 280-302+352- 333+313
Chlorotrimethylsilane	 Danger	225-301+331- 312-314-EUH014	210-233-280- 303+361+353- 304+340+310- 305+351+338
Copper(I) iodide	 Danger	302-315-317-318- 410	261-273-280- 301+312- 302+352- 305+351+338
Copper(II) bromide	 Danger	302-314	280- 305+351+338- 310
Decanoyl chloride	 Danger	314	280- 303+361+353- 304+340+310- 305+351+338- 363-405








Diazabicycloundecene	 Danger	301-314-412-290	273-280- 301+310+330- 301+330+331- 303+361+353- 305+351+338
Dichlorodimethylsilane	 Danger	225-302-314-331	280- 301+330+331- 303+361+353- 305+351+338- 310-210
Dichloromethane	 Warning	315-319-336-351	201-202-261- 302+352- 305+351+338- 308+313
Dicyanoimidazole 0.25 M in CH <sub>3</sub> CN	 Danger	225- 302+312+332- 315-318-335	210-280- 301+312- 303+361+353- 304+340+312- 305+351+338
Diethylether	 Danger	224	210-233-240- 241-403+233
Diethylmalonate	 Warning	319	264-280- 305+351+338- 337+313
Diisobutylaluminum hydride	 Danger	250-260-314- EUH014	210-222- 231+232-280- 303+361+353- 305+351+338



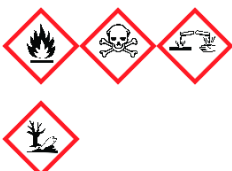


## Hazardous substance register

Diisopropylethylamine	 Danger	225-302-331-318-335	210-280-301+312+330-304+340+311-305+351+338+310
Dimethylsulfoxide	This substance is not classified as dangerous according to directive 67/548/EWG.		
Diphenylphosphite	 Danger	302-315-318-335	280-301+312+330-302+352-305+351+338-310
Diphenylphosphoryl azide	 Danger	301-310-330-315-319-335	280-302+352-304+340-310-332+313-337+313
Dirhodium tetraacetate	This substance is not classified as dangerous according to directive 67/548/EWG.		
Disuccinimidyl carbonate	 Warning	315-319-335	302+352-305+351+338
Di- <i>tert</i> -butyl dicarbonate	 Danger	226-315-317-318-330-335	210-233-280-303+361+353-304+340+310-305+351+338
endo-BCN-NHS carbonate	This substance is not classified as dangerous according to directive 67/548/EWG.		
Ethanol	 Danger	225-319	210-305+351+338







Ethyl acetate	 Danger	225-319-336- EUH066	210-233-240- 242- 305+351+338
Ethyl diazoacetate	 Warning	226-242-302-315- 319-351	210-301+312- 303+361+353- 308+313- 370+378- 403+235
Ethyl trifluoroacetate	 Danger	225-319-412	210-264-280- 303+361+353- 337+313
Ethylene glycol	 Warning	302-373	301+312+330
Ethylenediamine	 Danger	226-302+332- 311-314-317-334- 412	210-273-280- 303+361+353- 304+340+310- 305+351+338
Formamidine acetate	 Warning	317	280
HATU	 Danger	228-315-319-335	210-261- 305+351+338
Hexane	 Danger	225-304-315-336- 361f-373-411	210-260-273- 280-301+310- 331-302+352
Hexynoic acid	 Warning	315-319-335	261-264-271- 280-302+352- 305+351+338

## Hazardous substance register
















Hydrazine hydrate solution (80 % in water)	 Danger	301+311-314- 317-330-350-410	280- 301+330+331- 302+350- 305+351+338- 304+340-310
Hydrochloric acid (37 %)	 Danger	290-314-335	234-261-271- 280- 303+361+353- 305+351+338
Hydrogen chloride (4 M in 1,4-dioxane)	 Danger	225-290-315-319- 335-351-EUH019	202-210-233- 303+361+353- 308+318
Hydrogen peroxide (30 % in water)	 Danger	318-412	273-280- 305+351+338- 501
<i>Isobutyl</i> chloroformate	 Danger	226-302-314-331	210-280- 301+P312- 303+361+353- 304+340+310- 305+351+338
Methanesulfonyl chloride	 Danger	290-301+311- 314-317-330-335	234-260-280- 303 +361+353- 304+340+310- 305+351+338
Methanol	 Danger	225- 301+311+331- 370	210-280-233- 301+310- 303+361+353- 304+340+311

Methyl chloroformate	 Danger	225-300-312-330-314	210-280-301+330+331-303+361+353-305+351+338-310
<i>N</i> -( <i>tert</i> -Butoxycarbonyl)glycine	This substance is not classified as dangerous according to directive 67/548/EWG.		
<i>N,N</i> -dicyclohexylmethylamine	 Danger	302-314	270-280-301+312-303+361+353-304+340+310-305+351+338
<i>N,N</i> -Diisopropylethylamine	 Danger	225-302-318-331-335-411	210-273-280-301+312-304+340+311-305+351+338
<i>N</i> -Bromosuccinimide	 Warning	272-290-315-317-319-341-400	210-273-280-302+352-305+351+338-308+313
<i>N</i> -Bromosuccinimide	 Warning	272-290-315-317-319-341-400	210-273-280-302+352-305+351+338-308+318







## Hazardous substance register








n-Butyllithium (1.6 M in Hexan)	 Danger	2252-250-260- 304-314-336- 361f-411-EUH014	210-231+232- 280- 301+330+331- 303+361+353- 304+340+310- 305+351+338- 370+378
N-Chlorosuccinimide	 Danger	290-302-314-335- 410	260-273-280- 301+312- 303+361+353- 305+351+338
N-Hydroxysuccinimide	This substance is not classified as dangerous according to directive 67/548/EWG.		
Nicotinic acid	 Warning	319	305+351+338
N-Methyl pyrrolidone	 Danger	315-319-335- 360D	201-302+352- 305+351+338- 308+313
N-Methylimidazole	 Danger	302-311-314	270-280- 301+312- 301+330+331- 303+361+353- 305+351+338
Palladium(II) acetate	 Danger	317-318-361d- 410	202-273-280- 302+352- 305+351+338- 308+313










Petroleum ether (50 – 70 °C)	    Danger	225-304-315-336- 361f-373-411	201-210-273- 301+310- 303+361+353- 331
Phenyl iodonium diacetate	This substance is not classified as dangerous according to directive 67/548/EWG.		
Phosphoryl chloride	   Danger	302-314-330-372	280-301+312- 303+361+353- 304+340+310- 305+351+338- 314
Piperidine	   Danger	225-302- 311+331-314	210-280- 301+312- 303+361+353- 304+340+310- 305+351+338
Potassium acetate	This substance is not classified as dangerous according to directive 67/548/EWG.		
Potassium carbonate	 Warning	315-319-335	261-264-271- 280-302+352- 305+351+338
Propargylamine	   Danger	225-302-310-314	210-233-280- 301+312- 303+361+353- 305+351+338
<i>p</i> -Toluenesulfonic acid monohydrate	 Danger	290-314-412	234-260-273- 280- 303+361+353- 305+351+338








## Hazardous substance register

Pyridine	 Danger	225- 302+312+332- 315-319	210-280- 301+312- 303+361+353- 304+340+312- 305+351+338
Sodium bicarbonate	This substance is not classified as dangerous according to directive 67/548/EWG.		
Sodium carbonate	 Warning	319	264-280- 305+351+338- 337+313
Sodium chloride	This substance is not classified as dangerous according to directive 67/548/EWG.		
Sodium cyanide	 Danger	290- 300+310+330- 372-410-EUH032	262-273-280- 302+352+310- 304+340+310- 314
Sodium hydroxide	 Danger	290-314	234-260-280- 303+361+353- 304+340+310- 305+351+338
Sodium nitrite	 Danger	272-301-319-400	210-220-264- 273-301+310- 305+351+338
Sodium sulfate	This substance is not classified as dangerous according to directive 67/548/EWG.		
Substance	GHS pictograms	H statements	P statements
Sulfur	 Warning	315	264-280- 302+352- 332+313- 362+364



Tris-(3,6-dioxaheptyl)-amin, TDA-1	 Danger	314	280- 303+ 361+353- 304+340 +310- 305+351+338- 363-405
<i>tert</i> -Butyl hydroperoxide solution 5.5 M in decane	 Danger	226-242-302-304- 311-314-317-330- 335-341-411	210-280- 301+330+331- 303+361+353- 304+340+310- 305+351+338- 370+378
<i>tert</i> -Butyldimethylsilylchlorid	 Danger	228-314-411	210-273-280- 303+361+353- 305+351+338+3 10
Tetrabutylammonium dihydrogen phosphate (0.4 M in acetonitrile)	 Danger	225- 302+312+332- 319	210-280- 301+312- 303+361+353- 304+340+312- 305+351+338
Tetrabutylammonium fluoride (1 M in THF)	 Danger	225-302-315-319- 335-336-351-411- EUH019-EUH032	210-273- 301+312- 303+361+353- 305+351+338- 308+313
Tetrahydrofuran	 Danger	225-302-319-335- 336-351-EUH019	201-202-210- 301+312- 305+351+338- 308+313
Tetrakis(triphenylphosphine)- palladium(0)	 Warning	302	264-270- 301+312-501

## Hazardous substance register

Thionyl chloride	 Danger	302-331-314-335	280- 301+330+331- 304+340- 305+351+338- 308+310
Toluene	 Danger	225-304-315-336- 361d-373-412	202-210-273- 301+310- 303+361+353- 331
Tri(2-furyl)phosphine	This substance is not classified as dangerous according to directive 67/548/EWG.		
Tri(cyclohexyl)phosphine	 Warning	315-319-335	261-264-271- 280-302+352- 305+351+338
Tributyl(vinyl) tin	 Danger	226-301-312-315- 319-360FD-372- 410	210-273-280- 301+310- 303+361+353- 305+351+338
Triethylorthoacetate	 Warning	226	210-233-240- 241-242-243- 302+352
Triethylphosphate	 Warning	302	301+312
Triethylamine	 Danger	225-302- 311+331-314-335	210-280- 301+330+331- 303+361+353- 304+340+311- 305+351+338+3 10

Triethylamine trihydrofluoride	 Danger	300+310+330-314	260-270-280-303+361+353-304+340+310-305+351+338
Triethylammonium bicarbonate buffer (1 M)	This substance is not classified as dangerous according to directive 67/548/EWG.		
Trifluoroacetic anhydride	 Danger	314-332-412-EUH014	273-280-301+310+331-303+361+353-304+340+312-305+351+338-310
Trifluoromethanesulfonic anhydride	 Danger	272-302-314-335-EUH014	210-220-280-301+312-303+361+353-305+351+338
Trimethylphosphate	 Danger	302-315-319-340-351	201-301+312+330-302+352-305+351+338-308+313
Trimethylsilyl trifluoromethanesulfonate	 Danger	226-314	280-305+351+338-310
Trimethylsilylacetylene	 Danger	225-315-319	210-233-240-241-303+361+353-305+351+338
Triphenylphosphine	 Danger	302-317-373	280-301+312+330-333+313

Hazardous substance register

Tris(dibenzylideneacetone)- dipalladium(0)	  Warning	317-411	261-272-273- 280-302+352- 333+313
QPhos	This substance is not classified as dangerous according to directive 67/548/EWG.		
Zinc triflate	This substance is not classified as dangerous according to directive 67/548/EWG.		

## Acknowledgements

### Mein Dank gilt...

Herrn Prof. Dr. Chris Meier für die Bereitstellung des interessanten Themas und dem Vertrauen die Fragestellung in Freiheit erkunden zu können. Ich bedanke mich für die stete Unterstützung und für das offene Ohr.

Herrn Prof. Dr. Volkmar Vill für die freundliche Übernahme des Zweitgutachtens.

Herrn Dr. T. Hackl und Frau Dr. M. Riedner und ihren MitarbeiterInnen für die Anfertigung zahlreicher NMR- und MS-Spektren und für ihre Hilfsbereitschaft bei besonderen Wünschen oder langen Messzeiten.

Herrn Prof. J. Bosse und seinem Arbeitskreis am CSSB für die warme Aufnahme und die geduldige Einführung in ein neues wissenschaftliches Feld.

Herrn Prof. Dr. J. Hauber und Dr. M. Voges vom LIV für die lange Kooperation und die Durchführung zahlreicher Experimente.

Dr. Johanna Huchting für die zahlreichen beantworteten Fragen, dem steten Strom an Ideen und dem Interesse an dieser Arbeit. Danke für das Korrekturlesen dieser Arbeit!

Meinen PraktikantInnen Nils, Desiree, Benedikt, Jelena und insbesondere Iven, der viele Wochen meinen Abzug blockierte und bei dem ich die Weiterführung des Projektes in sicheren und ehrgeizigen Händen weiß.

Dr. Simon Weising, der mir während meiner „Masterzeit“ viel beigebracht hat und mir dadurch einen leichten Start für ein selbständiges Arbeiten ermöglichte.

Bei allen momentanen und ehemaligen Mitgliedern des AK Meier, die wussten eine Atmosphäre zu schaffen, die Leichtigkeit verspricht. Ich hatte eine gute Zeit, an die ich mich gerne zurück erinnern werde. Hier möchte ich besonders meinen „Laborehemann“ Stefan aus dem Exil im 4. Stock hervorheben. Es wurde nie langweilig!

Mein ganz besonderer Dank gilt all meinen FreundInnen und Wohngemeinschaftsmitgliedern, die sich (fast) alle nicht um Chemie scherrten und mir halfen das alles sein Ort hatte und Zuhause zu Hause ist.

Danke Familie, für die sichere und bedingungslose Unterstützung während meines ganzen Studiums – ohne Euch wäre dieser Abschluss nicht möglich.





---

## Declaration on Oath

I hereby declare on oath, that I have written the present dissertation by my own and have not used other than the acknowledged resources and aids. The submitted written version corresponds to the version on the electronic storage medium. I hereby declare that I have not previously applied or pursued for a doctorate (Ph.D. studies).

Hamburg, 08.03.2023

Place, Date



---

Vincente Tassilo Sterrenberg, M.Sc.